frontiers | Research Topics

The effects of climate change and anthropogenic activities on patterns, structures and functions of terrestrial ecosystems

Edited by
Guoqi Wen, Cuicui Jiao, Wei Zhao and Wenping Yuan

Coordinated by
Xiao Guo

Published in
Frontiers in Ecology and Evolution

ISSN 1664-8714
ISBN 978-2-8325-3796-1
DOI 10.3389/978-2-8325-3796-1

About Frontiers

Frontiers is more than just an open access publisher of scholarly articles: it is a pioneering approach to the world of academia, radically improving the way scholarly research is managed. The grand vision of Frontiers is a world where all people have an equal opportunity to seek, share and generate knowledge. Frontiers provides immediate and permanent online open access to all its publications, but this alone is not enough to realize our grand goals.

Frontiers journal series

The Frontiers journal series is a multi-tier and interdisciplinary set of open-access, online journals, promising a paradigm shift from the current review, selection and dissemination processes in academic publishing. All Frontiers journals are driven by researchers for researchers; therefore, they constitute a service to the scholarly community. At the same time, the *Frontiers journal series* operates on a revolutionary invention, the tiered publishing system, initially addressing specific communities of scholars, and gradually climbing up to broader public understanding, thus serving the interests of the lay society, too.

Dedication to quality

Each Frontiers article is a landmark of the highest quality, thanks to genuinely collaborative interactions between authors and review editors, who include some of the world's best academicians. Research must be certified by peers before entering a stream of knowledge that may eventually reach the public - and shape society; therefore, Frontiers only applies the most rigorous and unbiased reviews. Frontiers revolutionizes research publishing by freely delivering the most outstanding research, evaluated with no bias from both the academic and social point of view. By applying the most advanced information technologies, Frontiers is catapulting scholarly publishing into a new generation.

What are Frontiers Research Topics?

Frontiers Research Topics are very popular trademarks of the *Frontiers journals series*: they are collections of at least ten articles, all centered on a particular subject. With their unique mix of varied contributions from Original Research to Review Articles, Frontiers Research Topics unify the most influential researchers, the latest key findings and historical advances in a hot research area.

Find out more on how to host your own Frontiers Research Topic or contribute to one as an author by contacting the Frontiers editorial office: frontiersin.org/about/contact

The effects of climate change and anthropogenic activities on patterns, structures and functions of terrestrial ecosystems

Topic editors

Guoqi Wen — Laval University, Canada
Cuicui Jiao — Sichuan University of Science and Engineering, China
Wei Zhao — Institute of Geographic Sciences and Natural Resources Research, Chinese Academy of Sciences (CAS), China
Wenping Yuan — Sun Yat-sen University, China

Topic coordinator

Xiao Guo — Sichuan University of Science and Engineering, China

Citation

Wen, G., Jiao, C., Zhao, W., Yuan, W., Guo, X., eds. (2023). *The effects of climate change and anthropogenic activities on patterns, structures and functions of terrestrial ecosystems*. Lausanne: Frontiers Media SA.
doi: 10.3389/978-2-8325-3796-1

Table of contents

frontiers | Frontiers in Ecology and Evolution

TYPE Editorial
PUBLISHED 10 October 2023
DOI 10.3389/fevo.2023.1296292

OPEN ACCESS

EDITED AND REVIEWED BY
Dennis Murray,
Trent University, Canada

*CORRESPONDENCE
Cuicui Jiao
jiaocui_cui@163.com

RECEIVED 18 September 2023
ACCEPTED 02 October 2023
PUBLISHED 10 October 2023

CITATION
Jiao C (2023) Editorial: The effects of climate change and anthropogenic activities on patterns, structures and functions of terrestrial ecosystems. *Front. Ecol. Evol.* 11:1296292. doi: 10.3389/fevo.2023.1296292

Editorial: The effects of climate change and anthropogenic activities on patterns, structures and functions of terrestrial ecosystems

Cuicui Jiao*

Research Center of Agricultural Economy, School of Economics, Sichuan University of Science and Engineering, Zigong, China

KEYWORDS

climate change, anthropogenic activities, terrestrial ecosystems, carbon cycles, nitrogen cycles, ecological vulnerability, biodiversity

Editorial on the Research Topic:
The effects of climate change and anthropogenic activities on patterns, structures and functions of terrestrial ecosystems

Climate change and anthropogenic activities are two profound forces influencing terrestrial ecosystems. The extent, velocity, and interplay of their effects offer a rich tapestry for scientific exploration, as the myriad of interactions and feedbacks are both nuanced and wide-reaching. This Research Topic, comprising 17 meticulous studies, delves deep into the multifaceted impacts of these forces on various ecological parameters, offering insights, patterns, and predictions of potential futures.

In Eurasian grasslands, where precipitation and productivity share a complex relationship, the pioneering work by Zhang et al. elucidates how these dynamics can be instrumental in identifying ecosystem transitions. Extending this analysis to a global scale, Chen et al. evaluates the determinants of photosynthetic capacity in grasslands, shedding light on the intertwined nature of ecosystems and their climatic contexts.

The role of human intervention, often regarded as a primary perturbing force, is sometimes positive. Liu et al. provides evidence of how, under the ever-evolving climate change scenario, anthropogenic activities have bolstered ecosystem productivity between 1983 and 2018.

Urban sprawl and land use changes, while central to human needs, reverberate through ecological processes. The study by Tao et al. focused on the Nanjing metropolitan circle, dynamically simulates these impacts on carbon storage under various development trajectories. Meanwhile, Cheng et al., Zhao et al., Su et al., and Chen et al. deliver comprehensive assessments of China's forest carbon distribution, extreme temperatures

in the Qilian Mountains, the rich biodiversity of the evergreen-deciduous karst forests, and the merits of the National Key Ecological Function Areas, respectively.

Drought—a significant concern in the era of climate change—is examined through its impacts on microbial genes in alpine peatland (Yan et al.) and on critical enzyme genes in Scutellaria baicalensis (Li et al.). The role of rainfall and its influence on temperate forest ecosystem services is adeptly tackled in Liang et al., reiterating the significance of water as an ecological driver.

The systematic review by Liu et al., which collates insights from multiple ecological restoration studies in China, underscores the importance of policy-driven ecological initiatives. It serves as a precursor to Lv et al. and Tang et al., focusing on carbon sequestration and the vulnerabilities in the karst regions, offering a roadmap for sustainable restoration.

The technological integration of modern research techniques finds its representation in this Research Topic too. The study on maize by Peng et al. combines an optimized model to unravel the connections between photosynthesis, evapotranspiration, and dry matter distribution. Furthermore, the use of a hybrid machine learning model (He et al.) showcases the potential of modern computational tools in mapping seagrass habitats.

In conclusion, this Research Topic paints a vivid and comprehensive portrait of the myriad ways in which climate change and anthropogenic activities shape, mold, and sometimes challenge terrestrial ecosystems. It is our hope that these contributions not only enhance understanding but also guide future actions and policy decisions, ensuring a balanced coexistence of human aspirations and ecological imperatives.

Author contributions

CJ: Writing – original draft, Writing – review & editing.

Acknowledgments

As the guest editor of this Research Topic, I am deeply grateful to all contributors, reviewers, and the editorial team for their commitment and expertise. Our hope is that this Research Topic fosters collaboration, sparks further research, and informs policy decisions that guide humanity towards a sustainable coexistence with nature.

Conflict of interest

The author declares that the research was conducted in the absence of any commercial or financial relationships that could be construed as a potential conflict of interest.

Publisher's note

frontiers | Frontiers in Ecology and Evolution

TYPE Original Research
PUBLISHED 17 January 2023
DOI 10.3389/fevo.2023.1093135

OPEN ACCESS

EDITED BY
Cuicui Jiao,
Sichuan University of Science and Engineering, China

REVIEWED BY
Mengmeng Gou,
Chinese Academy of Forestry, China
Li Lipeng,
Ningxia University, China
Haimeng Liu,
Chinese Academy of Sciences (CAS), China

*CORRESPONDENCE
Mengyang Hou
houmengyang@hbu.edu.cn

SPECIALTY SECTION
This article was submitted to Population, Community, and Ecosystem Dynamics, a section of the journal Frontiers in Ecology and Evolution

RECEIVED 08 November 2022
ACCEPTED 02 January 2023
PUBLISHED 17 January 2023

CITATION
Chen H, Hou M, Xi Z, Zhang X and Yao S (2023) Co-benefits of the National Key Ecological Function Areas in China for carbon sequestration and environmental quality. *Front. Ecol. Evol.* 11:1093135. doi: 10.3389/fevo.2023.1093135

Co-benefits of the National Key Ecological Function Areas in China for carbon sequestration and environmental quality

Hanyu Chen[1,2], Mengyang Hou[1,2]*, Zenglei Xi[1,2], Xiao Zhang[3,4] and Shunbo Yao[3,4]

[1]School of Economics, Hebei University, Baoding, China, [2]Research Center of Resources Utilization and Environmental Conservation, Hebei University, Baoding, China, [3]College of Economics and Management, Northwest A&F University, Yangling, China, [4]Center for Resource Economics and Environment Management, Northwest A&F University, Yangling, China

Introduction: The National Key Ecological Functional Areas (NKEFAs) are location-oriented ecological engineering of China, which rely on the main functional area planning. The co-benefits of ecological product supply and ecological environment improvement of NKEFAs has not been fully assessed in the literature.

Methods: NKEFAs is considered a quasi-natural experiment, and the time-varying difference-in-differences (DID) model is used to assess the impact of NKEFAs on carbon sequestration (CS) and environmental quality (EQ) based on the panel data of 330 cities in China from 2001 to 2019. Then, we explore whether the co-benefits of ecological product supply and eco-environment protection can be achieved.

Results and discussion: NKEFAs can enhance CS and EQ and thus achieve co-benefits for both. NKEFAs can achieve the co-benefits of CS and EQ through territory spatial allocation and labor force aggregation, but industrial structure upgrading only positively mediates the impact of NKEFAs on CS. The co-benefits of CS and EQ are heterogeneous across functional area types, geospatial locations, and quantiles, while only CS at windbreak-sand fixation area, northwestern region, and low quantile regions is enhanced. This study makes a theoretical and methodological contribution to the existing literature on the policy effect assessment of ecological engineering. It also provides a comprehensive framework for evaluating the ecological effects of relevant policies in other countries by integrating the co-benefits of ecological products and eco-environment, analyzing regional heterogeneity, and exploring the underlying mechanisms.

KEYWORDS

National Key Ecological Function Areas, carbon sequestration, environmental quality, co-benefits, time-varying difference-in-differences, China

1. Introduction

The effectiveness of ecological policies and environmental regulation has received widespread global attention in recent decades, regarding that climate change and environmental degradation are already critical problems that threatening humankind (Dong et al., 2022). Facing the above threat, Chinese government has committed to reaching peak carbon emissions by 2030 and carbon neutrality by 2060 (Yu and Zhang, 2021). Therefore, achieving the goals of dual-carbon strategy and improving ecological environment are the basic need of high-quality green development. Territorial space use is mainly expressed as the interaction between ecosystems and human activities (Ball et al., 2010). Inappropriate ways and unreasonable structure of human activities induce terrestrial ecosystem degradation, which significantly explains the growing carbon emission intensity and environmental

problems (Gao et al., 2013). The rough expansion of industrialization and urbanization results in structural contradiction in land space utilization, encroaching on the ecological space (Lin et al., 2020).

In order to reasonably use the territory, China issued the National Main Function Area Planning in December 2010, which specifies the main functions of different regions (Liu J. et al., 2017; Liu W. et al., 2017), gradually form a spatial development pattern of the national territory in harmony with population, economy, resources and environment. According to the development content, the main functional areas can be divided into urbanized areas, main agricultural producing areas, and key ecological functional areas. Among them, the National Key Ecological Function Areas (NKEFAs) are important to ensure national ecological security, primarily for protecting the ecological environment and enhancing the ecological product supply. NKEFAs bear important ecological functions such as water conservation, soil conservation, windbreak sand fixation and biodiversity maintenance. Currently, China established the first batch of NKEFAs covering 436 counties at the end of 2010 (Xu et al., 2018), to which 240 new counties were added in 2016 (Figure 1). Since 2011, NKEFAs have become the largest regional ecological policy in China (Zhu and Chen, 2020).

Over the years since the establishment of NKEFAs, it is worthwhile to explore its ecological benefits in the context of the dual carbon strategy. The existing studies focus on the effect of fiscal transfer payments, the quantitative of ecosystem service changes in NKEFAs, etc. (Miao and Zhao, 2019; Xu et al., 2019; Liu et al., 2020). Early studies indicated that the ecological benefits of NKEFAs is unobvious, which is related to the precision and target matching of its transfer payment policy (Li et al., 2013, 2014; Li and Li, 2014). found that the transfer payment of NKEFAs promoted environment quality in the Qinba Mountains of Shaanxi, but relatively weak. In contrast, Xu and Zhang (2017) found that the positive ecological effect of transfer payment was relatively significant for NKEFAs in Shaanxi Province, with the ecological environment in the base period playing an indispensable role. Additionally, by comparing the environmental changes before and after the NKEFAs through GIS technology, its eco-environment shows an improvement trend (Liu et al., 2018; Zhang M. et al., 2022, Zhang T. et al., 2022), varying with different function area types (Hou et al., 2018). In addition, The afforestation area of NKEFAs received the attention of scholars (Bryan et al., 2018; Pan, 2021), and there is also literature focusing on the carbon reduction effect or air pollution control of ecological policies (Dong et al., 2022; Gao et al., 2022; Liu et al., 2022).

Existing studies have deeply investigated the ecological effect of NKEFAs but have limitations. First, the relevant literature focuses on transfer payment, most of which is the experience summary and theoretical discussion. Second, the quantitative analysis is mostly case studies, and the interference of other ecological policies is nearly unavoidable in GIS-based analysis. More importantly, existing studies focus more on the eco-environmental effect, but neglect the major goal of NKEFAs to enhance the ecological product supply (Zhang M. et al., 2022; Zhang T. et al., 2022). Carbon sequestration (CS) is the ability of vegetation to absorb and store carbon dioxide, which is an important ecological product (Liu and Song, 2022). So, the achievement of NKEFAs' ecological goals requires both enhancing CS and improving environmental quality (EQ), and to promote the joint improvement of both, which is also known as co-benefits. Therefore, it is necessary to assess the NKEFAs' CS capacity and co-benefits of CS and EQ.

Specifically, we consider the NKEFAs as a "quasi-natural experiment" (Zhang M. et al., 2022; Zhang T. et al., 2022). Then the

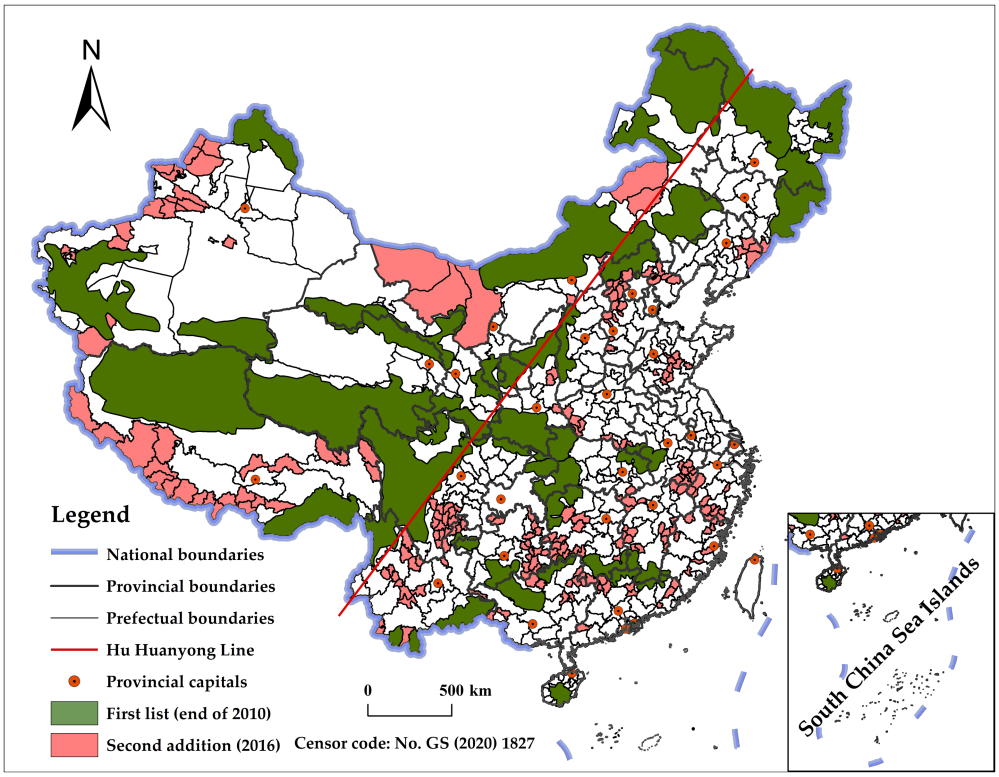

FIGURE 1
The distribution map of NKEFAs.

panel data of 330 cities in China from 2001 to 2019 and a time-varying difference-in-differences (DID) model are used to assess the impact of NKEFAs on CS and EQ, so as to identify the co-benefits of ecological product supply and ecological environment improvement. This study contributes to experience accumulation and institutional improvement to implement sustainable ecological policies in China. It also provides a reference for the synergistic balance between ecological product supply and eco-environmental protection in other countries.

This paper has the advantage of the policy stripping of DID model and large sample data to effectively assess the policy effect of NKEFAs. In addition, the marginal contributions are as follows. First, unlike previous studies, this paper integrates CS and EQ into a framework to investigate whether NKEFAs can achieve the co-benefits of ecological product supply and ecological environment. Second, existing assessments based on inter-provincial average treatment effect (ATE) can hardly accurately reflect individual differences in ecological features within provinces. So, a more detailed examination at a smaller-scale of prefecture level (Rosenthal and Strange, 2003) can eliminate the homogenization error in provincial macro data. Third, existing studies based on GIS technology to compare and analyze the changes of ecological effect before and after the policy implementation or between covered and non-covered areas are difficult to exclude the influence of other ecological policies. The identification using DID model can effectively strip the interference of other similar policies in the same period.

2. Materials and methods

2.1. Data sources

The panel data of 330 cities at the prefecture level and above in China from 2001 to 2019 are selected as the study samples. The areas covered by NKEFAs are manually collated according to relevant policy documents (Table 1). NPP is obtained from the MOD17A3HGF product based on the MODIS satellite launched by NASA, the spatial resolution is 500 m. EQ data came from the CHEQ dataset (2001–2019) released by China's National Earth System Science Data Center,[1] with a spatial resolution of 0.0089°. The land use data is derived from the global land cover product data[2] of the European Space Agency's (ESA) Climate Change Initiative (CCI), with a resolution of 300 m. The data of temperature, precipitation, and sunshine hours were obtained from the annual data set of China's surface climate data from the China Meteorological Data Network.[3] The socio-economic data is provided by the China City Statistical Yearbook, China Regional Economic Statistical Yearbook, and provincial statistical yearbooks of previous years.[4] The missing data is supplemented by prefecture statistical yearbooks or by interpolation. The variance inflation factor (VIF) of each variable is significantly <10, there is no obvious multicollinearity problem among the explanatory variables.

1 www.geodata.cn
2 www.esa-landcover-cci.org
3 www.data.cma.cn
4 https://data.cnki.net/Yearbook

2.2. Variable selection

2.2.1. Explained variables: Carbon sequestration and environmental quality

1. Carbon sequestration (CS). The scale of CS is measured by the net primary productivity (NPP) of vegetation, which can indicate the supply scale of ecological products. CS is mainly the process of absorbs CO_2 from the atmosphere through photosynthesis of plants (UNFCCC, 1997). NPP is the residual of gross primary productivity (GPP) minus the value of autotrophs respiration, which can be deduced from the CO_2 absorbed by plants and the dry matter produced (He et al., 2018). The chemical equation is $6CO_2 + 6H_2O \rightarrow C_6H_{12}O_6 + 6O_2$. Vegetation photosynthesis can fix 1.63 kg of CO_2 for 1 kg of dry matter produced, and the carbon content of dry matter is about 45% in the total NPP. Therefore, the CO_2 per unit area fixed by vegetation is $W_{CO2} = NPP/0.45 \times 1.63$ (g/m^2). The scale of CS is W_{CO2} multiplied by the vegetation cover area (Chen et al., 2020).
2. Environmental quality (EQ). EQ mainly reflects the overall condition of ecological environment, which is characterized by historical data from China's High-resolution Eco-Environmental Quality (CHEQ) dataset (Xu et al., 2021). The dataset is developed based on indicators such as habitat, greenness, dryness, heat, humidity, and abundance index, with a data range of 0–1. It is highly consistent with the environmental index provided by the Ministry of Ecology and Environment of China and can reflect the quality effect of environmental benefits.

2.2.2. Core explanatory variable: NKEFAs

1. The scope of cities covered. Given that the list in the policy document is at the county level, according to the summary and collation of counties, there are 171 prefecture-level cities covered by the NKEFAs (111 first list and 60 additional list).
2. The time node of policy implementation. According to the different times of policy introduction and new list, 2011 and 2016 are the starting time of the two batches, respectively.

2.2.3. Control variables

In the econometric model, exogenous variables of socio-economic and natural climatic variables need to be controlled (Zhang M. et al., 2022; Zhang T. et al., 2022). In this paper, the following are included, population density (*DEN*), reflects the expansion of population size; economic growth (GDP *per capita*, *PGDP*), reflects the general situation of regional economic (Tang et al., 2021a); urbanization rate (*URBAN*), reflects the expansion of urbanization; industrial structure adjustment (*STURC*), reflects the change in the share of the three industries in total output (Guo et al., 2020); urban–rural income gap (*GAP*), reflects the change in income of urban and rural residents; opening to trade (*OPEN*), reflects the level of openness to foreign trade; transportation conditions (*TRANS*), reflects the gradual improvement of transportation infrastructure. The variables of natural conditions select precipitation (*PRE*), temperature (*TEM*), and sunshine hours (*SUN*) to test the shock of climate change on eco-environment.

TABLE 1 Descriptive statistics of the variables.

Variables	Variable definition	*N*	Mean	SD	Min.	Max.
Explained variables						
CS	Carbon sequestration scale (Million tons)	6,270	31.734	35.868	0.061	430.523
EQ	Environmental quality index from CHEQ	6,270	0.541	0.131	0.096	0.861
Core explanatory variable						
DID	NKEFAs	6,270	0.198	0.398	0	1
Mediating variables						
TERRI	Ecological space/territory area	6,270	0.490	0.288	0.001	0.996
INDUS	Value added of tertiary industry/value added of secondary industry	6,270	0.958	0.542	0.026	5.500
LABOR	Agricultural labor force/total population	6,270	0.223	0.095	0.001	0.485
Control variables						
DEN	Total population/land area (people/km^2)	6,270	402.861	485.234	0.656	6729.490
lnPGDP	Logarithm of GDP *per capita* (2001 as base period)/RMB yuan	6,270	10.010	0.937	6.898	12.657
URBAN	Urbanization rate of resident population/%	6,270	42.574	19.694	7.435	100
STRUC	Gross secondary industry/GDP	6,270	0.384	0.094	0.086	0.835
GAP	Urban *per capita* disposable income/rural *per capita* net income	6,270	2.685	0.784	0.917	7.378
OPEN	Total import and export trade/GDP	6,270	0.187	0.375	0	6.966
TRANS	Road mileage/land area (km/km^2)	6,270	0.801	0.559	0.009	5.887
PRE	Average annual precipitation /mm	6,270	954.358	539.161	29.289	2680.360
TEM	Average annual temperature/°C	6,270	13.883	5.451	−2.908	25.636
SUN	Sunshine hours/h	6,270	2068.952	511.408	784.640	3407.62

2.3. Theoretical framework

As specific areas in the main function area plan to undertake ecological functions and maintain ecological security, the NKEFAs belong to the location-oriented ecological engineering in China (Lin and Qi, 2021). The positive incentives for NKEFAs are mainly formed by transfer payments to local governments. The ecological compensation transfer payment contract signed between central government and local governments form a principal-agent relationship, thus motivate local governments to invest more efforts in ecological governance (Zhang and Li, 2015), and also enhance the fiscal capacity of local governments to provide basic public services (Fu and Miao, 2015). The NKEFAs can mainly enhance the service function of ecological products and the eco-environment quality with government actions. To this end, we have established a framework system for NKEFAs to influence the co-benefits of CS and EQ (Figure 2).

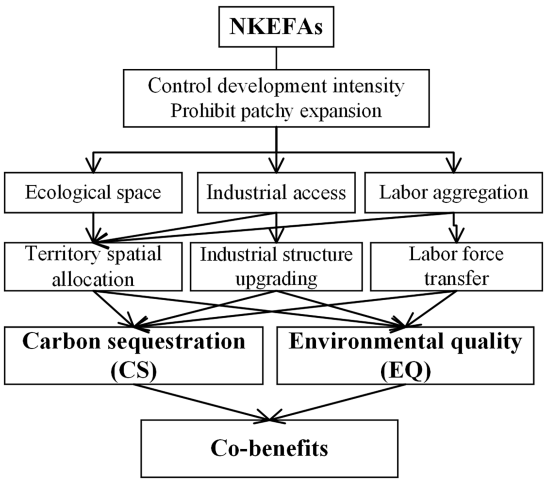

FIGURE 2
The framework of NKEFAs affecting CS and EQ.

Theoretically, fiscal support and social participation can help NEKFAs protect and restore the ecological environment, thereby enhancing CS and EQ. We argue that NKEFAs can influence the co-benefits of CS and EQ through territory space allocation, industrial structure upgrading, and labor force aggregation. First, the NKEFAs comprehensively delineate the ecological red line. This requires strict control of development intensity and scope in territorial development. Moreover, urban construction and industrial development should match the regional carrying capacity of resources and environments (Huang et al., 2021). Restricted development areas and ecological red lines assume different main functions, promote the optimization of the territorial utilization pattern, and help improve the efficiency of land spatial allocation (Jiang and Chen, 2021). The land spatial allocation reinforces the target requirement of prioritizing eco-environmental protection (DeFries et al., 2007), while the ecological space expansion contributes to co-benefits. Second, in NKEFA construction, a targeted negative list system is implemented for industrial access, which specifies a list of industries restricted and prohibited for suitable industry development. For industries that do not match the main function, strict industrial policy can promote the gradient transfer of polluting enterprises to areas with low environmental costs or to service industries with less pollution (Zhou et al., 2017; Luo and Qi, 2021). Then NKEFAs can promote industrial structure upgrading, conducive to pollutant emission reduction. In addition, the accompanying technical upgrade has also reduced the constraints of environment on economic

development (Liu and Lin, 2020). Third, the reallocation of NKEFAs to the territory space and industrial layout has accelerated the adjustment of factors and the mobility of labor. Territorial allocation and industrial upgrading enable the labor force to move orderly from restricted development areas to key development areas or urbanized areas (Zhang M. et al., 2022; Zhang T. et al., 2022). As a result, urban population clustering also alleviates employment pressure (Fan, 2016). Labor force aggregation in space with permissible environmental capacity promotes the reallocation and structural adjustment of factors. This is conducive to preventing environmental pollution and effectively using resources.

2.4. Baseline regression

The DID (difference in difference) model is a widely used method for evaluating policy effects in recent years (Tang et al., 2021b). Its basic idea is to set the implementation of a policy as an exogenous "quasi-natural experiment" (Wang and Ge et al., 2022), so as to strip the net effect of this specific policy. The NKEFAs can lead to ecological differences not only between the policy-covered and non-covered areas but also before and after the policy implementation (Zhang M. et al., 2022; Zhang T. et al., 2022). Therefore, DID model can be applied to assess the policy effects of the NKEFAs.

Considering that the National Plan for Main Functional Areas was launched at the end of December 2010, the first batch of NKEFAs was announced simultaneously. And the list of additional counties was announced in 2016. This paper selects 2011 as the starting year for the NKEFAs. Considering the difference in time for the establishment of NKEFAs, time-varying DID model is employed, which is constructed as follows:

$$Y_{it} = \alpha + \beta DID_{it} + \delta control_{it} + \mu_i + \gamma_t + \varepsilon_{it} \quad (1)$$

Where Y_{it} denotes the explained variable, including CS and EQ, DID_{it} denotes the core explanatory variable, i.e., a dummy variable for this ecological policy. If region i is established as an NKEFA in year t, $DID_{it} = 1$; otherwise, $DID_{it} = 0$. β reflects the net effect of NKEFAs, if the NKEFAs help to enhance CS and EQ, β is significantly positive. $control_{it}$ indicates the set of control variables, μ_i denotes the area-fixed effect, γ_t denotes the time-fixed effect, and ε_{it} is the random disturbance term.

The list in the document is at the county scale, while the scale of this research is at the prefecture level. In the DID model, for a prefecture-level city, if a NKEFA cover the county within its jurisdiction, this city belongs to the coverage of this NKEFA, then the list of counties can be summarized to the prefecture-level city. If the counties in a city are covered in both the first batch and the added batch, then the policy starting time of this city is 2011.

2.5. Parallel trend test and dynamic effect

DID model needs to satisfy the parallel trend hypothesis. Before the establishment of NKEFAs, the ecological effects of the treatment and control groups maintained basically the same trend of change. The parallel trend hypothesis test generally uses the event study approach (ESA), which also looks at the dynamic effect and persistence of policy impact. In this way, whether a significant difference exists in the changing trend can be accurately determined between the treatment and control groups in the NKEFAs (Wu et al., 2021). So, the ESA is applied to test the parallel trend hypothesis, and then analyze the dynamic policy effect (McGavock, 2021).

Considering that the Ministry of Finance promulgated the Transfer Payment (Pilot) Measures for NEKFAs in 2009, and some important ecological regions have started to pilot transfer payment. The year before the NKEFA implementation (2010) is used as the reference group for the parallel trend test. Referring to related studies (Chen, 2017; Tao et al., 2021), Eq. (1) is expanded as:

$$Y_{it} = \alpha_0 + \beta_t \sum_{t=2001, t\neq 2010}^{2019} treat_i \times year_t + \mu_i + \gamma_t + \varepsilon_{it} \quad (2)$$

Where $treat_i \times year_t$ is the interaction term of the grouping variable $treat_i$ and the year dummy variable $year_t$. The year before this policy (2010) is not introduced. β_t denotes the policy effect in each year. If β_t is not significant until 2010, the parallel trend hypothesis is satisfied.

3. Results

3.1. Baseline regression result

The baseline regression results show that (Table 2), whether or not controlling for city fixed effect and year fixed effect, or controlling for characteristic variables, the coefficients of DID are all positive

TABLE 2 Results of baseline regression.

Variables	Explained variable: CS				Explained variable: EQ			
	(1)	(2)	(3)	(4)	(5)	(6)	(7)	(8)
DID	3.5388***	2.3985***	2.1615***	2.1625***	0.0076***	0.0043***	0.0033***	0.0031***
	(0.1333)	(0.1683)	(0.1678)	(0.1743)	(0.0004)	(0.0005)	(0.0005)	(0.0010)
cons	31.6003***	28.6806***	19.6504***	25.4192***	0.5394***	0.5395***	0.5387***	0.5482***
	(1.7518)	(0.1896)	(2.3671)	(2.9588)	(0.0069)	(0.0006)	(0.0066)	(0.0083)
Controls	NO	NO	YES	YES	NO	NO	YES	YES
Adj-R^2	0.1062	0.1582	0.1424	0.1688	0.0621	0.1026	0.1316	0.1745
City FE	NO	YES	NO	YES	NO	YES	NO	YES
Year FE	NO	YES	NO	YES	NO	YES	NO	YES
No. of cities	330	330	330	330	330	330	330	330

***$p < 0.01$. **$p < 0.05$. *$p < 0.10$. Robust standard errors clustered at city level appear in parentheses.

significantly. NKEFAs exert a significant positive impact on CS, indicate that the NKEFAs enhanced the CS and EQ of the covered cities significantly, and achieve the ecological co-benefits. According to the coefficients of DID in columns (4) and (8), compared to that of cities in non-NKEFAs, the ATE of cities at the prefecture level is improved by about 2.1625 and 0.0031, respectively.

3.2. Parallel trend test and policy dynamic effect

The coefficients of the NKEFAs on CS and EQ are all insignificant, fluctuated around 0 for each year before 2010 (Figure 3). CS and EQ prior this policy was introduced did not differ significantly between treatment groups and control groups. Hence, the parallel trend hypothesis is satisfied, and the treatment and control groups are comparable ex ante, this policy is suitable for evaluation using DID model.

For dynamic effects, the coefficients of NKEFAs changed from negative to significantly positive, the positive contribution to ecological benefits gradually became prominent. After the establishment of NKEFAs, the impact on CS and EQ was significantly positive in the ATE, which showed a dynamic upward trend with time. For CS, the positive effect begins to stabilize 2 years after the establishment of the NKEFAs, and the obvious positive contribution after 2017 due to the second list of added regions, further contributing to the CS scale. For EQ, the positive effect basically maintained a stable upward trend. The dynamic effect results further showed that the NKEFAs promoted the co-benefits of CS and EQ in the covered areas.

3.3. Robustness test

3.3.1. Placebo test

The purpose of placebo test is to rule out the influence of omitted variables, randomness factors, etc., before and after this policy. Then a counterfactual framework is used to carry out the placebo test (Cisilino et al., 2019). Specifically, the non-parametric permutation test is employed with an unduplicated random sampling of all cities and times (Lu et al., 2021). Since there are 171 cities covered by the two batches, so 171 cities are first randomly selected from the overall samples as the treatment group and other cities as the control group. Then a certain year is randomly selected from 2001 to 2019 as the establishment time of the NKEFAs. Finally a quasi-randomized experiment at two levels of city-time is constructed. To improve the explanatory power of placebo test, this random process is repeated 500 times, and obtain the kernel density distribution map of the DID coefficients under multiple random shocks (Figure 4). The coefficient distribution of CS and EQ is slightly deviated from 0, most of the *p*-values are >0.1, and the DID coefficients of the baseline regression also are located in the low tail of the kernel distribution, which are obvious outliers. So, the placebo test based on

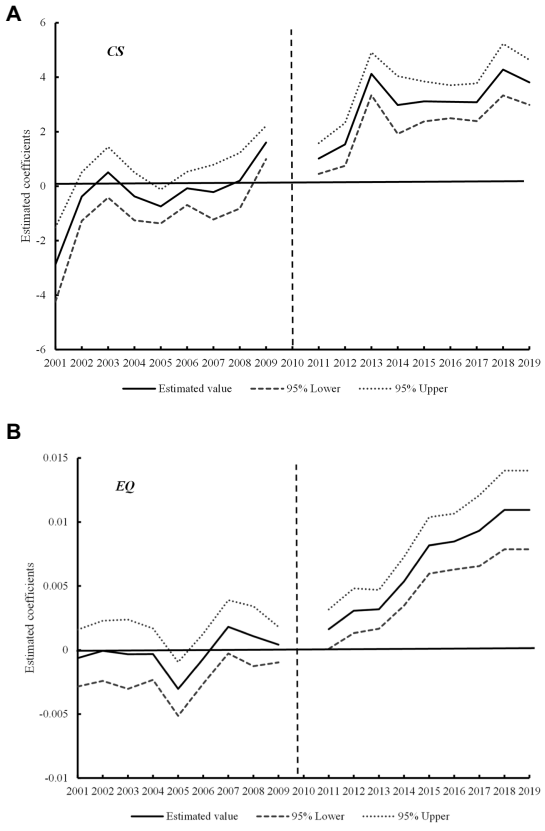

FIGURE 3
Parallel trend hypothesis and dynamic effects of NKEFAs on CS **(A)** and EQ **(B)**.

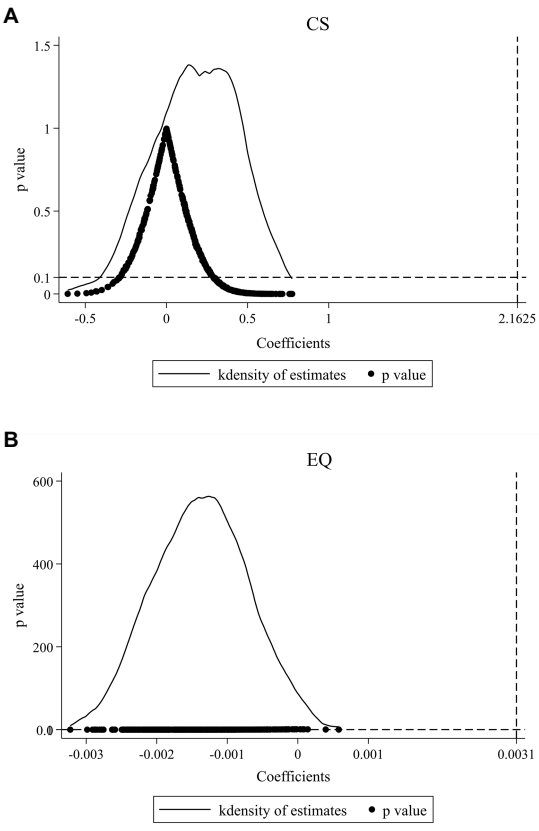

FIGURE 4
The placebo test of CS **(A)** and EQ **(B)**. The X-axis is the coefficients of DID for the 500 random processes. The vertical lines on the right side are the baseline coefficients of DID, all significantly located in the low-tailed of the kernel density distribution.

the counterfactual perspective confirms that the model setting is less disturbed by issues such as omitted variables or random factors, and does not affect the reliability of the baseline results.

3.3.2. PSM-DID

According to the goal of optimizing the spatial pattern of land use, the NKEFAs are important areas selected to undertake ecological functions and maintain ecological security, so their delineation may not be completely random (Lin and Qi, 2021), and prone to endogeneity caused by selection bias. If endogeneity exists, Propensity Score Matching (PSM) is an effective way to solve the problem under the non-randomized experiments (Shi et al., 2018). To reduce the selection bias of DID, the PSM combined with DID (PSM-DID) is used to assess the ecological co-benefits of NKEFAs. First, the control variables are used to predict the probability of each city being set as a NKEFA (Logit regression), and the treatment group is delineated. Second, the k-nearest neighbor matching method in the caliper (k takes 1, that is, matches according to 1:3) is used to match the control group for the treatment group, ensure that there is no significant systemic difference between the treatment group and the control group before the policy. Third, the matching sample is used for DID evaluation.

The regression results are shown in columns (1) and (2) of Table 3, the estimated coefficients of DID are 2.2004 and 0.0029 significantly, which are consistent with the baseline regression, respectively. So the positive promotion effects of NKEFAs on CS and EQ are robust.

3.3.3. Excluding other ecological policy interference

Some other ecological policies to improve the environment was underway at the same time when the NKEFAs was established. Other ecological policies such as the Grassland Ecological Protection Subsidy and Incentive Policy began in 2011, the New Round of Plans for Returning Farmland to Forests and Grasses in 2014, the Opinions on Accelerating the Construction of Ecological Civilization in 2015, may also affect the CS and EQ. To exclude the interference of other ecological policies, the interaction terms of the grouping variable (treat) with the time dummy variables for 2011, 2014, and 2015 are introduced in the baseline regression model (Tao et al., 2021). The results in column (3) and column (4) of Table 3 show that the impacts of NKEFAs on CS and EQ are still all significantly positive, the results are robust.

3.3.4. Substituting explained variables

Ecological improvement is positively correlated with vegetation change. Meanwhile, Normalized Difference Vegetation Index (NDVI) is closely related to vegetation cover, biomass and productivity, which can also indirectly reflect the supply capacity of ecological products. So, NDVI can be used as a proxy variable for CS. The EQ is mainly measured by the inverse indicator of atmospheric pollution level (Wang and Tang, 2019). In view of the availability of data, water environment-related indicators are not considered for the time being. The level of atmospheric pollution is characterized by $PM_{2.5}$ concentration from RS interpretation, and $PM_{2.5}$ is made positive by taking the inverse. It can be found that the estimated coefficients of DID on both NDVI and 1/PM2.5 are significantly positive. NKEFAs can significantly enhance NDVI and reduce haze pollution, indicating that the positive contribution of NKEFAs on CS and EQ remains robust.

3.3.5. Eliminating special samples

The NKEFAs is closely related to the ecological characteristics and environmental carrying capacity of the covered areas, while cities such as municipalities directly under the central government, provincial capitals, special economic zones may have obvious systematic differences in ecological endowments from other cities due to their own positioning. To further ensure reliability, the baseline models are re-estimated after eliminating these special samples (292 remaining). The results in columns (7) and (8) of Table 3 show that the coefficients of DID are still all significantly positive. After eliminating some samples, the positive effect of NKEFAs to CS and EQ remains robust.

3.4. Mechanism analysis

According to the framework system, the transmission mechanism of NKEFAs affecting CS and EQ is explored in terms of territorial spatial allocation, industrial structure upgrading, and labor force aggregation. For the model setting, the stepwise method is borrowed (Baron and

TABLE 3 Robustness tests.

Variables	PSM-DID		Excluding other policy interference		Substituting explained variables		Eliminating special samples	
	CS	*EQ*	*CS*	*EQ*	*NDVI*	1/*PM2.5*	*CS*	*EQ*
	(1)	(2)	(3)	(4)	(5)	(6)	(7)	(8)
DID	2.2004*** (0.0043)	0.0029*** (0.0005)	2.1679*** (0.1781)	0.0032*** (0.0005)	0.0185*** (0.0011)	0.0010* (0.0005)	1.9909*** (0.1895)	0.0028*** (0.0005)
cons	27.1356*** (3.2617)	0.5537*** (0.0089)	25.4126*** (2.9581)	0.5482*** (0.0083)	0.6039*** (0.0195)	0.0917*** (0.0102)	21.2040*** (3.1719)	0.5553*** (0.0088)
Controls	Yes	Yes	Yes	Yes	Yes	Yes	Yes	Yes
Adj-R^2	0.1757	0.1992	0.1696	0.1750	0.4931	0.4195	0.1692	0.1842
City FE	Yes	Yes	Yes	Yes	Yes	Yes	Yes	Yes
Year FE	Yes	Yes	Yes	Yes	Yes	Yes	Yes	Yes
No. of cities	330	330	330	330	330	330	292	292

***$p < 0.01$. **$p < 0.05$. *$p < 0.10$. Remove samples that do not satisfy the common support hypothesis after nearest neighbor matching. NDVI is derived from the Chinese annual vegetation index (NDVI) spatial distribution dataset of the Data Center for Resource and Environmental Sciences, Chinese Academy of Sciences, with a spatial resolution of 1 km. PM2.5 is obtained from Surface PM2.5 data (V5.GL.02) with 0.01° × 0.01° resolution (V5.GL.02; Aaron et al., 2021), which were made available to the public by the University of Washington.

Kenny, 1986; Chan et al., 2012; Tang et al., 2020): first test the impact of NKEFAs on mediating variables, second test the effects of NKEFAs and mediating variables on CS and EQ (Table 4).

Based on the theoretical framework, the mediating variables included territorial spatial allocation (TERRI), industrial structural upgrading (INDUS), and labor force transfer (LABOR). Ecological space mainly provides functions such as ecological products or ecological services, include forest land, grassland, water, et al. TERRI is characterized by the proportion of ecological space to the national territory. INDUS is characterized by the ratio of added-value of the tertiary industry to added-value of the secondary industry, so as to reflect the transformation trend of the leading industry to the service industry (Yu, 2015). Due to the high overlap in spatial distribution between counties covered by NKEFAs and national poverty-stricken counties (Wang and Gao, 2018), LABOR is characterized by the proportion of labor in agriculture, forestry, animal husbandry and fishery to the total population year-end, to reflect the rural labor mobility among urban–rural areas and industries.

3.4.1. Territory spatial allocation effect (TERRI)

The NKEFAs has a markedly positive impact on TERRI, and TERRI has an obvious positive influence on CS and EQ. Therefore, the territory space allocation positively mediates the co-benefits of NKEFAs on CS and EQ. NKEFAs can enhance CS and EQ by enhancing the share of ecological space to optimize the spatial allocation structure of the territory, thus achieving ecological co-benefits.

3.4.2. Industrial structure upgrading effect (INDUS)

NKEFAs has a remarkably positive influence on INDUS. However, INDUS only exerts a positive effect on CS but failed to obviously contribute to EQ in the covered areas. This indicates that INDUS only positively mediates the CS enhancement in NKEFAs. The industrial structure upgrading by increasing the tertiary industry proportion in the national economy only promotes the enhancement of CS in NKEFAs, instead of EQ, thus failing to realize ecological co-benefits.

3.4.3. Labor force aggregation effect (LABOR)

NKEFAs has a significant positive impact on the LABOR, which can increase the labor proportion in agriculture, forestry, animal husbandry, and fisheries. Meanwhile, NKEFAs makes a significant positive contribution to both CS and EQ. Therefore, labor force agglomeration positively mediates the effect of NKEFAs on CS and EQ. NKEFAs can enhance CS and EQ through inter-industrial mobility and labor agglomeration to achieve ecological co-benefits.

In summary, the NKEFAs can achieve ecological co-benefits of CS and EQ through territory spatial allocation and labor force aggregation, and industrial structure upgrading only plays a positive mediating role in the impact of NKEFAs on CS.

3.5. Heterogeneity analysis

The ecological co-benefits of NKEFAs vary according to ecological foundation, endowment conditions, geographical location and other factors, and it is necessary to understand them through heterogeneity analysis. Heterogeneity analysis is carried out from the following perspectives: different ecological function types, different geospatial locations, different quantiles of CS and EQ.

3.5.1. Differences in ecological function types

According to the differences in ecological product supply and functional positioning, NKEFAs can be classified into four types: water conservation, soil conservation, windbreak sand fixation, and biodiversity maintenance (Table 5). In summary, the NKEFAs of water conservation, soil conservation and biodiversity maintenance achieve co-benefits of CS and EQ. In contrast, the windbreak sand-fixation type

TABLE 4 The results of mechanism test.

Variables	*TERRI*			*INDUS*			*LABOR*		
	land	*CS*	*EQ*	*indus*	*CS*	*EQ*	*labor*	*CS*	*EQ*
	(1)	(2)	(3)	(4)	(5)	(6)	(7)	(8)	(9)
DID	0.0025*** (0.0003)	2.0658*** (0.1753)	0.0022*** (0.0005)	0.0121* (0.0065)	2.1437*** (0.1737)	0.0031*** (0.0005)	0.0070*** (0.0013)	2.1128*** (0.1745)	0.0030*** (0.0005)
TERRI		38.1633*** (8.4921)	0.3392*** (0.0236)						
INDUS					1.5487*** (0.2341)	−0.0008 (0.0007)			
LABOR								7.0843*** (1.7342)	0.0140*** (0.0049)
cons	0.4885*** (0.0045)	6.7750 (5.0929)	0.3825*** (0.0141)	0.3239** (0.1638)	24.9176*** (2.9491)	0.5485*** (0.0084)	0.2968*** (0.0222)	23.3168*** (2.9993)	0.5441*** (0.0085)
Controls	Yes	Yes	Yes	Yes	Yes	Yes	Yes	Yes	Yes
Adj-R^2	0.3338	0.1716	0.2024	0.6547	0.3345	0.1747	0.3305	0.1711	0.1756
City FE	Yes	Yes	Yes	Yes	Yes	Yes	Yes	Yes	Yes
Year FE	Yes	Yes	Yes	Yes	Yes	Yes	Yes	Yes	Yes
No. of cities	330	330	330	330	330	330	330	330	330

***$p < 0.01$. **$p < 0.05$. *$p < 0.10$. Robust standard errors clustered at city level appear in parentheses. The direct effect + mediated effect is slightly deviated from the total effect is the result of the retention of decimal points.

TABLE 5 Heterogeneity analysis: differences based on function type.

Variables	Water conservation		Soil conservation		Windbreak sand-fixation		Biodiversity maintenance	
	CS	*EQ*	*CS*	*EQ*	*CS*	*EQ*	*CS*	*EQ*
	(1)	(2)	(3)	(4)	(5)	(6)	(7)	(8)
DID	1.1967*** (0.2137)	0.0026*** (0.0006)	2.0411*** (0.2815)	0.0048*** (0.0008)	7.7708*** (0.3853)	−0.0098*** (0.0011)	0.6964*** (0.2543)	0.0023*** (0.0007)
cons	22.4709*** (2.9962)	0.5430*** (0.0168)	26.7325*** (3.0078)	0.5528*** (0.0084)	25.1438*** (2.8970)	0.5443*** (0.0083)	24.2242*** (2.9958)	0.5472*** (0.0084)
Controls	Yes	Yes	Yes	Yes	Yes	Yes	Yes	Yes
Adj-R^2	0.1516	0.1716	0.1546	0.1742	0.2020	0.1800	0.1482	0.1705
City FE	Yes	Yes	Yes	Yes	Yes	Yes	Yes	Yes
Year FE	Yes	Yes	Yes	Yes	Yes	Yes	Yes	Yes
No. of NKEFAs	95	95	40	40	18	18	52	52
No. of cities	330	330	330	330	330	330	330	330

***$p < 0.01$. **$p < 0.05$. *$p < 0.10$. The sum of functional areas number included in each type is not equal to 171, because some cities belong to two types.

only has the strongest enhancement effect on CS, followed by the soil conservation type. The soil conservation type showed the greatest improvement effect on EQ, followed by the water conservation type.

3.5.2. Differences in geospatial locations

According to the different geographical locations, the country is divided into six geographic regions, i.e., Northeast China (NEC), North China (NC), Northwest China (NWC), Southwest China (SWC), Middle and Lower Reaches of the Yangtze River regions (MLY), and Southeast Coastal regions (SEC). Among them, NEC, NC, and NWC belong to the North, while the SWC, MLY, and SEC are part of the South (Table 6).

Among the NKEFAs in the six geographic regions, the NKEFAs in SWC, MLY, and SEC of the South achieve co-benefits of CS and EQ, while NEC, NC, and NWC of the North only significantly enhance the CS. In comparison, NKEFAs represent the strongest enhancement effect on CS in NWC, followed by NEC; the NKEFAs show the strongest promotion effect on EQ in SWC and SEC, followed by MLY. Taken together, the enhancing effect of NKEFAs on CS is stronger in the North, while that on EQ is more obvious in the South.

3.5.3. Differences in quantiles of CS and EQ

There are differences in the degree of policy dependence and response among regions with different endowment conditions. The heterogeneity distribution of CS and EQ of NKEFAs is further examined by a panel quantile regression model (Table 7).

The NKEFAs show a rising and then declining positive effect on CS with the increasing quantile, and represent an overall growing trend. The highest positive effect appears near the 75% quantile, in areas with good ecological endowment base, the positive enhancement effect of NKEFAs on CS is higher. Regions with excellent ecological endowment have a larger scale of CS and can better absorb and store CO_2. The NKEFAs promote the optimization of national land space, limit large-scale and high-intensity urbanization and industrialization, which help to release more potential of carbon sink.

The effect of NKEFAs on EQ shows a "positive → negative → positive" U-shaped trend with the increasing quantile, with an obvious negative effect near the 25% quantile and a gradual change to a positive effect after the 40% quantile. This identifies that the NKEFAs do not tremendously improve the EQ in areas with relatively poor ecological endowment and high ecological vulnerability, consistent with the results of the windbreak sand-fixation area and NWC. Additionally, NKEFAs can better improve the EQ in areas with excellent eco-environment.

4. Discussions

4.1. Ecological co-benefits of NEKFAs and its mechanism

As a command-and-control ecological policy (Blackman et al., 2018), the distribution of NKEFAs forms an important ecological barrier of China. DID analysis can effectively capture the co-benefits of ecological product supply and the eco-environment quality of NKEFAs, consistent with Pan and Tang (2020). The coefficient of CS turned significantly positive in 2009. We found in 2009, China has begun to pilot ecological transfer payments in some important ecological regions to enhance environmental investment, relevant government departments responded in advance following the policy guidance. That is, the NKEFAs can produce an expected effect on CS and EQ (Du et al., 2020). Moreover, the improvement of CS is superior to that of EQ, and thus the environment quality improvement still has a long way to go, this is similar to Liu et al. (2022). In general, the co-benefit enhancement of CS and EQ is a long-term process that evolves gradually. The ecological effect of transfer payment and policy rollout to NKEFAs is relatively weak in the short term, but gradually increase in the long term. Through providing continuous vertical ecological compensation to NKEFAs, the co-benefits can be effectively promoted in a sustainable manner (Zhu and Chen, 2021).

The NKEFAs can achieve co-benefits of CS and EQ by optimizing the territory spatial pattern and promoting the labor force transformation. The expansion of ecological space is the primary means of NKEFA establishment, which inevitably require urbanization and industrial development to match the carrying capacity of resources and the environment (Huang et al., 2021). It also provides carriers and opportunities for industrial aggregation and labor mobility. However, restrictive development and industrial upgrading make it challenging for ecological functional areas to carry a larger labor force. Although the overloaded population has transferred in an orderly manner, the active population migration policy can increase population aggregation and

TABLE 6 Heterogeneity analysis: regional differences based on geographic space.

Variables	NEC		NC		NWC	
	CS	*EQ*	*CS*	*EQ*	*CS*	*EQ*
	(1)	(2)	(3)	(4)	(5)	(6)
DID	2.4679*** (0.4665)	0.0021 (0.0015)	2.0233*** (0.2149)	0.0001 (0.0009)	3.7120*** (0.7461)	−0.0007 (0.0011)
cons	41.7258*** (9.8409)	0.6805*** (0.0320)	26.0882*** (4.9821)	0.5214*** (0.0231)	16.5328*** (10.7054)	0.44445*** (0.0161)
Controls	Yes	Yes	Yes	Yes	Yes	Yes
Adj-R^2	0.3559	0.5762	0.5711	0.2147	0.2611	0.1990
City FE	Yes	Yes	Yes	Yes	Yes	Yes
Year FE	Yes	Yes	Yes	Yes	Yes	Yes
No. of cities	36	36	59	59	63	63
Variables	SWC		MLY		SEC	
	CS	*EQ*	*CS*	*EQ*	*CS*	*EQ*
	(7)	(8)	(9)	(10)	(11)	(12)
DID	0.7847* (0.4041)	0.0069*** (0.0012)	0.5737*** (0.1501)	0.0055*** (0.0008)	0.6091*** (0.2186)	0.0069*** (0.0011)
cons	53.7831*** (8.1748)	0.4621*** (0.0235)	28.3889*** (3.5909)	0.6579*** (0.0195)	38.7921*** (4.5361)	0.6245*** (0.0234)
Controls	Yes	Yes	Yes	Yes	Yes	Yes
Adj-R^2	0.3891	0.4182	0.3576	0.3834	0.2888	0.5850
City FE	Yes	Yes	Yes	Yes	Yes	Yes
Year FE	Yes	Yes	Yes	Yes	Yes	Yes
No. of cities	47	47	67	67	58	58

***$p < 0.01$. **$p < 0.05$. *$p < 0.10$. The six geographic regions specifically include the following provinces: Heilongjiang, Jilin and Liaoning in NEC, Beijing, Tianjin, Hebei, Henan, Shandong and Shanxi in NC, Inner Mongolia, Shaanxi, Gansu, Ningxia, Qinghai and Xinjiang in the NEC, Sichuan, Chongqing, Guizhou, Yunnan and Tibet in the SWC, Jiangsu, Shanghai, Anhui, Jiangxi, Hubei and Hunan in MLY, and Zhejiang, Fujian, Guangdong, Guangxi, Hainan and Hong Kong, Macao and Taiwan in SWC.

TABLE 7 Heterogeneity analysis: differences in distribution based on quantile levels.

Quantiles	Explained variable: CS	Explained variable: EQ
	DID	*DID*
0.05	4.2911*** (0.1783)	0.0114*** (0.0004)
0.25	6.0542*** (0.1052)	−0.0089** (0.0039)
0.50	17.4855*** (0.2128)	0.0018*** (0.0003)
0.75	35.0966*** (0.2275)	0.0132*** (0.0004)
0.95	16.5249*** (1.1962)	0.0156*** (0.0001)
Controls	Yes	Yes
City FE	Yes	Yes
Year FE	Yes	Yes
No. of cities	Yes	Yes

***$p < 0.01$. **$p < 0.05$. *$p < 0.10$. Bootstrap 1,000 times to obtain the coefficient covariance, and the optimization technique selects the adaptive MCMC method.

absorption capacity, and the development of ecological industries can also attract the return of outflowing labor. The NKEFAs encourage industries development to be compatible with the positioning of the main functional areas. Industrial upgrading enhances the ecological product supply capacity but minimally improves EQ in the short term.

In summary, the research findings make theoretical and methodological contributions to the scientific assessment of policy effect on ecological engineering. This article focuses on the ecological goals achievement of NKEFAs, and provides a complete framework for assessing the implementation effect of ecological engineering by integrating the co-benefits of ecological products supply and environment quality improvement. The assessment framework and policy insights can provide methodological reference and application value for ecological engineering in other countries. However, it should be noted that the selected indicators of policy assessment depend on the specific ecological engineering and socio-economic development reality in China. Once this framework is extended to other countries or regions, an appropriate assessment framework that fits the ecological conditions needs to be constructed according to the special operating dynamics of ecological engineering in this country or region.

4.2. Localization and precision in the management of NKEFAs

NKEFAs undertake important ecological functions, such as water and soil conservation, windbreak sand fixation, and biodiversity maintenance (Pan et al., 2021). The difference in the leading ecological function determines the direction of development and protection of each NKEFA (Zuo and Gao, 2021). The water conservation type can realize precipitation retention, runoff regulation, soil desertification control and vegetation restoration. The soil conservation type has the function of avoiding soil erosion through watershed management, restriction of resource development, returning farmland to forest and grass, etc. The biodiversity maintenance type has the function of maintaining and restoring the balance of wildlife species, preventing habitat changes due to ecological construction. All three types of NKEFAs can achieve co-benefits of CS and EQ, and similar to Liu et al.

(2020), the soil conservation type has the greatest improvement effect. In contrast, the windbreak sand-fixation type only positively contributes to CS, probably because deserts, as an important part of terrestrial ecosystems, can sequester large amounts of carbon dioxide and play a key role as carbon sinks (Yang et al., 2020). However, the windbreak sand-fixation type is generally located in fragile ecosystems with high desertification and severe grassland degradation, with limited environmental benefits and still has a long way to go.

NWC presents a more consistent performance of the windbreak sand-fixation type. The functions of different types in the NWC are intertwined, which can improve the capacity of CS. Nevertheless, most areas of NWC show arid and semi-arid climate characteristics, with a poorer ecological endowment base and more prominent environmental problem. In contrast, areas with better ecological conditions are mainly located near the Qinling Mountains in Shaanxi. Differently, NC is a traditional agricultural production area, where the contradiction between population, economy, and environmental carrying capacity induces prominent haze problems. Although air quality has gradually improved in recent years, improving EQ is an evolutionary process that needs sustained effort in the long term.

The performance of different ecological function areas and geospatial locations conform to the quantile heterogeneity law of the ecological environment. Areas with richer ecological foundation and environmental conditions are the key areas restricted and prohibited from development. NKEFAs with higher environmental carrying capacity can provide more ecological goods and services, then improve ecological co-benefits. In contrast, it is difficult for NEKFAs with poorer ecological endowment base to improve EQ greatly in a short time, and the improvement of environmental benefits is a lasting and stable process. In short, there is a need for differentiation and precision in the institutional arrangement of NKEFAs (Gao et al., 2021).

5. Conclusion

This study considers the NKEFAs as quasi-natural experiment, a time-varying DID model is used to assess the impact of NKEFAs on CS and EQ. In conclusion, the NKEFAs enhance both CS and EQ and achieve the ecological co-benefits. Compared to those of non-NKEFAs, the CS and EQ of NKEFAs are elevated by 2.1625 and 0.0031 in ATE, respectively. The NKEFAs can enhance CS and EQ through the positive mediating role of territory spatial allocation and labor force aggregation. Nevertheless, the NKEFAs only enhance CS by industrial structure upgrading. The policy effects of NKEFAs are heterogeneous across ecological function types, geospatial locations, and quantiles. Except for the NKEFAs of windbreak sand-fixation type, northwestern region and low quantiles where only promote CS, all other function areas can achieve the ecological co-benefits.

The conclusions have abundant policy implications: (1) Improving the sustainability and stability of NKEFAs. While the establishment of NKEFAs has achieved ecological co-benefits currently, effective sustainability incentives depend on local government action in ecological governance and protection. In order to form a long-term positive incentive, avoid the ecosystem rebound in NKEFAs, a mechanism of continuous support and supervision is necessary nation widely. (2) Implementing a more dynamic and efficient industrial policy. The covered areas can actively develop eco-agriculture and service industries. More policies about the active population migration and household registration management should be introduced to attract transferred labor to new industries. By doing this, market-oriented and cross-regional mobility of labor and other factors will be promoted. (3) Building a diversified and precise ecological governance and compensation system. Due to the existence of heterogeneity, the institutional arrangement of NKEFAs should be more adapted to local conditions and more precise. The NKEFAs need to focus on areas with lower ecological endowment base to maintain synergy between land utilization and eco-environment. For example, the northwestern region in China mainly belongs to the ecological functional area of windbreak sand fixation, the transfer funds of the central government need to be tilted more toward these areas. In this way, ecological governance and service functions are expected to be strengthened.

Data availability statement

The original contributions presented in the study are included in the article/supplementary material, further inquiries can be directed to the corresponding author.

Author contributions

HC: methodology, data curation, and writing—original draft. MH: conceptualization, writing—review and editing, and software. ZX: writing—review and editing, data curation, and validation. XZ: data curation, software, and visualization. SY: conceptualization, writing—review and editing, investigation, and supervision. All authors contributed to the article and approved the submitted version.

Funding

This research was funded by the Social Science Foundation of Hebei Province (no. HB22YJ053); Scientific Research Initiation Project for High-level Talents of Hebei University (no. 521100222017); National Social Science Foundation of China (no. 17BTJ029); and National Natural Science Foundation of China (no. 71773091).

Acknowledgments

The valuable comments and suggestions of editors and reviewers are gratefully acknowledged.

Conflict of interest

The authors declare that the research was conducted in the absence of any commercial or financial relationships that could be construed as a potential conflict of interest.

Publisher's note

References

Aaron, D., Melanie, S., Liam, B., Michael, B., Jeffery, R., Michael, J., et al. (2021). Monthly global estimates of fine particulate matter and their uncertainty. *Environ. Sci. Technol.* 55, 15287–15300. doi: 10.1021/acs.est.1c05309

Ball, B., Kominoski, J., Adams, H., Jones, S., Kane, E., Loecke, T., et al. (2010). Direct and terrestrial vegetation-mediated effects of environmental change on aquatic ecosystem processes. *Bioscience* 60, 590–601. doi: 10.1525/bio.2010.60.8.5

Baron, R., and Kenny, D. (1986). The moderator-mediator variable distinction in social psychological research: conceptual, strategic, and statistical considerations. *J. Pers. Soc. Psychol.* 51, 1173–1182. doi: 10.1037//0022-3514.51.6.1173

Blackman, A., Li, Z., and Liu, A. (2018). Efficacy of command-and-control and market-based environmental regulation in developing countries. *Annual Review of Resource Economics.* 10, 381–404. doi: 10.1146/annurev-resource-100517-023144

Bryan, B. A., Gao, L., Ye, Y., Sun, X., Connor, J. D., Crossman, N. D., et al. (2018). China's response to a national land-system sustainability emergency. *Nature* 559, 193–204. doi: 10.1038/s41586-018-0280-2

Chan, R., He, H., Chan, H., and Wang, W. (2012). Environmental orientation and corporate performance: the mediation mechanism of green supply chain management and moderating effect of competitive intensity. *Ind. Mark. Manag.* 41, 621–630. doi: 10.1016/j.indmarman.2012.04.009

Chen, S. (2017). The effect of a fiscal squeeze on tax enforcement: evidence from a natural experiment in China. *J. Public Econ.* 147, 62–76. doi: 10.1016/j.jpubeco.2017.01.001

Chen, J., Fan, W., Li, D., Liu, D., and Song, M. (2020). Driving factors of global carbon footprint pressure: based on vegetation carbon sequestration. *Appl. Energy* 267:114914. doi: 10.1016/j.apenergy.2020.114914

Cisilino, F., Bodini, A., and Zanoli, A. (2019). Rural development programs' impact on environment: an ex-post evaluation of organic farming. *Land Use Policy* 85, 454–462. doi: 10.1016/j.landusepol.2019.04.016

DeFries, R., Hansen, A., Turner, B., Reid, R., and Liu, J. (2007). Land use change around protected areas: management to balance human needs and ecological function. *Ecol. Appl.* 17, 1031–1038. doi: 10.1890/05-1111

Dong, Z., Xia, C., Fang, K., and Zhang, W. (2022). Effect of the carbon emissions trading policy on the co-benefits of carbon emissions reduction and air pollution control. *Energy Policy* 165:112998. doi: 10.1016/j.enpol.2022.112998

Du, J., Liu, H., and Wu, H. (2020). Impact of environmental supervision system on enterprises' investment in environmental protection. *China Population, Resources and Environment.* 30, 151–159. doi: 10.12062/cpre.20200423

Fan, J. (2016). Theoretical innovation in optimization of protection and development of China's territorial space and coping strategy of 13th five-year plan. *Bull. Chin. Acad. Sci.* 31, 1–12. doi: 10.16418/j.issn.1000-3045.2016.01.001

Fu, R., and Miao, X. (2015). A new financial transfer payment system in ecological function areas in China: based on the spillover ecological value measured by the expansion energy analysis. *Econ. Res. J.* 50, 47–61.

Gao, Y., He, N., and Wang, Y. (2013). Characteristics of carbon sequestration by ecosystem and progress in its research. *J. Nat. Resour.* 28, 1264–1274. doi: 10.11849/zrzyxb.2013.07.018

Gao, X., Liu, N., and Hua, Y. (2022). Environmental protection tax law on the synergy of pollution reduction and carbon reduction in China: evidence from a panel data of 107 cities. *Sustainable Prod. Consumption* 33, 425–437. doi: 10.1016/j.spc.2022.07.006

Guo, S., Pei, Y., and Wu, Y. (2020). Research on industrial structure adjustment and upgrading effect of the development of productive service industry. *J. Quant. Technol. Econ.* 37, 45–62. doi: 10.13653/j.cnki.jqte.2020.10.003

Gao, J., Zuo, L., and Liu, W. (2021). Environmental determinants impacting the spatial heterogeneity of karst ecosystem services in Southwest China. *Land Degradation & Development.* 32, 1718–1731. doi: 10.1002/ldr.3815

He, Q., Chen, Z., Peng, X., Liu, Y., and Zhang, M. (2018). An assessment of forest biomass carbon storage and ecological compensation based on surface area: a case study of Hubei province, China. *Ecological Indicators.* 90, 392–400. doi: 10.1016/j.ecolind.2018.03.030

Hou, P., Zhai, J., Cao, W., Yang, M., Cai, M., and Li, J. (2018). Evaluation on ecosystem changes and protection of the national key ecological function zones in mountainous areas of Central Hainan Island. *Acta Geograph. Sin.* 73, 429–441. doi: 10.11821/dlxb201803004

Huang, X., Chen, Y., Zhao, Y., Shi, M., and Li, T. (2021). Optimization on land spatial development pattern in the Yellow River Basin: from the perspective of land development intensity. *Geogr. Res.* 40, 1554–1564. doi: 10.11821/dlyj020200546

Jiang, H., and Chen, L. (2021). Spatial allocation efficiency and control strategy of county land resources based on main functional areas of territorial space: a case study of Ganyu, Jiangsu province. *J. Nat. Resour.* 36, 2424–2436. doi: 10.31497/zrzyxb.20210918

Li, G., and Li, X. (2014). Allocation mechanism of national key ecological function areas transfer payment. *China Popul. Resour. Environ.* 24, 124–130. doi: 10.3969/j.issn.1002-2104.2014.05.019

Li, G., Li, X., and Wang, H. (2013). Ecological compensation effect of national key ecological function areas transfers payment policy. *Modern Econ. Sci.* 35, 58–64.

Li, G., Wang, H., and Liu, Q. (2014). The dual objectives and performance evaluation of transfer payment in national key ecological function areas. *J. Northwest Univ. (Philos. Social Sci. Ed.)* 44, 151–155. doi: 10.16152/j.cnki.xdxbsk.2014.01.032

Li, G., Yang, L., and Liu, S. (2016). Study on spatial spillover effects of ecological environment quality at the county level in national key ecological function areas. *J. China Univ. Geosci. (Social Sci. Ed.).* 16, 10–19. doi: 10.16493/j.cnki.42-1627/c.2016.01.002

Lin, G., Jiang, D., Fu, J., Cao, C., and Zhang, D. (2020). Spatial conflict of production–living–ecological space and sustainable-development scenario simulation in Yangtze River Delta agglomerations. *Sustainability.* 12:2175. doi: 10.3390/su12062175

Lin, S., and Qi, Y. (2021). The incentive effect and strategy choice of location-oriented ecological environmental policy. *Public Finance Res.* 06, 85–103. doi: 10.19477/j.cnki.11-1077/f.2021.06.005

Liu, L., Cao, W., Wu, D., and Huang, L. (2018). Temporal and spatial variations of ecosystem services in national key ecological function zones. *Sci. Geogr. Sin.* 38, 1508–1515. doi: 10.13249/j.cnki.sgs.2018.09.014

Liu, H., Gao, J., Liu, X., Zhang, H., and Xu, X. (2020). Monitoring and assessment of the ecosystem services value in the national key ecological function zones. *Acta Ecol. Sin.* 40, 1865–1876. doi: 10.5846/stxb201903010382

Liu, Z., and Lin, Y. (2020). Structural transformation, TFP and high-quality development. *Manage. World* 36, 15–29. doi: 10.19744/j.cnki.11-1235/f.2020.0100

Liu, W., Liu, J., Kuang, W., and Ning, J. (2017). Examining the influence of the implementation of major function-oriented zones on built-up area expansion in China. *J. Geogr. Sci.* 27, 643–660. doi: 10.1007/s11442-017-1398-0

Liu, J., Liu, Y., and Li, Y. (2017). Classification evaluation and spatial-temporal analysis of "production-living-ecological" spaces in China. *Acta Geograph. Sin.* 72, 1290–1304. doi: 10.11821/dlxb201707013

Liu, B., and Song, M. (2022). Basic framework and value realization of carbon sink ecological products. *Nat. Resour. Econ. China* 35, 4–11. doi: 10.19676/j.cnki.1672-6995.000744

Liu, H., Wang, C., Zhang, M., and Wang, S. (2022). Evaluating the effects of air pollution control policies in China using a difference-in-differences approach. *Sci. Total Environ.* 845:157333. doi: 10.1016/j.scitotenv.2022.157333

Lu, S., Dong, R., and Ye, C. (2021). Does "the belt and road initiative" promote high-quality exports—evidence from firms in China. *China Ind. Econ.* 03, 80–98. doi: 10.19581/j.cnki.ciejournal.2021.03.012

Luo, Z., and Qi, B. (2021). The effects of environmental regulation on industrial transfer and upgrading and banking synergetic development—evidence from water pollution control in Yangtze River basin. *Econ. Res. J.* 56, 174–189.

McGavock, T. (2021). Here waits the bride? The effect of Ethiopia's child marriage law. *J. Dev. Econ.* 149:102580. doi: 10.1016/j.jdeveco.2020.102580

Miao, X., and Zhao, Y. (2019). Impact of transfer payment in eco-functional areas on eco-environmental improvement: capital compensation or institutional incentives? *Public Finance Res.* 05, 17–32. doi: 10.19477/j.cnki.11-1077/f.2019.05.003

Pan, D. (2021). The impact of command-and-control and market-based environmental regulations on afforestation area: quasi-natural experimental evidence from county data in China. *Resour. Sci.* 43, 2026–2041. doi: 10.18402/resci.2021.10.0

Pan, D., and Tang, J. (2020). The effects of heterogeneous environmental regulations on water pollution control: quasi-natural experimental evidence from China. *Sci. Total Environ.* 751:141550. doi: 10.1016/j.scitotenv.2020.141550

Pan, D., and Tang, J. (2021). The effects of heterogeneous environmental regulations on water pollution control: Quasi-natural experimental evidence from China. *Science of The Total Environment.* 751:141550. doi: 10.1016/j.scitotenv.2020.141550

Rosenthal, S., and Strange, W. (2003). Geography, industrial organization, and agglomeration. *Rev. Econ. Stat.* 85, 377–393. doi: 10.1162/003465303765299882

Shi, D., Ding, H., Wei, P., and Liu, J. (2018). Can smart city construction reduce environmental pollution? *China Ind. Econ.* 06, 117–135. doi: 10.19581/j.cnki.ciejournal.2018.06.008

Tang, K., Liu, Y., Zhou, D., and Qiu, Y. (2021a). Urban carbon emission intensity under emission trading system in a developing economy: evidence from 273 Chinese cities. *Environ. Sci. Pollut. Res.* 28, 5168–5179. doi: 10.1007/s11356-020-10785-1

Tang, K., Qiu, Y., and Zhou, D. (2020). Does command-and-control regulation promote green innovation performance? Evidence from China's industrial enterprises. *Sci. Total Environ.* 712:136362. doi: 10.1016/j.scitotenv.2019.136362

Tang, K., Zhou, Y., Liang, X., and Zhou, D. (2021b). The effectiveness and heterogeneity of carbon emissions trading scheme in China. *Environ. Sci. Pollut. Res.* 28, 17306–17318. doi: 10.1007/s11356-020-12182-0

Tao, F., Zhao, J., and Zhou, H. (2021). Does environmental regulation improve the quantity and quality of green innovation----evidence from the target responsibility system of environmental protection. *China Ind. Econ.* 02, 136–154. doi: 10.19581/j.cnki.ciejournal.2021.02.016

UNFCCC. (1997). *Kyoto protocol to the United Nations framework convention on climate change*. Kyoto Climate Change Conference.

Wang, X., and Gao, Y. (2018). The road to rural revitalization in poor counties in national key ecological function areas. *PRO* 04, 94–100. doi: 10.16501/j.cnki.50-1019/d.2018.04.012

Wang, F., and Ge, X. (2022). Can low-carbon transition impact employment: Empirical evidence from Low-carbon city pilot policy. *China Industrial Economics* 05, 81–99. doi: 10.19581/j.cnki.ciejournal.2022.05.004

Wang, D., and Tang, M. (2019). How does land urbanization affect ecological environment quality? Analysis based on dynamic optimization and spatially adaptive semi-parametric model. *Econ. Res. J.* 54, 72–85.

Wu, Y., Qi, J., Xian, Q., and Chen, J. (2021). The carbon emission reduction effect of China's carbon market-from the perspective of the coordination between market mechanism and administrative intervention. *China Ind. Econ.* 08, 114–132. doi: 10.19581/j.cnki.ciejournal.2021.08.007

Xu, J., Xie, G., Xiao, Y., Li, N., Jiang, Y., Chen, W., et al. (2019). Dynamic analysis of ecological environmental quality changes in national key ecological function areas in China. *Acta Ecol. Sin.* 39, 3039–3050. doi: 10.5846/stxb201806011227

Xu, J., Xie, G., Xiao, Y., Li, N., Yu, F., Pei, S., et al. (2018). Dynamic analysis of ecological environment quality combined with water conservation changes in National key Ecological Function Areas in China. *Sustainability.* 10:1202. doi: 10.3390/su10041202

Xu, D., Yang, F., Yu, L., Zhou, Y., Li, H., Ma, J., et al. (2021). Quantization of the coupling mechanism between eco-environmental quality and urbanization from multisource remote sensing data. *J. Clean. Prod.* 321:128948. doi: 10.1016/j.jclepro.2021.128948

Xu, H., and Zhang, W. (2017). Study on the ecological protection effect of the transfer payment of national key ecological function areas: an empirical study based on Shaanxi data. *China Popul. Resour. Environ.* 27, 141–148. doi: 10.12062/cpre.20170618

Yang, F., Huang, J., He, Q., Zheng, X., Zhou, C., Pan, H., et al. (2020). Impact of differences in soil temperature on the desert carbon sink. *Geoderma* 379:114636. doi: 10.1016/j.geoderma.2020.114636

Yu, B. (2015). Economic growth effects of industrial restructuring and productivity improvement-analysis of dynamic spatial panel model with Chinese city data. *China Ind. Econ.* 12, 83–98. doi: 10.19581/j.cnki.ciejournal.2015.12.007

Yu, Y., and Zhang, N. (2021). Low-carbon city pilot and carbon emission efficiency: Quasi-experimental evidence from China. *Energy Economics.* 96:105125. doi: 10.1016/j.eneco.2021.105125

Zuo, L., and Gao, J. (2021). Investigating the compounding effects of environmental factors on ecosystem services relationships for Ecological Conservation Red Line areas. *Land Degradation & Development.* 32, 4609–4623. doi: 10.1002/ldr.4059

Zhang, T., Hou, M., Chu, L., and Wang, L. (2022). Can the establishment of National key Ecological Function Areas enhance vegetation carbon sink? Quasi-natural experiment evidence from China. *Int. J. Environ. Res. Public Health* 19:12215. doi: 10.3390/ijerph191912215

Zhang, W., and Li, G. (2015). Dynamic incentive effect analysis of transfer payment in national key ecological function zone. *China Popul. Resour. Environ.* 25, 125–131. doi: 10.3969/j.issn.1002-2104.2015.10.017

Zhang, M., Zhang, L., He, H., Ren, X., Lv, Y., Niu, Z., et al. (2022). Improvement of ecosystem quality in National key Ecological Function Zones in China during 2000–2015. *J. Environ. Manag.* 324:116406. doi: 10.1016/j.jenvman.2022.116406

Zhou, X. Y., Lei, K., Meng, W., and Khu, S. T. (2017). Industrial structural upgrading and spatial optimization based on water environment carrying capacity. *Journal of Cleaner Production.* 165, 1462–1472. doi: 10.1016/j.jclepro.2017.07.246

Zhu, Y., and Chen, H. (2020). Did the transfer payment in key eco-functional areas improve the eco-environment? Based on PSM. *South China J. Econ.* 10, 125–140. doi: 10.19592/j.cnki.scje.371556

Zhu, Y., and Chen, H. (2021). Did the transfer payment in key eco-functional areas improve the eco-environment? Based on PSM. *South China Journal of Economics.* 10, 125–140. doi: 10.19592/j.cnki.scje.371556

frontiers | Frontiers in Ecology and Evolution

TYPE Original Research
PUBLISHED 19 January 2023
DOI 10.3389/fevo.2022.1101135

OPEN ACCESS

EDITED BY
Guoqi Wen,
Laval University, Canada

REVIEWED BY
Hui Yang,
Chinese Academy of Geological Sciences, China
Lili Jiang,
Key Laboratory of Tibetan Environment Changes and Land Surface Processes, Institute of Tibetan Plateau Research (CAS), China

*CORRESPONDENCE
Xiaoyong Bai
✉ baixiaoyong@vip.skleg.cn

SPECIALTY SECTION
This article was submitted to Population, Community, and Ecosystem Dynamics, a section of the journal Frontiers in Ecology and Evolution

RECEIVED 17 November 2022
ACCEPTED 28 December 2022
PUBLISHED 19 January 2023

CITATION
Liu M, Bai X, Tan Q, Luo G, Zhao C, Wu L, Chen F, Li C, Yang Y, Ran C, Luo X and Zhang S (2023) Climate change enhanced the positive contribution of human activities to net ecosystem productivity from 1983 to 2018.
Front. Ecol. Evol. 10:1101135.
doi: 10.3389/fevo.2022.1101135

Climate change enhanced the positive contribution of human activities to net ecosystem productivity from 1983 to 2018

Min Liu[1,2], Xiaoyong Bai[1,3,4]*, Qiu Tan[2], Guangjie Luo[5], Cuiwei Zhao[2], Luhua Wu[1,3,4], Fei Chen[1,3,4], Chaojun Li[1,3,4], Yujie Yang[6], Chen Ran[1,2], Xuling Luo[1,2] and Sirui Zhang[1,2]

[1]State Key Laboratory of Environmental Geochemistry, Institute of Geochemistry, Chinese Academy of Sciences, Guiyang, Guizhou, China, [2]School of Geography and Environmental Sciences, Guizhou Normal University, Guiyang, China, [3]CAS Center for Excellence in Quaternary Science and Global Change, Xi'an, Shanxi, China, [4]Puding Karst Ecosystem Observation and Research Station, Chinese Academy of Sciences, Anshun, Guizhou, China, [5]Guizhou Provincial Key Laboratory of Geographic State Monitoring of Watershed, Guizhou Education University, Guiyang, China, [6]College of Geography and Environmental Science, Lanzhou University, Lanzhou, Gansu, China

Introduction: Accurate assessment of the net ecosystem productivity (NEP) is very important for understanding the global carbon balance. However, it remains unknown whether climate change (CC) promoted or weakened the impact of human activities (HA) on the NEP from 1983 to 2018.

Methods: Here, we quantified the contribution of CC and HA to the global NEP under six different scenarios based on a boosted regression tree model and sensitivity analysis over the last 40 years.

Results and discussion: The results show that (1) a total of 69% of the areas showed an upward trend in the NEP, with HA and CC controlled 36.33 and 32.79% of the NEP growth, respectively. The contribution of HA (HA_con) far exceeded that of CC by 6.4 times. (2) The CO2 concentration had the largest positive contribution (37%) to NEP and the largest influence area (32.5%). It made the most significant contribution to the NEP trend in the range of 435–440 ppm. In more than 50% of the areas, the main loss factor was solar radiation (SR) in any control area of the climate factors. (3) Interestingly, CC enhanced the positive HA_con to the NEP in 44% of the world, and in 25% of the area, the effect was greater than 50%. Our results shed light on the optimal range of each climatic factor for enhancing the NEP and emphasize the important role of CC in enhancing the positive HA_con to the NEP found in previous studies.

KEYWORDS

climate change, NEP, human activity, CO_2 concentration, boosted regression tree

1. Introduction

Terrestrial ecosystems play an most important role in the carbon cycle (Keenan et al., 2016). Vegetation can fix atmospheric carbon through photosynthesis. The net ecosystem productivity (NEP) is the photosynthetic product that is deducted from the photosynthetic product of plant photosynthesis after deducting the consumption of the plant's autotrophic respiration and the consumption of microbial heterotrophic respiration (Steffen et al., 1998; You et al., 2020). Usually, it is an indicator used to check whether the ecosystem can fix or release carbon from the atmosphere (Grant et al., 2012; Yu et al., 2013; Kong et al., 2022; Wang et al., 2022). In previous studies, it has been generally believed that NEP ≥ 0 represents a carbon sink while NEP < 0 represents a carbon source (Luyssaert et al., 2008; Yu et al., 2014).

The contribution of internal variations in global carbon sinks is currently under debate. Several studies have shown that the global terrestrial carbon sink has gradually increased over the past decade (Keenan et al., 2016; Ballantyne et al., 2017), and it has experienced large inter-annual changes (Fu et al., 2017; Ni et al., 2017). The carbon sink capacity in the semi-arid regions of the world has been increasing during the last 34 years (Zhang L. et al., 2020). The average annual NEP was 0.007 Gt C/yr in China from 1981 to 2000 (Cao et al., 2003). Tao et al. (2007) found that the terrestrial ecosystem generally played the role of a carbon sink from 1981 to 2000 in China. Terrestrial carbon absorption in China accounts for 8–11% of the global carbon sink (Piao et al., 2009). Climatic factors were once seen as important constraints on terrestrial ecosystems. The increase in the CO_2 concentration in the atmosphere increases the net carbon uptake (Sitch et al., 2007). And the CO_2 concentration is the main climate factor leading to the net carbon absorption in China (Tian et al., 2011; Piao et al., 2012). Elevated CO_2 concentrations could increase productivity by increasing the water use efficiency (WUE) of plants in semi-arid areas (Fay et al., 2003; Izaurralde et al., 2011). The increase in the CO_2 concentration is positively correlated with the NEP in global (Zhang L. et al., 2020). In addition, climate warming usually increases carbon sequestration by extending the carbon sequestration period (Peng et al., 2013; Keenan et al., 2014). In the same ecosystem, carbon sinks exhibit regular growth and are weak in warm and humid environmental conditions and relatively dry and cold environmental conditions, respectively, suggesting that proper precipitation and temperature are important for increasing the NEP. Global warming may promote the increase in the capacity of carbon sinks in cold regions (Chuai et al., 2018). However, an increase in temperature will reduce the NEP by increasing soil respiration (Bond-Lamberty and Thomson, 2010; Chen S. T. et al., 2012). Therefore, continued warming may impair carbon sinks and may even transform them into carbon sources (Medvigy et al., 2010). Increased precipitation will increase cloud cover and reduce solar radiation (SR), which is very important for vegetation (Mathur, 2014). Previous studies have shown that the monsoon climate system, which is characterized by large changes in precipitation, may be an important driver of the changes in the global carbon cycle (Zhang et al., 2018). The impact of precipitation on the NEP was positively correlated in China (Fang et al., 2001), India (Nayak et al., 2013), Asia (Tian et al., 2003), and other places (Poulter et al., 2014). The severe drought caused by the continuous decrease in precipitation in southwestern China led to a significant reduction in carbon absorption in 2009 and 2010 (Chen S. et al., 2019; Li et al., 2019). In China's typical karst areas, vegetation carbon and water use efficiency is also an important factor affecting vegetation's role in climate change and land use (Xiao et al., 2023). Overall, high precipitation and temperature increase the NEP, but excess precipitation and temperature have a negative effect on the NEP. In addition, SR is considered to be an important factor affecting the annual NEP (Zhang et al., 2009; Kitamura et al., 2012). SR is considered to be an important factor contributing to the large carbon sinks of the subtropical forests in southwestern China (Tan et al., 2011). Precipitation (P), Temperature (T), and SR together affect about 10% of the NEP in the semi-arid regions of the world, and drought is a combination of precipitation and soil moisture decline (Zhang L. et al., 2020). As a result, soil moisture is also considered to be one of the important driving factors affecting the NEP (Krishnan et al., 2006; Ru et al., 2018). In ecosystems with limited water, the soil moisture has a greater impact on the NEP than the temperature (Liu et al., 2010), and they all have an important impact on the NEP. In the past, many scholars have paid attention to the impact of climate change on the NEP, but the vegetation carbon caused by human activities should not be ignored (Li et al., 2020). Piao et al. (2010) pointed out that climate change and the restoration of woodland and shrubs through human activities were mainly affected factors to carbon balance in China. In addition, the contributions of the various factors to the NEP may have offsetting and diluting effects.

However, there are two issues that cannot be ignored. First, few previous studies have quantitatively distinguished the impact of each factor on the NEP. In addition, the optimal range of the interactions of the climate factors, the pairwise factors affecting the NEP, and whether climate change impacts the HA to improve the NEP on large scales are not known, which to some extent affects the understanding of global NEP differences in the past 40 years. Thus, in this study, we aimed (1) to study the changes in the carbon sink/source regions, the NEP, and climate factors from 1983 to 2018; (2) to calculate the optimal intervals for the contribution of the climate factors to the NEP; and (3) to identify the controlling areas in which the CC and HA contribution to NEP increasing or decreasing. (4) The optimal interval for the contribution of a single climate factor to the NEP, and the change in the NEP when the two climate factors work together were investigated. (5) Whether CC has increased the

positive HA_con to the NEP was analyzed. If yes, where does this enhancement primarily occur? How strong is the enhancement? Understanding the spatial distribution of the global carbon sources/sinks and the mechanisms of influence could enhance our understanding of the global carbon cycle.

2. Materials and methods

2.1. Materials

2.1.1. Gross primary productivity dataset

Based on about 40 years of remote sensing Advanced Very High Resolution Radiometer (AVHRR) data and observations from hundreds of flux sites around the world, a long-term, global, high-resolution series of Gross Primary Productivity (GPP) data was generated from 1982 to 2018 (Wang and Zhang, 2020).[1] The resolution is 1 month, and the data unit is $gCm^{-2}d^{-1}$. Previous research has shown that NIRv was strongly correlated with GPP under various ecosystem and climate conditions based on hundreds of flux points and continuous ground-based observations (Badgley et al., 2019; Baldocchi et al., 2020; Dechant et al., 2020), with determination coefficient (R2) values higher than 0.6, and the mean values of fixed points and verification points were 0.71 and 0.70, respectively, and the root mean square error (RMSE) of the data are 0.02 and 1.95 $gCm^{-2}d^{-1}$. This dataset can be used for research on global climate change and the carbon cycle (Deng et al., 2021; Sun et al., 2021; Wang et al., 2021; Wu and Jiang, 2022). All of the data were analyzed at the spatial resolution of 0.25° × 0.25°.

2.1.2. Meteorological data

The Precipitation (P) and Temperature (T) data were obtained from GLDAS-2.1 datasets provided by the National Aeronautics and Space Administration (NASA),[2] with a spatial resolution of 0.25° from 01/1983 to 12/2018 (Li et al., 2022; Song et al., 2022; Xiong et al., 2022). The SR dataset derived from the THRGPU (Terrestrial Hydrology Research Group of Princeton University).[3] The CO_2 concentration data were obtained from the Climate Data Store,[4] which is an authoritative website that gathers data from several websites, including the European Commission Joint Research Centre, implemented by the ECMWF (European Centre for Medium-Range Weather Forecasts), and the Climate Change Service. The CO_2 concentration data were for the period 1979–2020 and have resolution of 3 h. The soil moisture (SM) data were derived from the Global Land Data Assimilation System (GLDAS) and were provided by NASA (see text footnote 2). The four land surface process models, including Noah, contain simulated SM products with various spatiotemporal resolutions based on surface observations and satellite remote sensing monitoring data (Rodell et al., 2004). In this study, the SM products from the Noah (version 2.7.1) model were used, which include four layers of SM data. The SM contents of the average layer (unit: kg/m^2) were used. This dataset has been used many times in soil moisture research (Deng et al., 2020).

2.2. Methods

2.2.1. Theil–Sen median trend analysis

The Theil–Sen Median Trend Analysis is a robust non-parametric statistical method for trend calculation (Sen, 1968; Tian et al., 2017). The formulas is as follows:

$$S_{NEP} = \text{mean}\left(\frac{NEP_j - NEP_i}{j\text{-}i}\right) \quad 1983 \le i \le j \le 2018 \tag{1}$$

Where i and j was time series data. The time series was showed an upward trend when SNEP was greater than 0, and vice versa.

The Mann–Kendall test was one of the most widely used non-parametric tests for trend and variation analysis of long-time series data (Mann, 1945; Kendall, 1975). The Mann–Kendall test focuses on the sequence than the number. The purpose was to compare the number of different sequences.

Set the $\{NEP_i\}$, i = 1983, 1984,..., 2018;

Define the Z-statistic as:

$$Z_{sta} = \begin{cases} \frac{S-1}{\sqrt{\text{var}(S)}}, S\rangle 0 \\ 0, S = 0 \\ \frac{S+1}{\sqrt{\text{var}(S)}}, S\langle 0 \end{cases} \tag{2}$$

$$S = \sum_{j=1}^{n-1} \sum_{i=j+1}^{n} \text{sg}\left(NEP_j - NEP_i\right) \tag{3}$$

$$\text{sg}\left(NEP_j - NEP_i\right) = \begin{cases} 1, NEP_j - NEP_i\rangle 0 \\ 0, NEP_j - NEP_i = 0 \\ -1, NEP_j - NEP_i\langle 0 \end{cases} \tag{4}$$

$$\text{var}\,(S) = \frac{n\,(n-1)\,(2n+5)}{18} \tag{5}$$

n is the number of data in the sequence, and NEP_i and NEP_j are the NEP value in the ith year and the jth year, respectively. sg is a symbolic function. In this study, the significance of the NEP trend was judged at a confidence level of a = 0.05. The results were divided into significant changes ($Z \ge 1.96$ or $Z \le 1.96$) and insignificant changes ($-1.96 < Z < 1.96$) according to the trend change characteristics and the results. According to the above criteria, we further divided the results into five grades: significant increase, slight increase, basically unchanged, slight decrease, and significant decrease (**Table 1**).

1 https://data.tpdc.ac.cn

2 https://www.nasa.gov/

3 http://hydrology.princeton.edu/home.php

4 https://ads.atmosphere.copernicus.eu

TABLE 1 The table of trend change rating.

Theil–Sen	Z	Trend
S ≤ 0.00005	≤ −1.96	Strong decrease
S ≤ 0.00005	−1.96 < Z < 1.96	Slight decrease
−0.00005 < S < 0.00005	−1.96 < Z < 1.96	No change
S ≥ 0.00005	−1.96 < Z < 1.96	Slight increase
S ≥ 0.00005	≥1.96	Strong increase

2.2.2. Mann–Kendall mutation test

Mann–Kendall Mutation test was applicable to the analysis of time series data with a continuous increasing or decreasing trend (monotonic trend). It is a nonparametric test that applies to all distributions (i.e., the assumption that the data need not satisfy a normal distribution). This method was usually used to check the reliability of the results of trend analysis. First, create an order column for X with n sample sizes.

$$y_k = \sum_{i=1}^{k} r_i, \left(r_i\right)0, 1 \le k \le n) \tag{6}$$

Under the assumption of the random independence of the time series, the statistic was defined as follows:

$$UF_k = \frac{y_k - E\left(y_k\right)}{\sqrt{var\left(y_k\right)}} \tag{7}$$

UF_k, E (y_k), and Var (y_k) are the mean values and variances of the cumulative number of y_k. When x_1, x_2,..., x_n are independently and interdependently, the computational formula is as follows:

$$E\left(y_k\right) = n(n + 0.25) \tag{8}$$

$$Var\left(y_k\right) = \frac{n\left(n - 1\right)\left(2n + 5\right)}{72} \tag{9}$$

Based on this method, the value passes the 0.05 significance test when UF > 0, indicating a continuous growth trend at the 0.05 significance level. Simultaneously, the UB curve was calculated. If the intersection of the UF and UB curves was within the confidence level interval [−1.96, 1.96], and the specific year of the intersection point was determined, the parameters of the year exhibited a sudden growth state. If the intersection point was not within the test range, the intersection point did not passed the 0.05 test. Therefore, the sudden increase in the parameter in this year did not exhibit a sudden change.

2.2.3. NEP

The concept of the NEP was first proposed by Woodwell et al. (1978). In previous studies, it was usually obtained by subtracting the autotrophic respiration (Ra) and heterotrophic respiration (Rh) from the GPP. The Re is the sum of the Ra and Rh. The GPP data used in this article were obtained through observations from hundreds of flux sites around the world. We refer to the research of Wang et al. (2015). On the small-scale, the calculation models for the NEP are simulated based on the local climate and hydrological conditions (Gong et al., 2017; Zhang X. Z. et al., 2020), and the differentiation of vegetation types is conducted using the statistics of the NEP algorithm (Yuan et al., 2009; Xiao et al., 2013; Chen S. et al., 2019). Considering the complexity of the global scale, we used a more recognized algorithm (Yu et al., 2013; Wang et al., 2015). The optimal approach for the Re was determined through the positive correlation of the spatial coupling between the GPP and Re. The formulae is as follows:

$$\begin{aligned} NPP &= GPP - Ra \\ NEP &= NPP - Rh \\ NEP &= GPP - (Ra + Rh) \\ NEP &= GPP - Re \end{aligned} \tag{10}$$

In previous research, it has been confirmed that there is a significant linear relationship between the GPP and Re, and the average Re/GPP ratio is always 0.87 ± 0.04 (Chen et al., 2013, 2015).

$$GPP = 107.02MAT + 2.18MAP - 0.10MAT \times MAP - 544.35 \tag{11}$$

$$Re = 54.08MAT + 1.19MAP - 0.05MAT \times MAP - 103.04 \tag{12}$$

$$Re = 0.68GPP + 81.9 \tag{13}$$

$$NEP = 48.98MAT + 0.79MAP - 0.05MAT \times MAP - 313.85 \tag{14}$$

Zhu et al. (2014) developed three kinds of assessment schemes to assess the spatial patterns of carbon fluxes based on the results from Yu et al. (2013). The results show that 68% of the per-unit GEP contributed to ER and 29% to NEP in terms of the spatial variations. Therefore, a carbon flux assessment scheme was recommended as the formula (13) (Zhu et al., 2014; Wang et al., 2015). The MAT (average annual temperature) and MAP (average annual temperature) refer to the average annual temperature and average annual Precipitation, respectively. This formula passed the correlation test. It has a high credibility, with correlation coefficients ranging from 0.8 to 0.9 (Zhu et al., 2014).

2.2.4. Statistical analysis

In this study, the least square method was used to determine the linear trend of each pixel.

$$\Delta NEP = \frac{\sum_{i=1}^{n}(i \times NEP_i) - \frac{1}{n}\sum_{i=1}^{n} i \times \sum_{i=1}^{n} NEP_i}{\sum_{i=1}^{n} j^2 - \frac{1}{n}\left(\sum_{i=1}^{n} j\right)^2} \tag{15}$$

Where n represents the 36-year time span from 1983 to 2018, NEP_i was the annual NEP value of year i, i = 1983, 1984,...,

2018. As same, ΔT,ΔP, ΔSR,ΔSMandΔCO_2 on behalf of the trends of T, P, SM, SR, and CO_2, respectively.

2.2.5. Sensitivity of NEP on climate change and human activities

Various methods have been used to isolate the contribution of factors, such as the residual trend (RESTREND) method (John et al., 2016; Zhou et al., 2018), the LPJ-GUESS ecosystem model (Smith et al., 2014) and Miami models (Krausmann et al., 2009; Zhou et al., 2015, 2017) was used to separate human activity and climate change from multiple influencing factors, Nevertheless, there was high uncertainty in the simulation results (Wu et al., 2020). After comparing various research methods, we finally chose the method from the research of Forzieri (Wang et al., 2014; Forzieri et al., 2018, 2020; Wu et al., 2020), this method assumes a linear interaction between response variables and predictive variables. Firstly, we derived the partial derivative sensitivity terms of NEP to five climate factors (precipitation (P), temperature (T), soil moisture (SM), solar radiation (SR) and CO_2 concentration, respectively) by multiple regression method. On the basis of defining the sensitivity of the four climate factors to NEP as the total derivative, the variation of single factor was separately expressed as a function of NEP. The sensitivity of NEP to changes in CC was computed between 1983 and 2018.

$$\Delta \mathrm{NEP} = HA_{\mathrm{con}} + CC_{\mathrm{con}} = HA_{\mathrm{con}} + \delta P^{NEP} + \delta T^{NEP} + \delta SR^{NEP} + \delta SM^{NEP} + \delta CO_2^{NEP} \quad (16)$$

Where δP^{NEP} was the P change associated with the long-term change of NEP, In the same way,δSM^{NEP}, δCO_2^{NEP}, δT^{NEP} and δSR^{NEP} represents the SM, CO_2 concentration, T and SR associated to NEP, respectively. Derived from Equation 15, variations in climate factors associated to NEP were expressed by the following equation:

$$\delta P^{NEP} = \frac{\partial NEP}{\partial P}\Delta P$$

$$\delta T^{NEP} = \frac{\partial NEP}{\partial T}\Delta T$$

$$\delta SR^{NEP} = \frac{\partial NEP}{\partial SR}\Delta SR$$

$$\delta SM^{NEP} = \frac{\partial NEP}{\partial SM}\Delta SM$$

$$\delta CO_2^{NEP} = \frac{\partial NEP}{\partial CO_2}\Delta CO_2 \quad (17)$$

Where ΔNEP, ΔT, ΔP,ΔSR, $\Delta SM$and ΔCO_2 represents the linear trend of the NEP, annually averaged T, P, SR, SM and CO_2 concentration, respectively (Zhou et al., 2001; Liu et al., 2021). $\frac{\partial NEP}{\partial P}$ was the sensitivity of P to NEP quantified between 1983 and 2018. The Equation 16 was extended to Equation 18 according to the rules of Equation 17.

$$\Delta \mathrm{NEP} = HA_{\mathrm{con}} + \frac{\partial \mathrm{NEP}}{\partial P}\Delta P + \frac{\partial NEP}{\partial T}\Delta T + \frac{\partial NEP}{\partial SR}\Delta SR + \frac{\partial NEP}{\partial SM}\Delta SM + \frac{\partial NEP}{\partial CO_2}\Delta CO_2 \quad (18)$$

The derived signal $\frac{\partial NEP}{\partial P}$ integrates the bidirectional interactions between P and NEP, the $\frac{\partial NEP}{\partial T}$ integrates between T and NEP, the $\frac{\partial NEP}{\partial SR}$ integrates between T and NEP. The $\frac{\partial NEP}{\partial SM}$ integrates between SM and NEP, the $\frac{\partial NEP}{\partial CO_2}$ integrates between CO_2 concentration and NEP.

2.2.6. The contribution of climate change and human activities of the NEP

In order to achieve a more accurate quantitative analysis of the contribution of Climate Change (CC_con) and Human Activities (HA_con), the CC_con and HA_con in this table differ from the contribution rates in Equations 15, 17, where the contribution rate represents the population, whereas here it is expressed by cases. Six typical scenarios were used to describe it (**Table 2**; Zhou et al., 2017; Yan et al., 2019): this paper define NI as the NEP increase of HA and CC, so, the HNI and CNI represents the NEP increase by HA and CC, respectively. The ND was NEP decrease by HA and CC, Breaking it down, the CND was NEP decrease by CC_con and the HND represents the decrease by HA. We have known the contribution of CC and HA to NEP through continuous comparison and analysis.

The relationship is expressed as Equation 18:

Where $Z > 0$ was represents the NEP increasing, and $Z < 0$ was represents the NEP decreasing. When $Z_{HA\,\mathrm{increasing}}$ and $Z_{HA_{\mathrm{dreasing}}}$ combine, that's HNI, they represent the positive HA_con and the negative HA_con to NEP, respectively. The same, When $Z_{CC\mathrm{increasing}}$ and $Z_{CC_{\mathrm{dreasing}}}$ combine, that's CNI, they represent the positive and negative CC_con to NEP, respectively.

$$Z_{NI} = Z_{HNI} + Z_{CNI}$$

$$Z_{HNI} = Z_{HA_{\mathrm{increasing}}} - Z_{HA_{\mathrm{dreasing}}}$$

$$Z_{CNI} = Z_{CC_{\mathrm{increasing}}} - Z_{CC_{\mathrm{dreasing}}} \quad (19)$$

2.2.7. Boosted regression tree

The boosted regression tree (BRT) machine learning method can effectively select the relevant variables and identify the nonlinear relationship between the input and output based on multivariate regression trees (Elith et al., 2008; Mitchell et al., 2018). The BRT was performed using the gem function in the dismo package in R studio (Pourghasemi and Rahmati, 2017). Nearly 50,000 points were selected to participate in the calculation. Furthermore, the number of trees, the learning rate, and the tree complexity were used to reduce model uncertainly.

TABLE 2 Different scenarios for estimate the CC_con and HA_con to NEP increase and decrease.

	Z	Scenario	CC_con	HA_con	Contribution proportion of CC (%)	Contribution proportion of HA (%)
X increasing	Z > 0	NI	>0	>0	$\frac{\lvert CC\_con\rvert}{\lvert CC\_con\rvert+\lvert HA\_con\rvert} \times 100$	$\frac{\lvert HA\_con\rvert}{\lvert CC\_con\rvert+\lvert HA\_con\rvert} \times 100$
		CNI	>0	<0	100	0
		HNI	<0	>0	0	100
X decreasing	Z < 0	ND	<0	<0	$\frac{\lvert CC\_con\rvert}{\lvert CC\_con\rvert+\lvert HA\_con\rvert} \times 100$	$\frac{\lvert HA\_con\rvert}{\lvert CC\_con\rvert+\lvert HA\_con\rvert} \times 100$
		CND	<0	>0	100	0
		HND	>0	<0	0	100

The highest AUC (area under the curve) of the training data, the optimal parameters of the number of trees, the tree complexity, and the learning rate were selected.

A five-fold cross-validation method was implemented for the BRT model, and we determined the best contribution relationship between the dependent variable (NEP) and all of the climate factors based on this model. We evaluated the accuracy of the model based on the AUC value. When AUC > 0.9, the accuracy of model is excellent; when 0.8 < AUC < 0.9, the accuracy of model is good; and if AUC < 0.7, the accuracy of model is poor (Swets, 1988). In addition, the fit is better if the ratio of the actual to the predicted NEP is close to one, the fitting effect is better. By this model can accurately identify the best contribution of all climate factors on the NEP interval, and the interval was conducted on the basis of 2.2.5 of determining if 2.2.5 part can get is the contribution of each factor to the NEP contribution in the size and spatial distribution, so this model, the precision will be able to get the best contribution of interval, and it is not limited to a single factor.

3. Results

3.1. The trend of NEP

A total of 69% of the areas showed an increase trend of NEP, and 20% exhibited a decrease from 1983 to 2018 based on the Theil–Sen and MK trend analysis results (**Figure 1A**). The average annual NEP increased from 228.62 g C m^{-2} yr^{-1} in 1983 to 256.71 g C m^{-2} yr^{-1} in 2018 (**Figure 1D**). The significant growth of the C sink area was mainly concentrated in the 60–69°N region, and the C source area was located in the 48–65°N region (**Figure 1B**). These results are similar to those of Chan et al. (2019). In a previous study, Luyssaert et al. (2007) found that the global NEP was 2.1 Pg C yr^{-1}. Piao et al. (2013) reported an average global NBP of 2.0 ± 0.8 Pg C yr^{-1} during 1980–2009. The growth rate of the global terrestrial carbon sink during 1998–2012 (0.17 ± 0.05 Pg C yr^{-2}) was 3 times that during 1980–1998 (Piao et al., 2018). The respiration of the terrestrial ecosystems was limited to 1.4 ± 0.1 Pg C yr^{-1} (Mahecha et al., 2010). The global NEP obtained in this study is 3.22–3.71 Pg C yr^{-1}. Results based on the updated time series are relatively closed compared to previous studies. On a regional scale, China's estimated NEP was determined to be 1.4–1.6 Pg C yr^{-1} (excluding desert values) in this study, which is slightly lower than the values obtained by Wang et al. (2015) (1.89 Pg C yr^{-1}) and the average NEP obtained by the author by redefining the relationship between NEP and NPP was 1.34 ± 0.12 PgC yr^{-1}. In addition, (Zhu et al., 2014) developed a statistical evaluation scheme to estimate the NEP of China in the 2000s as 1.91 ± 0.15 PgC yr^{-1}. And Wang et al. (2020) estimated that the average annual terrestrial carbon sink in China from 2010 to 2016 was 1.11 ± 0.38 Pg C yr^{-1}. Therefore, the results of this paper have a certain degree of credibility on a regional scale. In the future, with the improvement of relevant results, it is easy to improve the estimation results of NEP synchronously by using the estimation process of this study, such as the study on some provinces in China (Lu et al., 2013; Gong et al., 2017; Zhang X. Z. et al., 2020) and statistics of NEP algorithm for distinguishing vegetation types (Chen S. et al., 2019).

About 79.4–82.6% of the area served as a Carbon sink from 1983 to 2018 (**Supplementary Figure 1**), which was 3.9–4.7 times the Carbon source area. The largest increase (1.4%) in the Carbon sink area occurred in 1990 based on the changes in the areas of the Carbon sources and Carbon sinks (**Figure 1C**). **Supplementary Figure 1** and **Supplementary Table 1** show the dynamic changes and spatial trends of the NEP, SR, SM, T, P, and CO_2.

3.2. Contribution of climate change to the NEP

The spatial distribution of the climatic factors contribution to the NEP based on the sensitivity analysis is shown in **Figure 2**. The single factor correlation analysis revealed that the NEP has the strongest correlation with P (R = 0.84), followed by temperature (R = 0.56) (**Figure 2F**). This is similar to the results of Chen et al. (2013), Xiao et al. (2013), and Chen S. et al. (2019). Nonetheless, considering that there may be some autocorrelation problems in the correlation analysis between a single factor and NEP, we analyzed the contribution of each

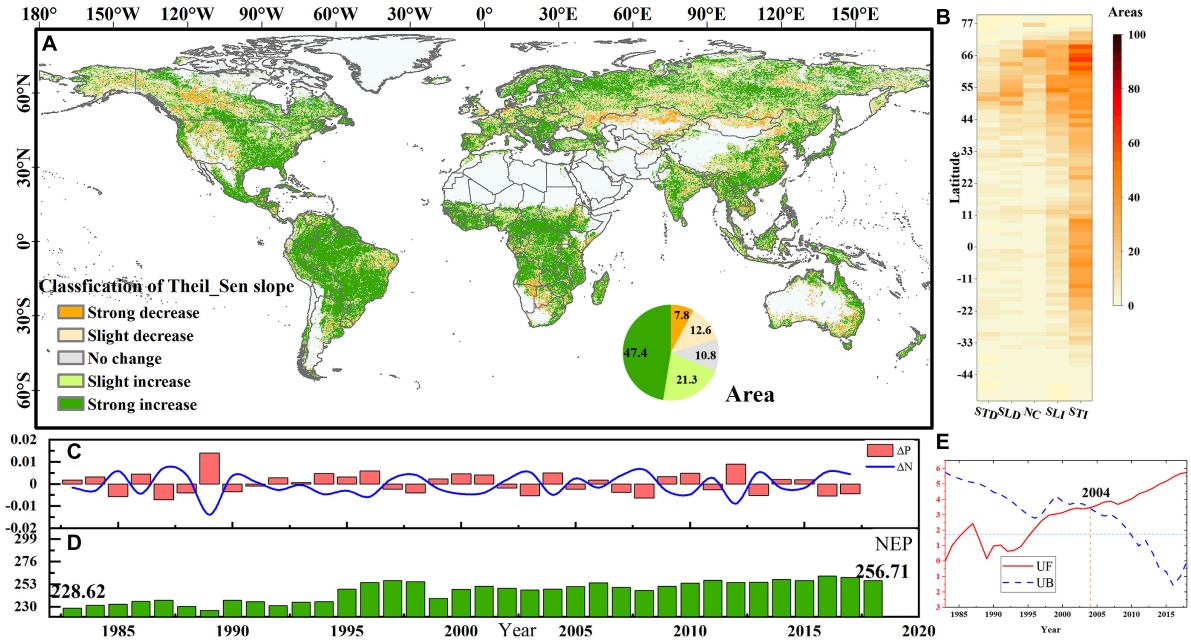

FIGURE 1
The trend of NEP. **(A)** Spatial pattern of the Theil–Sen trend of NEP between 1983 and 2018; **(B)** latitude map of NEP trend in different classification, strong decrease is STD, slight decrease is SLD, no change is NC, strong increase is STI, and slight increase is SLI; **(C)** the ΔP (the carbon sink areas difference between the current year and the previous year) and ΔN (the carbon source areas difference between the current year and the previous year) and **(D)** the mean value of NEP; **(E)** the Mann–Kendall mutation test of NEP.

climate factor to NEP through Equation 16, which excluded the interaction between factors and recognized this contribution in space (Figure 2A). The results show that the CO_2 concentration had the highest contribution rate (37%), although it made a negative contribution in many areas (Figure 2A). The SR made negative contributions in many areas in India, Africa, and North America, and its negative contribution rate was the highest (−11.7%) (Figure 2D). Although the correlation coefficient between P and NEP was the highest, it made a negative contribution to the NEP (−10.5%; Figure 2B). The negative contribution of T was mainly concentrated in the high latitude regions of the Northern hemisphere (Figure 2E). The SM made a large contribution in the high latitude regions such as Russia (Figure 2C).

3.3. Main area controlled and main load controlled by climatic factors

In order to identify the factors that play a key role in the NEP in different regions, we explored the major latitudes and regions for each climate factor. The results showed that the CO_2 concentration had the largest positive contribution (37%) to NEP and the largest influence area (32.5%; Figure 3). Although the main area controlled by the SR was the next largest, the SR made a negative contribution to the NEP (Figure 3B), and the SR made the lowest contribution to the NEP (−11.7%). Among the other factors, the main region controlled by T was the smallest, and it exhibits a divergent distribution. P mostly played an active role in the mosit and semi-humid terrestrial regions, and the main regions controlled by the SM were mostly located in the Northern Hemisphere. Interestingly, we found that in more than 50% of the areas, the main loss factor was the SR in any area controlled by the climate factors (T, P, SM, and CO_2).

3.4. Best ranges for climatic factors for the NEP

To explore the changes in the sensitivity of the NEP trend to the climate factors, we used boosting and regression tree (BRT) models to evaluate the optimal interval for the contribution of the climatic factor to the NEP. We adjusted the tree complexity (2, 3, and 4) and the learning rate (0.01, 0.05, and 0.001) to generate the best model (Supplementary Figure 3) according to Equation 6. The prediction accuracy was good when the AUC was 0.875 (i.e., >0.8). The ratio between the actual value and the predicted value was 0.86, which indicates a good prediction accuracy. Therefore, the BRT model was suitable for determining the optimal value of the climate factor for the NEP.

Figure 4 shows the best ranges for two climate factors for the NEP, as well as the optimal contribution interval for a single factor and the NEP calculated based on the BRT model

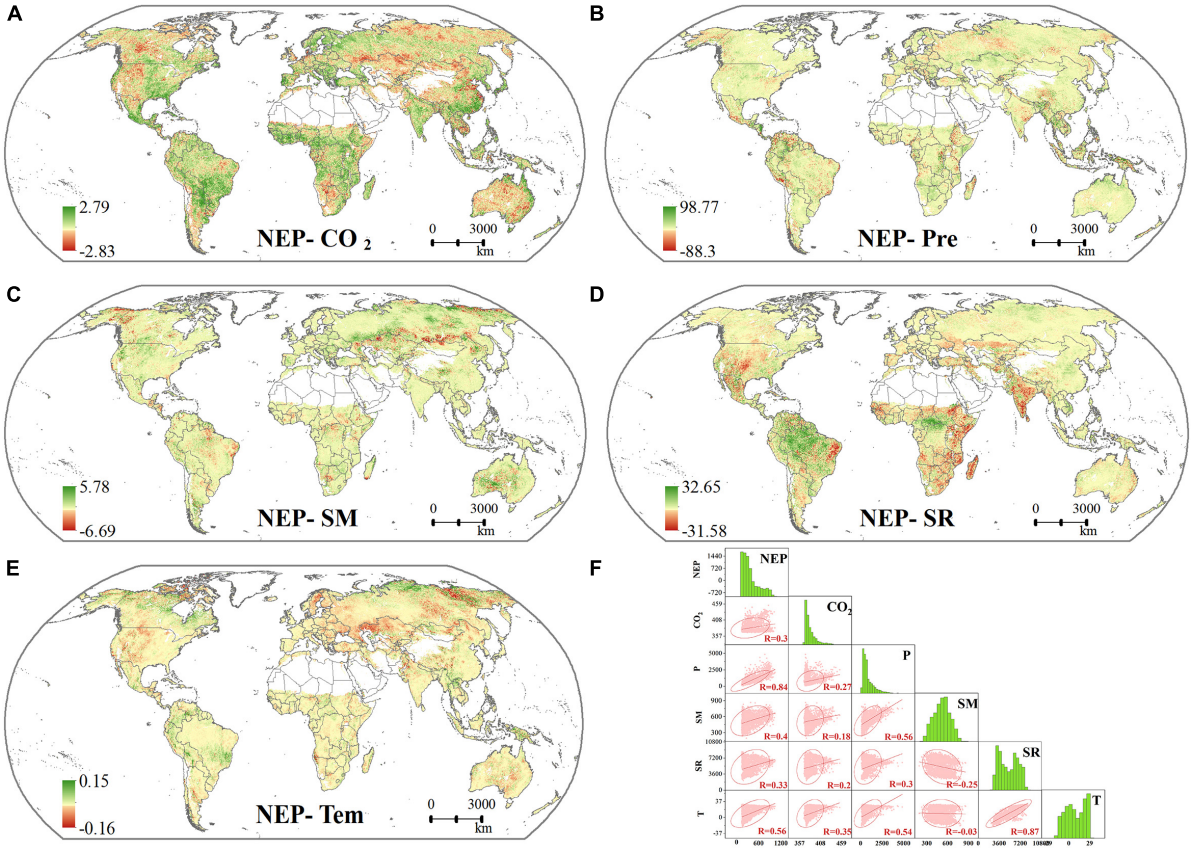

FIGURE 2
Sensitivity of NEP to climate factor. Sensitivity of NEP to changes in CO_2 concentration **(A)**, P **(B)**, SM **(C)**, SR **(D)**, and T **(E)**; correlation analysis between NEP and climate factors **(F)**.

(in the small diagram in Figure 4). In addition, in order to better view the optimal contribution interval of a single factor, a detailed version is listed in Supplementary Figure 3. When the precipitation was greater than 2000 mm and the SR was between 3500 and 7500 (Figure 4F and Supplementary Figures 3B, E), the NEP was relatively stable. An increase in temperature can promote an increase in the NEP, but the upward trend drops sharply after 25°C (Supplementary Figure 3F). However, the NEP is more likely to be lower in the areas with less precipitation. Interestingly, the NEP decreased with increasing SM (Supplementary Figure 3C). There is a well-defined positive gradient with increasing precipitation and temperature. In general, when the temperature was between 16 and 27.7°C, the annual precipitation reached 900 mm, the SR was 4295–7000, the SM was 550–800 kg/m^2, the CO_2 concentration was greater than 380 ppm, and the NEP was high. The NEP was particularly high when the precipitation was greater than 900 mm, the SR was greater than 5200, and the SM was greater than 350 kg/m^2. The CO_2 concentration was the most complicated factor, and its contribution to the NEP trend was the most significant between 435 and 440 ppm (Figure 4D). The contribution to the NEP was most significant when the CO_2 concentration increased and the precipitation exceeded 1200 mm.

3.5. The contribution of human activities and climate change to the NEP

Human activities and CC made positive contributions to the NEP in 57.6 and 60.3% of the area, respectively (Figures 5A, B). The HA_con to the NEP reached 86.48%, far exceeding the CC_con of 13.54% (i.e., by 6.4 times). So, HA was the main factor affecting the NEP.

In addition, for the purpose of this study, the CC_con and HA_con were quantitatively analyzed for increasing or decreasing NEP using the method of Table 1. The positive effect of HA_con was obvious in North America and India (Figure 5C), and the NEP in South America, southern-central Africa, northern Asia, and eastern China was mainly due to the CC_con (Figure 5E). Negative HA_con was mainly found in northern Asia, such as northern China, northern Kazakhstan

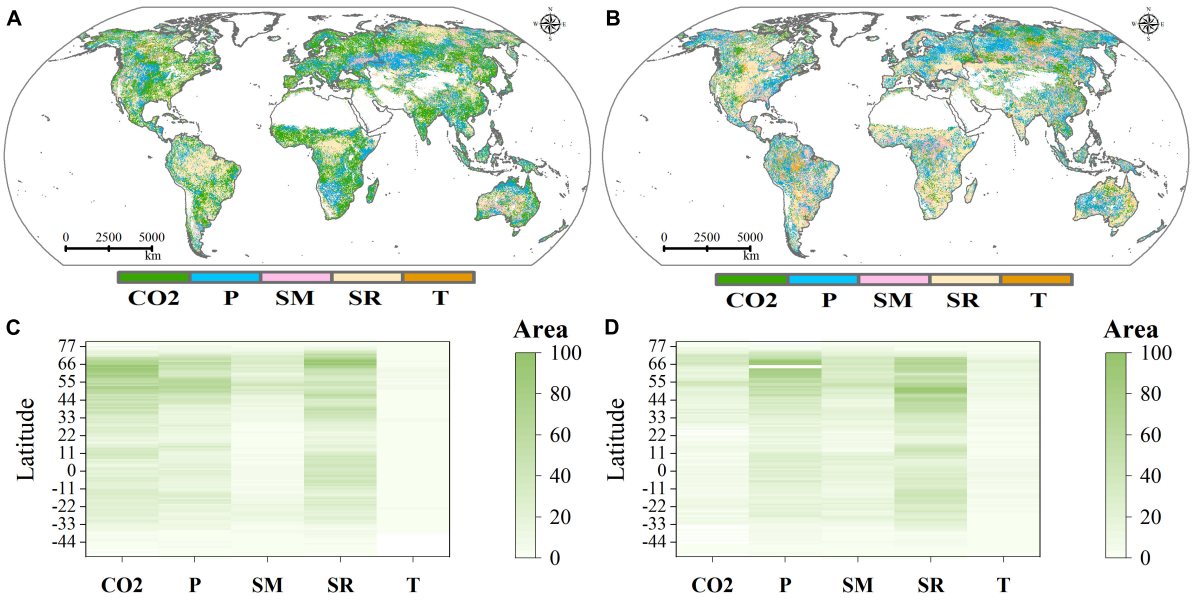

FIGURE 3
(A) The main controlling factors and **(B)** the main load controlling factor influencing the NEP. The five driving factors include CO_2 concentration, T, P, SR, and SM. **(C,D)** The contributions of the five driving factors at latitudes of 55°S–80°N.

and northern Russia (**Figure 5D**). In the Europe and Australia, CC_con played a negative role to NEP (**Figure 5F**). By studying the main controlled areas, the HA and CC controlled 36.33 and 32.79% of the NEP growth areas and controlled 11.76 and 16.13% of the NEP degradation areas (**Figures 5G, H**) in the world, respectively. In addition, the countries in **Figure 5K** are ranked according to their NEP trends. **Figure 5J** shows the proportions that CC enhances the HA_con the NEP and factor contributions for the 167 major countries of the world are shown in **Supplementary Table 1**. Moreover, when comparing the CC_con and HA_con, we found that the CC_con improved the positive HA_con in 44% of the world. In addition, in one-fifth of the regions, the enhancement effects reached more than half (**Figure 5I**). Understanding how the CC_con improves the HA_con will help us to further understand what role CC plays in promoting the NEP.

4. Discussion

4.1. Comparison with the driving mechanisms of GPP and NEP

In contrast to the research results, in this study it was found that the CO_2 concentration gives the highest contribution to the NEP trend, the T_con was very low and the main regions it controlled was the smallest. This is consistent with the results of previous studies (Chuai et al., 2018; Fernández-Martínez et al., 2019; Zhang L. et al., 2020). The NEP was controlled by a complex interplay between a range of climatic factors. Our further analysis revealed that the main factors driving the GPP were inconsistent with those driving the NEP, but the HA_con was consistentlymuch larger than the CC_con. The HA_con and CC_con to the NEP were 86.48 and 13.54%, respectively, while the GPP was almost entirely controlled by the HA. The CO_2 concentration made the largest positive contribution to the GPP (12%), T made the smallest contribution (0.04%), and SR made the largest negative contribution (−11%). Previous studies have shown that the sensitivities of the GPP and NEP to T and SR are not much different (You et al., 2020), and there is no significant relationship between the GPP and P (Chen W. et al., 2019). However, an increase in the annual average T will cause the vegetation growing season to be prolonged and cause an increase in the GPP, and the inter-annual variation in the GPP is not significantly correlated with T on a global scale (Piao et al., 2013). Our study shows that HA had a positive effect on the NEP, and we believe that CC deepened this positive contribution. Overall, assessing the impacts of the climatic factors on the NEP is critical to more accurately predicting the future dynamics of the global carbon cycle and its feedback on the climate system.

4.2. Regional differences

Of the six continents in the world, Australia has the lowest NEP trend and South America the highest (**Figure 6**). Interestingly, in North America, Africa, and Europe, the NEP was almost entirely controlled by HA, and the main negative

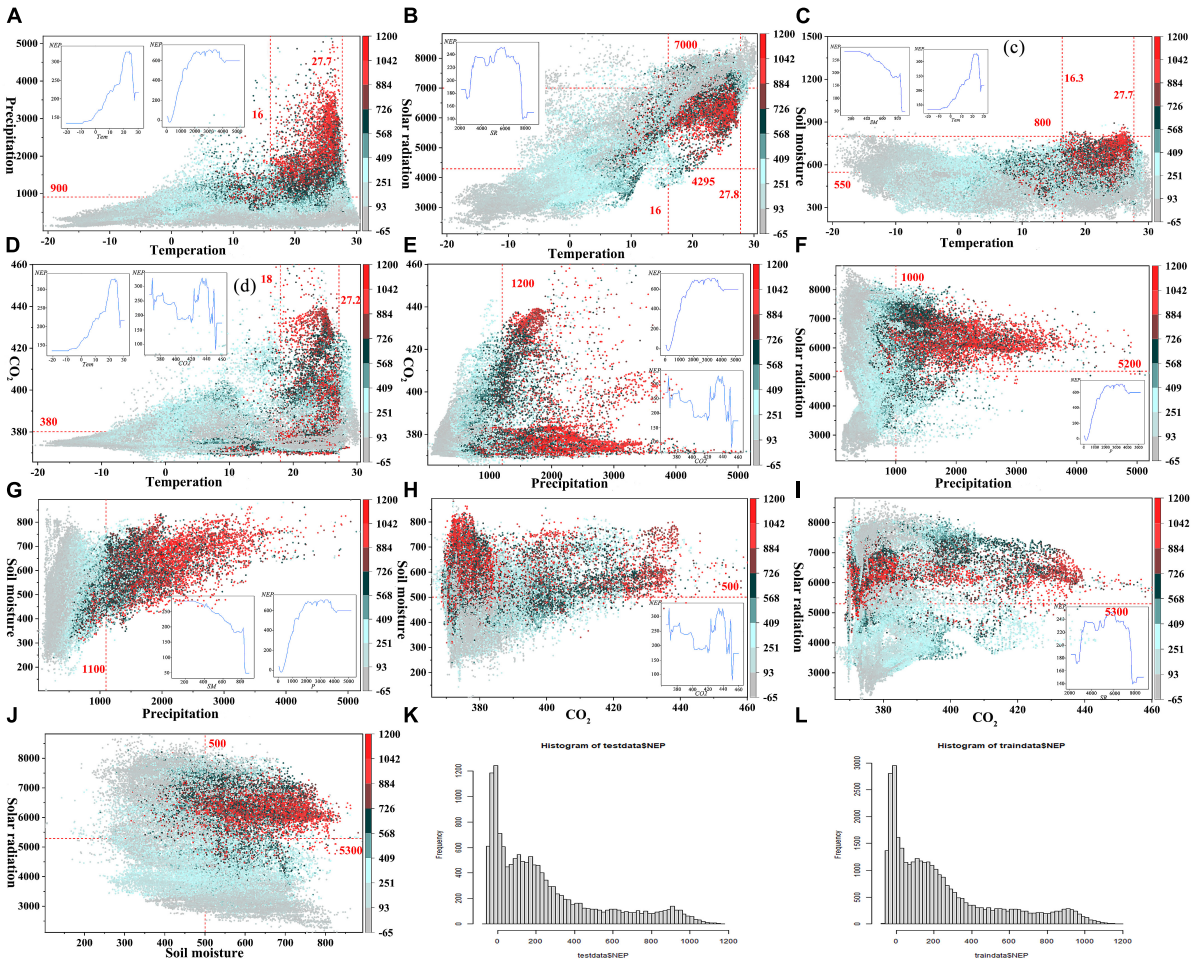

FIGURE 4
The best contribution interval of each climatic factor to the NEP. Annual NEP in the climate domains based on **(A)** T and P; **(B)** T and SR; **(C)** T and SM; **(D)** T and CO_2; **(E)** P and CO_2; **(F)** P and SR; **(G)** P and SM; **(H)** CO_2 and SM; **(I)** CO_2 and SR; **(J)** SM and SR; **(K)** NEP test data; and **(L)** NEP training data.

contributions of the climatic factors was from the SR. The NEP in South America was entirely controlled by CC, of which the SR_con was 85.42%. HA and CC both contributed positively to the NEP in Australia and Asia, and the HA_con to NEP also contributed positively to the NEP, with values of 85.25 and 81.25%, respectively. SR made a major negative contribution on these two continents, with values of −81.25 and −13.11%, respectively. Among climate factors, the CO_2 concentration had the highest positive contribution to the NEP on all six continents except South America.

Among the top seven countries in terms of land area in the world (Russia, Canada, China, the United States, Brazil, Australia, and India) (**Figure 6**), CC played the absolute dominant role in the NEP trend in Brazil, and the SR_con was the largest. CC also contributes positively to the NEP trend in China, with CO_2 concentration contributed 42.55%, while the opposite was true for the rest of the countries, where HA_con was the strongest. SR made the largest negative contribution to the NEP in India, Australia and the United States. Russia had the strongest negative P_con. The CO_2_con for the seven major countries was 43–59%. The CO_2 concentration contributed only made a small negative contribution in 10 of the 167 major countries in the world.

4.3. Uncertainties

Overall, the limitations of this study are mainly reflected in the following: Firstly, although climate factors (T, P, CO_2, SR, and SM) are closely related to NEP, some natural factors, such as forest age, vegetation type and growing season length, also have a definite impact on NEP (Tang et al., 2014; Migliavacca et al., 2015), which is the direction of our next research. In addition, considering that most of the factors causing nitrogen deposition are man-made factors, such as unreasonable fertilization in

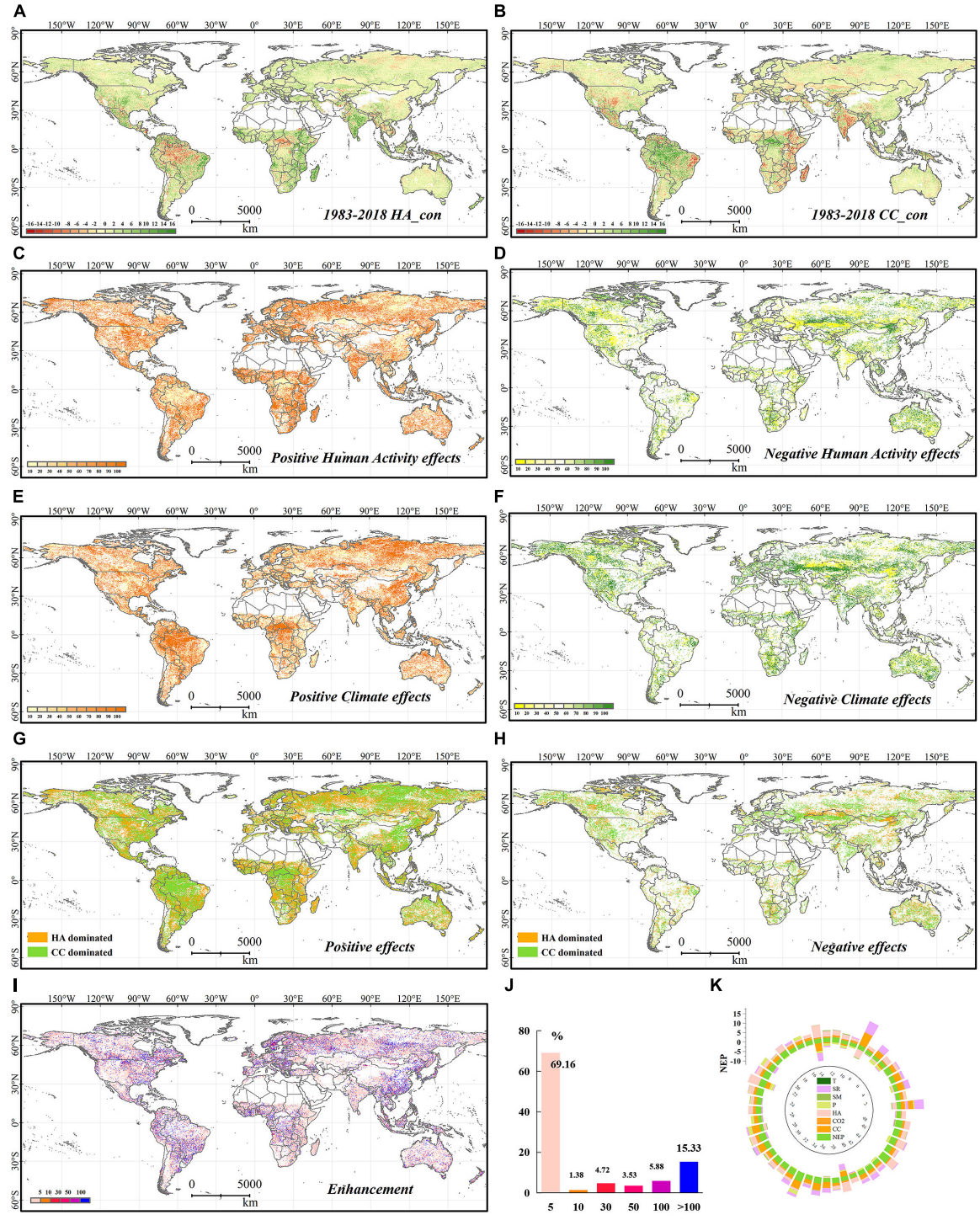

FIGURE 5
The HA_con **(A)** and the CC_con **(B)** to NEP, the CC_con and HA_con to NEP increasing **(C,E)** and decreasing **(D,F)**; spatial pattern of the CC and HA controlled the increasing **(G)** and decreasing **(H)** of the NEP; spatial diagram of the positive of CC_con to HA_con **(I)**; the proportions that CC enhances the HA_con **(J)**; the trend of NEP in the top 50 countries of global **(K)**.

farmland, poor management of livestock and poultry manure in livestock farms, coal burning, and automobile exhaust emissions, which will increase the emission of man-made reactive nitrogen into the atmosphere, nitrogen deposition can be summarized in human activities from this perspective. Even though the role of N deposition on NEP has been mentioned

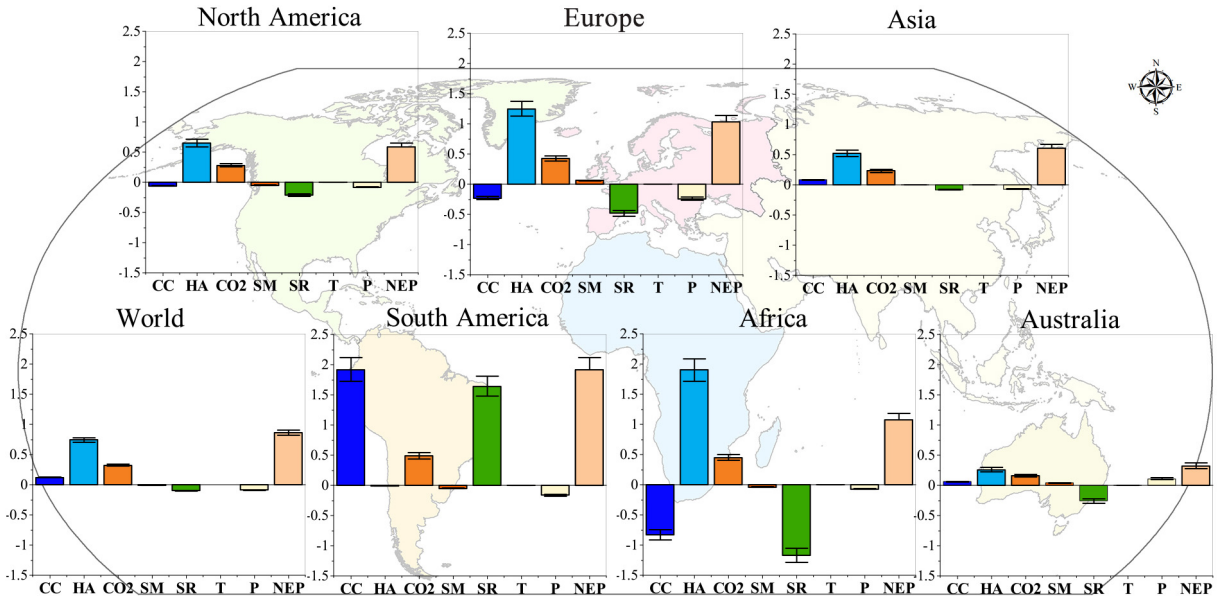

FIGURE 6
The HA_con and CC_con to NEP in the world and six continents.

in much literature, some studies have shown that the increase in global N deposition since 1981 has only weakly affected the Carbon sink area (Nadelhoffer et al., 1999; Chen H. et al., 2012; Chen J. M. et al., 2019). And, since the 21st century, nitrogen deposition has increased from 316.16 to 331.88, with little overall change. Therefore, the role of nitrogen deposition in HA is included in this paper. This involves the inclusion of other factors (including nitrogen deposition) in the scope of HA in this paper (although we believe that most of the causes of nitrogen deposition are still caused by human activities) will increase the contribution rate of HA to a certain extent, such as food collection, timber harvesting, burning of plant residues, fires (Yin et al., 2020), water erosion and other geological processes that cause carbon leakage. However, this paper is limited by the difficulty of obtaining data and the lack of long-term monitoring of human activities (such as ecological engineering and timber logging), which leads to the inadequacy of this part. Of course, in the next study it will be very necessary to include the effect of nitrogen deposition in the study of long time series. This is also a direction for our further research on how to more carefully quantify the contribution of various factors in human activities to the NEP. We believe that it is of scientific importance to clarify the main limiting factors affecting regional NEP. There are certain uncertainties in the generation of the GPP data products from the modeling results. These errors can be caused by a number of factors, including roughness of the meteorological data and different resolutions of this pixels. In addition, in this study, the spatial data used for the analysis were unified in a 0.25° space due to the limitations of the data. An attempt to evaluate with more fine-resolution multi-source data and measurements will be made in further studies. These limitations should be overcome in future studies. In addition, it is necessary to explore NEP and climate change on the monthly and quarterly scales. Moreover, since the important impact of CO_2 concentration on NEP has been obtained in this paper, it is instructive to clarify how the dynamic contribution of CO_2 concentration can be used to achieve the goal of carbon neutrality in different future emission scenarios.

In general, in this study, the global NEP from 1983 to 2018 was evaluated, the responses of the NEP to CC and HA were discussed, and detailed analysis was performed on different continents in 167 countries. Despite these uncertainties, this study is critical to improving the understanding of the carbon cycle, and it provides a theoretical understanding of how CC enhances the positive contributions of HA in the context of a changing climate.

5. Conclusion

In this study, the change in the global NEP and its responses to climate change and human activities over the last 40 years were assessed based on sensitivity analysis and BRT models. We choose temperature (T), precipitation (P), solar radiation (SR), soil moisture (SM), and CO_2 concentration as the most important climatic factors. A regression model and sensitivity analysis were used to evaluate the CC_con and HA_con to the NEP under six different scenarios on the global scale. The results of this study enhance our knowledge of the CC and HA to the global NEP. The conclusions of this study are as follows.

(1) The NEP increased in 69% of the world between 1983 and 2018, about 79.4–82.6% of the area served as a Carbon sink, i.e., 3.9–4.7 times greater than the carbon source area. And HA and CC controlled 36.33 and 32.79% of the NEP growth, respectively. However, the contribution of HA far exceeded that of CC (i.e., by 6.4 times).
(2) The CO_2 concentration had the largest positive contribution (37%) to NEP and the largest influence area (32.5%). Our paper use the BRT models to evaluate the optimal interval that the contribution of climate factor to NEP. We have further measured the optimal contribution interval of each factor, providing a more accurate guide to global NEP. It made the most significant contribution to the NEP trend in the range of 435–440 ppm. In more than 50% of the areas, the main loss factor was SR in any of the areas controlled by the climatic factors. HA and CC controlled 37.33 and 34.79% of the NEP growth, respectively. However, the contribution of HA far exceeded that of CC (i.e., by 6.4 times).
(3) The CC_con and HA_con have been identified in different countries, interestingly, CC improved the positive HA_con to the NEP in 44% of the world. Moreover, in 25% of the area, the enhancement effect reached more than 50%.

Our results clarify a long-standing problem and emphasize the important role of CC to the NEP. Therefore, this study quantitatively distinguishes the influence of each factor on NEP, and determined the best range of climate factor interaction. It is also understood that CC can affect HA to improve NEP on a large scale compared with previous studies.

Data availability statement

The original contributions presented in this study are included in this article/**Supplementary material**, further inquiries can be directed to the corresponding author.

Author contributions

XB designed the research. ML wrote the manuscript with support of QT, CZ, and LW. FC, YY, GL, and CR performed the data processing and picture making. CL, XL, and SZ performed the language editors and references. All authors contributed to the interpretation of the results and the writing of the manuscript.

Funding

This research work was supported jointly by the Western Light Cross-team Program of Chinese Academy of Sciences (No. xbzg-zdsys-202101), National Natural Science Foundation of China (No. 42077455), the Central Government Leading Local Science and Technology Development (QianKeZhongYinDi [2021]4028), Strategic Priority Research Program of the Chinese Academy of Sciences (Nos. XDB40000000 and XDA23060100), Guizhou Provincial Science and Technology Projects (No. 2022-198), High-level innovative talents in Guizhou Province (GCC[2022]015-1), and Opening Fund of the State Key Laboratory of Environmental Geochemistry (Nos. SKLEG2022206 and SKLEG2022208).

Conflict of interest

The authors declare that the research was conducted in the absence of any commercial or financial relationships that could be construed as a potential conflict of interest.

Publisher's note

Supplementary material

The Supplementary Material for this article can be found online at: https://www.frontiersin.org/articles/10.3389/fevo.2022.1101135/full#supplementary-material

References

Badgley, G., Anderegg, L. D., Berry, J. A., and Field, C. B. (2019). Terrestrial gross primary production: Using NIRV to scale from site to globe. *Glob. Change Biol.* 25, 3731–3740. doi: 10.1111/gcb.14729

Baldocchi, D., Ryu, Y., Dechant, B., Eichelmann, E., Hemes, K., Ma, S., et al. (2020). Outgoing near infrared radiation from vegetation scales with canopy photosynthesis across a spectrum of function, structure, physiological capacity and weather. *J. Geophys. Res. Biogeosci.* 125:e2019JG005534.

Ballantyne, A., Smith, W., Anderegg, W., Kauppi, P., Sarmiento, J., Tans, P., et al. (2017). Accelerating net terrestrial carbon uptake during the warming hiatus due to reduced respiration. *Nat. Clim. Change* 7, 148–152. doi: 10.1038/nclimate3204

Bond-Lamberty, B., and Thomson, A. (2010). Temperature-associated increases in the global soil respiration record. *Nature* 464, 579–582. doi: 10.1038/nature08930

Cao, M. K., Prince, S. D., Li, K. R., Tao, B., Small, J., and Shao, X. (2003). Response of terrestrial C uptake to climate interannual variability in China. *Glob. Change Biol.* 9, 536–546. doi: 10.1186/s13021-022-00215-9

Chen, H., Mo, J. M., Zhang, W., Lu, X. K., and Huang, J. (2012). Effects of nitrogen deposition on carbon sequestration in forest ecosystems. *Acta Ecol. Sin.* 32, 6864–6879. doi: 10.5846/stxb201109171363

Chen, S. T., Huang, Y., Zou, J. W., Shi, Y. S., Lu, Y. Y., Zhang, W., et al. (2012). Interannual variability in soil respiration from terrestrial ecosystems in China and its response to climate change. *Sci. China Earth Sci.* 55, 2091–2098. doi: 10.1007/s11430-012-4464-6

Chen, J. M., Ju, W., Ciais, P., Viovy, N., Liu, R., Liu, Y., et al. (2019). Vegetation structural change since 1981 significantly enhanced the terrestrial carbon sink. *Nat. Commun.* 10:4259. doi: 10.1038/s41467-019-12257-8

Chen, S., Zou, J., Hu, Z., and Lu, Y. (2019). Climate and vegetation drivers of terrestrial carbon fluxes: A global data synthesis. *Adv. Atmos. Sci.* 36, 679–696. doi: 10.1007/s00376-019-8194-y

Chen, W., Zhu, D., Huang, C., Ciais, P., and Zeng, N. (2019). Negative extreme events in gross primary productivity and their drivers in china during the past three decades. *Agric. For. Meteorol.* 275, 47–58. doi: 10.1016/j.agrformet.2019.05.002

Chen, Z., Yu, G. R., Zhu, X. J., Wang, Q., Niu, S., and Hu, Z. (2015). Covariation between gross primary production and ecosystem respiration across space and the underlying mechanisms: A global synthesis. *Agric. For. Meteorol.* 203, 180–190.

Chen, Z., Yu, G., Ge, J., Sun, X., Hirano, T., Saigusa, N., et al. (2013). Temperature and precipitation control of the spatial variation of terrestrial ecosystem carbon exchange in the Asian region. *Agric. For. Meteorol.* 182-183, 266–276. j.agrformet.2013.04.026 doi: 10.1016/

Chuai, X. W., Qi, X. X., Zhang, X. Y., Li, J. S., and Yuan, Y. (2018). Monitoring using terrestrial ecosystem C sinks/sources and their response to climate change in China. *Land Degrad. Dev.* 29, 3489–3502. doi: 10.1002/ldr.3117

Dechant, B., Ryu, Y., Badgley, G., Zeng, Y., Berry, J. A., Zhang, Y., et al. (2020). Canopy structure explains the relationship between photosynthesis and sun-induced chlorophyll fluorescence in crops. *Remote Sens. Environ.* 241:111733.

Deng, Y. H., Wang, S. J., Bai, X. Y., Luo, G., Wu, L., Cao, Y., et al. (2020). Variation trend of global soil moisture and its cause analysis. *Ecol. Indic.* 110:105939. doi: 10.1016/j.ecolind.2019.105939

Deng, Y., Li, X., Shi, F., and Hu, X. (2021). Woody plant encroachment enhanced global vegetation greening and ecosystem water-use efficiency. *Glob. Ecol. Biogeogr.* 30, 2337–2353. doi: 10.1111/geb.13386

Elith, J., Leathwick, J. R., and Hastie, T. (2008). A working guide to boosted regression trees. *J. Anim. Ecol.* 77, 802–813. doi: 10.1111/j.1365-2656.2008.01390.x

Fang, J., Piao, S., Tang, Z., Peng, C., and Ji, W. (2001). Interannual variability in net primary production and precipitation. *Science* 293:1723. doi: 10.1126/science.293.5536.1723a

Fay, P. A., Carlisle, J. D., Knapp, A. K., Blair, J. M., and Collins, S. L. (2003). Productivity responses to altered rainfall patterns in a C_4-dominated grassland. *Oecologia* 137, 245–251. doi: 10.1007/s00442-003-1331-3

Fernández-Martínez, M., Sardans, J., Chevallier, F., Ciais, P., Obersteiner, M., Vicca, S., et al. (2019). Global trends in carbon sinks and their relationships with CO2 and temperature. *Nat. Clim. Change* 9, 73–79. doi: 10.1038/s41558-018-0367-7

Forzieri, G., Alkama, R., Miralles, D. G., and Cescatti, A. (2018). Satellites reveal contrasting responses of regional climate to the widespread greening of earth. *Science* 1727, 1180–1184.

Forzieri, G., Miralles, D. G., Ciais, P., Alkama, R., and Cescatti, A. (2020). Increased control of vegetation on global terrestrial energy fluxes. *Nat. Clim. Change* 10, 356–362. doi: 10.1038/s41558-020-0717-0

Fu, Z., Dong, J., Zhou, Y., Stoy, P., and Niu, S. (2017). Long term trend and interannual variability of land carbon uptake–the attribution and processes. *Environ. Res. Lett.* 12:014018. doi: 10.1088/1748-9326/aa5685

Gong, J., Zhang, Y., and Qian, C. Y. (2017). Spatial-temporal changes of net ecosystem productivity in the Belongjiang River Basin, Gansu Province. *Acta Ecol. Sin.* 15, 5121–5128.

Grant, R. F., Baldocchi, D. D., and Ma, S. (2012). Ecological controls on net ecosystem productivity of a seasonally dry annual grassland under current and future climates: Modelling with ecosys. *Agric. For. Meteorol.* 152, 189–200. doi: 10.1016/j.agrformet.2011

Izaurralde, R. C., Thomson, A. M., Morgan, J. A., Fay, P. A., Polley, H. W., and Hatfield, J. L. (2011). Climate impacts on agriculture: Implications for forage and rangeland production. *Agron. J.* 103, 371–381. doi: 10.2134/agronj2010.0304

John, R., Chen, J. Q., Kim, Y., Ou-Yang, Z., Xiao, J., Park, H., et al. (2016). Differentiating anthropogenic modification and precipitation-driven change on vegetation productivity on the Mongolian Plateau. *Landsc. Ecol.* 31, 547–566.

Keenan, T. F., Prentice, I. C., Canadell, J. G., Williams, C. A., Wang, H., Raupach, M., et al. (2016). Recent pause in the growth rate of atmospheric CO2 due to enhanced terrestrial C uptake. *Nat. Commun.* 7:13428. doi: 10.1038/ncomms13428

Keenan, T., Gray, J., Friedl, M., Toomey, M., Bohrer, G., Hollinger, D., et al. (2014). Net carbon uptake has increased through warming-induced changes in temperate forest phenology. *Nat. Clim. Change* 4, 598–604. doi: 10.1038/nclimate2253

Kendall, M. G. (1975). *Rank correlation methods*. London: Griffin.

Kitamura, K., Nakai, Y., Suzuki, S., Ohtani, Y., Yamanoi, K., and Sakamoto, T. (2012). Interannual variability of net ecosystem production for a broadleaf deciduous forest in Sapporo, Northern Japan. *J. For. Res.* 17, 323–332. doi: 10.1007/s10310-012-0335-4

Kong, R., Zhang, Z. X., Huang, R. C., Tian, J., Feng, R., and Chen, X. (2022). Projected global warming-induced terrestrial ecosystem carbon across China under SSP scenarios. *Ecol. Indic.* 139:108963. doi: 10.1016/j.ecolind.2022.108963

Krausmann, F., Haberl, H., Erb, K., Wiesinger, M., Gaube, V., and Gingrich, S. (2009). What determines geographical patterns of the global human appropriation of net primary production? *J. Land Use Sci.* 4, 15–33. doi: 10.1093/nsr/nwaa145

Krishnan, P., Black, T. A., Grant, N. J., Barr, A. G., Hogg, E. H., Jassal, R. S., et al. (2006). Impact of changing soil moisture distribution on net ecosystem productivity of a boreal aspen forest during and following drought. *Agric. For. Meteorol.* 139, 208–223. doi: 10.1016/j.agrformet.2006.07.002

Li, C. J., Bai, X. Y., Tan, Q., Luo, G., Wu, L., Chen, F., et al. (2022). High-resolution mapping of the global silicate weathering carbon sink and its long-term changes. *Glob. Change Biol.* 28, 4377–4394. doi: 10.1111/gcb.16186

Li, X., Li, Y., Chen, A., Gao, M., Slette, I. J., and Piao, S. (2019). The impact of the 2009/2010 drought on vegetation growth and terrestrial carbon balance in Southwest China. *Agric. For. Meteorol.* 269–270, 239–248. doi: 10.1016/j.agrformet.2019.01.036

Li, Z., Chen, Y., Zhang, Q., and Li, Y. (2020). Spatial patterns of vegetation C sinks and sources under water constraint in central Asia. *J. Hydrol.* 590:125355. doi: 10.1016/j.jhydrol.2020.125355

Liu, M., Bai, X., Tan, Q., Luo, G., Zhao, C., Wu, L., et al. (2021). Monitoring impacts of ecological engineering on ecosystem services with geospatial techniques in karst areas of SW China. *Geocarto Int.* 10, 1–25. doi: 10.1080/10106049.2021.190

Liu, W., Zhang, Z., and Wan, S. (2010). Predominant role of water in regulating soil and microbial respiration and their responses to climate change in a semiarid grassland. *Glob. Change Biol.* 15, 184–195. doi: 10.1111/j.1365-2486.2008.01728.x

Lu, F., Zhang, Y., and Qin, Y. (2013). Spatial pattern of carbon source and sink in provincial regions of China. *Prog. Geogr.* 32:9.

Luyssaert, S., Jung, M., Richardson, A. D., Reichstein, M., Papale, D., Piao, S. L., et al. (2007). CO2 balance of boreal, temperate, and tropical forests derived from a global database. *Glob. Change Biol.* 13, 2509–2537. doi: 10.1111/j.1365-2486.2007.01439.x

Luyssaert, S., Schulze, E., Börner, A., Knohl, A., Hessenmöller, D., Law, B. E., et al. (2008). Old-growth forests as global carbon sinks. *Nature* 455, 213–215. doi: 10.1038/nature07276

Mahecha, M. D., Reichstein, M., Carvalhais, N., Lasslop, G., Lange, H., Seneviratne, S. I., et al. (2010). Global convergence in the temperature sensitivity of respiration at ecosystem level. *Science* 329, 838–840. doi: 10.1126/science.1189587

Mann, H. B. (1945). Nonparametric tests against trend. *Econometrica* 13, 245–259. doi: 10.2307/1907187

Mathur, M. (2014). Functional dynamics of energy variables and their impacts on growth and population attributes of a woody perennial at arid wasteland. *Aust. J. Bot.* 62, 490–498. doi: 10.1071/BT14180

Medvigy, D., Wofsy, S. C., Munger, J. W., and Moorcroft, P. R. (2010). Responses of terrestrial ecosystems and C budgets to current and future environmental variability. *Proc. Natl. Acad. Sci. U.S.A.* 107, 8275–8280. doi: 10.1073/pnas.0912032107

Migliavacca, M., Reichstein, M., Richardson, A. D., Colombo, R., Sutton, M. A., Lasslop, G., et al. (2015). Semiempirical modeling of abiotic and biotic factors controlling ecosystem respiration across eddy covariance sites. *Glob. Change Biol.* 17, 390–409. doi: 10.1111/j.1365-2486.2010.02243.x

Mitchell, M., Johansen, K., Maron, M., McAlpine, C. A., Wu, D., and Rhodes, J. R. (2018). Identification of fine scale and landscape scale drivers of urban aboveground carbon stocks using high-resolution modeling and mapping. *Sci. Total Environ.* 622–623, 57–70. doi: 10.1016/j.scitotenv.2017.11.255

Nadelhoffer, K., Emmett, B., Gundersen, P., Kjønaas, O., Koopmans, C., and Schleppi, P. (1999). Nitrogen deposition makes a minor contribution to carbon sequestration in temperate forests. *Nature* 398, 145–148. doi: 10.1038/18205

Nayak, R. K., Patel, N. R., and Dadhwal, V. K. (2013). Inter-annual variability and climate control of terrestrial net primary productivity over India. *Int. J. Climatol.* 33, 132–142. doi: 10.1002/joc.3414

Ni, S. L., Fu, Z., Luo, Y. Q., Stoy, P., Keenan, T. F., Poulter, B., et al. (2017). Interannual variability of ecosystem C exchange: From observation to prediction. *Glob. Ecol. Biogeogr.* 26, 1225–1237. doi: 10.1111/geb.12633

Peng, S., Piao, S., Ciais, P., Myneni, R., Chen, A., Chevallier, F., et al. (2013). Asymmetric effects of daytime and night-time warming on Northern Hemisphere vegetation. *Nature* 501, 88–92. doi: 10.1038/nature12434

Piao, S. L., Huang, M., Liu, Z., Wang, X., Ciais, P., Canadell, J., et al. (2018). Lower land-use emissions responsible for increased net land carbon sink during the slow warming period. *Nat. Geosci.* 11, 739–743. doi: 10.1038/s41561-018-0204-7

Piao, S. L., Ito, A., Li, S. G., Huang, Y., Ciais, P., Wang, X. H., et al. (2012). The carbon budget of terrestrial ecosystems in East Asia over the last two decades. *Biogeosciences* 9, 4025–4066. doi: 10.5194/bg-9-3571-2012

Piao, S. L., Sitch, S., Ciais, P., Friedlingstein, P., Peylin, P., Wang, X., et al. (2013). Evaluation of terrestrial carbon cycle models for their response to climate variability and to CO2 trends. *Glob. Change Biol.* 19, 2117–2132. doi: 10.1111/gcb.12187

Piao, S., Fang, J., Ciais, P., Peylin, P., Huang, Y., Sitch, S., et al. (2010). The carbon balance of terrestrial ecosystems in China. *China Basic Sci.* 458, 1009–1013.

Piao, S., Fang, J., Ciais, P., Peylin, P., Huang, Y., Sitch, S., et al. (2009). The carbon balance of terrestrial ecosystems in China. *Nature* 458, 1009–1013. doi: 10.1038/nature07944

Poulter, B., Frank, D., Ciais, P., Myneni, R. B., Andela, N., Bi, J., et al. (2014). Contribution of semi-arid ecosystems to interannual variability of the global carbon cycle. *Nature* 509, 600–603. doi: 10.1038/nature13376

Pourghasemi, H. R., and Rahmati, O. (2017). Prediction of the landslide susceptibility: Which algorithm, which precision? *CATENA* 162, 177–192. doi: 10.1016/j.catena.2017.11.022

Rodell, M., Houser, P. R., Jambor, U., Gottschalck, J., Mitchell, K., Meng, C., et al. (2004). The global land data assimilation system. *Bull. Am. Meteorol. Soc.* 85:381. doi: 10.1175/BAMS-85-3-381

Ru, J., Zhou, Y., Hui, D., Zheng, M., and Wan, S. (2018). Shifts of growing-season precipitation peaks decrease soil respiration in a semiarid grassland. *Glob. Change Biol.* 24, 1001–1011. doi: 10.1111/gcb.13941

Sen, P. K. (1968). Estimates of the regression coefficient based on Kendall's Tau. *J. Am. Stat. Assoc.* 63, 1379–1389. doi: 10.1080/01621459.1968.10480934

Sitch, S., Cox, P. M., Collins, W. J., and Huntingford, C. (2007). Indirect radiative forcing of climate change through ozone effects on the land-carbon sink. *Nature* 448, 791–794. doi: 10.1038/nature06059

Smith, B., Wårlind, D., Arneth, A., Hickler, T., Leadley, P., and Siltberg, J. (2014). Implications of incorporating n cycling and n limitations on primary production in an individual-based dynamic vegetation model. *Biogeosciences* 11, 2027–2054.

Song, F. J., Wang, S., Bai, X. Y., Wu, L., Wang, J., Li, C., et al. (2022). A new indicator for global food security assessment: Harvested area rather than cropland area. *Chin. Geogr. Sci.* 32, 204–217. doi: 10.1007/s11769-022-1264-6

Steffen, W., Noble, N., Canadell, J., Apps, M., Schulze, E., and Jarvis, P. G. (1998). The terrestrial carbon cycle: Implications for the Kyoto. *Protoc. Sci.* 280:1393. doi: 10.1126/science.280.5368.1393

Sun, H., Bai, Y., Lu, M., Wang, J., Tuo, Y., Yan, D., et al. (2021). Drivers of the water use efficiency changes in China during 1982–2015. *Sci. Total Environ.* 799:149145. doi: 10.1016/j.scitotenv.2021.149145

Swets, J. (1988). Measuring the accuracy of diagnostic systems. *Science* 240, 1285–1293. doi: 10.1126/science.3287615

Tan, Z. H., Zhang, Y. P., Schaefer, D., Yu, G. R., Liang, N. S., and Song, Q. H. (2011). An old-growth subtropical Asian evergreen forest as a large C sink. *Atmos. Environ.* 45, 1548–1554. doi: 10.1016/j.atmosenv.2010.12.041

Tang, J., Luyssaert, S., Richardson, A. D., Kutsch, W., and Janssens, I. (2014). Steeper declines in forest photosynthesis than respiration explain age-driven decreases in forest growth. *Proc. Natl. Acad. Sci. U.S.A.* 111, 8856–8860. doi: 10.1073/pnas.1320761111

Tao, B., Cao, M. K., Li, K. R., Gu, F., Ji, J., Mei, H., et al. (2007). Spatial patterns of terrestrial net ecosystem productivity in China during 1981–2000. *Sci. China Ser. D Earth Sci.* 50, 745–753. doi: 10.1007/s11430-007-0022-z

Tian, H. Q., Jerry, M., Lu, C. Q., Kicklighter, D., Liu, M., Ren, W., et al. (2011). China's terrestrial carbon balance: Contributions from multiple global change factors. *Glob. Biogeochem. Cycles* 25:GB1007. doi: 10.1029/2010GB003838

Tian, H., Melillo, J. M., Kicklighter, D. W., Pan, S., Liu, J., and McGuire, A. D. (2003). Regional carbon dynamics in monsoon Asia and its implications for the global carbon cycle. *Glob. Planet. Change* 37, 201–217. doi: 10.1016/S0921-8181(02)00205-9

Tian, Y. C., Bai, X. Y., Wang, S. J., Qin, L., and Li, Y. (2017). Spatial-temporal changes of vegetation cover in Guizhou Province, Southern China. *Chin. Geogr. Sci.* 27, 25–38. doi: 10.1007/s11769-017-0844-3

Wang, C., Zhao, W., and Zhang, Y. (2022). The change in net ecosystem productivity and its driving mechanism in a mountain ecosystem of arid regions, Northwest China. *Remote Sens.* 14:4046. doi: 10.3390/rs14164046

Wang, J., Feng, L., Palmer, P. I., Liu, Y., Fang, S., Bösch, H., et al. (2020). Large Chinese land carbon sink estimated from atmospheric carbon dioxide data. *Nature* 586, 720–723.

Wang, Q., Han, Z., Zhu, X., and Yu, G. (2015). Primary estimation of Chinese terrestrial C sequestration during 2001–2010. *Sci. Bull.* 60, 577–590. doi: 10.1007/s11434-015-0736-9

Wang, S., and Zhang, Y. (2020). Long-term (1982-2018) global gross primary production dataset based on NIRv. *Natl. Tibetan Plateau Data Center* doi: 10.6084/m9.figshare.12981977.v2

Wang, S., Zhang, Y., Ju, W., Qiu, B., and Zhang, Z. (2021). Tracking the seasonal and inter-annual variations of global gross primary production during last four decades using satellite near-infrared reflectance data. *Sci. Total Environ.* 755:142569. doi: 10.1016/j.scitotenv.2020.142569

Wang, X., Piao, S., Ciais, P., Friedlingstein, P., Myneni, R. B., Cox, P., et al. (2014). A two-fold increase of carbon cycle sensitivity to tropical temperature variations. *Nature* 506, 212–215. doi: 10.1038/nature12915

Woodwell, G. M., Whittaker, R. H., Reiners, W. A., Likens, G., Delwiche, C., and Botkin, D. (1978). The biota and the world carbon budget. *Science* 199, 141–146. doi: 10.1126/science.199.4325.141

Wu, L. H., Wang, S. J., Bai, X. Y., Tian, Y., Luo, G., Wang, J., et al. (2020). Climate change weakens the positive effect of human activities on karst vegetation productivity restoration in southern China. *Ecol. Indic.* 115:106392.

Wu, X., and Jiang, D. (2022). Probabilistic impacts of compound dry and hot events on global gross primary production. *Environ. Res. Lett.* 17:034049.

Xiao, B. Q., Bai, X. Y., Zhao, C. W., Tan, Q., Li, Y., Luo, G., et al. (2023). Responses of carbon and water use efficiencies to climate and land use changes in China's karst areas. *J. Hydrol.* 617:128968. doi: 10.1016/j.jhydrol.2022.128968

Xiao, J. F., Sun, G., Chen, J. Q., Chen, H., Chen, S., and Dong, G. (2013). Carbon fluxes, evapotranspiration, and water use efficiency of terrestrial ecosystems in China. *Agric. For. Meteorol.* 182–183, 76–90. doi: 10.1016/j.agrformet.2013.08.007

Xiong, L., Bai, X. Y., Zhao, C. W., Li, Y., Tan, Q., Luo, G., et al. (2022). High-resolution data sets for global carbonate and silicate rock weathering carbon sinks and their change trends. *Earths Future* 10:e2022EF002746. doi: 10.1029/2022EF002746

Yan, Y. C., Liu, X. P., Wen, Y. Y., and Ou, J. M. (2019). Quantitative analysis of the contributions of climatic and human factors to grassland productivity in Northern China. *Ecol. Indic.* 103, 542–553.

Yin, Y., Bloom, A. A., Worden, J., Saatchi, S., Yang, Y., Williams, M., et al. (2020). Fire decline in dry tropical ecosystems enhances decadal land carbon sink. *Nat. Commun.* 11:1900.

You, Y. F., Wang, S. Y., Pan, N. Q., Ma, Y., and Liu, W. (2020). Growth stage-dependent responses of Carbon fixation process of alpine grasslands to climate change over the Tibetan Plateau, China. *Agric. For. Meteorol.* 291:108085. doi: 10.1016/j.agrformet.2020.108085

Yu, G. R., Chen, Z., Piao, S. L., Peng, C., Ciais, P., Wang, Q., et al. (2014). High carbon dioxide uptake by subtropical forest ecosystems in the East Asian monsoon region. *Proc. Natl. Acad. Sci. U.S.A.* 111, 4910–4915. doi: 10.1073/pnas.1317065111

Yu, G. R., Zhu, X. J., Fu, Y. L., He, H. L., Wang, Q., Wen, X., et al. (2013). Spatial patterns and climate drivers of carbon fluxes in terrestrial ecosystems of China. *Glob. Change Biol.* 19, 798–810. doi: 10.1111/gcb.12079

Yuan, W. P., Luo, Y. Q., Richardson, A. D., Oren, R., Luyssaert, S., Janssens, I. A., et al. (2009). Latitudinal patterns of magnitude and interannual variability in net ecosystem exchange regulated by biological and environmental variables. *Glob. Change Biol.* 15, 2905–2920. doi: 10.1111/.1365-2486.2009.01870.x

Zhang, L., Ren, X., Wang, J., He, H., Wang, S., Wang, M., et al. (2018). Interannual variability of terrestrial net ecosystem productivity over China: Regional contributions and climate attribution. *Environ. Res. Lett.* 14:014003. doi: 10.1088/1748-9326/aaec95

Zhang, L., Xiao, J., Zheng, Y., Li, S., and Zhou, Y. (2020). Increased Carbon uptake and water use efficiency in global semi-arid ecosystems. *Environ. Res. Lett.* 15:034022. doi: 10.1088/1748-9326/ab68ec

Zhang, X. Z., Li, Y., Zhang, C. Q., and Liu, H. B. (2020). Analysis of changes in net ecosystem productivity in the shiyang river basin from 2000 to 2014. *J. Lanzhou Univ. (Nat. Sci. Ed.)* 486–492. doi: 10.13885/j.issn.0455-2059.2020.04.008

Zhang, Y. J., Xu, M., Chen, H., and Adams, J. (2009). Global pattern of NPP to GPP ratio derived from MODIS data: Effects of ecosystem type, geographical location and climate. *Glob. Ecol. Biogeogr.* 18, 280–290.

Zhou, L., Tucker, C. J., Kaufmann, R. K., Slayback, D., Shabanov, N. V., and Myneni, R. B. (2001). Variations in northern vegetation activity inferred from satellite data of vegetation index during 1981 to 1999. *J. Geophys. Res. Atmos.* 106, 20069–20083. doi: 10.1029/2000JD000115

Zhou, S., Yu, B., Schwalm, C. R., Ciais, P., Zhang, Y., and Fisher, J. B. (2017). Response of water use efficiency to global environmental change based on output from terrestrial biosphere models. *Glob. Biogeochem. Cycles* 31, 1639–1655. doi: 10.1002/2017GB005733

Zhou, W., Gang, C., Zhou, F., Li, J., Dong, X., and Zhao, C. (2015). Quantitative assessment of the individual contribution of climate and human factors to desertification in Northwest China using net primary productivity as an indicator. *Ecol. Indic.* 48, 560–569. doi: 10.1016/j.ecolind.2014.08.043

Zhou, X., Yamaguchi, Y., and Arjasakusuma, S. (2018). Distinguishing the vegetation dynamics induced by anthropogenic factors using vegetation optical depth and AVHRR NDVI: A cross-border study on the Mongolian Plateau. *Sci. Total Environ.* 616, 730–743. doi: 10.1016/j.scitotenv.2017.10.253

Zhu, X. J., Yu, G. R., He, H. L., Wang, Q., Chen, Z., Gao, Y., et al. (2014). Geographical statistical assessments of carbon fluxes in terrestrial ecosystems of China: Results from upscaling network observations. *Glob. Planet Change* 118, 52–61. doi: 10.1016/j.gloplacha.2014.04.003

frontiers | Frontiers in Ecology and Evolution

TYPE Original Research
PUBLISHED 02 February 2023
DOI 10.3389/fevo.2023.1116083

OPEN ACCESS

EDITED BY
Wei Zhao,
Institute of Geographic Sciences and Natural Resources Research (CAS),
China

REVIEWED BY
Babar Zahoor,
Smithsonian Conservation Biology Institute (SI), United States
Yingxin Huang,
Northeast Institute of Geography and Agroecology (CAS),
China

*CORRESPONDENCE
Wei Mao
✉ maowei@hainanu.edu.cn

†These authors have contributed equally to this work and share first authorship

SPECIALTY SECTION
This article was submitted to Population, Community, and Ecosystem Dynamics, a section of the journal Frontiers in Ecology and Evolution

RECEIVED 05 December 2022
ACCEPTED 16 January 2023
PUBLISHED 02 February 2023

CITATION
He B, Zhao Y, Liu S, Ahmad S and Mao W (2023) Mapping seagrass habitats of potential suitability using a hybrid machine learning model.
Front. Ecol. Evol. 11:1116083.
doi: 10.3389/fevo.2023.1116083

Mapping seagrass habitats of potential suitability using a hybrid machine learning model

Bohao He[1,2†], Yanghe Zhao[1,2†], Siyu Liu[1,2], Shahid Ahmad[1,2] and Wei Mao[1,2*]

[1]School of Ecology and Environment, Hainan University, Haikou, China, [2]Key Laboratory of Agro-Forestry Environmental Processes and Ecological Regulation of Hainan Province, Hainan University, Haikou, China

Seagrass meadows provide essential ecosystem services globally in the context of climate change. However, seagrass is being degraded at an accelerated rate globally due to ocean warming, ocean acidification, aquaculture, and human activities. The need for more information on seagrasses' spatial distribution and health status is a serious impediment to their conservation and management. Therefore, we propose a new hybrid machine learning model (RF-SWOA) that integrates the sinusoidal chaos map whale optimization algorithm (SWOA) with a random forest (RF) model to accurately model the suitable habitat of potential seagrasses. This study combines *in situ* sampling data with multivariate remote sensing data to train and validate hybrid machine learning models. It shows that RF-SWOA can predict potential seagrass habitat suitability more accurately and efficiently than RF. It also shows that the two most important factors affecting the potential seagrass habitat suitability on Hainan Island in China are distance to land (38.2%) and depth to sea (25.9%). This paper not only demonstrates the effectiveness of a hybrid machine learning model but also provides a more accurate machine learning model approach for predicting the potential suitability distribution of seagrasses. This research can help identify seagrass suitability distribution areas and thus develop conservation strategies to restore healthy seagrass ecosystems.

KEYWORDS

seagrass, machine learning, species distribution model, hybrid model, habitat suitability, niches

1. Introduction

Seagrasses are large submerged angiosperms with the general characteristics of vascular plants, a fully adapted aquatic environment, and the only angiosperm that can flower, fruit, and germinate in seawater (Hemminga and Duarte, 2000). Seagrasses are one of the extremely important marine resources that provide significant ecological value (Fourqurean et al., 2012; Cullen-Unsworth and Unsworth, 2018). Globally, seagrass habitats are rapidly degrading, and the loss of seagrass habitats will lead to multiple risks, such as the increased impacts of global climate change, shoreline destruction, and declining biodiversity (Orth et al., 2006; Waycott et al., 2009; Kendrick et al., 2019; Moksnes et al., 2021). Seagrass suitability habitat distribution patterns in the world are changing as the effects of global change severely threaten seagrass suitability habitats. The accurate knowledge of seagrass habitat and understanding of what factors limit or even threaten seagrass distribution has become an urgent issue (Short and Wyllie-Echeverria, 1996; Waycott et al., 2009). Unfortunately, many seagrass habitats around the world do not have clear spatial information (McKenzie et al., 2001; Short et al., 2007; He et al., 2022b), which seriously hinders marine environmental management and seagrass conservation. The traditional experimental method of mapping seagrass distribution requires large-scale field investigations, which are time consuming and cost-effective (McKenzie et al., 2001;

Krause-Jensen et al., 2004). In recent years, due to the development of remote sensing technology, a mushrooming number of data and methods have been applied to marine predictive modeling, such as satellite data, unmanned aerial vehicles (UAV), acoustic surveys, and Geographic Information Systems (GIS; Picart et al., 2014; Ouellette and Getinet, 2016; Fingas, 2019; Belkin, 2021).

Species distribution models (SDMs) are used to predict regional distribution maps (Gonzalez-Irusta et al., 2015; Bittner et al., 2020) and to assess the degree of habitat suitability (Miller, 2010; Zimmermann et al., 2010; Pollock et al., 2014). As SDM has been intensively studied, more and more studies have chosen to use machine learning for SDM modeling and have produced excellent results (Evans et al., 2011; Li and Wang, 2013). Downie et al. (2013) used GAM and MaxEnt models to predict seagrass distribution, and their results showed that machine learning could accurately predict seagrass distribution. However, Bittner et al. (2020) found the differences in the relative importance of environmental factors in predicting the distribution of seagrasses between machine learning models when predicting the distribution of species. Therefore, a more accurate and robust machine learning model should be selected for prediction, such as random forest model that is widely used in SDM modeling methods. As a very representative tree modeling algorithm, random forest model can provide high prediction accuracy and stability (Kosicki, 2017; Mi et al., 2017; Kosicki, 2020; Luan et al., 2020; Saranya et al., 2021).

In recent years, with the development of machine learning, hybrid machine learning models have been widely used (Bies et al., 2006; Ardabili et al., 2019). Meta-heuristic algorithms have been found to improve the classification accuracy of models significantly (Beheshti and Shamsuddin, 2013; Singh and Kottath, 2021). Further, population-based hybrid optimization algorithms can dramatically increase the speed and power of search algorithms by moving from many individuals to collaborative groups (Abdel-Basset et al., 2018; Dokeroglu et al., 2019). The excellent performance and optimal solutions of metaheuristic algorithms solve the puzzles of multidisciplinary research, ranging from engineering and social sciences to ecology (Yang, 2009, 2013). This led to the widespread use of metaheuristics in many studies (de Melo and Carosio, 2013; Talbi, 2016; Dokeroglu et al., 2019; Hassan and Pillay, 2019; Cruz-Duarte et al., 2021; Moya et al., 2021), e.g., the whale optimization algorithm (WOA; Mirjalili and Lewis, 2016; Kaur and Arora, 2018; He et al., 2022a).

Some applications have demonstrated the usability of hybrid machine learning models in providing insights into various knowledge's domains (Tsai and Chen, 2010; Pinter et al., 2020). Still, few have explored the use of hybrid machine learning models to predict species suitability distributions. This study combines WOA into a Sinusoidal (S) chaotic graph and couples it with Random Forest (RF) to form a new hybrid machine learning model (RF-SWOA). The model is able to more accurately model seagrass habitat suitability. Thus, the objectives of this study are: (1) to develop a hybrid machine learning model for more accurately predicting potential seagrass habitat; (2) to explore the effects of environmental variables on seagrass habitat; and (3) to evaluate the predictive advantages and limitations of the hybrid machine learning model.

2. Materials and methods

2.1. Seagrass occurrence data

Hainan Province, located in the southernmost island of China, is the largest province in China in terms of land area (land plus sea). Hainan Province has a latitude and longitude range of 3.30°N to 20.07°N and 108.15°E to 120.05°E, respectively. The climate of Hainan Island belongs to the monsoon tropical climate, which is between the two temperature zones of the tropics and subtropics. Its annual average temperature is 24°C. Hainan Island is rich in plant and animal resources, of which seagrass is one of the main aquatic seed plant resources.

Hainan Island accounts for 64% of China's total seagrass area (Zheng et al., 2013). Therefore, this study conducted a field survey to determine the distribution of seagrass on Hainan Island from March to August 2021 (Figure 1). The presence of seagrass was marked with latitude and longitude, and samples were collected to identify seagrass species according to the method advocated by international seagrass researchers (Kuo and Den Hartog, 2001). The literature and field survey data were also combined to form the known distribution of seagrass beds on Hainan Island. We used GPS (ICEGPS 610) to record seagrass bed boundaries, as well as the latitude and longitude coordinates at low tide, to determine the spatial extent of seagrass distribution on Hainan Island, when the large areas of seagrass beds are more easily exposed at low tide (Yang and Yang, 2009; Jiang et al., 2017). A total of 42 actual seagrass distribution sites were used in this study, including seven species of seagrass (i.e., *Halophila ovalis*, *Halophila minor*, *Thalassia hemprichii*, *Halodule uninervis*, *Halodule pinifolia*, *Enhalus acoroides*, and *Halophila beccarii*), while a random sampling of pseudo-absence in the Hainan seagrass distribution area produced a total of 31,700 records (Barbet-Massin et al., 2012).

2.2. Environmental data

The distribution of seagrasses is regulated by external environmental factors and key physiological processes. A total of 15 environmental prediction layers were used in this study (Table 1), each of which was important in determining the prediction of potentially suitable habitat for seagrasses (Dennison, 1987; Duarte, 1990, 1991; Nguyen et al., 2021).

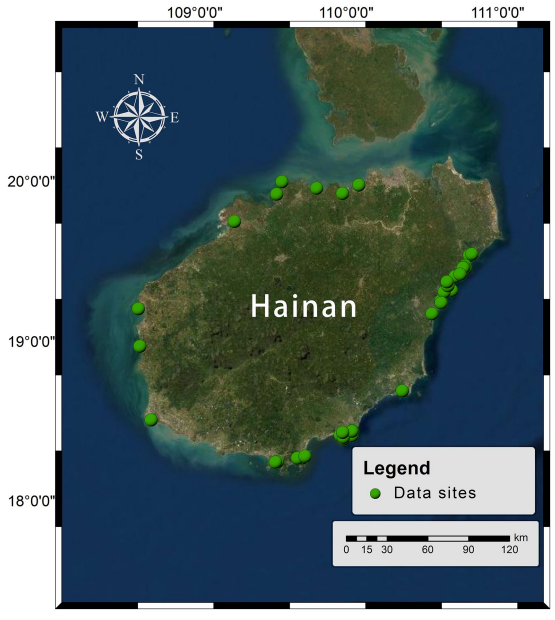

FIGURE 1
Study area and seagrass field distribution location sites.

TABLE 1 Environmental variables used in this study.

Notation	Description	Units
Silicate	Ocean silicate concentration	mol.m^{-3}
Attenuation	Diffuse attenuation	m^{-1}
Calcite	Constituent minerals in the ocean	mol.m^{-3}
Chlorophyll	Ocean chlorophyll-a concentration	mol.m^{-3}
Depth	Ocean depth	F
Land	Distance from land	F
Nitrate	Ocean nitrate concentration	mol.m^{-3}
Par	Photosynthetically active radiation	E.m^{-2}.day^{-1}
pH	Hydrogen ion concentration	1
Phosphate	Ocean phosphate concentration	mol.m^{-3}
Phytoplankton	Phytoplankton in the ocean	μmol.m^{-3}
Salinity	Ocean salinity	PSS
Slope	Ocean slope	F
Temperature	Ocean surface temperature	°C
Current	Currents velocity	m^{-1}

Temperature, salinity, velocity, nitrate, phosphate, silicate, phytoplankton, calcite, pH, and attenuation were obtained by Bio-ORACLE 2.2 version.[1] Ocean slope data are from GMED 2.0 version.[2] Ocean chlorophyll-*a* concentration data are from Google Earth Engine.[3] Photosynthetically active radiation data are from the Moderate-resolution Imaging Spectroradiometer (MODIS) aqua sensor.[4] Distance to nearest-shore data is from NASA's Ocean Biology Processing Group.[5] Bathymetric dataset is from The General Bathymetric Chart of the Oceans (GEBCO) global network.[6] Table 2 shows the minimum (MIN), maximum (MAX), mean (MEAN), and standard deviation (STD) of the 15 different environmental variables. All environmental variables were interpolated to 1 km spatial resolution using kriging interpolation in the ArcGIS 10.8 version of geostatistical analysis. To reduce spatial autocorrelation between variables (Legendre, 1993; Koenig, 1999; Dormann et al., 2007), correlation coefficients (r>0.7) were excluded using *spdep* R package (Bivand et al., 2015).

2.3. Machine learning models and evaluation

2.3.1. Random forest model

Random Forest (RF) algorithm is an extension of Bagging (Breiman, 1996, 2001), in which base learners are fixed as decision trees and a forest is made up of multiple trees (Figure 2). Compared with bagging integration of decision trees, RF has poor starting performance. However, as the number of base learners increases, RF tends to converge to a lower generalization error. Also, unlike bagging, in which the decision tree selects the optimal division attributes from all attribute sets, RF selects the division attributes from only a subset of the attribute set and thus is more efficient to train. In this study, the gini importance built-in algorithm of random forests was used to calculate the importance of the environmental features of the potentially suitable habitats for seagrasses.

2.3.2. Hybrid model

Whale Optimization Algorithm (WOA) was introduced by Mirjalili and Lewis (2016). Inspired by the way whales hunt, the predation behavior is organized into three mathematical models: prey encirclement, bubble net attack, and prey search (Mirjalili and Lewis, 2016; Aljarah et al., 2018). A whale encircles its prey while locating the best search position with an increasing number of iterations, while updating in real time. The mathematical expression of this behavior is

$$\begin{aligned} D &= \left|C * X_L(t) - X(t)\right|, \\ X(t+1) &= X_L(t) - A * D, \end{aligned} \tag{1}$$

where D represents the distance between whale and prey, A and C are the coefficient vectors, t indicates the current iteration, X_L is the position vector of the best solution obtained so far, X is the position vector, $|\ |$ is the absolute value, and * is an element-wise multiplication. A and C are calculated *via*

$$\begin{aligned} A &= 2a * r - a \\ C &= 2 * r \end{aligned} \tag{2}$$

where r is a random vector, and a is linearly decreased from 2 to 0 during iterating. A new position must be defined between the initial search position and the optimal search position so as to adjust the parameters. In this case, it is described as follows:

$$X(t+1) = \mathrm{D} * e^{bl} \cdot \cos(2\pi l) + X_L(\mathrm{t}), \tag{3}$$

where b is a constant coefficient, and l is a random vector whose items are all within [0, 1]. The whale contraction or spiral model approach is selected based on a 50% probability. Based on the mathematical model, the whale's prey is simulated in a spiral circle as follows:

$$X(t+1) = \begin{cases} X_L(t) - A * D & \text{if } p < 0.5 \\ D * e^{bl} * \cos(2\pi l) + X_L(t) & \text{if } p \geqslant 0.5 \end{cases} \tag{4}$$

Contraction envelope and spiral position updates are performed simultaneously, with contraction according to p and spiral wandering according to $1-p$, where $p \in [0,1]$.

As the whale searches for prey, it moves toward the local optimal location while expanding the global optimal location search, and this phase can be described as follows:

$$\begin{aligned} D &= |C * X_{\text{rand}} - X(t)|, \\ X(t+1) &= X_{\text{rand}} - A * D, \end{aligned} \tag{5}$$

1 https://www.bio-oracle.org/index.php, accessed on February 5, 2022.

2 https://gmed.auckland.ac.nz/index.html, accessed on February 6, 2022.

3 https://earthengine.google.com/, accessed on February 5, 2022.

4 https://oceancolor.gsfc.nasa.gov/data/aqua/, accessed on February 6, 2022.

5 https://oceancolor.gsfc.nasa.gov/docs/distfromcoast/, accessed on February 6, 2022.

6 https://www.gebco.net/, accessed on February 6, 2022.

where X_{rand} is a vector of random locations. A more detailed explanation of the WOA algorithm can be found in Mirjalili and Lewis (2016).

WOA becomes SWOA after adding a chaotic map to optimize global search capabilities. SWOA is mathematically described as follows:

TABLE 2 Statistical analysis results for different environmental variables.

Notation	Min	Max	Mean	Std
Silicate	5.87	13.12	8.13	1.96
Attenuation	0.04	0.27	0.15	0.06
Calcite	0.00	0.04	0.01	0.01
Chlorophyll	0.12	0.56	0.25	0.10
Depth	−100.09	−1.11	−30.82	18.70
Land	0.02	0.28	0.14	0.05
Nitrate	0.02	1.93	0.52	0.51
Par	36.04	42.37	39.21	1.54
pH	8.18	8.19	8.19	0.00
Phosphate	0.00	0.10	0.05	0.03
Phytoplankton	0.92	2.97	1.53	0.45
Salinity	32.94	33.31	33.18	0.08
Slope	0.02	0.19	0.09	0.04
Temperature	24.97	27.13	26.20	0.67
Current	0.12	0.55	0.24	0.09

$$p_{k+1} = ap_k^2 \sin(\pi p_k), p_0 \in [0,1], 0 < a \leqslant 4, \quad (6)$$

where k is the number of iterations, and a is the description parameter within $0 < a \leqslant 4$. For more information on SWOA algorithm, please refer to (He et al., 2022a).

The model in this study randomly selects 80% of the seagrass occurrence data for training and the remaining 20% for testing. The RF and RF-SWOA models were developed in Python 3.8 (Python, 2021).

2.3.3. Model evaluation

A comprehensive evaluation of the model was conducted using six evaluation metrics. They are AUC, Omission rate, Correct classification rate, Sensitivity, Specificity, Kappa.

$$AUC = \frac{1 + \frac{\text{True positive}}{\text{True positive} + \text{False negative}} - \frac{\text{False positive}}{\text{False positive} + \text{True negative}}}{\text{True number} * \text{False number}} \quad (7)$$

$$\text{Omission rate} = \frac{\text{False negative}}{\text{False negative} + \text{True negative}} \quad (8)$$

$$\text{Correct classification rate} = \frac{\text{True number}}{\text{Total sample}} \quad (9)$$

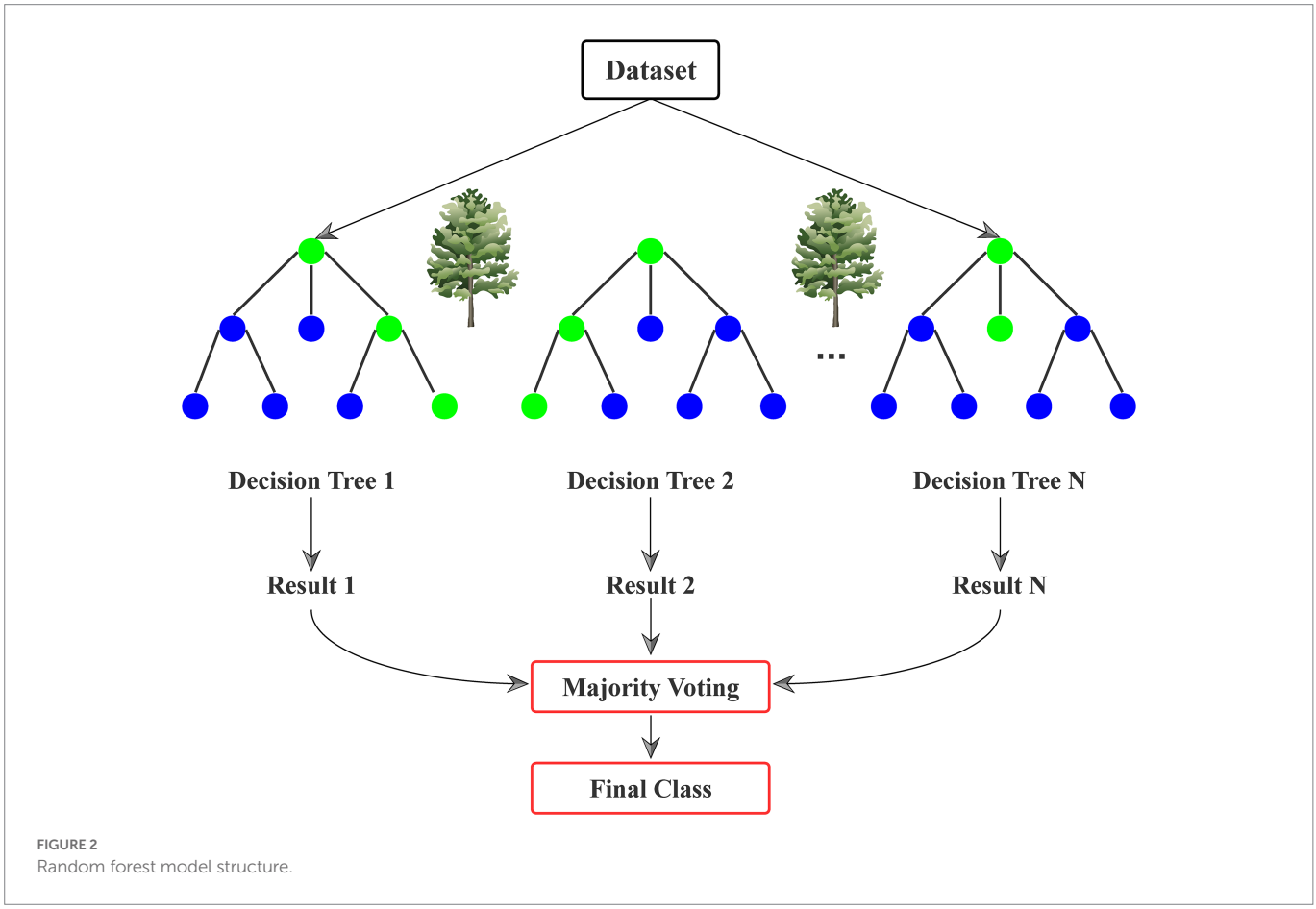

FIGURE 2
Random forest model structure.

$$\text{Sensitivity} = \frac{\text{True positive}}{(\text{True positive} + \text{False negative})} \quad (10)$$

$$\text{Specificity} = \frac{\text{True positive}}{(\text{False positive} + \text{True negative})} \quad (11)$$

$$\text{Kappa} = \frac{P_{\text{observed}} - P_{\text{bychance}}}{1 - P_{\text{bychance}}} \quad (12)$$

3. Results

3.1. Correlation analysis between environments

The results of the study clearly show the spatial autocorrelation among all environmental variables (Figure 3). Correlation analysis of environmental variables was used to identify and remove variables with high multicollinearity ($r > 0.7$) in order to prevent model over-fitting. After removing phosphate, phytoplankton, par, and attenuation environmental variables, and the remaining variables were introduced into the model training.

3.2. Importance of environment features

The results of the importance of environmental characteristics showed that the most important ones to predict the potential habitat of seagrass were the distance to land (38.2%) and the depth of the ocean (25.9%). The rest of the environmental variables showed small contribution values (<6%) to the prediction of the potential habitat of seagrass (Figure 4).

3.3. Potential seagrass habitat

Both models (RF and RF-SWOA) mapped potential seagrass habitat areas (Figure 5). RF model overestimates the potential habitat of

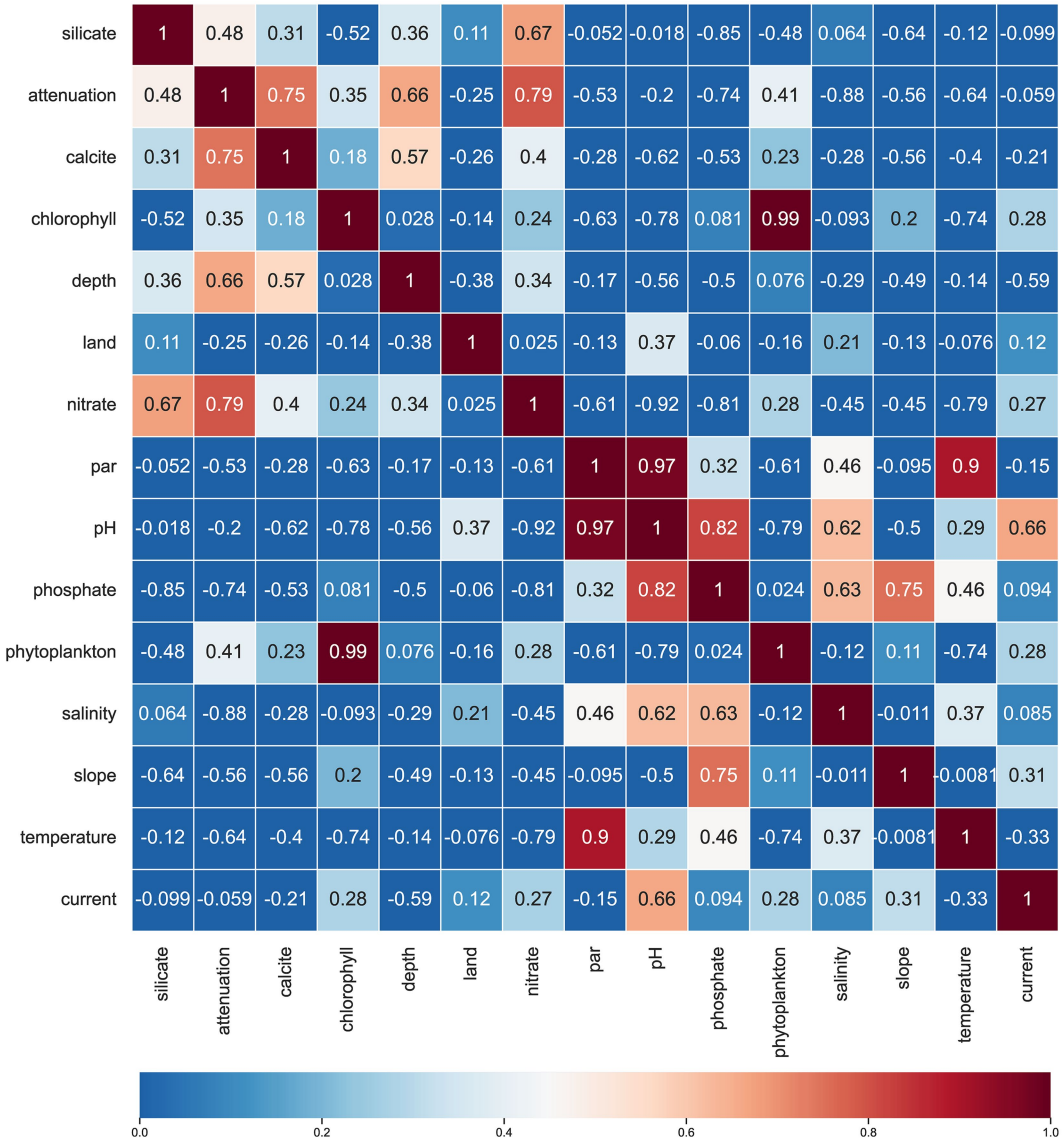

FIGURE 3
Correlation analysis matrix for different environmental variables.

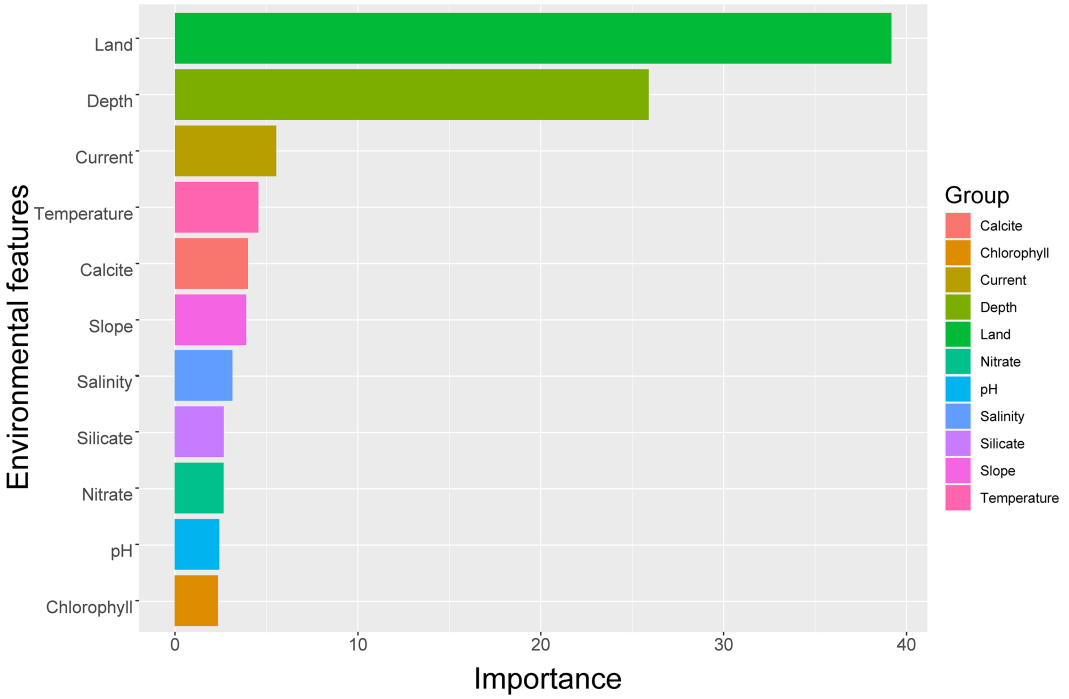

FIGURE 4
Importance analysis of 11 environmental features.

seagrass and makes a more optimistic prediction, but this is not consistent with actual observations (Figure 1). In contrast, the potential seagrass habitat areas estimated by RF-SWOA model are closer to actual observations. From Figure 5, it can be found that the further is the potential seagrass habitat from land, the less likely it exists. This is reflected in both models.

3.4. Model performance evaluation

RF-SWOA and RF models are compared in Figure 6. Their results show that RF-SWOA has a higher AUC, correct classification rate, Kappa, and lower omission rate than RF. RF-SWOA produced a more accurate and stable prediction of seagrass habitat than RF. In Figure 7, the sensitivity and specificity of the proposed model (RF-SWOA) are better than those of RF model. Hybrid machine learning algorithms with higher sensitivity and specificity in prediction can reduce errors in the potential distribution of seagrass, achieving more reliable results.

4. Discussion

4.1. SWOA hybrid model evaluation

Intelligent optimization algorithms are widely used in various engineering practices (Su et al., 2014; Wang et al., 2020; Li et al., 2021), and simple operation is one of the advantages of WOA algorithm. It has excellent optimization capabilities and few parameters, which can dramatically increase the accuracy of the solution and convergence speed in the process of optimizing machine learning functions (Sun et al., 2018; Chakraborty et al., 2021). Although WOA has obvious advantages compared with other intelligent algorithms, it has similar problems like other intelligent algorithms, such as being easily trapped into a local optimum. The SWOA algorithm proposed in this paper can update its position according to its adaptive parameter strategy while updating the optimal individual to achieve the ability of optimizing global search. This study further verified the performance of the SWOA algorithm through simulation experiments. Four standard test functions (Table 3) were used to assess the performance of the algorithm. F1 and F2 test functions were used to determine how quickly and efficiently the SWOA algorithm finds an optimal value (Figures 8A,B). F3 and F4 test functions were used to see if the algorithm can jump out of its local optimum (Figures 8C,D). Each simulation test is to solve the performance of a 1,000-dimensional test function. By testing the performance of the SWOA and WOA algorithms through simulations, the SWOA algorithm has better global convergence and robustness (Figure 8). In this study, a random forest model was also used, which is increasingly being used in ecology due to its predictive accuracy and stability (Cutler et al., 2007; Evans et al., 2011). In particular, random forest models are still very robust at predicting species distributions with limited sample sizes (Luan et al., 2020). After coupling SWOA with RF, we found that the SWOA algorithm greatly influenced the performance of RF on classification. Based on the above findings, hybrid machine learning models can improve predictions of marine species distributions (e.g., seagrasses).

4.2. Environmental drivers of seagrass habitat

The potential adaptability of seagrass habitat is influenced by a combination of environmental elements. In this study, those environmental variables were combined to model potential seagrass habitats. Our results show that the most critical environmental factors affecting seagrass habitat are the distance from land, ocean depth, and current velocity. It reflects the particular importance of physical environmental variables for seagrass habitats. However, this does not mean that chemical and biological types of environmental

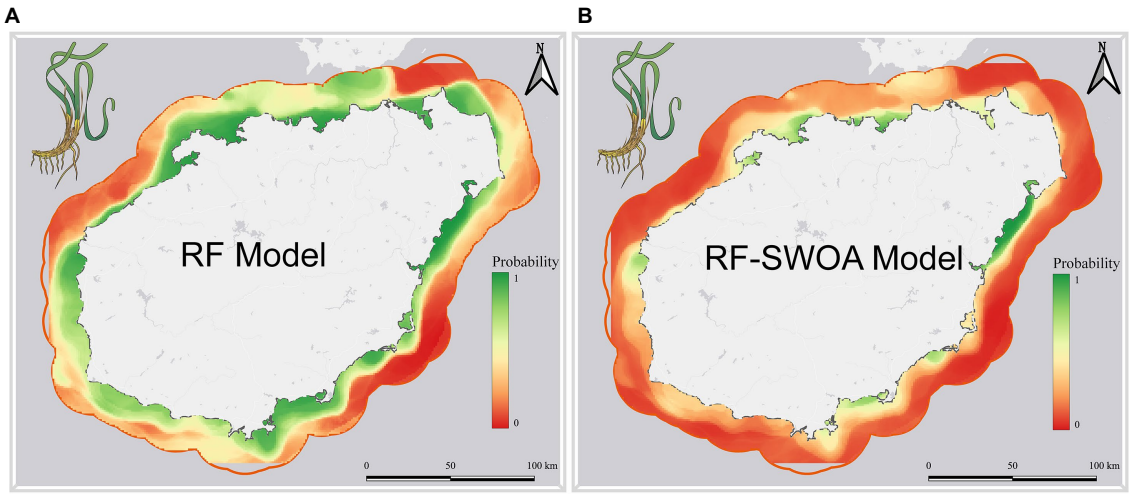

FIGURE 5
Potential habitat areas (Predicted by **(A)** RF model and **(B)** RF-SWOA model).

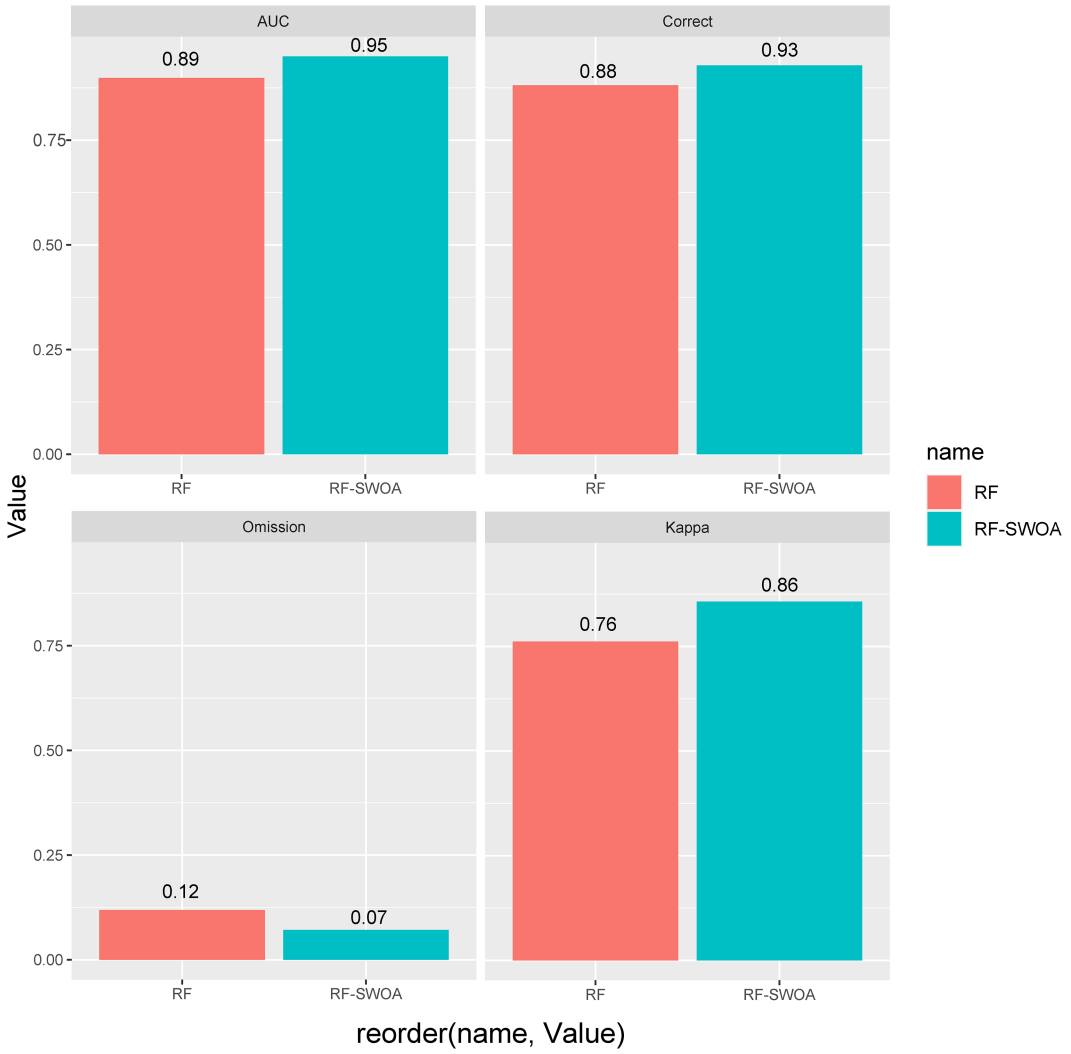

FIGURE 6
RF and RF-SWOA model performance evaluation.

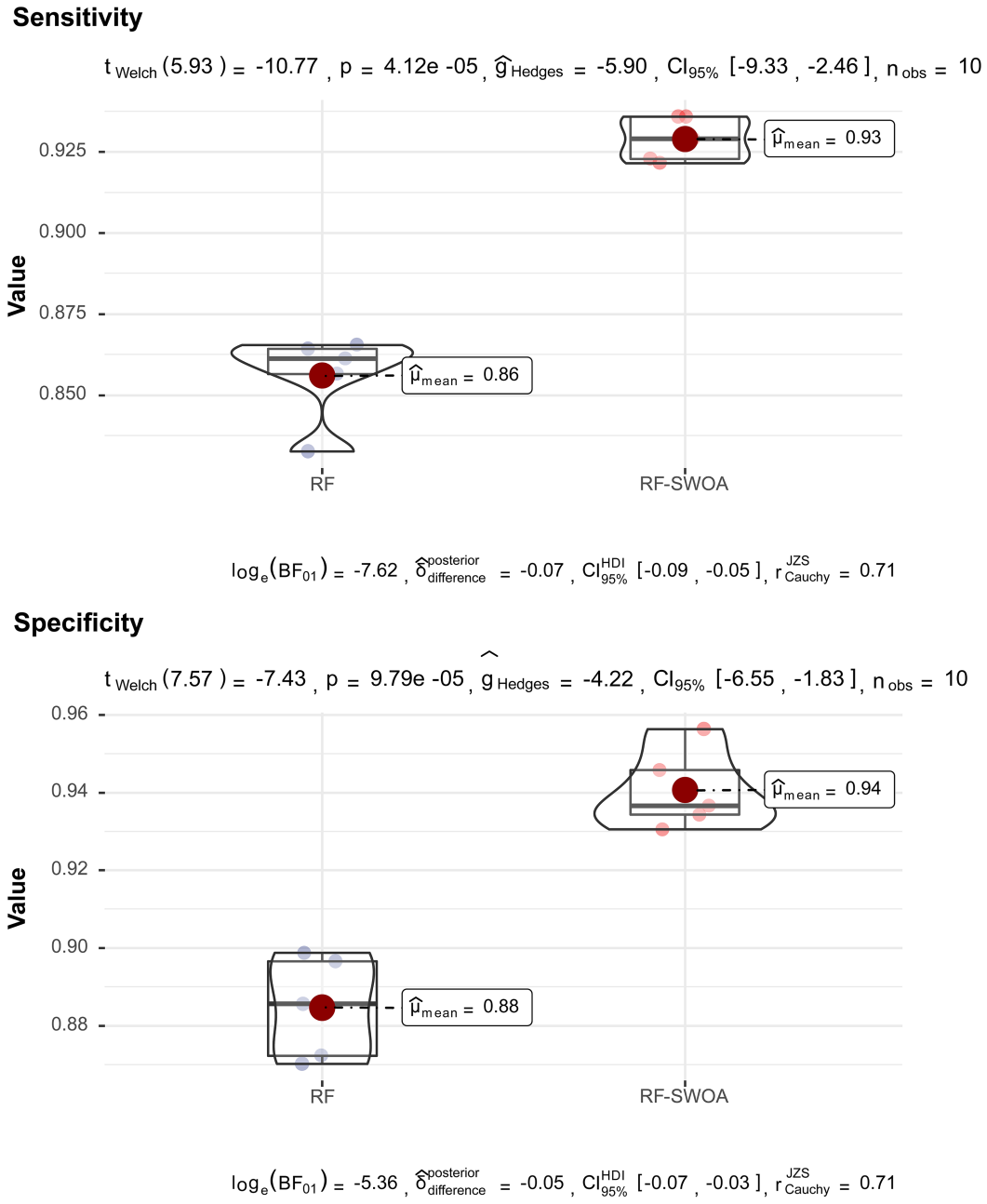

FIGURE 7
Sensitivity and specificity tests of RF and RF-SWOA models. The upper part of the panel shows the statistical test results of frequentist analysis, and the lower part of the panel shows the statistical test results of Bayesian analysis. The results follow the gold standard of statistical reporting (Patil, 2021).

variables do not affect seagrass survival. We found that modeling the distribution of seagrasses in different study areas and scales was influenced by different environmental drivers. A global model showed that the temperature of the sea surface and the distance to the land were the most important environmental variables to predict the distribution of seagrass (Jayathilake and Costello, 2018). At a regional scale, surface nitrate concentration and the availability of benthic light became the most important environmental variables for predicting seagrass distribution in a model of seagrass species distribution in the Gulf of Mexico, while in another sea area, the distance to the sandy shore and depth were the most important environmental drivers (Downie et al., 2013; Bittner et al., 2020). Therefore, we proposed to establish a seagrass habitat simulation in the local study area to identify which environmental factors will lead to seagrass distribution limitation in order to better target local seagrass conservation and restoration (Mao et al., 2022).

5. Conclusion

This study proposed a new hybrid machine learning model (RF-SWOA) to accurately predict suitable habitats for potential seagrasses. The results of this study indicated that the RF-SWOA model could effectively be applied to model seagrass distribution. The results of the RF-SWOA model compared with RF model showed that RF-SWOA was able to identify potential seagrass habitats more accurately and stably. This hybrid machine learning model was demonstrated to be effective in improving the prediction of SDM. The

TABLE 3 Four simulation test functions.

Simulation function expression	Function name	Search space	Global optimum	Characteristic
$F_1 = 1 + \sum_{i=1}^{n} \frac{x_i^2}{4000} - \prod_{i=1}^{n} \cos\left(\frac{x_i}{\sqrt{i}}\right) \sqrt{b^2 - 4ac}$	Griewank	[−600, 600]	0	Unimodal function
$F_2 = \sum_{i=1}^{n} \lvert x_i \rvert$	Schwefel 2.20	[−100, 100]	0	Unimodal function
$F_3 = -20\exp\left(-0.2\sqrt{\frac{1}{n}\sum_{i=1}^{n} x_i^2}\right) - \exp\left(\frac{1}{n}\sum_{i=1}^{n} \cos(2\pi x_i)\right) + 20 + \exp(1)$	Ackley	[−32, 32]	0	Bimodal function
$F_4 = 10n + \sum_{i=1}^{n} \left(x_i^2 - 10\cos(2\pi x_i)\right)$	Rastrigin	[−5.12, 5.12]	0	Bimodal function

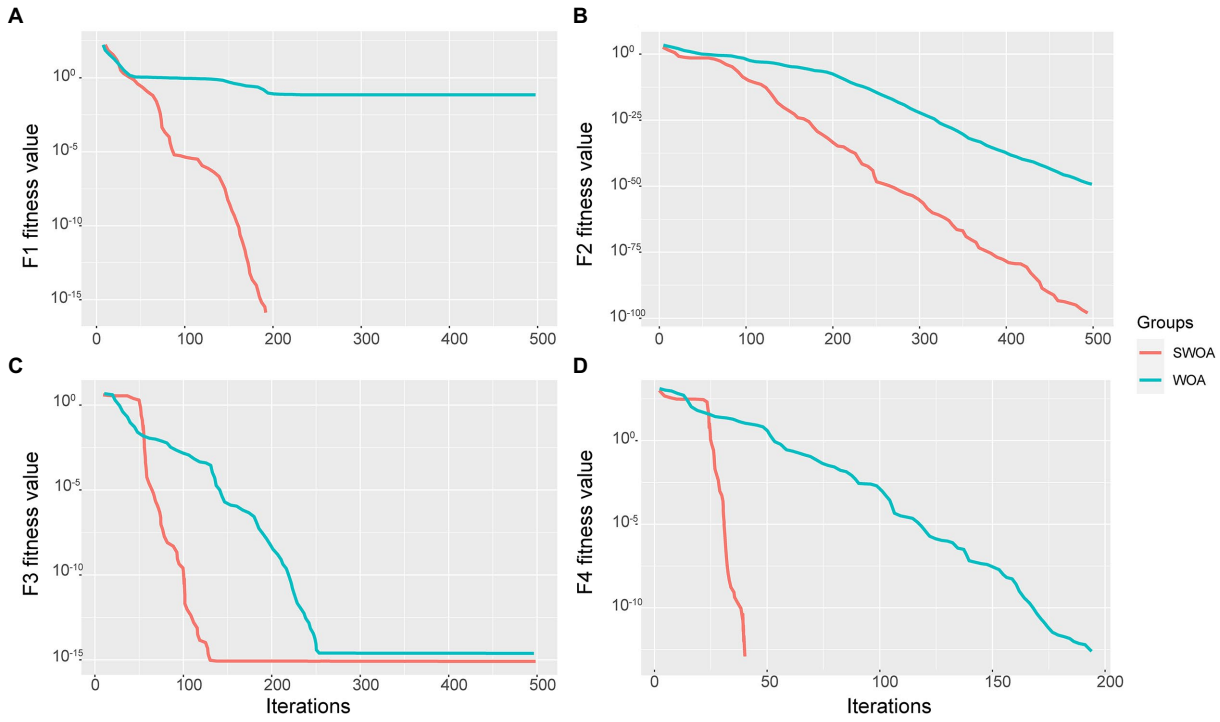

FIGURE 8
RF and RF-SWOA model performance evaluation. **(A)** Griewank simulation function; **(B)** Schwefel 2.20 simulation function; **(C)** Ackley simulation function; **(D)** Rastrigin simulation function.

most important environmental factors affecting seagrass distribution were the distance from land, ocean depth, and current velocity. Therefore, seagrass potential adaptability habitat maps based on the RF-SWOA model can assist in the adequate conservation and restoration of seagrass and provide scientific guidance for seagrass area planning.

Data availability statement

The original contributions presented in the study are included in the article/supplementary material, further inquiries can be directed to the corresponding author.

Author contributions

BH: conceptualization, methodology, software, validation, formal analysis, investigation, resources, data curation, writing—original draft, writing—review and editing, visualization, and funding acquisition. YZ: investigation, resources, data curation, and writing—original draft. SL: writing—review and editing, and supervision. SA: writing—review and editing, supervision, and project administration. WM: conceptualization, resources, data curation, writing—review and editing, supervision, project administration, and funding acquisition. All authors contributed to the article and approved the submitted version.

Funding

This research was supported by the Major Science and Technology Project of Hainan Province (ZDKJ202008-1-2), the National Natural Science Foundation of China (42276235), the Start-up funding from Hainan University (kyqd20035), the Innovative Research Projects for Graduate Students in Hainan Province (Qhys2021-16).

Acknowledgments

We would like to thank Biying Jia and Peng Wang for their help in data acquisition. BH sincerely thanks Yingshuai Liu for his help and advice on GIS and remote sensing. The authors would thank university of Maryland's integration and application network.

Conflict of interest

The authors declare that the research was conducted in the absence of any commercial or financial relationships that could be construed as a potential conflict of interest.

Publisher's note

All claims expressed in this article are solely those of the authors and do not necessarily represent those of their affiliated organizations, or those of the publisher, the editors and the reviewers. Any product that may be evaluated in this article, or claim that may be made by its manufacturer, is not guaranteed or endorsed by the publisher.

References

Abdel-Basset, M., Abdel-Fatah, L., and Sangaiah, A. K. (2018). "Chapter 10 - metaheuristic algorithms: a comprehensive review," in *Computational Intelligence for Multimedia Big Data on the Cloud with Engineering Applications*. eds. A. K. Sangaiah, M. Sheng and Z. Zhang (Academic Press) 185–231.

Aljarah, I., Faris, H., and Mirjalili, S. (2018). Optimizing connection weights in neural networks using the whale optimization algorithm. *Soft. Comput.* 22, 1–15. doi: 10.1007/s00500-016-2442-1

Ardabili, S., Mosavi, A., and Várkonyi-Kóczy, A. R. (2019). "Advances in machine learning modeling reviewing hybrid and ensemble methods", in *International Conference on Global Research and Education* (Springer), 215–227.

Barbet-Massin, M., Jiguet, F., Albert, C. H., and Thuiller, W. (2012). Selecting pseudo-absences for species distribution models: how, where and how many? *Methods Ecol. Evol.* 3, 327–338. doi: 10.1111/j.2041-210X.2011.00172.x

Beheshti, Z., and Shamsuddin, S. M. H. (2013). A review of population-based meta-heuristic algorithms. *Int. J. Adv. Soft Comput. Appl.* 5, 1–35.

Belkin, I. M. (2021). Remote sensing of ocean fronts in marine ecology and fisheries. *Remote Sens.* 13:883. doi: 10.3390/rs13050883

Bies, R. R., Muldoon, M. F., Pollock, B. G., Manuck, S., Smith, G., and Sale, M. E. (2006). A genetic algorithm-based, hybrid machine learning approach to model selection. *J. Pharmacokinet. Pharmacodyn.* 33, 195–221. doi: 10.1007/s10928-006-9004-6

Bittner, R. E., Roesler, E. L., and Barnes, M. A. (2020). Using species distribution models to guide seagrass management. *Estuar. Coast. Shelf Sci.* 240:106790. doi: 10.1016/j.ecss.2020.106790

Bivand, R., Altman, M., Anselin, L., Assunção, R., Berke, O., Bernat, A., et al. (2015). Package 'spdep'. The Comprehensive R Archive Network.

Breiman, L. (1996). Bagging predictors. *Mach. Learn.* 24, 123–140. doi: 10.1007/BF00058655

Breiman, L. (2001). Random forests. *Mach. Learn.* 45, 5–32. doi: 10.1023/A:1010933404324

Chakraborty, S., Saha, A. K., Sharma, S., Mirjalili, S., and Chakraborty, R. (2021). A novel enhanced whale optimization algorithm for global optimization. *Comput. Ind. Eng.* 153:107086. doi: 10.1016/j.cie.2020.107086

Cruz-Duarte, J. M., Amaya, I., Ortiz-Bayliss, J. C., Conant-Pablos, S. E., Terashima-Marin, H., and Shi, Y. (2021). Hyper-heuristics to customise metaheuristics for continuous optimisation. *Swarm Evol. Comput.* 66:100935. doi: 10.1016/j.swevo.2021.100935

Cullen-Unsworth, L. C., and Unsworth, R. (2018). A call for seagrass protection. *Science* 361, 446–448. doi: 10.1126/science.aat7318

Cutler, D. R., Edwards, T. C. Jr., Beard, K. H., Cutler, A., Hess, K. T., Gibson, J., et al. (2007). Random forests for classification in ecology. *Ecology* 88, 2783–2792. doi: 10.1890/07-0539.1

De Melo, V. V., and Carosio, G. L. C. (2013). Investigating multi-view differential evolution for solving constrained engineering design problems. *Expert Syst. Appl.* 40, 3370–3377. doi: 10.1016/j.eswa.2012.12.045

Dennison, W. C. (1987). Effects of light on seagrass photosynthesis, growth and depth distribution. *Aquat. Bot.* 27, 15–26. doi: 10.1016/0304-3770(87)90083-0

Dokeroglu, T., Sevinc, E., Kucukyilmaz, T., and Cosar, A. (2019). A survey on new generation metaheuristic algorithms. *Comput. Ind. Eng.* 137:106040. doi: 10.1016/j.cie.2019.106040

Dormann, C. F., McPherson, J. M., Araújo, M. B., Bivand, R., Bolliger, J., Carl, G., et al. (2007). Methods to account for spatial autocorrelation in the analysis of species distributional data: a review. *Ecography* 30, 609–628. doi: 10.1111/j.2007.0906-7590.05171.x

Downie, A.-L., Von Numers, M., and Boström, C. (2013). Influence of model selection on the predicted distribution of the seagrass *Zostera marina*. *Estuar. Coast. Shelf Sci.* 121–122, 8–19. doi: 10.1016/j.ecss.2012.12.020

Duarte, C. M. (1990). Seagrass nutrient content. Marine ecology progress series. *Oldendorf* 67, 201–207. doi: 10.3354/meps067201

Duarte, C. M. (1991). Seagrass depth limits. *Aquat. Bot.* 40, 363–377. doi: 10.1016/0304-3770(91)90081-F

Evans, J. S., Murphy, M. A., Holden, Z. A., and Cushman, S. A. (2011). "Modeling species distribution and change using random forest," in *Predictive Species and Habitat Modeling in Landscape Ecology: Concepts and Applications*, eds. C. A. Drew, Y. F. Wiersma and F. Huettmann (New York, NY: Springer), 139–159.

Fingas, M. (2019). "Chapter 5 - remote sensing for marine management," in *World Seas: An Environmental Evaluation (Second Edition)*. ed. C. Sheppard (Academic Press), 103–119.

Fourqurean, J. W., Duarte, C. M., Kennedy, H., Marbà, N., Holmer, M., Mateo, M. A., et al. (2012). Seagrass ecosystems as a globally significant carbon stock. *Nat. Geosci.* 5, 505–509. doi: 10.1038/ngeo1477

Gonzalez-Irusta, J. M., Gonzalez-Porto, M., Sarralde, R., Arrese, B., Almon, B., and Martin-Sosa, P. (2015). Comparing species distribution models: a case study of four deep sea urchin species. *Hydrobiologia* 745, 43–57. doi: 10.1007/s10750-014-2090-3

Hassan, A., and Pillay, N. (2019). Hybrid metaheuristics: an automated approach. *Expert Syst. Appl.* 130, 132–144. doi: 10.1016/j.eswa.2019.04.027

He, B., Jia, B., Zhao, Y., Wang, X., Wei, M., and Dietzel, R. (2022a). Estimate soil moisture of maize by combining support vector machine and chaotic whale optimization algorithm. *Agric. Water Manag.* 267:107618. doi: 10.1016/j.agwat.2022.107618

He, B., Zhao, Y., and Mao, W. (2022b). Explainable artificial intelligence reveals environmental constraints in seagrass distribution. *Ecol. Indic.* 144:109523. doi: 10.1016/j.ecolind.2022.109523

Hemminga, M. A., and Duarte, C. M. (2000). *Seagrass Ecology*. Cambridge: Cambridge University Press.

Jayathilake, D. R., and Costello, M. J. (2018). A modelled global distribution of the seagrass biome. *Biol. Conserv.* 226, 120–126. doi: 10.1016/j.biocon.2018.07.009

Jiang, Z., Liu, S., Zhang, J., Zhao, C., Wu, Y., Yu, S., et al. (2017). Newly discovered seagrass beds and their potential for blue carbon in the coastal seas of Hainan Island, South China Sea. *Mar. Pollut. Bull.* 125, 513–521. doi: 10.1016/j.marpolbul.2017.07.066

Kaur, G., and Arora, S. (2018). Chaotic whale optimization algorithm. *J. Comput. Des. Eng.* 5, 275–284. doi: 10.1016/j.jcde.2017.12.006

Kendrick, G. A., Nowicki, R. J., Olsen, Y. S., Strydom, S., Fraser, M. W., Sinclair, E. A., et al. (2019). A systematic review of how multiple stressors from an extreme event drove ecosystem-wide loss of resilience in an iconic seagrass community. *Front. Mar. Sci.* 6:455. doi: 10.3389/fmars.2019.00455

Koenig, W. D. (1999). Spatial autocorrelation of ecological phenomena. *Trends Ecol. Evol.* 14, 22–26. doi: 10.1016/S0169-5347(98)01533-X

Kosicki, J. Z. (2017). Should topographic metrics be considered when predicting species density of birds on a large geographical scale? A case of random Forest approach. *Ecol. Model.* 349, 76–85. doi: 10.1016/j.ecolmodel.2017.01.024

Kosicki, J. Z. (2020). Generalised additive models and random Forest approach as effective methods for predictive species density and functional species richness. *Environ. Ecol. Stat.* 27, 273–292. doi: 10.1007/s10651-020-00445-5

Krause-Jensen, D., Quaresma, A. L., and Cunha, A. H. (2004). How are seagrass distribution and abundance monitored. *European seagrasses: an introduction to monitoring and management*, 45–53.

Kuo, J., and Den Hartog, C. (2001). Seagrass taxonomy and identification key. *Glob. Seagrass Res. Methods* 33, 31–58. doi: 10.1016/B978-044450891-1/50003-7

Legendre, P. (1993). Spatial autocorrelation: trouble or new paradigm? *Ecology* 74, 1659–1673. doi: 10.2307/1939924

Li, X., and Wang, Y. (2013). Applying various algorithms for species distribution modelling. *Integr. Zool.* 8, 124–135. doi: 10.1111/1749-4877.12000

Li, W., Wang, G.-G., and Gandomi, A. H. (2021). A survey of learning-based intelligent optimization algorithms. *Arch. Comput. Methods Eng.* 28, 3781–3799. doi: 10.1007/s11831-021-09562-1

Luan, J., Zhang, C., Xu, B., Xue, Y., and Ren, Y. (2020). The predictive performances of random forest models with limited sample size and different species traits. *Fish. Res.* 227:105534. doi: 10.1016/j.fishres.2020.105534

Mao, W., Zhao, Y., He, B., Jia, B., and Li, W. (2022). Review on degradation mechanism and restoration strategies of seagrass ecosystem. *J. Desert Res.* 42:87.

Mckenzie, L. J., Finkbeiner, M. A., and Kirkman, H. (2001). "Chapter 5 - Methods for mapping seagrass distribution," in *Global Seagrass Research Methods*. eds. F. T. Short and R. G. Coles (Amsterdam: Elsevier Science), 101–121.

Mi, C., Huettmann, F., Guo, Y., Han, X., and Wen, L. (2017). Why choose random Forest to predict rare species distribution with few samples in large undersampled areas? Three Asian crane species models provide supporting evidence. *PeerJ.* 5:e2849. doi: 10.7717/peerj.2849

Miller, J. (2010). Species distribution modeling. *Geogr. Compass* 4, 490–509. doi: 10.1111/j.1749-8198.2010.00351.x

Mirjalili, S., and Lewis, A. (2016). The whale optimization algorithm. *Adv. Eng. Softw.* 95, 51–67. doi: 10.1016/j.advengsoft.2016.01.008

Moksnes, P. O., Röhr, M. E., Holmer, M., Eklöf, J. S., Eriander, L., Infantes, E., et al. (2021). Major impacts and societal costs of seagrass loss on sediment carbon and nitrogen stocks. *Ecosphere* 12:e03658. doi: 10.1002/ecs2.3658

Moya, I., Bermejo, E., Chica, M., and Cordon, O. (2021). Coral reefs optimization algorithms for agent-based model calibration. *Eng. Appl. Artif. Intell.* 100:104170. doi: 10.1016/j.engappai.2021.104170

Nguyen, H. M., Ralph, P. J., Marín-Guirao, L., Pernice, M., and Procaccini, G. (2021). Seagrasses in an era of ocean warming: a review. *Biol. Rev.* 96, 2009–2030. doi: 10.1111/brv.12736

Orth, R. J., Carruthers, T. J., Dennison, W. C., Duarte, C. M., Fourqurean, J. W., Heck, K. L., et al. (2006). A global crisis for seagrass ecosystems. *Bioscience* 56, 987–996. doi: 10.1641/0006-3568(2006)56[987:AGCFSE]2.0.CO;2

Ouellette, W., and Getinet, W. (2016). Remote sensing for marine spatial planning and integrated coastal areas management: achievements, challenges, opportunities and future prospects. *Remote Sens. Appl.* 4, 138–157. doi: 10.1016/j.rsase.2016.07.003

Patil, I. (2021). Visualizations with statistical details: The'ggstatsplot'approach. *J. Open Source Softw.* 6:3167. doi: 10.21105/joss.03167

Picart, S. S., Sathyendranath, S., Dowell, M., Moore, T., and Platt, T. (2014). Remote sensing of assimilation number for marine phytoplankton. *Remote Sens. Environ.* 146, 87–96. doi: 10.1016/j.rse.2013.10.032

Pinter, G., Felde, I., Mosavi, A., Ghamisi, P., and Gloaguen, R. (2020). COVID-19 pandemic prediction for Hungary; a hybrid machine learning approach. *Mathematics* 8:890. doi: 10.3390/math8060890

Pollock, L. J., Tingley, R., Morris, W. K., Golding, N., O'Hara, R. B., Parris, K. M., et al. (2014). Understanding co-occurrence by modelling species simultaneously with a joint species distribution model (JSDM). *Methods Ecol. Evol.* 5, 397–406. doi: 10.1111/2041-210X.12180

Python, W. (2021). Python. *Python Releases for Windows* 24.

Saranya, K. R. L., Lakshmi, T. V., and Reddy, C. S. (2021). Predicting the potential sites of Chromolaena odorata and Lantana camara in forest landscape of eastern Ghats using habitat suitability models. *Eco. Inform.* 66:101455. doi: 10.1016/j.ecoinf.2021.101455

Short, F., Carruthers, T., Dennison, W., and Waycott, M. (2007). Global seagrass distribution and diversity: a bioregional model. *J. Exp. Mar. Biol. Ecol.* 350, 3–20. doi: 10.1016/j.jembe.2007.06.012

Short, F. T., and Wyllie-Echeverria, S. (1996). Natural and human-induced disturbance of seagrasses. *Environ. Conserv.* 23, 17–27. doi: 10.1017/S0376892900038212

Singh, P., and Kottath, R. (2021). An ensemble approach to meta-heuristic algorithms: comparative analysis and its applications. *Comput. Ind. Eng.* 162:107739. doi: 10.1016/j.cie.2021.107739

Su, Z., Wang, J., Lu, H., and Zhao, G. (2014). A new hybrid model optimized by an intelligent optimization algorithm for wind speed forecasting. *Energy Convers. Manag.* 85, 443–452. doi: 10.1016/j.enconman.2014.05.058

Sun, Y., Wang, X., Chen, Y., and Liu, Z. (2018). A modified whale optimization algorithm for large-scale global optimization problems. *Expert Syst. Appl.* 114, 563–577. doi: 10.1016/j.eswa.2018.08.027

Talbi, E.-G. (2016). Combining metaheuristics with mathematical programming, constraint programming and machine learning. *Ann. Oper. Res.* 240, 171–215. doi: 10.1007/s10479-015-2034-y

Tsai, C.-F., and Chen, M.-L. (2010). Credit rating by hybrid machine learning techniques. *Appl. Soft Comput.* 10, 374–380. doi: 10.1016/j.asoc.2009.08.003

Wang, J., Du, P., Hao, Y., Ma, X., Niu, T., and Yang, W. (2020). An innovative hybrid model based on outlier detection and correction algorithm and heuristic intelligent optimization algorithm for daily air quality index forecasting. *J. Environ. Manag.* 255:109855. doi: 10.1016/j.jenvman.2019.109855

Waycott, M., Duarte, C. M., Carruthers, T. J., Orth, R. J., Dennison, W. C., Olyarnik, S., et al. (2009). Accelerating loss of seagrasses across the globe threatens coastal ecosystems. *Proc. Natl. Acad. Sci. U. S. A.* 106, 12377–12381. doi: 10.1073/pnas.0905620106

Yang, X.-S. (2009). "Harmony search as a metaheuristic algorithm," in *Music-Inspired Harmony Search Algorithm: Theory and Applications*. ed. Z. W. Geem (Berlin, Heidelberg: Springer), 1–14.

Yang, X.-S. (2013). Optimization and metaheuristic algorithms in engineering. *Metaheuristics in Water, Geotechnical and Transport Engineering* 1:23.

Yang, D., and Yang, C. (2009). Detection of seagrass distribution changes from 1991 to 2006 in Xincun Bay, Hainan, with satellite remote sensing. *Sensors* 9, 830–844. doi: 10.3390/s90200830

Zheng, F., Qiu, G., Fan, H., and Zhang, W. (2013). Diversity, distribution and conservation of Chinese seagrass species. *Biodivers. Sci.* 21, 517–526. doi: 10.3724/SP.J.1003.2013.10038

Zimmermann, N. E., Edwards, T. C. Jr., Graham, C. H., Pearman, P. B., and Svenning, J. C. (2010). New trends in species distribution modelling. *Ecography* 33, 985–989. doi: 10.1111/j.1600-0587.2010.06953.x

frontiers | Frontiers in Ecology and Evolution

TYPE Original Research
PUBLISHED 14 February 2023
DOI 10.3389/fevo.2023.1102015

OPEN ACCESS

EDITED BY
Wei Zhao,
Institute of Geographic Sciences and Natural Resources Research (CAS), China

REVIEWED BY
Cuicui Jiao,
Sichuan University of Science and Engineering, China
Preet Lal,
Michigan State University, United States

*CORRESPONDENCE
Chun Wang
✉ wangchun@chzu.edu.cn

†These authors have contributed equally to this work

SPECIALTY SECTION
This article was submitted to Population, Community, and Ecosystem Dynamics, a section of the journal Frontiers in Ecology and Evolution

RECEIVED 18 November 2022
ACCEPTED 16 January 2023
PUBLISHED 14 February 2023

CITATION
Tao Y, Tian L, Wang C and Dai W (2023) Dynamic simulation of land use and land cover and its effect on carbon storage in the Nanjing metropolitan circle under different development scenarios.
Front. Ecol. Evol. 11:1102015.
doi: 10.3389/fevo.2023.1102015

Dynamic simulation of land use and land cover and its effect on carbon storage in the Nanjing metropolitan circle under different development scenarios

Yu Tao[1,2†], Lei Tian[3†], Chun Wang[1,2*] and Wen Dai[4]

[1]School of Geographic Information and Tourism, Chuzhou University, Chuzhou, Anhui, China, [2]Anhui Province Key Laboratory of Physical Geographical Environment, Chuzhou, Anhui, China, [3]College of Forestry, Nanjing Forestry University, Nanjing, Jiangsu, China, [4]School of Geographical Sciences, Nanjing University of Information Science and Technology, Nanjing, Jiangsu, China

Land use and land cover (LULC) change is a pattern of alteration of the Earth's land surface cover by human society and have a significant impact on the terrestrial carbon cycle. Optimizing the distribution of LULC is critical for the redistribution of land resources, the management of carbon storage in terrestrial ecosystems, and global climate change. We integrated the patch-generating land use simulation (PLUS) model and integrated valuation of ecosystem services and trade-offs (InVEST) model to simulate and assess future LULC and ecosystem carbon storage in the Nanjing metropolitan circle in 2030 under four scenarios: natural development (ND), economic development (ED), ecological protection (EP), and collaborative development (CD). The results showed that (1) LULC and carbon storage distribution were spatially heterogenous in the Nanjing metropolitan circle for the different scenarios, with elevation, nighttime lights, and population being the main driving factors of LULC changes; (2) the Nanjing metropolitan circle will experience a carbon increase of 0.50 Tg by 2030 under the EP scenario and losses of 1.74, 3.56, and 0.48 Tg under the ND, ED, and CD scenarios, respectively; and (3) the CD scenario is the most suitable for the development of the Nanjing metropolitan circle because it balances ED and EP. Overall, this study reveals the effects of different development scenarios on LULC and ecosystem carbon storage, and can provide a reference for policymakers and stakeholders to determine the development patterns of metropolitan areas under a dual carbon target orientation.

KEYWORDS

carbon storage, land use and land cover, scenario simulation, PLUS model, InVEST model, Nanjing metropolitan circle

1. Introduction

Human society interacts with the natural environment through land use and land cover (LULC) change (Sleeter et al., 2017; Homer et al., 2020; Yee et al., 2021; Zhai et al., 2021; Lal et al., 2022). Scientific planning for LULC is essential for the achievement of global sustainable development goals, as it has a significant impact on global climate change, food security, biodiversity conservation, and carbon sources and sinks (Lambin and Meyfroidt, 2011; Arneth et al., 2014; Popp et al., 2014; Powers and Jetz, 2019). LULC and its dynamics are key scientific issues in the study of human carbon emissions in the current dual-carbon context (Tang et al., 2021; Bukoski et al., 2022; Wang et al., 2022) and global climate change (Winkler et al., 2021; Meyfroidt et al., 2022; Tian et al., 2022b).

Indeed, global climate change is already an indisputable fact (Wilfried, 2007; Gauthier et al., 2014; Lawal et al., 2019; Tian and Fu, 2020) and atmospheric concentrations of greenhouse gases (GHG; e.g., CO_2 and CH_4) directly influence the global average temperature (Solomon et al., 2009; Cramer et al., 2018; Tian et al., 2022a). Some research suggests that in order to prevent warming by more than 1.5°C, GHG emissions need to be reduced by 7.6% per year from 2019 to 2030 (Huppmann et al., 2018; Rogelj et al., 2018; United Nations Environment Programme, 2019). This will require joint efforts from governments worldwide. Over the past few decades, most of the world's major cities have expanded, with more than 50% of the population already living in cities, and by 2050, the urban population is expected to reach 66% (Ayanlade, 2016). However, as urbanization continues to accelerate, the driving force of economic development (ED) has gradually shifted from agriculture to industry and services and the increasing level of urbanization has led to dramatic changes in LULC, which significantly impacts terrestrial ecosystem functions and directly affects the carbon storage of terrestrial ecosystems (Feddema et al., 2005; Newbold et al., 2015; Li et al., 2019). Carbon storage in terrestrial ecosystems is widely recognized as an indicator of ecosystem services and plays a key role in the global carbon cycle (Lu et al., 2013; Wang et al., 2022). Reducing carbon emissions from land use and sequestering CO_2 from the atmosphere into terrestrial ecosystems is one of the most economical and environmentally friendly ways to mitigate global climate change (Molotoks et al., 2018; Dybala et al., 2019). For example, increasing the area of forest ecosystems through afforestation could contribute to increasing carbon storage in terrestrial ecosystems (Tian et al., 2022b).

Previous studies indicated that LULC changes are affected by climate change and human activity (Sleeter et al., 2017; Homer et al., 2020; Lal et al., 2021; Yee et al., 2021; Zhai et al., 2021). In recent decades, the conflict between humans and land has intensified and human activities have significantly affected changes in LULC, causing problems for ecosystems, climate, and biodiversity (Foley et al., 2005; Thonfeld et al., 2020; Lee, 2021). Since the implementation of the reform and opening-up policy, the urbanization process in China has accelerated significantly (Li et al., 2018), with a dramatic increase in the urbanization rate from 17.92 to 59.58% (Zhu et al., 2020). Liu et al. (2020) mapped the global annual urban dynamics from 1985–2015 using Landsat data, and the results showed urbanization accelerated in developing countries (for example, China, India, Saudi Arabia and a few urban clusters in Africa) but decelerated in developed countries (for example, United States, Canada, Japan and European countries). For example, in the Shanghai area of China, the average growth rate of urban lands is 49.5 km^2 $yr.^{-1}$, By contrast, in the Chicago area, one of the most urbanized regions in the United States, the mean increase in urban area during 1985–2015 is 21.3 km^2 $yr.^{-1}$. Furthermore, many Chinese cities are exhibiting an accelerated pace of urbanization due to the dependence of financial revenues on real estate and land transactions (Huang et al., 2017). Rapid ED and intensive land development have decreased the carbon storage in terrestrial ecosystems and destroyed local ecological environments, which further contributes to climate warming (Zhu et al., 2021; Tian et al., 2022b). Therefore, there is a need for anthropogenic planning of LULC development patterns to coordinate ED and ecological conservation, which is essential for optimizing future regional urban planning and maintaining ecosystem carbon balance (Liao et al., 2022; Sun et al., 2022; Tian et al., 2022b).

In the process of urbanization, cities develop to a mature stage and will form urban agglomerations, which is a new geographical unit (Schoenberger and Walker, 2017). It is a spatially compact, economically connected, and ultimately highly co-located and integrated group of cities formed by a well-developed transportation and communication infrastructure network. The Nanjing metropolitan circle, the first inter-provincial metropolitan area planned and built in China, its goal is to form an economic zone with Nanjing as the center and to develop and strengthen the zone as a whole; that is, to take one city as the leader to drive the development of surrounding cities and towns. The Nanjing metropolitan circle plays an important role in the construction of the "One Belt and Road," the integrated development of the Yangtze River Delta, the development of the Yangtze River Economic Belt, and other major strategies. With the continuous strengthening of policy guidance for the synergistic development of urban agglomerations, an optimal layout of urban agglomeration land use that reflects the national strategic intent and scientific, sustainable, and equitable development is urgently required. Therefore, integrated planning of the urban development pattern of the Nanjing metropolitan circle is necessary to optimize the future urban structure, protect local ecological environment, and maintain regional carbon balance.

Several models have been developed for land use simulation, such as the cellular automata (CA)-Markov model (Wu H. et al., 2019; Zhao et al., 2019), Logistic-CA-Markov model (Guan et al., 2019), Artificial Neural Network-CA model (Yang et al., 2016; Xu et al., 2019), Mixed-cell CA model (Liang et al., 2021a), CLUS-S model (Luo et al., 2010; Jiang et al., 2017), and FLUS model (Liu et al., 2017; Liang et al., 2018). Yet, in spite of some successful applications of the above models in land use simulation, the inability to effectively identify the factors affecting LULC and the inability to simulate land use units in a dynamic spatio-temporal manner, which clearly limits the application of LULC simulation under multi-factor-driven conditions (Wang et al., 2022). The patch-generating land use simulation (PLUS) model developed by Liang et al. (2021b) is a future land use simulation model used to improve the understanding of the driving factors of LULC change and has a higher simulation accuracy than other CA models. The model is capable of performing future land use change simulation by deciphering the deep relationships between sites and resolving land use change strategies, thereby improving land use simulation accuracy (Liang et al., 2021b). For example, Zhai et al. (2021) predicted the land distribution pattern in Wuhan, China, in 2029 using the PLUS model based on the spatiotemporal pattern of LULC changes during the urbanization process in the city from 2000 to 2019. Zhang et al. (2022) integrated the PLUS model with multiple linear regression and Markov chain models to predict the landscape patterns in the Fujian Delta region by 2050. Furthermore, studies have combined the PLUS model and integrated valuation of ecosystem services and trade-offs (InVEST) model to assess carbon storage changes in terrestrial ecosystems caused by changes in LULC (Wang et al., 2022; Tian et al., 2022b). Current urban land use layout optimization strategies can consider urban agglomerations as a whole or each city as an isolated individual. Denoting the regional synergistic development of urban agglomerations, establishing optimization objectives applicable to the urban agglomeration scale, and carrying out urban agglomeration land use layout optimization remains a major challenge in land use research. Therefore, it is important to explore the land use distribution patterns of future cities under different scenarios and their impacts on carbon storage to find the optimal solution for planning scenarios of metropolitan areas under the dual carbon target (i.e., carbon peaking and carbon neutrality) and to provide a leading and demonstration role for other metropolitan areas in China.

Here, we set four future development scenarios for the Nanjing metropolitan circle and integrated the PLUS and InVEST models to dynamically simulate land use distribution patterns under different

scenarios and assess the changes in carbon storage due to changes in LULC. Specifically, we aimed to (1) simulate the spatial distribution of LULC in the Nanjing metropolitan circle for a temporal range of 2020–2030 using the PLUS model; (2) assess the dynamics of carbon storage under different development scenarios; and (3) explore the optimal scenario of future urban development in the Nanjing metropolitan circle. Overall, this work is important for optimizing the land use development pattern of the Nanjing metropolitan circle, providing guidance to government departments and decision makers in urban planning, facilitating the formulation of reasonable policies, and for the rational use and synergistic development of land resources in urban agglomerations.

2. Materials and methods

2.1. Study area

The Nanjing metropolitan circle, an economic zone centered around Nanjing, in eastern China, covers a core area of the urban zone along the middle and lower reaches of the Yangtze River. It spans over the Jiangsu and Anhui provinces and is the first planned cross-provincial metropolitan circle in China. The Nanjing metropolitan circle ranges from 29°57'N–34°05'N and 117°09′ E–119°58′E and includes 33 municipal districts, 11 county-level cities, and 16 counties, with a total area of 66,000 km^2 (Figure 1). The Nanjing metropolitan circle connects the north, south, east, and west of China, with a special geographical location and various city types. It is an important conduction area for the Yangtze River Delta to drive the development of the central and western regions and has an important position in the national Yangtze River Economic Belt development strategy. In 2021, the Nanjing metropolitan circle had a resident population of 3,582.47 million and a regional gross domestic product (GDP) of 4.6 trillion RMB. It contains 0.7% of the country's land area and 2.5% of the resident population and generates 4.1% of China's GDP (National Bureau of Statistics, 2021).

The Nanjing metropolitan circle has a humid northern subtropical climate with four distinct seasons and abundant rainfall. The average annual rainfall days per year is 117, with an average annual precipitation and temperature of approximately 912 mm and 16.18°C, respectively. The topography of the Nanjing metropolitan circle is high in the south and low in the north and most cities in the region have flat terrain. The southern area has a high forest coverage rate with rich forestry resources. Moreover, the region has many river systems with large lakes and rivers, such as Hongze and Gaoyou Lakes and the Yangtze and Huai Rivers, and a large area of water and wetlands.

2.2. Data acquisition and preprocessing

The data used in this study include LULC data and its driving factors (i.e., socioeconomic data and natural environmental data), as shown in Table 1. Specifically, the LULC data for the Nanjing metropolitan circle for 2000, 2010, and 2020 were obtained from the GLOBELAND30 dataset produced by the National Geomatics Center of China. Based on the actual land use types in the study area, the LULC data (with a spatial resolution of 30 m) were reclassified into six categories: cropland, forest, grassland, water, artificial surface, and other (Figure 2). The socioeconomic data included population density, GDP, nighttime lights, government, residents, train station locations, and various levels of road vector data.

The natural environment data included temperature, precipitation, soil type, digital elevation model (DEM), and slope data, with the slope data being obtained by DEM processing. All the above driving factor data has been processed to 30 m spatial resolution after a series of preprocessing steps as requirement of PLUS Model (Liang et al., 2021b). These preprocessing steps included projection transformation, Euclidean distance generation, resampling, and cropping. The temporal range of the data was kept as close as possible to that of the LULC data in 2020; however, owing to data acquisition limitations, data from similar years were used for some factors (Long et al., 2013).

2.3. Methods

2.3.1. Scenarios setting

Historical LULC change trends and Markov chain methods have been used to estimate future land use demand (Munsi et al., 2012; Nor et al., 2017; Li et al., 2021). Specifically, land use dynamics changes and land use conversion matrices were used to adjust the conversion probabilities in Markov chains to estimate land use demand for different scenarios. In order to effectively evaluate the potential effects of future LULC changes on regional carbon storage, four LULC change scenarios were developed for the Nanjing metropolitan circle from 2020 to 2030 (Wang et al., 2018; Zhai et al., 2021; Zhang and Gu, 2022): natural development (ND), ED, ecological protection (EP), and collaborative development (CD) scenario. The four scenarios were set as follows:

2.3.1.1. ND scenario

On the basis of the historical change trends of each land use type from 2000 to 2020, this scenario makes a linear prediction of land use patterns in the Nanjing metropolitan circle in 2030. This scenario implies that each land use type's demand only evolves linearly in accordance with its historical evolutionary trajectory and is unaffected by other external causes (conversion probability matrix for the period 2000–2020), making it an ideal state land use development scenario.

2.3.1.2. ED scenario

As the core engine of ED in the Yangtze River Economic Belt, the Nanjing metropolitan circle is one of the most economically dynamic international urban agglomerations. The ED scenario simulates a land use structure that prioritizes ED, with the goal of maximizing economic benefits by availing all land use types. Under this scenario, the conversion probability of cropland, forest, grassland, and other land, except water, to artificial surfaces increases by 30% and the conversion probability of artificial surfaces to any other land type decreases by 40%. This scenario helps to scientifically grasp the risk of land use conflicts in the fast-growing Nanjing metropolitan circle, and reveals the potential menace of the "GDP-only" development model to social stability and environmental carrying capacity.

2.3.1.3. EP scenario

The dense population and rapidly developing economy in the Nanjing metropolitan circle have caused considerable real or potential harm to the local ecological environment. To promote further optimization and enhancement of the Nanjing metropolitan circle, it is necessary to place EP in a prominent position. The conversion of cropland, forest and grassland with ecological functions to Artificial surface was strictly controlled by referring to *the Ecological restoration planning of land space in Anhui Province (2021–2035)* and *the Draft of master plan of land and space of Nanjing Municipality (2021–2035)*. The

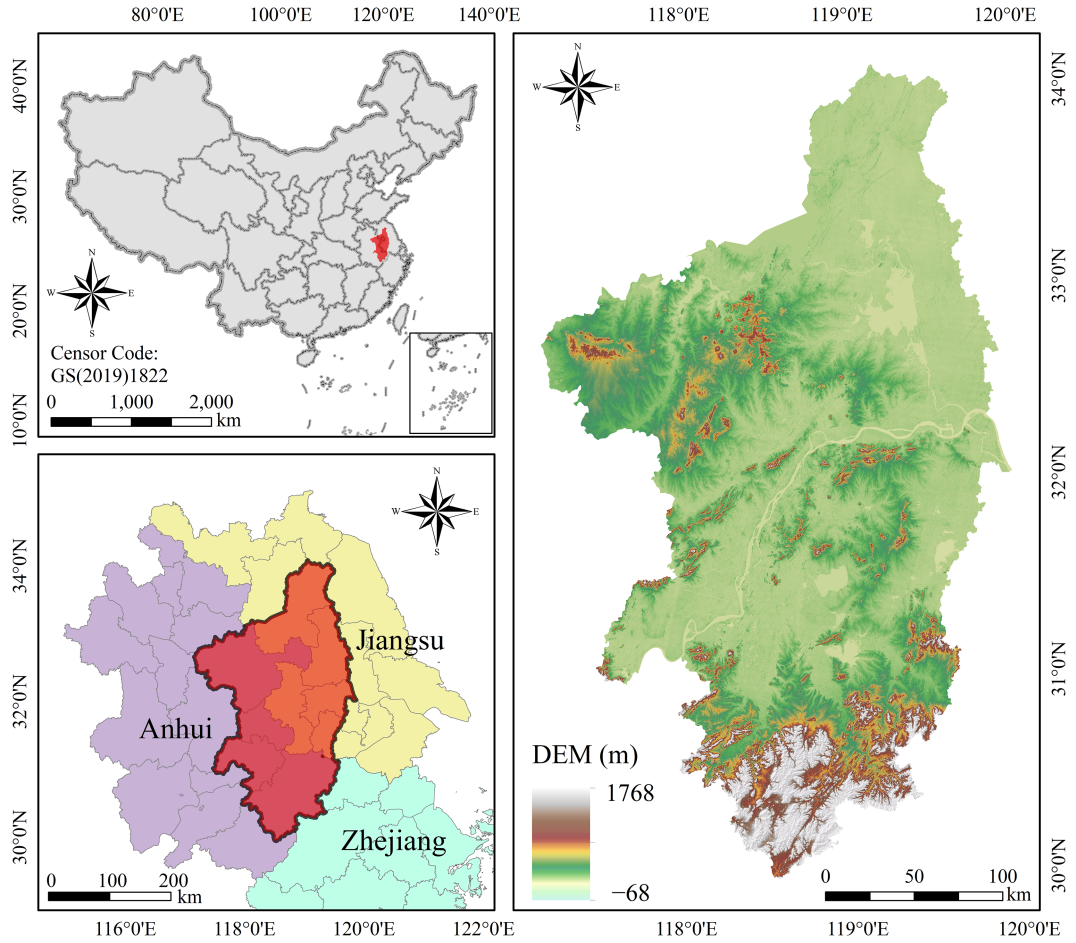

FIGURE 1
Location of Nanjing metropolitan circle with a digital elevation model (DEM).

EP scenario ensures that land types providing ecological services, such as forests, grasslands, and water bodies, are conserved and prioritized for development by setting ecological priority development strategies. Under this scenario, the expansion of urban areas is restricted and water is not transferred to other land uses; therefore, the conversion probability of forests, grasslands, and artificial surfaces decreases by 35%, the conversion probability of cropland to forests and grasslands increases by 25 and 20%, respectively, and the conversion probability of grassland to forest increases by 15%. This scenario is an important reference for mitigating land-use conflicts, promoting the delineation of ecological red lines, establishing a nature reserves mainly as national parks, and implementing the national main function zone system.

2.3.1.4. CD scenario

ED and EP are not opposites and can promote each other and develop together. With according to *the Territorial Spatial Planning of Anhui Province (2021–2035) (Draft for comments)* and *the Draft of master plan of land and space of Nanjing Municipality (2021–2035)*. The CD scenario takes into consideration high-quality ED while balancing good economic and ecological benefits of regional synergistic development. This scenario constructs a harmonious human-land relationship in the Nanjing metropolitan circle by harmonizing ED and EP. The transition probability of forest and grassland to artificial surfaces was reduced by 40%, the transition probability of cropland to artificial surfaces was reduced by 50%, the transition probability of cropland to other land was reduced by 20%, and the transition probability of other land to grassland and forest land increased by 50%. This scenario is important for coordinating economic and ecological benefits, promoting the development of the Nanjing metropolitan circle in harmonious economic and ecological conditions, and promoting high quality development of homeland space.

2.3.2. LULC simulation using PLUS model

The PLUS model was used to simulate the distribution pattern of LULC in Nanjing metropolitan circle in 2030 under different scenarios, which consists of two main components: (1) land expansion analysis strategy (LEAS) model for obtaining the development probabilities of various land use types; (2) CA model based on the multi-type random patch seeds (CARS) model for spatio-temporal dynamics simulation of land patches (Liang et al., 2021b). The LEAS module first extracts the fraction of expansion of each land type between the two periods of LULC change and samples it together with the responding driving factors, and uses the random forest (RF) algorithm to obtain the contribution of the driving factors and the development potential of each land category. Subsequently, the CARS model incorporates stochastic seeding and a threshold decreasing mechanism for land use simulation under the constraint of development probability. Previous studies confirmed that the PLUS model can mine the potential linkages between various driving factors and geographic units to develop future land use change patterns with higher accuracy and more realistic landscape patterns (Zhai et al., 2021; Wang et al., 2022; Tian et al., 2022b).

TABLE 1 Spatial driving factors of the land use change in this study.

Category	Data	Year	Original resolution	Data resource
Land use and land cover data	Land use and land cover data	2000, 2010, 2020	30 m	GLOBELAND30 dataset
Socioeconomic driver data	Population	2019	1000 m	https://www.resdc.cn
	GDP	2019	1000 m	
	Nighttime lights	2020	30 m	https://eogdata.mines.edu/products/vnl/
	Distance to governments	2020	30 m	https://lbs.amap.com
	Distance to train stations			
	Distance to highways	2020	30 m	OpenStreetMap (https://www.openstreetmap.org)
	Distance to primary roads			
	Distance to secondary roads			
	Distance to tertiary roads			
	Distance to trunk roads			
	Distance to railroads	2020	30 m	https://www.webmap.cn
	Distance to residents			
Natural environmental driver data	Distance to water	2020	30 m	LULC in 2020
	DEM	2009	30 m	ASTER GDEM 30 M dataset
	Slope			
	Soil types	1995	30 m	https://www.resdc.cn
	Average annual temperature	2000–2020	1000 m	http://www.geodata.cn
	Average annual precipitation			

In this study, 18 driving factors (Figure 3) were collected to facilitate LULC simulations, as described in Section 2.2. First, the 2020 LULC data were simulated based on the 2000 and 2010 LULC data (Figure 2) to assess the model accuracy. Moreover, the PLUS model based on the RF algorithm was used to assess the contribution of each driving factor to future land use patterns, which aids in understanding the effect of the driving factors on future land use changes.

2.3.3. InVEST model for carbon storage estimation

The InVEST model estimates terrestrial ecosystem carbon storage by the carbon density of each land use type and the corresponding area (Sharp et al., 2020). We set the carbon densities of the LULC ecosystem using values from previous studies, as shown in Table 2 (Wang et al., 2011; Xu et al., 2014; Fang et al., 2021). Furthermore, the economic value of sequestering one ton of carbon is assumed to be 57.50 RMB (from the carbon market trading price in China on September 30, 2022), with the annual rate of change in carbon prices and the market discount rate of 0 and 3%, respectively (Babbar et al., 2021). Specifically, we combined the PLUS model with the InVEST model to explore the effects of land use change on the carbon storage of the Nanjing metropolitan circle from 2020 to 2030 under the different scenarios. The general research framework included (1) simulation of LULC data based on the PLUS model and (2) assessment of ecosystem carbon storage changes due to LULC changes using the InVEST model (Figure 4).

3. Results

3.1. Contribution of the driving factors for land use change

The contributions of the driving factors for each land use type based on the RF algorithm, as illustrated in Figure 5. It should be noted that the contribution of the driving factor of the water body is not given in Figure 5 due to the small area of change in the water, which was mainly affected by a single driving factor, which is the distance to the water (96.73%). The main driving factors for the change in cropland were nighttime light (12.90%), distance to water (12.39%), and temperature (10.30%). Nighttime lights are indicators of urban development and can represent the rate of urban expansion. The loss of cropland was mainly due to urban expansion and agricultural restructuring. The main driving factors affecting forests were elevation (13.68%), population (13.09%), and nighttime lights (9.73%). Specifically, forests are mainly distributed in the higher elevation areas in the southern part of the study area (Figures 1, 3) and elevation may have affected the interconversion of forest to non-forest land use types. Elevation (17.48%) is the main driving factor for grassland changes. Distance from water (16.50%), nighttime lights (14.72%), and elevation (12.70%) were the main driving factors for artificial surface expansion. The water area generally does not convert to other land use types and urban expansion tends to avoid water areas. Elevation (12.70%) was also the primary driving factor for other land use types. In conclusion, the main driving factors of LULC change in the Nanjing metropolitan circle are elevation, nighttime lights, and population.

3.2. Simulation of LULC spatiotemporal distribution

Overall accuracy (OA) and Kappa coefficients were used to evaluate the accuracy of the PLUS model. The comparison of the simulated 2020 LULC data with the actual 2020 LULC data shows that the OA and Kappa coefficient are 91.8% and 0.85, respectively, which indicates that the PLUS model simulates land use data with high accuracy and can be reliably applied to simulate LULC.

Subsequently, the 2030 LULC data for the Nanjing metropolitan circle under four development scenarios were successfully simulated

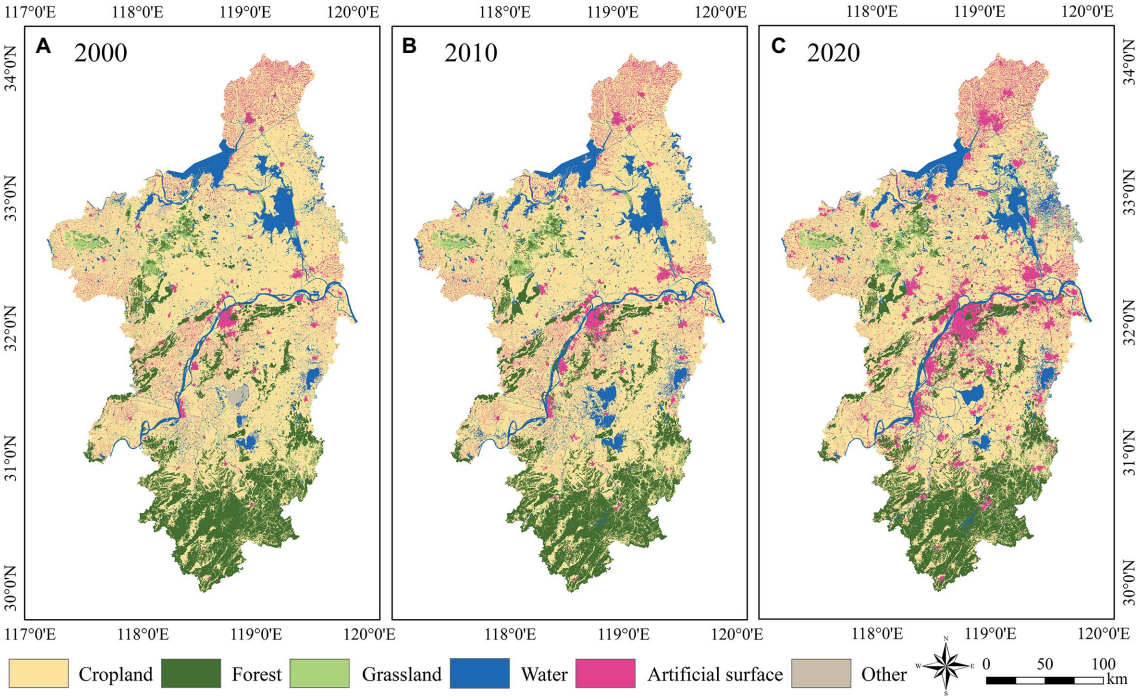

FIGURE 2
Historic LULC data in **(A)** 2000, **(B)** 2010, and **(C)** 2020 for the Nanjing metropolitan circle.

using the PLUS model (Figure 6), and its statistics are shown in Table 3. Furthermore, Figure 7 illustrates the different land use type conversions for the period of 2020–2030 under the different scenarios. Specifically, under the ND scenario, the land use pattern in 2030 for the Nanjing metropolitan circle was similar to that of the historical (i.e., 2010–2020 land use change trend, which was consistent with our expectations). The artificial surface maintained relatively high growth, with an increase of 1597.40 km^2, which was achieved by encroaching on cropland, forest land, and grassland. Under the ED scenario, the artificial surface area expanded sharply, reaching 11,554.77 km^2, which is an increase of 3,400.07 km^2 (41.69%) compared to 2020. The urban expansion pattern emerged in the form of Nanjing as the center, with neighboring cities expanding in all directions (Figure 6B). As forests and grasslands were not effectively protected under this scenario, the area of cropland significantly decreased, and water and other land areas saw varying degrees of decrease. Overall, the ED scenario demonstrated a future land-use development pattern with economic primacy and unrestricted urban expansion.

Under the EP scenario, the area of artificial surface increases only 265.93 km^2 by 2030. Forest land and grassland were effectively protected, with an increase in area of 861.27 km^2 and 13.42 km^2, respectively. The area of water remained virtually unchanged and other land areas showed a slight increase. The land use pattern under the CD scenario was more balanced than those under the other three scenarios because this scenario integrates the consideration of EP and ED, which is reflected in the land use change pattern that the artificial surface is maintained with a certain increase, while the forest and grassland are effectively protected. This scenario is of great significance to the Nanjing metropolitan circle for implementing EP, high-speed ED policies, optimizing urban functions and spatial structure, and empowering high-quality and sustainable urban development.

3.3. Spatiotemporal patterns of carbon storage

The distribution of carbon storage in the Nanjing metropolitan circle in 2030 under different scenarios is illustrated in Figure 8, and the carbon storage under different scenarios is significantly different (Figure 9; Table 4). Under the ND scenario, the carbon storage of other land slightly increased in 2030 (0.04 Tg); however, the other land use types showed varying degrees of decrease in carbon storage: cropland, forest land, and grassland decreased by 1.42, 0.34, and 0.02 Tg, respectively, resulting in a net total decrease in carbon storage of 1.74 Tg. This implies that if the Nanjing metropolitan circle is developed according to the ND scenario, the carbon storage of vegetation will continue to decrease, which is not beneficial for stabilizing the carbon balance.

The ED scenario resulted in a significant decrease in total carbon storage of 3.56 Tg by 2030, with the carbon storage of cropland, forest land, and grassland decreasing by 2.89, 1.57, and 0.03 Tg, respectively. Under this scenario, the Nanjing metropolitan circle showed a spatial distribution pattern of decreasing carbon storage over a wide range (Figure 8B). Evidently, the ED scenario critically affected the carbon balance of the Nanjing metropolitan circle. Under the EP scenario, the ecological condition of the Nanjing metropolitan circle has improved significantly and the total carbon storage increased by 0.50 Tg. By 2030, forest land, grassland, and other land carbon storage increased by 1.74, 0.01, and 0.03 Tg, respectively, while that of cropland decreased by 1.16 Tg. As can be seen, the increased carbon storage mainly came from forest land, which offset the decrease in that of cropland and contributes to carbon sequestration in ecosystems.

The CD scenario strikes a balance between ED and EP by preserving the local ecosystem as much as possible while ensuring a certain level of ED. Under the CD scenario, the carbon storage of forest land and other land increased by 0.51 and 0.01 Tg, respectively, that of cropland decreased by

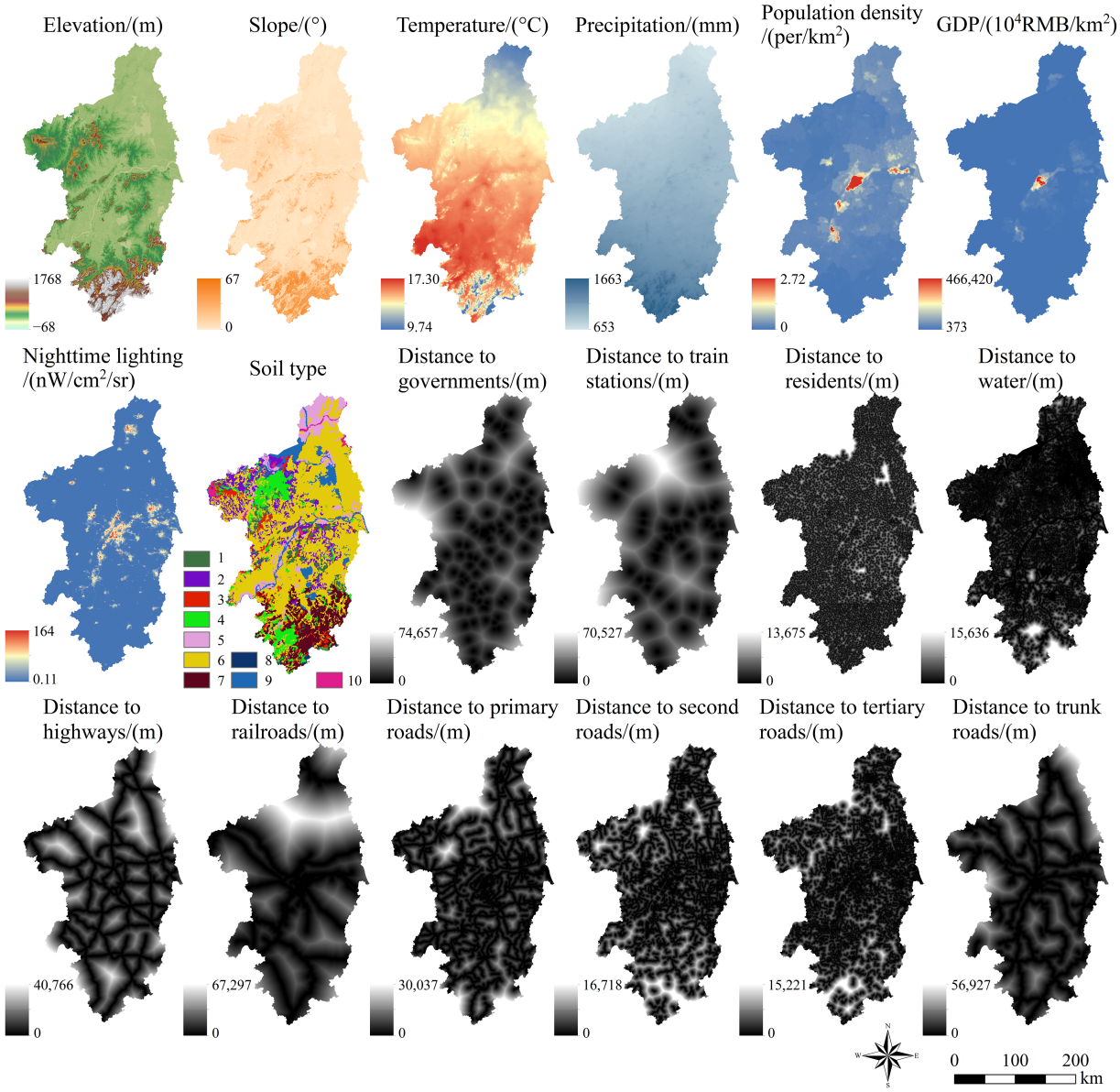

FIGURE 3
The 18 driving factors affecting LULC. Note: The legend of soil type represents, 1: yellow-brown soils; 2: yellow-cinnamon soils; 3: limestone soils; 4: chisley soils; 5: fluvo-aquic soils; 6: paddy soils; 7: red earths; 8: yellow earths; 9: water; and 10: others.

TABLE 2 Carbon density for each LULC (kg/m²).

Land use types	C_{above}	C_{below}	C_{soil}	C_{dead}
Cropland	1.19	0.13	8.03	0.12
Forest	2.38	0.78	15.27	0.56
Grassland	0.15	0.54	6.33	0.21
Water	/	/	/	/
Artificial surface	/	/	/	/
Other	0.05	/	6.21	/

1.00 Tg, while that of grassland remained stable. Although the total carbon storage in the Nanjing metropolitan circle decreased by 0.48 Tg under the CD scenario, the trend of decreasing carbon storage under the CD scenario was effectively mitigated compared to that of the ND and ED scenarios. According to this scenario, the Nanjing metropolitan circle is expected to have a positive increase in total carbon storage by 2040. This indicates that the trend of decreasing carbon storage in the Nanjing metropolitan circle could be reversed through integrated and coordinated development.

Figure 10 illustrates the economic value of carbon sequestration in terrestrial ecosystems under different scenarios, with positive values representing carbon sequestration and negative values representing carbon loss. In this study, we assumed that the future carbon sequestration and current carbon sequestration values were the same and the discount rate of carbon sequestration and social value were constant (i.e., 3%). The economic values of carbon loss of Nanjing metropolitan circle in 2020–2030 under ND and ED scenarios were 96.83 million and 201.38 million RMB, respectively. Under the EP scenario, the carbon sequestration economy of the Nanjing metropolitan circle will be positive in 2020–2030, with a value of 32.03

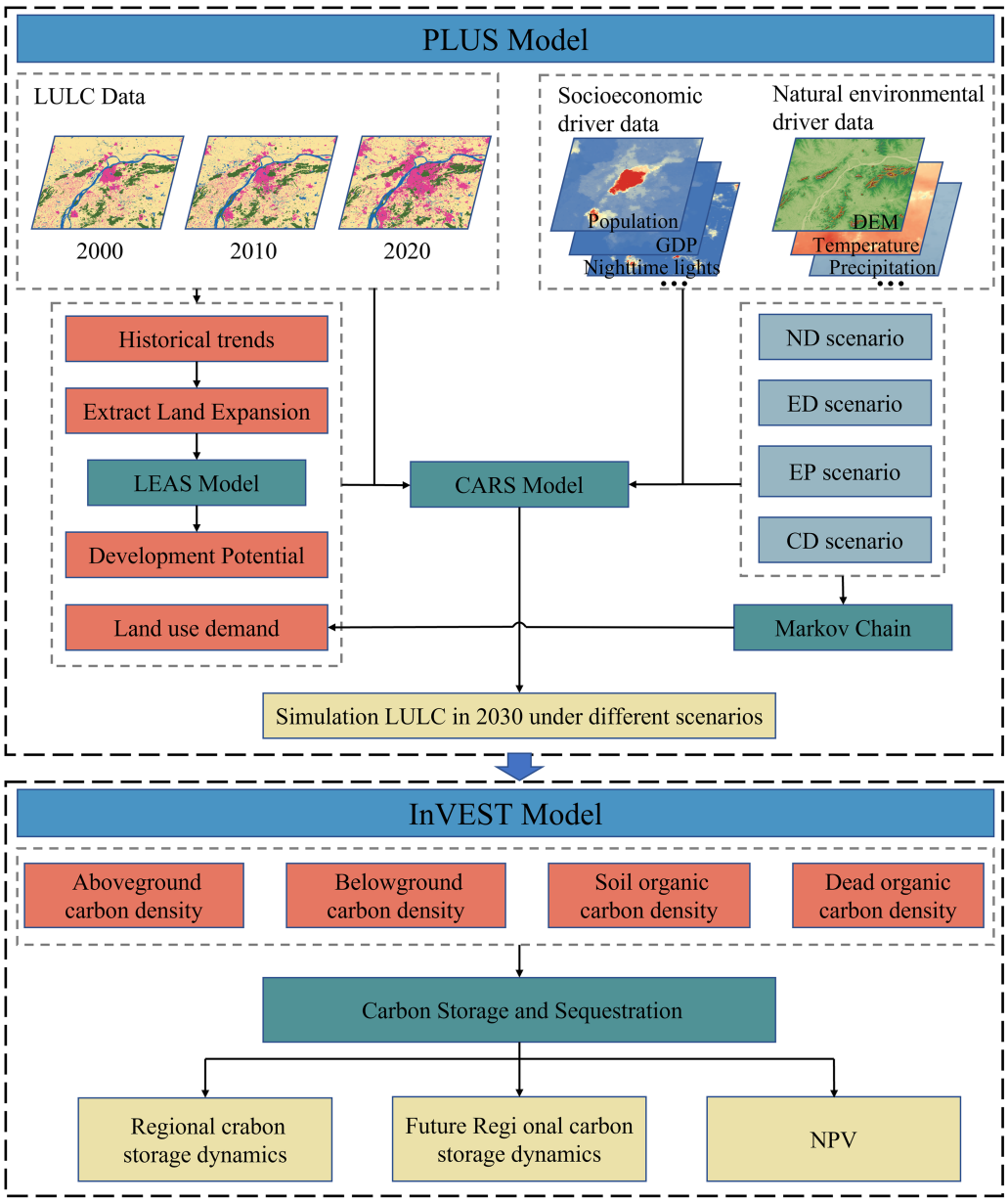

FIGURE 4
Research framework.

million RMB. Under the CD scenario, the economic value of carbon loss in the Nanjing metropolitan circle in 2020–2030 was 24.59 million. Although the sequestration economy was still negative compared with the EP model, the economic value of carbon loss was significantly lower than those under the ND and ED scenarios. Overall, this ecosystem carbon sequestration function, expressed as a monetary value, can effectively demonstrate the value of ecosystem services and convey it to policymakers (Babbar et al., 2021).

4. Discussion

4.1. Impact of LULC on carbon storage

We evaluated the impacts of four future development scenarios on LULC and carbon storage in the Nanjing metropolitan circle. Significant spatial heterogeneity was observed in the distribution of LULC changes and carbon storage in 2020–2030 under the four scenarios. The effects of different drivers on LULC were reflected in the impact of LULC on carbon storage changes.

Forest land had the highest carbon density in this study, followed by cropland and grassland (Table 2), which implies that forest land, cropland, and grassland accumulated more carbon storage than other land use types (Li et al., 2020). The area of cropland decreased under all scenarios, but by different degrees; in contrast, the artificial surface showed the opposite result, instead of increasing under all scenarios (Table 3). The change in the cropland area was driven more by nighttime lights, whereas the expansion of the artificial surface was mainly affected by the distance to water, nighttime lights, and elevation (Figure 5). Nighttime lights are indicators of urban development and can represent the rate of urban expansion (Liu et al., 2012; Ma et al., 2012; Zhang and Su, 2016). Previous studies have

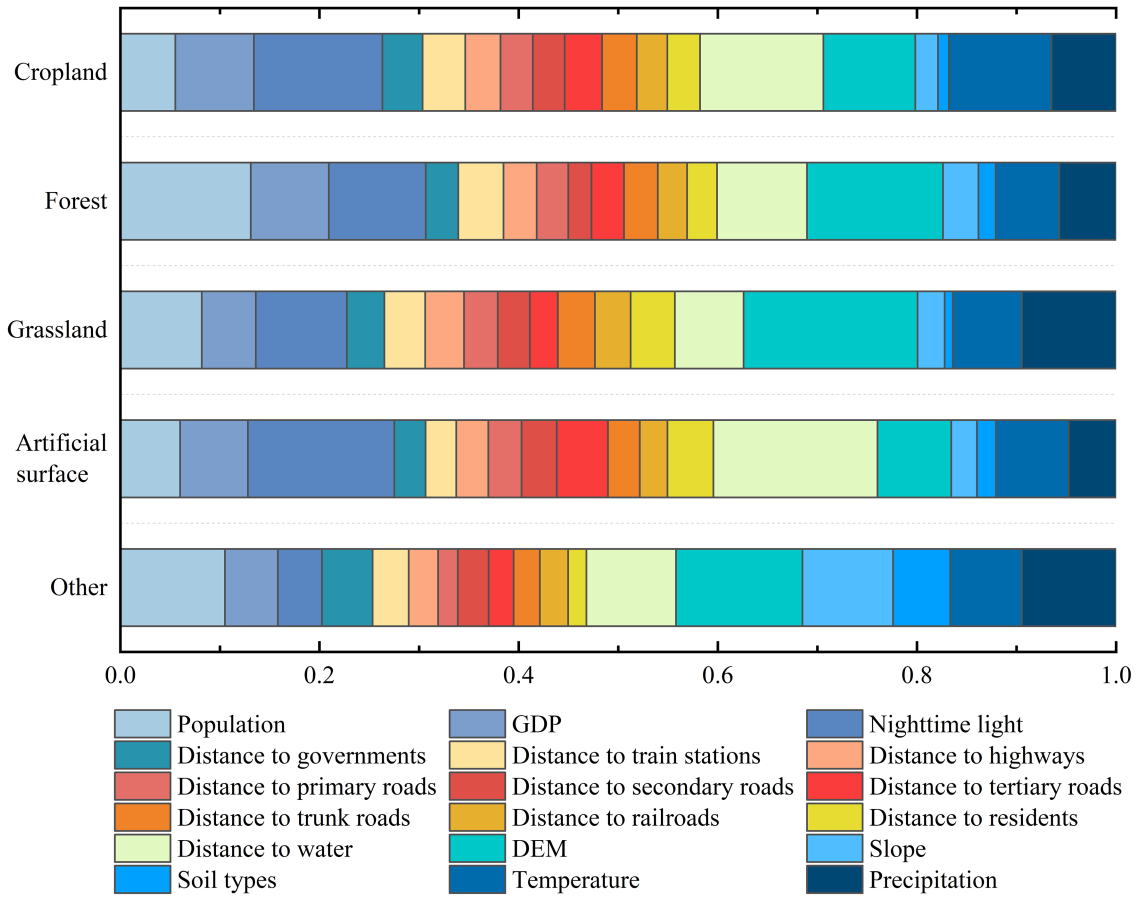

FIGURE 5
Contributions of driving factors.

shown that nighttime lights are positively correlated with regional GDP and population (Shi et al., 2014; Bennett and Smith, 2017; Lan et al., 2020). Increased GDP and population growth require larger urban areas (capacity), while urban expansion usually occurs through encroachment on natural land and cropland, which results in a vicious circle. Similar results were reported in other studies. He et al. (2016) and Jiang et al. (2017) also reported great carbon storage losses, and the occupation of natural land and farmland is the main reason for the losses of carbon storage in the Beijing and Changsha-Zhuzhou-Xiangtan urban agglomerations. Moreover, another study on the loss and loss rate of carbon storage in the Yangtze River Delta urban agglomeration from 1990 to 2015 also showed that the reduction of natural land and arable land surrounding the urban area was the main reason for the loss of carbon storage (Gao and Wang, 2019). In addition, topographical factors influence the difficulty and cost of urban construction, which also determine urban expansion. Generally, cities are established in areas with flat topography, fertile soil, and easy access to agriculture, which facilitates transportation links and saves on building investments, thus urban expansion avoids large topographic undulations (e.g., mountains; Zhai et al., 2021). The general pattern of urban development determines that the expanded artificial surface is mainly distributed in flat areas with relatively low topographic relief (Figure 6). Under the ED scenario, carbon storage in terrestrial ecosystems decreases by 35.07 Mg, which is due to the increase in artificial surface. Urban expansion, which provides more jobs and rapidly increases GDP, seems profitable, but will reduce carbon storage in regional ecosystems in the long term (Weisberg et al., 2007; Eigenbrod et al., 2011).

The expansion of forest land differed between the development scenarios, with a decrease in forest land area under the ND and ED scenarios and an increase in area under the EP and CD scenarios. Correspondingly, different forest land area changes resulted in different carbon storage patterns. Specifically, under the ND and ED scenarios, 222.52 and 313.56 km^2 of forest land are projected to be converted to other types of land by 2030, decreasing the forest ecosystem carbon storage by 2.47 and 5.95 Mg, respectively. Under the EP scenario, 655.53 km^2 of cropland is expected to be converted to forest land by 2030, increasing carbon storage by 6.24 Mg. This was confirmed by the study of Zhang et al. (2010) that the ecological engineering of grain to feed conversion can significantly increase the carbon sink of soil ecosystems in China. In addition, 222.65 km^2 of grassland will be converted to forest land, increasing carbon storage by 2.62 Mg. Overall, the conversion from other land use types to forest land contributes 8.86 Mg of carbon storage under the EP scenario. The CD scenario is similar to the EP scenario, with a projected increase in forest land area of 285.74 km^2 by 2030 and increase in carbon storage of 2.72 Mg. Balancing urban expansion and ecological conservation can maintain woodland and grassland areas, slow urban sprawl (Yang et al., 2020), and contribute to the growth of carbon storage in forest ecosystems (Zhao et al., 2019).

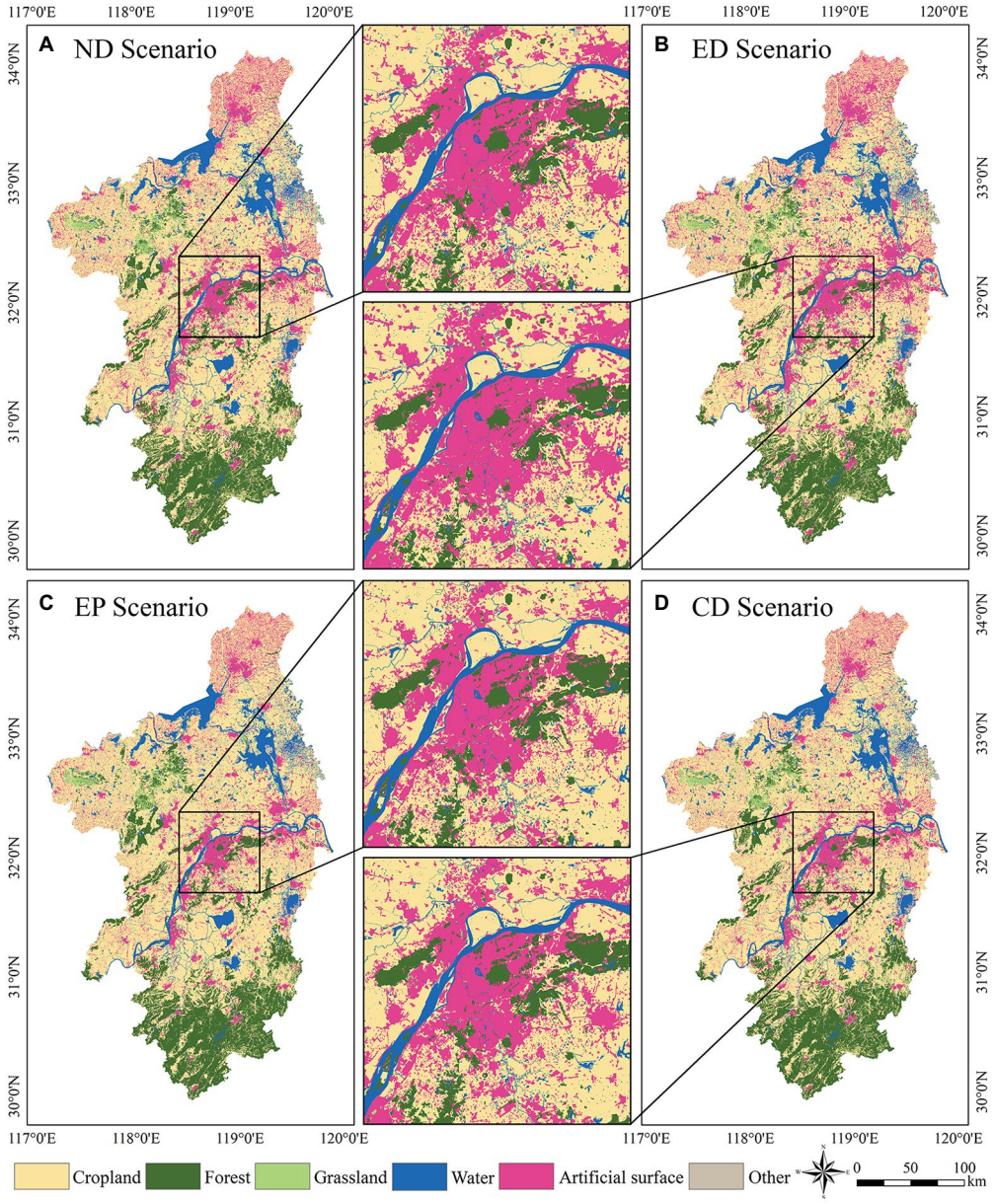

FIGURE 6
Simulation results of LULC in 2030 under four scenarios: **(A)** ND; **(B)** ED; **(C)** EP; and **(D)** CD.

TABLE 3 LULC area for four scenarios (km^2).

Land use types	2020	2030			
		ND scenario	ED scenario	EP scenario	CD scenario
Cropland	38,936.61	37,437.12	35,879.18	37,704.64	37,879.10
Forest	10,722.06	10,542.54	10,390.70	11,583.33	10,990.00
Grassland	1283.96	1265.51	1249.43	1297.38	1284.93
Water	6044.46	6036.43	6031.97	6041.58	6031.97
Artificial surface	8154.70	9752.10	11,554.77	8420.63	8885.39
Other	310.26	364.29	291.94	350.43	326.60

In the study area, forests were mainly distributed at higher elevations of the mountains. Zhang and Xie (2019) believe that population expansion not only requires forests to provide more forestry products, but people also need to enjoy the value of ecological services provided by forests, which may explain the impact of population expansion on forests. Moreover, previous studies have shown that the growth of forest

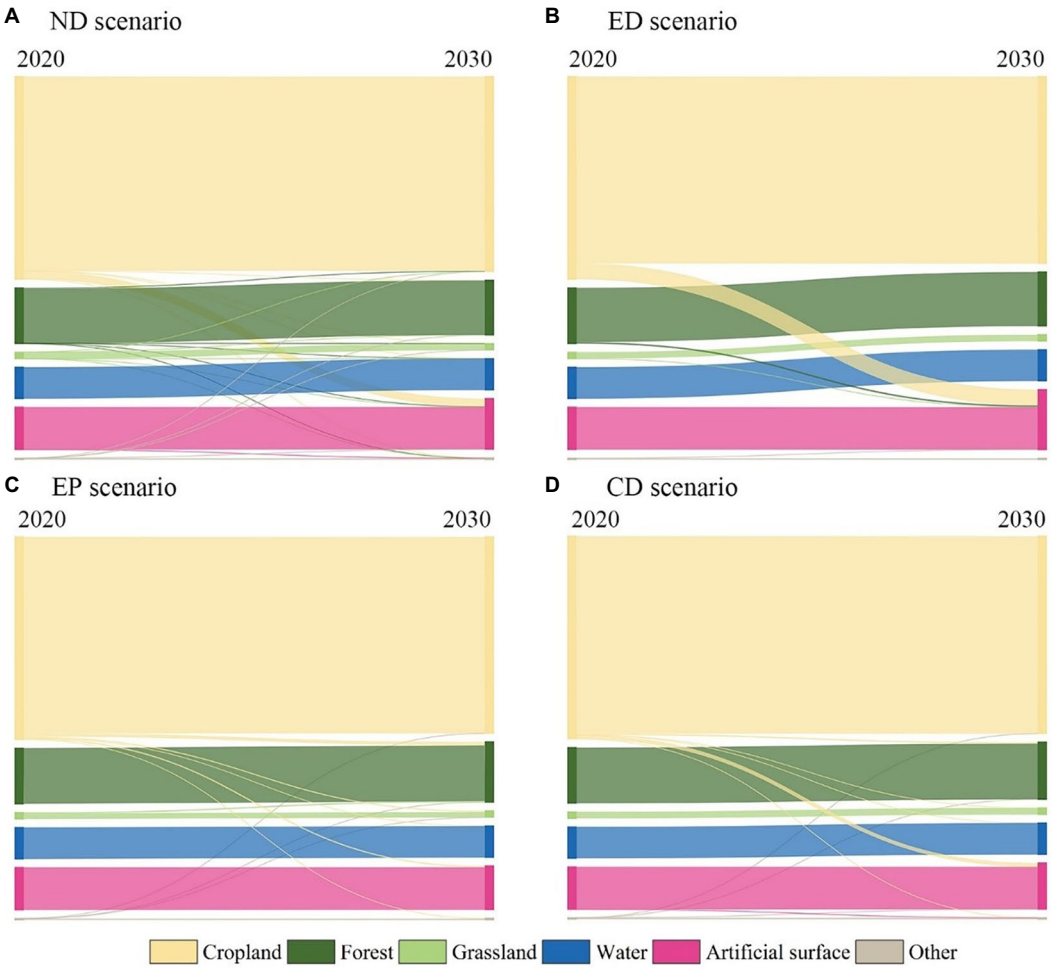

FIGURE 7
Land use type conversions from 2020–2030 under four scenarios: **(A)** ND; **(B)** ED; **(C)** EP; and **(D)** CD.

land area benefits from lower economic growth rates and more stable climatic conditions (Angelsen and Kaimowitz, 1999; Noss, 2001; Tian et al., 2022b) and that and that areas with higher ecological quality are more suitable for forest growth (Weisberg et al., 2007). Forest ecosystems tend to be more influenced by various factors, and have the greatest impact on carbon storage in terrestrial ecosystems. Therefore, protection of forests from destruction and increasing the area of forested land through measures such as natural restoration and artificial afforestation would help increase the carbon sink capacity of forest ecosystems and increase the carbon storage of the entire terrestrial ecosystem (Tian et al., 2022b).

4.2. Suggestions for future development

Urban development patterns are particularly important in the context of increased climate and socioeconomic uncertainty in the future, especially for urban agglomerations such as the Nanjing metropolitan circle, which are nationally planned and built at the inter-provincial level. If urban expansion is carried out according to the ND or ED scenarios, the artificial surface area of the Nanjing metropolitan circle will continue to increase and natural vegetation land use types, such as forest land, will continue to degrade, leading to an increasingly fragile ecological environment. Carbon storage in terrestrial ecosystems will also be significantly reduced in recent decades. If urban expansion is carried out according to the EP scenario, there will be an increase in the forest and grassland area of the Nanjing metropolitan circle will increase, artificial surface area, and carbon storage of terrestrial ecosystems. However, this scenario ignores the demonstration role of the Nanjing metropolitan circle as the leading city in the ED of the Yangtze Delta region of China, which is not conducive to the realization of future ED of the Nanjing metropolitan circle and the national development strategy.

The CD scenario balances the ED and EP of the Nanjing metropolitan circle and maintains a balance of local carbon storage with stable economic growth. Although the terrestrial ecosystem carbon storage will decrease by 0.48 Tg by 2030 under this scenario, the carbon storage reduction of the scenario will decrease significantly and the terrestrial ecosystem carbon storage under the scenario will be positive by 2040. Therefore, reasonable planning of the future urban structure, optimization of land use types, and an increase in carbon storage are particularly important for the future urban development of the Nanjing metropolitan circle. The results of this study show that rapid economic growth will lead to a continuous decrease in carbon storage and a gradual deterioration of the ecological environment. Therefore, slowing the rate of economic growth and promoting ED from “high speed” to

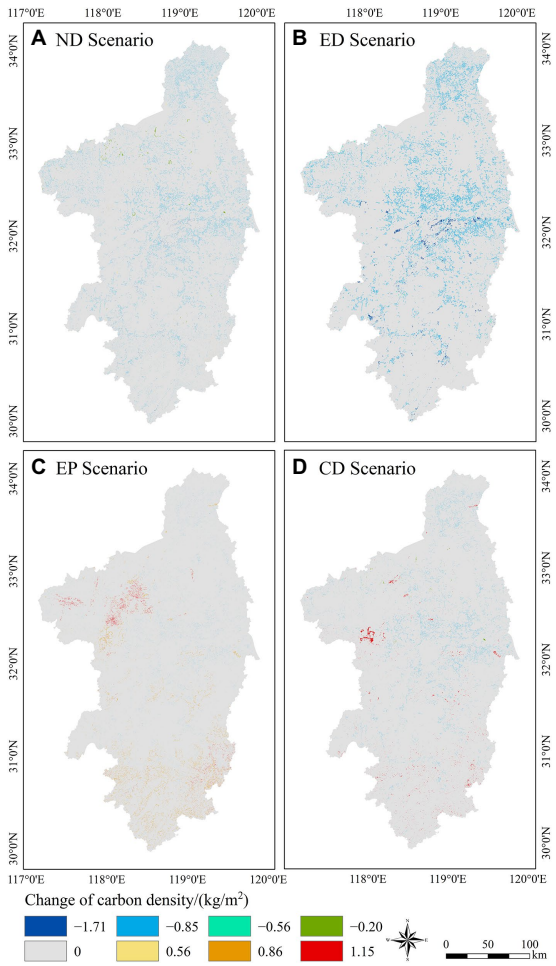

FIGURE 8
Carbon storage distribution in 2030 under four scenarios: **(A)** ND; **(B)** ED; **(C)** EP; and **(D)** CD.

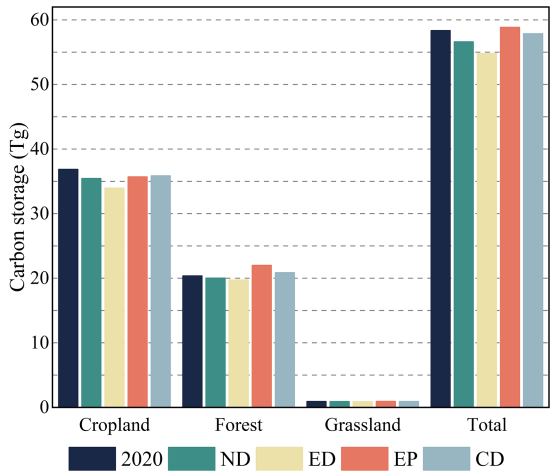

FIGURE 9
Sequestered carbon content of different land uses over 2020–2030 under four scenarios.

"high quality" could improve the carbon storage and ecosystem service value of the study area (Wang et al., 2022). Limiting the disorderly expansion of urban boundaries and constructing ecological red lines can help stabilize the structure of local ecosystems and improve EP (Wu Y. et al., 2019). Moreover, in order to mitigate the effects of climate change, it is necessary to further increase the proportion of clean energy use in the energy structure and reduce the use of fossil fuels (Tian et al., 2022b). More importantly, protecting forests from destruction and increasing the area of forest land can contribute to increasing carbon storage in terrestrial ecosystems (Cao et al., 2009; Xiao, 2014).

4.3. Strengths and uncertainties

In this work, we developed a novel approach for spatial simulation and carbon storage assessment of future LULC based on four set future development scenarios of the Nanjing metropolitan circle and land use demand combining the PLUS and InVEST models (Figure 2). We determined the most suitable future urban development scenario for the Nanjing metropolitan circle to be the CD scenario and simulated a reasonable spatial distribution of LULC and carbon storage. This framework provides relatively accurate spatial and temporal simulations of LULC and carbon storage, and is useful for assessing the distribution of LULC and the impact on carbon storage under different scenarios, which is important for LULC management of urban agglomerations (Gao and Wang, 2019). Our study reveals the model for the dynamic evolution of factors controlling carbon storage in a key area of urban agglomerations, which provides support for decision-making on sustainable regional urbanization. China has three national urban agglomerations and several small urban agglomerations. The rapid growth of urban agglomerations affects carbon storage and threatens other multi-ecosystems, such as water yields, biodiversity conservation, and recreation opportunities (Nelson et al., 2009). Therefore, future research should focus on the following aspects: (1) Different regions have different geographic environments, development patterns, and cultural climates, etc. Scenarios should be set according to the individual characteristics of the regions. Therefore, it is necessary to explore the different driving mechanisms of urban agglomerations in other regions. (2) Besides carbon storage, other ecosystem services can also be assessed by the InVEST model (Nelson et al., 2010; Gao and Wang, 2019). PLUS model combined with InVEST model is meaningful and feasible for simulating LULC and carbon storage changes under different scenarios. Future studies should also examine the spatiotemporal variation of LULC and carbon storage in different regions.

However, the setting of different development scenarios needs to consider more factors, such as the urban planning layout and national forest park reserve planning (Liang et al., 2021b). In addition, the GDP, population, temperature, and precipitation data in this work were resampled to 30 m. This scale difference may cause some uncertainty in the results (Fang et al., 2022). Additionally, the limitations of the InVEST model remain a major challenge in current carbon storage estimations. The model assumes that the carbon storage of the LULC type does not change over time and is equal to the mean value of the carbon storage of the LULC type, which obviously simplifies the carbon cycle process. A second limitation is that the accuracy of the model in estimating carbon storage is dependent on the carbon density estimates for each LULC type. However, the acquisition of carbon density for each land use type is labor-intensive, and regional carbon density values usually cannot be applied to other regions (Sharp et al., 2020). For this purpose, carbon density data were collected for all land use types in the study area to the extent possible to minimize uncertainty in the assessment of carbon storage. Despite these limitations, our work revealed the spatial and temporal distribution patterns of possible future LULCs and the

TABLE 4 Carbon storage dynamic changes of LULC under four scenarios in Nanjing metropolitan circle over 2020–2030 (Unit: Tg).

Scenarios		Cropland	Forest	Grassland	Other	Total	Change vs. 2020
2020		36.87	20.36	0.93	0.19	58.36	/
2030	ND	35.45	20.02	0.91	0.23	56.62	−1.74
	ED	33.98	19.73	0.90	0.18	54.80	−3.56
	EP	35.71	22.00	0.94	0.22	58.86	0.50
	CD	35.87	20.87	0.93	0.20	57.87	−0.48

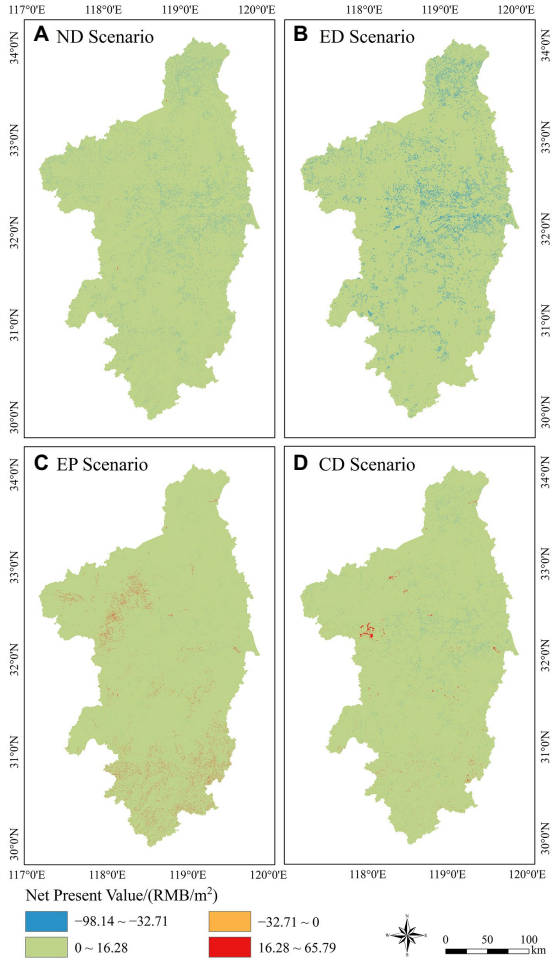

FIGURE 10
Net present value (unit RMB) of Nanjing metropolitan circle in 2020–2030 under four scenarios: **(A)** ND; **(B)** ED; **(C)** EP; and **(D)** CD.

dynamics of carbon storage in the Nanjing metropolitan circle. Based on the results of this study, we explored an optimal future urban development scenario for the Nanjing metropolitan circle, which can aid the Nanjing metropolitan circle achieve a win-win situation for both ED and EP, formulate policies for sustainable socio-ED, and achieve a reasonable future urban LULC layout.

5. Conclusion

We analyzed and simulated the spatial and temporal changes in LULC and its caused ecosystem carbon storage in the Nanjing metropolitan circle under four scenarios for 2020–2030 using the PLUS and InVEST models. The driving factors of LULC changes and the spatial and temporal differences in carbon storage were discussed and the main conclusions were as follows. (1) integrating the PLUS and InVEST models can effectively simulate LULC changes and the resulting carbon storage changes under different development scenarios. (2) The dominant driving factors for LULC changes in the Nanjing metropolitan circle were elevation, nighttime lights, and population. (3) The Nanjing metropolitan circle agglomeration experienced a carbon storage increase of 0.50 Tg under the EP scenario and losses of 1.74, 3.56, and 0.48 Tg under the ND, ED, and CD scenarios from 2020–2030. (4) The conversion of cropland and forest land to artificial surface in Nanjing metropolitan circle is the main cause of carbon storage loss, and this reduced ecosystem carbon storage can be effectively offset by increasing forest ecosystem carbon storage. Overall, the CD scenario was the most appropriate for the future development of the Nanjing metropolitan circle as it balanced ED and EP. Increasing the area of forested land through afforestation can improve the carbon sink capacity of forest ecosystems and increase carbon storage in terrestrial ecosystems. The results provide new perspectives for future land resource reallocation and ED strategies on a regional scale and provide data to support the achievement of China's carbon neutrality goals.

Data availability statement

The original contributions presented in the study are included in the article/supplementary material, further inquiries can be directed to the corresponding author.

Author contributions

YT, LT, and CW: conceptualization and writing—review and editing. YT and LT: methodology, software, and writing—original draft preparation. WD: formal analysis. LT and CW: funding acquisition. All authors contributed to the article and approved the submitted version.

Funding

This work was supported by the Major Project of Natural Science Research of Anhui Provincial Department of Education (no. KJ2021ZD0130), the Project of Physical Geographic Environment Intelligent Technology Industry Innovation, the Scientific Research Projects of Anhui Higher Education Institutions (no. 2022AH010066),

and the Postgraduate Research and Practice Innovation Program of Jiangsu Province (KYCX22_1114).

Conflict of interest

The authors declare that the research was conducted in the absence of any commercial or financial relationships that could be construed as a potential conflict of interest.

Publisher's note

References

Angelsen, A., and Kaimowitz, D. (1999). Rethinking the causes of deforestation: lessons from economic models. *World Bank Res. Obs.* 14, 73–98. doi: 10.1093/wbro/14.1.73

Arneth, A., Brown, C., and Rounsevell, M. D. A. (2014). Global models of human decision-making for land-based mitigation and adaptation assessment. *Nat. Clim. Chang.* 4, 550–557. doi: 10.1038/nclimate2250

Ayanlade, A. (2016). Seasonality in the daytime and night-time intensity of land surface temperature in a tropical city area. *Sci. Total Environ.* 557-558, 415–424. doi: 10.1016/j.scitotenv.2016.03.027

Babbar, D., Areendran, G., Sahana, M., Sarma, K., Raj, K., and Sivadas, A. (2021). Assessment and prediction of carbon sequestration using Markov chain and InVEST model in Sariska Tiger Reserve. *J. Clean. Prod.* 278:123333. doi: 10.1016/j.jclepro.2020.123333

Bennett, M. M., and Smith, L. C. (2017). Advances in using multitemporal night-time lights satellite imagery to detect, estimate, and monitor socioeconomic dynamics. *Remote Sens. Environ.* 192, 176–197. doi: 10.1016/j.rse.2017.01.005

Bukoski, J. J., Dronova, I., and Potts, M. D. (2022). Net loss statistics underestimate carbon emissions from mangrove land use and land cover change. *Ecography* 2022:e05982. doi: 10.1111/ecog.05982

Cao, S. X., Chen, L., and Liu, Z. D. (2009). An investigation of Chinese attitudes toward the environment: case study using the grain for green project. *Ambio* 38, 55–64. doi: 10.1579/0044-7447-38.1.55

Cramer, W., Guiot, J., Fader, M., Garrabou, J., Gattuso, J. P., Iglesias, A., et al. (2018). Climate change and interconnected risks to sustainable development in the Mediterranean. *Nat. Clim. Chang.* 8, 972–980. doi: 10.1038/s41558-018-0299-2

Dybala, K. E., Steger, K., Walsh, R. G., Smart, D. R., Gardali, T., and Seavy, N. E. (2019). Optimizing carbon storage and biodiversity co-benefits in reforested riparian zones. *J. Appl. Ecol.* 56, 343–353. doi: 10.1111/1365-2664.13272

Eigenbrod, F., Bell, V. A., Davies, H. N., Heinemeyer, A., Armsworth, P. R., and Gaston, K. J. (2011). The impact of projected increases in urbanization on ecosystem services. *Proce. R. Soc. Lond. Ser. B Biol. Sci.* 278, 3201–3208. doi: 10.1098/rspb.2010.2754

Fang, Z., Ding, T. H., Chen, J. Y., Xue, S., Zhou, Q., Wang, Y. D., et al. (2022). Impacts of land use/land cover changes on ecosystem services in ecologically fragile regions. *Sci. Total Environ.* 831:154967. doi: 10.1016/j.scitotenv.2022.154967

Fang, J.Y., Zhu, J.X., Li, P., Ji, C.J., Zhu, J.L., Jiang, L., et al. (2021). *Carbon Budgets of Forest Ecosystems in China*. Beijing, China: Science Press.

Feddema, J. J., Oleson, K. W., Bonan, G. B., Mearns, L. O., Buja, L. E., Meehl, G. A., et al. (2005). The importance of land-cover change in simulating future climates. *Science* 310, 1674–1678. doi: 10.1126/science.1118160

Foley, J. A., DeFries, R., Asner, G. P., Barford, C., Bonan, G., Carpenter, S. R., et al. (2005). Global consequences of land use. *Science* 309, 570–574. doi: 10.1126/science.1111772

Gao, J., and Wang, L. C. (2019). Embedding spatiotemporal changes in carbon storage into urban agglomeration ecosystem management - a case study of the Yangtze River Delta. *J. Clean. Prod.* 237:117764. doi: 10.1016/j.jclepro.2019.117764

Gauthier, S., Bernier, P., Burton, P. J., Edwards, J., Isaac, K., Isabel, N., et al. (2014). Climate change vulnerability and adaptation in the managed. *Environ. Rev.* 22, 256–285. doi: 10.1139/er-2013-0064

Guan, D. J., Zhao, Z. L., and Tan, J. (2019). Dynamic simulation of land use change based on logistic-CA-Markov and WLC-CA-Markov models: a case study in three gorges reservoir area of Chongqing. *Umweltwissenschaften und Schadstoff-Forschung* 26, 20669–20688. doi: 10.1007/s11356-019-05127-9

He, C. Y., Zhang, D., Huang, Q. X., and Zhao, Y. Y. (2016). Assessing the potential impacts of urban expansion on regional carbon storage by linking the LUSD-urban and InVEST models. *Environ. Model. Softw.* 75, 44–58. doi: 10.1016/j.envsoft.2015.09.015

Homer, C., Dewitz, J., Jin, S. M., Xian, G., Costello, C., Danielson, P., et al. (2020). Conterminous United States land cover change patterns 2001-2016 from the 2016 National Land Cover Database. *Photogrammetria* 162, 184–199. doi: 10.1016/j.isprsjprs.2020.02.019

Huang, X., Wen, D. W., Li, J. Y., and Qin, R. J. (2017). Multi-level monitoring of subtle urban changes for the megacities of China using high-resolution multi-view satellite imagery. *Remote Sens. Environ.* 196, 56–75. doi: 10.1016/j.rse.2017.05.001

Huppmann, D., Rogelj, J., Kriegler, E., Krey, V., and Riahi, K. (2018). A new scenario resource for integrated 1.5 degrees C research. *Nat. Clim. Chang.* 8, 1027–1030. doi: 10.1038/s41558-018-0317-4

Jiang, W. G., Deng, Y., Tang, Z. H., Lei, X., and Chen, Z. (2017). Modelling the potential impacts of urban ecosystem changes on carbon storage under different scenarios by linking the CLUE-S and the InVEST models. *Ecol. Model.* 345, 30–40. doi: 10.1016/j.ecolmodel.2016.12.002

Lal, P., Dubey, A. K., Kumar, A., Kumar, P., and Dwivedi, C. S. (2022). Measuring the control of landscape modifications on surface temperature in India. *Geocarto Int.* 1-18, 1–18. doi: 10.1080/10106049.2022.2102224

Lal, P., Shekhar, A., and Kumar, A. (2021). Quantifying temperature and precipitation change caused by land cover change: a case study of India using the WRF model. *Front. Environ. Sci.* 9:588. doi: 10.3389/fenvs.2021.766328

Lambin, E. F., and Meyfroidt, P. (2011). Global land use change, economic globalization, and the looming land scarcity. *PNAS Nexus* 108, 3465–3472. doi: 10.1073/pnas.1100480108

Lan, F., Gong, X. Y., Da, H. L., and Wen, H. Z. (2020). How do population inflow and social infrastructure affect urban vitality? Evidence from 35 large-and medium-sized cities in China. *Cities* 100:102454. doi: 10.1016/j.cities.2019.102454

Lawal, S., Lennard, C., and Hewitson, B. (2019). Response of southern African vegetation to climate change at 1.5 and 2.0 degrees global warming above the pre-industrial level. *Clim. Serv.* 16, 100134–100116. doi: 10.1016/j.cliser.2019.100134

Lee, R. J. (2021). Vacant land, flood exposure, and urbanization: examining land cover change in the Dallas-Fort Worth metro area. *Landsc. Urban Plan.* 209:104047. doi: 10.1016/j.landurbplan.2021.104047

Li, S. C., Bing, Z. L., and Jin, G. (2019). Spatially explicit mapping of soil conservation Service in Monetary Units due to land use/cover change for the three gorges reservoir area, China. *Remote Sens.* 11:468. doi: 10.3390/rs11040468

Li, J. Y., Chen, X., Kurban, A., Van de Voorde, T., De Maeyer, P., and Zhang, C. (2021). Coupled SSPs-RCPs scenarios to project the future dynamic variations of water-soil-carbon-biodiversity services in Central Asia. *Ecol. Indic.* 129:107936. doi: 10.1016/j.ecolind.2021.107936

Li, J. Y., Gong, J., Guldmann, J. M., Li, S. C., and Zhu, J. (2020). Carbon dynamics in the northeastern Qinghai-Tibetan plateau from 1990 to 2030 using Landsat land use/cover change data. *Remote Sens.* 12:528. doi: 10.3390/rs12030528

Li, X. C., Zhou, Y. Y., Zhu, Z. Y., Liang, L., Yu, B. L., and Cao, W. T. (2018). Mapping annual urban dynamics (1985-2015) using time series of Landsat data. *Remote Sens. Environ.* 216, 674–683. doi: 10.1016/j.rse.2018.07.030

Liang, X., Guan, Q. F., Clarke, K. C., Chen, G. Z., Guo, S., and Yao, Y. (2021a). Mixed-cell cellular automata: a new approach for simulating the spatio-temporal dynamics of mixed land use structures. *Landscape Urban Plan.* 205:103960. doi: 10.1016/j.landurbplan.2020.103960

Liang, X., Guan, Q. F., Clarke, K. C., Liu, S. S., Wang, B. Y., and Yao, Y. (2021b). Understanding the drivers of sustainable land expansion using a patch-generating land use simulation (PLUS) model: a case study in Wuhan. *Comput. Environ. Urban. Syst.* 85:101569. doi: 10.1016/j.compenvurbsys.2020.101569

Liang, X., Liu, X. P., Li, X., Chen, Y. M., Tian, H., and Yao, Y. (2018). Delineating multi-scenario urban growth boundaries with a CA-based FLUS model and morphological method. *Landscape Urban Plan.* 177, 47–63. doi: 10.1016/j.landurbplan.2018.04.016

Liao, Q. P., Liu, X. R., and Xiao, M. Z. (2022). Ecological restoration and carbon sequestration regulation of mining areas-a case study of Huangshi City. *Int. J. Env. Res. Public Health* 19:4175. doi: 10.3390/ijerph19074175

Liu, Z. F., He, C. Y., Zhang, Q. F., Huang, Q. X., and Yang, Y. (2012). Extracting the dynamics of urban expansion in China using DMSP-OLS nighttime light data from 1992 to 2008. *Landscape Urban Plan.* 106, 62–72. doi: 10.1016/j.landurbplan.2012.02.013

Liu, X. P., Huang, Y. H., Xu, X. C., Li, X. C., Li, X., Ciais, P., et al. (2020). High-spatiotemporal-resolution mapping of global urban change from 1985 to 2015. *Nat. Sustain.* 3, 564–570. doi: 10.1038/s41893-020-0521-x

Liu, X. P., Liang, X., Li, X., Xu, X. C., Ou, J. P., Chen, Y. M., et al. (2017). A future land use simulation model (FLUS) for simulating multiple land use scenarios by coupling human and natural effects. *Landscape Urban Plan.* 168, 94–116. doi: 10.1016/j.landurbplan.2017.09.019

Long, Y., Han, H. Y., Lai, S. K., and Mao, Q. Z. (2013). Urban growth boundaries of the Beijing metropolitan area: comparison of simulation and artwork. *Cities* 31, 337–348. doi: 10.1016/j.cities.2012.10.013

Lu, M., Zhou, X. H., Yang, Q., Li, H., Luo, Y. Q., Fang, C. M., et al. (2013). Responses of ecosystem carbon cycle to experimental warming: a meta-analysis. *Ecology* 94, 726–738. doi: 10.1890/12-0279.1

Luo, G. P., Yin, C. Y., Chen, X., Xu, W. Q., and Lu, L. (2010). Combining system dynamic model and CLUE-S model to improve land use scenario analyses at regional scale: a case study of Sangong watershed in Xinjiang, China. *Ecol. Complex.* 7, 198–207. doi: 10.1016/j.ecocom.2010.02.001

Ma, T., Zhou, C., Pei, T., Haynie, S., and Fan, J. (2012). Quantitative estimation of urbanization dynamics using time series of DMSP/OLS nighttime light data: a comparative case study from China's cities. *Remote Sens. Environ.* 124, 99–107. doi: 10.1016/j.rse.2012.04.018

Meyfroidt, P., de Bremond, A., Ryan, C. M., Archer, E., Aspinall, R., Chhabra, A., et al. (2022). Ten facts about land systems for sustainability. *P. Natl. Acad. Sci. U. S. A.* 119:e2109217118. doi: 10.1073/pnas.2109217118

Molotoks, A., Stehfest, E., Doelman, J., Albanito, F., Fitton, N., Dawson, T. P., et al. (2018). Global projections of future cropland expansion to 2050 and direct impacts on biodiversity and carbon storage. *Glob. Chang. Biol.* 24, 5895–5908. doi: 10.1111/gcb.14459

Munsi, M., Areendran, G., and Joshi, P. K. (2012). Modeling spatio-temporal change patterns of forest cover: a case study from the Himalayan foothills (India). *Reg. Environ. Chang.* 12, 619–632. doi: 10.1007/s10113-011-0272-3

National Bureau of Statistics (2021). *China Statistical Yearbook*. Beijing: China Statistics Press.

Nelson, E., Mendoza, G., Regetz, J., Polasky, S., Tallis, H., Cameron, D. R., et al. (2009). Modeling multiple ecosystem services, biodiversity conservation, commodity production, and tradeoffs at landscape scales. *Front. Ecol. Environ.* 7, 4–11. doi: 10.1890/080023

Nelson, E., Sander, H., Hawthorne, P., Conte, M., Ennaanay, D., Wolny, S., et al. (2010). Projecting global land-use change and its effect on ecosystem service provision and biodiversity with simple models. *PLoS One* 5:e14327. doi: 10.1371/journal.pone.0014327

Newbold, T., Hudson, L. N., Hill, S. L. L., Contu, S., Lysenko, I., Senior, R. A., et al. (2015). Global effects of land use on local terrestrial biodiversity. *Nature* 520, 45–50. doi: 10.1038/nature14324

Nor, A. N. M., Corstanje, R., Harris, J. A., and Brewer, T. (2017). Impact of rapid urban expansion on green space structure. *Ecol. Indic.* 81, 274–284. doi: 10.1016/j.ecolind.2017.05.031

Noss, R. F. (2001). Beyond Kyoto: Forest management in a time of rapid climate change. *Conserv. Biol.* 15, 578–590. doi: 10.1046/j.1523-1739.2001.015003578.x

Popp, A., Humpenöder, F., Weindl, I., Bodirsky, B. L., Bonsch, M., Lotze-Campen, H., et al. (2014). Land-use protection for climate change mitigation. *Nat. Clim. Chang.* 4, 1095–1098. doi: 10.1038/nclimate2444

Powers, R. P., and Jetz, W. (2019). Global habitat loss and extinction risk of terrestrial vertebrates under future land-use-change scenarios. *Nat. Clim. Chang.* 9, 323–329. doi: 10.1038/s41558-019-0406-z

Rogelj, J., Shindell, D., Jiang, K., Fifita, S., Forster, P., Ginzburg, V., et al. (2018). "Mitigation pathways compatible with 1.5°C in the context of sustainable development," in *Global Warming of 1.5°C. An IPCC Special Report on the Impacts of Global Warming of 1.5°C Above Pre-industrial Levels and Related Global Greenhouse Gas Emission Pathways, in the Context of Strengthening the Global Response to the Threat of Climate Change, Sustainable Development, and Efforts to Eradicate Poverty.* eds. V. Masson-Delmotte, P. Zhai, H.-O. Pörtner, D. Roberts, J. Skea, P. R. Shukla, et al. (Geneva, Switzerland: Intergovernmental Panel on Climate Change/World Meteorological Organization), 93–174.

Schoenberger, E., and Walker, R. A. (2017). Beyond exchange and agglomeration: resource flows and city environments as wellsprings of urban growth. *J. Econ. Geogr.* 17, lbw012–lbw958. doi: 10.1093/jeg/lbw012

Sharp, R., Douglass, J., Wolny, S., Arkema, K., Bernhardt, J., Bierbower, W., et al. (2020). *InVEST 3.10.2 User's Guide, the Natural Capital Project*. Stanford University: Stanford, CA, USA; University of Minnesota: Minneapolis, MN, USA; The Nature Conservancy, and World Wildlife Fund: Arlington, VI, USA.

Shi, K. F., Yu, B. L., Huang, Y. X., Hu, Y. J., Yin, B., Chen, Z. Q., et al. (2014). Evaluating the ability of NPP-VIIRS nighttime light data to estimate the gross domestic product and the electric power consumption of China at multiple scales: a comparison with DMSP-OLS data. *Remote Sens.* 6, 1705–1724. doi: 10.3390/rs6021705

Sleeter, B. M., Wilson, T. S., Sharygin, E., and Sherba, J. T. (2017). Future scenarios of land change based on empirical data and demographic trends. *Earths Future* 5, 1068–1083. doi: 10.1002/2017ef000560

Solomon, S., Plattner, G. K., Knutti, R., and Friedlingstein, P. (2009). Irreversible climate change due to carbon dioxide emissions. *Proc. Natl. Acad. Sci. U. S. A.* 106, 1704–1709. doi: 10.1073/pnas.0812721106

Sun, L. L., Cui, H. J., and Ge, Q. S. (2022). Will China achieve its 2060 carbon neutral commitment from the provincial perspective? *Adv. Clim. Chang. Res.* 13, 169–178. doi: 10.1016/j.accre.2022.02.002

Tang, X. J., Woodcock, C. E., Olofsson, P., and Hutyra, L. R. (2021). Spatiotemporal assessment of land use/land cover change and associated carbon emissions and uptake in the Mekong River basin. *Remote Sens. Environ.* 256:112336. doi: 10.1016/j.rse.2021.112336

Thonfeld, F., Steinbach, S., Muro, J., Hentze, K., Games, I., Naschen, K., et al. (2020). The impact of anthropogenic land use change on the protected areas of the Kilombero catchment. *ISPRS J. Photogramm. Remote Sens.* 168, 41–55. doi: 10.1016/j.isprsjprs.2020.07.019

Tian, L., and Fu, W. (2020). Bi-temporal analysis of spatial changes of boreal Forest cover and species in Siberia for the years 1985 and 2015. *Remote Sens.* 12:4116. doi: 10.3390/rs12244116

Tian, L., Fu, W. X., Tao, Y., Li, M. Y., and Wang, L. (2022a). Dynamics of the alpine timberline and its response to climate change in the Hengduan mountains over the period 1985-2015. *Ecol. Indic.* 135:108589. doi: 10.1016/j.ecolind.2022.108589

Tian, L., Tao, Y., Fu, W. X., Li, T., Ren, F., and Li, M. Y. (2022b). Dynamic simulation of land use/cover change and assessment of Forest ecosystem carbon storage under climate change scenarios in Guangdong Province, China. *Remote Sens.* 14:2330. doi: 10.3390/rs14102330

United Nations Environment Programme (2019). *Emissions Gap Report 2019*. Nairobi: UNEP.

Wang, Z. Y., Li, X., Mao, Y. T., Li, L., Wang, X. R., and Lin, Q. (2022). Dynamic simulation of land use change and assessment of carbon storage based on climate change scenarios at the city level: a case study of Bortala, China. *Ecol. Indic.* 134:108499. doi: 10.1016/j.ecolind.2021.108499

Wang, Y., Li, X. M., Zhang, Q., Li, J. F., and Zhou, X. W. (2018). Projections of future land use changes: multiple scenarios-based impacts analysis on ecosystem services for Wuhan city, China. *Ecol. Indic.* 94, 430–445. doi: 10.1016/j.ecolind.2018.06.047

Wang, Z. H., Liu, H. M., Guan, Q. W., Wang, X. J., Hao, J. P., Ling, N., et al. (2011). Carbon storage and density of urban forest ecosystems in Nanjing. *J. Nanjing For. Univ.* 35, 18–22. doi: 10.3969/j.issn.1000-2006.2011.04.004

Weisberg, P. J., Lingua, E., and Pillai, R. B. (2007). Spatial patterns of pinyon-juniper woodland expansion in Central Nevada. *Rangel. Ecol. Manag.* 60, 115–124. doi: 10.2111/05-224r2.1

Wilfried, T. (2007). Biodiversity: climate change and the ecologist. *Nature* 448, 550–552. doi: 10.1038/448550a

Winkler, K., Fuchs, R., Rounsevell, M., and Herold, M. (2021). Global land use changes are four times greater than previously estimated. *Nat. Commun.* 12:2501. doi: 10.1038/s41467-021-22702-2

Wu, H., Li, Z., Clarke, K. C., Shi, W. Z., Fang, L. C., Lin, A. Q., et al. (2019). Examining the sensitivity of spatial scale in cellular automata Markov chain simulation of land use change. *Int. J. Geogr. Inf. Sci.* 33, 1040–1061. doi: 10.1080/13658816.2019.1568441

Wu, Y., Tao, Y., Yang, G. S., Ou, W. X., Pueppke, S., Sun, X., et al. (2019). Impact of land use change on multiple ecosystem services in the rapidly urbanizing Kunshan City of China: past trajectories and future projections. *Land Use Policy* 85, 419–427. doi: 10.1016/j.landusepol.2019.04.022

Xiao, J. F. (2014). Satellite evidence for significant biophysical consequences of the "grain for green" program on the loess plateau in China. *J. Geophys. Res. Biogeosci.* 119, 2261–2275. doi: 10.1002/2014jg002820

Xu, T. T., Gao, J., and Coco, G. (2019). Simulation of urban expansion via integrating artificial neural network with Markov chain - cellular automata. *Int. J. Geogr. Inf. Sci.* 33, 1960–1983. doi: 10.1080/13658816.2019.1600701

Xu, L., He, N. P., and Yu, G. R. (2014). A dataset of carbon density in Chinese terrestrial ecosystems (2010s). *China Science Data* 4, 90–96.

Yang, X., Chen, R., and Zheng, X. Q. (2016). Simulating land use change by integrating ANN-CA model and landscape pattern indices. *Geomat. Nat. Haz. Risk* 7, 918–932. doi: 10.1080/19475705.2014.1001797

Yang, H., Huang, J. L., and Liu, D. F. (2020). Linking climate change and socioeconomic development to urban land use simulation: analysis of their concurrent effects on carbon storage. *Appl. Geogr.* 115:102135. doi: 10.1016/j.apgeog.2019.102135

Yee, S. H., Paulukonis, E., Simmons, C., Russell, M., Fulford, R., Harwell, L., et al. (2021). Projecting effects of land use change on human well-being through changes in ecosystem services. *Ecol. Model.* 440:109358. doi: 10.1016/j.ecolmodel.2020.109358

Zhai, H., Lv, C. Q., Liu, W. Z., Yang, C., Fan, D. S., Wang, Z. K., et al. (2021). Understanding Spatio-temporal patterns of land use/land cover change under urbanization in Wuhan, China, 2000-2019. *Remote Sens.* 13:3331. doi: 10.3390/rs13163331

Zhang, K., Dang, H., Tan, S., Cheng, X., and Zhang, Q. (2010). Change in soil organic carbon following the 'grain-for-green' programme in China. *Land Degrad. Dev.* 21, 13–23. doi: 10.1002/ldr.954

Zhang, X., and Gu, R. X. (2022). Spatio-temporal pattern and multi-scenario simulation of land use conflict: a case study of the Yangtze River Delta urban agglomeration. *Geogr. Res.* 41:16. doi: 10.11821/dlyj020210375

Zhang, Q. W., and Su, S. L. (2016). Determinants of urban expansion and their relative importance: a comparative analysis of 30 major metropolitans in China. *Habitat Int.* 58, 89–107. doi: 10.1016/j.habitatint.2016.10.003

Zhang, Y. W., and Xie, H. L. (2019). Interactive relationship among urban expansion, economic development, and population growth since the reform and opening up in China: an analysis based on a vector error correction model. *Land* 8:153. doi: 10.3390/land8100153

Zhang, S. H., Zhong, Q. L., Cheng, D. L., Xu, C. B., Chang, Y. N., Lin, Y. Y., et al. (2022). Landscape ecological risk projection based on the PLUS model under the localized shared

socioeconomic pathways in the Fujian Delta region. *Ecol. Indic.* 136:108642. doi: 10.1016/j.ecolind.2022.108642

Zhao, M. M., He, Z. B., Du, J., Chen, L. F., Lin, P. F., and Fang, S. (2019). Assessing the effects of ecological engineering on carbon storage by linking the CA-Markov and InVEST models. *Ecol. Indic.* 98, 29–38. doi: 10.1016/j.ecolind.2018.10.052

Zhu, S. Y., Kong, X. S., and Jiang, P. (2020). Identification of the human-land relationship involved in the urbanization of rural settlements in Wuhan city circle, China. *J. Rural Stud.* 77, 75–83. doi: 10.1016/j.jrurstud.2020.05.004

Zhu, G. F., Qiu, D. D., Zhang, Z. A. X., Sang, L. Y., Liu, Y. W., Wang, L., et al. (2021). Land-use changes lead to a decrease in carbon storage in arid region, China. *Ecol. Indic.* 127:107770. doi: 10.1016/j.ecolind.2021.107770

frontiers | Frontiers in Ecology and Evolution

TYPE Original Research
PUBLISHED 20 February 2023
DOI 10.3389/fevo.2023.1110594

OPEN ACCESS

EDITED BY
Cuicui Jiao,
Sichuan University of Science and Engineering, China

REVIEWED BY
Xulin Guo,
University of Saskatchewan, Canada
Wei Zhao,
Institute of Geographic Sciences and Natural Resources Research (CAS), China

*CORRESPONDENCE
Guoliang Liu
✉ gliu@aitree.ltd
Zhonghui Zhang
✉ zzhgiszzh@163.com

†These authors have contributed equally to this work and share first authorship

SPECIALTY SECTION
This article was submitted to Population, Community, and Ecosystem Dynamics, a section of the journal Frontiers in Ecology and Evolution

RECEIVED 29 November 2022
ACCEPTED 31 January 2023
PUBLISHED 20 February 2023

CITATION
Cheng F, Tian J, He J, He H, Liu G, Zhang Z and Zhou L (2023) The spatial and temporal distribution of China's forest carbon. *Front. Ecol. Evol.* 11:1110594. doi: 10.3389/fevo.2023.1110594

The spatial and temporal distribution of China's forest carbon

Fushan Cheng[1†], Jiaxin Tian[2†], Jingyuan He[1], Huaijiang He[3,4], Guoliang Liu[1,5*], Zhonghui Zhang[3,4*] and Liping Zhou[6]

[1]College of Forestry, Beijing Forestry University, Beijing, China, [2]College of Forestry, Northeast Forestry University, Harbin, China, [3]Jilin Provincial Academy of Forestry Sciences, Jilin, China, [4]Jilin Province Degraded Forest Ecosystem Restoration and Reconstruction Interregional Cooperation Science and Technology Innovation Center, Jilin, China, [5]Nanjing Jialin System Engineering Ltd, Nanjing, China, [6]Shenyang Forestry Management Institute of China Railway Shenyang Bureau Group Co. Ltd, Shenyang, China

Introduction: China's forests have sequestrated a significant amount of carbon over the past two decades. However, it is not clear whether China's forests will be able to continue to have as much carbon sequestration potential capacity in the future.

Methods: In order to research China's forest carbon storage and carbon sequestration potential capacities at spatial and temporal scales, we built a digital forest model for each province of China using the data from The China Forest Resources Report (2014– 2018) and calculated the carbon storage capacity and sequestration potential capacity of each province with the current management practices without considering natural successions.

Results: The results showed that the current forest carbon storage is 10.0 Pg C, and the carbon sequestration potential in the next 40 years (from year 2019 to 2058) will be 5.04 Pg C. Since immature forests account for the majority of current forests, the carbon sequestration capacity of the forest was also high (0.202 Pg C year–1). However, the forest carbon storage reached the maximum with the increase of stand maturity. At this time, if scenarios such as afforestation and reforestation, human and natural disturbances, and natural succession are not considered, the carbon sequestration capacity of forests will continue to decrease. After 90 years, all stands will develop into mature and over-mature forests, and the forest carbon sequestration capacity is 0.008 Pg year–1; and the carbon sequestration rate is ~4% of what it is nowadays. The change trend of forest carbon in each province is consistent with that of the country. In addition, considering the large forest coverage area in China, the differences in tree species and growing conditions, the forest carbon storage and carbon sequestration capacities among provinces were different. The growth rate of carbon density in high-latitude provinces (such as Heilongjiang, Jilin, and Inner Mongolia) was lower than that in the south (Guangdong, Guangxi, or Hunan), but the forest carbon potential was higher.

Discussion: Planning and implementing targeted forest management strategies is the key to increasing forest carbon storage and extending the service time of forest carbon sinks in provinces. In order to reach the national carbon neutrality goals, we recommend that each province have an informative strategic forest management plan.

KEYWORDS

forest carbon storage, carbon sequestration, forest carbon modeling, national and provincial scale, spatial–temporal distribution

1. Introduction

Since the Industrial Revolution, a large amount of fossil fuel has been utilized and a significant amount of carbon dioxide has been released into the atmosphere. The carbon emission is far more than the amount absorbed by the marine and terrestrial ecosystems. Forest carbon sequestration is the most cost effective nature-based way to reduce the CO_2 in the atmosphere (Münnich Vass, 2017). Accurate estimates of carbon storage and the carbon sequestration potential of forests are critical for achieving the strategic goal of carbon neutrality (Broadstock et al., 2021). In order to reduce CO_2 emission, many countries and regions have promised to achieve carbon neutrality within certain time frames. At the United Nations Climate Action Summit in September 2019, 66 parties committed to achieve net-zero emissions, and China committed to achieve carbon neutrality by the year 2060 (UNFCCC, 2019). The carbon sequestration capacity depends on the photosynthesis (P) and respiration (R) potential of the trees (Jiang et al., 2020). E.P.Odum's ecological succession hypothesis is one of the main hypotheses to explain the overall development of forest community. Trees sequestrated CO_2 through photosynthesis and released carbon through respiration. According to the hypothesis, the biomass increases in the early stage of ecological succession when $P/R > 1$. The value of P/R will be close to 1 when the stands in the forest reach mature growth. The carbon budget of the ecosystem will reach a balance, and the forest biomass will reach the maximum limit (Odum Eugene, 1969). In other words, the forest carbon sink tends to be zero when the stands in the forest reach mature stages. Meanwhile, a crucial issue has emerged for our world: if forests lost the function of doing carbon sequestration, what would be the fate of the CO_2 emitted by the industry? This is why scientists need to estimate and predict future changes in forest carbon storage and carbon sequestration capacity.

There are 4.1 billion ha forests in the world, and the annual forest carbon sequestration is about 1.1 ± 0.8 Pg C year^{-1} (Pan et al., 2011). Existing forests will continue to absorb large amounts of CO_2, but the future sequestration capacities will depend on forest management. Studies have shown signs of carbon sequestration saturation in tropical rainforests in Africa and in the Amazon (Hubau et al., 2020), tropical Borneo (Qie et al., 2017) and in parts of Europe (Nabuurs et al., 2013). The carbon sequestration rate of forests is closely related to their age structure (Pan et al., 2004). The carbon sequestration rate of young and middle-aged forest is relatively high, and the carbon sequestration capacity rate begins to decline gradually (Pregitzer and Euskirchen, 2004; Zhou et al., 2015) because of stand aging. In theory, by the end of the life cycle, trees will eventually die and become a carbon source, resulting in carbon release (Maia et al., 2020).

Since the 1970s, China has implemented large-scale afforestation and reforestation programs to protect the ecological environment. At present, the area of plantation forests in China ranks the first in the world, and the forest area has increased from 12.7% in early 1970 to 21.6% in 2013. China's forests are making a positive response to global carbon neutralization (China, S.F.A.O, 2014). Previous forest carbon sequestration studies have predicted the future carbon sequestration capacities, for example, He et al. (2017) predicted the change of carbon storage and carbon sequestration rate of Chinese forests from 2010 to 2050, Cai et al. (2022) predicted carbon sequestration rate for the time period 2010–2060, while Xu et al. (2010) predicted carbon sequestration rates for the period 2000–2050, and Yao et al. (2018) predicted carbon sequestration rate for the period 2010–2040. These results show that Chinese forests will be able to maintain a higher carbon sequestration rate and absorb more CO_2 from the atmosphere in the next 30–50 years. These studies play an important role in the specific contribution of forests to conduct carbon neutralization by the year 2060. However, how the forest carbon sequestration capacity will change after 2060 is unknown. We need to learn more about the forest carbon sequestration capacity to make smart forest management decisions to achieve and maintain carbon neutrality after the year 2060.

The Bonn Challenge[1] launched in 2011, encourages countries to restore 150 million ha of forest by 2020 and 350 million ha (Hawes, 2018) by 2030, and countries around the world have actively responded to global climate change. China has implemented a series of measures since the 1970s, such as the Three-North Shelter Forest program, the Natural Forest Protection program and many other programs. From 2001 to 2010, the total carbon sequestration of these programs was 132 Tg C year^{-1} (Lu et al., 2018), which made a significant contribution to China's current and future CO_2 emission reduction (Wang et al., 2018). So far, China has nearly 60 million ha of plantation forests, accounting for 31.76% of the total forest area in China, and most areas are still in the juvenile stages. Due to excessive deforestation over the last decades, more than 60% of the second growth natural forests are still at young and middle-age stages (Dai et al., 2018). The potential carbon sequestration capacity for the near future (from 2010 to 2060) will be significant, however, the carbon sequestration capacity for the distant future (after 2060) is not clear yet. Therefore, the analysis of forest carbon storage and carbon sequestration capacity is required at both a national scale and provincial scales.

The carbon storage and carbon sequestration capacities are particularly important for China's long-term forest management. The objectives of this research are to predict the carbon storage and sequestration capacities of China in the long-term based on the current management practice and the data of the China Forest Resources Report (2014–2018).

2. Data and Methods

2.1. Data collection and compilation

China is located in the northern hemisphere, with forests covering a wide range of latitudes from north to south. The latitude and climatic differences between the north and south of China make the country's climate complex and diverse. The latitudinal spatial of forests makes China's forest types diverse, such as tropical rain forests, subtropical evergreen broad-leaved forests, warm temperate deciduous broad-leaved forests, temperate coniferous and broad-leaved mixed forests, and cold temperate coniferous forests. The longitude spatial makes the country's forests mainly concentrated in the east, and the west is mostly grassland and desert.

Since the 1970s, every 5 years, the State Forestry Administration of China has published statistics about forest resources. According to the data, forests are divided into three major categories: arborescence forest, economic forests and bamboo forests (this study does not include economic forests or bamboo forests). Furthermore, according

1 www.bonnchallenge.org

to the dominant tree species, the forest was divided into 36 forest types, and each forest type was divided into five age classes: young forest, middle-aged forest, premature forest, mature forest and over-mature forest. The classification of age classes will be carried out with the age classes and age groups of main tree species in the Technical Regulations on Forest Resource Inventory of China (Supplementary Table 1; Administration, C.S.F, 2014). The study covers the entire national forest area of 31 provinces of China.

The key to the prediction of forest carbon storage is to understand the relationship between biomass accumulation and forest ages. In recent years, many studies have found that the Logistic equation can better describe the relationship between biomass density and forest ages (Zhou et al., 2014; He et al., 2017). Xu et al. (2010) used the logistic function to fit the biomass growth curves statistically. In this study, we used the logistic curves of forest stand types by Xu, combined with the latest national forest inventory data in China, to calculate and predict the forest carbon storage capacities of each province.

$$B = \frac{w}{1 + ke^{ct}} \tag{1}$$

where B is the biomass density (Mg C ha^{-1}); t is the forest age (year); w k and c are the model parameters. Xu used China's forest data to fit logistic curves of biomass and age of different forest types. We can see the fitted parameter values (w k and c) for each forest type in Supplementary Table 2.

2.2. Carbon storage calculations

China Certified Emission Reduction (CCER) was launched in 2011, from which the development of forestry carbon sequestration projects has attracted widespread attention from around the world (Ye et al., 2021). At present, the CCER forestry carbon sequestration project is divided into Afforestation carbon sequestration methodology, forest management and carbon sequestration methodology, bamboo afforestation carbon sequestration methodology, and bamboo management and carbon sequestration methodology. Those methodologies accord with the present situation of ecological development in China, and have the characteristics of being universal, cost effective, and environmentally integrated as well as being scientific and reasonable (Li L. et al., 2019).

Forest management and carbon calculation methodology was used to calculate the carbon storage amount of each province. The carbon storage amount mainly included four carbon pools, living trees, dead trees, litter, and harvested wood production. The carbon storage of this study was calculated and predicted based on the current forest area without considering afforestation and reforestation, or any human and natural disturbances in the future using Eq. 2.

$$C_{Forest} = \sum_{j=1}^{M}\sum_{t=0}^{T}\sum_{i=1}^{N}\begin{pmatrix} C_{Tree,jti} + C_{CDW,jti} \\ +C_{Litter,jti} + C_{HWP,jti} \end{pmatrix} \times A_i \tag{2}$$

where C_{Forest} is the total forest carbon of the country; C_{Tree}, C_{CDW}, C_{Litter}, C_{HWP} represent the carbon pools of live trees, dead wood, litter carbon, and harvested wood production, respectively; A is the total area of each forest stand type; i, t, and j parameters represent the forest stand types, age groups, and provinces. C_{Tree} is generally calculated as the biomass multiplied by the carbon density of each tree species. Many studies used the default values of 0.5 to transfer biomass to carbon storage (Taeroe et al., 2017; Cai et al., 2022; Chen et al., 2022), but there were significant differences in carbon density among different species. The average carbon density of the deciduous species was <0.5, and the coniferous species was higher than 0.5. We calculated the carbon storage using the average carbon density of each tree species based on the Forestry Standard—Standing tree Biomass Model and Carbon parameters (forestry standard number: LY/T2258-2014, LY/T2259-2014, LY/T2260-2014, LY/T2261-2014, LY/T2262-2014, LY/T2263-2014, LY/T2264-2014, LY/T2655-2016, LY/T2654-2016, LY/T2659-2016, LY/T2661-2016, LY/T2660-2016, LY/T2656-2016, LY/T2657-2016, LY/T2658-2016). In addition, C_{HWP} is equal to zero because forest harvesting was not involved in this study.

The biomass of the whole tree was mainly composed of two parts: aboveground biomass and belowground biomass. Most studies ignore the belowground biomass or use the average ratio of 0.25 given by FAO (Chen et al., 2022). We calculated the belowground carbon according to the ratio of belowground biomass to aboveground biomass of each tree species given by the National Greenhouse Gas Inventory Report of China 2005 (Commission, N.D.a.r, 2014) as Eqs 3, 4.

$$C_{Tree,i} = B_{Tree,i} \times CF_i \tag{3}$$

$$B_{Tree} = B_{AGB}\left(1 + \frac{B_{BGB}}{B_{AGB}}\right) \tag{4}$$

where CF_i is the carbon density of the tree species i. B_{Tree} is the live tree biomass. B_{AGB} and B_{BGB} represent aboveground biomass and belowground biomass, respectively.

$$C_{CWD,i} = C_{Tree,i} \times DF_{CWD,i} \tag{5}$$

where $C_{CWD,i}$ is the dead wood carbon of tree species i; $C_{Tree,i}$ is live tree carbon; $DF_{CWD,i}$ is the ratio of dead wood carbon and live tree carbon of tree species i.

According to the Chinese forest biomass database, we discovered that the correlation between the ratio of litter biomass to the aboveground biomass and aboveground biomass was given by Eq. 6.

$$C_{Litter,i} = f_{Litter}\left(B_{AGB}\right) \times CF_{Litter,i} \tag{6}$$

where C_{Litter} is litter carbon of the tree species i; $CF_{Litter,i}$ is the carbon rate of litter in tree species i, and 0.37 is the amount of C per kg of dry litter biomass; $f_{Litter}\left(B_{AGB}\right)$ is the percentage of litter biomass to the aboveground biomass (%).

2.3. Carbon storage predictions

In our study, the entire carbon pool change was affected by the changes of trees, dead wood, and litter. We did not consider the

changes of soil organic carbon pool and carbon storage of shrub and grass under the forest. In addition, the change of carbon pool caused by extreme climate (fire, flood, and drought) was not within the scope of our study. This function was used to determine forest carbon sequestration capacity:

$$C_{Total\_t1} = C_{t0} + \Delta C_{Tree\_t1-t0} + \Delta C_{CDW\_t1-t0} + \Delta C_{Litter\_t1-t0} \quad (7)$$

where C_{Total_t1} is the total carbon stock in year t1; C_{t0} is the current carbon storage; ΔC_{CDW_t1-t0}, and ΔC_{Litter_t1-t0} represent the variation of the change of carbon storage of trees, dead wood, and litter during t1-t0, respectively. Forest Simulation and Optimization System (FSOS)[2] were used for the analysis in this study (Liu et al., 2006). FSOS is a forest planning system with artificial intelligence algorithm to balance and optimize multiple forest functions using cloud computing. FSOS is a widely used decision support system with stand dynamic modeling and landscape modeling.

3. Results

3.1. Temporal patterns of forest carbon storage and carbon sequestration capacity

The current forest carbon storage in China is 10.0 Pg, and this rate will continue to increase in the future. The total carbon storage will increase from 10.0 Pg to 16.2 Pg, with a total growth potential of 62% in the next 200 years (Figure 1). The total forest carbon storage will increase gradually and attain a stable stage with the increase of time. On the national scale, the carbon sequestration capacity has already reached its peak and has begun to gradually decrease. Forest carbon sequestration capacity is currently the greatest (0.202 Pg year^{-1}), and the decline of forest carbon sequestration capacity has changed from fast to slow, which is what it will be in the future. If forests continue to develop at this trend, they will play a smaller role in achieving the goal of carbon neutrality.

Using the age and age classification of each forest type, we drew a national forest age structure figure. At present, the forest area of each age class accounts for 32.67% (young forest), 30.39% (middle-aged forest), 15.59% (premature forest), 14.11% (mature forest), and 7.24% (overmature forest) of the total forest area, respectively (Figure 2). Combined with the changes of forest carbon sequestration capacity, the current forests are mainly young, and the carbon sequestration capacity is at its peak. The proportion of young and middle-aged forests gradually decreased with stands beginning to age. The forest will change from a young state to a mature state, and the carbon sequestration capacity also will decrease. After 35 years, all the young forests will have been transformed into middle-aged forests, and the carbon sequestration capacity will drop from 0.202 Pg year^{-1} to 0.063 Pg year^{-1}; additionally, the carbon sequestration rate might decrease 69%. The middle-aged forest will develop into premature forests over the next 70 years, the carbon sequestration capacity of the forest will be 0.016 Pg year^{-1}, and the carbon sequestration capacity will decrease by 92%. After 90 years, all the stands will have developed into mature and overmature forests, and the carbon sequestration capacity of forest will be 0.008 Pg year^{-1}, and the carbon sequestration rate will be ~4% of the current forest carbon sequestration capacity. When the forest is all overmature (after 130 years), the carbon sequestration capacity will be 0.0017 Pg year^{-1}, and the carbon sequestration rate will be reduced by 99%.

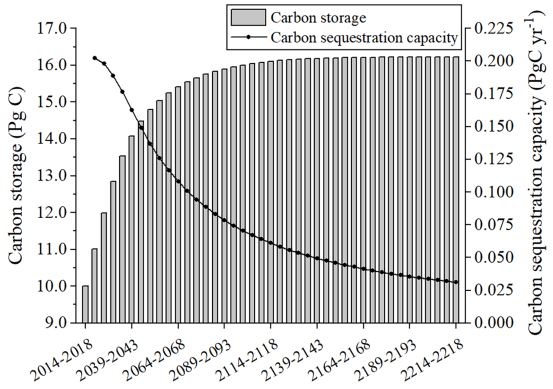

FIGURE 1
The carbon storage and carbon sequestration capacity of China's forests in contemporary times and in the future.

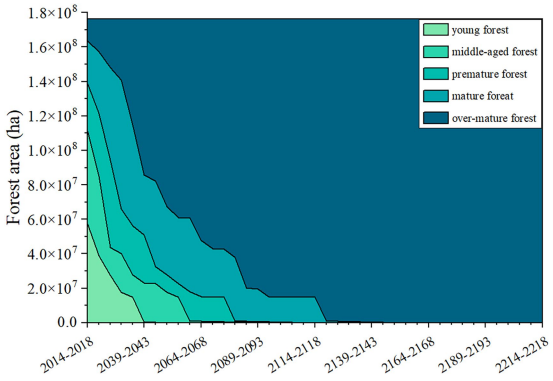

FIGURE 2
The age structure of China's forests in currently and in the future.

3.2. Spatial patterns of forest carbon storage and carbon sequestration capacity

There are great differences in carbon storage capacities among the different provinces (Figure 3). The regions with higher carbon storage capacities are mainly in northeastern and southwestern China. Heilongjiang province has the highest carbon storage of 1.49 Pg C, followed by Sichuan (1.28 Pg C), Inner Mongolia (1.16 Pg C) and Yunnan (0.87 Pg C). The forest carbon storage of the eastern coastal provinces is lower than that in the northeastern or southwestern provinces. The lowest carbon storage was in the central area (Henan, Anhui, Shandong, Shanxi, Jiangsu, and Shanghai) of China, which ranged from 0.002 Pg to 0.16 Pg. Although the land area of this western regions is very large, the forest area is relatively small. Due to the harsh environment, there are few types of woodlands suitable for

2 http://forestcloud.ca

tree growth, the trees grow slowly, and the forest carbon storage potential is lower than that in other areas.

The carbon sequestration capacities in forest ecosystems were distributed heterogeneously across China. The current forest carbon sequestration capacities in the southwestern and eastern regions are at their peaks, and have greatly reduced with stand aging (Figure 4). Most regions in the central-southern region (Guangdong, Guangxi, Hunan, Hubei et al.) have not yet reached the maximum carbon sequestration capacities yet and they will reach the maximum around the year 2028. Through the comparative analysis of carbon storage and the carbon sequestration capacity of 31 provinces in China, generally speaking, there is a positive correlation between forest carbon sequestration capacity and carbon storage, such as in Heilongjiang or in Inner Mongolia, Sichuan or the Yunnan provinces. The corresponding carbon sequestration capacity is also higher than that of other provinces. Interestingly, although the carbon sequestration capacity of forests in the Guangxi Province is lower than that in the Yunnan Province, it is still higher than that in Heilongjiang, Inner Mongolia or Sichuan. In addition, the carbon sequestration capacity of other provinces in the southern regions (Guangdong, Hunan, Hubei) is also higher than that of most other provinces in China.

3.3. Spatial and temporal patterns of future forest carbon densities

At present, the average carbon density of all forest is 56.69 Mg C ha^{-1} in China, and only 9 provinces are above the average level (Figure 5). The areas with higher carbon densities are mainly concentrated in the northeast, northwest and southwest of China, and the lower carbon density areas are in the eastern and south-central regions. The forest carbon density (91.68 Mg C ha^{-1}) of Xinjiang is the highest, followed by Tibet (84.78 Mg C ha^{-1}), Sichuan (83.18 Mg C ha^{-1}), Jilin (75.57 Mg C ha^{-1}), Heilongjiang (75.07 Mg C ha^{-1}) and other regions. The carbon density in Tianjin, Jiangsu and Guangxi is much lower than other provinces, and the forests of Guangxi are mainly young plantation forests. The carbon density of provinces in the eastern and southeastern regions is low, and the carbon density is between 20 and 40 Mg C ha^{-1}, but the future growth rate is expected to be faster.

In the next 40 years, the average forest carbon density of China will increase greatly in the eastern, central and southern regions of China, from 56.69 Mg C ha^{-1} in 2018 to 86.38 Mg C ha^{-1} in 2058. We also found that the increment rate of carbon density in most provinces in southern China was higher than that in the north, but the

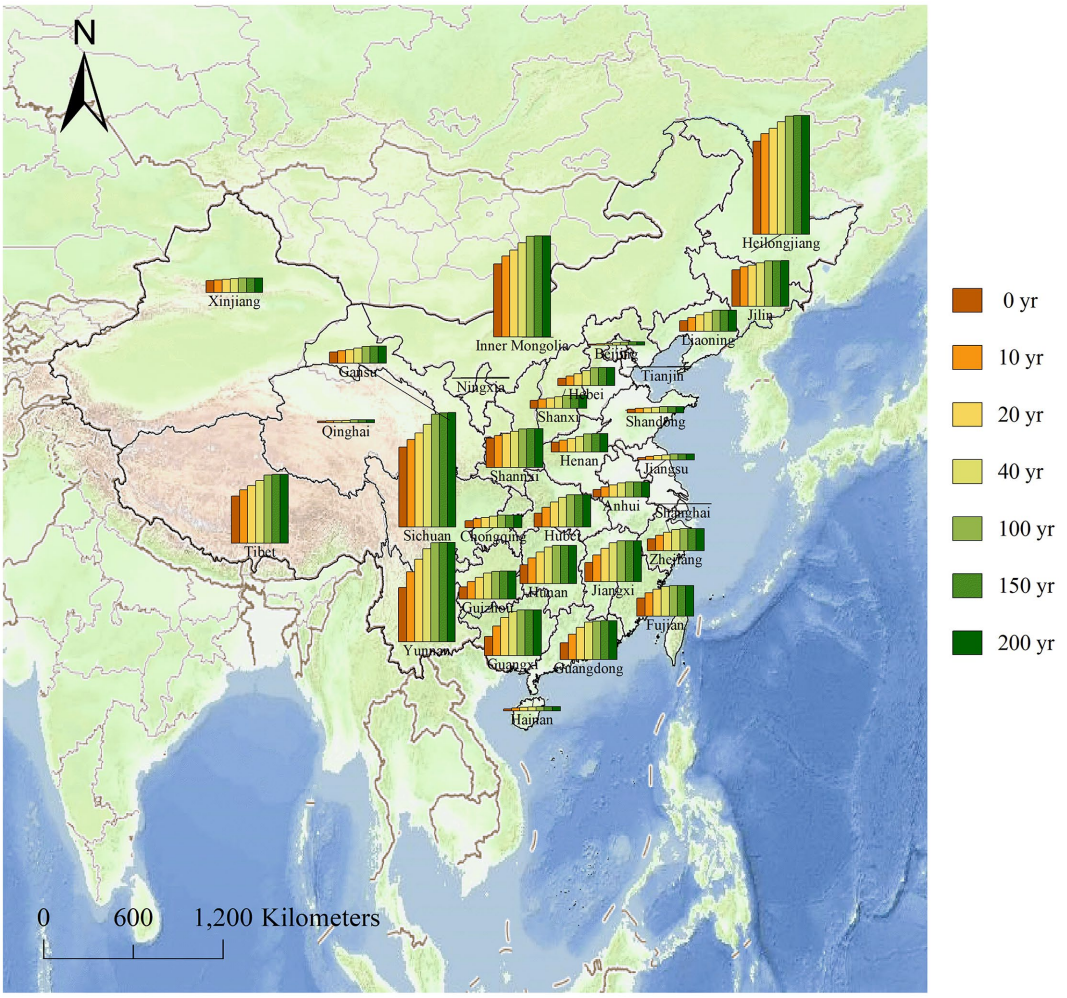

FIGURE 3
Carbon storage of China's forests by the provinces.

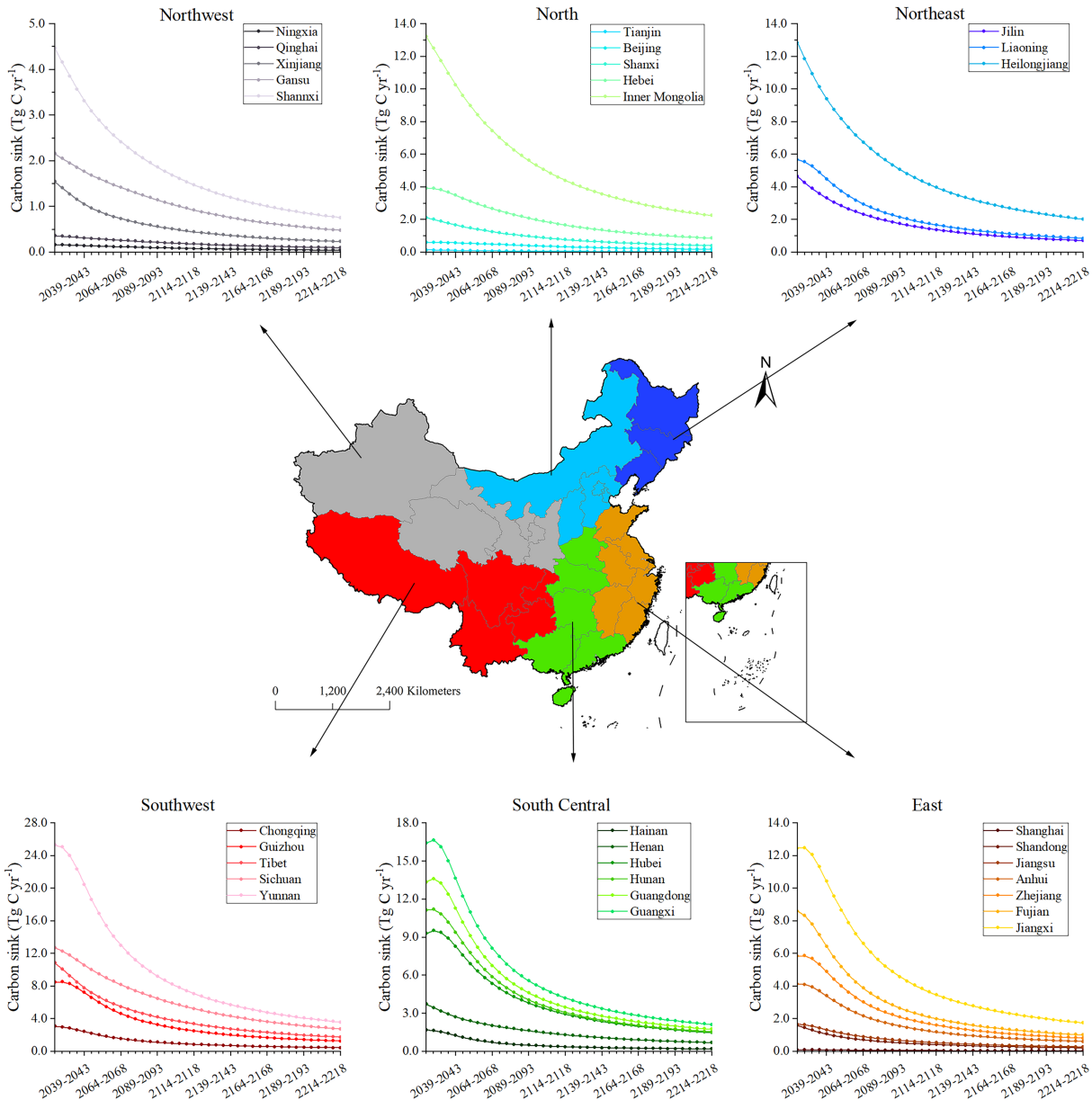

FIGURE 4
Carbon sequestration capacities (Tg C year^{-1}) of 31 provinces over the next 200years. Forests in China are divided into six regions: Northwestern region (Shaanxi, Gansu, Xinjiang, Qinghai, and Ningxia), Northern region (Inner Mongolia, Hebei, Inner Mongol, Shanxi, Beijing, and Tianjin), Northeastern region (Heilongjiang, Jilin, and Liaoning), Southwestern region (Sichuan, Yunnan, Tibet, Guizhou, and Chongqing), Central southern region (Guangxi, Guangdong, Hubei, Hunan, Henan, and Hainan), and Eastern region (Fujian, Jiangxi, Zhejiang, Shanghai, Anhui, Shandong, and Jiangsu).

potential of forest carbon sequestration in southern China will likely account for a major part of the whole carbon uptake process in the future.

4. Discussion

4.1. Uncertainties of future forest carbon storages

Forest carbon sequestration provides a low-cost, nature-based solution for national carbon neutral strategies with enormous potential capacities for the future. Piao et al. (2022a) compared and analyzed four large-scale ecosystem carbon storage and carbon sequestration capacity methods. The existing carbon storage estimation methods of forest vegetation have been relatively mature. Our study uses the inventory method to calculate the carbon storage of China's forests without including economic forests and bamboo forests. The total carbon storage is 10.0 Pg C of various vegetation types of 31 provinces. Tang et al. (2018) also calculated the carbon storage of China's forests by vegetation types. The carbon storage of Chinese forests is 10.5 ± 2.0 Pg C. Chen et al. (2022) calculated that the carbon storage of natural forest of China was 9.4 ± 1.45 Pg C using a similar method and the data of 762 natural forest sites in 2010. The

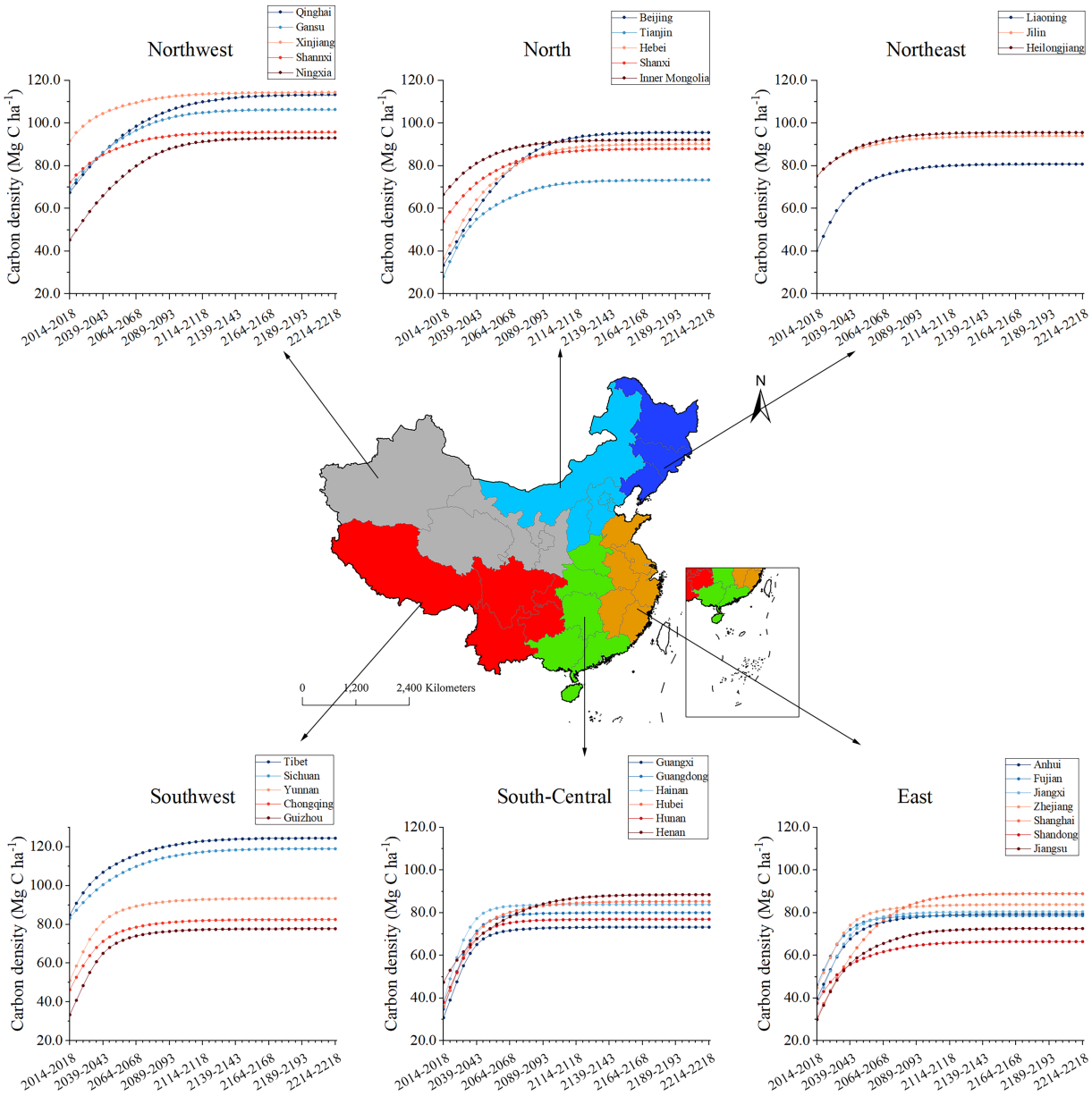

FIGURE 5
Carbon density (Mg C ha^{-1}) of 31 provincial regions.

previous studies estimated that the carbon storage is 1.4 Pg C in the plantation forests (Zhang et al., 2015), and 10.8 Pg C in the natural forests. The results of all these studies are consistent with those of this study. Due to the lack of economic forest and bamboo forest data, the total carbon storage of this study is slightly lower than that of other studies.

4.2. Temporal changes of carbon storage and carbon sequestration capacity of provinces

To better understand the characteristics of forest carbon sequestration and the contribution to carbon neutrality, based on the calculation of carbon storage, we forecasted the forest carbon storage and sequestration capacities of China for the next 200 years. From 2019 to 2048, the increment of forest carbon storage will be 4.48 Pg C, and the average carbon sequestration will be 0.15 Pg C year^{-1}. He et al. (2017) predicted that the increment of carbon storage of forest vegetation of China will be 13.92 Pg C and the average carbon sequestration will be 0.34 Pg C year^{-1} from 2010 to 2050, which is much higher than our results. While Yao et al. (2018) predicted that the increment from 2010 to 2050 will be 6.69 Pg C (the average carbon sequestration is 0.17 Pg C year^{-1}). Xu et al. (2010) predicted 7.23Pg C (0.14 Pg C year^{-1}) from 2000 to 2050, and Cai et al. (2022) predicted 0.211 Pg C year^{-1} from 2010 to 2060. These results are similar to ours. Our results showed that in the next 40 years, the carbon storage will increase from 10.0 Pg C to 15.04 Pg C, and the average carbon

sequestration will be only 0.13 Pg C year^{-1}. However, it is worth noting that after 90 years, when all forests have transitioned to a mature state, the carbon sequestration capacity of forests will be only 4% of the current level, and forests almost lost their carbon sequestration capacity. Our results supported E.P.Odum's ecological succession hypothesis. The forests will gradually enter the old seral stages, the carbon sequestration capacities will decrease greatly, and the carbon storage of the whole forest will gradually reach the upper limit in stable environment conditions (Odum Eugene, 1969; Hubau et al., 2020; Piao et al., 2022b). Of course, our research object is only the current forests in China. In the future, due to afforestation and reforestation, human management, natural succession of forests, and natural disturbances such as hurricanes, floods, droughts, and wildfires that forests may suffer. These factors will affect the carbon storage and carbon sequestration capacity of forests (Fekete et al., 2017; Ceccherini et al., 2020; Walker et al., 2020; Anderegg et al., 2022; Phillips et al., 2022). Studies showed that China's terrestrial carbon sequestrations will offset 2.8%–18.7% of fossil fuel emissions by the year 2060 (Cai et al., 2022; Yang et al., 2022). However, China will also face more severe challenges in achieving the goal of carbon neutrality because of the decrease in forest carbon sequestration capacities. The carbon sequestration capacity will tend to be zero as the forest gradually enters the mature stage (Odum Eugene, 1969).

4.3. Spatial distribution of carbon storage and carbon sequestration capacities

The study showed that the carbon storage and carbon sequestration capacities have large spatial heterogeneity in China, and the carbon storage capacity in the northeastern and southwestern regions is much higher than that in other regions. The difference in carbon storage among the different provinces is mainly related to the forest areas of each province. In the last 20–25 years, carbon storage in the northeast of China has increased from 1.79 Pg C from 1994 to 1998 to 2.17 Pg C from 1997 to 1999 (Fang et al., 2001), a 45.95% increase because of plantations (Luo et al., 2020), mainly due to the 3-North Shelter Forest Program that has been implemented by China since 1979. The project requires that the afforestation areas in the three northern areas increase from 5.05% to 15.95% by 2050. The fast-growing trees absorb CO_2 quickly because of the good climatic conditions in the southeast of the Tibet Plateau, with suitable temperature and sufficient precipitation. Another main reason for the carbon storage increase is that the area is less disturbed (Keith et al., 2009). Forest disturbances have always been the major factors affecting forest carbon storage and carbon sequestration capacity (Seidl et al., 2014). Storms, droughts, pests, wildfires and human disturbances have a great impact on the global carbon storage. For example, Kurz et al. (2008) predicted that continued insect outbreaks in British Columbia will lead to forest loss of about 374,000 square kilometers of forest area between 2000 and 2020, and they also indicated that the forest fires in western Canada have also released a huge amount of carbon. With global warming, climate extremes such as droughts and storms can decrease the regional ecosystem carbon stocks (Reichstein et al., 2013). Lasslop et al. (2020) used simulations from seven global vegetation models to estimate the fire impacts on global tree cover and the carbon cycle, and found that global fires reduce forest cover and vegetation carbon storage by 10%. In addition, there is sufficient evidence to prove that deforestation has reduced forest carbon stocks in the Amazon by 5.1 ± 3.7% (Li et al., 2022).

According to the 2014 IPCC's report, forest carbon sequestration is the most cost-effective way for national carbon neutral strategies. Forest carbon sequestration capacities can be increased by reducing deforestation, sustainable management and afforestation (IPCC, 2004). In China, forests are widely distributed, with large latitude and longitude spans, and complex terrain. In general, the national forest area, the forest carbon storage and the carbon sequestration capacity have been positively correlated. In areas with high carbon storage, forest carbon sequestration capacity will also be stronger. However, it is worth noting that some low-latitude provinces have lower carbon storage than high-latitude provinces, but their carbon sequestration capacity is stronger than that of high-latitude provinces. For example, the total carbon storage of the Guangxi Province is lower than that of Heilongjiang and Inner Mongolia, but its carbon sequestration capacity is also greater. The reasons may be as follows: First, the proportion of young and middle-aged forests in the Guangxi Province is 84% higher than that in Heilongjiang (61%) and in Inner Mongolia (53%), and the carbon sequestration capacity of young and middle-aged forests is still relatively strong. Second, there are great differences in forest types among the provinces. The southern forests are dominated by short-life cycle tree species with a short maturity period, while the northern tree species have a longer life cycle. The southern forests mainly have the fastest growth and shortest rotation species (*Populus* spp., *Cunninghamia lanceolata*, *Eucalyptus robusta*, *Larix* spp.), which have greater carbon sequestration capacities if we manage them properly. Third, the environment in the southern region is more suitable for tree growth, with suitable temperatures and precipitation enabling trees to grow year-round, while the annual growth of the cycle of trees in the northern region is short. Here, we also found that although the current carbon sequestration capacity of some south-central provinces (Guangdong, Hunan, and Hubei) is not much different from that of Heilongjiang and Inner Mongolia, the carbon sequestration capacity in the future will decline much more rapidly than in these other provinces. This is related to the growth characteristics of the forest ecosystems in each province. Long life-cycle tree species have a longer carbon sink service time. To maintain a higher level of forest carbon sequestration capacity after achieving the carbon neutralization, China needs to manage forests more effectively to improve forest carbon sequestration capacity as much as possible. Ameray et al. (2021) proposed three management strategies for boreal, temperate and tropical forests: extensive forest management, intensive forest management and old-growth forest conservation. Old-growth forests can store more carbon than young forests, and although older forests have a slower rate of carbon sequestration, old-growth forest will release more carbon after logging (Harmon et al., 1990). Intensive forest management is one way to increase the carbon sequestration capacity of fast-growing tree species. Extensive forest management increases forest carbon sequestration capacity and soil carbon storage through partial cutting (Dalmonech et al., 2022). Due to the strong spatial heterogeneity of China's forest carbon, it is very necessary to implement corresponding management strategies for forest conditions in different regions. For example, forests in Guangxi, Guangdong, and Fujian should focus on intensive forest management to improve the carbon sequestration capacity of fast-growing species such as *Cunninghamia lanceolata* and *Eucalyptus robusta*. Provinces such as Heilongjiang, Inner Mongolia, Jilin, and

Liaoning have long forest life cycles. It is recommended to adopt extensive forest management and increase forest and soil carbon storage through partial cutting. Forests in Yunnan, Sichuan and Tibet are less disturbed and have higher carbon density, so it is recommended to focus on protection.

Currently, the forests of China will have largest carbon storage potential and strongest carbon sequestration capacities by the year 2058, but the role of forest carbon sequestration will decline gradually. Therefore, the key to maintaining the high carbon sequestration capacity of forests lies in two points. First, increase the forest area as much as possible and increase the carbon storage potential. From the late 1990s to 2010, the cumulative afforestation area of six key forests projects begun in China increased by 106.31×10^6 ha. The potential afforestation area in the future (2010–2050) is about 300,000 ha, and the carbon sequestration potential of afforestation may reach 2.52 Pg. These afforestation projects are the key to increasing carbon storage in China's forest ecosystems (Huang et al., 2012). Second, maintain a reasonable forest age structure and maintain a certain proportion of young and middle-aged forests through forest management measures. Here we suggest that national-scale forest planning should implement targeted measures on a province-by-province basis. For forests with fast growing trees in the south, high-intensity management and reforestation methods are used to maintain the high carbon sequestration capacity of forests (Busch et al., 2019; Veldkamp et al., 2020). Aiming at the slow-growing forests in the north, increasing the forest area is not the main goal, but improving forest quality through low-intensity management is the key (Canadell and Raupach, 2008; Feng et al., 2022; Kreier, 2022). The objectives of this research are to comprehensively analyze forest carbon reserves and carbon sequestration potential at a national scale as well as to understand the changes of forest carbon sequestration capacities, and provide a reference for decision-makers so that they can make more effective and more intelligent decisions.

4.4. Carbon density in forest ecosystems

Forest stand ages are important factors for the carbon sequestration capacities of forest ecosystems because the carbon accumulation greatly depends on forest stand ages (Yao et al., 2018). At present, 63.06% of China's forests are young and middle-aged forests, so China's forests currently maintain a high forest carbon sequestration capacity. But the carbon sequestration capacity declines rapidly with the succession of ecosystems. When the forest is fully succeeded to a mature state (after 90 years), the carbon sequestration capacity of the forest decreases by 68%. Therefore, to maintain the high carbon sequestration capacity of forests, a certain proportion of young forests must be maintained. The forest carbon sequestration capacities of China have increased by 34% through afforestation and reforestation after the forests were destroyed before the 1990s (Pan et al., 2011). The high proportion of young and middle-age forests make China's current forest carbon density (56.69 Mg C ha^{-1}) lower than the United States (88 Mg C ha^{-1}; Pan et al., 2011; Nelson et al., 2017). The areas with high carbon densities in China are mainly concentrated in the Northeast, Northwest and Southwest, and the carbon densities in South-Central and Eastern areas are relatively small. The mature and over-mature forests are mainly located in the Northeast, Northwest and Southwest.

The current forest is dominated by immature forest stands, with strong carbon sequestration capacities, and the carbon density will increase from 56.69 Mg C ha^{-1} to 86.38 Mg C ha^{-1} over the next 40 years (by 2058). However, the forest carbon sequestration capacities will decrease after the stands reach the mature and over-mature stageswithin the next 40 years. The average carbon density of the national forest will reach the stable stage 91.93 Mg C ha^{-1} after 100 years, and the carbon density of New Zealand's natural forest will be 227 Mg C ha^{-1} when it reaches the stable stage. There are two main reasons for the differences: the natural forest of New Zealand Forest Inventory is mainly composed of primordial forest, which has a more stable structure and a higher carbon storage capacity with a longer growing season and good rainfall (Paul et al., 2021). Reasonable age structure is the key to maintaining high carbon sequestration capacity of forests (Li Y. et al., 2019).

5. Conclusion

The results of this study analyzed the changes of forest carbon storage and carbon sequestration capacities in China. The current forest carbon storage in China is 10.0 Pg C. Before the national carbon neutrality strategic goal is achieved in 2060, the forest still has 5.04 Pg increment space. However, in the next 40 years, the carbon sequestration capacity will be greatly reduced, from 0.202 Pg $year^{-1}$ to 0.050 Pg $year^{-1}$, and the carbon sequestration capacity will decrease by 75%. These changes in the trends of forest carbon in the provinces are basically the same as those in the country, and as the new forests, the possible disturbances in the future, and the forest succession are not considered, the carbon sequestration capacity of forest tends to zero with the forest age. Therefore, in order to maintain a high forest carbon sequestration capacity and a longer service time for forest carbon sinks, we have to make more comprehensive strategic plans for our forests. At present, restoration, afforestation, reforestation and sustainable forest development will be the main methods through which to extend the service time of forest carbon sinks. Because of the strong spatial–temporal heterogeneity of forest carbon in China, to formulate and implement afforestation and management strategies according to the changes of forest carbon pools and the carbon sequestration capacity in each province, strategies need to be developed and implemented.

We suggest that the carbon trades should include the carbon storage amount and time in the future because the carbon sequestration of all forests will be gradually reduced to zero when the forests recover to the stable stages. Paying fees by carbon storage amount and time will be a more effective way to keep carbon in the forests and reduce the amount of carbon in the atmosphere. The combination of carbon storage fee and the carbon sequestration fee can be a long-term effective way to reduce the greenhouse gas amount in the atmosphere.

Data availability statement

The raw data supporting the conclusions of this article will be made available by the authors, without undue reservation.

Author contributions

FC and JT: conceptualization, methodology, formal analysis, investigation, data curation, writing–original draft, and writing–review. JH: data curation and writing–review. HH: conceptualization, writing–review and editing. GL: methodology, formal analysis, investigation, project administration, and funding acquisition. ZZ: investigation, project administration, and funding acquisition. LZ: writing–review and editing. All authors contributed to the article and approved the submitted version.

Funding

This project was supported by the Jilin Scientific and Technological Development Program: Impact of Harvesting Disturbance on the Relationship between Coniferous and Broadwood Mixed Forest Productivity and Biodiversity (20210508012RQ); Jilin Scientific and Technological Development Program: Research and Demonstration of Natural Secondary Forest Management Technology in Eastern Mountainous Mountains of Jilin Province (20220202097NC); Jilin Scientific and Technological Development Program: Jilin Province Degraded Forest Ecosystem Restoration and Reconstruction Cross-regional Cooperation Science and Technology Innovation Center (20200602006ZP); Jilin Scientific and Technological Development Program: Research and demonstration of key Technologies for Ecological Restoration of degraded Natural Forest ecosystem (20190303072SF).

Acknowledgments

We thank numerous who contributed to data collecting. We also thank the editors and reviewers for their very helpful comments.

Conflict of interest

LZ is employed by Shenyang Forestry Management Institute of China Railway Shenyang Bureau Group Co. Ltd. GL is employed by Nanjing Jialin System Engineering Ltd.

The remaining authors declare that the research was conducted in the absence of any commercial or financial relationships that could be construed as a potential conflict of interest.

Publisher's note

Supplementary material

The Supplementary material for this article can be found online at: https://www.frontiersin.org/articles/10.3389/fevo.2023.1110594/full#supplementary-material

References

Administration, C.S.F (2014). "*Technical provisions for continuous inventory of National Forest Resources*". (Beijing: China Forestry Publishing House).

Ameray, A., Bergeron, Y., Valeria, O., Montoro Girona, M., and Cavard, X. (2021). Forest carbon management: a review of Silvicultural practices and management strategies across boreal, temperate and tropical forests. *Curr. For. Rep.* 7, 245–266. doi: 10.1007/s40725-021-00151-w

Anderegg, W. R. L., Chegwidden, O. S., Badgley, G., Trugman, A. T., Cullenward, D., Abatzoglou, J. T., et al. (2022). Future climate risks from stress, insects and fire across US forests. *Ecol. Lett.* 25, 1510–1520. doi: 10.1111/ele.14018

Broadstock, D., Ji, Q., Managi, S., and Zhang, D. (2021). Pathways to carbon neutrality: challenges and opportunities. *Resour. Conserv. Recycl.* 169:105472. doi: 10.1016/j.resconrec.2021.105472

Busch, J., Engelmann, J., Cook-Patton, S. C., Griscom, B. W., Kroeger, T., Possingham, H., et al. (2019). Potential for low-cost carbon dioxide removal through tropical reforestation. *Nat. Clim. Chang.* 9, 463–466. doi: 10.1038/s41558-019-0485-x

Cai, W., He, N., Li, M., Xu, L., Wang, L., Zhu, J., et al. (2022). Carbon sequestration of Chinese forests from 2010 to 2060: spatiotemporal dynamics and its regulatory strategies. *Sci. Bull.* 67, 836–843. doi: 10.1016/j.scib.2021.12.012

Canadell, J. G., and Raupach, M. R. (2008). Managing forests for climate change mitigation. *Science* 320, 1456–1457. doi: 10.1126/science.1155458

Ceccherini, G., Duveiller, G., Grassi, G., Lemoine, G., Avitabile, V., Pilli, R., et al. (2020). Abrupt increase in harvested forest area over Europe after 2015. *Nature* 583, 72–77. doi: 10.1038/s41586-020-2438-y

Chen, S., Lu, N., Fu, B., Wang, S., Deng, L., and Wang, L. (2022). Current and future carbon stocks of natural forests in China. *For. Ecol. Manag.* 511:120137. doi: 10.1016/j.foreco.2022.120137

China, S.F.A.O (2014). *Forest resource statistics of China (2009–2013)*. Beijing: China Forestry Publishing House.

Commission, N.D.a.r (2014). *National Greenhouse gas Inventory Report of China (2005)*. Beijing: China Environmental Science Press.

Dai, L., Li, S., Zhou, W., Qi, L., Zhou, L., Wei, Y., et al. (2018). Opportunities and challenges for the protection and ecological functions promotion of natural forests in China. *For. Ecol. Manag.* 410, 187–192. doi: 10.1016/j.foreco.2017.09.044

Dalmonech, D., Marano, G., Amthor, J. S., Cescatti, A., Lindner, M., Trotta, C., et al. (2022). Feasibility of enhancing carbon sequestration and stock capacity in temperate and boreal European forests via changes to management regimes. *Agric. For. Meteorol.* 327:109203. doi: 10.1016/j.agrformet.2022.109203

Fang, J., Chen, A., Peng, C., Zhao, S., and Ci, L. (2001). Changes in forest biomass carbon storage in China between 1949 and 1998. *Science* 292, 2320–2322. doi: 10.1126/science.1058629

Fekete, I., Lajtha, K., Kotroczó, Z., Várbíró, G., Varga, C., Tóth, J. A., et al. (2017). Long-term effects of climate change on carbon storage and tree species composition in a dry deciduous forest. *Glob. Chang. Biol.* 23, 3154–3168. doi: 10.1111/gcb.13669

Feng, Y., Schmid, B., Loreau, M., Forrester, D. I., Fei, S., Zhu, J., et al. (2022). Multispecies forest plantations outyield monocultures across a broad range of conditions. *Science* 376, 865–868. doi: 10.1126/science.abm6363

Harmon, M. E., Ferrell, W. K., and Franklin, J. F. (1990). Effects on carbon storage of conversion of old-growth forests to young forests. *Science* 247, 699–702. doi: 10.1126/science.247.4943.699

Hawes, M. (2018). Planting carbon storage. *Nat. Clim. Chang.* 8, 556–558. doi: 10.1038/s41558-018-0214-x

He, N., Wen, D., Zhu, J., Tang, X., Xu, L., Zhang, L., et al. (2017). Vegetation carbon sequestration in Chinese forests from 2010 to 2050. *Glob. Chang. Biol.* 23, 1575–1584. doi: 10.1111/gcb.13479

Huang, L., Liu, J., Shao, Q., and Xu, X. (2012). Carbon sequestration by forestation across China: past, present, and future. *Renew. Sust. Energ. Rev.* 16, 1291–1299. doi: 10.1016/j.rser.2011.10.004

Hubau, W., Lewis, S. L., Phillips, O. L., Affum-Baffoe, K., Beeckman, H., Cuní-Sanchez, A., et al. (2020). Asynchronous carbon sink saturation in African and Amazonian tropical forests. *Nature* 579, 80–87. doi: 10.1038/s41586-020-2035-0

IPCC (2004). Annex II: glossary *Climate change 2014: Synthesis report. Contribution of working groups I, II and III to the fifth assessment report of the intergovernmental panel on climate change* K. J. Mach, S. Planton and C. von Stechow (IPCC, Geneva, Switzerland) 151.

Jiang, M., Medlyn, B. E., Drake, J. E., Duursma, R. A., Anderson, I. C., Barton, C. V. M., et al. (2020). The fate of carbon in a mature forest under carbon dioxide enrichment. *Nature* 580, 227–231. doi: 10.1038/s41586-020-2128-9

Keith, H., Mackey, B. G., and Lindenmayer, D. B. (2009). Re-evaluation of forest biomass carbon stocks and lessons from the world's most carbon-dense forests. *Proc. Natl. Acad. Sci. U. S. A.* 106, 11635–11640. doi: 10.1073/pnas.0901970106

Kreier, F. (2022). Tropical forests have big climate benefits beyond carbon storage. *Nature*. doi: 10.1038/d41586-022-00934-6

Kurz, W. A., Dymond, C. C., Stinson, G., Rampley, G. J., Neilson, E. T., Carroll, A. L., et al. (2008). Mountain pine beetle and forest carbon feedback to climate change. *Nature* 452, 987–990. doi: 10.1038/nature06777

Lasslop, G., Hantson, S., Harrison, S. P., Bachelet, D., Burton, C., Forkel, M., et al. (2020). Global ecosystems and fire: multi-model assessment of fire-induced tree-cover and carbon storage reduction. *Glob. Chang. Biol.* 26, 5027–5041. doi: 10.1111/gcb.15160

Li, Y., Bao, W., Bongers, F., Chen, B., Chen, G., Guo, K., et al. (2019). Drivers of tree carbon storage in subtropical forests. *Sci. Total Environ.* 654, 684–693. doi: 10.1016/j.scitotenv.2018.11.024

Li, Y., Brando, P. M., Morton, D. C., Lawrence, D. M., Yang, H., and Randerson, J. T. (2022). Deforestation-induced climate change reduces carbon storage in remaining tropical forests. *Nat. Commun.* 13:1964. doi: 10.1038/s41467-022-29601-0

Li, L., Ye, F., Li, Y., and Chang, C.-T. (2019). How will the Chinese certified emission reduction scheme save cost for the national carbon trading system? *J. Environ. Manag.* 244, 99–109. doi: 10.1016/j.jenvman.2019.04.100

Liu, G., Han, S., Zhao, X., Nelson, J. D., Wang, H., and Wang, W. (2006). Optimisation algorithms for spatially constrained forest planning. *Ecol. Model.* 194, 421–428. doi: 10.1016/j.ecolmodel.2005.10.028

Lu, F., Hu, H., Sun, W., Zhu, J., Liu, G., Zhou, W., et al. (2018). Effects of national ecological restoration projects on carbon sequestration in China from 2001 to 2010. *Proc. Natl. Acad. Sci. U. S. A.* 115, 4039–4044. doi: 10.1073/pnas.1700294115

Luo, W., Kim, H. S., Zhao, X., Ryu, D., Jung, I., Cho, H., et al. (2020). New forest biomass carbon stock estimates in Northeast Asia based on multisource data. *Glob. Chang. Biol.* 26, 7045–7066. doi: 10.1111/gcb.15376

Maia, V. A., Santos, A. B. M., De Aguiar-Campos, N., De Souza Cléber, R., De Oliveira, M. C. F., Coelho, P. A., et al. (2020). The carbon sink of tropical seasonal forests in southeastern Brazil can be under threat. *Sci. Adv.* 6:eabd4548. doi: 10.1126/sciadv.abd4548

Münnich Vass, M. (2017). Renewable energies cannot compete with forest carbon sequestration to cost-efficiently meet the EU carbon target for 2050. *Renew. Energy* 107, 164–180. doi: 10.1016/j.renene.2017.01.034

Nabuurs, G.-J., Lindner, M., Verkerk, P. J., Gunia, K., Deda, P., Michalak, R., et al. (2013). First signs of carbon sink saturation in European forest biomass. *Nat. Clim. Chang.* 3, 792–796. doi: 10.1038/nclimate1853

Nelson, R., Margolis, H., Montesano, P., Sun, G., Cook, B., Corp, L., et al. (2017). Lidar-based estimates of aboveground biomass in the continental US and Mexico using ground, airborne, and satellite observations. *Remote Sens. Environ.* 188, 127–140. doi: 10.1016/j.rse.2016.10.038

Odum Eugene, P. (1969). The strategy of ecosystem development. *Science* 164, 262–270. doi: 10.1126/science.164.3877.262

Pan, Y., Birdsey, R. A., Fang, J., Houghton, R., Kauppi, P. E., Kurz, W. A., et al. (2011). A large and persistent carbon sink in the world's forests. *Science* 333, 988–993. doi: 10.1126/science.1201609

Pan, Y., Luo, T., Birdsey, R., Hom, J., and Melillo, J. (2004). New estimates of carbon storage and sequestration in China'S forests: effects of age–class and method on inventory-based carbon estimation. *Clim. Chang.* 67, 211–236. doi: 10.1007/s10584-004-2799-5

Paul, T., Kimberley, M. O., and Beets, P. N. (2021). Natural forests in New Zealand – a large terrestrial carbon pool in a national state of equilibrium. *For. Ecosyst.* 8, 1–21. doi: 10.1186/s40663-021-00312-0

Phillips, C. A., Rogers, B. M., Elder, M., Cooperdock, S., Moubarak, M., Randerson, J. T., et al. (2022). Escalating carbon emissions from north American boreal forest wildfires and the climate mitigation potential of fire management. *Sci. Adv.* 8:eabl7161. doi: 10.1126/sciadv.abl7161

Piao, S., He, Y., Wang, X., and Chen, F. (2022a). Estimation of China's terrestrial ecosystem carbon sink: methods, progress and prospects. *Sci. China Earth Sci.* 65, 641–651. doi: 10.1007/s11430-021-9892-6

Piao, S., Yue, C., Ding, J., and Guo, Z. (2022b). Perspectives on the role of terrestrial ecosystems in the 'carbon neutrality' strategy. *Sci. China Earth Sci.* 65, 1178–1186. doi: 10.1007/s11430-022-9926-6

Pregitzer, K. S., and Euskirchen, E. S. (2004). Carbon cycling and storage in world forests: biome patterns related to forest age. *Glob. Chang. Biol.* 10, 2052–2077. doi: 10.1111/j.1365-2486.2004.00866.x

Qie, L., Lewis, S. L., Sullivan, M. J. P., Lopez-Gonzalez, G., Pickavance, G. C., Sunderland, T., et al. (2017). Long-term carbon sink in Borneo's forests halted by drought and vulnerable to edge effects. *Nat. Commun.* 8:1966. doi: 10.1038/s41467-017-01997-0

Reichstein, M., Bahn, M., Ciais, P., Frank, D., Mahecha, M. D., Seneviratne, S. I., et al. (2013). Climate extremes and the carbon cycle. *Nature* 500, 287–295. doi: 10.1038/nature12350

Seidl, R., Schelhaas, M. J., Rammer, W., and Verkerk, P. J. (2014). Increasing forest disturbances in Europe and their impact on carbon storage. *Nat. Clim. Chang.* 4, 806–810. doi: 10.1038/nclimate2318

Taeroe, A., Mustapha, W. F., Stupak, I., and Raulund-Rasmussen, K. (2017). Do forests best mitigate CO2 emissions to the atmosphere by setting them aside for maximization of carbon storage or by management for fossil fuel substitution? *J. Environ. Manag.* 197, 117–129. doi: 10.1016/j.jenvman.2017.03.051

Tang, X., Zhao, X., Bai, Y., Tang, Z., Wang, W., Zhao, Y., et al. (2018). Carbon pools in China's terrestrial ecosystems: new estimates based on an intensive field survey. *Proc. Natl. Acad. Sci. U. S. A.* 115, 4021–4026. doi: 10.1073/pnas.1700291115

UNFCCC (2019). Climate ambition alliance: nations renew their push to upscale action by 2020 and achieve net zero CO2 emissions by 2050. (UNFCCC, Madrid, Bonn).

Veldkamp, E., Schmidt, M., Powers, J. S., and Corre, M. D. (2020). Deforestation and reforestation impacts on soils in the tropics. *Nat. Rev. Earth Environ.* 1, 590–605. doi: 10.1038/s43017-020-0091-5

Walker, W. S., Gorelik, S. R., Baccini, A., Aragon-Osejo, J. L., Josse, C., Meyer, C., et al. (2020). The role of forest conversion, degradation, and disturbance in the carbon dynamics of Amazon indigenous territories and protected areas. *Proc. Natl. Acad. Sci. U. S. A.* 117, 3015–3025. doi: 10.1073/pnas.1913321117

Wang, K., Hu, D., Deng, J., Shangguan, Z., and Deng, L. (2018). Biomass carbon storages and carbon sequestration potentials of the grain for green program-covered forests in China. *Ecol. Evol.* 8, 7451–7461. doi: 10.1002/ece3.4228

Xu, B., Guo, Z., Piao, S., and Fang, J. (2010). Biomass carbon stocks in China's forests between 2000 and 2050: a prediction based on forest biomass-age relationships. *Sci. China Life Sci.* 53, 776–783. doi: 10.1007/s11427-010-4030-4

Yang, Y., Shi, Y., Sun, W., Chang, J., Zhu, J., Chen, L., et al. (2022). Terrestrial carbon sinks in China and around the world and their contribution to carbon neutrality. *Sci. China Life Sci.* 65, 861–895. doi: 10.1007/s11427-021-2045-5

Yao, Y., Piao, S., and Wang, T. (2018). Future biomass carbon sequestration capacity of Chinese forests. *Sci. Bull.* 63, 1108–1117. doi: 10.1016/j.scib.2018.07.015

Ye, F., Xiong, X., Li, L., and Li, Y. (2021). Measuring the effectiveness of the Chinese certified emission reduction scheme in mitigating CO2 emissions: a system dynamics approach. *J. Clean. Prod.* 294:125355. doi: 10.1016/j.jclepro.2020.125355

Zhang, C., Ju, W., Chen, J. M., Wang, X., Yang, L., and Zheng, G. (2015). Disturbance-induced reduction of biomass carbon sinks of China's forests in recent years. *Environ. Res. Lett.* 10:114021. doi: 10.1088/1748-9326/10/11/114021

Zhou, W., Lewis, B. J., Wu, S., Yu, D., Zhou, L., Wei, Y., et al. (2014). Biomass carbon storage and its sequestration potential of afforestation under natural forest protection program in China. *Chin. Geogr. Sci.* 24, 406–413. doi: 10.1007/s11769-014-0702-5

Zhou, T., Shi, P., Jia, G., Dai, Y., Zhao, X., Shangguan, W., et al. (2015). Age-dependent forest carbon sink: estimation via inverse modeling. *J. Geophys. Res. Biogeo.* 120, 2473–2492. doi: 10.1002/2015jg002943

frontiers | Frontiers in Ecology and Evolution

TYPE Original Research
PUBLISHED 20 February 2023
DOI 10.3389/fevo.2023.1105150

OPEN ACCESS

EDITED BY
Cuicui Jiao,
Sichuan University of Science and Engineering, China

REVIEWED BY
Zhiwei Xu,
National School of Geographical Sciences, France
Xingliang Xu,
Institute of Geographic Sciences and Natural Resources Research (CAS), China

*CORRESPONDENCE
Yanlong Jia
✉ jyl198620@163.com

SPECIALTY SECTION
This article was submitted to Population, Community, and Ecosystem Dynamics, a section of the journal Frontiers in Ecology and Evolution

RECEIVED 22 November 2022
ACCEPTED 25 January 2023
PUBLISHED 20 February 2023

CITATION
Yang X, Yang L, Li Q, Li X, Xu G, Xu Z and Jia Y (2023) Short-term responses of soil nutrients and enzyme activities to nitrogen addition in a *Larix principis-rupprechtii* plantation in North China. *Front. Ecol. Evol.* 11:1105150. doi: 10.3389/fevo.2023.1105150

Short-term responses of soil nutrients and enzyme activities to nitrogen addition in a *Larix principis-rupprechtii* plantation in North China

Xiaocong Yang[1], Liu Yang[1], Qianru Li[2], Xiao Li[3], Guoqiao Xu[3], Zhongqi Xu[1] and Yanlong Jia[1]*

[1]College of Forestry, Hebei Agricultural University, Baoding, China, [2]College of Economics and Management, Hebei Agricultural University, Baoding, China, [3]Mulanweichang National Forestry Administration of Hebei Province, Chengde, China

Atmospheric nitrogen (N) deposition is among the main manifestations of global change and has profoundly affected forest biogeochemical cycles. However, the threshold of N deposition to soil nutrient contents and enzyme activities has rarely been studied in a forest. In this study, we explored the effects of N deposition on soil nutrients and enzyme activities in a *Larix principis-rupprechtii* plantation on the northern Yanshan Mountain through multigradient N addition experiments (0, 5, 10, 20, 40, 80, and 160 kg N ha^{-1} $year^{-1}$) after fertilization for 2 years. Compared with the controls, N addition first led to a decrease in soil NH_4^+-N and NO_3^--N, which then increased significantly. N addition had no significant effects on other soil nutrients. N addition overall elevated soil β-glucosidase activity. N application of >40 kg N ha^{-1} $year^{-1}$ significantly reduced soil leucine aminopeptidase activity but had no significant effects on soil acid phosphatase, N-acetyl-β-D-glucosidase, and urease activities. N addition increased the overall stoichiometry ratio of EEA C:N and EEA C:P, but EEA N:P started decreasing after N application of 40 kg N ha^{-1} $year^{-1}$. The ratios of C, N, and P acquisition activities changed from 1:1.2:1 under the control conditions to 1:1.1:1 under the N application of 160 kg N ha^{-1} $year^{-1}$. N addition increased the overall vector length and had no significant effects on the vector angle. Correlation and redundancy analyses revealed that N addition-induced change in available soil N was the main factor affecting soil enzyme activity and stoichiometry. In general, different enzyme activities had different sensitivities to N addition. Moderate N addition or atmospheric N deposition (e.g., <40 kg N ha^{-1} $year^{-1}$) had beneficial effects on soil nutrient cycling and microorganisms in a *Larix principis-rupprechtii* plantation.

KEYWORDS

nitrogen addition, *Larix principis-rupprechtii*, soil nutrients, soil enzyme activity, North China

1. Introduction

With industrial development, increases in population, and excessive use of fossil fuels, atmospheric nitrogen (N) deposition is increasing year by year. Some studies have predicted that the global nitrogen deposition rate will increase by 2.5 times in the twenty-first century (Davidson, 2009). By the end of the twentieth century, China had become among the three major N deposition regions globally. Although recent studies have shown that N deposition

in China has exhibited a stabilizing or even decreasing trend (Yu et al., 2019; Wen et al., 2020), it remains at a high level. Increased N deposition affects the growth and diversity of ecosystem plants and alters the species and structure of soil microorganisms, thereby affecting soil enzyme activity and nutrient cycling (Isbell et al., 2013). Carbon, nitrogen, and phosphorus acquisition enzymes are widely present in soil and have a crucial role in organic matter decomposition and nutrient cycling in soil (Burns et al., 2013), which reflect the microbial requirement for C, N, P, and other nutrient elements and changes in the soil environment (Gutknecht et al., 2010; Guo et al., 2022; Wang et al., 2022). Therefore, they are often used to indicate the response of soil microorganisms to global changes (Kelley et al., 2011) and have a profound terrestrial ecosystem biogeochemical cycle (Sinsabaugh et al., 2009; López-Aizpún et al., 2017). Investigating the effect of N addition on soil nutrients and enzyme activity is crucial for a deeper understanding of soil nutrient cycling in the background of increasing atmospheric N deposition.

The results of studies on the effect of N addition on soil nutrients are generally consistent. Most of them have reported that N addition increases the content of forest soil organic carbon, soluble organic carbon, total nitrogen (TN), and available nitrogen (AN) (Liu and Greaver, 2010), whereas excessive nitrogen input leads to phosphorus limitation (Elser et al., 2009; Deng et al., 2017) and loss of calcium, magnesium, and other nutrients (Huang et al., 2015; Lu et al., 2018). However, the results of studies investigating the effect of N addition on the activity of soil carbon, nitrogen, and phosphorus acquisition enzymes differed considerably. For example, with N addition, the activity of carbon acquisition-related β-1,4-glucosidase (BG) showed an increasing trend in one study (Sinsabaugh et al., 2005), no significant change in another study (Zeglin et al., 2007), and a decreasing trend in other studies (Ramirez et al., 2012; Zhang et al., 2017). Moreover, different enzyme species responded differently to the same N addition treatment. For example, Fan et al. (2018) found that N addition (40 and 80 kg N ha^{-1} $year^{-1}$) increased acid phosphatase (ACP) activity but decreased N-acetyl-β-D-glucosidase (NAG) activity in a subtropical *Castanopsiscarlesii* forest soil. The differential effects of N addition on the activities of different soil enzymes may be closely related to N application rates. However, most current experimental gradients of forest N addition are few (generally 3–4) (Sinsabaugh et al., 2005; Zhang et al., 2017), and the starting fertilizer application is high (generally >40 kg N ha^{-1} $year^{-1}$) (Fan et al., 2018), which limits us to determine the sensitivity of soil enzyme activity to nitrogen addition. Finding the threshold at which nitrogen addition starts to influence a certain enzyme activity is difficult.

Larix principis-rupprechtii is among the major silvicultural species on the northern Yanshan Mountain and is widely distributed in warm temperate areas in China. Simultaneously, North China has gradually become one of the new high deposition areas in China (Yu et al., 2019), and studying the effect of N deposition on *Larix principis-rupprechtii* plantations is important. In this study, we conducted a multigradient N addition experiment in a typical *Larix principis-rupprechtii* plantation and measured soil nutrients, microbial biomass, and activities of soil carbon and phosphorus acquisition enzymes after 2 years of fertilizer application. We hypothesized that different soil nutrients and enzyme activities have different sensitivities and threshold values to N addition. Available nutrients, such as NH_4^+ or NO_3^-, and nitrogen acquisition enzymes have high sensitivity and low threshold values to N addition. This study clarified the response and threshold values of soil nutrients and enzyme activities to N addition and thus provided a scientific basis for long-term management of *Larix principis-rupprechtii* plantations under the N deposition background.

2. Methods

2.1. Study sites

The study area is located in Mulanweichang National Forestry Administration of Hebei Province (41°35′N–42°40′N, 116°32′E–118°14′E). This area is in the transition zone between the Inner Mongolia Plateau and the northern mountains of Hebei Province and has a flat terrain and altitude of 1,200–2,000 m. The area has a typical temperate continental plateau monsoon climate. This climate is characterized by cold and dry winters and cool and heat-free summers, with an average annual temperature of ∼3.3°C. The average annual precipitation is 445 mm, mostly concentrated in July and August.

In this study, one side of a hill with consistent stand conditions was selected as the experimental sample site for N addition. The stand type was a *Larix principis-rupprechtii* plantation on the northern slope of the hill, a shady slope of ∼15°. This 30-year-old stand has an average tree diameter at a breast height of 13.2 cm, an average tree height of 10.5 m, and a density of ∼1,575 trees hm^{-2}. The understory shrubs mainly include *Rosa dahurica*, *Lespedeza bicolor*, *Armeniacasibirica*, and *Spiraea pubescens Turcz*. The main herbs are *Carex siderosticta*, *Campanula punctata*, *Moehringia trinervia*, *Artemisia mongolicau*, etc.

2.2. Experimental design

In July 2018, 28 sample plots (area of each plot: 20 m × 20 m) were set up in a row along the slope's contour. The plots were separated by a 10-m separation zone to avoid the interaction between different N application treatments. All plots were fenced to exclude human and animal interference. Before fertilization, 0–10 cm of surface soil was collected from each site by using a five-point sampling method, and soil indices such as pH, soil organic carbon (SOC), TN, total phosphorus (TP), available phosphorus (AP), ammonium nitrogen (NH_4^+-N), nitrate nitrogen (NO_3^--N), and available nitrogen (AN) were measured (Table 1). No significant differences were observed in the soil background of each site and were moderate for the nutrient addition control experiments.

The N addition gradient fertilization experiments were conducted in August 2019. N addition was divided into seven levels with four replications for each treatment in a randomized block design. Using the rain gauge method, we found that the annual atmospheric wet N deposition flux in this area is 5.03 kg

TABLE 1 Background data of soil nutrients in nitrogen addition plots.

Treatment	N0	N5	N10	N20	N40	N80	N160
SOC (g kg^{-1})	69.45 ± 3.40a	67.19 ± 4.89a	63.98 ± 2.31a	66.06 ± 5.60a	69.46 ± 3.75a	64.38 ± 2.08a	67.07 ± 7.39a
TN (g kg^{-1})	5.62 ± 0.73a	5.79 ± 0.12a	5.52 ± 1.07a	5.59 ± 0.13a	5.40 ± 0.57a	5.25 ± 0.35a	5.45 ± 0.49a
TP (g kg^{-1})	1.02 ± 0.23a	0.96 ± 0.19a	0.92 ± 0.27a	0.92 ± 0.07a	0.92 ± 0.07a	0.92 ± 0.19a	0.92 ± 0.09a
AP (mg kg^{-1})	10.98 ± 2.00a	10.95 ± 0.22a	13.92 ± 6.13a	10.43 ± 1.55a	11.52 ± 1.29a	12.62 ± 2.91a	12.18 ± 1.65a
NH_4^+-N (mg kg^{-1})	7.55 ± 2.66a	11.04 ± 2.66a	15.69 ± 9.06a	13.94 ± 7.60a	11.62 ± 2.01a	10.45 ± 3.49a	8.72 ± 1.74a
NO_3^--N (mg kg^{-1})	25.56 ± 10.51a	18.01 ± 8.77a	26.73 ± 9.91a	22.66 ± 3.49a	23.24 ± 1.01a	23.24 ± 1.01a	25.56 ± 2.66a
pH	6.11 ± 0.19a	6.01 ± 0.07a	5.94 ± 0.14a	6.12 ± 0.05a	6.06 ± 0.12a	6.02 ± 0.11a	5.99 ± 0.10a

The letters "a" in the same row indicate that there is no significant differences between different nitrogen addition gradients ($p > 0.05$).

N ha^{-1} $year^{-1}$, and 88% of it is deposited in the growing season from May to September. Thus, N concentrations for addition to the seven levels were 0 (N0), 5 (N5), 10 (N10), 20 (N20), 40 (N40), 80 (N80), and 160 (N160) kg N ha^{-1} yr^{-1} from low to high, and the fertilizer type was urea (CH_4N_2O). Urea was dissolved in 40 L of water in each sample plot and sprayed in each plot evenly. Equal amounts of water were sprayed in the control sample plot. The soil was fertilized every month in the growing season.

2.3. Field sampling

Soil surface (0–10 cm) sampling was conducted in September 2020, 2 years after fertilization was completed in the sample plots. Soil from five points on each plot was sampled and mixed into one sample. The soil were passed through a 2-mm soil sieve to remove debris such as animal residues and stones. A part of the sieved soil sample was stored in a refrigerator at 4°C to determine soil enzyme activity and microbial carbon. Another part of the soil was stored at room temperature and dried naturally to determine basic soil nutrient indices.

2.4. Measurement methods

2.4.1. Soil chemical properties

Soil organic carbon was determined using the potassium dichromate-external heating method; recalcitrant organic carbon (ROC) was determined through acid hydrolysis; soil easily oxidized organic carbon (EOC) was determined using the potassium permanganate colorimetric method; and microbial quantity carbon (MBC) was determined using the chloroform fumigation-potassium sulfate leaching method. Soil TN was determined through potassium dichromate-sulfuric acid digestion; ammonium nitrogen (NH_4^+-N) and nitrate nitrogen (NO_3^--N) were extracted with 2 mol L^{-1} KCI and determined using a continuous flow analyzer (Skalar san++, Skalar, Netherlands); AN was a sum of NH_4^+-N and NO_3^--N. Soil TP and AP were detected using the continuous flow analyzer (Hedley et al., 1982). Soil pH was determined using an acidity meter with the soil–water ratio (1:2.5). These methods can be seen in Bao (2000).

2.4.2. Determination of enzyme activity and calculation of enzyme stoichiometric ratio

Soil urease (UE), soil leucine aminopeptidase (LAP), soil ACP, soil NAG, and soil β-glucosidase (BG) were determined using the microplate fluorometric method (Chen et al., 2018). According to the requirements of the test kit, soil samples were placed in 96-well cell culture plates with the corresponding reagents and detected using a microplate reader (Thermo Scientific™, USA). The substrates of BG, NAG, UE, LAP, and ACP are 4-MUB-β-D-glucopyranoside, 4-MUB-N-acetyl-β-D-glucosaminide, urea, L-leucine-7-amino-4-methylcoumarin, and 4-MUB-phosphate, respectively.

The equations for determining the stoichiometry of soil extracellular enzymes (Keeler et al., 2009) are as follows:

$$EEA_{C:N} = \frac{\ln(BG)}{\ln(LAP + NAG)} \quad (1)$$

$$EEA_{C:P} = \frac{\ln(BG)}{\ln(ACP)} \quad (2)$$

$$EEA_{N:P} = \frac{\ln(LAP + NAG)}{\ln(ACP)} \quad (3)$$

where EEA represents the soil extracellular enzyme activity, BG represents soil β-glucosidase, NAG represents soil N-acetyl-β-D-glucosidase, LAP represents leucine aminopeptidase, and ACP represents acid phosphatase.

2.4.3. Vector characteristics of enzyme activity

To quantify the limitation of microbial metabolism of C, N, and P, vector analysis was performed on the relative proportion of enzyme activity. Vector length represents the C limitation, and the vector angle represents relative P and N limitations. Microbial C limitation increases with the vector length. A vector angle of >45° represents microbial P limitation, and that of <45° represents N limitation (Fanin et al., 2016; Moorhead et al., 2016).

$$Length = \sqrt{(EEA_{C:N})^2 + (EEA_{C:P})^2}$$
$$Angle(\circ) = Degrees\left[Atant2\left(EEA_{C:P}\right), \left(EEA_{C:N}\right)\right].$$

2.5. Data analysis

Data statistics and analysis were performed using Microsoft Excel 2019 and SPSS 22.0. One-way ANOVA and Duncan multiple

comparisons of enzyme activities for N addition treatments were performed at a significance level of $p < 0.05$ and plotted using SigmaPlot 14.0 software. The Pearson correlation analysis analyzed the correlation between soil enzyme activities and their stoichiometric ratios with soil physicochemical properties and other indicators. Redundancy analysis (RDA) was performed using Canoco 5.0 software to determine the inter-relationships between soil enzyme activities and their environmental conditions. In the forward selection step, the variable was excluded due to its collinearity with the currently selected variable. The constrained step based on a Monte Carlo permutation moved unimportant explanatory variables, and significant variables ($p < 0.05$) were used in the final analyses.

3. Results and analysis

3.1. Effects of N addition on soil chemical properties

Table 2 and Figure 1 present the effects of N addition on total soil nutrients, effective nutrients, and pH. SOC, TN, and TP with their ratios, pH, AP, and MBC exhibited no significant difference among the different levels of N added ($p > 0.05$). Soil EOC content tended to increase with increasing N addition, but it did not reach a significant level ($p > 0.05$). Soil NH_4^+-N and NO_3^--N displayed a decreasing trend with low N applications and tended to increase after the N20 or N40 treatment (Figure 1), and soil AN also exhibited the same trend as soil NO_3^--N.

3.2. Effects of N addition on soil enzyme activity and enzyme stoichiometry

Figure 2 presents the effects of N addition on the activity of each soil enzyme. Among them, N addition influenced BG activity, with an overall trend of increase and then decrease, with the highest activity observed after the N5 treatment (Figure 2A). NAG, LAP, and UE presented different responses to N addition. NAG displayed large variations in activity among N treatments and showed no obvious regularity with an increase in N addition. LAP activity first increased and then decreased with the increase in N addition, reaching its peak after the N40 treatment. No significant change was observed in UE activity after the N treatments. ACP activity also did not exhibit significant changes (Figure 2D).

Figure 3 presents the influences of N addition on the stoichiometric ratio of soil enzymes. With an increase in N addition, EEA C:N and EEA C:P presented a trend of first increasing and then decreasing. At the same time, EEA N:P exhibited an overall trend of decreasing and reached its highest value after the N10 treatment (Figure 3C).

3.3. Effect of N addition on vector characteristics of soil enzyme activity

Overall, the vector length increased with N addition ($p < 0.05$), except after the N80 treatment (Figure 4A). The vector length was the longest after the N5 treatment, thereby indicating that microorganisms experience the largest carbon limitation at the N5 level. Compared with the controls, N addition had no significant effects on the vector angle (Figure 4B). Vector angles under different gradient N addition enzymes were all <45°. This indicates that microbial communities experience nitrogen limitation to some extent, and short-term N addition did not significantly change this status.

3.4. Analysis of soil enzyme activities and stoichiometric ratios with soil environmental factors

3.4.1. Correlation analysis

The results of correlation analysis between soil enzyme activities, stoichiometric ratios, and soil environmental factors in a *Larix principis-rupprechtii* plantation after N addition are presented in Table 3. Soil BG activity significantly and negatively correlated with pH and EOC and significantly and positively correlated with MBC ($p < 0.05$). Soil LAP activity was significantly and negatively correlated with NO_3^--N and AN. Soil ACP activity was extremely and positively correlated with TP ($p < 0.01$) and significantly and negatively correlated with MBC. Soil UE activity was significantly and positively correlated with NH_4^+-N. Soil NAG activity was not significantly correlated with any of the environmental factors ($p > 0.05$).

EEA C:N was significantly and positively correlated with soil MBC. EEA C:P was significantly and negatively correlated with AN and significantly and positively correlated with MBC. EEA N:P significantly and positively correlated with soil NH_4^+-N and ROC ($p < 0.05$).

3.4.2. Redundancy analysis

As shown in Figure 5, the total interpretation rate of environmental variables on soil enzyme activities was 65.66%. The total interpretation rates on the first and second axes were 57.65% and 8.01%, respectively. NH_4^+-N and ROC were the first two factors for explaining the variation in soil enzyme activities and enzyme stoichiometry, and their interpretation rates were 20.6% and 18.6%, respectively.

4. Discussion

4.1. Effects of N addition on soil chemical properties

In this study, short-term fertilizer application exhibited no significant effect on soil SOC, TN, TP, TK, ROC, and pH but had significant effects on AN, NH_4^+-N, NO_3^--N, and MBC (Figure 1; Table 2). Most studies have reported an increase in soil AN, NH_4^+-N, and NO_3^--N contents with high N addition (Fang et al., 2009; Hu et al., 2009; Xu et al., 2009). In the present study, these factors also increased with high N addition, but they first decreased with low N application. This phenomenon has rarely been reported in forest ecosystems because the starting fertilizer application rate

TABLE 2 Effects of nitrogen addition on soil chemical properties.

Treatment	N0	N5	N10	N20	N40	N80	N160
SOC (g kg^{-1})	77.98 ± 4.53a	67.90 ± 6.12bc	70.87 ± 3.04abc	64.41 ± 3.12abc	69.97 ± 5.04c	72.55 ± 5.74abc	75.56 ± 5.21abc
TN (g kg^{-1})	6.00 ± 0.23a	5.34 ± 0.42a	5.38 ± 0.10a	5.27 ± 0.41a	5.16 ± 0.43a	5.41 ± 0.48a	5.98 ± 0.76a
TP (g kg^{-1})	0.62 ± 0.02c	0.62 ± 0.46c	0.73 ± 0.00a	0.65 ± 0.34bc	0.72 ± 0.07ab	0.62 ± 0.04c	0.68 ± 0.03abc
SOC:TN	12.99 ± 0.38a	12.82 ± 2.20a	13.15 ± 0.73a	12.25 ± 1.26a	13.66 ± 2.02a	13.40 ± 0.17a	12.81 ± 2.21a
TN:TP	9.60 ± 0.70a	8.63 ± 1.25ab	7.32 ± 0.09b	8.07 ± 0.94ab	7.11 ± 0.80b	8.64 ± 0.55ab	8.70 ± 0.92ab
SOC:TP	124.64 ± 10.19a	108.91 ± 2.95bc	96.22 ± 4.39c	98.10 ± 2.07c	96.80 ± 15.37c	115.83 ± 7.06ab	110.10 ± 7.28abc
AN (mg kg^{-1})	25.75 ± 0.76b	22.19 ± 1.02c	21.38 ± 0.16c	20.46 ± 0.76c	25.62 ± 1.43b	25.44 ± 0.24b	28.38 ± 0.33a
AP (mg kg^{-1})	7.01 ± 0.48a	6.70 ± 0.76a	7.11 ± 0.15a	6.84 ± 0.62a	6.70 ± 0.15a	6.25 ± 1.50a	6.88 ± 0.58a
ROC (g kg^{-1})	3.43 ± 0.03b	3.45 ± 0.05ab	3.47 ± 0.07ab	3.53 ± 0.03a	3.53 ± 0.04a	3.52 ± 0.02a	3.49 ± 0.01ab
EOC (g kg^{-1})	4.00 ± 0.48a	4.01 ± 0.26a	4.00 ± 0.67a	4.96 ± 0.72a	4.52 ± 0.62a	4.64 ± 0.13a	5.05 ± 0.61a
MBC (mg kg^{-1})	752.30 ± 2.00b	857.63 ± 22.97a	704.15 ± 54.09b	724.30 ± 63.23b	695.26 ± 16.91b	765.04 ± 22.87ab	718.37 ± 43.76b
pH	6.25 ± 0.04a	6.23 ± 0.16a	6.13 ± 0.06a	6.28 ± 0.09a	6.26 ± 0.05a	6.23 ± 0.01a	6.16 ± 0.51a

Different letters in the same row indicate significant differences between different nitrogen addition gradients ($p < 0.05$).

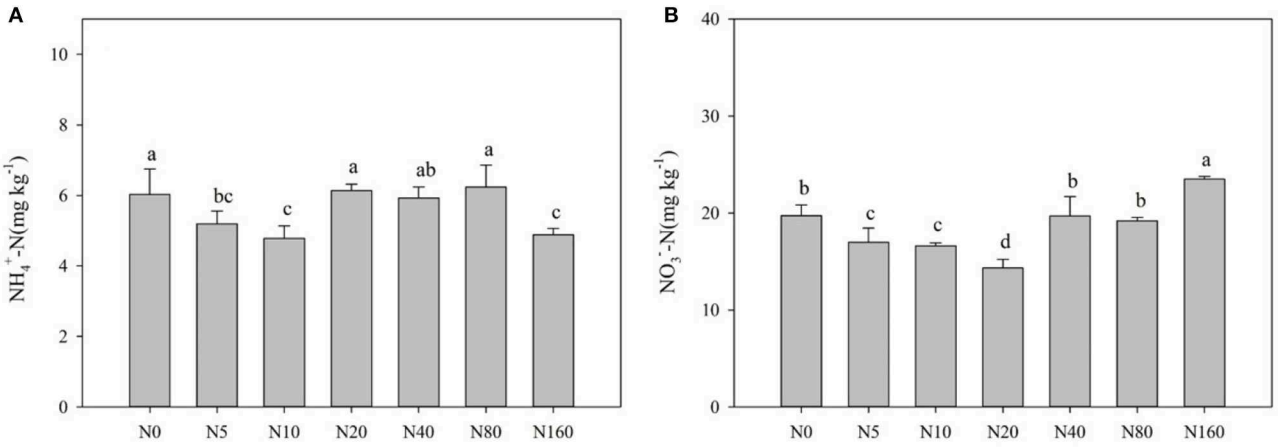

FIGURE 1
Effects of nitrogen addition on soil ammonium nitrogen **(A)** and nitrate nitrogen **(B)** in a *Larix principis-rupprechtii* plantation in North China.

was usually high in previous studies (Fan et al., 2018). Boreal forests are typically nitrogen-deficient ecosystems (Du et al., 2020). A study also found that nitrogen addition increased plant N uptake and plant biomass in North China (Du et al., 2014). N addition stimulated *Larix principis-rupprechtii* growth, but this effect was greater at a low N addition level (<40 kg N ha^{-1} year^{-1}) and lower with high N addition (unpublished data). Therefore, high N uptake by trees with low N addition is possibly the main reason for the decreased available N. Simultaneously, N addition promotes the mineralization of soil organic N, and decomposition of soil organic N after exogenous N addition directly increases the soil NH_4^+-N content (Aber, 2002) and the nitrification reaction (Bejarano et al., 2014). Therefore, when the content of available soil N exceeds the range that plants could absorb, soil NH_4^+-N and NO_3^--N accumulate and increase with high N addition.

Soil microorganisms are the most active part of soil organic matter, and MBC is a sensitive index that reflects small changes in the soil environment. Most studies have indicated that N addition causes a reduction in soil MBC content (Treseder, 2008; Janssens et al., 2010; Liu and Greaver, 2010; Zhang et al., 2017), whereas N addition did not reduce soil MBC content in this study (Table 2). In a meta-analysis, Treseder (2008) concluded that two main reasons lead to a decrease in MBC content with N addition. The first is "aluminum toxicity" in soil due to the decrease in soil pH with N addition, and the second is the microbial "carbon starvation" caused by the decrease in lignose activity, increase in melanin content, or decrease in plant carbon allocation to the subsurface with N addition. Soil MBC did not decrease in the present study because, on the one hand, short-term fertilizer application had not led to soil acidification, and on the other hand, the herbaceous plant community under the larch

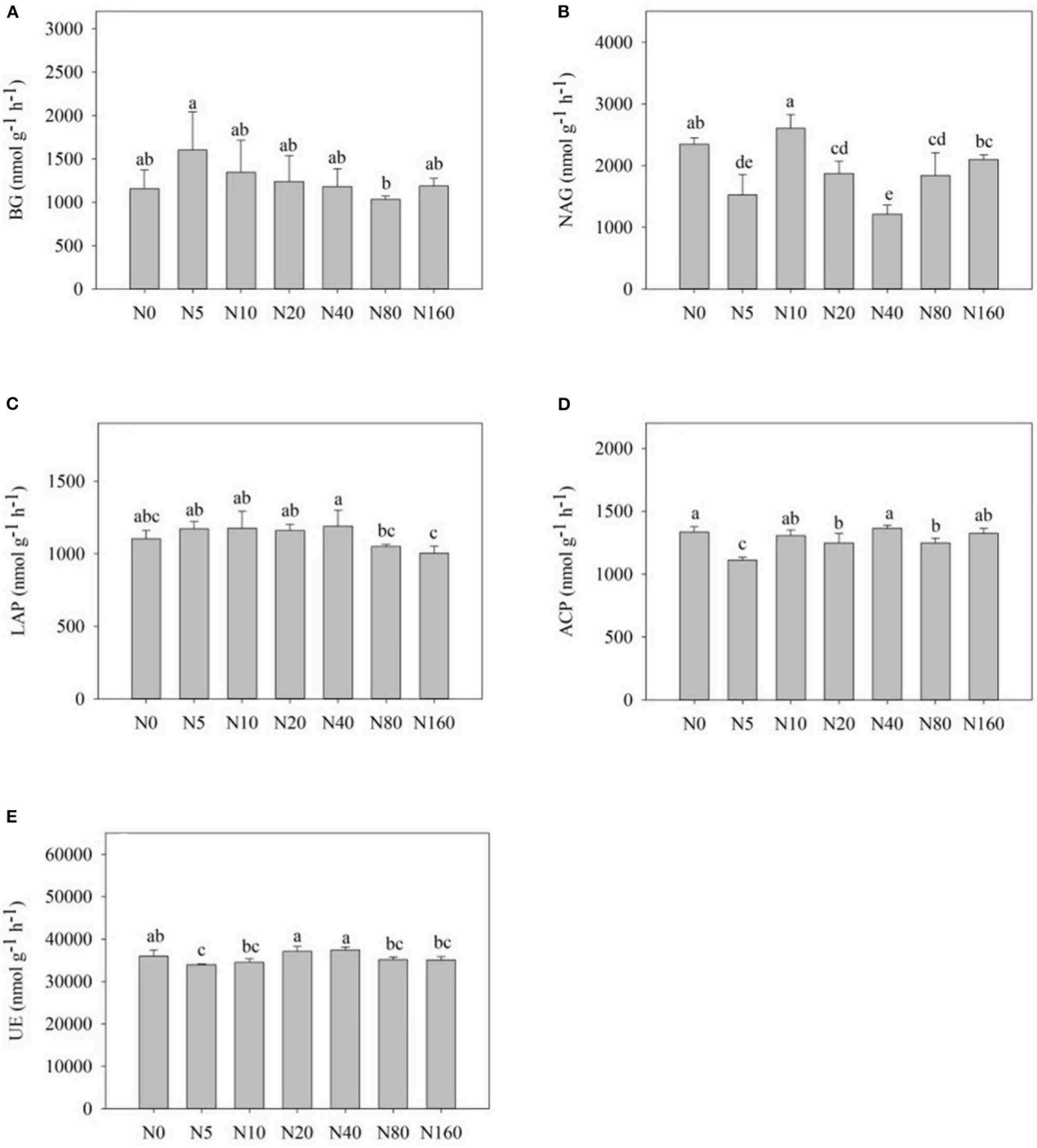

FIGURE 2
Effects of nitrogen addition on soil enzyme activity of a *Larix principis-rupprechtii* plantation in North China. **(A–E)** BG, NAG, LAP, ACP, and UE, respectively.

forest in North China was growing vigorously, and N addition significantly increased its biomass (unpublished data). The rapid turnover of herbaceous plants might have increased the soil EOC (Table 2), thereby alleviating the microbial "carbon starvation" possibly after N addition. Therefore, the role of understory plants in connection to the effect of N addition on soil nutrients needs to be further explored.

4.2. Effect of N addition on soil enzyme activities and stoichiometric ratios

Atmospheric N deposition can affect the balance of energy flow and nutrient cycle within forest ecosystems (Liu et al., 2017). Soil enzymes are more sensitive to environmental changes, so they act as an indicator of the soil response to N deposition

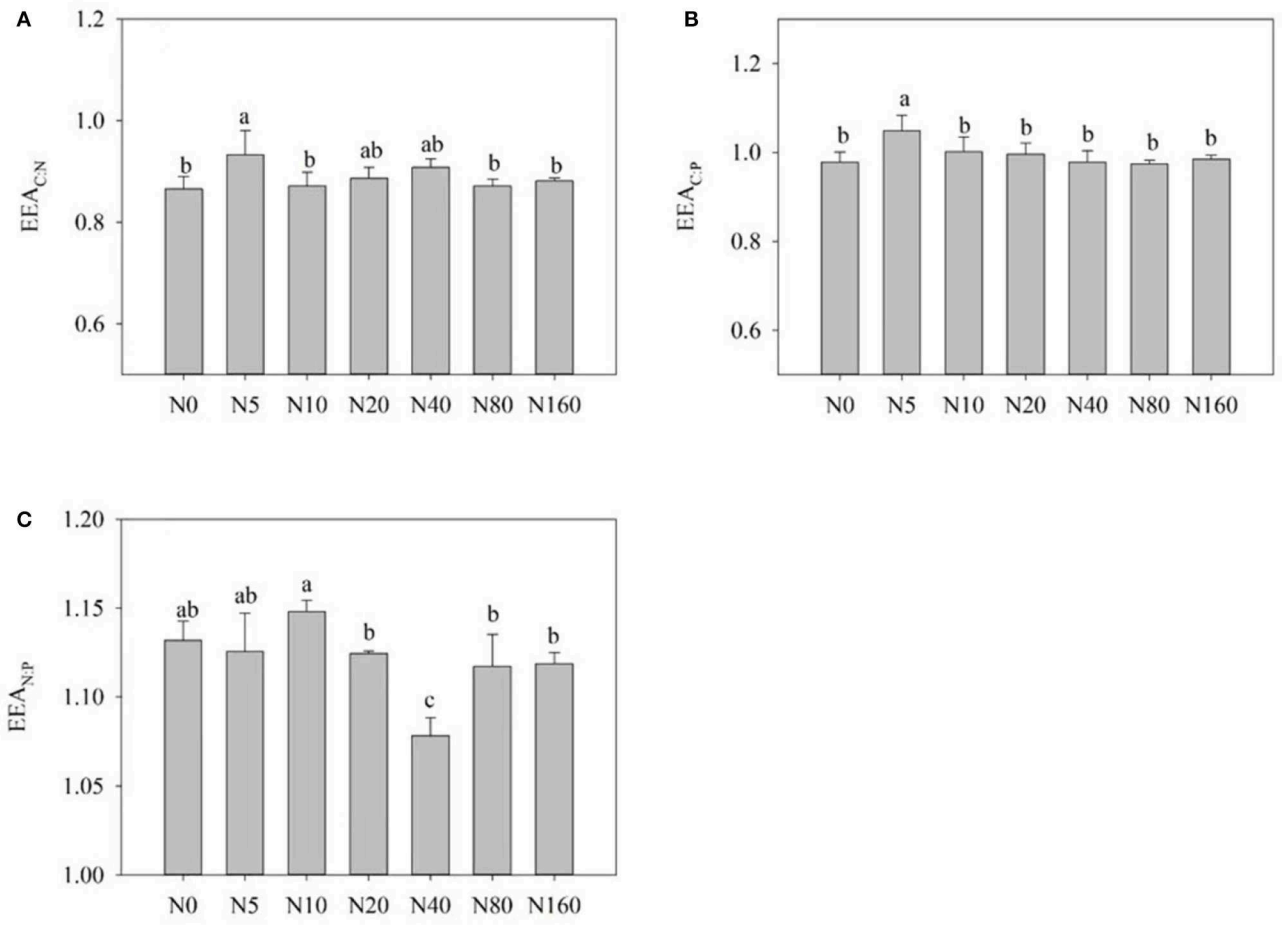

FIGURE 3
Effects of nitrogen addition on soil enzyme stoichiometry in a *Larix principis-rupprechtii* plantation in North China. **(A–C)** BG: (LAP+NAG), BG:ACP, and (LAP+NAG):ACP, respectively.

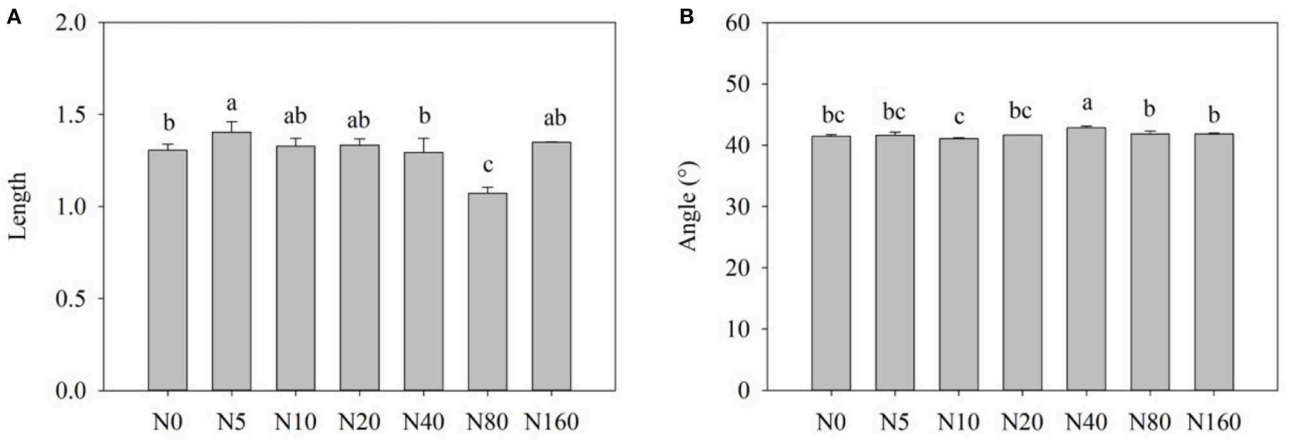

FIGURE 4
Effect of nitrogen addition on the length **(A)** and angle **(B)** of enzyme activity vector.

(Sinsabaugh et al., 2005). We here focused on the activities of five soil carbon, nitrogen, and phosphorus acquisition enzymes. A total of 2 years after N addition, BG and LAP activities exhibited regular changes, whereas NAG, UE, and ACP activities exhibited no significant regular changes. LAP activity was significantly lower after high N treatment (>80 kg N ha^{-1} year^{-1}) than in the control

TABLE 3 Pearson correlation between soil enzymes, stoichiometric ratios, and soil physicochemical properties.

	BG	NAG	LAP	UE	ACP	EEA C:N	EEA C:P	EEA N:P
pH	−0.450*	−0.197	0.126	0.163	−0.187	−0.283	−0.263	−0.043
SOC	0.130	0.379	−0.223	−0.077	0.388	−0.137	−0.080	0.138
TN	−0.265	0.430	−0.297	−0.015	0.194	−0.145	−0.428	0.304
TP	0.162	0.055	0.090	0.323	0.557**	0.295	0.118	−0.241
AP	0.114	0.402	−0.025	−0.052	0.079	0.090	−0.109	0.349
AN	−0.427	−0.096	−0.490*	0.379	−0.052	−0.251	−0.497*	−0.355
NH_4^+-N	−0.278	−0.395	−0.047	0.460*	0.101	−0.252	−0.028	−0.438*
NO_3^--N	−0.349	0.000	−0.464*	−0.159	0.344	−0.311	−0.237	−0.241
MBC	0.557*	−0.219	0.111	−0.258	−0.480*	0.448*	0.548*	0.053
SOC:TN	0.364	−0.104	0.084	−0.045	0.031	0.042	0.352	−0.193
SOC:TP	−0.041	0.231	−0.228	−0.110	−0.328	−0.320	−0.155	0.262
TN:TP	−0.286	0.261	−0.258	−0.230	−0.225	−0.274	−0.367	0.367
EOC	−0.481*	−0.257	−0.336	−0.087	−0.228	−0.372	−0.251	−0.240
ROC	−0.013	−0.428	−0.124	0.157	0.116	0.038	0.213	−0.529*

*Significant correlation between two different variables ($p < 0.05$); **An extremely significant correlation ($p < 0.01$).

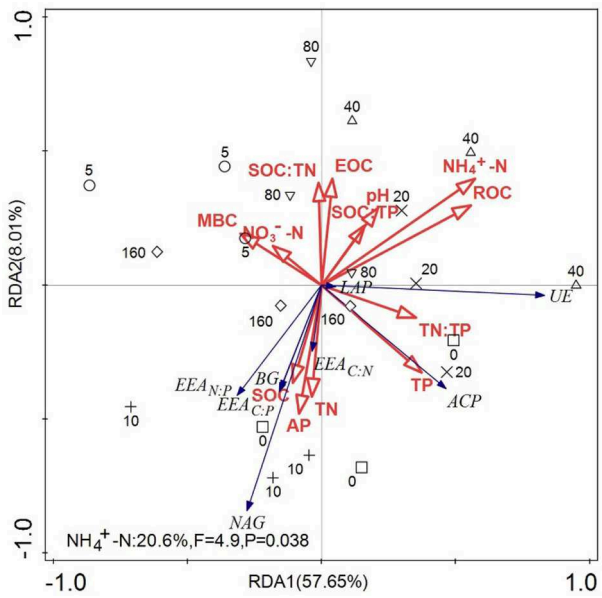

FIGURE 5
Redundant analysis diagram of the influence of soil nutrients on soil enzyme activity and stoichiometric ratios. Soil enzyme activity and the ecological enzyme stoichiometric ratio were used as response variables, and soil environmental factors were used as explanatory variables for redundancy analysis (RDA). The arrows connecting soil microbial enzyme activities and enzyme stoichiometric ratios are in blue, and the arrows connecting the soil environmental factors are in red.

and low N groups. High N addition reduced N acquisition enzyme activity, which is consistent with the results of most studies (Dong et al., 2019). According to the resource allocation model (Allison and Vitousek, 2005), N addition can alter soil enzyme activity by affecting the effectiveness of soil nutrients (Wallenius et al., 2011), and enzyme activity associated with N acquisition decreases because of an increase in the effective soil N content under N addition conditions (Berg and Matzner, 2011). The correlation analysis results revealed that the increase in soil AN and NO_3^--N after N addition was the primary cause of the decreased LAP activity (Table 3).

The resource allocation model also suggested that the activities of carbon acquisition enzymes increase after N addition. The increase in BG activity after N addition, in this study, is consistent with the results obtained from the USA (Sinsabaugh et al., 2005). N application generally stimulates microbial activity, thereby increasing the demand for carbon and the activity of carbon-associated soil enzymes (Keeler et al., 2009). In the present study, pH was negatively correlated with BG activity, which agrees with the results of a meta-analysis (Sinsabaugh et al., 2008). The decreased pH and the high H^+ concentration could inhibit the biomass of soil microorganisms, which in turn had an inhibitory effect on enzyme activity. In addition, the change in pH induces a change in the binding state of soil particles, thus leading to a consequent change in soil enzyme activity. In this study, EOC was negatively correlated with BG activity. This may be because when the content of EOC, as a more active part of organic carbon, increases, the organic carbon-decomposing extracellular enzymes would have negative feedback. Soil microorganisms reduce the energy required to synthesize enzymes to a certain extent. This would allow the effective promotion of microbial growth by nutrients, thereby limiting the release of nutrients and inhibiting carbon hydrolase activity in the soil (Enrique et al., 2008).

At the global scale, the ratio of specific C, N, and P acquisition activities is 1:1:1 (Sinsabaugh et al., 2008). In this study, this ratio changed from 1:1.2:1 under the control condition to 1:1.1:1 after treatment with 160 kg N ha^{-1} $year^{-1}$, thereby indicating that N limitation occurred in this area. The vector angle also exhibited this

phenomenon (Figure 4B). Short-term N addition alleviated this N limitation to some extent but led to no change in this situation. In the present study, the overall increase in BG activity, enzyme EEA C:N, and enzyme vector length with N addition also indicated that N addition exacerbated carbon limitation, which accorded to the "optimal allocation" principle of ecological economics (Sinsabaugh and Moorhead, 1994). Therefore, soil microorganisms in this area were simultaneously under C and N limitation, and N addition aggravated the C limitation. These results were obtained due to short-term N addition, and we believe that it can be alleviated when plant litter increases after long-term N addition.

4.3. Implication for forest ecosystem management

Notably, in this study, the sensitivities of enzyme activities related to carbon, nitrogen, and phosphorus differed in response to N addition in *Larix principis-rupprechtii* plantation soils. The activities of carbon acquisition enzymes (e.g., BG) were altered with low N addition, and those of nitrogen acquisition enzymes (e.g., LAP) responded significantly with medium N addition ($\sim$40 kg N ha^{-1} yr^{-1}). By contrast, the activities of phosphorus acquisition enzymes (e.g., ACP) did not change significantly. The different sensitivities of these soil enzymes to the N addition rate had important implications for ecosystem management. Unlike plants, which are typically limited from accessing nitrogen in terrestrial ecosystems (LeBauer and Treseder, 2008), heterotrophic microorganisms are more susceptible to carbon limitation. In this study, soil microorganisms were simultaneously under C and N limitations. Moreover, with high N addition (>40 kg N ha^{-1} $year^{-1}$), the soil enzyme N:P ratio decreased, and the vector angle increased slightly, thereby indicating a risk of phosphorus limitation. A healthy forest needs a nutritive element balance between C, N, and P. Therefore, in this study, moderate N addition or atmospheric N deposition had beneficial effects on soil microbial growth and nutrient cycling and promoted forest growth with positive ecological effects on the ecosystem.

5. Conclusion

In this study, the effects of 2 years of N addition on soil nutrients, enzyme activities, and stoichiometric ratios were investigated in a *Larix principis-rupprechtii* plantation on the northern Yanshan Mountain in China. Our results revealed that short-term N addition had no significant effects on total nutrients, AP, soil pH, or MBC in larch plantations. Soil AN, NH_4^+-N, and NO_3^--N contents decreased with low N addition and significantly increased with high N addition. The sensitivities of different enzyme activities in response to N addition varied. BG activity increased with low N treatment, and LAP activity started to decrease significantly with medium N application (40 kg N ha^{-1} $year^{-1}$) treatment. The other three enzymes exhibited no sensitivity to short-term N addition. Soil NH_4^+-N and NO_3^--N contents were the main environmental factors influencing soil enzyme activity and altered enzyme stoichiometric ratios under N addition. In general, moderate N addition or atmospheric N deposition was beneficial for soil nutrient cycling and microorganisms in *Larix principis-rupprechtii* plantations.

Data availability statement

The original contributions presented in the study are included in the article/supplementary material, further inquiries can be directed to the corresponding author.

Author contributions

YJ and ZX contributed to the design of the study. XY, LY, XL, and GX performed the experiment. XY performed the statistical analysis. XY, QL, and YJ wrote the first draft of the manuscript. All authors contributed to the manuscript revision and reading and approved the submitted version.

Funding

This study was supported by the National Natural Science Foundation of China (31700377) and the Natural Science Foundation of Hebei (C2018204096).

Conflict of interest

The authors declare that the research was conducted in the absence of any commercial or financial relationships that could be construed as a potential conflict of interest.

Publisher's note

References

Aber, J. D. (2002). Nitrogen saturation in temperate forest ecosystems: current theory, remaining questions and recent advances. *Prog. Nutr.* 98: 179–188. doi: 10.1007/978-94-017-2789-1-13

Allison, S. D., and Vitousek, P. M. (2005). Responses of extracellular enzymes to simple and complex nutrient inputs. *Soil Boil. Biochem.* 37: 937–944. doi: 10.1016/j.soilbio.2004.09.014

Bao, S. D. (2000). *Soil and Agricultural Chemistry Analysis*. Beijing: China Agricultural Press.

Bejarano, M., Etchevers, J. D., Ruíz-Suárez, G., and Julio, C. (2014). The effects of increased N input on soil C and N dynamics in seasonally dry tropical forests: an experimental approach. *Appl. Soil Ecol.* 73, 105–115. doi: 10.1016/j.apsoil.2013.08.015

Berg, B., and Matzner, E. (2011). Effect of N deposition on decomposition of plant litter and soil organic matter in forest systems. *Environ. Rev.* 5, 1–25. doi: 10.1139/er-5-1-1

Burns, R. G., Deforest, J. L., Marxsen, J., Sinsabaugh, R. L., Stromberger, M. E., Wallenstein, M. D., et al. (2013). Soil enzymes in a changing environment: current knowledge and future directions. *Soil Biol. Biochem.* 58, 216–234. doi: 10.1016/j.soilbio.2012.11.009

Chen, H., Li, D. J., Xiao, K. C., and Wang, K. L. (2018). Soil microbial processes and resource limitation in karst and non-karst forests. *Funct. Ecol.* 32, 1400–1409. doi: 10.1111/1365-2435.13069

Davidson, E. A. (2009). The contribution of manure and fertilizer nitrogen to atmospheric nitrous oxide since 1860. *Nat. Geosci*. 2, 659–662. doi: 10.1038/ngeo608

Deng, Q., Hui, D. F., Dennis, S., and Reddy, C. (2017). Responses of terrestrial ecosystem phosphorus cycling to nitrogen addition: a meta-analysis. *Glob. Ecol. Biogeogr.* 26, 713–728. doi: 10.1111/geb.12576

Dong, C. C., Wang, W., Liu, H. Y., Xu, X. T., and Zeng, H. (2019). Temperate grassland shifted from nitrogen to phosphorus limitation induced by degradation and nitrogen deposition: evidence from soil extracellular enzyme stoichiometry. *Ecol. Indic.* 101, 453–464. doi: 10.1016/j.ecolind.2019.01.046

Du, E. Z., César, T., Adam, F. A. P., Anders, A., Lissa, C. J., Zhang, X., et al. (2020). Global patterns of terrestrial nitrogen and phosphorus limitation. *Nat. Geosci.* 13, 221–226. doi: 10.1038/s41561-019-0530-4

Du, Z. H., Wang, W., Zeng, W. J., and Zeng, H. (2014). Nitrogen deposition enhances carbon sequestration by plantations in Northern China. *PLoS ONE* 9, e87975. doi: 10.1371/journal.pone.0087975

Elser, J. J., Andersen, T., Baron, J. S., Bergström, A. K., Jansson, M., Kyle, M., et al. (2009). Shifts in lake N:P stoichiometry and nutrient limitation driven by atmospheric nitrogen deposition. *Science* 326, 835–837. doi: 10.1126/science.1176199

Enrique, A., Bruno, C., Christopher, A., Virgile, C., and Stéven, C. (2008). Effects of nitrogen availability on microbial activities, densities and functional diversities involved in the degradation of a Mediterranean evergreen oak litter (*Quercus ilex L.*). *Soil Boil. Biochem*. 40, 1654–1661. doi: 10.1016/j.soilbio.2008.01.020

Fan, Y. X., Lin, F., Yang, L. M., Zhong, X. J., Wang, M. H., Zhou, J. C., et al. (2018). Decreased soil organic P fraction associated with ectomycorrhizal fungal activity to meet increased P demand under N application in a subtropical forest ecosystem. *Biol. Fert. Soils* 54, 149–161. doi: 10.1007/s00374-017-1251-8

Fang, Y. T., Gundersen, P., Mo, J. M., and Zhu, W. X. (2009). Nitrogen leaching in response to increased nitrogen inputs in subtropical monsoon forests in southern China. *Forest Ecol. Manag.* 257, 332–342. doi: 10.1016/j.foreco.2008.09.004

Fanin, N., Moorhead, D., and Bertrand, I. (2016). Eco-enzymatic stoichiometry and enzymatic vectors reveal differential C, N, P dynamics in decaying litter along a land-use gradient. *Biogeochemistry* 129, 21–36. doi: 10.1007/s10533-016-0217-5

Guo, D. L., Ou, Y. S., Zhou, X. H., Wang, X., Zhao, Y. F., Li, J., et al. (2022). Response of soil enzyme activities to natural vegetation restorations and plantation schemes in a landslide-prone region. *Forests* 13, 880. doi: 10.3390/f13060880

Gutknecht, J. L. M., Henry, H. A. L., and Balser, T. C. (2010). Inter-annual variation in soil extra-cellular enzyme activity in response to simulated global change and fire disturbance. *Pedobiologia* 53, 283–293. doi: 10.1016/j.pedobi.2010.02.001

Hedley, M. J., Stewart, J. W. B., and Chauhan, B. S. (1982). Changes in inorganic and organic soil phosphorus fractions induced by cultivation practices and by laboratory incubations. *Soil Sci. Soc. Am. J.* 46, 970–976. doi: 10.2136/sssaj1982.03615995004600050017x

Hu, Y. L., Han, S. J., Li, X. F.,Zhao, Y. T., and Li, T. (2009). Responses of soil available nitrogen of natural forest and secondary forest to simulated N deposition in Changbai Mountain (in Chinese). *J. Northeast For. Univ.* 37. 36–38. doi: 10.1016/j.elecom.2008.10.019

Huang, Y. M., Kang, R. H., Mulder, J., Zhang, T., and Duan, L. (2015). Nitrogen saturation, soil acidification, and ecological effects in a subtropical pine forest on acid soil in southwest China. *J. Geophys Res-Biogeo.* 120, 2457–2472. doi: 10.1002/2015JG003048

Isbell, F., Reich, P. B., Tilman, D., Hobbie, S. E., Polasky, S., and Binder, S. (2013). Nutrient enrichment, biodiversity loss, and consequent declines in ecosystem productivity. *Proc. Natl. Acad. Sci. USA* 110, 11911–11916. doi: 10.1073/pnas.1310880110

Janssens, I. A., Dieleman, W., Luyssaert, S., Subke, J. A., Reichstein, M., Ceulemans, R., et al. (2010). Reduction of forest soil respiration in response to nitrogen deposition. *Nat. Geosci.* 3, 315–322. doi: 10.1038/ngeo844

Keeler, B. L., Hobbie, S. E., and Kellogg, L. E. (2009). Effects of long-term nitrogen addition on microbial enzyme activity in eight forested and grassland sites: implications for litter and soil organic matter decomposition. *Ecosystems* 12, 1–15. doi: 10.1007/s10021-008-9199-z

Kelley, A. M., Fay, P. A., Polley, H. W., Gill, R. A., and Jackson, R. B. (2011). Atmospheric CO_2 and soil extracellular enzyme activity: a meta-analysis and CO_2 gradient experiment. *Ecosphere* 2, 1–20. doi: 10.1890/ES11-00117.1

LeBauer, D. S., and Treseder, K. K. (2008). Nitrogen limitation of net primary productivity in terrestrial ecosystems is globally distributed. *Ecology* 89: 371–379. doi: 10.1890/06-2057.1

Liu, L., and Greaver, T. L. (2010). A global perspective on belowground carbon dynamics under nitrogen enrichment. *Ecol. Lett.* 13, 819–828. doi: 10.1111/j.1461-0248.2010.01482.x

Liu, X. F., Yang, Z. J., Lin, C. F., Giardina, C. P., Xiong, D. C., Chen, G. S., et al. (2017). Will nitrogen deposition mitigate warming-increased soil respiration in a young subtropical plantation? *Agric. For. Meteorol*. 246, 78–85. doi: 10.1016/j.agrformet.2017.06.010

López-Aizpún, M., Arango-Mora, C., Santamaría, C., Elustondo, D., Lasheras, E., Santamaria, J. M., et al. (2017). Atmospheric ammonia concentration modulates soil enzyme and microbial activity in an *oak* forest affecting soil microbial biomass. *Soil Boil. Biochem*. 116, 378–387. doi: 10.1016/j.soilbio.2017.10.020

Lu, X. K., Vitousek, P. M., Mao, Q. G., Gilliam, F. S., Luo, Y., Zhou, G., et al. (2018). Plant acclimation to long-term high nitrogen deposition in an N-rich tropical forest. *Proc. Natl. Acad. Sci. USA* 115, 5187–5192. doi: 10.1073/pnas.1720777115

Moorhead, D. L., Sinsabaugh, R. L., Hill, B. H., and Weintraub, M. N. (2016). Vector analysis of ecoenzyme activities reveal constraints on coupled C, N and P dynamics. *Soil Boil Biochem* 93, 1–7. doi: 10.1016/j.soilbio.2015.10.019

Ramirez, K. S., Craine, J. M., and Fierer, N. (2012). Consistent effects of nitrogen amendments on soil microbial communities and processes across biomes. *Glob. Change Biol.* 18, 1918–1927. doi: 10.1111/j.1365-2486.2012.02639.x

Sinsabaugh, R. L., Gallo, M. E., Lauber, C., Waldrop, M. P., and Zak, D. R. (2005). Extracellular enzyme activities and soil organic matter dynamics for northern hardwood forests receiving simulated nitrogen deposition. *Biogeochemistry* 75, 201–215. doi: 10.1007/s10533-004-7112-1

Sinsabaugh, R. L., Hill, B. H., and Shah, J. J. F. (2009). Ecoenzymatic stoichiometry of microbial organic nutrient acquisition in soil and sediment. *Nature* 462: 795–798. doi: 10.1038/nature08632

Sinsabaugh, R. L., Lauber, C. L., Weintraub, M. N., Ahmed, B., Allison, S. D., Crenshaw, C., et al. (2008). Stoichiometry of soil enzyme activity at global scale. *Ecol. Lett.* 11, 1252–1264. doi: 10.1111/j.1461-0248.2008.01245.x

Sinsabaugh, R. L., and Moorhead, D. L. (1994). Resource allocation to extracellular enzyme production: a model for nitrogen and phosphorus control of litter decomposition. *Soil Biol. Biochem.* 26, 1305–1311. doi: 10.1016/0038-0717(94)90211-9

Treseder, K. K. (2008). Nitrogen additions and microbial biomass: a meta-analysis of ecosystem studies. *Ecol. Lett*. 11, 1111–1120. doi: 10.1111/j.1461-0248.2008.01230.x

Wallenius, K., Rita, H., Mikkonen, A., Lappi, K., Lindström, K., Hartikainen, H., et al. (2011). Effects of land use on the level, variation and spatial structure of soil enzyme activities and bacterial communities. *Soil Boil. Biochem*. 43, 1464–1473. doi: 10.1016/j.soilbio.2011.03.018

Wang, M. W., Li, J., Shen, F. Y., Meng, J., Wang, J. L., Shan, C. F., et al. (2022). Differential responses of soil extracellular enzyme activity and stoichiometric ratios under different slope aspects and slope positions in *Larix olgensis* plantations. *Forests* 13, 845. doi: 10.3390/f13060845

Wen, Z., XU, W., Li, Q., Han, M. J., Tang, A. H., Zhang, Y., et al. (2020). Changes of nitrogen deposition in China from 1980 to 2018. *Environ. Int.* 144, 106022. doi: 10.1016/j.envint.2020.106022

Xu, X. K., Lin, H., Luo, X. B., and Liu, Z. R. (2009). Effects of nitrogen addition on dissolved N_2O and CO_2, dissolved organic matter, and inorganic nitrogen in soil solution under a temperate old-growth forest. *Geoderma* 151, 370–377. doi: 10.1016/j.geoderma.2009.05.008

Yu, G. R., Jia, Y. L., He, N. P., Zhu, J. X., Chen, Z., Wang, Q. F., et al. (2019). Stabilization of atmospheric nitrogen deposition in China over the past decade. *Nat. Geosci.* 12, 424–429. doi: 10.1038/s41561-019-0352-4

Zeglin, L. H., Stursova, M., Sinsabaugh, R. L., and Collins, S. L. (2007). Microbial responses to nitrogen addition in three contrasting grassland ecosystems. *Oecologia* 154, 349–359. doi: 10.1007/s00442-007-0836-6

Zhang, C., Zhang, X. Y., Zou, H. T., Kou, L., Yang, Y., Wen, X. F., et al. (2017). Contrasting effects of ammonium and nitrate additions on the biomass of soil microbial communities and enzyme activities in subtropical China. *Biogeosciences* 14, 4815–4827. doi: 10.5194/bg-14-4815-2017

frontiers | Frontiers in Ecology and Evolution

TYPE Original Research
PUBLISHED 24 February 2023
DOI 10.3389/fevo.2023.1135895

OPEN ACCESS

EDITED BY
Wei Zhao,
Institute of Geographic Sciences and Natural Resources Research (CAS), China

REVIEWED BY
Zengyun Hu,
Xinjiang Institute of Ecology and Geography (CAS), China
Sergio Noce,
Foundation Euro-Mediterranean Center on Climate Change (CMCC), Italy

*CORRESPONDENCE
Zhibin He
✉ hzbmail@lzb.ac.cn

SPECIALTY SECTION
This article was submitted to Population, Community, and Ecosystem Dynamics, a section of the journal Frontiers in Ecology and Evolution

RECEIVED 02 January 2023
ACCEPTED 01 February 2023
PUBLISHED 24 February 2023

CITATION
Zhao P, He Z, Ma D and Wang W (2023) Evaluation of ERA5-Land reanalysis datasets for extreme temperatures in the Qilian Mountains of China.
Front. Ecol. Evol. 11:1135895.
doi: 10.3389/fevo.2023.1135895

Evaluation of ERA5-Land reanalysis datasets for extreme temperatures in the Qilian Mountains of China

Peng Zhao[1,2], Zhibin He[1]*, Dengke Ma[1,2] and Wen Wang[1,2]

[1]Linze Inland River Basin Research Station, Key Laboratory of Inland River Basin Science, Northwest Institute of Eco-Environment and Resource, Chinese Academy of Sciences, Lanzhou, China, [2]University of Chinese Academy of Sciences, Beijing, China

An increase in extreme temperature events could have a significant impact on terrestrial ecosystems. Reanalysis temperature data are an important data set for extreme temperature estimation in mountainous areas with few meteorological stations. The ability of ERA5-Land reanalysis data to capture the extreme temperature index published by the Expert Team on Climate Change Detection and Indices (ETCCDI) was evaluated by using the observational data from 17 meteorological stations in the Qilian Mountains (QLM) during 1979–2017. The results show that the ERA5-Land reanalysis temperature data can capture well for the daily maximum temperature, two warm extremes (TXx and TX90p) and one cold extreme (FD0) in the QLM. ERA5-Land's ability to capture temperature extremes is best in summer and worst in spring and winter. In addition, ERA5-Land can capture trends in all extreme temperature indices except the daily temperature range (DTR). The main bias of ERA5-Land is due to the difference in elevation between the ground observation station and the ERA5-Land grid point. The simulation accuracy of ERA5-Land increases with the decrease of elevation difference. The results can provide a reference for the study of local extreme temperature by using reanalysis data.

KEYWORDS

reanalysis, extreme temperature, ERA5-Land, Qilian Mountains, climate change

1. Introduction

Between 2011 and 2020, the average temperature of the global surface was 1.1°C warmer than it was at the end of the 19th century (before the Industrial Revolution) (IPCC, 2021). Since the 1950s, all inhabited regions have seen more frequent and more intense heat waves, while extreme cold temperatures have become fewer and milder, which affects people's lives and property safety (Shtober-Zisu and Wittenberg, 2021). Global warming has also led to the spread of extreme events to places where they have not been common before. The extent of warming projected by models after the 2050s is associated with taking action against climate change. If carbon dioxide emissions are drastically and rapidly reduced from now on and throughout the 21st century, warming will stop around the middle of the century, and warming will be around 1.5°C or 2°C by the end of the century. With global warming, heat waves, heavy rainfall and droughts will continue to become more severe and frequent (Ruml et al., 2017; Sun et al., 2017; Supari et al., 2017).

Generally, previous research on extreme temperatures utilized observational data (Lin et al., 2017; Ruml et al., 2017; Sun et al., 2017; Supari et al., 2017). However, in mountainous

areas with complex climatic conditions and terrain, there are few meteorological stations, limiting the availability of data. Reanalysis data such as ERA-Interim, ERA5, and NCEP have been extensively applied because of their higher resolution and longer time series (Zhao P. et al., 2020; Virman et al., 2021; Araujo et al., 2022; Zhao and He, 2022b; Zou et al., 2022). However, biases between observations and reanalysis data may exist, suggesting that it is necessary to compare reanalysis error with observations (Liu L. et al., 2020; Huai et al., 2021; Rakhmatova et al., 2021; Wu et al., 2021a,b; Xin et al., 2021; Li et al., 2022). European Centre for Medium-Range Weather Forecasts (ECMWF) implements the Copernicus Climate Change Service (C3S) on behalf of the European Union. As part of the Copernicus project, ECMWF has provided ERA5-Land, a state-of-the-art reanalysis data set for land applications, which is available for free in the Copernicus Climate Data Store (Joaquín et al., 2021). ERA5-Land reanalysis data have finer resolution ($0.1° \times 0.1°$) than ERA5 and ERA-Interim reanalysis data (Alexander and Gregor, 2020; Cao et al., 2020; Jiang et al., 2020; Liu J. et al., 2020; Luis and Johannes, 2020; Pelosi et al., 2020; Konstantinos et al., 2021; Pelosi and Chirico, 2021). Several studies evaluated ERA5-Land data (Cao et al., 2020; Pelosi et al., 2020; Zandler et al., 2020; Jiao et al., 2021; Rakhmatova et al., 2021; Ruqing et al., 2021; Wu et al., 2021b; Jintao et al., 2022). For example, Zou et al. (2022) found that ERA5-Land underestimated the observed temperature of coastal urban agglomerations in southeast China with a mean bias of 0.90°C. Araujo et al. (2022) found that the ERA5-Land reanalysis temperature was reliable for Pernambuco, Brazil. Hong et al. (2021) found that the performance of ERA5 precipitation products in Jiangxi Province, China was worse than that of ERA5-Land in 2019.

The Qilian Mountains are an important ecological protection barrier in northwest China and an important water source for Hexi Corridor (Deng et al., 2013; Yang et al., 2021). Due to the complex terrain and climatic conditions of the QLM, meteorological stations are rare, especially above 3,500 m (Lin et al., 2017; Wang L. et al., 2019; Wang X. et al., 2019; Zhou et al., 2019), necessitating the use of reanalysis data. Zhao and He (2022a) assessed ERA5-Land reanalysis monthly average temperature for the QLM and found that the observed temperature variation was captured very well. Li et al. (2022) found that ERA5-Land was more suitable than China Meteorological Forcing Dataset for analyzing temperature trends in the QLM. However, previous studies which evaluated reanalysis data for the QLM were primarily focused on monthly averages but rarely examined extreme temperature events. The Qilian Mountains and Hexi Corridor are affected by different circulation systems, and the local climate changes are more complicated, with frequent meteorological disasters such as drought, flood, sandstorm, dry hot air, low temperature freezing damage and snow disaster. Therefore, evaluating the reliability of ERA5-Land data is necessary in understanding extreme temperature events in the QLM.

Here, we used temperature data for the years 1979 to 2017 from 17 meteorological stations in the QLM to evaluate the ability of ERA5-Land reanalysis data to capture extreme temperature events. Evaluation of the extremes of temperature with reanalysis datasets provides a reference for the research on climate change in the QLM.

2. Data and methods

2.1. ERA5-Land temperature data (T_e)

ERA5-Land hourly data were downloaded from the website of ECMWF (link:[1]). We used ERA5-Land hourly 2 m temperature data for years 1979 to 2017 in this study. The location of cell grid points ranged from 35.8 to 40°N and from 93.5 to 104°E, which covered the entire QLM region (Figure 1). According to the latitude and longitude coordinates of the 17 stations, the ERA5-Land cell closest to each station is selected to avoid spatial interpolation (Zhao and He, 2022a). ERA5-Land hourly reanalysis data is given for UTC time, with an 8-h difference from Beijing time in China; we matched the times of observation and ERA5-Land reanalysis with a time-difference conversion method (Zhao P. et al., 2020; Xu et al., 2022). ERA5-Land grid elevation is extracted from the Digital Elevation Model (DEM) of Geospatial data cloud,[2] with the information of ASTER GDEM 30 m. The spatial range of DEM used in this study is 33.94–45.29°N, 88.81–107.24°E, which can cover the entire the Qilian Mountains (Table 1; Figure 1).

2.2. Observations (T_o)

In this study, observational daily temperature data including daily mean temperature (T_mean), daily maximum temperature (T_max) and daily minimum temperature (T_min) at 17 meteorological stations in the QLM were obtained from China Meteorological Data Sharing Service of National Meteorological Information Center.[3] These data can be directly used in scientific research after strict quality control by provider from five aspects: climate limit value and allowable value checking, extreme value checking, internal consistency checking between timing value, daily average, and daily extreme value, time consistency checking, and space consistency checking (Zhao C. et al., 2020; Zhao P. et al., 2020; Zhao and He, 2022a). Spatial distribution and specific information on the meteorological stations can be found in Figure 1 and Table 1, respectively.

2.3. Extreme temperature indices

Eleven extreme temperature indices were selected from ETCCDI (Yin and Sun, 2017) based on their application in climatology research in the region (Hu et al., 2017; Yin and Sun, 2017; Yu et al., 2020; Xu et al., 2022). These indices were grouped into four types: (1) absolute indices (TNx, TNn, TXn, and TXx), (2) threshold indices (ID0 and FD0), (3) percentile-based indices (TN10p, TX10p, TN90p, and TX90p), and (4) other indices (DTR) (Table 2).

1 https://cds.Climate.copernicus.eu/cdsapp#!/dataset/reanalysis-era5-land?tab=form

2 https://www.gscloud.cn

3 http://cdc.cma.gov.cn/index.jsp

TABLE 1 Geographical information about meteorological stations used in this study (Zhao and He, 2022a).

No	Site name	Latitude (°)	Longitude (°)	Altitude (m)	H_{ERA} (m)	H_{ERA}-H_{Obs} (m)
1	Jiu Quan	39.67	98.72	1,470	1,397	−73
2	Gao Tai	39.38	99.72	1,357	1,342	−15
3	Zhang Ye	38.92	100.58	1,550	1,500	−50
4	Shan Dan	38.78	101.08	1,760	1801	41
5	Yong Chang	38.23	101.97	1,987	2022	35
6	Wu Wei	38.08	102.92	1,525	1,498	−27
7	Wu Shaoling	37.2	102.87	3,045	3,431	386
8	Gao Lan	36.55	103.67	2,032	2033	1
9	Leng Hu	38.75	93.58	2,762	3,244	482
10	Tuo Te	38.87	98.37	3,460	3,621	161
11	Ye Niugou	38.62	99.35	3,200	3,575	375
12	Qi Lian	38.18	100.3	2,800	3,098	298
13	Da Chaidan	37.83	95.28	3,000	3,257	257
14	De Lingha	37.25	97.13	2,762	2,914	152
15	Gang Cha	37.33	100.17	3,100	3,275	175
16	Men Yuan	37.45	101.62	2,800	4,109	1,309
17	Min He	36.23	102.93	1,900	2,144	244

H_{ERA} is the ERA5-Land grid point height (m), H_{Obs} is the altitude of meteorological stations.

2.4. Evaluation methods

In this study, we used DISO (the distance between indices of simulation and observation) indicator combined with correlation coefficient (r) and mean absolute error (MAE) to assess the reliability of ERA5-Land in capturing daily temperature data and 11 extreme temperature indices in the QLM (Hu et al., 2019; Zhou et al., 2021; Hu et al., 2022; Xu et al., 2022). The equation of DISO is shown in Table 3. DISO is more flexible in expressing the quality of data than other indices (Zhou et al., 2021). The results of DISO value can be divided into two categories in this study: above 0.5 and 0.0–0.5 to analyze the reliability of ERA5-Land in capturing extreme temperature events in the QLM (Hu et al., 2019). It is suggested that ERA5-Land can capture extreme temperature events well when DISO is less than 0.5 (Hu et al., 2019). DISO greater than 0.5 indicates a poor simulation (worst if greater than 1.0), and less than 0.5 indicates a good simulation (best if close to 0.0). In addition, RB was divided into two groups: below 0.0 and above 0.0. The RB below 0.0 or above 0.0 was considered to indicate that ERA5-Land relatively underestimates or overestimates the observational data, respectively. NRMSE shows the mean error of ERA5-Land. NMAE can eliminate the effect of positive and negative offsetting of ERA5-Land errors. The CC is a important indicator of the correlation between ERA5-Land and Observations (Lei et al., 2022).

3. Results and discussion

3.1. Comparisons of daily temperatures

The correlation coefficient (r) between ERA5-Land and observed T_mean, T_max, and T_min was all larger than 0.9 (Table 4), the determination coefficient (R^2) between ERA5-Land and observed T_mean, T_max, and T_min was 0.99, 0.99, and 0.98, respectively (Figure 2), indicating excellent agreement between ERA5-Land daily temperature and observational daily temperature. The average MAE of T_mean, T_max, and T_min at all stations was 2.24, 3.52 and 2.69, respectively (Table 4). Station No.16 has the smallest r value and the largest MAE, which may be due to the larger altitude difference (1,309 m) between T_e and T_o at Station No.16 (Table 1). The DISO value for T_mean and T_max was <0.5 for 47 and 53% of the stations, respectively (Table 5). The DISO value of T_min at all stations is greater than 0.5. The average DISO at all stations of T_mean, T_max, and T_min was 2.44, 0.62, and 2.19, respectively. The spatial distribution of DISO value for T_mean and T_max is shown in Figure 3. In general, the DISO value was higher within the QLM than in the Hexi Corridor, indicating that the ability of ERA5-Land to capture T_mean and T_max in this mountainous area was worse than that in the oasis area. In general, reliability of ERA5-Land to capture T_max is best in the QLM.

3.2. Comparisons of extreme temperatures

High correlation coefficient (r) of 11 extreme temperature indices between T_e and T_o indicates that ERA5-Land can capture the extreme temperature indices well (Table 6). Only the average r at all stations of DTR is less than 0.8, and the average r at all stations of other extreme temperature indexes is above 0.85. After comparing the MAE of 11 extreme temperature indices between T_e and T_o, we can learn that TX90p have MAE smaller than 1 at all stations (Table 7). DISO of DTR at individual stations ranged from 0.28 to 0.69 with an average across the stations of 0.46, indicating that ERA5-Land simulates DTR

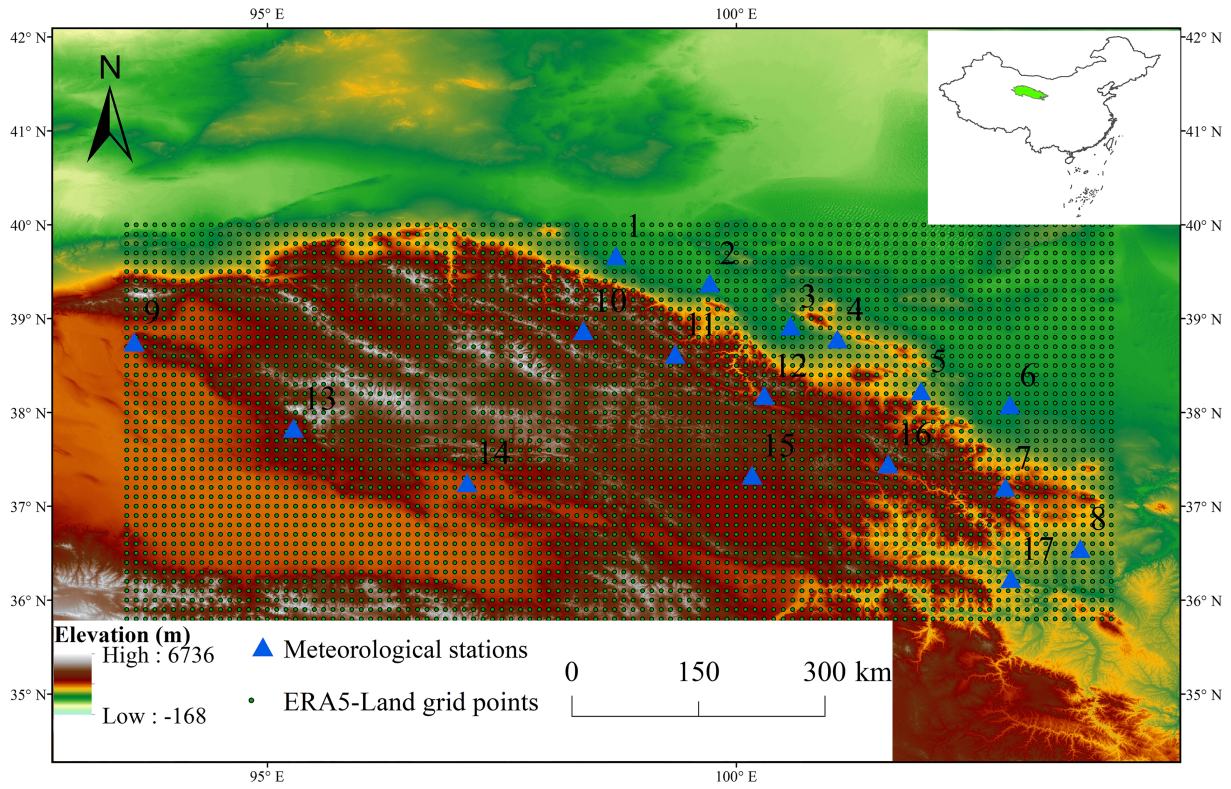

FIGURE 1
Distribution of ERA5-Land grid points and 17 meteorological stations in the QLM.

TABLE 2 Description of extreme temperature indices.

Index	Name	Definition	Unit
TXx	Max T_{max}	Monthly maximum of maximum daily temperatures	°C
TNx	Max T_{min}	Monthly maximum of minimum daily temperatures	°C
TXn	Min T_{max}	Monthly minimum of maximum daily temperatures	°C
TNn	Min T_{min}	Monthly minimum of minimum daily temperatures	°C
FD0	Frost days	Number of days per year when TN (daily minimum) < 0°C	d
ID0	Ice days	Number of days per year when TX (daily maximum) < 0°C	d
TN10p	Cool nights	Percentage of days when TN < 10th percentile	d
TX10p	Cool days	Percentage of days when TX < 10th percentile	d
TN90p	Warm nights	Percentage of days when TN > 90th percentile	d
TX90p	Warm days	Percentage of days when TX > 90th percentile	d
DTR	Diurnal temperature range	Monthly mean difference between TX and TN	°C

in the QLM well (Table 8). ERA5-Land captured FD0 very accurately, with DISO <0.5 for 15 meteorological stations and an average of 0.27. ERA5-Land reanalysis performed better for TXx than for TXn, TNn, and TNx. DISO for TXx was <0.5 at 12 stations accounting for approximately 71% of all stations. TX90p performed better than TN90p, TX10p and TN10p. DISO for TX90p was <0.5 at 9 stations accounting for approximately 53% of all stations. Zhu et al. (2016) found that ERA-Interim and 20CR reanalysis can capture intensity indices better than frequency indices over China, in agreement with this study. The mean DISO values of the warmest days (TXx) in spring, summer, autumn and winter were 0.31, 0.16, 0.32, and 0.93, respectively (Table 9). The spring DISO values of TXn, TNn and TNx were the largest. Overall, ERA5-Land reanalysis performed well in summer and poorly in spring and winter, similar to previous studies (Zhao P. et al., 2020; Xu et al., 2022). Figure 3 shows the spatial distribution of DISO values of extreme temperature index. In general, FD0 has the best performance within the Qilian Mountains region.

3.3. Trends in daily and extreme temperatures

Figures 4–7 shows trends in daily temperature and extreme temperature indices based on ERA5-Land and observations during

TABLE 3 Evaluation criteria used in this study.

Metric	Name	Formula	Optimal value	Unit
NRMSE	Normalized root mean square error	$\frac{1}{\bar{O}}\sqrt{\frac{1}{n}\sum_{i=1}^{n}(E_i-O_i)^2}$	0	/
NMAE	Normalized mean absolute error	$\frac{1}{n\bar{O}}\sum_{i=1}^{n}\lvert E_i-O_i\rvert$	0	/
RB	Relative bias	$\frac{\sum_{i=1}^{n}(E_i-O_i)}{\sum_{i=1}^{n}O_i}\times 100$	0	%
CC	Pearson correlation coefficient	$\frac{\sum_{i=1}^{n}(E_i-\bar{E})(O_i-\bar{O})}{\sqrt{\sum_{i=1}^{n}(E_i-\bar{E})^2}\sqrt{\sum_{i=1}^{n}(O_i-\bar{O})^2}}\times 100$	1	/
DISO	Distance between indices of simulation and observation	$\sqrt{NRMSE_i^2+NMAE_i^2+RB_i^2+(CC_i-1)^2}$	0	/
RMSE	Root-mean-square-error	$\sqrt{\frac{1}{n}\sum_{i=1}^{n}(E_i-O_i)^2}$	0	°C

n represents the number of samples; $\bar{E}$ and $\bar{O}$ represent the mean values of extreme temperature indices obtained from ERA5-Land and observations, respectively; and E_i and O_i are values of extreme temperature indices obtained from ERA5-Land and observations, respectively.

TABLE 4 Correlation coefficient (*r*) and mean absolute error (MAE) between observational daily temperature and ERA5-Land daily temperature at 17 stations in the QLM from 1979 to 2017.

		r			MAE	
No	T_mean	T_max	T_min	T_mean	T_max	T_min
1	0.992	0.991	0.976	1.20	1.80	2.06
2	0.989	0.990	0.972	1.89	1.40	2.55
3	0.991	0.986	0.978	1.38	1.45	2.09
4	0.992	0.987	0.980	1.20	2.49	1.86
5	0.988	0.987	0.969	1.26	2.03	2.03
6	0.992	0.988	0.981	1.21	1.35	1.66
7	0.977	0.978	0.953	1.57	1.52	2.55
8	0.982	0.983	0.963	2.25	4.62	2.43
9	0.991	0.993	0.971	1.75	4.30	2.21
10	0.970	0.969	0.949	2.83	4.85	2.94
11	0.968	0.961	0.941	4.63	7.29	4.36
12	0.969	0.960	0.944	4.48	7.01	4.25
13	0.987	0.990	0.961	2.50	4.80	2.65
14	0.988	0.987	0.966	1.23	1.39	2.52
15	0.983	0.982	0.961	1.26	2.22	1.97
16	0.960	0.949	0.925	5.65	8.51	4.86
17	0.987	0.983	0.963	1.72	2.74	2.70
Average	0.983	0.980	0.962	2.24	3.52	2.69

TABLE 5 Statistics of DISO for ERA5-Land daily temperature at 17 stations in the QLM from 1979 to 2017.

Statistics	T_mean	T_max	T_min
0–0.5 (%)	47	53	0
> 0.5 (%)	53	47	100
Average	2.44	0.62	2.19

1979–2017 in the QLM. Daily temperature data obtained from ERA5-Land reanalysis and observation datasets showed significant positive trends from 1979 to 2017. This indicated that the warming trend in observed data at daily scale was captured accurately by the ERA5-Land reanalysis temperature. TXx (warmest day), TNx (warmest night), TX90p (warm days), and TN90p (warm nights) exhibited a significant positive trend. With global warming, extreme heat events are increasing in intensity and frequency (Xu et al., 2022). Also, extreme high-temperature indices were captured by ERA5-Land well. In addition, TX10p (cool days), TN10p (cool nights), ID0 (ice days), and FD0 (frost days) based on observations and ERA5-Land exhibited negative trends. Both TNn (coldest night) and TXn (coldest day) calculated from T_e and T_o showed a positive trend, showing that the intensity of extreme low temperature events in the QLM increases with global warming. Zhou et al. (2016) analyzed the variation in extreme temperature indices over China using high-resolution gridding data (CN05), and found that the coldest day (TXn) had less variability than the coldest night (TNn), and the warmest day (TXx) had less variability than the warmest night (TNx), similar to the results of this study. Our conclusion is that the trend in extreme

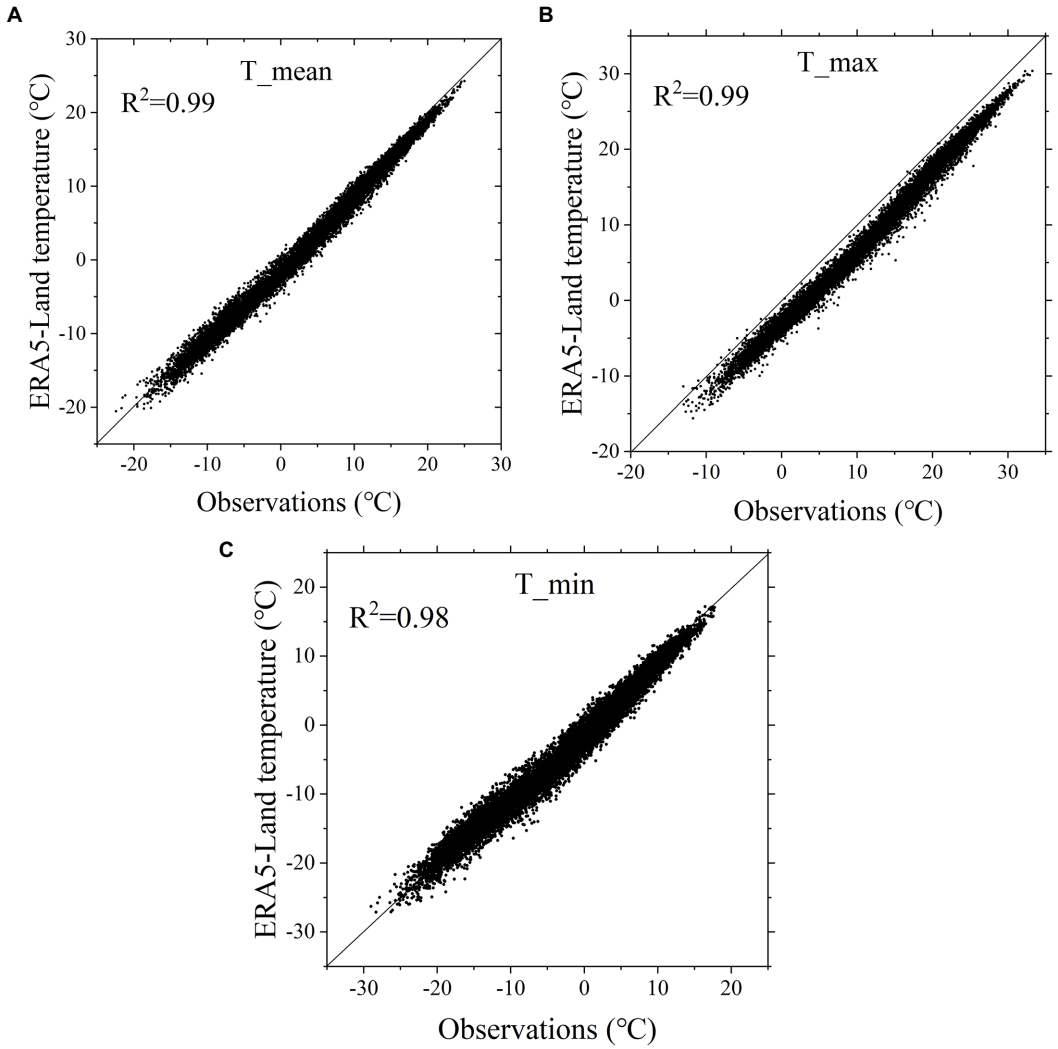

FIGURE 2
Scatter plots of ERA5-Land daily temperature and observed values of T_mean **(A)**, T_max **(B)**, and T_min **(C)**. The solid line is 1 :1 line.

low-temperature indices can be captured by ERA5-Land well. The observational DTR showed a large decreasing trend (−0.162°C/decade), while DTR of ERA5-Land showed only a slightly decreasing trend (−0.009°C/decade), indicating that ERA5-Land did not capture the trend in DTR well (Table 10). Generally, all tendencies in extreme temperature events except DTR were captured well by ERA5-Land in the QLM.

3.4. Possible bias analysis

Observational data in the QLM were underestimated by ERA5-Land for daily temperature, DTR, and absolute indices of extreme temperature (Figures 4, 5). Our results are similar to previous studies. (Zhao P. et al., 2020; Huai et al., 2021; Zou et al., 2022; Zhao and He, 2022a). Many studies indicated that the main reason for bias in reanalysis temperature data is the elevation difference between T_e and T_o (Gao et al., 2014, 2018; Xu et al., 2022). The linear relationship between T_e and T_o bias and elevation difference is shown in Figure 8, the R^2 values of T_mean, T_max and T_min were 0.541, 0.454, and 0.469, respectively. The daily biases were related to the elevation difference between T_e and T_o, especially for T_mean. The simulation reliability of ERA5-Land increased with a decrease in the elevation difference (Zhao and He, 2022a). Therefore, it is possible to correct ERA5-Land reanalysis temperature through a temperature lapse-rate model to further reduce the error and improve the precision of temperature reanalysis (Dee and Uppala, 2009; Gao et al., 2012; Di Giuseppe et al., 2013; Gao et al., 2017). The number of meteorological stations used in this study is small, especially above 3,500 m. However, many studies have shown that the limited number of meteorological stations is sufficient to effectively and accurately evaluate the applicability of reanalysis data (Huai et al., 2021; Jiao et al., 2021). We believe that the bias is mainly caused by the elevation difference between T_e and T_o. Other factors, such as the interpolation method, terrain complexity, and glaciers, are also potential sources of bias (Huang et al., 2022; Zhao and He, 2022a). The DISO values of T_mean, T_max and T_min were 2.44, 0.62 and 2.19, respectively. Due to the high altitude of the Qilian Mountain, complex terrain and few meteorological observation

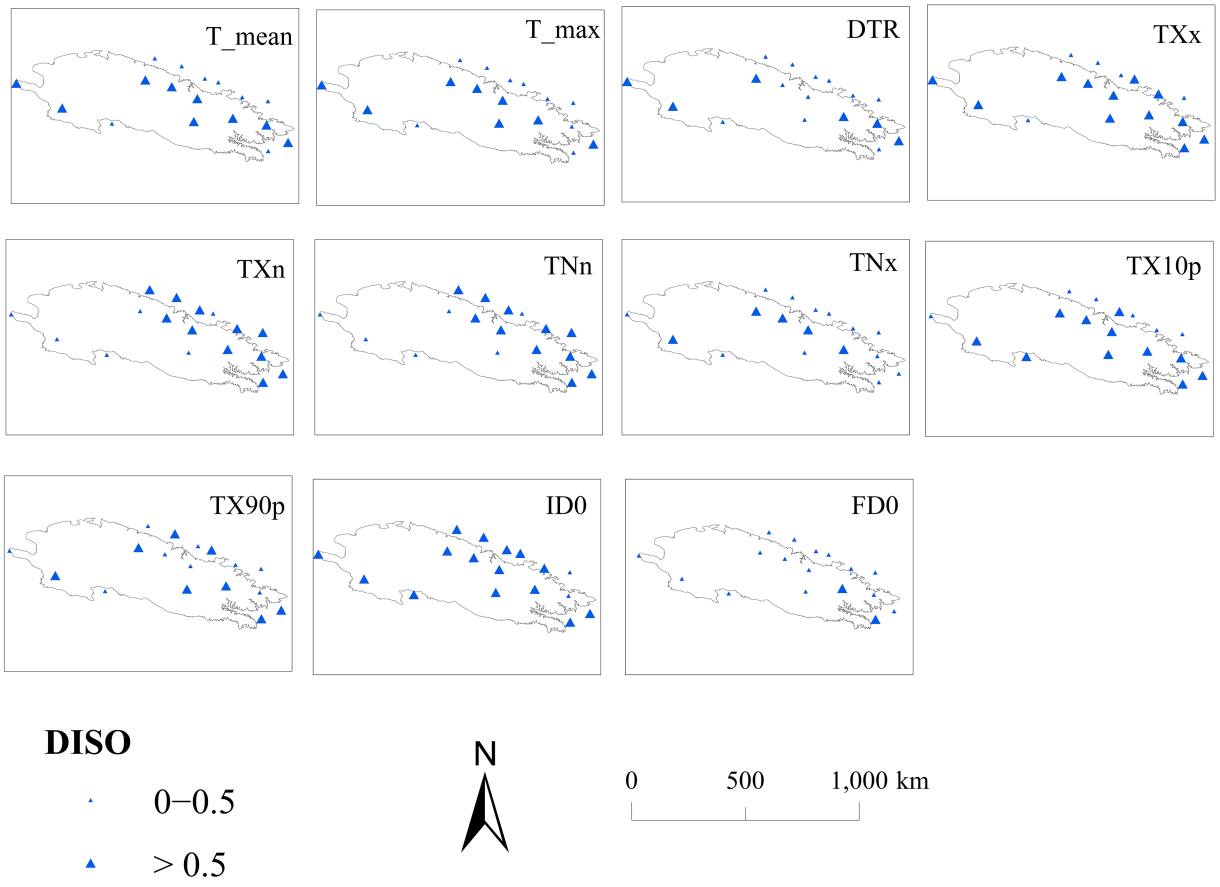

FIGURE 3
Distribution of DISO for T_mean,T_max and extreme temperature indices of 17 meteorological stations in the QLM.

TABLE 6 Correlation coefficient (*r*) between observational extreme temperature indices and ERA5-Land extreme temperature indices at 17 stations in the QLM from 1979 to 2017.

No	DTR	TXn	TNn	TXx	TNx	TX10p	TN10p	TN90p	TX90p	ID0	FD0
1	0.746	0.991	0.984	0.994	0.980	0.980	0.955	0.943	0.977	0.967	0.989
2	0.808	0.988	0.978	0.992	0.985	0.974	0.932	0.946	0.965	0.972	0.982
3	0.790	0.984	0.980	0.991	0.982	0.965	0.941	0.956	0.974	0.962	0.986
4	0.825	0.987	0.986	0.991	0.985	0.977	0.936	0.965	0.963	0.966	0.986
5	0.829	0.988	0.967	0.989	0.982	0.977	0.891	0.961	0.967	0.965	0.981
6	0.839	0.988	0.984	0.991	0.984	0.988	0.952	0.921	0.969	0.984	0.989
7	0.718	0.987	0.960	0.979	0.978	0.937	0.828	0.963	0.977	0.978	0.987
8	0.819	0.982	0.980	0.988	0.979	0.962	0.925	0.945	0.954	0.895	0.983
9	0.663	0.994	0.986	0.995	0.980	0.976	0.882	0.968	0.973	0.909	0.994
10	0.727	0.973	0.922	0.980	0.971	0.872	0.827	0.960	0.968	0.884	0.949
11	0.760	0.971	0.912	0.964	0.974	0.915	0.763	0.965	0.973	0.755	0.896
12	0.743	0.976	0.926	0.961	0.975	0.850	0.762	0.963	0.967	0.769	0.937
13	0.650	0.991	0.975	0.992	0.973	0.964	0.928	0.948	0.965	0.889	0.970
14	0.669	0.985	0.982	0.992	0.980	0.964	0.952	0.965	0.973	0.978	0.970
15	0.669	0.978	0.949	0.990	0.977	0.921	0.875	0.974	0.971	0.956	0.960
16	0.591	0.963	0.934	0.948	0.970	0.853	0.767	0.945	0.957	0.688	0.891
17	0.786	0.983	0.954	0.987	0.981	0.954	0.889	0.952	0.967	0.927	0.946
Average	0.743	0.983	0.962	0.984	0.979	0.943	0.882	0.955	0.968	0.909	0.964

TABLE 7 Mean absolute error (MAE) between observational extreme temperature indices and ERA5-Land extreme temperature indices at 17 stations in the QLM from 1979 to 2017.

No	DTR	TXn	TNn	TXx	TNx	TX10p	TN10p	TN90p	TX90p	ID0	FD0
1	2.93	1.72	2.23	1.83	1.60	0.47	0.72	0.96	0.53	1.34	0.96
2	2.96	1.61	2.50	1.40	1.83	0.56	0.91	0.84	0.63	0.84	1.12
3	2.41	1.59	2.16	1.36	1.90	0.70	0.88	0.81	0.56	0.69	0.99
4	2.30	2.03	1.55	2.92	1.64	0.53	0.90	0.70	0.66	1.65	1.12
5	2.17	1.60	2.25	2.23	1.71	0.52	1.24	0.75	0.62	1.59	1.33
6	1.94	1.27	1.45	1.39	1.48	0.43	0.77	1.05	0.60	0.54	0.94
7	2.43	1.26	3.56	1.58	1.85	0.91	1.59	0.74	0.51	1.65	1.11
8	4.55	4.33	1.72	4.46	2.54	0.72	1.01	0.91	0.79	2.86	1.33
9	4.55	4.20	1.94	4.42	2.40	0.51	1.26	0.66	0.57	3.70	0.76
10	4.09	4.32	3.79	5.46	2.55	1.31	1.59	0.74	0.66	4.74	2.48
11	4.00	6.78	6.07	7.68	4.39	1.09	1.93	0.67	0.64	8.19	4.08
12	3.74	6.99	6.48	7.57	3.74	1.45	1.93	0.72	0.66	7.45	3.13
13	4.03	4.58	2.13	4.98	2.62	0.63	0.98	0.88	0.66	4.70	1.68
14	2.38	1.30	1.65	1.57	2.24	0.66	0.84	0.71	0.57	1.25	1.87
15	2.66	1.78	2.39	2.90	1.62	1.02	1.35	0.63	0.65	2.56	1.87
16	4.70	8.12	6.29	9.09	5.17	1.43	1.89	0.96	0.84	9.81	4.28
17	2.21	2.78	3.03	3.03	2.05	0.69	1.21	0.79	0.61	1.57	2.57
Average	3.18	3.31	3.01	3.76	2.43	0.80	1.24	0.79	0.63	3.24	1.86

TABLE 8 Statistics of DISO for ERA5-Land extreme temperature indices at 17 stations in the QLM from 1979 to 2017.

Statistics	DTR	TXn	TNn	TXx	TNx	TX10p	TN10p	TN90p	TX90p	ID0	FD0
0–0.5 (%)	71	29	35	71	35	35	0	0	53	12	88
>0.5 (%)	29	71	65	29	65	65	100	100	47	88	12
Average	0.46	8.80	0.68	0.39	1.87	0.67	1.02	0.65	0.51	1.54	0.27

TABLE 9 DISO for ERA5-Land daily temperature and extreme temperature indices at seasonal scales from 1979 to 2017.

	Spring	Summer	Autumn	Winter	Annual
mean	0.70	0.13	0.55	0.21	0.58
max	0.46	0.20	0.48	25.79	0.46
min	2.68	0.19	0.84	0.16	0.84
DTR	0.29	0.25	0.40	0.46	0.48
TXn	1.39	0.30	1.24	0.61	1.22
TNn	0.52	0.50	0.36	0.15	0.30
TXx	0.31	0.16	0.32	0.93	0.32
TNx	0.84	0.17	0.59	0.38	0.72

points, the accuracy of simulation is influenced (Xu et al., 2022). Large DISO values have been found at those stations located within the QLM. Therefore, the bias between the observed values and the reanalysis values within the QLM is higher than that in the surrounding areas such as Hexi Corridor. This may be due to the complicated terrain inside the Qilian Mountains (Zhao and He, 2022a).

4. Conclusions

In this study, we evaluated the ability of ERA5-Land reanalysis to capture extreme temperatures in the Qilian Mountains. The R^2 between ERA5-Land and observed T_mean, T_max, and T_min was 0.99, 0.99, and 0.98, respectively, which indicates that ERA5-Land can capture observational daily temperature data well. However, an average DISO at all stations of T_mean, T_max, and T_min was 2.44, 0.62, and 2.19, respectively, indicating that the reliability of capturing the T_max of ERA5-Land reanalysis temperature data is better than that of the T_mean and T_min in the QLM. ERA5-Land performed well in capturing extreme temperature indices TXx, TX90p and FD0. DISO for TXx was <0.5 at 12 stations accounting for approximately 71% of all stations. DISO for TX90p was <0.5 at 9 stations accounting for approximately 53% of all stations. ERA5-Land captured FD0 very well, with DISO <0.5 for 15 meteorological stations and an average of 0.27. The mean DISO values of the warmest days (TXx) in spring, summer, autumn and winter were 0.31, 0.16, 0.32 and 0.93, 131 respectively, showing that evaluation results of the extreme temperature index on the seasonal scale show that the capture results of ERA5-Land

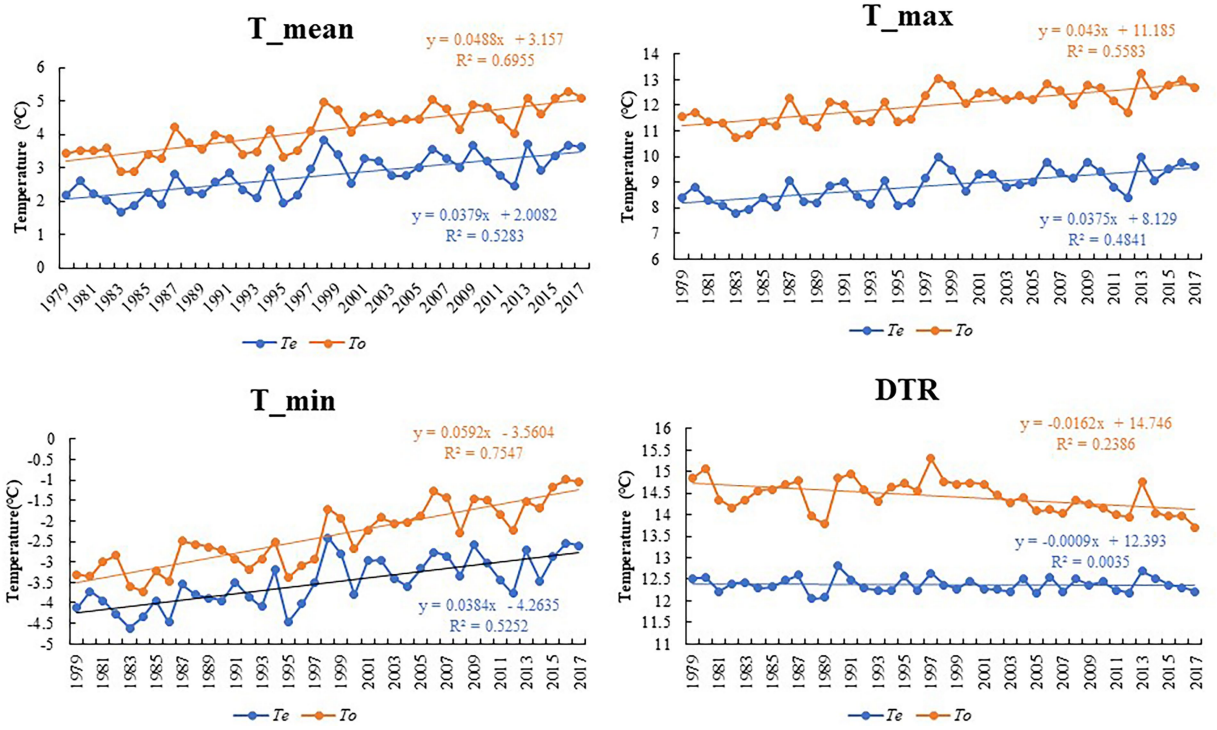

FIGURE 4
Trends in daily temperature and DTR in observation and ERA5-Land datasets from 1979 to 2017 in the QLM.

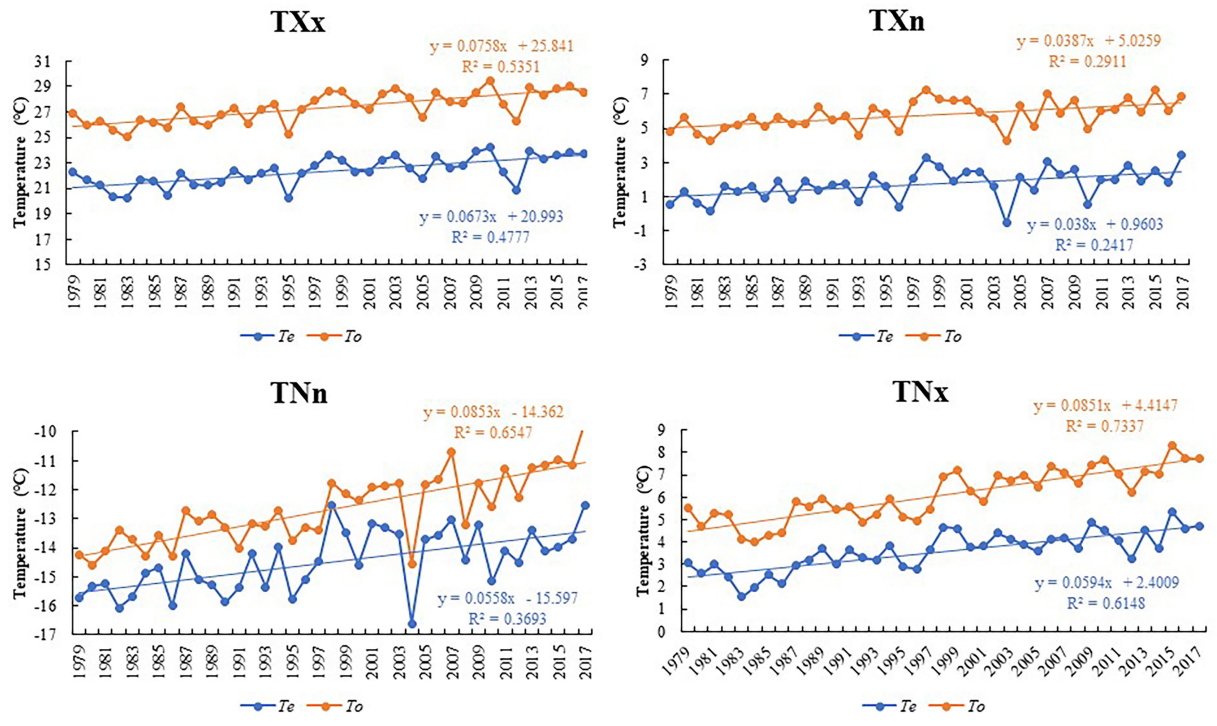

FIGURE 5
Trends in absolute indices of extreme temperature in observation and ERA5-Land datasets from 1979 to 2017 in the QLM.

on the extreme temperature index are best in summer. Furthermore, our results show that ERA5-Land is able to capture trends in all extreme temperature indices except DTR, for the observational DTR showed a large decreasing trend (−0.162°C/decade), while

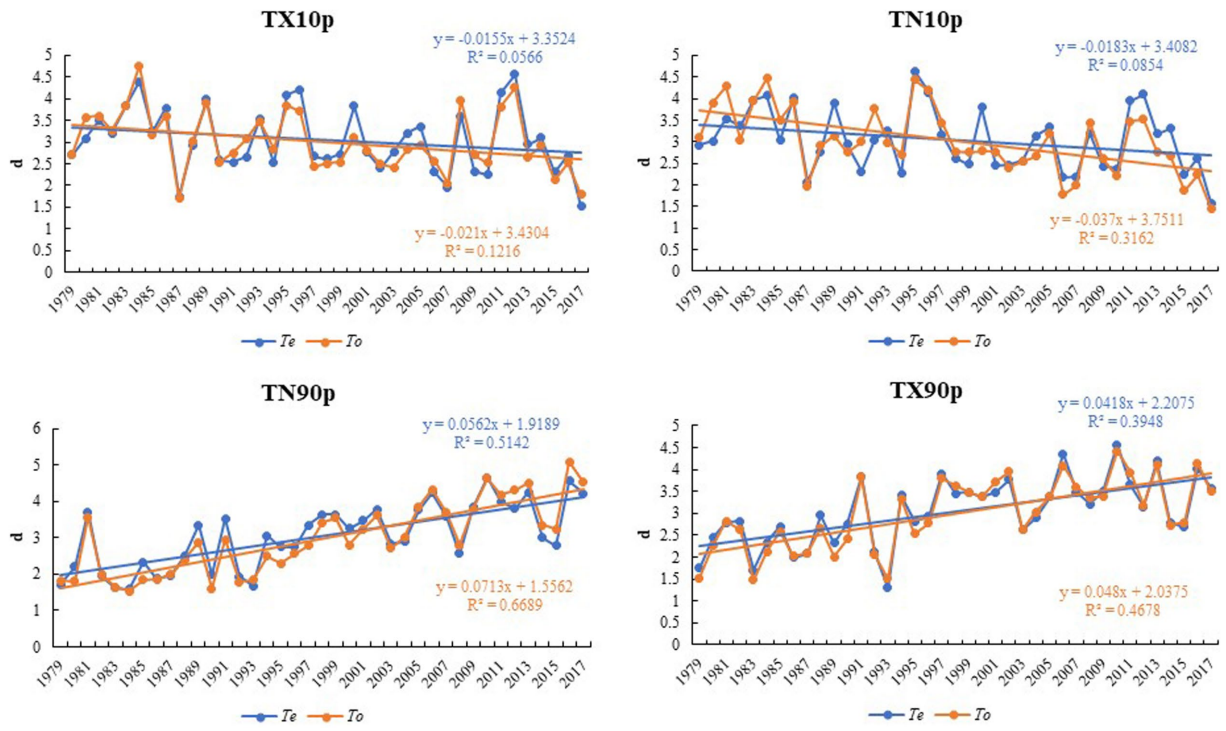

FIGURE 6
Trends in percentile-based indices of extreme temperature in observation and ERA5-Land datasets from 1979 to 2017 in the QLM.

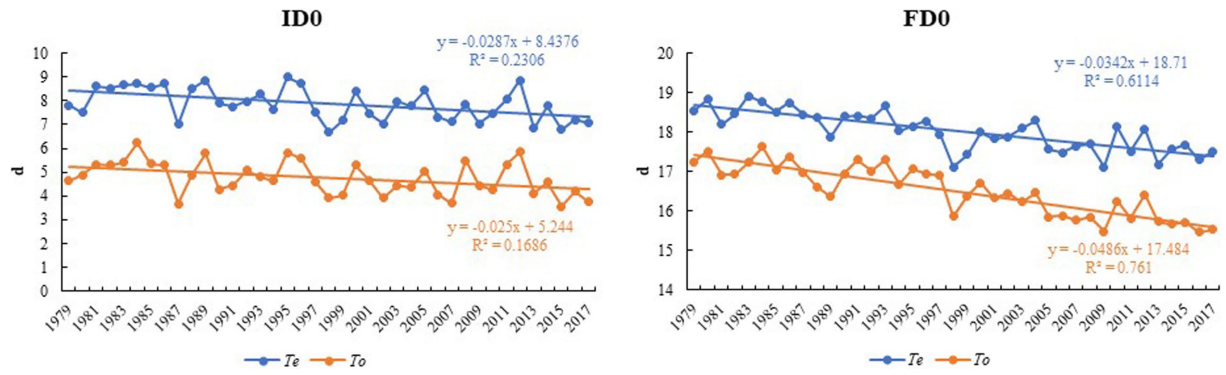

FIGURE 7
Trends in threshold indices of extreme temperature in observation and ERA5-Land datasets from 1979 to 2017 in the QLM.

TABLE 10 Trends in daily temperature and extreme temperature indices in ERA5-Land and observation datasets in the QLM from 1979 to 2017 (The units of T_mean, T_max, T_min, TXn, TNn, TXx, TNx, and DTR are°C/decade; the units of TX10p, TN10p, TX90p, TN90p, ID0, and FD0 are day/decade).

Temperature	T_ mean	T_ max	T_ min	DTR	TXn	TNn	TXx	TNx	TX10p	TN10p	TN90p	TX90p	ID0	FD0
T_e	0.379	0.375	0.384	−0.009	0.38	0.558	0.673	0.594	−0.155	−0.183	0.562	0.418	−0.287	−0.342
T_o	0.488	0.43	0.592	−0.162	0.387	0.853	0.758	0.851	−0.21	−0.37	0.713	0.48	−0.25	−0.486
T_o-T_e	0.109	0.055	0.208	−0.153	0.007	0.295	0.085	0.257	−0.055	−0.187	0.151	0.062	0.037	−0.144

DTR of ERA5-Land showed only a slightly decreasing trend (−0.009°C/decade). The R^2 values between temperature bias and elevation difference of T_mean, T_max, and T_min were 0.541, 0.454 and 0.469, respectively, showing that the elevation difference

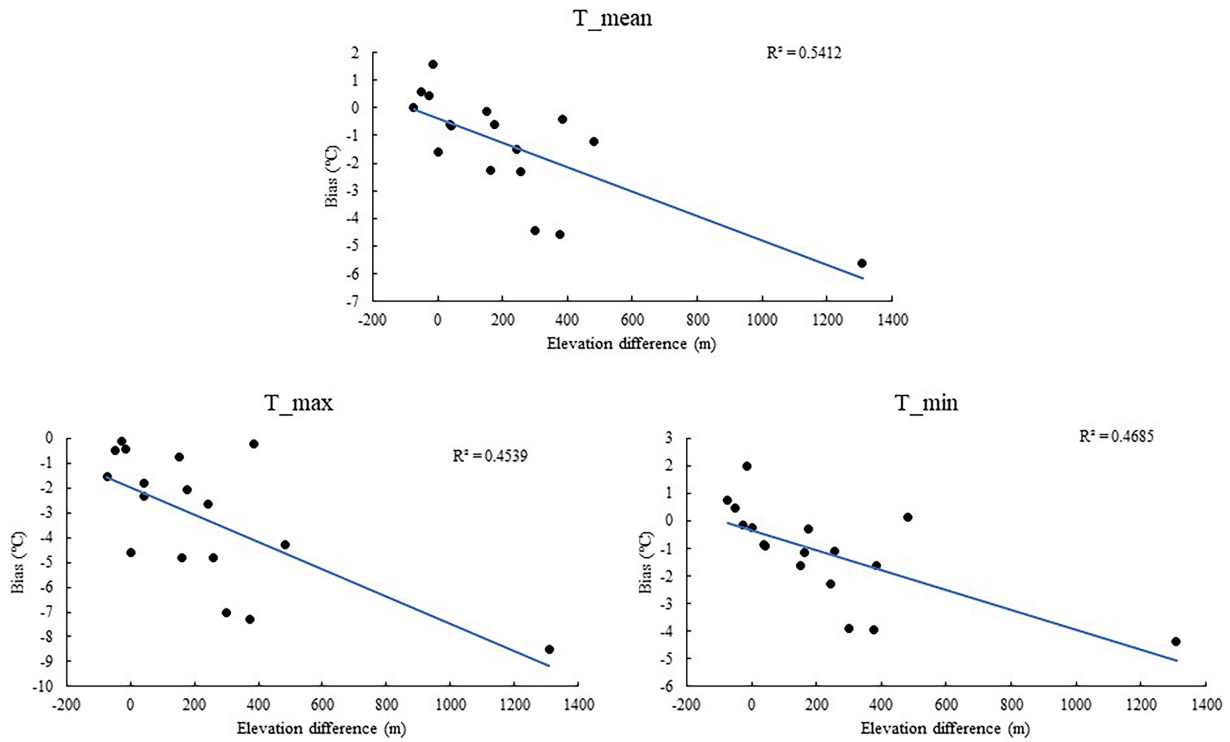

FIGURE 8
Relationship of bias and elevation differences between ERA5-Land daily temperature and daily observations in the QLM during the period of 1979–2017.

between ERA5-Land reanalysis temperature data and observation data may be the main cause of temperature bias. Generally, ERA5-Land reanalysis temperature data were reliable in simulating temperature data and identifying extreme temperature events; we conclude that ERA5-Land can be applied in the QLM for climate change research.

Data availability statement

The datasets presented in this study can be found in online repositories. The names of the repository/repositories and accession number (s) can be found below: https://cds.Climate.copernicus.eu/cdsapp#!/dataset/reanalysis-era5-land?tab=form.

Author contributions

PZ: designed study, collected meteorological data, and write article. DM and WW: final edit. ZH: provide fund support. All authors contributed to the article and approved the submitted version.

Funding

This study was supported by the National Natural Science Foundation of China, No. 41621001, and the Strategic Priority Research Program of the Chinese Academy of Sciences, No. XDA23060301.

Conflict of interest

The authors declare that the research was conducted in the absence of any commercial or financial relationships that could be construed as a potential conflict of interest.

Publisher's note

All claims expressed in this article are solely those of the authors and do not necessarily represent those of their affiliated organizations, or those of the publisher, the editors and the reviewers. Any product that may be evaluated in this article, or claim that may be made by its manufacturer, is not guaranteed or endorsed by the publisher.

References

Alexander, M., and Gregor, B. (2020). Demystifying the use of ERA5-land and machine learning for wind power forecasting. *IET Renew. Power Gen.* 14, 4159–4168. doi: 10.1049/iet-rpg.2020.0576

Araujo, C. S. P., Silva, I., Ippolito, M., and Almeida, C. (2022). Evaluation of air temperature estimated by ERA5-land reanalysis using surface data in Pernambuco. *Brazil Environ. Monit. Assess.* 194:381. doi: 10.1007/s10661-022-10047-2

Cao, B., Gruber, S., Zheng, D., and Li, X. (2020). The ERA5-land soil temperature bias in permafrost regions. *Cryosphere* 14, 2581–2595. doi: 10.5194/tc-14-2581-2020

Dee, D. P., and Uppala, S. (2009). Variational bias correction of satellite radiance data in the ERA-interim reanalysis. *Q. J. R. Meteorol. Soc.* 135, 1830–1841. doi: 10.1002/qj.493

Deng, S.-F., Yang, T.-B., Zeng, B., Zhu, X.-F., and Xu, H.-J. (2013). Vegetation cover variation in the Qilian Mountains and its response to climate change in 2000–2011. *J. Mt. Sci.* 10, 1050–1062. doi: 10.1007/s11629-013-2558-z

Di Giuseppe, F., Molteni, F., and Dutra, E. (2013). Real-time correction of ERA-interim monthly rainfall. *Geophys. Res. Lett.* 40, 3750–3755. doi: 10.1002/grl.50670

Gao, L., Bernhardt, M., and Schulz, K. (2012). Elevation correction of ERA-interim temperature data in complex terrain. *Hydrol. Earth Syst. Sci.* 16, 4661–4673. doi: 10.5194/hess-16-4661-2012

Gao, L., Bernhardt, M., Schulz, K., and Chen, X. (2017). Elevation correction of ERA-interim temperature data in the Tibetan plateau. *Int. J. Climatol.* 37, 3540–3552. doi: 10.1002/joc.4935

Gao, L., Hao, L., and Chen, X.-W. (2014). Evaluation of ERA-interim monthly temperature data over the Tibetan plateau. *J. Mt. Sci.* 11, 1154–1168. doi: 10.1007/s11629-014-3013-5

Gao, L., Wei, J., Wang, L., Bernhardt, M., Schulz, K., and Chen, X. (2018). A high-resolution air temperature data set for the Chinese Tian Shan in 1979–2016. *Earth Syst. Sci. Data* 10, 2097–2114. doi: 10.5194/essd-10-2097-2018

Hong, T., Li, H., and Chen, M. (2021). Comprehensive evaluations on the error characteristics of the state-of-the-art gridded precipitation products over Jiangxi Province in 2019. *Earth Space Sci.* 8. doi: 10.1029/2021EA001787

Hu, Z., Chen, D., and Chen, X. (2022). CCHZ-DISO: a timely new assessment system for data quality or model performance from Da Dao Zhi Jian. *Geophys. Res. Lett.* 49:e2022GL100681. doi: 10.1029/2022GL100681

Hu, Z., Chen, X., Zhou, Q., Chen, D., and Li, J. (2019). DISO: a rethink of Taylor diagram. *Int. J. Climatol.* 39, 2825–2832. doi: 10.1002/joc.5972

Hu, L., Huang, G., and Hu, K. (2017). The performance of multiple datasets in characterizing the changes of extreme air temperature over China during 1979. *Theor. Appl. Climatol.* 133, 619–632. doi: 10.1007/s00704-017-2215-5

Huai, B., Wang, J., Sun, W., Wang, Y., and Zhang, W. (2021). Evaluation of the near-surface climate of the recent global atmospheric reanalysis for Qilian Mountains, Qinghai-Tibet plateau. *Atmos. Res.* 250:105401. doi: 10.1016/j.atmosres.2020.105401

Huang, X., Han, S., and Shi, C. (2022). Evaluation of three air temperature reanalysis datasets in the alpine region of the Qinghai–Tibet plateau. *Remote Sens.* 14, 1–24. doi: 10.3390/rs14184447

IPCC (2021). Climate Change 2021: The Physical Science Basis. V. Masson-Delmotteet al. ed. Contribution of Working Group I to the Sixth assessment report of the intergovernmental panel on climate change Cambridge, United Kingdom: Cambridge University Press.

Jiang, L., Tawia, H. D. F., and Yi, L. (2020). Global land surface temperature change (2003–2017) and its relationship with climate drivers: AIRS, MODIS, and ERA5-land based analysis. *Remote Sens.* 13, 1–20. doi: 10.3390/rs13010044

Jiao, D., Xu, N., Yang, F., and Xu, K. (2021). Evaluation of spatial-temporal variation performance of ERA5 precipitation data in China. *Sci. Rep.* 11:17956. doi: 10.1038/s41598-021-97432-y

Jintao, X., Ziqiang, M., Songkun, Y., and Jie, P. (2022). Do ERA5 and ERA5-land precipitation estimates outperform satellite-based precipitation products? A comprehensive comparison between state-of-the-art model-based and satellite-based precipitation products over mainland China. *J. Hydrol.* 605, 1–16. doi: 10.1016/j.jhydrol.2021.127353

Joaquín, M. S., Emanuel, D., Anna, A. P., Clément, A., Gabriele, A., Gianpaolo, B., et al. (2021). ERA5-land: a state-of-the-art global reanalysis dataset for land applications. *Earth Syst. Sci. Data* 13, 4349–4383. doi: 10.5194/essd-13-4349-2021

Konstantinos, S., George, V., Aikaterini, V., Anastasios, P., and Elias, D. (2021). Delineating the relative contribution of climate related variables to chlorophyll-a and phytoplankton biomass in lakes using the ERA5-land climate reanalysis data. *Water Res.* 196, 1–16. doi: 10.1016/j.watres.2021.117053

Lei, X., Xu, W., Chen, S., Yu, T., Hu, Z., Zhang, M., et al. (2022). How well does the ERA5 reanalysis capture the extreme climate events over China? Part I: extreme precipitation. *Front. Environ. Sci.* 10:921658. doi: 10.3389/fenvs.2022.921658

Li, Y., Qin, X., Liu, Y., Jin, Z., Liu, J., Wang, L., et al. (2022). Evaluation of long-term and high-resolution gridded precipitation and temperature products in the Qilian Mountains, Qinghai–Tibet plateau. *Front. Environ. Sci.* 10:906821. doi: 10.3389/fenvs.2022.906821

Lin, P., He, Z., du, J., Chen, L., Zhu, X., and Li, J. (2017). Recent changes in daily climate extremes in an arid mountain region, a case study in northwestern China's Qilian Mountains. *Sci. Rep.* 7:2245. doi: 10.1038/s41598-017-02345-4

Liu, L., Gu, H., Xie, J., and Xu, Y. P. (2020). How well do the ERA-interim, ERA-5, GLDAS-2.1 and NCEP-R2 reanalysis datasets represent daily air temperature over the Tibetan plateau? *Int. J. Climatol.* 41, 1484–1505. doi: 10.1002/joc.6867

Liu, J., Hagan, D. F. T., and Liu, Y. (2020). Global land surface temperature change (2003–2017) and its relationship with climate drivers: AIRS, MODIS, and ERA5-land based analysis. *Remote Sens.* 13, 1-20. doi: 10.3390/rs13010044

Luis, R. C., and Johannes, S. (2020). Simulation of multi-annual time series of solar photovoltaic power: is the ERA5-land reanalysis the next big step? *Sustain. Energy Technol. Assess.* 42, 1–12. doi: 10.1016/j.seta.2020.100829

Pelosi, A., and Chirico, G. B. (2021). Regional assessment of daily reference evapotranspiration: can ground observations be replaced by blending ERA5-land meteorological reanalysis and CM-SAF satellite-based radiation data? *Agric. Water Manag.* 258:107169. doi: 10.1016/j.agwat.2021.107169

Pelosi, A., Terribile, F., D'Urso, G., and Chirico, G. B. (2020). Comparison of ERA5-land and UERRA MESCAN-SURFEX reanalysis data with spatially interpolated weather observations for the regional assessment of reference evapotranspiration. *Water* 12, 1–22. doi: 10.3390/w12061669

Rakhmatova, N., Arushanov, M., Shardakova, L., Nishonov, B., Taryannikova, R., Rakhmatova, V., et al. (2021). Evaluation of the perspective of ERA-interim and ERA5 Reanalyses for calculation of drought indicators for Uzbekistan. *Atmos.* 12, 1–14. doi: 10.3390/atmos12050527

Ruml, M., Gregorić, E., Vujadinović, M., Radovanović, S., Matović, G., Vuković, A., et al. (2017). Observed changes of temperature extremes in Serbia over the period 1961-2010. *Atmos. Res.* 183, 26–41. doi: 10.1016/j.atmosres.2016.08.013

Ruqing, Z., Li, L., Zhang, Y., Huang, F. N., Li, J. D., Liu, W., et al. (2021). Assessment of agricultural drought using soil water deficit index based on ERA5-land soil moisture data in four southern provinces of China. *Agriculture* 11, 1–19. doi: 10.3390/agriculture11050411

Shtober-Zisu, N., and Wittenberg, L. (2021). Long-term effects of wildfire on rock weathering and soil stoniness in the Mediterranean landscapes. *Sci. Total Environ.* 762:143125. doi: 10.1016/j.scitotenv.2020.143125

Sun, X.-B., Ren, G. Y., Shrestha, A. B., Ren, Y. Y., You, Q. L., Zhan, Y. J., et al. (2017). Changes in extreme temperature events over the Hindu Kush Himalaya during 1961–2015. *Adv. Clim. Chang. Res.* 8, 157–165. doi: 10.1016/j.accre.2017.07.001

Supari, T. F., Juneng, L., and Aldrian, E. (2017). Observed changes in extreme temperature and precipitation over Indonesia. *Int. J. Climatol.* 37, 1979–1997. doi: 10.1002/joc.4829

Virman, M., Bister, M., Räisänen, J., Sinclair, V. A., and Järvinen, H. (2021). Radiosonde comparison of ERA5 and ERA-interim reanalysis datasets over tropical oceans. *Dynam. Meteorol. Oceanogr.* 73, 1–7. doi: 10.1080/16000870.2021.1929752

Wang, L., Chen, R., Han, C., Wang, X., Liu, G., Song, Y., et al. (2019). Change characteristics of precipitation and temperature in the Qilian Mountains and Hexi oasis, northwestern China. *Environ. Earth Sci.* 78, 1–13. doi: 10.1007/s12665-019-8289-x

Wang, X., Chen, R., Han, C., Yang, Y., Liu, J., Liu, Z., et al. (2019). Response of frozen ground under climate change in the Qilian Mountains, China. *Quat. Int.* 523, 10–15. doi: 10.1016/j.quaint.2019.06.006

Wu, Z., Feng, H., He, H., Zhou, J., and Zhang, Y. (2021a). Evaluation of soil moisture climatology and anomaly components derived from ERA5-land and GLDAS-2.1 in China. *Water Resour. Manag.* 35, 629–643. doi: 10.1007/s11269-020-02743-w

Wu, Z., Feng, H., He, H., Zhou, J., and Zhang, Y. (2021b). Evaluation of soil moisture climatology and anomaly components derived from ERA5-land and GLDAS-2.1 in China. *Water Resour. Manag.* 35, 629–643. doi: 10.1007/s11269-020-02743-w

Xin, Y., Lu, N., Jiang, H., Liu, Y., and Yao, L. (2021). Performance of ERA5 reanalysis precipitation products in the Guangdong-Hong Kong-Macao greater Bay Area, China. *J. Hydrol.* 602:126791. doi: 10.1016/j.jhydrol.2021.126791

Xu, W., Lei, X. Y., Chen, S. T., Yu, T. T., Hu, Z. Y., Zhang, M., et al. (2022). How well does the ERA5 reanalysis capture the extreme climate events over China? Part II: extreme temperature. *Front. Environ. Sci.* 10, 1–15. doi: 10.3389/fenvs.2022.921659

Yang, L., Feng, Q., Adamowski, J. F., Alizadeh, M. R., Yin, Z., Wen, X., et al. (2021). The role of climate change and vegetation greening on the variation of terrestrial evapotranspiration in Northwest China's Qilian Mountains. *Sci. Total Environ.* 759:143532. doi: 10.1016/j.scitotenv.2020.143532

Yin, H., and Sun, Y. (2017). Characteristics of extreme temperature and precipitation in China in based on ETCCDI indices. *Adv. Clim. Chang. Res.* 9, 218–226. doi: 10.1016/j.accre.2019.01.001

Yu, X., Ren, G., Zhang, P., Hu, J., Liu, N., Li, J., et al. (2020). Extreme temperature change of the last 110 years in Changchun Northeast China. *Adv. Atmos. Sci.* 37, 347–358. doi: 10.1007/s00376-020-9165-z

Zandler, H., Senftl, T., and Vanselow, K. A. (2020). Reanalysis datasets outperform other gridded climate products in vegetation change analysis in peripheral conservation areas of Central Asia. *Sci. Rep.* 10:22446. doi: 10.1038/s41598-020-79480-y

Zhao, P., Gao, L., Wei, J., Ma, M., Deng, H., Gao, J., et al. (2020). Evaluation of ERA-interim air temperature data over the Qilian Mountains of China. *Adv. Meteorol.* 2020, 1–11. doi: 10.1155/2020/7353482

Zhao, C., Gong, J., Wang, H., Wei, S., Song, Q., et al. (2020). Changes of temperature and precipitation extremes in a typical arid and semiarid zone: observations and multi-model ensemble projections. *Int. J. Climatol.* 40, 5128–5153. doi: 10.1002/joc.6510

Zhao, P., and He, Z. (2022a). A first evaluation of ERA5-land reanalysis temperature product over the Chinese Qilian Mountains. *Front. Earth Sci.* 10. doi: 10.3389/feart.2022.907730

Zhao, P., and He, Z. (2022b). Temperature change characteristics in Gansu Province of China. *Atmos.* 13, 1–13. doi: 10.3390/atmos13050728

Zhou, Q., Chen, D., Hu, Z., and Chen, X. (2021). Decompositions of Taylor diagram and DISO performance criteria. *Int. J. Climatol.* 41, 5726–5732. doi: 10.1002/joc.7149

Zhou, J., Li, Q., Wang, L., Lei, L., Huang, M., Xiang, J., et al. (2019). Impact of climate change and land-use on the propagation from meteorological drought to hydrological drought in the eastern Qilian Mountains. *Water* 11, 1–19. doi: 10.3390/w11081602

Zhou, B., Xu, Y., Wu, J., Dong, S., and Shi, Y. (2016). Changes in temperature and precipitation extreme indices over China: analysis of a high-resolution grid dataset. *Int. J. Climatol.* 36, 1051–1066. doi: 10.1002/joc.4400

Zhu, J., Huang, D.-Q., Yan, P.-W., Huang, Y., and Kuang, X.-Y. (2016). Can reanalysis datasets describe the persistent temperature and precipitation extremes over China? *Theor. Appl. Climatol.* 130, 655–671. doi: 10.1007/s00704-016-1912-9

Zou, J., Lu, N., Jiang, H., Qin, J., Yao, L., Xin, Y., et al. (2022). Performance of air temperature from ERA5-land reanalysis in coastal urban agglomeration of Southeast China. *Sci. Total Environ.* 828:154459. doi: 10.1016/j.scitotenv.2022.154459

frontiers | Frontiers in Ecology and Evolution

TYPE Review
PUBLISHED 23 March 2023
DOI 10.3389/fevo.2023.1152907

OPEN ACCESS

EDITED BY
Wei Zhao,
Institute of Geographic Sciences and Natural Resources Research (CAS),
China

REVIEWED BY
Zhuo Wu,
Guangzhou University,
China
Ümüt Halik,
Xinjiang University,
China

*CORRESPONDENCE
Yan Wu
✉ wuyan@cib.ac.cn
Tingfa Dong
✉ dongfar@163.com

†These authors have contributed equally to this work

SPECIALTY SECTION
This article was submitted to Population, Community, and Ecosystem Dynamics, a section of the journal Frontiers in Ecology and Evolution

RECEIVED 28 January 2023
ACCEPTED 06 March 2023
PUBLISHED 23 March 2023

CITATION
Liu J, Du J, Zhang C, Zhang J, Yang H, Donald ML, Wu Y and Dong T (2023) Ecosystem service assessment under ecological restoration programs: A systematic review of studies from China.
Front. Ecol. Evol. 11:1152907.
doi: 10.3389/fevo.2023.1152907

Ecosystem service assessment under ecological restoration programs: A systematic review of studies from China

Junyan Liu[1,2†], Jie Du[3†], Chenfeng Zhang[2], Jindong Zhang[2], Hongbo Yang[4], Marion L. Donald[5], Yan Wu[1*] and Tingfa Dong[2*]

[1]Chengdu Institute of Biology, Chinese Academy of Sciences, Chengdu, China, [2]Key Laboratory of Southwest China Wildlife Resources Conservation, Ministry of Education, China West Normal University, Nanchong, Sichuan, China, [3]Jiuzhaigou Nature Reserve Administrative Bureau, Jiuzhaigou, China, [4]State Key Laboratory of Urban and Regional Ecology, Research Center for Eco-Environmental Sciences, Chinese Academy of Sciences, Beijing, China, [5]Manaaki Whenua Landcare Research, Lincoln, New Zealand

With a growing body of literature on the topic of ecosystem service (ES), there is an urgent need to summarize ES research in the context of ecological restoration programs (ERPs) in China and identify knowledge gaps for future directions. We conducted a systematic literature review of articles to examine the use of ES approaches for ERP assessments. Our results showed that previous studies mainly focused on the Shaanxi Province, and more than half of the reviewed studies considered no more than three ES types simultaneously. All ES categories were not covered equally; most of the studies focused on provisioning and regulating services, while cultural services have received little attention. Although regional-scale and short-term assessments dominated the reviewed papers, we suggest that multiple temporal and spatial scales for ERP assessments should be given more attention in future work. Moreover, we highlight that an oversimplified land use/land cover (LULC) categorization scheme may potentially lead to inaccuracies and biases in ESs detection under restoration programs. Based on this review, our findings can guide future ERP assessments by using the ES approach. Meanwhile, given the global LULC change brought by the proliferation of plantations under ERPs, our results are also expected to provide a path forward to assess ESs associated with LULC change globally.

KEYWORDS

China, ecological restoration program, ecosystem services, LULC, systematic review

1. Introduction

Ecosystem services (ESs) are widely defined as the benefits that people derive from ecosystems (Millennium Ecosystem Assessment (MEA), 2005). ESs are grouped into four categories including provisioning services (e.g., food, water, and timber), regulating services (e.g., carbon sequestration, water purification, and soil conservation), supporting services (e.g., biodiversity conservation, biomass production, and nutrient cycling) and cultural services (e.g., education, recreation, aesthetic; Zheng et al., 2013; Jiang et al., 2018; Cui et al., 2021). Sustainably managing and utilizing the ESs can improve human well-being (Millennium Ecosystem Assessment (MEA), 2005). However, intensive interference from human activities (e.g., extensive deforestation, cropland, and urban expansion) has dramatically altered ecosystems (Xu W. et al.,

2017), causing reductions in two-thirds of all ESs over the last few decades (Millennium Ecosystem Assessment (MEA), 2005; Gao et al., 2017). Ecological restoration has become a major strategy to restore the degraded ecosystem and improve ESs (Chazdon, 2008; Bullock et al., 2011; Keesstra et al., 2018).

Since the beginning of this century, the Chinese government has implemented several ecological restoration programs (ERPs), including the Grain-for-Green Program (GTGP), Natural Forest Conservation Program (NFCP), Soil and Water Conservation Programs (SWCP), and so on (Li et al., 2016; Zhang et al., 2016; Bryan et al., 2018; Jiang et al., 2021). Correspondingly, increasing interest has been focused on temporal and spatial changes in ecosystem services in the context of ecological restoration (Wang et al., 2017; Lu et al., 2018; Zhou et al., 2021). Currently, applications of remote sensing monitoring and biophysical model simulation have demonstrated that these restoration programs promoted vegetation restoration (Li et al., 2015; Zhang et al., 2018, 2019), carbon sequestration (Zhou et al., 2020), biomass increase (Brandt et al., 2018), and soil conservation (Xia et al., 2021). With the continuous implementation of ERPs, it is important to monitor the efficiency and impacts of these ERPs (Hua et al., 2018). A review of previous ERP assessments is particularly important for adjusting current and planning for future ERPs more effectively and efficiently.

Evaluating ERPs has attracted extensive attention and a growing number of studies have been carried out in China for this purpose (Wang et al., 2017; Liu et al., 2019; Tang et al., 2019; Qi et al., 2021). A variety of methodological approaches are available to assess ERPs, such as monetary valuation (Geng et al., 2020), field measurements (Guo et al., 2021), or modeling approaches (Liang et al., 2021). In addition, these studies assess changes in ES caused by ERPs at different scales: Qi et al. (2021) at the county scale, Zhou et al. (2021) at the regional scale, and Wang et al. (2021) at the national scale. Previous review papers related to ERP assessment using ES approaches have been carried out by D'Amato et al. (2016) and Wen and Théau (2020). However, the former focused primarily on monetary valuation studies of forest ES between 2000 and 2012 rather than on the approaches themselves used to assess the ERPs; the latter examined the use of ES approaches by selecting only the peer-reviewed English journal articles and assessed the only two ERPs (i.e., GTGP and NFCP), which may lead to biases in ERPs assessment results. Therefore, integrating local publications and more restoration projects is necessary to obtain a fuller picture of ERP assessment.

In this context, we conducted a more comprehensive systematic review of the literature on ERP assessments using ES approaches in China. Particularly, we focused on answering the following two questions: (1) What is the prevalence of using ES approach on ERP assessments in China? (2) What are the methodological approaches employed to assess ERP? Here, we address these questions by systematically reviewing the relevant literature published in both English and Chinese journals. Our objective was to provide a basis for assessing ERP using ES approaches, identify current challenges and offer recommendations for future research directions.

Several important national or provincial ecological policies in China are relevant to the reviewed papers; they are described briefly below. As one of China's largest ecological restoration projects, the GTGP, which consists of 10 subprograms covering >73% of China's territory, has been devoted to converting sloping farmland (farmland land with a slope great than 25°) to forest and grassland since 2000 (Zhou et al., 2020). The NFPP, as another large-scale restoration program, is aimed to protect natural vegetation for sustainable development (Ouyang et al., 2016). The SWCP, which is designed and implemented to reduce soil loss and enhance the soil retention function of the ecosystem (e.g., Duan et al., 2020; Jiang et al., 2021), has gradually developed into a national key ecological construction project. The emerging Ecological Conservation Red Line (ECRL) policy, which was initiated in 2011, aimed to protect ecologically fragile areas and important ecological functional zones, and enhance various ecosystem services (Zhou et al., 2021). The Three-North Shelter Forest Program, which is known as the "Green Great Wall" because its massive area spans half of northern China, has led to desired reductions in local land desertification and soil erosion as well as decreases in airborne sand and dust regionally (Li et al., 2021). The Beijing-Tianjin Sand Source Control Project was initiated in 2001 to promote environmental conservation near the capital of China (Beijing) by controlling the risk of wind-sand and soil erosion disasters. The Returning Grazing Land to Grassland Project was launched in 2003 to reduce the impacts of overgrazing and promote grassland productivity (Lu et al., 2018).

2. Methods

We conducted a systematic literature review of peer-reviewed articles published in English and Chinese journals, using the ISI Web of Science (WOS) database and the China Academic Journal Network Publishing Database of the China National Knowledge Infrastructure (CNKI). Keywords for the search in WOS included a combination of the following: "ecosystem service*" AND ("forest recovery" OR "forest restoration" OR "ecological restoration" OR "vegetation recovery" OR "vegetation restoration") AND ("China" OR "Chinese"). Additionally, we search CNKI using the combining sets of "生态系统服务" AND ("生态恢复" OR "森林恢复" OR "植被恢复"; the translation of the search terms in WOS) in the topic. We limited the search to the timeframe of 2005–2021 because few ES studies were conducted before the publication of the Millennium Ecosystem Assessment (Dade et al., 2019; Zheng et al., 2019), and China has implemented numerous forest restoration projects since 2000 (Qi et al., 2019). We defined two specific criteria to select papers to be reviewed in this study. First, we only consider papers that assess the ERPs using ES approaches because assessment of ES change could reveal the successes and limitations of the ERPs geared toward enhancing ES (Tallis et al., 2008; Jenerette et al., 2011). Second, we grouped ES assessments into two categories based on De Groot et al. (2012): economic and non-economic assessment. Though economic valuation is easy for implementation and requires minimal data, it generally suffers from measurement and generalization errors, possibly leading to invalid and unreliable results (TEEB, 2010; Jiang, 2017). In addition, since the non-economic valuation encompasses the health state of the ecosystem, which is more applicable to the sustainability evaluation of ecosystem services than the economic assessment (Fu et al., 2013), we only included studies on non-economic assessment of ESs. Our review consisted of a two-step screening process (Figure 1). We first screened article abstracts for relevancy and, if relevant, we then read the entire paper in the second stage of screening. We identified 640 scientific articles meeting the search criteria and 542 articles after the first screening, which removed review articles, conceptual papers, or ones that lacked consideration of ES changes driven by ERPs (Figure 1). We then excluded papers that

did not our screening criteria and resulted in 100 papers. See the Appendix for a full list of papers included.

From each of the selected publications, we retrieved the following information: geographical location, driver factors, ESs that were assessed, and spatial and temporal scales (Table 1). We also reviewed assessment methodologies used to assess the ERPs. Methodologies were categorized into three classes: (1) field measurement refers to the use of field observations or laboratory analysis to provide information on ESs, (2) model simulation refers to the incorporation of representations of physical processes underpinning the functioning of the ecosystem to map ESs, and (3) questionnaire survey refers to the evaluation using a perception study that presented a questionnaire or interview, which is often used to evaluate cultural services. We further recorded whether to consider interactions among ESs in each study. Finally, we recorded the changes in ESs related to ERPs based on the findings reported in the literature (i.e., increased, decreased, or no change), considering the differences in the response of ESs to ERPs (Wilson et al., 2017; Benra et al., 2019; Wu et al., 2019). This classification allowed us to synthesize results consistently from different methodological approaches.

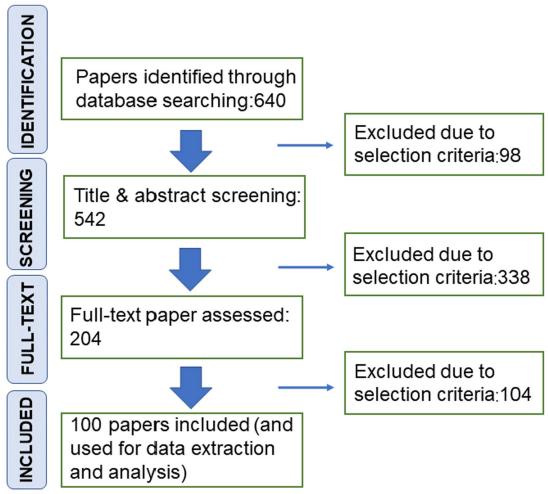

FIGURE 1
Overview of the selection process of the peer-reviewed publications identified in the review.

3. Results and discussion

3.1. The publication trends and geographical distribution

We identified 100 papers in total on the topic of ERP assessments using ES approaches in China in the WOS and CNKI from 2005 to 2021 that met our specific criteria. The first paper was published in 2007 (Wu et al., 2007), and it assessed the change in soil conservation brought about by the ecological restoration in the karst region. Figure 2 shows the number of related studies per year on this topic. It shows that since 2015, the number of studies has dramatically increased. Furthermore, nearly a quarter of the studies were published in 2019 and no studies were published from 2008 to 2010. Although the ES research work became popular and exponentially increase after the publication of the millennium assessment report in 2005 (Schägner et al., 2013), the ES approach used to assess ERPs started rather late in China. China implemented multiple ERPs in the 2000s, and the high number of publications two decades later may reflect the intense interest in understanding these programs' outcomes.

The spatial distribution of ES study regions within China was heterogeneous (Figure 3). Nearly half of the reviewed papers chose a case study located in Shaanxi Province, of which Bojie Fu and his research team from Research Center for Eco-Environmental Sciences, Chinese Academy of Sciences made the biggest contribution to ES research related to ERPs assessment within this province, of 16 percentage points. The Qinghai Province was the next most studied area (38% of studies).

TABLE 1 Details of variables extracted from each paper during the literature review.

Variables extracted	Categories
Geographical location	Province(s) where the study was located
Consideration of the ES relationship	Whether to consider interactions among ESs
Driver factors	Ecological restoration program(s) the study evaluated
ESs that were assessed	Categorized based on Millennium Ecosystem Assessment (MEA) (2005) and De Groot et al. (2002), group level: regulating services (i.e., air-quality regulation, climate regulation, pollination, erosion regulation, water regulation and water purification); provisioning services (i.e., food production, fresh water provision, fiber and timber, genetic resources, biochemicals and ornamental resources), supporting services (i.e., nutrient cycling, primary production, soil formation, and biodiversity/habitat for species); cultural services (i.e., aesthetic values, cultural diversity, educational values, knowledge systems, recreation and ecotourism, spiritual and religious values)
Changes in ESs	Increased, decreased, or no change
Assessment methodologies	Categorized based on previous reviews (Andrew et al., 2015; Thom and Seidl, 2016), group level: field measurement, model simulation and questionnaire survey
Spatial scale	Categorized based on Wen and Théau (2020), group level: the county level assessment refers to the evaluation of ERPs in a specific county; the regional level assessment refers to watershed or catchment, and provincial scales; the national level assessment refers to the assessment of ERPs across China
Temporal scale	As for the period covered, we defined two classes: the short-term evaluation (<20 years); the long-term evaluation (more than 20 years)

However, the eastern coastal regions (e.g., Fujian, Shandong and Jiangsu Province) received the least amount of attention in terms of ERP assessment. This is likely because these regions were not covered by the two largest ERPs (i.e., GTGP and NFCP). Moreover, studies in the southwestern and northeastern regions also received less attention, as each province accounted for <16% of the reviewed paper considered. As the southwestern and northeastern regions are the two largest forested areas in China, massive deforestation for timber production in the past has led to the deterioration of the ecological environment in these regions, which may induce severe catastrophic events (Li, 1999; Cai et al., 2014). Indeed, a large-scale flood occurred in the Yangtze River basin in 1998, and the southwestern and northeastern regions were the source areas of this flood, indicating the importance of these regions in water conservation (Li, 1999). Since then, the Chinese government has launched a series of ERPs in these regions, which has resulted in a significant increase in tree cover (Hua et al., 2018). Despite the clear importance of ES on environmental impacts, the changes in ES under restoration programs remain poorly understood because of the paucity of studies for this purpose conducted in these regions. Thus, we need more studies in these regions to determine if the impacts and effectiveness of restoration programs are similar or different across China.

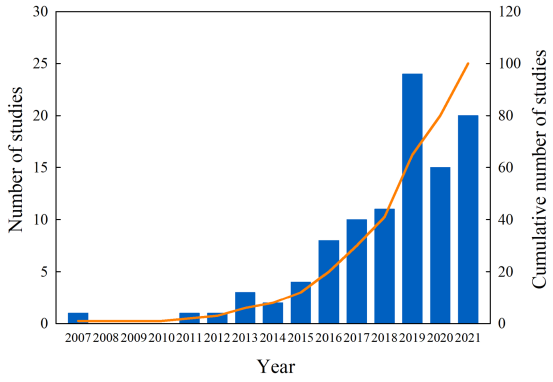

FIGURE 2
Number of studies on ecosystem services in China has increased in recent years. The line is the cumulative number of studies.

3.2. Findings through the review analysis

3.2.1. Number of ecosystem service considered

The number of ES considered concurrently in each study varied from 1 to 11 (Figure 4). However, most studies considered between

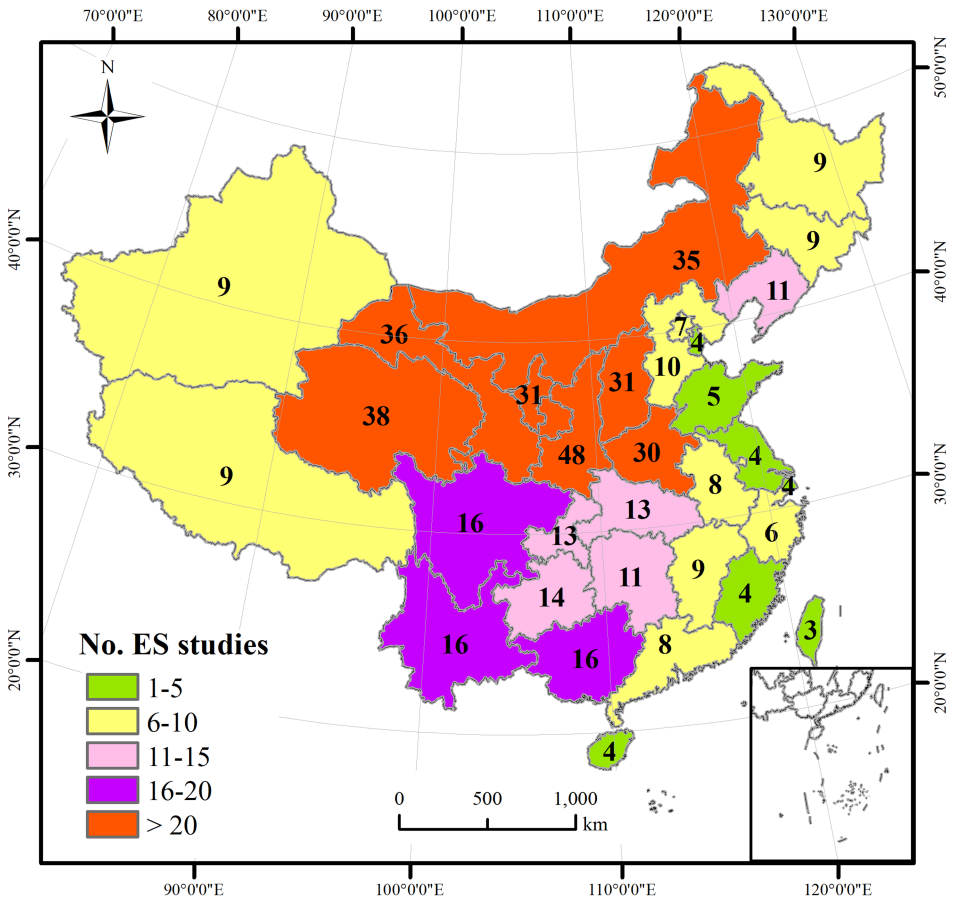

FIGURE 3
Geographical distribution of case studies included in the review. Colors represent the number of ecosystem service case studies (as a few studies consider several regions, the sum of studies in this figure exceeds the total number of studies reviewed).

one and five ES types. More than two-thirds of all studies (71%) considered only three or fewer ES types simultaneously, with 42% only considering a single ES, while only 8% of studies considered more than five ES types (Figure 4). The ecosystem should be considered as a whole because the changes or impacts on one part of an ecosystem can have consequences for the whole system (Wen and Théau, 2020). The narrow focus on one or a few ES types may provide little information to policymakers for an appropriate management of ES, and therefore a comprehensive assessment of a broad array of ES is necessary.

Change of ESs under ecological restoration programs has revealed interactions (i.e., trade-off and synergy) between multiple ES types (Fu et al., 2015): a single service's supply might have a positive or negative impact on the supply of another ES. Although an increasing number of studies have begun to focus on the relationships among ESs, nearly half of the reviewed papers, which excluded the studies considered a single ES, analyzed ESs in isolation (i.e., without considering any interactions; Figure 4). Given that identifying interrelations of ESs is critical to the sustainable management of ES (Raudsepp-Hearne and Peterson, 2016), interactions of multiple ESs need to be further examined to maintain ecosystem health.

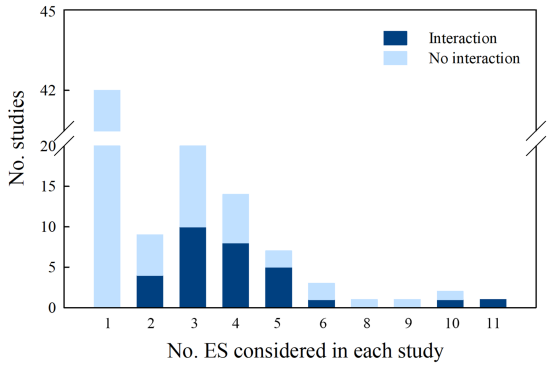

FIGURE 4
Frequency distribution of the number of ecosystem services evaluated in each case study. The proportion of studies that considered no interaction among ecosystem services is in gray, while the proportion that considered interactions among ecosystem services is in dark gray.

3.2.2. Types of ecosystem service

Following the Millennium Ecosystem Assessment (MEA) (2005) and De Groot et al. (2002), ESs are grouped into four broad categories: provisioning, regulating, cultural and supporting ES. Even though ES approaches have been widely used to analyze the ecological impact of ERPs, reviewed ERP assessment studies showed that not all ESs were considered (Figure 5). Specifically, five types of ESs (i.e., genetic resources, biochemicals, ornamental resources, pollination, and knowledge systems) were not evaluated in the reviewed papers, whereas 77% of studies evaluated the impact of ERPs on regulation services. In addition, reviewed studies primarily focused on provisioning services, particularly services associated with agricultural activities (i.e., fresh water provision and food provision), which has also been evaluated in other studies (Foley et al., 2005; Paudyal et al., 2019; Sylla et al., 2020). However, the reviewed papers showed little interest in evaluating the impacts of ERPs on cultural services, with only 7% of the studies related to these topics. Also, we observed an uneven distribution of types of ESs within each category: of the regulating services, 62 studies estimated the impacts of ERPs on erosion regulation, but only 10 studies focused on air quality regulation; of the cultural services, most studies mainly looked at spiritual and religious values, whereas few studies considered other cultural services (e.g., education and aesthetic). Similarly, studies evaluating provisioning services mostly focused on fresh water provision, and studies evaluating supporting services mostly focused on opportunities for soil formation (Figure 5). Ecosystem services provide benefits to people across various dimensions. While much focus has been placed on the ES categories of provisioning and regulating, cultural services have

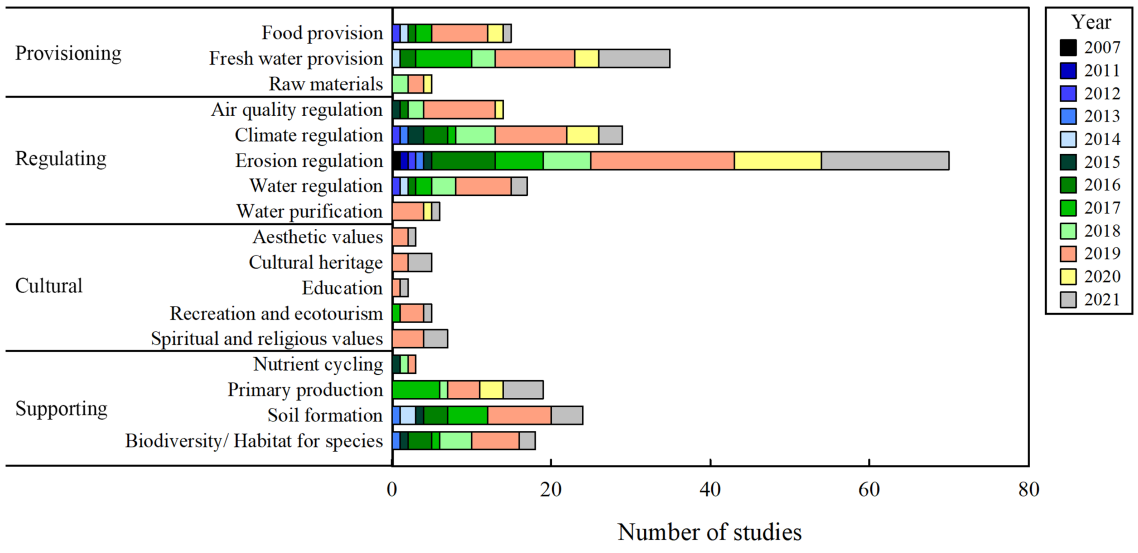

FIGURE 5
The number of studies that address each type of ecosystem service and their distribution across each year (because most of the studies consider several ecosystem services, the sum of studies in this figure exceeds the total number of studies reviewed).

received little attention in previous studies. One reason often cited is the difficulty in assessing cultural ESs because of their subjective and intangible character (Daniel et al., 2012; Schirpke et al., 2018; Kalinauskas et al., 2021). Cultural services are of great importance, not only for understanding the human-nature relationship but also for policy development (Jiang, 2017). We suggest that future research should take cultural services into account to build a more comprehensive assessment of ESs.

To summarize the features of regionalized differences, we further analyzed the focus of existing literature and the gaps of major ecosystem services within each region or province by taking into account the spatial distribution of the key ecological function zones (KEFZs) in China. Given that KEFZs are categorized by their functions of fresh water provision, sand fixation, soil and water conservation, water regulation, and biodiversity conservation (from the Resource and Environment Science and Data Center, https://www.resdc.cn; Figure 6A), we analyzed the spatial coverage of its corresponding ESs (i.e., fresh water provision, air quality regulation, erosion regulation, water regulation and biodiversity/habitat for species) in the reviewed papers. We found that the study site selection in the reviewed papers was not evenly distributed throughout KEFZs. Specifically, many papers chose Shaanxi Province as the case study sites to assess changes in fresh water provision and erosion regulation caused by ERPs (Figures 6B,C), which was in line with major local ecological characteristics or problems (e.g., water shortage and soil erosion; Cao et al., 2009). However, the northwest regions of China (e.g., Xinjiang and Tibet) and the southwestern regions (e.g., Guizhou, Guangxi and Chongqing) received less attention in terms of fresh water provision and erosion regulation evaluations, respectively, although there are a few KEFZs located in these regions (Figures 6B,C). Similarly, uneven distribution was detected in air quality regulation and water regulation evaluations related to ERPs assessments (Figures 6D,E). Moreover, we observed that the research on biodiversity conservation in some specific regions like Yunnan, Xinjiang and Tibet was still rare (Figure 6F). So there need to be more studies in these regions to better understand the effect of ecological restoration on biodiversity maintenance, especially for biodiversity hotspots such as Yunnan Province. Due to the importance of the KEFZs that contain degraded ecosystems and affect the ecological security of the entire country or large regions within it (Fan et al., 2017; Sun et al., 2021), we recommend that full consideration should be given to the regions with different ecosystem service functions, to provide targeted regional ecological restoration strategies.

3.2.3. Spatial and temporal scales

Scale plays an important role in estimating ESs and analyzing their interactions (Gret-Regamey et al., 2014). This is not surprising because ESs and their interactions in response to ERPs vary across spatiotemporal scales (Haines-Young et al., 2012; Costanza et al., 2014; Locatelli et al., 2014; Sannigrahi et al., 2019). We found that regional-level assessments account for 80% of the review papers, followed by county-level assessment (13%). Only 7% of studies considered national scales (see Appendix). Studies focused on the regional and national scales can detect the dynamic changes of ESs at large geographical extents but are limited in their ability to provide detailed information on local scale changes in ES (Raudsepp-Hearne and Peterson, 2016). However, studies focused on small spatial scales limit the ability of policy-makers to assess the full ecological impacts of restoration programs because ecological restoration could provide substantial influences to areas outside the region through the flow of ESs (Wolff et al., 2015). For instance, some specific ESs are provided locally but the benefits can accrue at different scales, ranging from local (e.g., food) to global (e.g., carbon sequestration; Xu S. et al., 2017). Certain ESs may be best considered at specific scales (Millennium Ecosystem Assessment (MEA), 2005). Generally, regulating and provisioning services may be best considered on a broad and small scale, respectively, while some specific services (e.g., carbon sequestration, climate regulation) should be considered on a national or global scale (Fu et al., 2011).

Additionally, the spatial patterns of ESs and their interactions are closely associated with the spatial scale (Sannigrahi et al., 2019), and thus findings from studies conducted in the same regions but on different spatial scales may not be consistent (Qiao et al., 2019). For instance, a study conducted in the floodplain of the Piedra River in central Spain found that the scale effects on changes in ES change will increase with spatial scale, as a higher pairwise correlation was observed at a larger scale (Felipe-Lucia et al., 2014). However, other studies identified a high correlation between changes in ES at fine spatial scales, with this trend disappearing as the spatial scale increases (Hou et al., 2017; Xu W. et al., 2017; Xu S. et al., 2017). Despite the differences in response to different spatial scales, few studies in the reviewed papers examined the variations in relationships among ESs across multiple spatial scales. Given that ecosystems are complex, and some ecological processes may occur across multiple scales (Agarwal et al., 2002), the single-scale observations may capture, miss, or distort ES interactions (Raudsepp-Hearne and Peterson, 2016). Therefore, determining the spatial patterns of ES and identifying associations that exist among them at multiple spatial scales is a critical need of future research aimed at accurately assessing the impacts of ERPs.

The temporal scale is also critical for ES research about ERPs as ESs vary from the short-term (e.g., amenity services) to the long-term (e.g., carbon sequestration; Turner et al., 2000; Limburg et al., 2002). Understanding the temporal changes in multiple ESs and their interactions contributes to assessing the long-term environmental impact of restoration programs (Hein et al., 2016). However, our results indicated that studies covered temporal scales unevenly; 76% of the total reviewed papers evaluated the changes in ESs related to the ERPs in the short term (<20 years; see Appendix), and 28% papers focused on evaluating <10 years of temporal extent. Only 24% papers analyzed more than 20 years of data. Furthermore, 45% of studies in the reviewed papers are based on static or semi-static (two-time points) analysis, without considering a temporal dynamic (at several time intervals or a continuous time series). These studies may ignore the uncertainty in analyzing changes in ESs and their interactions. For instance, changes in modeled ES may likely be dominated or overwhelmed by the external environment (e.g., fluctuations in weather in 1 year), which may result in detecting biased interactions between ESs (Li et al., 2017). Instead, studies based on temporal dynamic analysis may help detect continuous changes in ecosystem services and threshold or lag effects in interactions among ES (Li et al., 2017; Yin et al., 2019).

3.2.4. Changes in ESs and driver factors

Changes in ESs related to ERPs were different among multiple ESs (Figure 6). Generally, after the implementation of ERPs, all the studies in reviewed papers showed an increase in raw materials, air quality

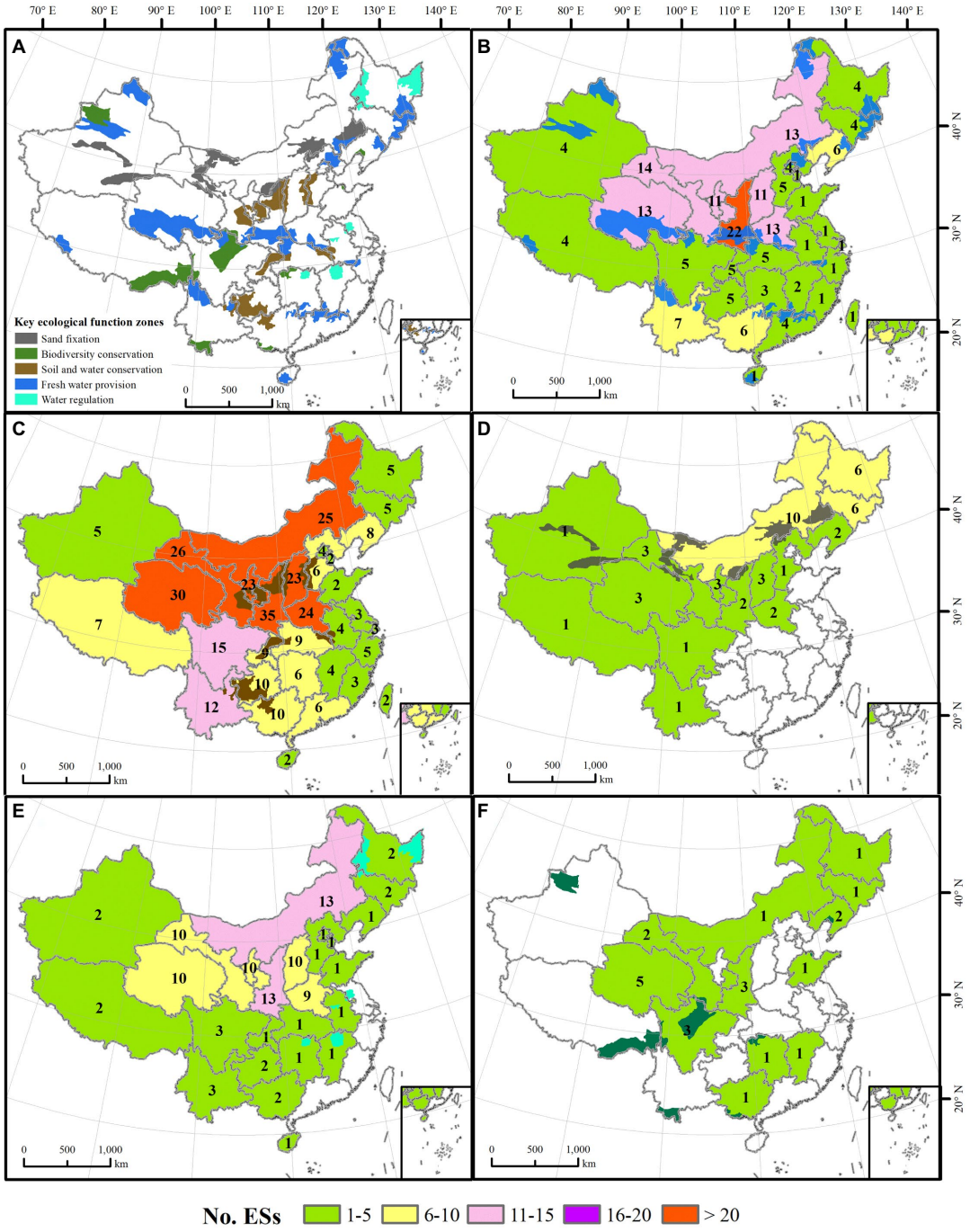

FIGURE 6
The key ecological function zones in China **(A)**, the number of ESs and their geographical distribution. **(B–F)** Stand for fresh water provision, air quality regulation, erosion regulation, water regulation and biodiversity/habitat for species, respectively.

regulation, water purification, education and nutrient cycling, followed by erosion regulation (93%), climate regulation (90%), and biodiversity/habitat for species (89%) (Figure 7). However, more than half of the studies (60%) showed that the ERPs resulted in a decrease in fresh water provision. There are also studies demonstrating that no change in ESs is related to ERPs, for instance, 11% of studies found no change in primary production. Overall, ecological restoration was beneficial to improving ESs (except for fresh water provision in some areas). This is likely because ecological restoration can improve the environment of the region (Chen et al., 2020; Tan et al., 2021). In addition, the landscape diversity caused by ecological restoration, and the consequent livelihood changes may make the public perceive more cultural ESs in several ways (Xian et al., 2020). However, our results also indicated that previous studies have yielded inconsistent results regarding ERPs' effect on ESs. This may be explained by geographical differences, historical factors, and economic conditions of the study regions. In China, most of the ERPs were not tailored for the local hydrological, climate, and land conditions of all regions covered by the

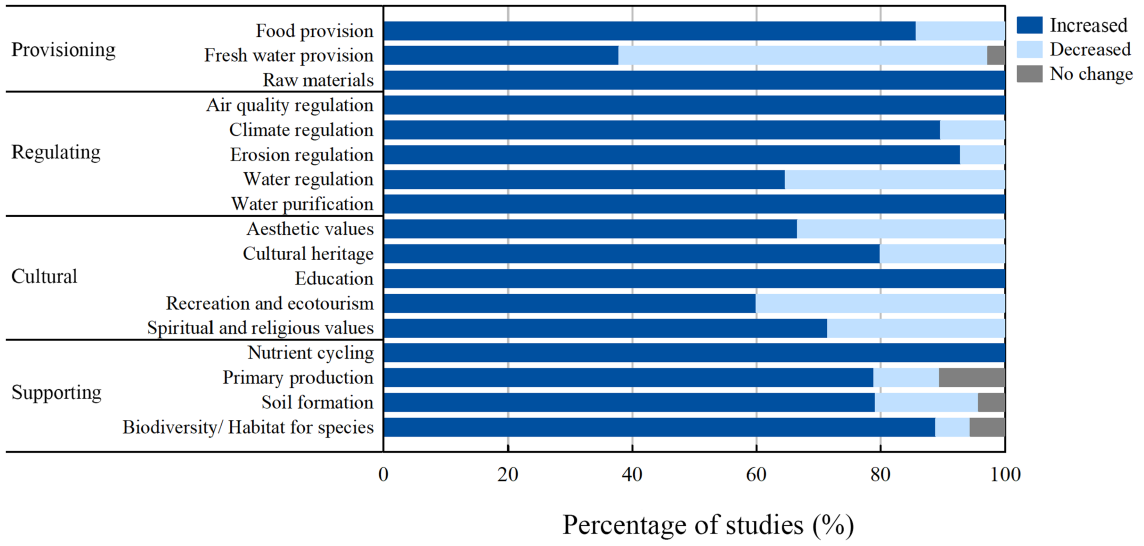

FIGURE 7
Changes in ecosystem services after ERPs.

program (Cao et al., 2011), and therefore, these programs may have negative impacts on ESs in some areas. More studies are needed to examine the interactions between multiple ESs and the mechanism behind these relationships, which could help improve the program's effectiveness.

Changes in ESs mentioned above were mainly driven by the implementation of ERPs. Indeed, ecological restoration engineering, including the GTGP, NFCP, SWCP, was the main factor that is responsible for improving ESs in China. However, previous reviews assessed only two ERPs (GTGP and NFCP; Wen and Théau, 2020), neglecting other ERPs' impacts. Our review found that there was a wide variety in the type of driver factors identified in the reviewed papers (see Appendix). The most identified driver was GTGP ($n = 53$), followed by NFCP ($n = 10$) and SWCP ($n = 6$). However, 33 studies in the reviewed papers did not specify the restoration programs. Although there was considerable variation in the number of papers focusing on each driver, GTGP and NFCP were two of the most studied drivers in ERPs assessment. This is likely because NFPP and GTGP are the two largest ERPs almost cover two-thirds of the Chinese territory (Liu et al., 2008) and have raised wider attention (Lu et al., 2018; Liu et al., 2019; Niu and Shao, 2020; Tan et al., 2021). However, to obtain a fuller picture of the influences of ERPs on ESs, restoration projects with different emphases (e.g., the emerging Ecological Conservation Red Line policy, ecological restoration after earthquake and the Three-North Shelter Forest Program) should be included in ERP assessments.

3.2.5. Methodologies used to assess the ERPs

Eighty-two reviewed papers assessed the ERPs based on model simulation, which shows the dominance of using simulation models in ES assessment (see Appendix). In particular, relatively simple ES models like the Integrated Valuation of Ecosystem Services and Tradeoffs (InVEST; https://naturalcapitalproject.stanford.edu/software/invest) or other comprehensive hydrological models such as the Soil Water Assessment Tool (SWAT; Arnold et al., 1998) can generate maps of the delivery and temporal distribution of water-related ESs across the landscape (Leh et al., 2013). The soil conservation assessment methods are mainly based on empirical soil erosion models, i.e., the Revised Universal Soil Loss Equation (RUSLE; Renard, 1997) or the Universal Soil Loss Equation (USLE; Wischmeier and Smith, 1978). Carbon sequestration mapping was commonly modeled using the CASA (Carnegie-Ames-Stanford Approach) model, which is fundamental to vegetation carbon sequestration assessment (Lü et al., 2012). Moreover, 16 reviewed papers used field observations or laboratory analysis to assess the ERPs. This approach can collect information directly from sample plots and is usually used to assess the soil formation services (e.g., soil moisture, soil organic carbon and soil nutrient elements) and biodiversity (e.g., Li L. et al., 2018; Li Y. et al., 2018). Only two papers used a questionnaire survey and the application focused on evaluating cultural ESs after ERPs.

Although our results indicated that model-based assessments have been widely used to evaluate ESs about ERPs, some uncertainties identified from the process of modeling physical quantities remain in these model-based studies that may affect the accuracy of results (Qiao et al., 2019). For example, using undifferentiated modeling parameter values can lead to uncertainties due to spatial heterogeneity in the environmental conditions (e.g., climate and soil; Jiang and Zhang, 2016). Using the land use/land cover (LULC) data as the main source of input data can be another possible source of uncertainty. Since the availability of LULC data depends largely on the spatial resolution of the remotely sensed images (Ghassemian, 2016), the broad categories of LULC obtained from the interpretation of the remote sensing images may cause the loss of some critical information (Su and Fu, 2013). Specifically, ERPs are usually achieved by afforestation and conservation of native forests, while current LULC classifications of forest cover do not differentiate between plantations and native forests. This can be problematic for assessing ERPs impacts on ES, as previous research has shown that plantations and native forests differ in their capacity to provide ESs; for example, plantations may support lower biodiversity, and lower soil and water provisioning

services compared with native forests (Wilson et al., 2017; Hua et al., 2018, 2022). Therefore, using the oversimplified LULC categorization scheme may potentially lead to inaccuracies and biases in ESs detection under restoration programs.

Similarly, uncertainties also exist in field measurement because these plot-level studies can often not account for the heterogeneity of complex landscapes and therefore do not sufficiently represent all the study areas (Birkhofer et al., 2015). Additionally, observations at large spatial scales and long-term, consecutive temporal-scale are usually scarce (Martínez-Harms and Balvanera, 2012), which may bring a difficulty to assess ERPs at large scales. This can be resolved by adding more field experiments, but they are usually time-consuming and labor-intensive. In addition, our results indicated that a questionnaire survey is usually used to identify the influences of ERPs on cultural ESs from human perceptions. Unlike some ESs that can be quantified based on the objective units of measure (e.g., the mass of pollutants sequestered per acre per year as a measure of the regulating service), the concept of cultural ESs is more difficult to quantify because they are subjective and driven by personal preferences (Booth et al., 2017), which potentially causes results uncertainties.

The uncertainties associated with the use of simulation models and the loss of information when using the oversimplified LULC categorization scheme may limit the accuracy and precision of evaluation results. Thus, it is necessary to find ways to reduce such uncertainties to improve the accuracy of results. First, a combination of methodology (e.g., field measurement and modeling) could be a possible solution. Model parameters for a regional scale or smaller spatial scale should be adjusted by using the results from field measurements which could provide direct on-ground data for parameterization and parameter optimization of ecosystem process models (Yu et al., 2018). Second, a more rigorous LULC categorization scheme that classifies the subtypes of forests (i.e., plantations versus native forests) is necessary. This is of particular importance as China's remarkable increase in forest cover has been dominated by tree plantations, usually monocultures following restoration (Hua et al., 2016), while native forests continue to decrease (Zhai et al., 2014). A multi-source data integration strategy that results from the comparison of historical aerial photographs and remote sensing data with high resolutions can be applied to reduce the imprecision and inconsistencies in LULC detection (Balthazar et al., 2015). Additionally, other datasets such as the China National Forestry Inventory should be considered as important Supplementary material, which not only can help us to differentiate between plantations and native forests (Hua et al., 2018) but also can be used to validate the results whether the simulation results or questionnaire survey results to improve the accuracy and precision of evaluation results.

4. Conclusion

This study reviewed 100 papers to evaluate ERPs using ES approaches in China. Our results show that most studies focused on specific regions and specific ES types (e.g., provisioning service and regulating service). Many studies did not consider the association among ES types, which may lead to an incomprehensive understanding of the ecological impact of China's restoration programs. In addition, the oversimplified LULC categorization scheme used in previous studies may limit the accuracy and precision of ERPs assessment results. Although our review showed that ES approaches have been widely used to analyze the ecological impact of ERPs in China, we identify some major elements that can improve future ERPs assessments. Priority should be given to performing studies on different regions, especially southwestern and northeastern China. Additionally, we suggest that multiple ESs, particularly cultural services, the interactions between multiple ESs, and multiple temporal and spatial scales for ERP assessments should be given more attention in future work. Further, we recommend that future studies should develop a more detailed LULC categorization scheme that differentiates the plantations from native forests to improve the accuracy and precision of evaluation results.

Author contributions

JL: conceptualization, formal analysis, writing an original draft. JD: conceptualization and review and editing. CZ: investigation and methodology. JZ, HY, and MD: review and editing. TD: conceptualization, supervision, and writing–review and editing. YW: project administration and supervision. All authors contributed to the article and approved the submitted version.

Funding

This study was supported by the National Key Research and Development Program of China (no. 2017YFC0505005), the Project of Jiuzhaigou National Nature Reserve (no. 5132202020000046), and (no. 22kE024).

Acknowledgments

We are very grateful to Heng-Xing Zou for his helpful suggestions.

Conflict of interest

The authors declare that the research was conducted in the absence of any commercial or financial relationships that could be construed as a potential conflict of interest.

Publisher's note

Supplementary material

The Supplementary material for this article can be found online at: https://www.frontiersin.org/articles/10.3389/fevo.2023.1152907/full#supplementary-material

References

Andrew, M. E., Wulder, M. A., Nelson, T. A., and Coops, N. C. (2015). Spatial data, analysis approaches, and information needs for spatial ecosystem service assessments: a review. *GISci. Remote Sens.* 52, 344–373. doi: 10.1080/15481603.2015.1033809

Agarwal, C., Green, G. M., Grove, J. M., Evans, T. P., and Schweik, C. M. (2002). A review and assessment of land-use change models: dynamics of space, time, and human choice. Gen tech rep NE-297 Newton Square, US Department of Agriculture, Forest Service, Northeastern Research Station

Arnold, J. G., Srinivasan, R., Muttiah, R. S., and Williams, J. R. (1998). Large area hydrologic modeling and assessment part I: model development. *J. Am. Water Resour. Assoc.* 34, 73–89. doi: 10.1111/j.1752-1688.1998.tb05961.x

Balthazar, V., Vanacker, V., Molina, A., and Lambin, E. F. (2015). Impacts of forest cover change on ecosystem services in high Andean mountains. *Ecol. Indic.* 48, 63–75. doi: 10.1016/j.ecolind.2014.07.043

Benra, F., Nahuelhual, L., Gaglio, M., Gissi, E., Aguayo, M., Jullian, C., et al. (2019). Ecosystem services tradeoffs arising from non-native tree plantation expansion in southern Chile. *Landscape Urban Plan.* 190:103589. doi: 10.1016/j.landurbplan.2019.103589

Birkhofer, K., Diehl, E., Andersson, J., Ekroos, J., Früh-Müller, A., Machnikowski, F., et al. (2015). Ecosystem services—current challenges and opportunities for ecological research. *Front. Ecol. Evol.* 2:87. doi: 10.3389/fevo.2014.00087

Booth, P. N., Law, S. A., Ma, J., Buonagurio, J., Boyd, J., and Turnley, J. (2017). Modeling aesthetics to support an ecosystem services approach for natural resource management decision making. *Integr. Environ. Assess. Manag.* 13, 926–938. doi: 10.1002/ieam.1944

Brandt, M., Yue, Y., Wigneron, J. P., Tong, X., Tian, F., Jepsen, M. R., et al. (2018). Satellite-observed major greening and biomass increase in South China karst during recent decade. *Earth Future* 6, 1017–1028. doi: 10.1029/2018EF000890

Bryan, B. A., Gao, L., Ye, Y., Sun, X., Connor, J. D., Crossman, N. D., et al. (2018). China's response to a national land-system sustainability emergency. *Nature* 559, 193–204. doi: 10.1038/s41586-018-0280-2

Bullock, J. M., Aronson, J., Newton, A. C., Pywell, R. F., and ReyBenayas, J. M. (2011). Restoration of ecosystem services and biodiversity: conflicts and opportunities. *Trend Ecol. Evol.* 26, 541–549. doi: 10.1016/j.tree.2011.06.011

Cai, W., Borlace, S., Lengaigne, M., van Rensch, P., Collins, M., Vecchi, G., et al. (2014). Increasing frequency of extreme El Niño events due to greenhouse warming. *Nat. Clim. Chang.* 4, 111–116. doi: 10.1038/nclimate2100

Cao, S. X., Chen, L., and Liu, Z. (2009). An investigation of Chinese attitudes towards the environment: case study using the grain for Green project. *Ambio* 38, 55–64. doi: 10.1579/0044-7447-38.1.55

Cao, S. X., Sun, G., Zhang, Z., Chen, L., Feng, Q., Fu, B., et al. (2011). Greening China naturally. *Ambio* 40, 828–831. doi: 10.1007/s13280-011-0150-8

Chazdon, R. L. (2008). Beyond deforestation: restoring forests and ecosystem services on degraded lands. *Science* 320, 1458–1460. doi: 10.1126/science.1155365

Chen, Y., Chen, L., Cheng, Y., Ju, W., Chen, H. Y., and Ruan, H. (2020). Afforestation promotes the enhancement of forest LAI and NPP in China. *For. Ecol. Manag.* 462:117990. doi: 10.1016/j.foreco.2020.117990

Costanza, R., de Groot, R., Sutton, P., van der Ploeg, S., Anderson, S. J., Kubiszewski, I., et al. (2014). Changes in the global value of ecosystem services. *Glob. Environ. Change* 26, 152–158. doi: 10.1016/j.gloenvcha.2014.04.002

Cui, F., Wang, B., Zhang, Q., Tang, H., De Maeyer, P., Hamdi, R., et al. (2021). Climate change versus land-use change—what affects the ecosystem services more in the forest-steppe ecotone? *Sci. Total Environ.* 759:143525. doi: 10.1016/j.scitotenv.2020.143525

D'Amato, D., Rekola, M., Li, N., and Toppinen, A. (2016). Monetary valuation of forest ecosystem services in China: a literature review and identification of future research needs. *Ecol. Econ.* 121, 75–84. doi: 10.1016/j.ecolecon.2015.11.009

Dade, M. C., Mitchell, M. G. E., McAlpine, C. A., and Rhodes, J. R. (2019). Assessing ecosystem service trade-offs and synergies: the need for a more mechanistic approach. *Ambio* 48, 1116–1128. doi: 10.1007/s13280-018-1127-7

Daniel, T. C., Muhar, A., Arnberger, A., Aznar, O., Boyd, J. W., Chan, K. M. A., et al. (2012). Contributions of cultural services to the ecosystem services agenda. *Proc. Natl. Acad. Sci. U. S. A.* 109, 8812–8819. doi: 10.1073/pnas.1114773109

De Groot, R., Brander, L., Ploeg, S., Costanza, R., Bernard, F., Braat, L., et al. (2012). Global estimates of the value of ecosystems and their services in monetary units. *Ecosyst. Serv.* 1, 50–61. doi: 10.1016/j.ecoser.2012.07.005

De Groot, R., Wilson, M. A., and Bouman, R. M. J. (2002). A typology for the classification, description and valuation of ecosystem services, goods and services. *Ecol. Econ.* 41, 393–408. doi: 10.1016/S0921-8009(02)00089-7

Duan, X., Bai, Z., Li, R., Li, Y., Ding, J., Tao, Y., et al. (2020). Investigation method for regional soil erosion based on the Chinese soil loss equation and high-resolution spatial data: case study on the mountainous Yunnan Province, China. *Catena* 184:104237. doi: 10.1016/j.catena.2019.104237

Fan, J., Wang, Y. F., Ouyang, Z. Y., Li, L. J., Xu, Y., Zhang, W. Z., et al. (2017). Risk forewarning of regional development sustainability based on a natural resources and environmental carrying index in China. *Earth Future* 5, 196–213. doi: 10.1002/2016EF000490

Felipe-Lucia, M. R., Comín, F. A., and Bennett, E. M. (2014). Interactions among ecosystem services across land uses in a floodplain agroecosystem. *Ecol. Soc.* 19:20. doi: 10.5751/ES-06249-190120

Foley, J. A., De Fries, R., Asner, G. P., Barford, C., Bonan, G., Carpenter, S. R., et al. (2005). Global consequences of land use. *Science* 309, 570–574. doi: 10.1126/science.1111772

Fu, B., Su, C., Wei, Y., Willett, I. R., Lü, Y., and Liu, G. (2011). Double counting in ecosystem services valuation: causes and countermeasures. *Ecol. Res.* 26, 1–14. doi: 10.1007/s11284-010-0766-3

Fu, B., Wang, S., Su, C., and Forsius, M. (2013). Linking ecosystem processes and ecosystem services. *Curr. Opin. Environ. Sust.* 5, 4–10. doi: 10.1016/j.cosust.2012.12.002

Fu, B., Zhang, L., Xu, Z., Zhao, Y., Wei, Y., and Skinner, D. (2015). Ecosystem services in changing land use. *J. Soils Sediments* 15, 833–843. doi: 10.1007/s11368-015-1082-x

Gao, J., Li, F., Gao, H., Zhou, C., and Zhang, X. (2017). The impact of land-use change on water-related ecosystem services: a study of the Guishui River basin, Beijing, China. *J. Clean Prod.* 163, S148–S155. doi: 10.1016/j.jclepro.2016.01.049

Geng, Q., Ren, Q., Yan, H., Li, L., Zhao, X., Mu, X., et al. (2020). Target areas for harmonizing the grain for Green Programme in China's loess plateau. *Land Degrad. Dev.* 31, 325–333. doi: 10.1002/ldr.3451

Ghassemian, H. (2016). A review of remote sensing image fusion methods. *Inform. Fusion* 32, 75–89. doi: 10.1016/j.inffus.2016.03.003

Gret-Regamey, A., Weibel, B., Bagstad, K. J., Ferrari, M., Geneletti, D., Klug, H., et al. (2014). On the effects of scale for ecosystem services mapping. *PLoS One* 9:e112601. doi: 10.1371/journal.pone.0112601

Guo, Z., Zhang, X., Dungait, J. A. J., Green, S. M., Wen, X., and Quine, T. A. (2021). Contribution of soil microbial necromass to SOC stocks during vegetation recovery in a subtropical karst ecosystem. *Sci. Total Environ.* 761:143945. doi: 10.1016/j.scitotenv.2020.143945

Haines-Young, R., Potschin, M., and Kienast, F. (2012). Indicators of ecosystem service potential at European scales: mapping marginal changes and trade-offs. *Ecol. Indic.* 21, 39–53. doi: 10.1016/j.ecolind.2011.09.004

Hein, L., van Koppen, C. S. A., van Ierland, E. C., and Leidekker, J. (2016). Temporal scales, ecosystem dynamics, stakeholders and the valuation of ecosystems services. *Ecosyst. Serv.* 21, 109–119. doi: 10.1016/j.ecoser.2016.07.008

Hou, Y., Lu, Y., Chen, W., and Fu, B. (2017). Temporal variation and spatial scale dependency of ecosystem service interactions: a case study on the central loess plateau of China. *Landsc. Ecol.* 32, 1201–1217. doi: 10.1007/s10980-017-0497-8

Hua, F., Bruijnzeel, L. A., Meli, P., Martin, P. A., Zhang, J., Nakagawa, S., et al. (2022). The biodiversity and ecosystem service contributions and trade-offs of forest restoration approaches. *Science* 376, 839–844. doi: 10.1126/science.abl464

Hua, F., Wang, L., Brendan, F., Zheng, X., Wang, X., Yu, D. W., et al. (2018). Tree plantations displacing native forests: the nature and drivers of apparent forest recovery on former croplands in southwestern China from 2000 to 2015. *Biol. Conserv.* 222, 113–124. doi: 10.1016/j.biocon.2018.03.034

Hua, F., Wang, X., Zheng, X., Fisher, B., Wang, L., Zhu, J., et al. (2016). Opportunities for biodiversity gains under the world's largest reforestation programme. *Nat. Commun.* 7:12717. doi: 10.1038/ncomms12717

Jenerette, G. D., Harlan, S. L., Stefanov, W. L., and Martin, C. A. (2011). Ecosystem services and urban heat riskscape moderation: water, green spaces, and social inequality in Phoenix, USA. *Ecol. Appl.* 21, 2637–2651. doi: 10.1890/10-1493.1

Jiang, W. (2017). Ecosystem services research in China: a critical review. *Ecosyst. Serv.* 26, 10–16. doi: 10.1016/j.ecoser.2017.05.012

Jiang, C., Guo, H., Wei, Y., Yang, Z., Wang, X., Wen, M., et al. (2021). Ecological restoration is not sufficient for reconciling the trade-off between soil retention and water yield: a contrasting study from catchment governance perspective. *Sci. Total Environ.* 754:142139. doi: 10.1016/j.scitotenv.2020.142139

Jiang, C., and Zhang, L. (2016). Ecosystem change assessment in the three-river headwater region, China: patterns, causes, and implications. *Ecol. Eng.* 93, 24–36. doi: 10.1016/j.ecoleng.2016.05.011

Jiang, C., Zhang, H., and Zhang, Z. (2018). Spatially explicit assessment of ecosystem services in China's loess plateau: patterns, interactions, drivers, and implications. *Glob. Planet. Change* 161, 41–52. doi: 10.1016/j.gloplacha.2017.11.014

Kalinauskas, M., Miksa, K., Inacio, M., Gomes, E., and Pereira, P. (2021). Mapping and assessment of landscape aesthetic quality in Lithuania. *J. Environ. Manag.* 286:112239. doi: 10.1016/j.jenvman.2021.112239

Keesstra, S., Nunes, J., Novara, A., Finger, D., Avelar, D., Kalantari, Z., et al. (2018). The superior effect of nature based solutions in land management for enhancing ecosystem services. *Sci. Total Environ.* 610-611, 997–1009. doi: 10.1016/j.scitotenv.2017.08.077

Leh, M. D. K., Matlocka, M. D., Cummingsa, E. C., and Nalley, L. L. (2013). Quantifying and mapping multiple ecosystem services change in West Africa. *Agric. Ecosyst. Environ.* 165, 6–18. doi: 10.1016/j.agee.2012.12.001

Li, W. (1999). Flood of Yantze river and ecological restoration. *J. Nat. Res* 14, 1–8. (in Chinese with English Abstract. doi: 10.11849/zrzyxb.1999.01.001

Li, Q., Chen, D., Zhao, L., Yang, X., Xu, S., and Zhao, X. (2016). More than a century of grain for Green program is expected to restore soil carbon stock on alpine grassland revealed by field ^{13}C pulse labeling. *Sci. Total Environ.* 550, 17–26. doi: 10.1016/j.scitotenv.2016.01.060

Li, Z., Liu, X., Niu, T., Kejia, D., Zhou, Q., Ma, T., et al. (2015). Ecological restoration and its effects on a regional climate: the source region of the Yellow River, China. *Environ. Sci. Technol.* 49, 5897–5904. doi: 10.1021/es505985q

Li, Y., Piao, S., Li, L., Chen, A., Wang, X., Ciais, P., et al. (2018). Divergent hydrological response to large-scale afforestation and vegetation greening in China. *Sci. Adv.* 4:eaar4182. doi: 10.1126/sciadv.aar4182

Li, L., Tietze, D. T., Fritz, A., Lü, Z., Bürgi, M., and Storch, I. (2018). Rewilding cultural landscape potentially puts both avian diversity and endemism at risk: a Tibetan plateau case study. *Biol. Conserv.* 224, 75–86. doi: 10.1016/j.biocon.2018.05.008

Li, Y., Zhang, L., Qiu, J., Yan, J., Wan, L., Wang, P., et al. (2017). Spatially explicit quantification of the interactions among ecosystem services. *Landsc. Ecol.* 32, 1181–1199. doi: 10.1007/s10980-017-0527-6

Li, R., Zheng, H., O'Connor, P., Xu, H., Li, Y., Lu, F., et al. (2021). Time and space catch up with restoration programs that ignore ecosystem service trade-offs. *Sci. Adv.* 7:eabf8650. doi: 10.1126/sciadv.abf8650

Liang, Y., Hashimoto, S., and Liu, L. (2021). Integrated assessment of land-use/land-cover dynamics on carbon storage services in the loess plateau of China from 1995 to 2050. *Ecol. Indic.* 120:106939. doi: 10.1016/j.ecolind.2020.106939

Limburg, K. E., O'Neill, R. V., Costanza, R., and Farber, S. (2002). Complex systems and valuation. *Ecol. Econ.* 41, 409–420. doi: 10.1016/S0921-8009(02)00090-3

Liu, J., Li, S., Ouyang, Z., Tam, C., and Chen, X. (2008). Ecological and socioeconomic effects of China's policies for ecosystem services. *Proc. Natl. Acad. Sci. U. S. A.* 105, 9477–9482. doi: 10.1073/pnas.0706436105

Liu, Y., Lü, Y., Fu, B., Harris, P., and Wu, L. (2019). Quantifying the spatio-temporal drivers of planned vegetation restoration on ecosystem services at a regional scale. *Sci. Total Environ.* 650, 1029–1040. doi: 10.1016/j.scitotenv.2018.09.082

Locatelli, B., Imbach, P., and Wunder, S. (2014). Synergies and trade-offs between ecosystem services in Costa Rica. *Environ. Conserv.* 41, 27–36. doi: 10.1017/S0376892913000234

Lü, Y., Fu, B., Feng, X., Zeng, Y., Liu, Y., Chang, R., et al. (2012). A policy-driven large scale ecological restoration: quantifying ecosystem services changes in the loess plateau of China. *PLoS One* 7:e31782. doi: 10.1371/journal.pone.0031782

Lu, F., Hu, H., Sun, W., Zhu, J., Liu, G., Zhou, W., et al. (2018). Effects of national ecological restoration projects on carbon sequestration in China from 2001 to 2010. *Proc. Natl. Acad. Sci. U. S. A.* 115, 4039–4044. doi: 10.1073/pnas.1700294115

Martínez-Harms, M. J., and Balvanera, P. (2012). Methods for mapping ecosystem service supply: a review. *Inter. J. Biodiver. Sci. Ecosyst. Serv. Manage.* 8, 17–25. doi: 10.1080/21513732.2012.663792

Millennium Ecosystem Assessment (MEA). (2005). *Ecosystems and human well-being*. Washington, DC: Island Press.

Niu, L., and Shao, Q. (2020). Soil conservation service spatiotemporal variability and its driving mechanism on the Guizhou plateau, China. *Remote Sens.* 12:2187. doi: 10.3390/rs12142187

Ouyang, Z., Zheng, H., Xiao, Y., Polasky, S., Liu, J., Xu, W., et al. (2016). Improvements in ecosystem services from investments in natural capital. *Science* 352, 1455–1459. doi: 10.1126/science.aaf2295

Paudyal, K., Baral, H., Bhandari, S. P., Bhandarie, A., and Keenan, R. J. (2019). Spatial assessment of the impact of land use and land cover change on supply of ecosystem services in Phewa watershed. *Nepal. Ecosyst. Serv.* 36:100895. doi: 10.1016/j.ecoser.2019.100895

Qi, X., Li, Q., Yue, Y., Liao, C., Zhai, L., Zhang, X., et al. (2021). Rural–urban migration and conservation drive the ecosystem services improvement in China karst: a case study of HuanJiang County, Guangxi. *Remote Sens.* 13:566. doi: 10.3390/rs13040566

Qi, W., Li, H., Zhang, Q., and Zhang, K. (2019). Forest restoration efforts drive changes in land-use/land-cover and water-related ecosystem services in China's Han River basin. *Ecol. Engineer* 126, 64–73. doi: 10.1016/j.ecoleng.2018.11.001

Qiao, X., Gu, Y., Zou, C., Xu, D., Wang, L., Ye, X., et al. (2019). Temporal variation and spatial scale dependency of the trade-offs and synergies amongmultiple ecosystemservices in the Taihu Lake Basin of China. *Sci. Total Environ.* 651, 218–229. doi: 10.1016/j.scitotenv.2018.09.135

Raudsepp-Hearne, C., and Peterson, G. D. (2016). Scale and ecosystem services: how do observation, management, and analysis shift with scale —lessons from Québec. *Ecol. Soc.* 21:16. doi: 10.5751/ES-08605-210316

Renard, K. G. (1997). *Predicting soil erosion by water: a guide to conservation planning with the revised universal soil loss equation (RUSLE)*. Washington DC: United States Government Printing.

Sannigrahi, S., Chakraborti, S., Joshi, P. K., Keesstra, S., Sen, S., Paul, S. K., et al. (2019). Ecosystem service value assessment of a natural reserve region for strengthening protection and conservation. *J. Environ. Manag.* 244, 208–227. doi: 10.1016/j.jenvman.2019.04.095

Schägner, J. P., Brander, L., Maes, J., and Hartje, V. (2013). Mapping ecosystem services' values: current practice and future prospects. *Ecosyst. Serv.* 4, 33–46. doi: 10.1016/j.ecoser.2013.02.003

Schirpke, U., Meisch, C., Marsoner, T., and Tappeiner, U. (2018). Revealing spatial and temporal patterns of outdoor recreation in the European Alps and their surroundings. *Ecosyst. Serv.* 31, 336–350. doi: 10.1016/j.ecoser.2017.11.017

Su, C., and Fu, B. (2013). Evolution of ecosystem services in the Chinese loess plateau under climatic and land use changes. *Glob. Planet. Change* 101, 119–128. doi: 10.1016/j.gloplacha.2012.12.014

Sun, M., Yang, R., Li, X., Zhang, L., and Liu, Q. (2021). Designing a path for the sustainable development of key ecological function zones: a case study of Southwest China. *Glob. Ecol. Conserv.* 31:e01840. doi: 10.1016/j.gecco.2021.e01840

Sylla, M., Hagemann, N., and Szewrański, S. (2020). Mapping trade-offs and synergies among peri-urban ecosystem services to address spatial policy. *Environ. Sci. Pol.* 112, 79–90. doi: 10.1016/j.envsci.2020.06.002

Tallis, H., Kareiva, P., Marvier, M., and Chang, A. (2008). An ecosystem services framework to support both practical conservation and economic development. *Proc. Natl. Acad. Sci. U. S. A.* 105, 9457–9464. doi: 10.1073/pnas.0705797105

Tan, Q., Gong, C., Li, S., Ma, N., Ge, F., and Xu, M. (2021). Impacts of ecological restoration on public perceptions of cultural ecosystem services. *Environ. Sci. Pollut. Res.* 28, 60182–60194. doi: 10.1007/s11356-021-14793-7

Tang, Y., Shao, Q., Liu, J., Zhang, H., Yang, F., Cao, W., et al. (2019). Did ecological restoration hit its mark? Monitoring and assessing ecological changes in the grain for Green program region using multi-source satellite images. *Remote Sens.* 11:358. doi: 10.3390/rs11030358

TEEB (2010). *The economics of ecosystems and biodiversity*. Ecological and Economic Foundations. Earthscan, London and Washington.

Thom, D., and Seidl, R. (2016). Natural disturbance impacts on ecosystem services and biodiversity in temperate and boreal forests. *Biol. Rev. Camb. Philos. Soc.* 91, 760–781. doi: 10.1111/brv.12193

Turner, R. K., van den Bergh, J. C. J. M., Söderqvist, T., Barendregt, A., van der Straaten, J., Maltby, E., et al. (2000). Ecological-economic analysis of wetlands: scientific integration for management and policy. *Ecol. Econ.* 35, 7–23. doi: 10.1016/S0921-8009(00)00164-6

Wang, J., Peng, J., Zhao, M., Liu, Y., and Chen, Y. (2017). Significant trade-off for the impact of grain-for-Green Programme on ecosystem services in North-Western Yunnan, China. *Sci. Total Environ.* 574, 57–64. doi: 10.1016/j.scitotenv.2016.09.026

Wang, H., Zhao, W., Li, C., and Pereira, P. (2021). Vegetation greening partly offsets the water erosion risk in China from 1999 to 2018. *Geoderma* 401:115319. doi: 10.1016/j.geoderma.2021.115319

Wen, X., and Théau, J. (2020). Assessment of ecosystem services in restoration programs in China: a systematic review. *Ambio* 49, 584–592. doi: 10.1007/s13280-019-01214-w

Wilson, S. J., Schelhas, J., Grau, R., Nanni, A. S., and Sloan, S. (2017). Forest ecosystem-service transitions: the ecological dimensions of the forest transition. *Ecol. Soc.* 22:38. doi: 10.5751/ES-09615-220438

Wischmeier, W. H., and Smith, D. D. (1978). Predicting rainfall erosion losses – A guide to conservation planning. Agriculture handbook no. 537 USDA/science and education administration, US Govt. Printing Office, Washington, DC.

Wolff, S., Schulp, C. J. E., and Verburg, P. H. (2015). Mapping ecosystem services demand: a review of current research and future perspectives. *Ecol. Indic.* 55, 159–171. doi: 10.1016/j.ecolind.2015.03.016

Wu, K. Y., Jiang, Z. C., and Luo, W. Q. (2007). Techniques of ecological restoration and evaluation of economic value of their results in Guohua demonstration area. *Earth Environ.* 35, 159–165. doi: 10.3969/j.issn.1672-9250.2007.02.011

Wu, D., Zou, C., Cao, W., Xiao, T., and Gong, G. (2019). Ecosystem services changes between 2000 and 2015 in the loess plateau, China: a response to ecological restoration. *PLoS One* 14:e0209483. doi: 10.1371/journal.pone.0209483

Xia, H., Kong, W., Zhou, G., and Sun, O. (2021). Impacts of landscape patterns on water-related ecosystem services under natural restoration in Liaohe River reserve, China. *Sci. Total Environ.* 792:148290. doi: 10.1016/j.scitotenv.2021.148290

Xian, J., Xia, C., and Cao, S. (2020). Cost–benefit analysis for China's grain for Green program. *Ecol. Eng.* 151:105850. doi: 10.1016/j.ecoleng.2020.105850

Xu, S., Liu, Y., Wang, X., and Zhang, G. (2017). Scale effect on spatial patterns of ecosystem services and associations among them in semi-arid area: a case study in Ningxia Hui autonomous region, China. *Sci. Total Environ.* 598, 297–306. doi: 10.1016/j.scitotenv.2017.04.009

Xu, W., Xiao, Y., Zhang, J., Yang, W., Zhang, L., Hull, V., et al. (2017). Strengthening protected areas for biodiversity and ecosystem services in China. *Proc. Natl. Acad. Sci. U. S. A.* 114, 1601–1606. doi: 10.1073/pnas.1620503114

Yin, L., Wang, X., Zhang, K., Xiao, F., Cheng, C., and Zhang, X. (2019). Trade-offs and synergy between ecosystem services in National Barrier Zone. *Geogr. Res.* 38, 2162–2172. (in Chinese with English Abstract. doi: 10.11821/dlyj020180578

Yu, G., He, H., and Zhou, Y. (2018). Ecosystem observation and research under background of big data. *Bull. Chin. Acad. Sci.* 33, 832–837. (in Chinese with English Abstract. doi: 10.16418/j.issn.1000-3045.2018.08.010

Zhai, D., Xu, J., Dai, Z., Cannon, C. H., and Grumbine, R. E. (2014). Increasing tree cover while losing diverse natural forests in tropical Hainan, China. *Reg. Environ. Change* 14, 611–621. doi: 10.1007/s10113-013-0512-9

Zhang, B., He, C., Burnham, M., and Zhang, L. (2016). Evaluating the coupling effects of climate aridity and vegetation restoration on soil erosion over the loess plateau in China. *Sci. Total Environ.* 539, 436–449. doi: 10.1016/j.scitotenv.2015.08.132

Zhang, M., Wang, K., Liu, H., Zhang, C., Yue, Y., and Qi, X. (2018). Effect of ecological engineering projects on ecosystem services in a karst region: a case study of Northwest Guangxi, China. *J. Clean. Prod.* 183, 831–842. doi: 10.1016/j.jclepro.2018.02.102

Zhang, Y., Xu, X., Li, Z., Liu, M., Xu, C., Zhang, R., et al. (2019). Effects of vegetation restoration on soil quality in degraded karst landscapes of Southwest China. *Sci. Total Environ.* 650, 2657–2665. doi: 10.1016/j.scitotenv.2018.09.372

Zheng, H., Robinson, B. E., Liang, Y.-C., Polasky, S., Ma, D.-C., Wang, F.-C., et al. (2013). Benefits, costs, and livelihood implications of a regional payment for ecosystem service program. *Proc. Natl. Acad. Sci. U. S. A.* 110, 16681–16686. doi: 10.1073/pnas.1312324110

Zheng, H., Wang, L., and Wu, T. (2019). Coordinating ecosystem service trade-offs to achieve win-win outcomes: a review of the approaches. *J. Environ. Sci.* 82, 103–112. doi: 10.1016/j.jes.2019.02.030

Zhou, M., Deng, J., Lin, Y., Zhang, L., He, S., and Yang, W. (2021). Evaluating combined effects of socio-economic development and ecological conservation policies on sediment retention service in the Qiantang River basin, China. *J. Clean. Prod.* 286:124961. doi: 10.1016/j.jclepro.2020.124961

Zhou, J., Zhao, Y., Huang, P., Zhao, X., Feng, W., Li, Q., et al. (2020). Impacts of ecological restoration projects on the ecosystem carbon storage of inland river basin in arid area, China. *Ecol. Ind.* 118:106803. doi: 10.1016/j.ecolind.2020.106803

frontiers | Frontiers in Ecology and Evolution

TYPE Original Research
PUBLISHED 04 April 2023
DOI 10.3389/fevo.2023.1113823

OPEN ACCESS

EDITED BY
Wei Zhao,
Institute of Geographic Sciences and Natural Resources Research (CAS),
China

REVIEWED BY
Wei Song,
Peking Union Medical College Hospital (CAMS),
China
Wei Zhou,
Zhejiang Chinese Medical University,
China

*CORRESPONDENCE
Chunsheng Liu
✉ max_liucs@263.net
Dan Jiang
✉ jiangdan1027@163.com

SPECIALTY SECTION
This article was submitted to Population, Community, and Ecosystem Dynamics, a section of the journal Frontiers in Ecology and Evolution

RECEIVED 13 January 2023
ACCEPTED 08 March 2023
PUBLISHED 04 April 2023

CITATION
Li P, Ren G, Wu F, Chen J, Jiang D and Liu C (2023) Root-specific flavones and critical enzyme genes involved in their synthesis changes due to drought stress on *Scutellaria baicalensis*.
Front. Ecol. Evol. 11:1113823.
doi: 10.3389/fevo.2023.1113823

Root-specific flavones and critical enzyme genes involved in their synthesis changes due to drought stress on *Scutellaria baicalensis*

Ping Li, Guangxi Ren, Fei Wu, Jiaxin Chen, Dan Jiang* and Chunsheng Liu*

School of Chinese Materia Medica, Beijing University of Chinese Medicine, Beijing, China

Introduction: *Scutellaria baicalensis* is rich in bioactive flavonoid, which are widely used in clinical therapy. Many environmental factors, such as water and temperature, affect gene expression and secondary metabolites accumulation in plants.

Methods: In this study, to explore the effect of drought stress on the accumulation of flavonoids and gene expression in *S. baicalensis* seedlings, 4-week-old *Scutellaria baicalensis* seedlings were treated with different concentrations of PEG6000 to simulate drought stress. The contents of four root-specific flavones (baicalein, wogonin, baicalin, and wogonoside) in samples under different treatments were quantitatively analyzed by high performance liquid chromatography (HPLC). The expression levels of flavonoid biosynthesis-related genes (P*AL1*, *PAL2*, *CHS,* and *UBGAT*) were determined by real-time quantitative PCR (qRT-PCR). Also, a correlation analysis between flavonoid contents and gene expression levels was made.

Results: The HPLC results revealed that 5 and 10% PEG6000 treatments significantly increased the content of four flavonoids, with 5% PEG 6000 treatment being the most beneficial to the flavonoids accumulation. The qRT-PCR results showed that *PAL2* and *CHS* gene expressions differed significantly in different organs, while *PAL1* and *UBGAT* had poor organ-specific. For genes in roots, the expression of *PAL1* and *UBGAT* was the highest in 5% PEG6000 treatment, and *PAL2* and *CHS* were the highest in 10% PEG6000 treatment. Compared with other concentrations of PEG6000, 5 and 10% PEG6000 were more advantageous for gene expression. Collectively, PEG6000 at a low concentration promoted the accumulation of flavonoids and the expression of related genes. Additionally, the correlation results demonstrated that *PAL1*, *PAL2*, *CHS*, and *UBGAT* genes in roots stimulated the formation and accumulation of the four flavonoids to varying degrees, while the exception of *PAL2* gene expression in roots was negatively correlated with wogonin content.

Discussion: This study for the first time investigated the effect of drought stress on the downstream gene *UBGAT* in *S.baicalensis* seedlings as well as the correlation between gene expression and flavonoid content in *S. baicalensis* seedlings under drought stress, providing a new sight for studying the effects of drought stress on flavonoid accumulation and related gene expression in *S. baicalensis*.

KEYWORDS

***Scutellaria baicalensis*, drought stress, gene expression, qRT-PCR, HPLC, flavonoids**

1. Introduction

Scutellaria baicalensis (Baikal skullcap), known locally as Huangqin, is a perennial herb native to East Asia (Vrabec et al., 2022). Its dried roots have been an important herb in traditional Chinese medicine for a long time (Wu et al., 2022; Zhou et al., 2022). It has significant therapeutic effects on a wide range of illnesses, including various cancers, inflammation, diabetic nephropathy, oxidative stress (Men et al., 2021; Zhou et al., 2021). Baicalein, wogonin, baicalin, and wogonoside are called as root-specific flavones of *S. baicalensis* (Zhao et al., 2018). There is a lack of 4′-hydroxy (4′-deoxyflavone) in ring B, which is mainly responsible for the pharmacological activities of *S. baicalensis* (Zhao et al., 2016). Baicalein has been shown to suppress lipopolysaccharide-induced acute lung injury, ameliorate osteoporosis, and exert an antitumor effect on cervical cancer (Cai et al., 2021; Luo et al., 2021; Jiang et al., 2022). It has been reported that wogonin inhibits cardiac hypertrophy and alleviates kidney tubular epithelial injury (Lei et al., 2021; Shi et al., 2021). Baicalin has been proven to have remarkable effects on various cancer treatments and cardiovascular, hepatic, and renal protection (Singh et al., 2021; Yang et al., 2021; Zhao et al., 2021). Wogonoside can also treat cancer and inflammation (Gu et al., 2021; Huang et al., 2021). Thus, the accumulation of root-specific flavones is an essential aspect of studying *S. baicalensis*.

Flavonoid synthesis and accumulation depend on the crucial enzymes in their synthesis pathway (Zhao et al., 2018; Wang S. et al., 2019). Studying crucial enzyme genes of the biosynthetic pathway can provide a theoretical basis for the molecular mechanism of active flavonoid accumulation. Flavonoids are usually synthesized through the phenylpropanoid pathway (Ahmed et al., 2021). Their biosynthetic routes are shown in Figure 1. Phenylalanine ammonia-lyase (PAL) catalyzes the first and rate-limiting step of the phenylpropanoid pathway, which provides precursors for a diversity of secondary metabolites, including flavonoids (Liu et al., 2006). It converts primary metabolism into secondary metabolism (Olsen et al., 2008). Chalcone synthase (CHS) is a crucial enzyme that catalyzes the first rate-limiting step of the flavonoid biosynthesis pathway (Wang et al., 2018). UDP-glucuronate (baicalein 7-O-glucuronosyltransferase, UBGAT) is responsible for catalyzing the formation of flavonoid glycosides. Nagashima analyzed the properties of UBGAT purified from cultured cells of *S. baicalensis* and catalyzed the reaction with various glycosides. The outcomes demonstrated that it only reacted with UDP-glucuronide, baicalein, and wogonin as substrates (Nagashima et al., 2000). Studies show that the flavonoid content of the planted *S. baicalensis* is lower than that of wild resources (Li et al., 2018; Tian et al., 2018). Therefore, exploring the method to improve the flavonoid content of cultivated medicinal materials is conducive to protecting the wild medicinal resources and preventing the wild resources from being excessively excavated. It has been proven crucial gene expression correlates with flavonoid accumulation (Ma et al., 2014). Accordingly, it is of practical significance for protecting medicinal plant resources and improving the quality of herbs to explore active compound accumulation and crucial enzyme gene expression.

Abiotic factors are fundamental components of the environment that determine plant distribution and productivity (Zhang H. et al., 2022). In nature, plants are constantly challenged by adverse abiotic environmental conditions such as drought, heat, and excess salt levels

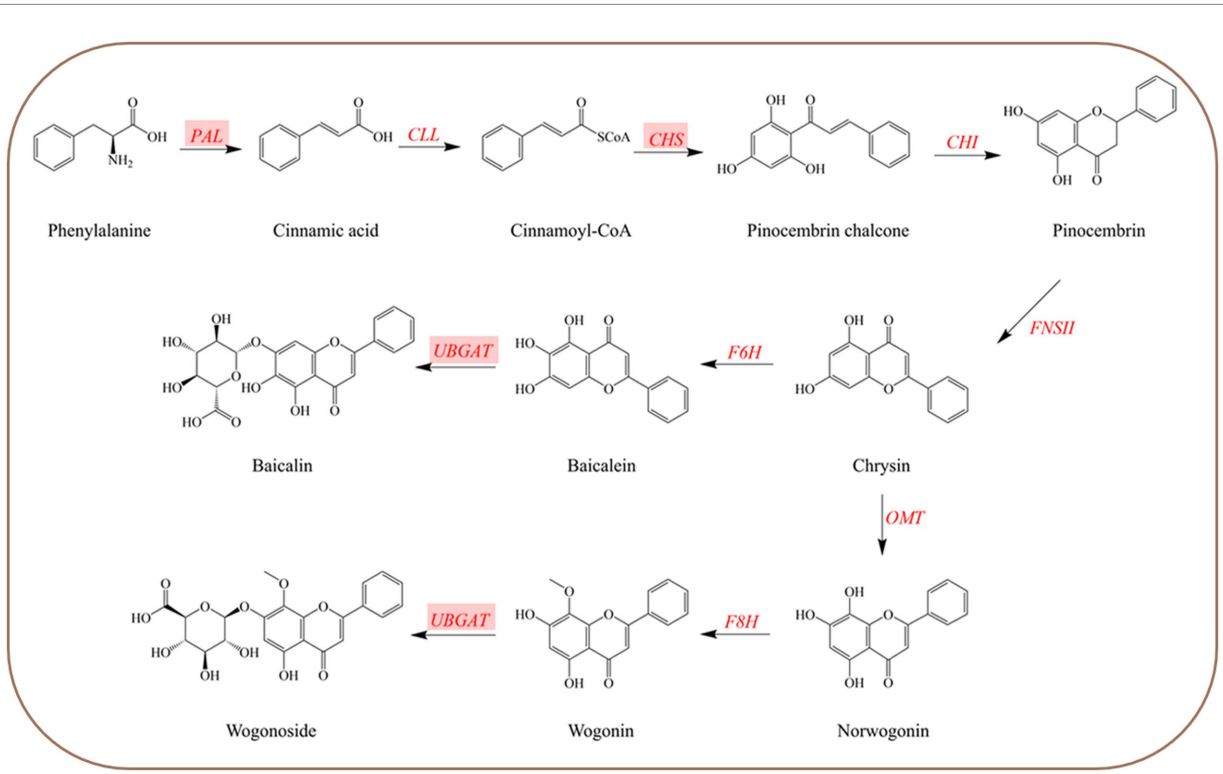

FIGURE 1
Biosynthetic pathways of four root-specific flavones (baicalin, baicalein, wogonin, and wogonoside) in *Scutellaria baicalensis*. Highlighted genes are the studied genes in this paper.

in the soil, which negatively affect crop productivity (Xie et al., 2021; Mahecha et al., 2022; Paparella et al., 2022). The gene expression and bioactive component accumulation are affected by environmental stress (Xu et al., 2020; Jiang et al., 2021; Xu et al., 2021). Accumulating evidence has proven that appropriate drought stress has the potential to promote the production of bioactive metabolites like flavonoids (Jia et al., 2018; Jia and Wang, 2019; Yang et al., 2020; Zhang et al., 2020). Thus, comprehending how plants respond to abiotic stresses and adverse environmental conditions is critical for protecting the ecology and evolution of living systems.

Polyethylene glycol (PEG) is composed of a large molecular size and is nontoxic (Chen et al., 2020). It can reduce the water potential of the surrounding environment of the cells, causing and cause drought (Wang et al., 2020). PEG6000 is often used to simulate drought stress treatments (Jian et al., 2022; Tang et al., 2022). Thus, this study proposed the hypothesis that appropriate drought treatment can promote the accumulation of flavonoids and gene expression in *S. baicalensis* seedlings. PEG6000 was used to treat seedlings to simulate drought stress. The accumulation of four bioactive root-specific flavones in roots during drought stress was determined by high performance liquid chromatography (HPLC). Simultaneously, the expression of four crucial genes related to flavonoid synthesis in the roots, stems, and leaves of *S. baicalensis* was determined by real-time quantitative PCR (qRT-PCR). And the effect of drought on the expression of related genes was comprehensively analyzed. This study would provide meaningful information on the accumulation of compounds in *S. baicalensis* and insights into the study of quality improvement under stressed conditions.

2. Materials and methods

2.1. Plant material and chemicals

The seeds of *S. baicalensis* were collected from Inner Mongolia, China. Healthy seeds were selected for the pot experiment. They were sown in a 16.8 cm × 15.5 cm (height × upper diameter) pot and cultured in an artificial illumination incubator (25°C, 16 h of light, and 8 h of dark light).

Compounds wogonoside (CAS: 51059–44-0), baicalin (CAS: 21967–41-9), wogonin (CAS: 632–85-9), and baicalein (CAS: 491–67-8) were procured from Yuanye (Shanghai, China) and had purity >98%. Acetonitrile (CAS: 75–05-8, HPLC) and formic acid (CAS:6449-79-2, LC/MS) were acquired from Fischer Scientific (Hampton, NJ, United States). The remaining reagents were bought locally and were of analytical grade.

2.2. Drought stress treatment

Four-week-old healthy seedlings were selected to be subjected to the follow-up treatment. There were six groups in each of the three replicates (three pots per replicate, 30 seedlings per pot). The six experimental groups were treated with 0, 5, 10, 15, 20, and 25% PEG 6000 under drought stress (Meher and Shivakrishna, 2018; Wang Z.Y. et al., 2019; Batool et al., 2022). The drought stress experiment lasted 5 days, and the solution was poured every other day for three times. Immediately after the experiment, the seedlings were frozen in liquid nitrogen and stored at −80°C.

2.3. Content determination

Thirty seedlings of similar growth were selected per replicate for each treatment for content determination. Dried the roots of *S. baicalensis* at 55–60°C and rushed them (Zhang L.W. et al., 2022). The powder was precisely weighed to approximately 0.1 g and placed in a triangular flask. Then, flavonoids from *S. baicalensis* were extracted by the extraction method optimized by our research group. 1 mL of 50% ethanol was added. The sample was accurately weighed and extracted with an ultrasonic step for 23 min. The sample was then filtered through a 0.22 μm filter.

The content of flavonoids in *S. baicalensis* was determined by HPLC established by our research group. The mobile phase was acetonitrile (A) −0.1% formic acid aqueous solution (B). The gradient elution was used under the following conditions: 0.01–4 min, 10–20% A; 4–12 min, 20–22% A; 12–22 min, 22–24% A; 22–49 min, 24–28% A; 49–52 min, 28–35% A; 52–60 min, 35–45% A; 60–64 min, 45% ~ A; 64–70 min, 55–10% A; 70–85 min, 10% A. The volume flow rate was 0.8 mL/min. The detection wavelength was 274 nm. The injection volume was 10 μL. The column temperature was 30°C.

2.4. Total RNA extraction, cDNA synthesis, and qRT-PCR

Total RNA was extracted from the roots, stems, and leaves of *S. baicalensis* according to TRNzol Universal Total RNA Extraction Reagent Operation Guide (Tiangen, Beijing, China). RNase-free water was used to dissolve the purified RNA. Using the extracted RNA as a template, cDNA was obtained by reverse transcription based on the instructions of the Evo M-MLV Mix Kit with gDNA Clean for qPCR kit (AGBio, Hunan, China) and carried out qRT-PCR following the instructions of the ChamQ Universal SYBR qPCR Master Mix (Vazyme, Nanjing, China) using an SYBR Green-based PCR assay. The information on primers used in this research is shown in Table 1. The expression levels of *PAL1*, *PAL2*, *CHS*, and *UBGAT* were determined using CT values and calculated using the $2^{-\triangle\triangle Ct}$ method (Liu et al., 2019). Each qRT-PCR reaction technique was three replicates. Each experiment has three biological repetitions.

2.5. Statistical analysis

The HPLC results were monitored and analyzed through Lab Solutions 5.92 (Shimadzu Scientific Instruments INC.). GraphPad Prism 8.3.0 (GraphPad Software INC.) and Adobe Illustrator 2020 (Adobe INC.) were applied to mapping analyses. OriginPro 2021 (OriginLab Corporation.) and IBM SPSS® Statistics 25 (International Business Machines Corporation) were used in this research work for data evaluation. All the biological samples were three replicates.

3. Results

3.1. Accumulation of root-specific flavones in roots *Scutellaria baicalensis* under drought stress

The significance of the Levene variance homogeneity test was greater than the significance level of 0.05 (Table 2), so it can

TABLE 1 The information on primers used in this research.

	Forward primer	Reverse primer	Accession number
Actin	TTGATCTTGCTGGTCGTGATCTCA	TGTTTCTAGCTCTTGCTCGTAGTCG	HQ847728
CHS	GAGCTAGGGTTCTCGTCGTC	AAGAGGGAGTTCCAGTCGG	AB008748
PAL1	GGCAAACCCTGTGACGAA	GCCTGGCATAGAGCGACTA	OP018668
PAL2	TCTACGGCACTTGGAGGAG	CATCAACGGATAGTTCACGCT	OP018669
UBGAT	CCCGACATCACGGACAA	AAATGAGGGGCAAACCAG	OP018670

TABLE 2 Results of statistical analysis of four root-specific flavones content.

Flavonoids	Variance homogeneity test results of mean		Results of one-way ANOVA between groups			
	Levene statistic	Sig.	Sum of squares	Mean square	*F*	Sig.
Baicalein	2.829	0.065	206.223	41.245	7889.677	0.000
Wogonin	2.069	0.140	56.172	11.234	2116.112	0.000
Baicalin	2.572	0.084	415.735	83.147	1530.721	0.000
Wogonoside	2.311	0.109	20.578	4.116	14569.957	0.000

be considered that the variance between sample data is homogeneous. The result indicated that one-way ANOVA could be used. The significance of the *F* value for all four compounds was 0.000, which was lower than the significance level of 0.05 (Table 2). It demonstrated that drought stress significantly affected the accumulation of four flavonoids.

In the LSD test, the mean difference results of each group showed that different PEG6000 concentrations treatments could lead to significant differences in flavonoid content. There was no significant difference in baicalein between 15 and 25% PEG6000 groups, but there were significant differences among other groups. For baicalin, there was no significant difference between 15, 20, and 25% PEG6000, but there were significant differences between other groups. As to wogonin and wogonoside, different treatments resulted in significant differences among all groups.

The contents of baicalein, wogonin, baicalin, and wogonoside were shown in Figure 2. The concentrations of baicalein under drought stress of 10% PEG6000 and 15% PEG6000 were 8.124 and 7.502 mg/g, respectively, which increased by 20.44 and 11.22% compared with the control group (0% PEG6000). Compared with 0% PEG6000, baicalin in the treated group of 10% PEG6000 and 15% PEG6000 was 68.72 and 35.86% higher. Correspondingly, the content of wogonoside increased by 82.75 and 56.59%, respectively, under the two treatments. Compared with the control group, the 5% PEG6000 group increased the content of wogonin by 45.81%.

3.2. Expression of crucial genes in roots, stems, and leaves of *Scutellaria baicalensis* under drought stress

Under drought stress, the RNA of the samples was extracted and the RNA quality is shown in Supplementary Figure S1 and Supplementary Table S1. Then the expression of four crucial enzyme genes was detected in different organs of *S. baicalensis* (Figure 3). The effects of different organs of *S. baicalensis* and the concentration of PEG6000 on gene expression were analyzed by multivariate analysis of variance (Table 3). Results of tests of between-subjects effects revealed that the effects of different concentrations of PEG6000 on *CHS, PAL1, PAL2,* and *UBGAT* were significant, and the expression levels of *CHS*, *PAL1*, and *PAL2* were significantly different in various organs of *S. baicalensis*.

The LSD results suggested that the relative expression of *CHS* was significantly different from other treatments when treated with 10% PEG6000. Compared with other treatment groups (except 10%), the relative expression of *PAL1* in the 5% PEG6000 treatment group was significantly different. Between the 5% PEG6000 treatment group and the other treatment concentration groups, the relative expression of *UBGAT* was considerably different. In the case of *PAL2*, the 10% PEG6000 treatment group was significantly different from the control group, as were the 15% PEG6000 and 25% PEG6000 treatment groups. In addition, the gene expression levels of genes in roots treated with different concentrations of PEG6000 were compared to explore the best treatment of four genes that affect the production of root-specific flavones. For *PAL1* and *UBGAT*, gene expression was highest when 5% treatment was used.

Meanwhile, the highest expression of *PAL1* and *UBGAT* genes was observed in the 5% treatment, and the highest expression of *PAL2* and *CHS* genes was observed in the 10% treatment, suggesting that low concentration (5 and 10%) of PEG6000 treatment was preferable for the expression of the four crucial enzyme genes. To further explore the gene function, these two concentrations of PEG6000 can be selected to treat samples to increase gene expression.

3.3. Correlation analysis

Pearson correlation method was used to analyze the association between gene expression and flavonoid accumulation by OriginPro 2021 (Figure 4). The findings demonstrated that the amounts of the four flavonoid components were highly positively connected, which indicated that the accumulation patterns of the four flavonoid components were similar under the treatment of PEG6000.

The expression of the *CHS* in roots was positively correlated with the content of baicalein, which indicated that the *CHS* could promote

10.3389/fevo.2023.1113823

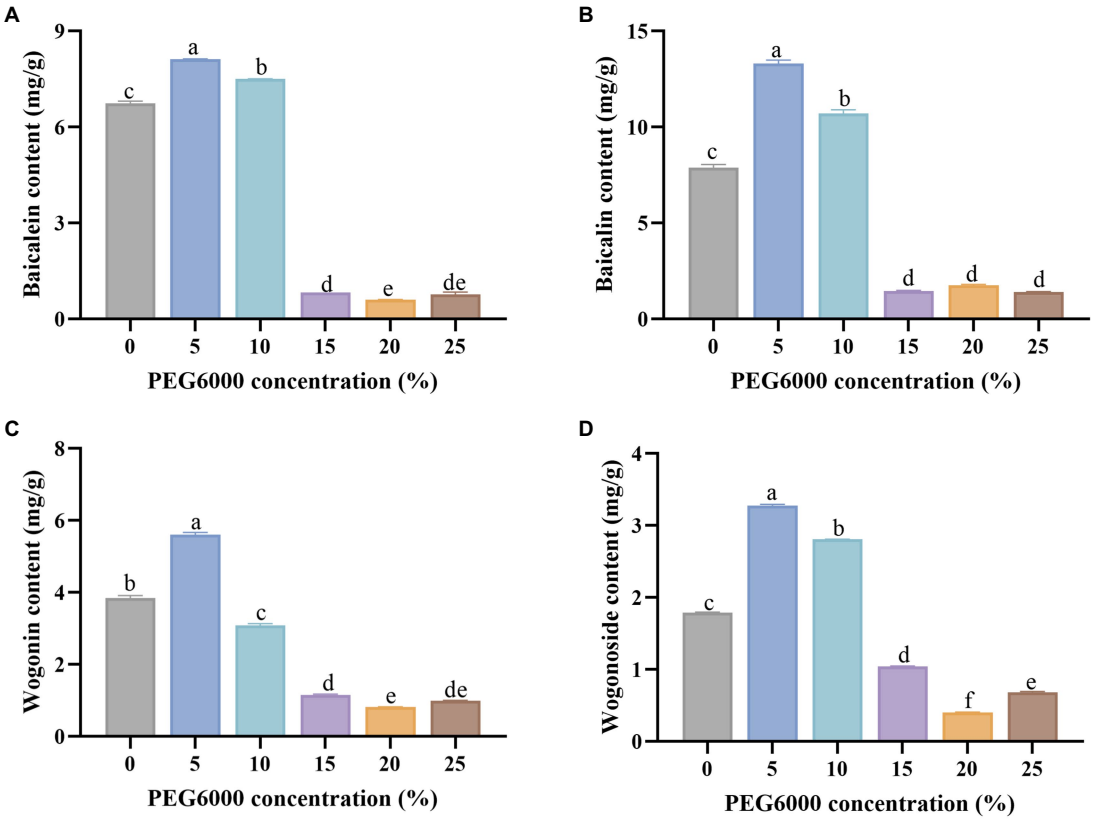

FIGURE 2
The contents of baicalein **(A)**, baicalin **(B)**, wogonin **(C)**, and wogonoside **(D)** under different concentrations of PEG6000 solution treatment. Different letters indicate significant differences by t-test between different treatment (p<0.05).

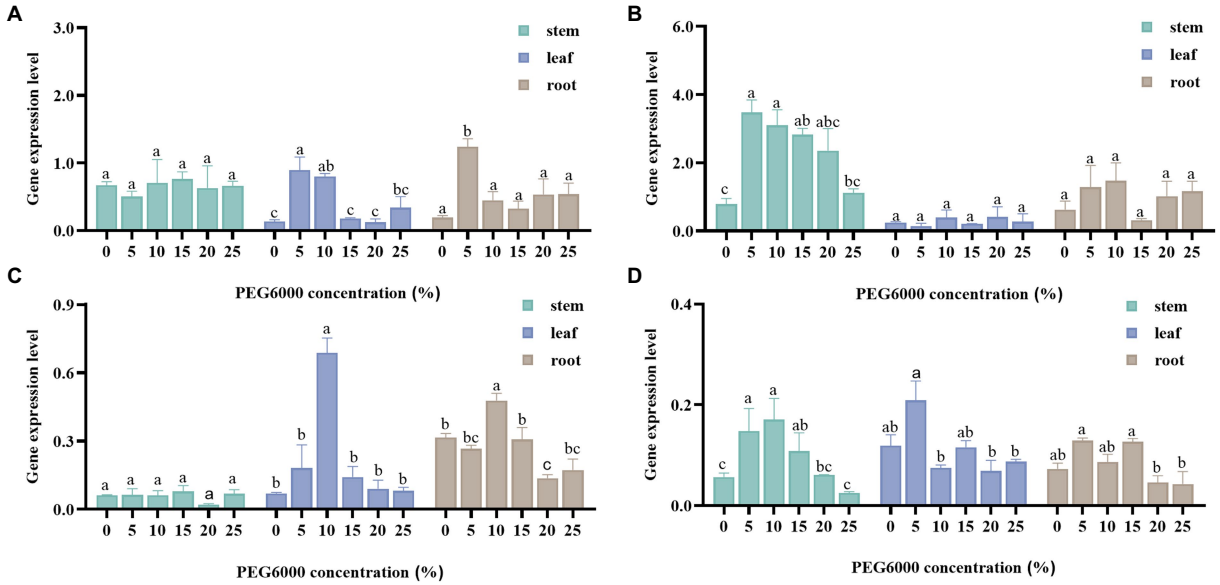

FIGURE 3
The results of the expression levels of *PAL1* **(A)**, *PAL2* **(B)**, *CHS* **(C)**, and *UBGAT* **(D)** in stems, leaves, and roots under drought stress. Different letters indicate significant differences by t-test between different treatment (p<0.05).

the accumulation of baicalein. The expression of *CHS* and *PAL1* in roots was positively correlated with baicalin content, which indicated that these genes played a critical role in regulating the accumulation of baicalin content. Correlation analysis showed that *PAL1* and *UBGAT* in roots were also essential regulators of wogonin accumulation. Moreover, *PAL1*, *CHS*, and *UBGAT* in roots had

TABLE 3 Significance results for tests of between-subjects effects.

	PEG6000				Organs			
	CHS	*PAL1*	*PAL2*	*UBGAT*	*CHS*	*PAL1*	*PAL2*	*UBGAT*
sig	0	0.002	0.005	0	0	0.038	0	0.1

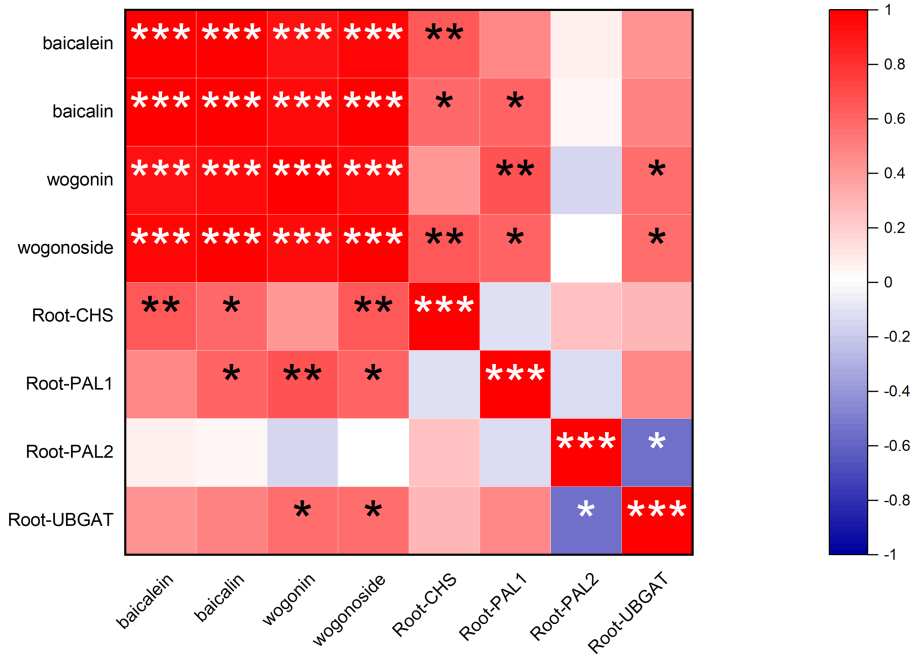

FIGURE 4
The results of correlation analysis between the indicators in this study. The correlation type is Pearson. *p<0.05, **p<0.01, and ***p<0.001.

significant effects on the accumulation of wogonoside. The most crucial enzyme gene expression positively impacted the amount of flavonoid. Only *PAL2* and wogonin have a negative correlation. It was speculated that *PAL2* might inhibit the accumulation of wogonin.

4. Discussion

Plants respond physiologically to environmental changes to maintain their individual or reproductive fitness. Flavonoid is a very significant class of secondary metabolites. Their synthesis and accumulation are related to the growing environment of plants, and they are involved in the process of plant resistance (Rodriguez-Calzada et al., 2019). They are essential protective substances for plants against the adverse external environment. Secondary metabolism is crucial for coping with environmental changes and maintaining plant homeostasis. Compared with primary metabolism, it is more susceptible to environmental changes (Yang et al., 2020). Previous studies have confirmed drought stress influenced flavonoid accumulation in *S. baicalensis*. The effects of PEG6000 stress on the accumulation of baicalin and baicalein in the suspension system of *S. baicalensis* were studied (Yang et al., 2011). Cheng et al., showed the accumulation of baicalin in the root of *S. baicalensis* under drought stress through controlled irrigation (Cheng et al., 2018). However, these studies only focused on the content of baicalin and baicalein. Wang et al., studied the PEG effect on the contents of baicalin, wogonoside, baicalein, and wogonin, while the object was suspension cells (Wang et al., 2020). Therefore, the response of four root-specific flavones in seedlings to drought stress was studied in this study. The results showed that proper drought stress could promote the accumulation of flavonoids in *S. baicalensis*. However, when the concentration of PEG6000 was increased, the content of flavonoids in *S. baicalensis* decreased significantly (Figure 2). This could be due to extreme drought reducing the plant's metabolic capacity. The best concentration for accumulating root-specific flavones out of all those tested was 5%.

Many interconnected metabolic branches constitute the biosynthesis pathway of plant flavonoids, which involves multiple enzyme genes whose expression is highly dependent on tissue type and responses to internal or external signals (Sun et al., 2022). The synthesis and accumulation of flavonoids depend on crucial enzymes in its synthesis pathway (Ahmad et al., 2019). These enzymes are usually located at the bifurcation of the metabolic branch in the plant secondary metabolites synthesis pathway and can further determine the metabolic flow direction (Zhao et al., 2018; Wang S. et al., 2019). In this study, PEG6000 was used to treat *S. baicalensis* seedlings to explore how drought stress affected the related gene expression. The data showed that crucial enzyme genes in the flavonoid biosynthesis pathway responded to abiotic stress differently. The effects of progressive drought stress on the expression patterns of key enzymes

upstream of baicalin biosynthesis were investigated during the vegetative period in 2-year-old *S. baicalensis*. And it was found that appropriate drought treatment resulted in increased gene expression, and over-treatment caused decreased expression (Cheng et al., 2018). This result is similar to our results, but it does not study the downstream key enzyme genes. Yang et al., studied the effects of PEG6000 stress on the expression of *PAL*, *CHS,* and *UBGAT* genes in the *S. baicalensis* suspension system. It was found that 10% PEG treatment of suspension cells significantly increased the expression of *PAL* and 20% PEG treatment significantly increased the expression of *UBGAT*, while there was no significant change in the expression of *CHS*, which was different from our results (Yang et al., 2011). In this paper, seedlings of *S. baicalensis* were used for the study. The newly discovered genes *PAL1*, *PAL2*, and *UBGAT* of *S. baicalensis* were reported. And the effect of drought stress on the downstream gene *UBGAT* in *S.baicalensis* seedlings was studied for the first time. The highest expression levels of four genes in roots were found at 5 and 10%, respectively, which indicated that these concentrations were more favorable for gene expression (Figure 3). These findings shed light on variations in the secondary metabolism of medicinal plants.

The biosynthesis of plant secondary metabolites is regulated by the spatial and temporal expression of biosynthesis genes (Lan et al., 2016). LSD results revealed significant differences in the relative expression levels of the *PAL2* and *CHS* genes among organs. Expression results displayed that the expression level of *PAL2* showed the highest gene expression level in stems, followed by the root and, finally, the leaf (Figures 3B,C). It may be because *PAL* is closely related not only to flavonoid synthesis but also to lignin formation. And the lignification of stems and roots was higher than that of leaves (Li et al., 2019). The expression of *CHS* in roots was the highest (Figure 3C). Generally, flavonoid biosynthesis genes were more strongly expressed in roots with higher flavonoid concentrations. As the medicinal organs, the taproots of *Polygonum minus* had a higher expression level of *CHS* (Roslan et al., 2012). The only organs in purple-fleshed sweet potato for anthocyanin biosynthesis are the purple tuberous roots, where *CHS* expression levels are significantly higher than in any other organ (Mano et al., 2007). However, the relative expression of the *UBGAT* gene differed significantly only between leaf and root, and the relative expression of the *PAL1* gene only differed significantly between stem and leaf (Figures 3A,D). It means that the expression of these two genes was not organ-specific. PAL is the first rate-limiting enzyme in the metabolism of phenylpropanes. CHS is the first rate-limiting enzyme in flavonoid synthesis. Both catalyze the rate-limiting step and affect the speed and direction of the metabolic pathway. And UBGAT is responsible for synthesizing aglycone into glycoside. Therefore, this study selected these four genes as representatives to study the effects of drought stress. Moreover, there are other key enzymes (e.g. CLL, CHI, F8H, OMT, and FNSII) in the flavonoid biosynthesis pathway (Lu et al., 2022). Among them, *CHI* and *OMT* have been proven to be able to respond to drought stress in other species (Castellarin et al., 2007; Gharibi et al., 2019). Subsequent experiments may be able to carry out more extensive research on the genes related to flavonoid biosynthesis in *S. baicalensis*.

There is some previous information on the effect of drought on the flavonoids or genes of *S. baicalensis*. However, up to now, there is no study on the correlation between the four root-specific flavones and crucial gene expression in *S. baicalensis* seedlings under drought stress. Therefore, we studied the correlation for the first time and found that there was a positive correlation between gene expression and flavonoid content, except for the negative correlation between *PAL2* and wogonin. And the correlation between the expression of *CHS*, *PAL1*, and *UBGAT* and flavonoid content was more significant (Figure 4). Therefore, it is suggested that *CHS*, *PAL1*, and *UBGAT* made a greater contribution to the drought-promoted flavonoid biosynthesis in *S. baicalensis* seedlings. These results showed that the increase in flavonoid content is related to the expression of the enzymes. Proving the relationship between flavonoids and gene expression may provide a theoretical basis for the gene function research. Given that 5% is the most suitable concentration for flavonoid accumulation and gene expression, subsequent experiments can use this as the optimal concentration to treat samples, and in-depth screen and verify gene function by multiple methods including comparing transcriptome and genetic engineering.

Altogether, this study found that drought stress had a significant effect on the accumulation of four flavonoids as well as the expression of four related genes in the medicinal and edible plant *S. baicalensis*. These findings deepen the understanding of the drought stress regulating function in *S. baicalensis,* which regulates the accumulation of flavonoids and gene expression. Overall, this research establishes a theoretical foundation for further exploration into the molecular mechanism of *S. baicalensis* in response to abiotic stresses, and it provides new insights into the metabolic regulation mechanism of *S. baicalensis* flavonoids.

Data availability statement

The datasets presented in this study can be found in online repositories. The names of the repository/repositories and accession number(s) can be found at: https://www.ncbi.nlm.nih.gov/genbank/, HQ847728, AB008748, OP018668, OP018669, and OP018670.

Author contributions

PL contributed to the methodology and writing of the original draft. DJ and CL contributed to the project administration, supervision, and draft review. GR, FW, and JC were responsible for resource collection. All authors contributed to the article and approved the submitted version.

Funding

This work was supported by the project National Natural Science Foundation of China (81903740).

Acknowledgments

This work gratefully acknowledges the financial support provided by the project National Natural Science Foundation of China (81903740).

Conflict of interest

The authors declare that the research was conducted in the absence of any commercial or financial relationships that could be construed as a potential conflict of interest.

Publisher's note

All claims expressed in this article are solely those of the authors and do not necessarily represent those of their affiliated organizations, or those of the publisher, the editors and the reviewers. Any product that may be evaluated in this article, or claim that may be made by its manufacturer, is not guaranteed or endorsed by the publisher.

Supplementary material

The Supplementary material for this article can be found online at: https://www.frontiersin.org/articles/10.3389/fevo.2023.1113823/full#supplementary-material

References

Ahmad, N., Liu, J. Y., Tian, X., Noman, M., Jameel, A., Yao, N., et al. (2019). Overexpression of a novel cytochrome P450 promotes flavonoid biosynthesis and osmotic stress tolerance in transgenic Arabidopsis. *Gene* 10:756. doi: 10.3390/genes10100756

Ahmed, U., Rao, M. J., Qi, C., Xie, Q., Noushahi, H. A., Yaseen, M., et al. (2021). Expression profiling of flavonoid biosynthesis genes and secondary metabolites accumulation in Populus under drought stress. *Molecules* 26:5546. doi: 10.3390/molecules26185546

Batool, M., El-Badri, A. M., Wang, Z. K., Mohamed, I. A. A., Yang, H. Y., Ai, X. Y., et al. (2022). Rapeseed Morpho-physio-biochemical responses to drought stress induced by PEG-6000. *Agronomy* 12:579. doi: 10.3390/agronomy12030579

Cai, P., Lu, Y., Yin, Z. F., Wang, X. H., Zhou, X. X., and Li, Z. K. (2021). Baicalein ameliorates osteoporosis via AKT/FOXO1 signaling. *Aging* 13, 17370–17379. doi: 10.18632/aging.203227

Castellarin, S. D., Pfeiffer, A., Sivilotti, P., Degan, M., Peterlunger, E., and Di Gaspero, G. (2007). Transcriptional regulation of anthocyanin biosynthesis in ripening fruits of grapevine under seasonal water deficit. *Plant Cell Environ.* 30, 1381–1399. doi: 10.1111/j.1365-3040.2007.01716.x

Chen, Z. K., Xu, W. W., Nie, J., Khan, A., Cao, C. G., and Li, P. (2020). Drought stress intensity, duration and its resistance impact on rice (ORYZA sativa l.) seedling. *Appl. Ecol. Environ. Res.* 18, 469–486. doi: 10.15666/aeer/1801_469486

Cheng, L., Han, M., Yang, L. M., Yang, L., Sun, Z., and Zhang, T. (2018). Changes in the physiological characteristics and baicalin biosynthesis metabolism of Scutellaria baicalensis Georgi under drought stress. *Ind. Crop. Prod.* 122, 473–482. doi: 10.1016/j.indcrop.2018.06.030

Gharibi, S., Tabatabaei, B. E. S., Saeidi, G., Talebi, M., and Matkowski, A. (2019). The effect of drought stress on polyphenolic compounds and expression of flavonoid biosynthesis related genes in Achillea pachycephala Rech.F. *Phytochemistry* 162, 90–98. doi: 10.1016/j.phytochem.2019.03.004

Gu, Q., Zhu, C. H., Wu, X., Peng, L. H., Huang, G. Y., and Hu, R. (2021). Wogonoside promotes apoptosis and ER stress in human gastric cancer cells by regulating the IRE1 alpha pathway. *Exp. Ther. Med.* 21:10. doi: 10.3892/etm.2021.9842

Huang, H., Li, X., Li, Y., Liu, L., Zhu, H. W., Cao, W., et al. (2021). Wogonoside inhibits TNF receptor-associated factor 6 (TRAF6) mediated-tumor microenvironment and prognosis of pancreatic cancer. *Ann. Transl. Med.* 9:15. doi: 10.21037/atm-21-4164

Jia, X., Sun, C. S., and Li, G. Y. (2018). Effect of drought stress on the growth and physiological characteristics and the accumulation of Astragaloside IV secondary metabolites of Astragalus membranaceus(Fisch.)var.mongholicus(Bge.)Hsiao. *Acta Botan. Boreali-Occiden. Sin.* 38, 501–509. doi: 10.7606/j.issn.1000-4025.2018.03.0501

Jia, X., and Wang, X. Q. (2019). Effects of salt and drought cross stress on growth and development and accumulation of Total flavonoids in Astragalus membranaceus var. mongholicus seedlings. *J. Chin. Med. Mater.* 42, 1215–1221. doi: 10.13863/j.issn1001-4454.2019.06.002

Jian, H. J., Sun, H. N., Liu, R. R., Zhang, W. Z., Shang, L. N., Wang, J. C., et al. (2022). Construction of drought stress regulation networks in potato based on SMRT and RNA sequencing data. *BMC Plant Biol.* 22:17. doi: 10.1186/s12870-022-03758-8

Jiang, D., Li, P., Yin, Y., Ren, G. X., and Liu, C. S. (2021). Molecular cloning and functional characterization of UGTs from Glycyrrhiza uralensis flavonoid pathway. *Int. J. Biol. Macromol.* 192, 1108–1116. doi: 10.1016/j.ijbiomac.2021.09.136

Jiang, C., Zhang, J. C., Xie, H. W., Guan, H. T., Li, R., Chen, C. X., et al. (2022). Baicalein suppresses lipopolysaccharide-induced acute lung injury by regulating Drp1-dependent mitochondrial fission of macrophages. *Biomed. Pharmacother.* 145:14. doi: 10.1016/j.biopha.2021.112408

Lan, X., Quan, H., Xia, X., Yin, W., and Zheng, W. (2016). Molecular cloning and transgenic characterization of the genes encoding chalcone synthase and chalcone isomerase from the Tibetan herbal plant Mirabilis himalaica. *Biotechnol. Appl. Biochem.* 63, 419–426. doi: 10.1002/bab.1376

Lei, L., Zhao, J., Liu, X. Q., Chen, J., Qi, X. M., Xia, L. L., et al. (2021). Wogonin alleviates kidney tubular epithelial injury in diabetic nephropathy by inhibiting PI3K/Akt/NF-kappa B signaling pathways. *Drug Design Dev. Therap.* 15, 3131–3150. doi: 10.2147/DDDT.S310882

Li, E., Liu, Y., Liu, Y., Jiang, S., and Wang, Y. (2018). Simultaneous determination of six components in Scutellaria baicalensisGeorgi from different districts by HPLC. *Chin. J. Hosp. Pharm.* 38, 946–948. doi: 10.13286/j.cnki.chinhosppharmacyj.2018.09.10

Li, G., Wang, H., Cheng, X., Su, X., Zhao, Y., Jiang, T., et al. (2019). Comparative genomic analysis of the PAL genes in five Rosaceae species and functional identification of Chinese white pear. *PeerJ* 7:e8064. doi: 10.7717/peerj.8064

Liu, F. R., Xie, L. F., Yao, Z. Y., Zhou, Y. L., Zhou, W. F., Wang, J. H., et al. (2019). Caragana korshinskii phenylalanine ammonialyase is up-regulated in the phenylpropanoid biosynthesis pathway in response to drought stress. *Biotechnol. Biotechnol. Equip.* 33, 842–854. doi: 10.1080/13102818.2019.1623718

Liu, R. R., Xu, S. H., Li, J. L., Hu, Y. L., and Lin, Z. P. (2006). Expression profile of a PAL gene from Astragalus membranaceus var. Mongholicus and its crucial role in flux into flavonoid biosynthesis. *Plant Cell Rep.* 25, 705–710. doi: 10.1007/s00299-005-0072-7

Lu, Y. M., Cao, B., Su, Y. Y., Yang, J. J., Xue, Y., Zhang, M., et al. (2022). Inter-specific differences of medicinal bioactive products are correlated with differential expressions of key enzyme genes in Scutellaria baicalensis and Scutellaria viscidula. *Ind. Crop. Prod.* 189:13. doi: 10.1016/j.indcrop.2022.115758

Luo, Y. H., Wang, M. Y., Zhang, L., Jia, W. N., Wengu, E. Z., Xia, J. Y., et al. (2021). Baicalein exerts antitumor effect in cervical cancer. *Mater. Express* 11, 1347–1353. doi: 10.1166/mex.2021.2042

Ma, D. Y., Sun, D. X., Wang, C. Y., Li, Y. G., and Guo, T. C. (2014). Expression of flavonoid biosynthesis genes and accumulation of flavonoid in wheat leaves in response to drought stress. *Plant Physiol. Biochem.* 80, 60–66. doi: 10.1016/j.plaphy.2014.03.024

Mahecha, M. D., Bastos, A., Bohn, F. J., Eisenhauer, N., Feilhauer, H., Hartmann, H., et al. (2022). Biodiversity loss and climate extremes — study the feedbacks. *Nature* 612, 30–32. doi: 10.1038/d41586-022-04152-y

Mano, H., Ogasawara, F., Sato, K., Higo, H., and Minobe, Y. (2007). Isolation of a regulatory gene of anthocyanin biosynthesis in tuberous roots of purple-fleshed sweet potato. *Plant Physiol.* 143, 1252–1268. doi: 10.1104/pp.106.094425

Meher, P., and Shivakrishna, K. A. Reddy and D. M. Rao (2018). "Effect of PEG-6000 imposed drought stress on RNA content, relative water content (RWC), and chlorophyll content in peanut leaves and roots." *Saudi J. Biol. Sci.* 25, 285–289. doi: 10.1016/j.sjbs.2017.04.008

Men, L. H., Pi, Z. F., Hu, M. X., Liu, S., Liu, Z. Q., Song, F. R., et al. (2021). Serum metabolomics coupled with network pharmacology strategy to explore therapeutic effects of Scutellaria Baicalensis Georgi on diabetic nephropathy. *Chin. J. Anal. Chem.* 49:13.

Nagashima, S., Hirotani, M., and Yoshikawa, T. (2000). Purification and characterization of UDP-glucuronate: baicalein 7-O-glucuronosyltransferase from Scutellaria baicalensis Georgi. Cell suspension cultures. *Phytochemistry* 53, 533–538. doi: 10.1016/S0031-9422(99)00593-2

Olsen, K. M., Lea, U. S., Slimestad, R., Verheul, M., and Lillo, C. (2008). Differential expression of four Arabidopsis PAL genes; PAL1 and PAL2 have functional specialization in abiotic environmental-triggered flavonoid synthesis. *J. Plant Physiol.* 165, 1491–1499. doi: 10.1016/j.jplph.2007.11.005

Paparella, F., D'Agostino, D., and Burt, J. (2022). Long–term, basin–scale salinity impacts from desalination in the Arabian/Persian gulf. *Sci. Rep.* 12:20549. doi: 10.1038/s41598-022-25167-5

Rodriguez-Calzada, T., Qian, M. J., Strid, A., Neugart, S., Schreiner, M., Torres-Pacheco, I., et al. (2019). Effect of UV-B radiation on morphology, phenolic compound production, gene expression, and subsequent drought stress responses in chili pepper (capsicum annuurn L.). *Plant Physiol. Biochem.* 134, 94–102. doi: 10.1016/j.plaphy.2018.06.025

Roslan, N. D., Yusop, J. M., Baharum, S. N., Othman, R., Mohamed-Hussein, Z.-A., Ismail, I., et al. (2012). Flavonoid biosynthesis genes putatively identified in the aromatic

plant Polygonum minus via expressed sequences tag (EST) analysis. *Int. J. Mol. Sci.* 13, 2692–2706. doi: 10.3390/ijms13032692

Shi, X. W., Zhang, B., Chu, Z. L., Han, B. J., Zhang, X. P., Huang, P., et al. (2021). Wogonin inhibits cardiac hypertrophy by activating Nrf-2-mediated antioxidant responses. *Cardiovasc. Ther.* 2021:13. doi: 10.1155/2021/9995342

Singh, S., Meena, A., and Luqman, S. (2021). Baicalin mediated regulation of key signaling pathways in cancer. *Pharmacol. Res.* 164:21. doi: 10.1016/j.phrs.2020.105387

Sun, G., Liu Jianyu, W., Found, Z. Q., Xintong, M., Xinyue, Z., Yingqi, H., et al. (2022). Correlation analysis between expression of CYP450s gene in Carthamus tinctorius and total flavonoids content in young leaves under stress. *Chin. Tradit. Herb. Drug* 53, 222–230. doi: 10.7501/j.issn.0253-2670.2022.01.025

Tang, D. F., Quan, C. Q., Lin, Y., Wei, K. H., Qin, S. S., Liang, Y., et al. (2022). Physio-morphological, biochemical and transcriptomic analyses provide insights into drought stress responses in Mesona chinensis Benth. *Front. Plant Sci.* 13:20. doi: 10.3389/fpls.2022.809723

Tian, T., Han, R., and Liang, Z. (2018). Study on HPLC fingerprint of Scutellaria baicalensis Georgi from different habitats and different years. *J. Zhejiang Agri. Sci.* 59, 370–376. doi: 10.16178/j.issn.0528-9017.20180304

Vrabec, R., Vokurkova, D., Tumova, L., and Cheel, J. (2022). Ex-vivo immune-stimulating activity of *Scutellaria baicalensis* and its major flavonoids on human immune cells. *Rec. Nat. Products* 16, 188–193. doi: 10.25135/rnp.264.21.02.1976

Wang, Z. Y., Pan, X., Meng, Z. J., Gao, Y., Dang, X. H., and Wang, J. (2019). Response of Chamecytisus palmensis to drought stress induced by polyethylene glycol during germination. *J. Plant Nutr.* 42, 2814–2823. doi: 10.1080/01904167.2019.1659335

Wang, S., Wang, R. S., Liu, T., Lv, C. G., Liang, J. W., Kang, C. Z., et al. (2019). CYP76B74 catalyzes the 3 -hydroxylation of Geranylhydroquinone in Shikonin biosynthesis. *Plant Physiol.* 179, 402–414. doi: 10.1104/pp.18.01056

Wang, Z. B., Yu, Q. B., Shen, W. X., El Mohtar, C. A., Zhao, X. C., and Gmitter, F. G. (2018). Functional study of CHS gene family members in citrus revealed a novel CHS gene affecting the production of flavonoids. *BMC Plant Biol.* 18:13. doi: 10.1186/s12870-018-1418-y

Wang, B., Zhang, T. X., Du, H. W., Zhao, Q., and Meng, X. C. (2020). Effect of PEG on secondary metabolites in suspension cells of *Scutellaria baicalensis* georgi. *Acta Med. Mediterr.* 36, 2307–2312. doi: 10.19193/0393-6384_2020_4_359

Wu, Q., Zhao, W. L., Chen, G. L., Yao, A. R., Yang, C., Zhao, Y., et al. (2022). Mechanistic study of endothelium independent vasodilation effects of wogonin. *Indian J. Exp. Biol.* 60, 34–40. doi: 10.56042/ijeb.v60i01.58773

Xie, H. Y., Li, M. R., Chen, Y. J., Zhou, Q. P., Liu, W. H., Liang, G. L., et al. (2021). Important physiological changes due to drought stress on oat. *Front. Ecol. Evol.* 9:14. doi: 10.3389/fevo.2021.644726

Xu, Z. C., Wang, M., Ren, T. T., Li, K. Y., Li, Y. Q., Marowa, P., et al. (2021). Comparative transcriptome analysis reveals the molecular mechanism of salt tolerance in Apocynum venetum. *Plant Physiol. Biochem.* 167, 816–830. doi: 10.1016/j.plaphy.2021.08.043

Xu, Z., Zhou, J., Ren, T., Du, H., Liu, H., Li, Y., et al. (2020). Salt stress decreases seedling growth and development but increases quercetin and kaempferol content inApocynum venetum. *Plant Biol.* 22, 813–821. doi: 10.1111/plb.13128

Yang, J. Y., Li, M., Zhang, C. L., and Liu, D. (2021). Pharmacological properties of baicalin on liver diseases: a narrative review. *Pharmacol. Rep.* 73, 1230–1239. doi: 10.1007/s43440-021-00227-1

Yang, L. L., Yang, L., Yang, X., Zhang, T., Lan, Y. M., Zhao, Y., et al. (2020). Drought stress induces biosynthesis of flavonoids in leaves and saikosaponins in roots of Bupleurum chinense DC. *Phytochemistry* 177:112434. doi: 10.1016/j.phytochem.2020.112434

Yang, Z. C., Yuan, Y., Chen, M., Shuai, L. F., Xiao, Q., and Lin, S. F. (2011). Effects of PEG stress on flavonoids accumulation and related gene expression in suspension of Scutellaria baicalensis. *Zhongguo Zhong Yao Za Zhi* 36, 2157–2161. doi: 10.4268/cjcmm20111601

Zhang, Q. Q., Li, Y. G., Su, Y. L., and Chen, G. L. (2020). Accumulation of flavonoids in different organs of Astragalus membranaceus (Fisch.) Bge.Var.mongholicus (Bge.) Hsiao and Astragalus membranaceus (Fisch.) Bge seedlings under drought stress. Acta Botanica Boreali-Occidentalia Sinica. *Acta Botan. Boreali-Occiden. Sin.* 40, 1201–1208. doi: 10.7606/j.issn.1000-4025.2020.07.1201

Zhang, L. W., Zhang, X. M., Begum, N., Xia, P. G., Liu, J. L., and Liang, Z. S. (2022). Effects of different processing methods based on different drying conditions on the active ingredients of salvia miltiorrhiza Bunge. *Molecules* 27:4860. doi: 10.3390/molecules27154860

Zhang, H., Zhu, J., Gong, Z., and Zhu, J.-K. (2022). Abiotic stress responses in plants. *Nat. Rev. Genet.* 23, 104–119. doi: 10.1038/s41576-021-00413-0

Zhao, Q., Cui, M. Y., Levsh, O., Yang, D. F., Liu, J., Li, J., et al. (2018). Two CYP82D enzymes function as flavone hydroxylases in the biosynthesis of root-specific 4 '-Deoxyflavones in Scutellaria baicalensis. *Mol. Plant* 11, 135–148. doi: 10.1016/j.molp.2017.08.009

Zhao, Q., Zhang, Y., Wang, G., Hill, L., Weng, J. K., Chen, X. Y., et al. (2016). A specialized flavone biosynthetic pathway has evolved in the medicinal plant, Scutellaria baicalensis. *Sci. Adv.* 2:e1501780. doi: 10.1126/sciadv.1501780

Zhao, F. C., Zhao, Z. X., Han, Y. R., Li, S. J., Liu, C. L., and Jia, K. (2021). Baicalin suppresses lung cancer growth phenotypes via miR-340-5p/NET1 axis. *Bioengineered* 12, 1699–1707. doi: 10.1080/21655979.2021.1922052

Zhou, X., Fu, L., Wang, P. L., Yang, L., Zhu, X. S., and Li, C. G. (2021). Drug-herb interactions between Scutellaria baicalensis and pharmaceutical drugs: insights from experimental studies, mechanistic actions to clinical applications. *Biomed. Pharmacother.* 138:18. doi: 10.1016/j.biopha.2021.111445

Zhou, J. L., Luo, Y. S., Kang, X. C., Bian, F. Z., and Liu, D. B. (2022). The root extract of Scutellaria baicalensis Georgi promotes beta cell function and protects from apoptosis by inducing autophagy. *J. Ethnopharmacol.* 284:6. doi: 10.1016/j.jep.2021.114790

frontiers | Frontiers in Ecology and Evolution

TYPE Original Research
PUBLISHED 06 April 2023
DOI 10.3389/fevo.2023.1132396

OPEN ACCESS

EDITED BY
Guoqi Wen,
Laval University,
Canada

REVIEWED BY
Zi-jian Xie,
Chinese Research Academy of Environmental Sciences,
China
Serge Rambal,
UMR5175 Centre d'Ecologie Fonctionnelle et Evolutive (CEFE),
France

*CORRESPONDENCE
Ruonan Li
✉ rnli@rcees.ac.cn

SPECIALTY SECTION
This article was submitted to Population, Community, and Ecosystem Dynamics, a section of the journal Frontiers in Ecology and Evolution

RECEIVED 27 December 2022
ACCEPTED 13 March 2023
PUBLISHED 06 April 2023

CITATION
Liang M, Han T, Ma J, Li R, Yang Y, Qiu X, Sun H and Zheng H (2023) Response of temperate forest ecosystem services to rainfall: A case study in the forest nature reserves of northern China.
Front. Ecol. Evol. 11:1132396.
doi: 10.3389/fevo.2023.1132396

Response of temperate forest ecosystem services to rainfall: A case study in the forest nature reserves of northern China

Mei Liang[1,2], Tian Han[1,3], Jinfeng Ma[1,2], Ruonan Li[1,2]*, Yanzheng Yang[1,2], Xiao Qiu[4], Hailian Sun[5] and Hua Zheng[1,2]

[1]State Key Laboratory of Urban and Regional Ecology, Research Center for Eco-Environmental Sciences, Chinese Academy of Sciences, Beijing, China, [2]University of Chinese Academy of Sciences, Beijing, China, [3]School of Geosciences & Surveying Engineering, China University of Mining & Technology, Beijing, China, [4]Inner Mongolia Academy of Agricultural and Animal Husbandry Sciences, Hohhot, China, [5]Baotou Teachers' College, Baotou, China

In the context of global climate change, temperate forests in climate-sensitive areas are inevitably affected. To deepen the understanding of the impact on precipitation changes into the relationship between key ecosystem services (ESs), this study selected net primary productivity (NPP), soil conservation (SC) and water yield (WY) of temperate forest in northern China as objects, and the Spearman correlation test and redundancy analysis were applied to analyze the response of ESs relationship to precipitation gradient. The results show that precipitation is the meteorological factor with the greatest impact (contribution 21.2%, $p<0.01$) on ESs and their relationships in temperate forests. The 600-700 mm precipitation gradient is the key turning point in the change of ESs relationship of WY with NPP and SC. This indicates that attention should be paid to the spatial variation of the 600-700 mm precipitation region in the future warm-wet in northern China, which should be used as a dividing line of forest management and policy development. Based on the results, future restoration projects in northern temperate forest should focus on (1) in areas with less than 600-700 mm of precipitation, attention should be paid to the selection of tree species for afforestation to maintain regional water balance; (2) in areas with more than 700 mm of precipitation, soil and water conservation projects need to be planned, especially in mountainous area. The research can not only support the management of temperate forest ecosystems in northern China, but also provide reference to other forest ecosystems to cope with climate change.

KEYWORDS

temperate forest, forest ecosystem services, trade-offs and synergies, precipitation gradients, northern China, climate change

1. Introduction

Forest ecosystems cover 30% of Earth's land surface and are the primary ecosystems supporting terrestrial life (FAO, 2020). As the source of essential ecosystem services (ESs) such as timber supply, soil conservation, carbon sequestration, and climate regulation (Gamfeldt et al., 2013; Brockerhoff et al., 2017; Ding et al., 2022), forest ecosystems are susceptible and vulnerable to global climate change (Seidl et al., 2017; Wan et al., 2018; Anderegg et al., 2022). Changes in precipitation are an important indicator of global climate

change, which can directly or indirectly affect the growth and distribution of forests, altering their structure and function, and thus affecting ESs and their interrelationships (Weltzin et al., 2003; Xu et al., 2020; Chen J. et al., 2021; Liu et al., 2022). From the perspective of the impact path on ESs on forest ecosystem, the intensity and duration of precipitation can affect the flow production mechanism and water yield, along with soil properties (Balasubramanian, 2017; Li M. et al., 2021; Wu et al., 2022); Spatial and temporal variations of precipitation can affect vegetation growth, change vegetation productivity and biomass (Wang et al., 2020), and then affect the carbon sequestration of forest. Forest canopy density and fine root distribution, which are affected by precipitation, can also impact on water yield and soil conservation (Lozano-Parra et al., 2015; Jiang et al., 2016; Thompson et al., 2016). In addition, temperate forest growth and ESs are more sensitive to water restriction (Gilliam, 2016; Seidl et al., 2020; Zhang et al., 2020). Therefore, exploring the response of temperate forest ESs and their inter-relationships to precipitation can not only support local forest management, but also provide basis for forest ecosystems to cope with global climate change.

Forest ecosystems provide a variety of ESs to human beings. Till now, most research on forest ESs focuses on the spatio-temporal changes and the cold and hot spots identification (Ditt et al., 2010; Mamat et al., 2018; Vatandaslar, 2022). Also, there are studies on forest ESs under different water conditions. In water-scarce temperate drylands, more attention has been paid to the dynamic interactions between rainfall and vegetation coverage and the ESs they provide (Wang et al., 2011; Rohatyn et al., 2018; Wang H. et al., 2022). In areas with abundant hydrothermal conditions, studies have revealed the effects of forest supply and support services on precipitation gradients (Alamgir et al., 2016; Thomas et al., 2021). In addition, the influence of temporal variation in precipitation on forest ESs is also one of the hotspots, e.g., the effects of inter-annual and intra-annual temporal dynamics of precipitation on forest area and regulation services (soil erosion, nutrient retention and etc.) in eco-sensitive zones (Suescún et al., 2017; Nelson et al., 2018; Rodrigues et al., 2020).

However, tradeoffs and synergies of ESs exist extensively in forest ecosystem (Liu et al., 2019; Wang et al., 2021; Feng et al., 2022; Jia et al., 2022), the dynamic of which can significantly affect the forest growth and management (Biber et al., 2020). Compared with the impact of precipitation on forest ESs (Hely et al., 2006; Lu et al., 2014), we still have relatively little understanding of the effects of precipitation on the interrelationships of forest ESs, especially the interconversion between tradeoffs and synergies. Due to the various response of different ESs and precipitation, the interrelationships among ESs with precipitation should be diverse. Therefore, it is of necessity to clarify the response of forest ES relationships to precipitation variation, especially in the temperate zone which is sensitive to climate change (Galicia et al., 2015; Wang et al., 2019).

The temperate forests of northern China are selected as the study area, of which is important national ecological security barriers. Forests in this area play the important role in regulating the local and regional carbon and water cycles and mitigating climate change (Thom et al., 2017; Jiao et al., 2021). In addition, the temperate zone is climate sensitive (Wan et al., 2017, 2018), and water conditions are the primary limiting factor for forest growth and ESs supply (Fang et al., 2005; Galicia et al., 2015). Therefore, in this study, three ESs, e.g., Net Primary Product (NPP), soil conservation (SC) and water yield (WY), which closely related to water resources in temperate forests were selected. The specific objectives are (1) to identify the relationship between the three ESs and precipitation; (2) quantify the interrelationships of ESs in response to precipitation gradients; and (3) assess the contribution of precipitation to interrelationship of ESs. The results can provide insight into the impact of precipitation changes on ES relationships and the information for coping with possible damage to forest due to climate change.

2. Materials and methods

2.1. Study area

To cover the overall temperature zone, the study area covers the Songliao River Basin and Haihe River Basin in the north of China (Figure 1). The area has warm-rainy summer and cold-dry winter with 445–973 mm in annual average rainfall and −7 to 13°C in annual average air temperature. Based on the statistical results of national weather stations in the study area, there was a significant downward trend in precipitation in the region, with a precipitation change rate of −7.35 mm/10a during the period 1960–2018[1]. However, existing models predict that the precipitation trend in the region will reverse in the future (Jiang et al., 2020; Jiang R. et al., 2021). The model simulations combined with IPCC SRES A2 scenario also indicate an increasing precipitation trend of 0.08-2 mm/d in the future (2035–2044) (Tang et al., 2009).

The forests of this region are not only capable of providing high-quality supplies and support services, but are also essential for local and regional regulation services (Mao et al., 2019). Climate fluctuations at large spatial and temporal scales will have irreversible effects on the distribution and function of forest ecosystems. In order to remove the influence of human disturbance, forest in 77 nature reserves were selected as typical objects (Xu et al., 2017), and the forest types are mainly coniferous broad-leaved mixed forest and deciduous broad-leaved forest. Based on dry-wet boundary, precipitation is divided into five gradients every 100 mm (i.e., <500, 500–600, 600–700, 700–800, and >800 mm).

2.2. Quantification of ecosystem services

Based on the previous studies on temperate forest ESs, three major ESs were selected, i.e., net primary product (NPP), soil conservation (SC), and water yield (WY) (Li et al., 2020; Li X. et al., 2021; Wang R. et al., 2022).

2.2.1. Net primary productivity

Net primary productivity (NPP) refers to the total amount of dry organic matter accumulated by vegetation per unit of time and area. It measures the net amount of carbon fixed in vegetation by photosynthesis of CO_2 (Field et al., 1998). NPP is an important

1 http://data.cma.cn

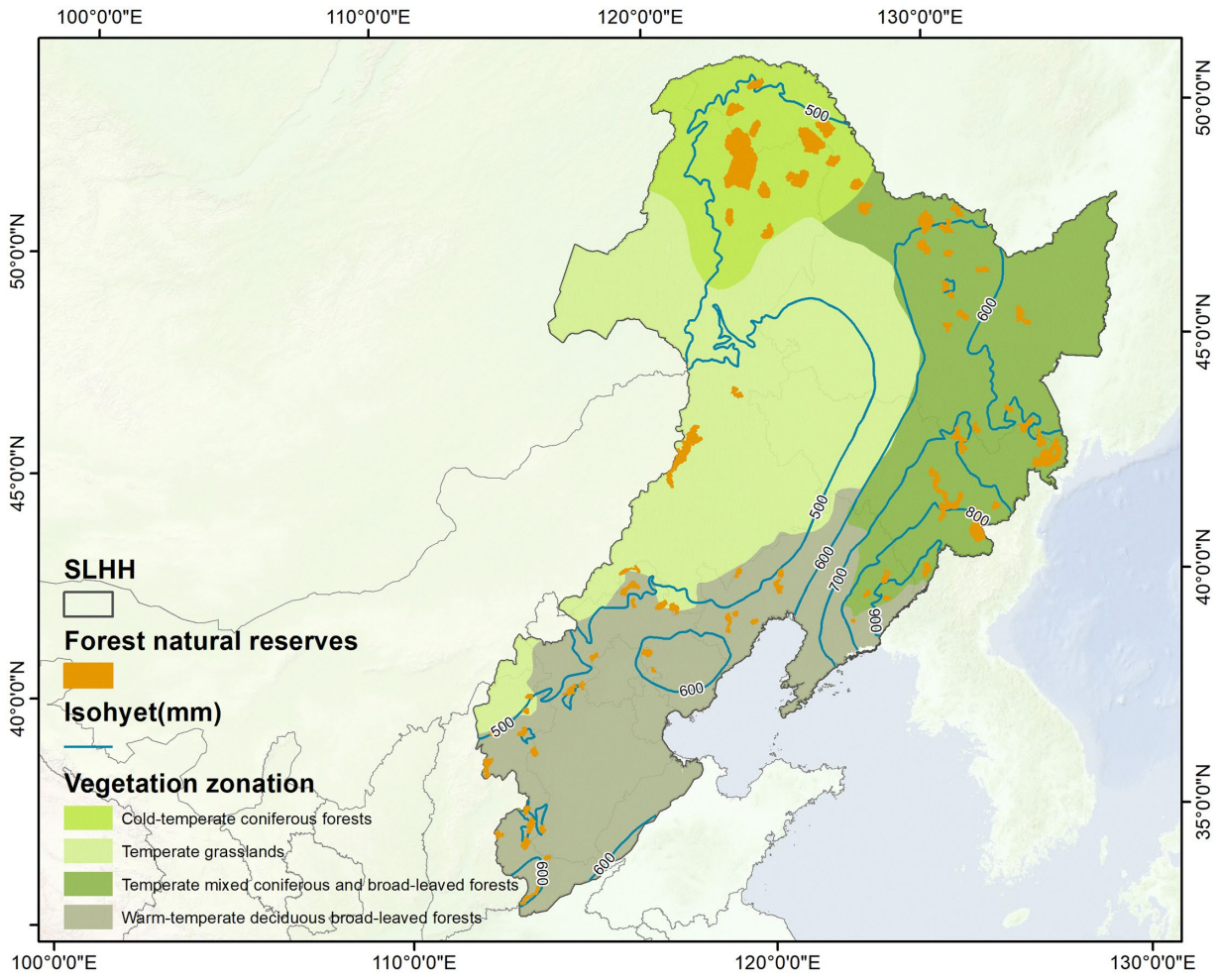

FIGURE 1
Distribution of precipitation gradients and forest natural reserves in the Songliao River Basin and Haihe River Basin, Northern China.

component of the terrestrial carbon cycle, not only directly reflecting the production capacity of vegetation communities under natural environmental conditions, representing the quality of the land ecosystem, but also determining the main factors of the carbon source and sink and regulating the ecological process, playing an important role in global change and carbon balance (Zhao and Running, 2010; Ji et al., 2020).

2.2.2. Soil conservation

Soil conservation service is the regulatory capacity of an ecosystem to prevent soil erosion. In this study, soil conservation is calculated based on the Revised Universal Soil Loss Equation (RUSLE), using the difference between actual and potential soil erosion (Ouyang et al., 2016). The calculation method is as follows:

$$SC = RKLS - USLE = R \times K \times LS \times (1 - C \times P)$$

where, R is the rainfall erosion force factor ($MJ\ mm\ hm^{-2}\ h^{-1}\ a^{-1}$); K is the soil erodibility factor ($t\ hm^{-2}\ h\ hm^{-2}\ MJ^{-1}\ mm^{-1}$); LS is the slope length slope factor; C is the cover and management factor; P is the soil conservation measure factor.

2.2.3. Water yield

In this study, the water yield module of the InVEST model was used for the simulation estimation of water yield (Sharp et al., 2018). The module is based on the Budyko curve and the average annual rainfall (Hamel and Guswa, 2015). The principle is briefly defined as the amount of precipitation per calculation unit minus the amount of water lost to storage and evapotranspiration, and the difference is the water yield (Ouyang et al., 2016), as follows:

$$Y_{x,j} = \left(1 - \frac{AET_{xj}}{P_x}\right) \times P_x$$

where, Y_x is the average annual water supply in raster x, P_x is the average multi-year precipitation in raster x, AET_{xj} is the average annual evaporation in raster x of the *jth* land use and land cover type.

2.3. Data sources

Based on regional precipitation frequency analysis, the year 2015, which is closest to the precipitation frequency $p = 50\%$ (around

617.8 mm), is selected as the reference year. The datasets involved used for assessing ESs based on the ArcGIS platform were listed in Table 1. ANUSPLIN interpolation was used for station data, and the spatial scale of raster data was finally unified to 1 km.

2.4. Analysis of trade-offs and synergies of ecosystem services

To derive trade-off/synergistic relationships between multiple ecosystem services, we analyzed the correlation between the two ecosystem services using the Spearman correlation test using the R language. A negative correlation coefficient indicates a trade-off between the two ESs, which means that as one ES increases, the other decreases. In contrast, a positive value indicates a synergistic relationship that grows or synergizes. The larger the absolute value of the correlation coefficient, the stronger the trade-off/synergy between the ESs and vice versa.

$$r_{ab(n)} = \frac{\sum_1^{ni}(ESa_{(n)} - \overline{ESa_{(n)}}) \times \sum_1^{n}(ESb_{(n)} - \overline{ESb_{(n)}})}{\sqrt{\sum_1^{n}(ESa_{(n)} - \overline{ESa_{(n)}})^2 \times \sum_1^{n}(ESb_{(n)} - \overline{ESb_{(n)}})^2}}$$

where, ES_a and ES_b represent the rank of two ESs, r_{ab} is the correlation coefficient between ES_a and ES_b; n is the rainfall gradient; $r_{ab(n)}$ is the correlation coefficient between ES_a and ES_b at rainfall gradient n. $r_{ab(n)} > 0$ indicates a synergistic relationship between ES_a and ES_b; $r_{ab(n)} = 0$ indicates no correlation between ES_a and ES_b; $r_{ab(n)} < 0$ indicates a trade-off relationship between ES_a and ES_b; a more significant of $r_{ab(n)}$ indicates a stronger correlation between ES_a and ES_b.

2.5. Redundancy analysis

Redundancy analysis (RDA) is a direct gradient analysis extension of principal components analysis (Šmilauer and Lepš, 2014). It can identify trends in the scatter of data points that are maximally and linearly related to a set of constraining (explanatory) variables (Makarenkov and Legendre, 2002). Mostly used by researchers to test hypotheses relating response (e.g., species data) to explanatory (e.g., environmental) variables (Legendre and Anderson, 1999; Dai et al., 2020). In this study, ES were clustered to better understand the analysis of the relationships between ES under different rainfall gradients (trade-offs and synergies) and their relations to other environmental factors.

3. Results

3.1. Correlations between ESs and precipitation

Throughout the study area (Figure 2), there was a significantly synergistic correlation with ecosystem services, with NPP having the strongest correlation, followed by WY and SC. Between ESs, WY had a significant synergy relationship with NPP and SC, respectively, and there was no significant correlation between NPP and SC.

Under different precipitation gradients, the heterogeneity of the relationships among ESs and precipitation was obvious. Precipitation has a synergistic correlation with NPP only at 500-600 mm gradient, and with water yield at >800 mm gradient. From the perspective of internal relations between ESs, synergistic relationship was found only between soil conservation and water yield at 600–700 mm gradient. Besides, NPP exhibited trade-off relationship with the other ESs at 500–600 and 600–700 mm gradients.

3.2. Characteristics of ESs along the precipitation gradients

As shown in Figure 3, all three ESs upraised with the increase of precipitation, but there was significant variability in the growth trend. By the analysis of variance between groups, it was also found that there was considerable variability in the service values between different precipitation gradients. The mean values of NPP under different rainfall gradients were 481.4 g C/m^2, 546.1 g C/m^2, 657.2 g C/m^2, 694.5 g C/m^2, and 710.7 g C/m^2, respectively, with the growth rate decreased significantly over 600–700 mm of gradient. The mean values of soil conservation under different rainfall gradients were 77.7 t/km^2, 139.8 t/km^2, 259.5 t/km^2, 441.9 t/km^2, and 535.4 t/km^2, respectively, with the growth rate increased significantly over 600–700 mm of precipitation. The mean values of WY under five rainfall gradients were 8.4, 30.8, 50.9, 67.4, and 118.2 mm, respectively, with a significantly increased growth rate over the 600–700 mm of precipitation.

TABLE 1 Data sources for ecosystem services assessment.

Data set	Data sources and description
NPP	Data for 2015 were derived from the Global Land Surface Satellite (GLASS) Products (Index of /NPP/AVHRR/GLASS_NPP_005D_YEAR)
Land use	Land use data in 2015 was taken from the Resources and Environmental Science Data Center (https://www.resdc.cn/)
Meteorological Data	Acquired from China Meteorological Administration (http://data.cma.cn/), including precipitation, temperature and evapotranspiration.
NDVI	Data for 2015 was obtained from the Resources and Environmental Science Data Center (https://www.resdc.cn/)
Elevation	Acquired from Resources and Environmental Science Data Center (https://www.resdc.cn/)
Potential evapotranspiration	Acquired from National Tibetan Plateau/Third Pole Environment Data Center (https://data.tpdc.ac.cn/)
Vegetation type	Acquired from National Tibetan Plateau Data Center (http://www.tpdc.ac.cn/zh-hans/)
Soil property	Acquired from National Tibetan Plateau Data Center (http://www.tpdc.ac.cn/zh-hans/)

Overall	**Precipitation**	0.76***	0.409***	0.643***
<500		0.179	0.143	0.536
500-600		0.45**	-0.155	-0.104
600-700		0.079	0.118	0.260
700-800		0.100	-0.500	0.100
>800		0.107	0.250	0.786*
Overall	0.76***	**NPP**	0.000	0.253*
<500	0.179		-0.643	0.393
500-600	0.450**		-0.521**	-0.458**
600-700	0.079		-0.494*	-0.687***
700-800	0.100		-0.300	-0.300
>800	0.107		0.536	0.357
Overall	0.409***	0.000	**Soil conservation**	0.592***
<500	0.143	-0.643		-0.179
500-600	-0.155	-0.521**		0.209
600-700	0.118	-0.494*		0.800***
700-800	-0.500	-0.300		0.200
>800	0.250	0.536		-0.107
Overall	0.643***	0.253*	0.592***	**Water yield**
<500	0.536	0.393	-0.179	
500-600	-0.104	-0.458**	0.209	
600-700	0.260	-0.687***	0.800***	
700-800	0.100	-0.300	0.200	
>800	0.786*	0.357	-0.107	

FIGURE 2
Relationship between ESs and precipitation. ***p<0.001; **p<0.01; *p<0.05. Blue and red represent significant positive and negative, respectively. Gray represents all the study areas, and successive ones represent different precipitation gradients.

3.3. Ecosystem services relationships under different precipitation gradients

The relationships between NPP, SC, and WY showed different trends under precipitation gradients (Figures 4A–C). The relation between NPP and SC showed a shift from tradeoff to synergy with rainfall increase. The relations of NPP with soil conservation and water yield showed an upward parabolic and downward parabolic trend, respectively, along the rainfall gradient. The peak and valley values of the relationship both appear in the precipitation gradient of 600-700 mm.

RDA results (Figure 4D) showed that precipitation was the most contributing meteorological factor (with contribution of 21.2%), after the slope (with contribution of 68.5%), followed by NDVI (4.5%) and Potential evapotranspiration (3.2%). Precipitation showed a positive correlation with all three ESs, while WY and SC showed more distinct clustering than NPP at different precipitation gradients. ESs under 600 mm precipitation are more distributed in the third quadrant, which also indicated that ESs are relatively small in these gradients. Under a 600–700 mm gradient, ESs are distributed in the second or fourth quadrant, meaning that there is a clear trade-off between NPP, WY, and SC. Meanwhile, in areas with precipitation less than 700, WY and SC are significantly influenced by slope, temperature and potential evapotranspiration. In areas with precipitation greater than 700, ESs are all in the first quadrant, which indicates that the ESs are relatively high, and the increasing trend is reflected in SC and WY driven by NDVI and slope.

4. Discussion

4.1. Response of key ESs and their relations to precipitation gradient

Our results quantify NPP, SC, and WY in temperate forest ecosystem, which are consistent with previous studies in northern China (Wang C. et al., 2020; Qi et al., 2021; Yan et al., 2021). Although the three ESs showed an increasing trend with precipitation, there was a clear difference in the rate of increase with the 600–700 mm gradient as the dividing line (Figure 3). As precipitation increased, NPP tended to increase faster and then slower, on the contrary, WY and SC showed a increase of slow first and then fast. The main reason for this difference is that the water limitation threshold in the climax community of temperate forest is about 700 mm (Chi et al., 2018). In the area where the rainfall is less than 700 mm, the forest community gradually succeed from shrubbery to arboreal forest, which leads to rapid increase in vegetation productivity and NPP. However, the vegetation cover is not yet high, and the water surplus is low after meeting the needs of vegetation growth, the growth of SC and WY is slow. In areas where rainfall is greater than 700 mm, the vegetation community structure is stable and the growth of NPP slows down. Moisture conditions in this area are already adequate for forest growth, so WY has increased significantly. Although increased precipitation also intensified the risk of soil erosion, these negative effects were offset by changes in forest structure and improvements in the water-holding capacity of the litter and soil water storage capacity,

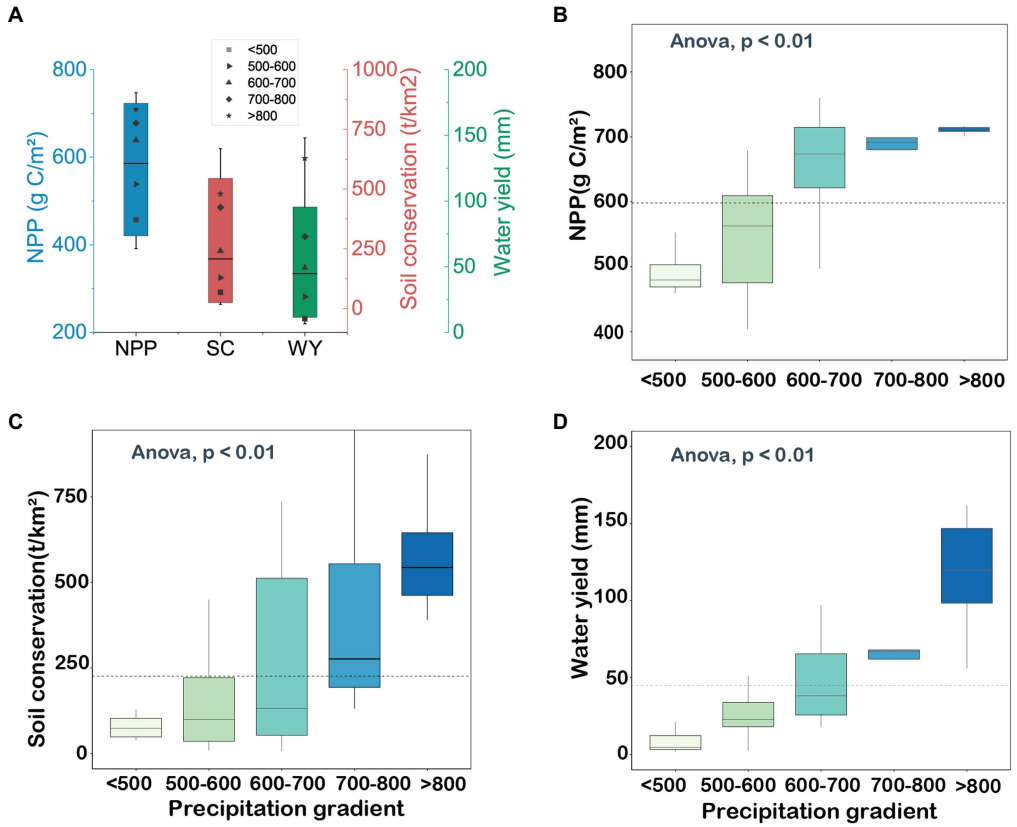

FIGURE 3
Three ESs in the forest natural reserves and the average of ESs under each precipitation gradient **(A)**; Variation of ESs along the precipitation gradients (**B:** NPP; **C:** Soil conservation; **D:** Water yield).

minimizing actual soil erosion (Hart and Frasier, 2003; Wu et al., 2020).

In addition, the relationship between the three ESs showed different trends with the precipitation gradient (Figure 4). As precipitation increased, the relationship between NPP and SC changed from a trade-off to synergy, while the synergy and trade-off between WY with SC and NPP reached the maximum on the 600–700 mm precipitation gradient. For NPP and SC, increased precipitation improved vegetation cover, while increased temperature and vegetation uptake accelerated soil water evaporation and soil erosion (Lu et al., 2014; Wang H. et al., 2020), resulting in the relationship between NPP and SC changing from a trade-off to a synergy (Figure 4D). For NPP and WY, NPP increased significantly with precipitation, and the succession of shrubbery to arboreal forest led to a relative decrease in WY, which intensifies the trade-off; after the community structure stabilized (above the 600–700 mm precipitation gradient), NPP and WY gradually reverted to synergy. For WY and SC, in areas with less precipitation, where shrubs still account for a certain proportion, and the combined effects of vegetation structure succession, temperature and other environmental factors keep SC and WY at a low level, showing a synergy between them; in areas with high precipitation (>700 mm), the growth of forest has been less restricted by water conditions (Chi et al., 2018), and excessive precipitation will cause soil erosion, making the synergistic relationship between SC and WY gradually weakened (Dai et al., 2022; Li et al., 2022).

4.2. Response of ESs and their relations to other environment factors

Slope (contribution = 68.5%; $p < 0.01$) was the most important factor influencing the relationship between ESs and ESs, and had a strong impact on ESs in areas with rainfall greater than 600–700 mm. Under this gradient, water demand of forest has stabilized, and slope can directly influence runoff velocity, alter infiltration, and have a positive correlation with erosion rates (Sun et al., 2018; Vanacker et al., 2019). Larger slope enhance the possibility for runoff generation (Hümann et al., 2011; Balasubramanian, 2017), increase the scouring force on the soil surface (Emmett, 1968), and change the relationship between WY and SC from synergy to trade-off. Also, slope is an important factor influencing local meteorological factor, which is closely related to precipitation (contribution = 1.0%; $p < 0.05$).

NDVI can reflect the state of vegetation coverage and biomass, and is influenced by environmental conditions such as precipitation and temperature (Defries and Townshend, 1994; Seidl et al., 2020). In the RDA results, NDVI (contribution = 4.5%; $p < 0.01$) was the important vegetation factor affecting NPP and WY, and was correlated with precipitation significantly and positively. Under the gradient of less than 600–700 mm, vegetation growth and carbon sequestration in temperate forest are limited by water (Mao et al., 2014; Higgins et al., 2023); when rainfall is greater than 700 mm, community succession and vegetation cover

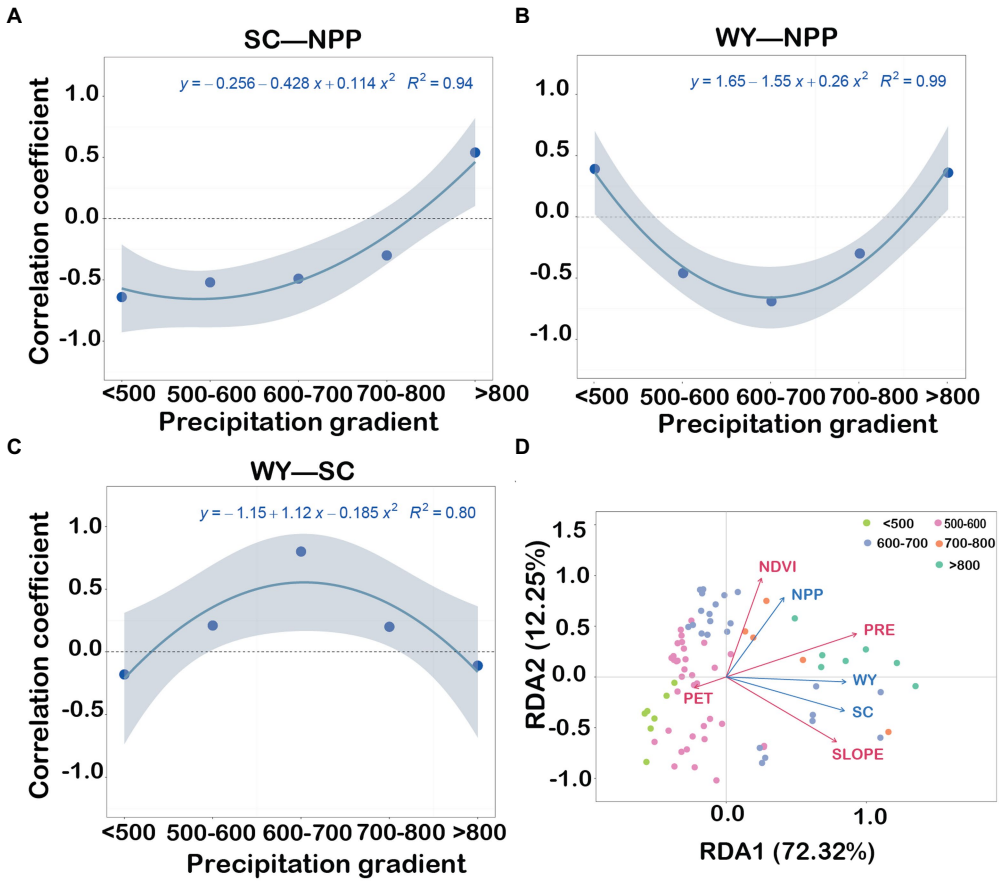

FIGURE 4
Changes in ES relationships between precipitation gradients [**(A)** soil conservation and NPP; **(B)** water yield and NPP; **(C)** water yield and soil conservation and RDA analysis **(D)**]. SC, soil conservation; WC, water yield; and PET, potential evapotranspiration. Explanation of ESs by influences in RDA and the permutation test result is 0.002, the explanatory variables account for 85.1% (adjusted explained variation is 83.3%).

in temperate forests stabilize, and ESs become progressively less influenced by NDVI.

Potential evapotranspiration (PET) is comprehensively affected by meteorological factors, higher PET means less water resources available (Donohue et al., 2010; Tu and Yang, 2022). In the RDA results, PET (contribution = 3.2%; $p < 0.01$) had a significant negative effect on ESs in areas with less than 600 precipitation, indicating that in areas with less precipitation, precipitation has difficulty in meeting the water requirements of vegetation growth, which limit the provision of temperate forest ESs (Rohatyn et al., 2018), and will also exacerbates trade-off between ESs.

Except for the four environmental factors SLOPE, PRE, NDVI, and PET that have outstanding contributions, the influence of other environmental factors is not significant: temperature (contribution = 1.0%; $p = 0.042$), vegetation type (contribution = 0.2%; $p = 0.8$) and soil type (contribution = 0.7%; $p = 0.1$). At the same time, based on the multi-year average temperature gradient, and it was found that there was no inter-group difference in WY under different temperature gradients (ANOVA; $p = 0.085$) (Supplementary Figure S1). It can be inferred when precipitation increases and the vegetation community tends to be stable, the sensitivity of forest water yield changes to temperature will be weakened (Zhou et al., 2015; Chen X. et al., 2021).

4.3. Implications of ESs interrelations for forest restoration and managements

Since 1960, both Northeast China and North China have experienced a shift from wet to dry climates (Fu et al., 2009; Shi et al., 2014), however, in the context of global climate change, it has been predicted that the future climate change in northern China will tend to be more wetter than warmer (Wu et al., 2010; Liu et al., 2017; Hui et al., 2018).

The increase in rainfall and temperature will favor the growth of promote the increase in the extent of coniferous and broad-leaf forests and broadleaf forests (Zhao et al., 2013; Zhang et al., 2022). The future increase of precipitation will bring westward shift of precipitation contour in northern China. For the new area with rainfall from 400 mm to 700 mm, it is vital to select vegetation types based on matching environmental elements such as temperature and topography with plant characteristics. Besides, Higher soil erosion rate may also be closely related to local topography, slope, temperature and other environmental factors (Fang and Guo, 2015). In areas with a future rainfall gradient of below 600 mm, the scrub-dominated vegetation types require less water for growth and are less capable of soil conservation, promoting a shift to a trade-off between the two ESs, and therefore

further soil conservation measures are needed in this part of the area. Moreover, in the area where rainfall may increase to more than 700 mm, there is still a need to focus on the construction of soil and water conservation forests to cope with the potential for increased trade-offs. In addition, to better capture the inflection points and thresholds of ESs trade-offs, it is suggested that additional ground-based data monitoring sites should be added in the future, to avoid possible errors in ESs assessment of this study. For other regions that are significantly affected by global climate change, e.g., the forest area of the southeast Tibetan Plateau, attention should also be paid to the changes in ES relationships. Studies predict that the alpine meadows in the hinterland of the plateau will be converted to shrub areas on a large scale (Korcz et al., 2021). Our results reveal that in the region dominated by shrubs, particular attention should be paid to the trade-offs between vegetation growth and water related ESs (Jiang C. et al., 2021; Jia et al., 2022). Therefore, in the restoration and management of vegetation in these areas, it is necessary to comprehensively consider the vegetation selection, the trade-off between vegetation water use and other water uses such as grain production, in order to reduce the trade-off between ESs.

5. Conclusion

This study revealed the response of major ESs interrelationships to precipitation gradient in temperate forest of northern China. The results show that 600–700 mm is a clear inflection point of the ESs and their correlations. The tradeoff between the regulation services (SC and NPP) gradually turned into synergy with the increase in precipitation, while the relationship between supply (WY) and regulation services (SC and NPP) presents a parabolic relationship.

The results indicated that afforestation and forest management should pay attention to the selection of tree species and the density of planting in areas where precipitation is less than 700 mm; while in high precipitation area, especially in mountainous areas, soil and water conservation projects should be paid focused. This study improve the current understanding of the impact of rainfall on ESs and relationships in temperate forests and provide predictive information to proactively address the potential damage to ESs in temperate forests from climate change.

Data availability statement

The raw data supporting the conclusions of this article will be made available by the authors, without undue reservation.

Author contributions

ML and RL: conceptualization. ML, JM, and RL: methodology. ML, TH, RL, XQ, HS, and YY: investigation and data. ML, RL, and HZ: writing – original draft preparation. ML, TH, JM, RL, YY, XQ, HS, and HZ: writing—review and editing. All authors have read and agreed to the published version of the manuscript.

Funding

This work was supported by the National Natural Science Foundation of China (42171099 and 41871218).

Conflict of interest

The authors declare that the research was conducted in the absence of any commercial or financial relationships that could be construed as a potential conflict of interest.

Publisher's note

All claims expressed in this article are solely those of the authors and do not necessarily represent those of their affiliated organizations, or those of the publisher, the editors and the reviewers. Any product that may be evaluated in this article, or claim that may be made by its manufacturer, is not guaranteed or endorsed by the publisher.

Supplementary material

The Supplementary material for this article can be found online at: https://www.frontiersin.org/articles/10.3389/fevo.2023.1132396/full#supplementary-material

References

Alamgir, M., Turton, S. M., Macgregor, C. J., and Pert, P. L. (2016). Assessing regulating and provisioning ecosystem services in a contrasting tropical forest landscape. *Ecol. Indic.* 64, 319–334. doi: 10.1016/j.ecolind.2016.01.016

Anderegg, W. R. L., Wu, C., Acil, N., Carvalhais, N., Pugh, T. A. M., Sadler, J. P., et al. (2022). A climate risk analysis of Earth's forests in the 21st century. *Science* 377, 1099–1103. doi: 10.1126/science.abp9723

Balasubramanian, A., (2017). *Surface water runoff*. India: Centre for Advanced Studies in Earth Science, University of Mysore.

Biber, P., Felton, A., Nieuwenhuis, M., Lindbladh, M., Black, K., Bahýl', J., et al. (2020). Forest biodiversity, carbon sequestration, and Wood production: modeling synergies and trade-offs for ten Forest landscapes across Europe. *Front. Ecol. Evol.* 8:547696. doi: 10.3389/fevo.2020.547696

Brockerhoff, E. G., Barbaro, L., Castagneyrol, B., Forrester, D. I., Gardiner, B., González-Olabarria, J. R., et al. (2017). Forest biodiversity, ecosystem functioning and the provision of ecosystem services. *Biodivers. Conserv.* 26, 3005–3035. doi: 10.1007/s10531-017-1453-2

Chen, X., Liu, L., Su, Y., Yuan, W., Liu, X., Liu, Z., et al. (2021). Quantitative association between the water yield impacts of forest cover changes and the biophysical effects of forest cover on temperatures. *J. Hydrol.* 600:126529. doi: 10.1016/j.jhydrol.2021.126529

Chen, J., Wang, Y., Sun, J., Liang, E., Shen, M., Yang, B., et al. (2021). Precipitation dominants synergies and trade-offs among ecosystem services across the Qinghai-Tibet plateau. *Glob. Ecol. Conserv.* 32:e01886. doi: 10.1016/j.gecco.2021.e01886

Chi, D., Wang, H., Li, X., Liu, H., and Li, X. (2018). Estimation of the ecological water requirement for natural vegetation in the Ergune River basin in northeastern China from 2001 to 2014. *Ecol. Indic.* 92, 141–150. doi: 10.1016/j.ecolind.2017.04.014

Dai, X., Wang, L., Huang, C., Fang, L., Wang, S., and Wang, L. (2020). Spatio-temporal variations of ecosystem services in the urban agglomerations in the middle reaches of the Yangtze River, China. *Ecol. Indic.* 115:106394. doi: 10.1016/j.ecolind.2020.106394

Dai, E., Wang, X., Zhu, J., and Tian, Q. (2022). Quantifying co-benefits and trade-offs between Forest ecosystem Services in the Gan River Basin of South China. *Sustainability* 14:8271. doi: 10.3390/su14148271

Defries, R. S., and Townshend, J. R. G. (1994). NDVI-derived land cover classifications at a global scale. *Int. J. Remote Sens.* 15, 3567–3586. doi: 10.1080/01431169408954345

Ding, Z., Zheng, H., Wang, J., O'Connor, P., Li, C., Chen, X., et al. (2022). Integrating top-down and bottom-up approaches improves practicality and efficiency of large-scale ecological restoration planning: insights from a social-ecological system. *Engineering*. doi: 10.1016/j.eng.2022.08.008

Ditt, E. H., Mourato, S., Ghazoul, J., and Knight, J. (2010). Forest conversion and provision of ecosystem services in the Brazilian Atlantic Forest. *Land Degrad. Dev.* 21, 591–603. doi: 10.1002/ldr.1010

Donohue, R. J., McVicar, T. R., and Roderick, M. L. (2010). Assessing the ability of potential evaporation formulations to capture the dynamics in evaporative demand within a changing climate. *J. Hydrol.* 386, 186–197. doi: 10.1016/j.jhydrol.2010.03.020

Emmett, W. W. (1968). "The hydraulics of overland flow on hillslopes" in *Dynamic and Descriptive Studies of Hillslopes (Geological Survey Professional Paper 662-A)*. U.S. Govt. Print. Off. Available at: https://doi.org/10.3133/pp662A

Fang, H., and Guo, M. (2015). Aspect-induced differences in soil erosion intensity in a gullied hilly region on the Chinese loess plateau. *Environ. Earth Sci.* 74, 5677–5685. doi: 10.1007/s12665-015-4648-4

Fang, J., Piao, S., Zhou, L., He, J., Wei, F., Myneni, R. B., et al. (2005). Precipitation patterns alter growth of temperate vegetation. *Geophys. Res. Lett.* 32:L21411. doi: 10.1029/2005GL024231

FAO. (2020). Global Forest Resources Assessment 2020. Food and Agriculture Organization of the United Nations (FAO). Available at: https://doi.org/10.4060/ca8753en

Feng, J., Chen, F., Tang, F., Wang, F., Liang, K., He, L., et al. (2022). The trade-offs and synergies of ecosystem Services in Jiulianshan National Nature Reserve in Jiangxi Province, China. *Forests* 13:416. doi: 10.3390/f13030416

Field, C. B., Behrenfeld, M. J., Randerson, J. T., and Falkowski, P. (1998). Primary production of the biosphere: integrating terrestrial and oceanic components. *Science* 281, 237–240. doi: 10.1126/science.281.5374.237

Fu, G., Charles, S. P., Yu, J., and Liu, C. (2009). Decadal climatic variability, trends, and future scenarios for the North China plain. *J. Clim.* 22, 2111–2123. doi: 10.1175/2008JCLI2605.1

Galicia, L., Gómez-Mendoza, L., and Magaña, V. (2015). Climate change impacts and adaptation strategies in temperate forests in Central Mexico: a participatory approach. *Mitig. Adapt. Strateg. Glob. Change* 20, 21–42. doi: 10.1007/s11027-013-9477-8

Gamfeldt, L., Snäll, T., Bagchi, R., Jonsson, M., Gustafsson, L., Kjellander, P., et al. (2013). Higher levels of multiple ecosystem services are found in forests with more tree species. *Nat. Commun.* 4:1340. doi: 10.1038/ncomms2328

Gilliam, F. S. (2016). Forest ecosystems of temperate climatic regions: from ancient use to climate change. *New Phytol.* 212, 871–887. doi: 10.1111/nph.14255

Hamel, P., and Guswa, A. J. (2015). Uncertainty analysis of a spatially explicit annual water-balance model: case study of the cape fear basin, North Carolina. *Hydrol. Earth Syst. Sci. Discuss.* 19, 839–853. doi: 10.5194/hess-19-839-2015

Hart, R. H., and Frasier, G. W. (2003). Bare ground and litter as estimators of runoff on short- and mixed-grass prairie. *Arid Land Res. Manage.* 17, 485–490. doi: 10.1080/713936119

Hely, C., Bremond, L., Alleaume, S., Smith, B., Sykes, M. T., and Guiot, J. (2006). Sensitivity of African biomes to changes in the precipitation regime. *Glob. Ecol. Biogeogr.* 15, 258–270. doi: 10.1111/j.1466-822X.2006.00235.x

Higgins, S. I., Conradi, T., and Muhoko, E. (2023). Shifts in vegetation activity of terrestrial ecosystems attributable to climate trends. *Nat. Geosci.* 16, 147–153. doi: 10.1038/s41561-022-01114-x

Hui, P., Tang, J., Wang, S., Niu, X., Zong, P., and Dong, X. (2018). Climate change projections over China using regional climate models forced by two CMIP5 global models. Part II: projections of future climate: Projections of climate over China with multi-RCM driven by CMIP5 GCM. *Int. J. Climatol.* 38, e78–e94. doi: 10.1002/joc.5409

Hümann, M., Schüler, G., Müller, C., Schneider, R., Johst, M., and Caspari, T. (2011). Identification of runoff processes – the impact of different forest types and soil properties on runoff formation and floods. *J. Hydrol.* 409, 637–649. doi: 10.1016/j.jhydrol.2011.08.067

Ji, Y., Zhou, G., Luo, T., Dan, Y., Zhou, L., and Lv, X. (2020). Variation of net primary productivity and its drivers in China's forests during 2000–2018. *For. Ecosyst.* 7:15. doi: 10.1186/s40663-020-00229-0

Jia, G., Dong, Y., Zhang, S., He, X., Zheng, H., Guo, Y., et al. (2022). Spatiotemporal changes of ecosystem service trade-offs under the influence of forest conservation project in Northeast China. *Front. Ecol. Evol.* 10:978145. doi: 10.3389/fevo.2022.978145

Jiang, C., Guo, H., Wei, Y., Yang, Z., Wang, X., Wen, M., et al. (2021). Ecological restoration is not sufficient for reconciling the trade-off between soil retention and water yield: a contrasting study from catchment governance perspective. *Sci. Total Environ.* 754:142139. doi: 10.1016/j.scitotenv.2020.142139

Jiang, C., Li, D., Wang, D., and Zhang, L. (2016). Quantification and assessment of changes in ecosystem service in the Three-River headwaters region, China as a result of climate variability and land cover change. *Ecol. Indic.* 66, 199–211. doi: 10.1016/j.ecolind.2016.01.051

Jiang, R., Sun, L., Sun, C., and Liang, X.-Z. (2021). CWRF downscaling and understanding of China precipitation projections. *Clim. Dyn.* 57, 1079–1096. doi: 10.1007/s00382-021-05759-z

Jiang, Z., Tian, Z., Dong, G., Sun, L., Zhang, P., Buonomo, E., et al. (2020). High-resolution projections of mean and extreme precipitation over China by two regional climate models. *J. Meteorol. Res.* 34, 965–985. doi: 10.1007/s13351-020-9208-5

Jiao, Y., Bu, K., Yang, J., Li, G., Shen, L., Liu, T., et al. (2021). Biophysical effects of temperate forests in regulating regional temperature and precipitation pattern across Northeast China. *Remote Sens.* 13:4767. doi: 10.3390/rs13234767

Korcz, N., Koba, J., Kobyłka, A., Janeczko, E., and Gmitrowicz-Iwan, J. (2021). Climate change and informal education in the opinion of Forest users in Poland. *Sustainability* 13:7892. doi: 10.3390/su13147892

Legendre, P., and Anderson, M. J. (1999). Distance-based redundancy analysis: testing multispecies responses in multifactorial ecological experiments. *Ecol. Monogr.* 69, 1–24. doi: 10.1890/0012-9615(1999)069[0001:DBRATM]2.0.CO;2

Li, M., Liang, D., Xia, J., Song, J., Cheng, D., Wu, J., et al. (2021). Evaluation of water conservation function of Danjiang River basin in Qinling Mountains, China based on InVEST model. *J. Environ. Manage.* 286:112212. doi: 10.1016/j.jenvman.2021.112212

Li, Z., Lu, Y., Wang, Y., and Liu, J. (2022). The Spatio-temporal evolution of the soil conservation function of ecosystems in the north–south transition zone in China: a case study of the Qinling-Daba Mountains. *Sustainability* 14:5829. doi: 10.3390/su14105829

Li, J., Wang, Y., and Liu, L. (2020). Responses of the terrestrial ecosystem productivity to droughts in China. *Front. Earth Sci.* 8:59. doi: 10.3389/feart.2020.00059

Li, X., Zhang, C., Zhang, B., Wu, D., Zhu, D., Zhang, W., et al. (2021). Nitrogen deposition and increased precipitation interact to affect fine root production and biomass in a temperate forest: implications for carbon cycling. *Sci. Total Environ.* 765:144497. doi: 10.1016/j.scitotenv.2020.144497

Liu, J., Du, H., Wu, Z., He, H. S., Wang, L., and Zong, S. (2017). Recent and future changes in THE combination of annual temperature and precipitation throughout China: changes in the combination of temperature and precipitation over China. *Int. J. Climatol.* 37, 821–833. doi: 10.1002/joc.4742

Liu, L., Wang, Z., Wang, Y., Zhang, Y., Shen, J., Qin, D., et al. (2019). Trade-off analyses of multiple mountain ecosystem services along elevation, vegetation cover and precipitation gradients: a case study in the Taihang Mountains. *Ecol. Indic.* 103, 94–104. doi: 10.1016/j.ecolind.2019.03.034

Liu, Z., Ye, L., Wei, Z., Jiang, J., Zhang, Q., and Lv, X. (2022). Water use by trees is linked to precipitation: a case study of a mixed forest in a hilly area in southern China. *Ecol. Indic.* 143:109343. doi: 10.1016/j.ecolind.2022.109343

Lozano-Parra, J., Schnabel, S., and Ceballos-Barbancho, A. (2015). The role of vegetation covers on soil wetting processes at rainfall event scale in scattered tree woodland of Mediterranean climate. *J. Hydrol.* 529, 951–961. doi: 10.1016/j.jhydrol.2015.09.018

Lu, N., Fu, B., Jin, T., and Chang, R. (2014). Trade-off analyses of multiple ecosystem services by plantations along a precipitation gradient across loess plateau landscapes. *Landsc. Ecol.* 29, 1697–1708. doi: 10.1007/s10980-014-0101-4

Makarenkov, V., and Legendre, P. (2002). Nonlinear redundancy analysis and canonical correspondence analysis based on polynomial regression. *Ecology* 83, 1146–1161. doi: 10.1890/0012-9658(2002)083[1146:NRAACC]2.0.CO;2

Mamat, Z., Halik, Ü., Keyimu, M., Keram, A., and Nurmamat, K. (2018). Variation of the floodplain forest ecosystem service value in the lower reaches of Tarim River, China. *Land Degrad. Rehab.* 29, 47–57. doi: 10.1002/ldr.2835

Mao, D., He, X., Wang, Z., Tian, Y., Xiang, H., Yu, H., et al. (2019). Diverse policies leading to contrasting impacts on land cover and ecosystem services in Northeast China. *J. Clean. Prod.* 240:117961. doi: 10.1016/j.jclepro.2019.117961

Mao, D., Wang, Z., Wu, C., Song, K., and Ren, C. (2014). Examining forest net primary productivity dynamics and driving forces in northeastern China during 1982–2010. *Chin. Geogr. Sci.* 24, 631–646. doi: 10.1007/s11769-014-0662-9

Nelson, H. P., Devenish-Nelson, E. S., Rusk, B. L., Geary, M., and Lawrence, A. J. (2018). A call to action for climate change research on Caribbean dry forests. *Reg. Environ. Chang.* 18, 1337–1342. doi: 10.1007/s10113-018-1334-6

Ouyang, Z., Zheng, H., Xiao, Y., Polasky, S., Liu, J., Xu, W., et al. (2016). Improvements in ecosystem services from investments in natural capital. *Science* 352, 1455–1459. doi: 10.1126/science.aaf2295

Qi, L., Zhang, Y., Xu, D., Zhu, Q., Zhou, W., Zhou, L., et al. (2021). Trade-offs and synergies of ecosystem services in forest barrier belt of Northeast China. *Chin. J. Ecol.* 40, 3401–3411. doi: 10.13292/j.1000-4890.202111.020

Rodrigues, A. R., Botequim, B., Tavares, C., Pécurto, P., and Borges, J. G. (2020). Addressing soil protection concerns in forest ecosystem management under climate change. *For. Ecosyst.* 7:34. doi: 10.1186/s40663-020-00247-y

Rohatyn, S., Rotenberg, E., Ramati, E., Tatarinov, F., Tas, E., and Yakir, D. (2018). Differential impacts of land use and precipitation on "ecosystem water yield.". *Water Resour. Res.* 54, 5457–5470. doi: 10.1029/2017WR022267

Seidl, R., Honkaniemi, J., Aakala, T., Aleinikov, A., Angelstam, P., Bouchard, M., et al. (2020). Globally consistent climate sensitivity of natural disturbances across boreal and temperate forest ecosystems. *Ecography* 43, 967–978. doi: 10.1111/ecog.04995

Seidl, R., Thom, D., Kautz, M., Martin-Benito, D., Peltoniemi, M., Vacchiano, G., et al. (2017). Forest disturbances under climate change. *Nat. Clim. Chang.* 7, 395–402. doi: 10.1038/nclimate3303

Sharp, R., Chaplin-Kramer, R., Wood, S., Guerry, A., Tallis, H., Ricketts, T., et al. (2018). InVEST3.2.0: *User's Guide*. The Natural Capital Project, Stanford University, University of Minnesota, The Nature Conservancy, and World Wildlife Fund. Available at: https://doi.org/10.13140/RG.2.2.32693.78567

Shi, P., Sun, S., Wang, M., Li, N., Wang, J., Jin, Y., et al. (2014). Climate change regionalization in China (1961–2010). *Sci. China Earth Sci.* 57, 2676–2689. doi: 10.1007/s11430-014-4889-1

Šmilauer, P., and Lepš, J. (2014). *Multivariate analysis of ecological data using CANOCO 5. 2nd* Edn Cambridge University Press.

Suescún, D., Villegas, J. C., León, J. D., Flórez, C. P., García-Leoz, V., and Correa-Londoño, G. A. (2017). Vegetation cover and rainfall seasonality impact nutrient loss via runoff and erosion in the Colombian Andes. *Reg. Environ. Chang.* 17, 827–839. doi: 10.1007/s10113-016-1071-7

Sun, J., Fan, D., Yu, X., and Li, H. (2018). Hydraulic characteristics of varying slope gradients, rainfall intensities and litter cover on vegetated slopes. *Hydrol. Res.* 49, 506–516. doi: 10.2166/nh.2017.097

Tang, J., Chen, X., Zhao, M., and Su, B. (2009). Numerical simulation of regional climate change under IPCC A2 scenario in China. *J. Meteorol. Res.* 23, 29–42.

Thom, D., Rammer, W., and Seidl, R. (2017). The impact of future forest dynamics on climate: interactive effects of changing vegetation and disturbance regimes. *Ecol. Monogr.* 87, 665–684. doi: 10.1002/ecm.1272

Thomas, E., Jansen, M., Chiriboga-Arroyo, F., Wadt, L. H. O., Corvera-Gomringer, R., Atkinson, R. J., et al. (2021). Habitat quality differentiation and consequences for ecosystem service provision of an Amazonian Hyperdominant tree species. *Front. Plant Sci.* 12:621064. doi: 10.3389/fpls.2021.621064

Thompson, A., Davis, J. D., and Oliphant, A. J. (2016). Surface runoff and soil erosion under eucalyptus and oak canopy: surface runoff and soil erosion under eucalyptus and oak canopy. *Earth Surf. Process. Landf.* 41, 1018–1026. doi: 10.1002/esp.3881

Tu, Z., and Yang, Y. (2022). On the estimation of potential evaporation under wet and dry conditions. *Water Resour. Res.* 58. doi: 10.1029/2021WR031486

Vanacker, V., Ameijeiras-Mariño, Y., Schoonejans, J., Cornélis, J.-T., Minella, J. P. G., Lamouline, F., et al. (2019). Land use impacts on soil erosion and rejuvenation in southern Brazil. *Catena* 178, 256–266. doi: 10.1016/j.catena.2019.03.024

Vatandaslar, C. (2022). Spatial assessment of ecosystem services provisioning changes in a forest-dominated protected area in NE Turkey. *Environ. Monit. Assess.* 194:539. doi: 10.1007/s10661-022-10212-7

Wan, J.-Z., Wang, C.-J., Qu, H., Liu, R., and Zhang, Z.-X. (2018). Vulnerability of forest vegetation to anthropogenic climate change in China. *Sci. Total Environ.* 621, 1633–1641. doi: 10.1016/j.scitotenv.2017.10.065

Wan, J.-Z., Wang, C.-J., and Yu, F.-H. (2017). Spatial conservation prioritization for dominant tree species of Chinese forest communities under climate change. *Clim. Chang.* 144, 303–316. doi: 10.1007/s10584-017-2044-7

Wang, Y., Dai, E., Ge, Q., Zhang, X., and Yu, C. (2021). Spatial heterogeneity of ecosystem services and their trade-offs in the Hengduan Mountain region, Southwest China. *Catena (Amst)* 207:105632. doi: 10.1016/j.catena.2021.105632

Wang, S., Fu, B.-J., He, C.-S., Sun, G., and Gao, G.-Y. (2011). A comparative analysis of forest cover and catchment water yield relationships in northern China. *For. Ecol. Manage.* 262, 1189–1198. doi: 10.1016/j.foreco.2011.06.013

Wang, C., Jiang, Q., Deng, X., Lv, K., and Zhang, Z. (2020). Spatio-temporal evolution, future trend and phenology regularity of net primary productivity of forests in Northeast China. *Remote Sens.* 12:3670. doi: 10.3390/rs12213670

Wang, R., Peng, Q., Zhang, W., Zhao, W., Liu, C., and Zhou, L. (2022). Ecohydrological service characteristics of Qilian Mountain ecosystem in the next 30 years based on scenario simulation. *Sustainability* 14:1819. doi: 10.3390/su14031819

Wang, H., Sun, B., Yu, X., Xin, Z., and Jia, G. (2020). The driver-pattern-effect connection of vegetation dynamics in the transition area between semi-arid and semi-humid northern China. *Catena* 194:104713. doi: 10.1016/j.catena.2020.104713

Wang, H., Wang, W. J., Liu, Z., Wang, L., Zhang, W., Zou, Y., et al. (2022). Combined effects of multi-land use decisions and climate change on water-related ecosystem services in Northeast China. *J. Environ. Manage.* 315:115131. doi: 10.1016/j.jenvman.2022.115131

Wang, C.-J., Zhang, Z.-X., and Wan, J.-Z. (2019). Vulnerability of global forest ecoregions to future climate change. *Glob. Ecol. Conserv.* 20:e00760. doi: 10.1016/j.gecco.2019.e00760

Weltzin, J. F., Loik, M. E., Schwinning, S., Williams, D. G., Fay, P. A., Haddad, B. M., et al. (2003). Assessing the response of terrestrial ecosystems to potential changes in precipitation. *Bioscience* 53:941. doi: 10.1641/0006-3568(2003)053[0941:ATROTE]2.0.CO;2

Wu, C., Qiu, D., Gao, P., Mu, X., and Zhao, G. (2022). Application of the InVEST model for assessing water yield and its response to precipitation and land use in the Weihe River basin, China. *J. Arid. Land* 14, 426–440. doi: 10.1007/s40333-022-0013-0

Wu, X., Shi, W., Guo, B., and Tao, F. (2020). Large spatial variations in the distributions of and factors affecting forest water retention capacity in China. *Ecol. Indic.* 113:106152. doi: 10.1016/j.ecolind.2020.106152

Wu, S., Zheng, D., Yin, Y., Lin, E., and Xu, Y. (2010). Northward-shift of temperature zones in China's eco-geographical study under future climate scenario. *J. Geogr. Sci.* 20, 643–651. doi: 10.1007/s11442-010-0801-x

Xu, W., Xiao, Y., Zhang, J., Yang, W., Zhang, L., Hull, V., et al. (2017). Strengthening protected areas for biodiversity and ecosystem services in China. *Proc. Natl. Acad. Sci.* 114, 1601–1606. doi: 10.1073/pnas.1620503114

Xu, H., Zhao, C., and Wang, X. (2020). Elevational differences in the net primary productivity response to climate constraints in a dryland mountain ecosystem of northwestern China. *Land Degrad. Dev.* 31, 2087–2103. doi: 10.1002/ldr.3587

Yan, M., Xue, M., Zhang, L., Tian, X., Chen, B., and Dong, Y. (2021). A Decade's change in vegetation productivity and its response to climate change over Northeast China. *Plan. Theory* 10:821. doi: 10.3390/plants10050821

Zhang, L., Sun, P., Huettmann, F., and Liu, S. (2022). Where should China practice forestry in a warming world? *Glob. Change Biol. Bioenergy.* 28, 2461–2475. doi: 10.1111/gcb.16065

Zhang, X., Xing, Y., Wang, Q., Yan, G., Wang, M., Liu, G., et al. (2020). Effects of long-term nitrogen addition and decreased precipitation on the fine root morphology and anatomy of the main tree species in a temperate forest. *For. Ecol. Manag.* 455:117664. doi: 10.1016/j.foreco.2019.117664

Zhao, M., and Running, S. W. (2010). Drought-induced reduction in global terrestrial net primary production from 2000 through 2009. *Science* 329, 940–943. doi: 10.1126/science.1192666

Zhao, D., Wu, S., and Yin, Y. (2013). Responses of terrestrial ecosystems' net primary productivity to future regional climate change in China. *PLoS One* 8:e60849. doi: 10.1371/journal.pone.0060849

Zhou, G., Wei, X., Chen, X., Zhou, P., Liu, X., Xiao, Y., et al. (2015). Global pattern for the effect of climate and land cover on water yield. *Nat. Commun.* 6:5918. doi: 10.1038/ncomms6918

frontiers | Frontiers in Ecology and Evolution

TYPE Original Research
PUBLISHED 28 April 2023
DOI 10.3389/fevo.2023.1126659

OPEN ACCESS

EDITED BY
Wei Zhao,
Chinese Academy of Sciences (CAS), China

REVIEWED BY
Manob Das,
University of Gour Banga, India
Fengtai Zhang,
Chongqing University of Technology, China

*CORRESPONDENCE
Kangning Xiong
✉ xiongkn@gznu.edu.cn

RECEIVED 18 December 2022
ACCEPTED 10 April 2023
PUBLISHED 28 April 2023

CITATION
Tang J, Xiong K, Wang Q, Chen Y and Wu Q (2023) Village ecosystem vulnerability in karst desertification control: evidence from South China Karst.
Front. Ecol. Evol. 11:1126659.
doi: 10.3389/fevo.2023.1126659

Village ecosystem vulnerability in karst desertification control: evidence from South China Karst

Jiuhan Tang, Kangning Xiong*, Qi Wang, Yue Chen and Qinglin Wu

School of Karst Science, Guizhou Normal University/State Engineering Technology Institute for Karst Desertification Control, Guiyang, China

Against the background of global environmental changes and the intensification of human activity, the village ecosystem faces enormous challenges. In particular, the rural areas in South China Karst face serious problems, such as karst desertification and human–land conflicts. In recent decades, the Chinese government and scientific researchers have committed to controlling karst desertification. However, village ecosystems in the context of karst desertification control (KDC) remain fragile. To promote the sustainable development of villages in KDC, this study considered village ecosystems in different karst desertification areas as study cases. Based on the model of susceptibility-exposure-lack of resilience, we constructed an index system of vulnerability research, used the entropy method to determine the weight, and introduced a contribution model to clarify the vulnerability level and vulnerability driving factors to recommend related governance strategies. We found that (1) the village ecosystem vulnerability levels under KDC were different. Village ecosystems were mildly vulnerable in none-potential KDC areas, moderately vulnerable in potential-mild areas, and moderately and highly vulnerable in moderate–severe KDC areas. (2) The combined effects of the natural environment and human activity have led to the vulnerability of village ecosystems in KDC in South China Karst. Among them, topography, climate, forest coverage, landscape pattern, soil erosion, karst desertification, economic development level, and production and living activity are the main factors affecting the village ecosystem vulnerability of KDC in South China Karst, and the differences in these factors lead to differences in vulnerability levels of different village ecosystems. (3) We designed adaptive governance strategies for village ecosystems based on the factors influencing the characteristics and vulnerability of different karst desertification areas, with the primary goal of sustainable development. They provide a decision-making basis for promoting sustainable development of the village ecosystems in KDC.

KEYWORDS

karst desertification, ecological governance, village ecosystem, vulnerability, influencing factors, sustainability

1. Introduction

Global environmental changes, social and economic development, a decrease in species diversity, an increase in desertification, extreme weather events, and other issues of ecosystem degradation seriously threaten the sustainability of society, the economy and the survival of human beings (Easterling et al., 2000; Guo et al., 2020; Li et al., 2021). Concurrently, the rapid

urbanization, environmental pollution and waste of resources places ecosystems under tremendous pressure, which further exacerbates the degradation of ecosystems (Meng et al., 2018). The increase in human activity and global climate change have led to tremendous pressure on the ecosystem (Li and Song, 2021; Wang et al., 2023), aggravating the expression of ecosystem vulnerability and destroying the supply capacity of ecosystem services. It is estimated that 60% of ecosystem services worldwide are degraded because of human activity (Zhang et al., 2018), resulting in ecological problems such as the degradation of water, loss of biodiversity (Vitousek et al., 1997; Foley et al., 2005), and land degradation. The contradiction and conflict between humankind's pursuit of social and economic prosperity and the ecological environment have become the main challenges facing current global sustainable development. Therefore, the environment, development, and sustainability have become major issues of concern worldwide (Nandy et al., 2015; Zhang et al., 2022).

Driven by globalization, industrialization, and urbanization, the countryside is undergoing a holistic reconstruction. In particular, rural areas in developing countries generally experience population reduction, economic non-agricultural transformation, and environmental pollution, which lead to rural decline and affects the sustainability of rural economic and social development (Li, 2020). Rural populations have declined, and village labor shortages, economic recession, and social degradation have caused rural decline to become global issues (Liu and Li, 2017). Villages are more at risk due to poor infrastructure, low human development, high dependence on agriculture, and lack of government attention, which places villages more at risk (Jamshed et al., 2020). In the past few decades, rural areas worldwide have faced tremendous pressure due to land-use changes that threaten ecosystem services and environmental sustainability (Yu, 2022). In the context of rapid urbanization, many villages are experiencing a sharp increase in the proportion of construction land, leading to a reduction in ecosystem services (Zhang et al., 2020), and the destruction of the ecological environment. Currently, the elements and functions of village systems have undergone transformation and restructuring, while simultaneously, the stability of the villages has been disrupted, which makes them vulnerable (Yang and Pan, 2021). The driving factors of village ecosystem vulnerability differ across geographical environments. For example, coastal villages are vulnerable because of the disturbance caused by hurricanes, storm surges, tsunamis, and the lack of adaptability of the villages themselves (Colburn et al., 2016; Karuppusamy et al., 2021). The impact of extreme weather events, earthquakes, and harsh natural environments has contributed to the vulnerability of Himalayan villages (Pandey et al., 2017; Dasgupta and Badola, 2020). Villages in river regions are adversely affected by repeated flooding and riverbank erosion, which destroy property, agricultural land, and habitat, and cause social and economic crises and food security problems, leading to the vulnerability of villages (Ahmad and Afzal, 2021). Drought-type villages are affected by the high variability of seasonal water and long-term, frequent droughts, which intensify the exposure and sensitivity of the ecosystem (Tessema et al., 2021). In areas with frequent geological disasters, the higher the altitude, the more fragile is the village ecosystem (Liu et al., 2020). However, approximately half of the world's population lives in rural regions (Bavinck et al., 2017). The livelihoods of rural populations directly dependent on ecosystem services are particularly at risk (Malmborg et al., 2018). Village ecosystems provide ecosystem services, such as water filtration, carbon absorption, and wildlife habitat, as well as food, freshwater, and energy that sustain both rural and urban residents (Miller Hesed et al., 2020). Concurrently, rural areas also provide the functions of supporting the population, maintaining culture, sightseeing tourism, and providing for the older urban residents (Huang, 2019). As an indispensable part of the global ecosystem, village ecosystems are of great significance for the sustainability of global development. Therefore, it is necessary to study the vulnerability of villages to provide scientific guidance for improving the service capacity of village ecosystems and promoting their sustainable development.

Therefore, it is of great scientific significance to construct a scientific and adequate vulnerability research index system, analyze the vulnerability level of village ecosystems, and reveal the driving factors of vulnerability. However, previous studies on the vulnerability of karst areas have neglected the analysis of the vulnerability of the human-land coupling system and its driving factors in karst desertification control villages. Therefore, they provide weak guidance to the consolidation of poverty alleviation achievements and the implementation of rural revitalization in karst desertification areas. To study the vulnerability of KDC villages, enhance their ecosystem service capacity, and promote the coordinated and sustainable development of their socio-economic and natural environment to consolidate the achievements of poverty alleviation and help rural revitalization, this paper provides a scientific and technological reference. As research cases, we selected villages in three different levels of KDC in the karst plateau mountainous areas, representing the overall structure of the karst desertification ecological environment type in South China Karst. The aim was to explore the level and influencing factors of village ecosystem vulnerability in the context of KDC and propose an adaptive management strategy for the KDC village ecosystem to provide a scientific and technological reference for the overall coordination and sustainable development of the KDC village ecosystem.

2. Literature review

Environmental changes are one of the biggest threats to global ecosystems in the coming decades, and currently scholars believe that vulnerability research should be incorporated into protection and planning to deal with the threat of environmental change to the sustainability of ecosystems (Lee et al., 2018). As one of the research themes in regional sustainable development, vulnerability assessment originates from the study of natural disasters. Since then, it has been widely used in geography, ecology, management, and other disciplines (Tai et al., 2020). Broadening of research on human factors in ecosystems led to the evolution of the concept of vulnerability from natural vulnerability to multi-dimensional vulnerability, which includes nature, the environment, society, the economy, and other factors (Wang et al., 2019). Research on the vulnerability of the social-ecological system, which considers the human-earth system to be the core, has become the focus of regional sustainable development research (Tian et al., 2013). Current research on the vulnerability of socio-ecological systems has focused on mountainous area (Brunner and Grêt-Regamey, 2016; Li et al., 2022), arid and semiarid areas (Liu et al., 2016; Chen et al., 2018), coastal areas (Hagenlocher et al., 2018; Silva et al., 2019; Koehn et al., 2022), and tourist areas (Jia et al., 2021; Li et al., 2022).

Studying the driving mechanisms of regional ecosystem vulnerability will be helpful in formulating ecological environment governance guidelines (Kang et al., 2018). Many international scientific programs (International Geosphere–Biosphere Program, Man and the Biosphere Program, and International Biological Program) have also included vulnerability as a topic of sustainability research in the context of global environmental changes (Hong et al., 2016). The current frameworks of vulnerability research mainly include the "pressure-state-response" (P-S-R; Hu et al., 2021), "exposure-sensitivity-adaptability" (V-S-D; Polsky et al., 2007), "sensitivity-resilience-pressure" (S-R-P; Li et al., 2015; Chen X. et al., 2021), driving force-pressure-state-impact-response (DPSIR; Malekmohammadi and Jahanishakib, 2017) and exposure-susceptibility-lack of resilience (E-S-LoR; Birkmann et al., 2013) models. Research methods used include principal component analysis (Xenarios et al., 2016), fuzzy evaluation method (Liu H. et al., 2014), analytic hierarchy process (Chen et al., 2022), comprehensive evaluation method (Guo and Huang, 2016), grey relational analysis (Luo and Zhang, 2018) and entropy method (Tai et al., 2020). Because the research purposes, regional characteristics, and foci may be very different, there is no unified indicator system (Li et al., 2021). However, sustainable governance strategies based on large-scale regions are not applicable to the village ecosystems. Scholars in all disciplines have conducted studies on village ecosystems in different types of ecological environments. Ghosh and Ghosal (2021) proposed improving the adaptability of residents through education, migration, increase in income, crop diversification, infrastructure and disaster early warning system construction aimed at the vulnerability factors of rural households in the Himalayan foothills. Farmers' resistance to drought in arid rural areas can be enhanced by increasing income and crop diversification, promoting non-agricultural employment, and other strategies (Keshavarz and Moqadas, 2021). Villages in geological disaster risk areas should establish disaster warning systems, publicise and educate farmers about disaster reduction, and strengthen professional personnel and infrastructure construction at the grassroots level (Xu et al., 2020). Villages in coastal areas that are susceptible to meteorological disasters should adjust their industrial structure, choose more favorable places to live and produce, cultivate a variety of skills, and develop diversified livelihoods to enhance farmers' adaptability to climate change (Touza et al., 2021). Poor villages in rocky desertification areas should establish a regional economic system, abandon extensive and predatory development at the expense of the environment and resources, and promote the transformation of rural development from a backward model to high-quality and sustainable development (Zuo et al., 2022). Thus far, research on rural sustainability has mainly analyzed rural adaptability to poverty, sustainable livelihood of farmers, and resilience of rural families to cope with disasters. Studies on the sustainability of village ecosystems from the perspective of human–environment coupling systems are lacking. However, the sustainability of villages in the KDC areas is mainly influenced by human activity and the natural environment, and the sensitive basic environment is fragile under the pressure of unsustainable human activity. Therefore, to promote sustainable development of the village ecosystem in the KDC, we must study its vulnerability characteristics.

Studying ecosystem vulnerability can effectively assist in monitoring environmental changes and mastering the motivation for environmental evolution to guide the rational protection and governance of the environment (Kang et al., 2018), At present, research on the vulnerability of karst areas includes the vulnerability of water resources (Marín et al., 2015; Zhu et al., 2019), nature reserve vulnerability (Chen Y. et al., 2021), vulnerability of mountain ecosystem (Guo et al., 2020), ecological environment vulnerability (Liu C. et al., 2014), livelihood vulnerability (Ren et al., 2020; Wang C. et al., 2022), vulnerability of land system (Lu et al., 2019), grassland ecosystem vulnerability (Guo et al., 2014), and vulnerability of the agricultural ecological environment vulnerability (Shu et al., 2020). However, current research on the vulnerability of karst areas cannot provide scientific guidance for sustainable development of village ecosystems in the KDC region. A large numbers of people live in karst mountain villages with poor soil and steep terrain, poor transportation infrastructure, and underdeveloped production technologies (Zhao and Hou, 2019), and the entire system is fragile. Karst landforms are formed by the development of soluble rocks such as limestone, dolomite, and gypsum. Karsts occur in over 10–15% of continental areas and are inhabited by approximately 17% of the world's population (Ford and Williams, 2013; Zhang et al., 2018). Because of special natural conditions and dense human activity, the karst ecosystem has degraded, which is mainly reflected in karst desertification, the most obvious outcome in South China Karst (Xiong and Chen, 2010). Karst desertification has resulted in fragile soil, vegetation, hydrology, and human environment in karst areas (Xiong and Chi, 2015). This seriously restricts the sustainability of the development of karst areas. Therefore, local governments and scientific researchers have actively promoted the control of karst desertification and achieved considerable results. However, the existing governance strategies designed for large-scale ecosystems are not applicable to village ecosystems. Therefore, it is necessary to study the vulnerability of village ecosystems and provide a scientific basis for the design of management strategies in for KDC.

3. Materials and methods

3.1. Study area

The South China Karst region, centered on the Guizhou Plateau, is the largest and most concentrated karst ecological vulnerable zone in the world and is facing serious karst desertification (Cheng et al., 2017; Chen Q. et al., 2021). This case study was conducted in the karst mountainous area of the Guizhou Plateau. Karst landforms are typical in Guizhou Province; there are karst distribution areas in 95% of the counties of the province, and 91.7% of the cultivated land, 88.3% of the rural population, 94% of the grain output, and 95.7% of the gross national product come from counties with karst distribution. The industry, agriculture, transportation, urban construction, tourism, ecology, and other aspects of the province are directly or indirectly affected by karst (Su and Zhu, 2000). Excessive human activities, such as deforestation and rapid population growth, have contributed to the degradation of the ecosystem quality in the region (Han et al., 2020). We selected village ecosystems at different levels of KDC as research cases (two villages selected in each KDC area) to investigate vulnerability levels and influencing factors. The none-potential KDC area is located in the east of Guizhou Province, it is typical dolomite karst, and it belongs to the subtropical humid monsoon climate. The potential-mild KDC area is located in the northwest Guizhou

Province. The landform type is mainly plateau mountain, and the rock type is mainly carbonate limestone. The moderate–severe KDC area is located on both sides of the Beipan River Canyon at the junction north of Zhenfeng County and south of Guanling County, Guizhou Province (Figure 1). The landform type is mainly a plateau canyon, the terrain fluctuates significantly, and the rock is mainly carbonate limestone.

3.2. Research framework and indicator system construction

The combination of human society and the environment has resulted in ecosystem vulnerability, and the factors influencing different ecosystem vulnerabilities vary (Kang et al., 2018). South China Karst has broken terrain, steep slopes, high vegetation sensitivity, low environmental carrying capacity, and poor land quality (Yang, 1990). Strongly developed underground cave systems lead to a lack of surface runoff, groundwater utilization is difficult, and engineering drought may occur (Liu C. et al., 2014; Qiu et al., 2021). According to the sensitive basic environmental characteristics, there is high system exposure and low resilience of village ecosystems in KDC. Therefore, we referred to relevant literature and selected the framework of E–S–LoR (Birkmann et al., 2013), and constructed an evaluation index system for the village ecosystem vulnerability of KDC with three dimensions of "exposure, susceptibility, and lack of resilience" and 26 indicators (Table 1). The details of the dimensions were as follows: (1) Susceptibility is the degree to which a system changes easily when disturbed, which reflects the stability of the underlying environment. Therefore, we chose the annual average temperature, annual precipitation, annual sunshine hours, altitude, average slope, terrain undulation, proportion of karst desertification area, soil erodibility K, landscape fragmentation, landscape diversity, and forest coverage as the indicators to measure susceptibility. (2) Lack of resilience is the system's self-adaptive capacity to deal with risk stress, including pre-event risk reduction for prevention, and post-event adaptive strategies. Herefore, we chose the length of roads open to traffic, livelihood strategies, net income per inhabitant, proportion of the population with high school education or above, number of pools, food production per unit of arable land area, area of returning farmland to forest, and annual control rate of karst desertification to reflect resilience. (3) Exposure reflects the extent to which an ecosystem is exposed to human activity and the external environment. The most direct manifestation is the pressure on production and population activity in the environment. We chose population density, population dependency ratio, proportion of building area, amount of fertilizer used on farmland, amount of pesticide used on farmland, proportion of labor outflow, and *per capita* cultivated land area to measure exposure.

3.3. Data sources

Basic natural and socio-economic data were used in this study. Basic natural data included meteorological, topographic, land-use type, and soil texture data. Socioeconomic data included demographic, economic income, production and population, and ecological governance-related data. Meteorological data were obtained from The

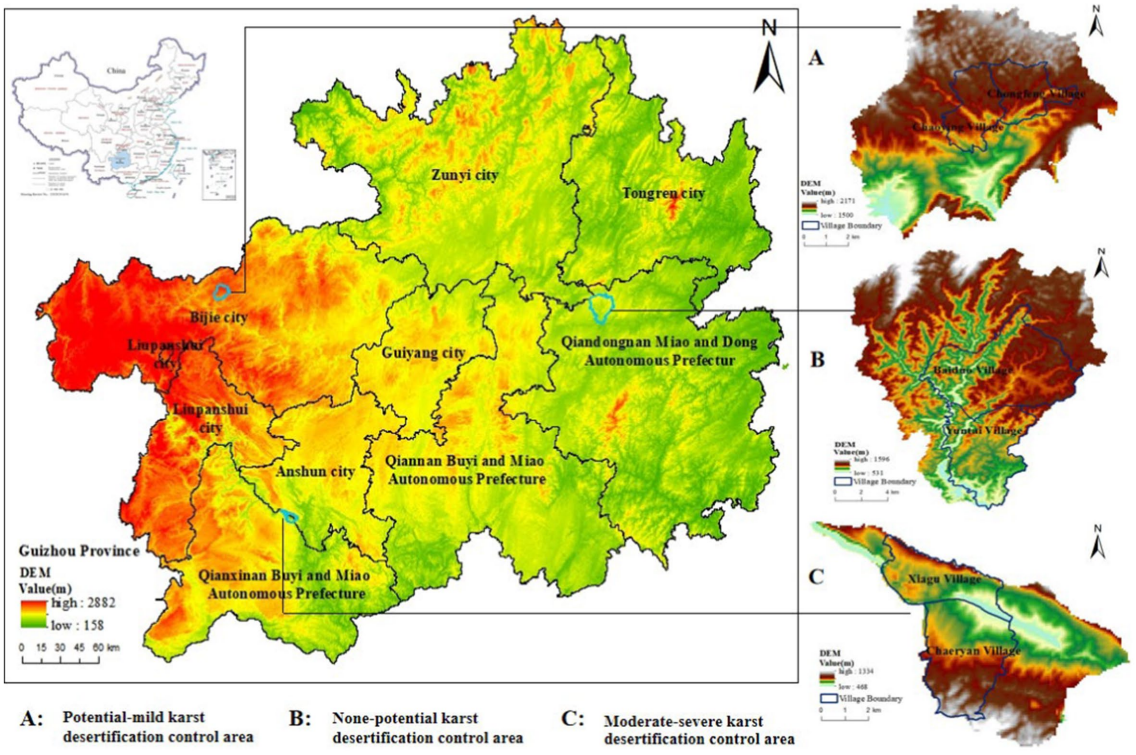

FIGURE 1
Location of study area.

10.3389/fevo.2023.1126659

TABLE 1 Village ecosystem vulnerability indicator weights.

Dimension layer	Indicator	Indicator attributes and numbers	Weights	Description of indicator
Susceptibility	Annual average temperature	X1 (−)	0.069	Indicates impact on villages of climate, light, temperature and precipitation factors affecting the quality of the ecosystem
	Annual precipitation	X2 (−)	0.044	
	Annual sunshine hours	X3 (−)	0.021	
	Altitude	X4 (+)	0.077	Indicates impact of terrain on ecosystem. The slope and terrain undulation will affect the stability of slope materials, and the altitude will affect the temperature and precipitation
	Average slope	X5 (+)	0.031	
	Terrain undulation	X6 (+)	0.042	
	Proportion of karst desertification area	X7 (+)	0.045	Indicates the degree of karst desertification of the village
	Soil erodibility-K	X8 (−)	0.029	Indicates the sensitivity to soil erosion
	Landscape fragmentation	X9 (+)	0.038	Reflects the degree of human disturbance on the landscape
	Landscape diversity	X10 (−)	0.046	Represents the richness and complexity of landscape types and reflects the diversity of ecosystem structure
	Forest coverage	X11 (+)	0.053	Reflects the vegetation and ecological environment under the KDC environment
Lack of resilience	Length of road open to traffic	X12 (−)	0.02	Reflects the interference intensity of human activity on the ecological environment. Data based on the statistics of village committees
	Livelihood strategies	X13 (−)	0.046	Indicates the degree of diversification of farmers' livelihood sources. Data based on interviews with farmers
	Net income per inhabitant	X14 (−)	0.043	Reflects the risk response ability of farmers. Data based on interviews with farmers
	Proportion of population with high school education or above	X15 (−)	0.02	Represents the education level of residents. Data based on the statistics of village committees
	Number of pools	X16 (−)	0.019	Reflects degree of residential water safety. Data based on the statistics of village committees
	Food production per unit of arable land area	X17 (−)	0.018	Indicates village land production capacity. Data based on the statistics of village committees
	Area of returning farmland to forest	X18 (−)	0.026	Reflects efforts of ecosystem governance. Data based on the statistics of village committees
	Annual control rate of karst desertification	X19 (−)	0.031	Reflects effect of karst desertification control. Data based on remote sensing image interpretation
Exposure	Density of population	X20 (+)	0.029	Reflects pressure of population on village ecological environment and resources. Data based on the statistics of village committees
	Dependency ratio of population	X21 (+)	0.028	Reflects the pressure of residents' life. Data based on the statistics of village committees
	Proportion of building area	X22 (−)	0.079	Represents the interference of human activities to the ecological environment. Data based on remote sensing image interpretation
	Amount of fertilizer used on farmland	X23 (+)	0.031	Use of chemical fertilizers and pesticides pollute the soil and water, thus damaging the ecosystem. Data based on interviews with farmers
	Amount of pesticide used on farmland	X24 (+)	0.051	
	Proportion of labor outflow	X25 (+)	0.041	Represents the loss of village labor force. Data based on the statistics of village committees
	Per capita cultivated land area	X26 (+)	0.023	Reflects the pressure of population on cultivated land resources. Data based on the statistics of village committees

"+" indicates that the indicator is positively correlated with vulnerability; "−" indicates that the indicator is negatively correlated with vulnerability.

China Meteorological Data Service Center.[1] We downloaded the 30 m resolution digital elevation model from the geospatial data cloud[2] and then used ArcGIS10.2 to extract the elevation, slope, and topographic relief. The land-use type data were interpreted using 30 m resolution remote sensing image data downloaded from the geospatial data cloud. Based on land-use data, we calculated landscape diversity and landscape fragmentation using Fragstats 4.2. We referred to the classification standard of karst desertification (Xiong et al., 2002) to extract karst desertification data in the study area. Soil type data were obtained from the Resource and Environment Science and Data Center of the Chinese Academy of Sciences.[3] Demographic, economic income, production, and ecological governance-related data were obtained through village group statistics and interviews with farmers. All the data were obtained in December 2020.

3.4. Methods

3.4.1. Data standardization

Because each indicator has different attributes and dimensions, it is necessary to standardize the original data before assessment. There are two types of relationships between an indicator and vulnerability: positive and negative (Zhao et al., 2018). Therefore, this study referred to relevant research and selected the following formula to normalize the indicators (Kan et al., 2018).

Positive indicators: (1).

$$X_{ij} = \frac{X - X_{\min}}{X_{\max} - X_{\min}} \tag{1}$$

Negative indicators: (2).

$$X_{ij} = \frac{X_{\max} - X}{X_{\max} - X_{\min}} \tag{2}$$

where X_{ij} is the standardized indicator value, X is the original value of the indicator, $X_{\min}$ is the minimum value of the original indicator, and $X_{\max}$ is the maximum value of the original indicator.

3.4.2. Weight calculation

The methods used to determine the weight of the indicator include the expert scoring method, analytic hierarchy process, entropy method, and principal component analysis (PCA). However, the entropy method is more objective and accurate. Therefore, this study used the entropy method to determine the weight coefficients of the indicators.

$$P_{ij} = \frac{X_{ij}}{\sum_{i=1}^{m} X_{ij}} \tag{3}$$

$$E_j = -\frac{1}{\ln m} \sum_{i=1}^{m} \mathrm{P_{ij}} \ln \mathrm{P_{ij}} \tag{4}$$

$$W_j = \frac{1 - E_j}{\sum_{i=1}^{n} (1 - E_j)} \tag{5}$$

where P_{ij} is the proportion of each indicator; E_j is the information entropy value of the indicator; W_j is the indicator weight; m is the sample size; and n is the number of indicators.

3.4.3. Vulnerability calculation

Based on the above weight calculation, we used Equation (6) to calculate the ecosystem vulnerability value of the village ecosystem of the KDC.

$$V = \sum_{j}^{n} W_j \cdot X_{ij} \tag{6}$$

where V is the vulnerability value: the higher the value of V, the higher the vulnerability level, W_j is the weight of the jth indicator, and X_{ij} is the standardized value of the jth indicator of the ith village.

3.4.4. Contribution calculation

In addition to analyzing its vulnerability level and spatial distribution, research on vulnerability should also analyze the causes of ecosystem vulnerability. To clarify the driving factors of the village ecosystem vulnerability of the KDC, we referred to the relevant literature to introduce a factor contribution model (Wang L. et al., 2022), Based on the results of the study, we selected the indicators with a contribution of more than 5% as the main contributing factors.

$$C_j = \frac{W_j \cdot I_j}{\sum_{j=1}^{m} W_j \cdot I_j} \times 100\% \tag{7}$$

$$U_r = \sum_{j=i}^{m} C_j \tag{8}$$

where C_j represents the contribution of the jth indicator to vulnerability, U_r represents the contribution of the rth element layer to vulnerability, I_j is the standardized value of the jth indicator, and W_j is the weight of the jth indicator.

4. Results

4.1. Village ecosystem vulnerability characteristics in KDC

The vulnerability values of the three KDC areas (six villages) are listed in Table 2. The average village ecosystem vulnerability values was 0.468, with a minimum value of 0.29, and the maximum value was 0.646. We referred to the relevant research (Zhang et al., 2017), and divided the vulnerability into five levels according to the vulnerability values: slight (0–0.2), mild (0.2–0.4), moderate (0.4–0.6), high (0.6–0.8), and extreme vulnerability (0.8–1). The vulnerability values of the Baiduo and Yuntai Villages in the none-potential KDC area were 0.318 and 0.29, respectively, indicating mild vulnerability. The vulnerability values of Chaoying and Chongfeng Villages in the potential-mild

1 http://data.cma.cn
2 http://www.gscloud.cn
3 http://www.resdc.cn

KDC area were 0.494 and 0.532, respectively, indicating moderate vulnerability. The vulnerability values of Chaeryan and Xiagu Villages in the moderate–severe KDC area were 0.527 and 0.646, respectively, indicating moderate and high vulnerability. Overall, the village ecosystem vulnerability of the KDC area was mild, moderate, and high.

4.2. Susceptibility value and contribution analysis

Based on statistical results (Figure 2A), the susceptibility values of Baiduo and Yuntai Villages in the none-potential KDC area were 0.167 and 0.105, respectively, whereas those of Chaoying and Chongfeng Villages in the potential-mild KDC area were 0.266 and 0.314, respectively. The susceptibility values of Chaeryan and Xiagu Villages in the moderate–severe KDC area were 0.204 and 0.289, respectively. We found that the susceptibility of the village ecosystem in the none-potential KDC area was the smallest, whereas that of the mild-potential KDC area was the highest. The village ecosystem susceptibility contributions in the none-potential karst desertification areas were 52.5 and 36.3%, and in the potential-mild karst desertification areas were 53.9 and 58.9%, respectively. The contributions in the moderate–severe karst desertification areas were 38.7 and 44.8%, respectively (Figure 2B).

TABLE 2 Village ecosystem vulnerability level.

The study area		Vulnerability value	Vulnerability level
None-potential KDC area	Baiduo Village	0.318	Mild vulnerability
	Yuntai Village	0.29	Mild vulnerability
Potential-mild KDC area	Chaoying Village	0.494	Moderate vulnerability
	Chongfeng Village	0.532	Moderate vulnerability
Moderate-severe KDC area	Chaeryan Village	0.527	Moderate vulnerability
	Xiagu Village	0.646	High vulnerability

4.3. Lack of resilience value and contribution analysis

The lack of resilience values for village ecosystems in the different KDC areas differed (Figure 3A). The lack of resilience values were smallest for Baiduo and Yuntai Villages in the none-potential KDC area at 0.072 and 0.078, respectively. The lack of resilience values were largest in Chaoying and Chongfeng Villages in the potential-mild KDC area, at 0.154 and 0.171, respectively. The lack of resilience values of Chaeryan and Xiagu Villages in the moderate–severe KDC area were 0.121 and 0.145, respectively, which fall between the other two grades of karst desertification areas. The contributions of the lack of resilience of the village ecosystems of the none-potential KDC areas were 22.7 and 27%, respectively, in the potential-mild KDC area were 31.1 and 32.1%, respectively, and 23 and 22.4% in the moderate–severe KDC area, respectively (Figure 3B).

4.4. Exposure value and contribution analysis

Through the analysis of the exposure of the study area (Figure 4A), we found that the exposure values between the village ecosystems of the KDC displayed large differences, with a minimum exposure value of 0.048 and a maximum value of 0.211. The exposure values of the

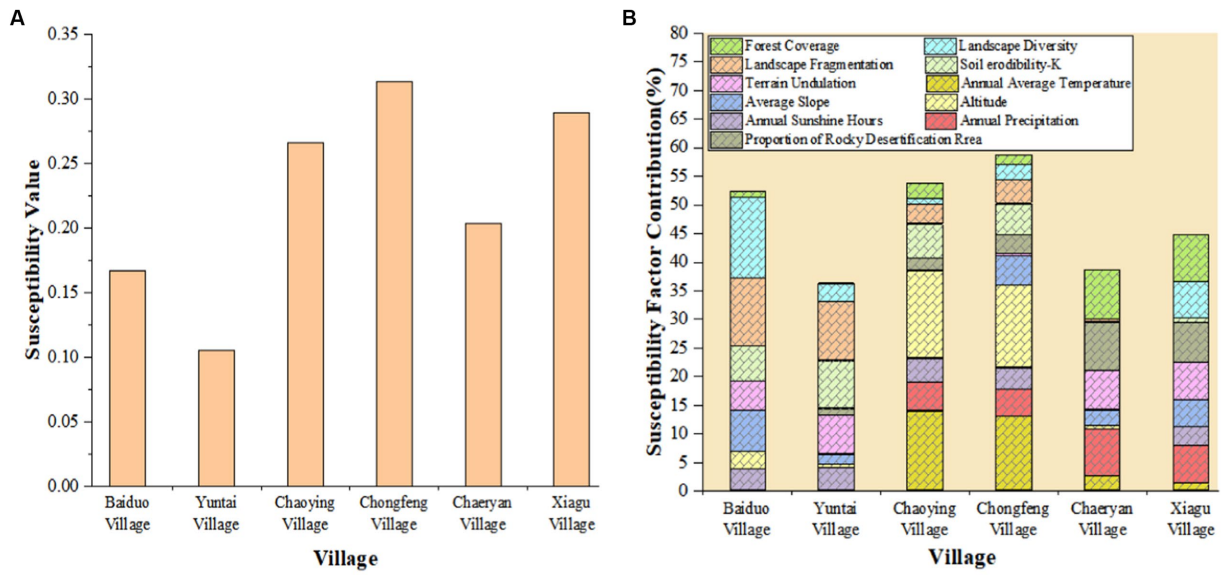

FIGURE 2
Susceptibility analysis of villages ecosystem in the KDC. **(A)** susceptibility values. **(B)** Contribution of susceptibility factor.

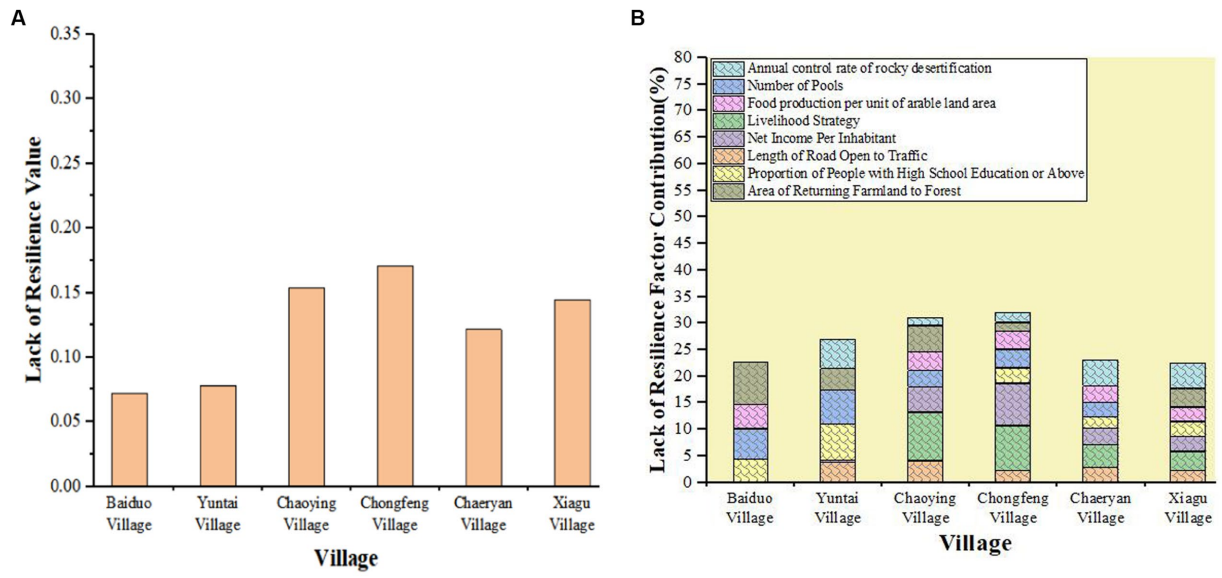

FIGURE 3
Lack of resilience analysis of villages ecosystem in the KDC. **(A)** Lack of resilience values. **(B)** Lack of resilience factors contribution.

Baiduo and Yuntai Villages in the none-potential KDC area were 0.079 and 0.106, respectively. The exposure values of the village ecosystems in the potential-mild karst desertification area were the lowest, and the exposure values of the Chaoying and Chongfeng Villages were 0.074 and 0.048, respectively. The exposure values of the village ecosystem in the moderate–severe KDC area were the largest, and the exposure values of the Chaeryan and Xiagu Villages were 0.202 and 0.211, respectively. In general, there was little difference in the exposure values of village ecosystems in the same KDC area. The exposure values of village ecosystems in different KDC areas were in the order of moderate–severe KDC areas > none-potential KDC areas > potential-mild KDC areas. The contribution of exposure differs from that of vulnerability. The exposure contribution of the village ecosystems in the none-potential KDC area was 24.8 and 36.7%, respectively, in the potential-mild KDC area, it was 15 and 9%, respectively, and in the moderate–severe KDC areas, it was 38.3 and 32.7%, respectively (Figure 4B).

5. Discussion

5.1. Causes of village ecosystem vulnerability

It is very important to reveal the level and influencing factors of village ecosystem vulnerability in KDC to further restore vulnerable karst ecosystems. The differences in the natural and socio-economic conditions of village ecosystems in different KDC areas lead to significant spatial differences in vulnerability. According to our research, the vulnerability level of the village ecosystems of KDC in South China Karst showed mild and moderate vulnerability. The unique geology and lithology are the basis of ecosystem vulnerability, and the unreasonable human social and economic activities are the external pressure factors of ecosystem vulnerability in the South China Karst (Li et al., 2002).

We calculated the contribution rate of each indicator to the vulnerability of the village ecosystem and screened factors with a large contribution rate. In the none-potential KDC area, the maximum contribution rates of landscape diversity, landscape crushing, soil corrosive factor, slope (Figure 2B), and labor loss factors were 14.3, 11.8, 8.4, 7.1, and 14.1%, respectively. The maximum contribution rates of pesticide and fertilizer use were 8 and 9.7%, respectively (Figure 4B). In the potential-mild KDC area, the maximum contribution rates of the annual average temperature, altitude factor, maximum soil corrosive factor (Figure 2B), livelihood strategies, *per capita* net income (Figure 3B), and population density were 14.1, 15.2, 5.9, 9.2, 8, and 5.8%, respectively (Figure 4B). In the moderate–severe KDC area, the maximum contribution rates of precipitation, topography, karst desertification, landscape diversity, forest coverage (Figure 2B), construction land, and pesticides were 8.3, 6.9, 8.3, 6.3, 8.7, 15, and 7.9%, respectively (Figure 4B). The terrain significantly affects the stability of the slope material and conditions for agricultural farming. Rainfall and temperature have an important impact on ecosystem stability. The landscape pattern index, degree of karst desertification, and forest coverage were the main factors that causeing ecosystem sensitivity. Soil erodibility is an important factor affecting soil and water loss. The use of chemical fertilizers and pesticides affects the quality of cultivated land. Livelihood strategies, population density, and labor loss have caused pressure on local residents, increasing their exposure. A low *per capita* income leads to a lower adaptability of farmers.

In none-potential KDC areas, local residents have a low level of education. To increase agricultural output, farmers use more pesticides and fertilizers during cultivation. There are few employment opportunities in the countryside; many young people choose to go away for work, leaving behind many older adults and children who are exposed to uncertain risks. The potential-mild KDC area is high in altitude, the average annual temperature is low, and the annual precipitation is insufficient. Serious soil erosion, low labor efficiency, and low economic income mainly rely on labor exports and

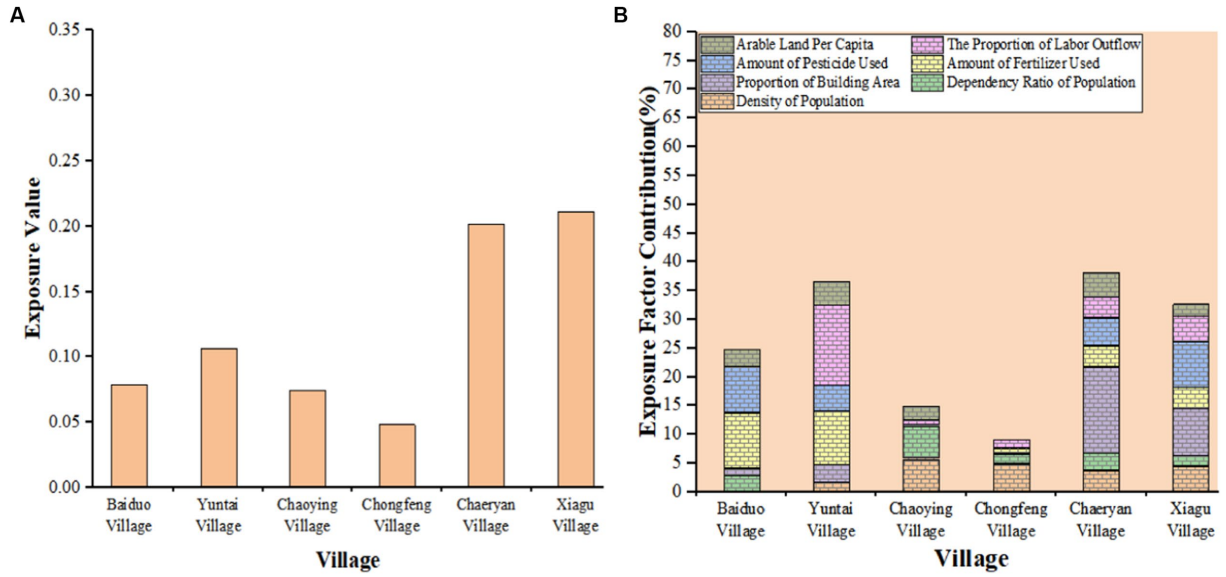

FIGURE 4
Exposure analysis of villages ecosystem in the KDC. **(A)** Exposure values. **(B)** Exposure factors contribution.

small-scale farming, and the incidence of poverty is extremely high (Ji et al., 2020; Ren et al., 2020). Our survey found that most local farmers' livelihoods came from labor output acquisition income, and small-scale planting and breeding industries, while the population pressure was high. The moderate–severe KDC area surface is crushed, the terrain of the area is steep, the surface soil and soil reservation capacity is insufficient (Mu et al., 2021), and annual precipitation is low. Karst in the region has a strong role; the soil formation rate is low, and a large amount of unreasonable reclamation in the early days has led to poor soil and discontinuous soil cover (Ren et al., 2020). This results in poor landscape diversity and forest cover. This shows serious karst desertification, which is difficult to control. To facilitate water access and agricultural cultivation, many people are concentrated in the valley area, accompanied by many construction facilities. Farmers use many pesticides to increase the output of Chinese red pepper and dragon fruit. According to the analysis of the difference in indicator vulnerability values (Figure 5), we found that topography, climate, forest coverage, landscape pattern, karst desertification degree, soil erodibility, KDC rate, production and construction activity, livelihood, and *per capita* net income were the key factors leading to the differences in village ecosystem vulnerability in the three different levels of KDC areas.

5.2. Comparison with previous studies

In recent years, scholars have conducted relevant research on karst ecological vulnerability. These studies included vulnerability and impact-factor analyses. Chen (2007) pointed out that owing to the deep soil layer and continuous soil cover in the karst trough area, there is a slight vulnerability. This is consistent with the results of our study of the karst plateau trough area (none-potential KDC area). Wang et al. (2021) studied the ecological vulnerability of karst areas in Yunnan Province, China, and revealed high vulnerability and extreme vulnerability in moderate-to-severe karst desertification areas. However, our results show that the moderate-to-severe karst desertification areas are moderately vulnerable and highly vulnerable. This may be due to the differences in KDC measures, leading to different ecological restoration effects and different degrees of vulnerability. Guo et al. (2017) analyzed the vulnerability level and influencing factors were analyzed of mountain ecosystem in Southwest China Karst using the remote sensing method, and found that the vulnerability of regions with strong karst development, low vegetation coverage, and high bedrock exposure rate was higher than that of regions with high vegetation coverage, low karst desertification and better ecological environment in karst mountain areas in southwest China. The results of this study are consistent with the actual vulnerability of the village ecosystems in the three KDC areas. Many studies demonstrated that vegetation cover factors, precipitation, topography, soil erosion factors, and the degree of karst desertification on the impact of karst ecosystem vulnerability is more significant (Wang and Yu, 2005; Chen, 2007; Wang et al., 2021). However, the KDC village ecosystem was characterized by karst ecosystem vulnerability. Owing to the differences in spatial scale, data accuracy, and measurement indicators, large-scale studies cannot reflect the characteristics of small-scale ecosystem vulnerability. For example, the influence mechanism of farmers' production activities, living activities, and socio-economic development on the vulnerability of karst ecosystems is a problem that has not been investigated in current large-scale research. The study of vulnerability at the village ecosystem scale can accurately reveal the factors influencing vulnerability. This has important significance for providing guidance to the government in formulating planning policies, which is also the significance and necessity of small-scale research.

5.3. Adaptive governance measures

Various ecosystem problems caused by karst desertification seriously affect the lives of local residents and hinder the coordinated development of the local socioeconomic and ecological environments

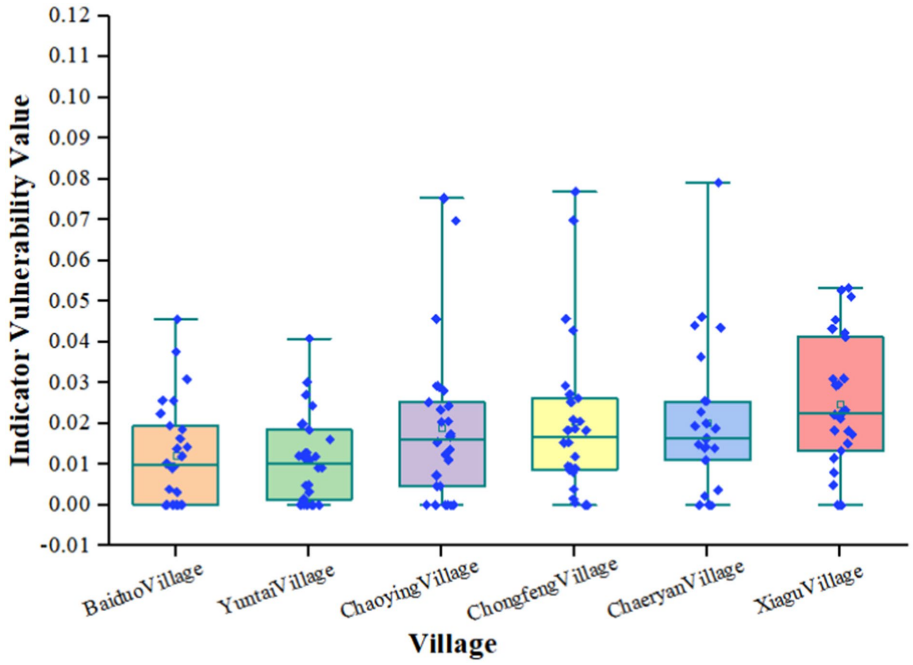

FIGURE 5
Indicator vulnerability value difference.

(Xiong and Chi, 2015). Over time, humans have attempted to control the deterioration of karst desertification in karst areas. For example, the Italian government restricts the cutting of firewood and prohibits goat breeding (Ford and Williams, 2013). KDC mainly adopts the measures of water storage, land management, returning farmland to forest and grassland, afforestation, three-dimensional ecological agriculture, and agricultural and forestry management development in the South China Karst (Xiong et al., 2006; Jiang et al., 2009). However, different levels of vulnerability still exist in rural areas of the KDC environment. Therefore, in view of the current situation of the village ecosystems of KDC, we should concentrate on both ecological management and socio-economic development, focusing on the sustainability of village development and proposing feasible adaptive management measures. In none-potential KDC areas, existing vegetation coverage should be maintained, the population scale should be controlled, population quality should be improved, and the rural labor force should be retained. Organic fertilizers and non-residual pesticides should be popularized and the use of stereoscopic agriculture in mountains should be developed. Forestry should be developed on mountain tops, the middle area of the mountain should be used for fruit industry development, and crop cultivation and livestock and poultry breeding should be carried out at the foot of the mountain and in low flat areas. The development of eco-tourism and the promotion of the sale of ecological products could promote economic development of the eco-industry. In mild-potential and moderate–severe KDC areas, the population size should be controlled, population quality should be improved, and population skills training should be strengthened along with the implementation of ecological and water storage irrigation engineering measures. The selection of an economic fruit forest with drought tolerance, calcium preference, and developed root systems for planting, implementing mountain closures for afforestation, and returning farmland to forests to increase vegetation coverage and reduce water and soil loss are recommended while popularizing the use of organic fertilizers and non-residual pesticides and developing stereoscopic agriculture on mountains. Projects for transforming slopes into terraces and building of water-saving, intensive agricultural production systems should be implemented. In addition, unreasonable human activities, such as grazing and felling of trees, should be prohibited in stone and semi-stone mountainous areas. Local scientific research departments should increase their investments in scientific and technological research and investigate new processed agricultural products to increase their added value. Local governments should take advantage of local natural conditions to build research and tourism bases with karst characteristics and promote local employment while simultaneously promoting the coordinated development of socio-economic and ecological factors.

In general, it is necessary to change the current development mode and concurrently improve the ecological and socio-economic benefits to promote high-quality and sustainable development of rural areas in karst desertification areas. Talents, technology, capital, and superior management modes are necessary to achieve high-quality and sustainable development, enhancing the management ability of grassroots leaders, strengthening the training of farmers' knowledge and skills, and comprehensively enhancing the production skills and environmental awareness of residents. Based on the advantages of rural resource endowment, we should optimize the allocation of resources, build a sustainable production system, integrate various industries, strengthen the construction of rural industrial chains, and promote the transformation and upgrading of the industrial structure and technological innovation. A reciprocal mechanism between rural industry development and farmers' interests should be established to promote the integration and development of the rural industry. We should vigorously develop the ecological industry and promote the

specialization and integration of production, processing, storage, transportation, and sales of ecological products. Furthermore, amendments to the quality requirements of ecological products should focus on improvements in product quality and economic benefits. We should rationally plan land-use patterns and optimize the spatial structure of rural production, life, and ecology. The quality of the ecological environment and the service function of the system should be improved. We should abandon the development model of destroying the environment for economic benefit, build a virtuous rural system, and form a local sustainable and high-quality development model.

5.4. Future research

Current vulnerability research has been applied to ecological, natural, and societal subsystems, and coupled socio-ecological systems (Gallopín, 2006). Research on the vulnerability of coupled socio-ecological systems has not yet resulted in the formulation of a perfect theoretical system, and is not unified in terms of concept connotation, research framework, and evaluation methods. Analysis of the process and mechanism of human–environment coupling is still an unresolved issue in research on ecosystem vulnerability (Tian and Chang, 2012). Currently, empirical research is mostly quantitative, the research methods are immature, existing models are used to build the index system, and there is a lack of innovation and lack of pertinence (Tang et al., 2022). Moreover, there is a lack of analysis on the formation process and internal mechanisms of ecosystem vulnerability. The research mainly focuses on a particular spatial and temporal scale and lacks a dynamic comparative analysis of vulnerability at different spatial and temporal scales (Huang et al., 2014). In future research, it is necessary to improve the indicator system, research models, and innovative research methods. We should pay attention to the process of the comprehensive action of human and natural factors and analyze the impact of the human–environment coupling mechanism on the formation mechanism of ecosystem vulnerability. We need to extend the spatial and temporal scales of research and use the 3S technology to reveal the spatial and temporal dynamic change processes of ecosystem vulnerability to realize dynamic monitoring and prediction. We should analyze the interaction mechanisms of material flow, energy flow, information flow, and ecological processes in the social-ecological system, and the relationship between stakeholders and ecological processes, to reveal the coupling mode of social economic factors and ecological environment factors. We should explore the breakthrough point of the social-ecological system from one steady state to another to reveal the threshold of vulnerability of the social-ecological system. The mutual feedback mechanism of the relationship between social activities and ecological environment degradation or restoration should be studied to explore the mode of balance and coordination between human production, living activities, and ecological restoration to combine theoretical research and practical applications and provide a decision-making basis for promoting sustainable governance of fragile ecosystems.

6. Conclusion

In this study, we analyzed the vulnerability level and driving factors of village ecosystems in different KDC based on the framework of "exposure–susceptibility–lack of resilience." Finally, we propose sustainable governance strategies for the village ecosystems of KDC areas. The results showed that topography, climate, and land cover were the main natural factors affecting the vulnerability of villages to KDC. Social and economic activities are external stress factors for of village ecosystem vulnerability in KDC. Due to differences in geographical factors, the level and influencing factors of village ecosystem vulnerability in different KDC may vary. Villages in the none-potential KDC have a mild vulnerability level, villages in the potential-mild KDC are moderately vulnerable, and villages in moderate–severe KDC have moderate and high vulnerability levels. Landscape diversity, fragmentation, soil erodibility, labor loss rate, slope, and the use of pesticides and fertilizers are the main reasons for the vulnerability of village ecosystems in the none-potential KDC. The average annual temperature, altitude, soil erodibility, livelihood strategies, *per capita* income, and population density were the main factors affecting village ecosystem vulnerability in the potential-mild KDC. Annual precipitation, topographic relief, karst desertification degree, landscape diversity, forest coverage, construction land proportion, and pesticide usage are the main factors affecting village ecosystem vulnerability in moderate–severe KDC. We found that terrain, climate, forest coverage, landscape pattern, karst desertification degree, soil erodibility, KDC effect, production and construction activity, livelihood strategies, and *per capita* net income were the key factors influencing the differences in village ecosystem vulnerability in KDC. Finally, our suggestions for the sustainable development of village ecosystems in KDC are to govern the ecological environment, control population size, improve population quality, retain more labor, develop local characteristic industries, increase employment opportunities, increase residents' economic income, promote the development of the ecological industry to drive economic increase, and promote sustainable development of village ecosystems in KDC.

Data availability statement

The original contributions presented in the study are included in the article/Supplementary material, further inquiries can be directed to the corresponding author.

Author contributions

KX conceived the framework, secured funding, and oversaw the entire project. JT, QWa, YC, and QWu collected data. JT analyzed the data and wrote the manuscript. KX provided comments. KX and JT reviewed the final manuscript. All authors have read and agreed to the published version of the manuscript.

Funding

This research was supported by the Key Science and Technology Program of Guizhou Province (no. 5411 2017 Qiankehe Pingtai Rencai), the China Overseas Expertise Introduction Program for Discipline Innovation (D17016) and Natural Science Foundation of Guizhou Province (grant no. Qiankehe Jichu -ZK[2022]317).

Conflict of interest

The authors declare that the research was conducted in the absence of any commercial or financial relationships that could be construed as a potential conflict of interest.

Publisher's note

All claims expressed in this article are solely those of the authors and do not necessarily represent those of their affiliated organizations, or those of the publisher, the editors and the reviewers. Any product that may be evaluated in this article, or claim that may be made by its manufacturer, is not guaranteed or endorsed by the publisher.

Supplementary material

The Supplementary material for this article can be found online at: https://www.frontiersin.org/articles/10.3389/fevo.2023.1126659/full#supplementary-material

References

Ahmad, D., and Afzal, M. (2021). Flood hazards, human displacement and food insecurity in rural riverine areas of Punjab, Pakistan: policy implications. *Environ. Sci. Pollut. Res.* 28, 10125–10139. doi: 10.1007/s11356-020-11430-7

Bavinck, M., Berkes, F., Charles, A., Dias, A. C. E., Doubleday, N., Nayak, P., et al. (2017). The impact of coastal grabbing on community conservation–a global reconnaissance. *Marit. Stud.* 16, 1–17. doi: 10.1186/s40152-017-0062-8

Birkmann, J., Cardona, O. D., Carreño, M. L., Barbat, A. H., Pelling, M., Schneiderbauer, S., et al. (2013). Framing vulnerability, risk and societal responses: the MOVE framework. *Nat. Haz.* 67, 193–211. doi: 10.1007/s11069-013-0558-5

Brunner, S. H., and Grêt-Regamey, A. (2016). Policy strategies to foster the resilience of mountain social-ecological systems under uncertain global change. *Environ. Sci. Pol.* 66, 129–139. doi: 10.1016/j.envsci.2016.09.003

Chen, H. (2007). The fragility characteristics and ecological control of karst ecological environment—a case study of Guizhou provinc. *J. Mt. Agric. Biol.* 3, 244–247+260. doi: 10.3969/j.issn.1008-0457.2007.03.013

Chen, X., Li, X., Eladawy, A., Yu, T., and Sha, J. (2021). A multi-dimensional vulnerability assessment of Pingtan Island (China) and Nile Delta (Egypt) using ecological sensitivity-resilience-pressure (SRP) model. *Hum. Ecol. Risk Assess. Int. J.* 27, 1860–1882. doi: 10.1080/10807039.2021.1912585

Chen, Q., Lu, S., Xiong, K., and Zhao, R. (2021). Coupling analysis on ecological environment fragility and poverty in South China karst. *Environ. Res.* 201:111650. doi: 10.1016/j.envres.2021.111650

Chen, Y., Xiong, K., Ren, X., and Cheng, C. (2021). Vulnerability comparison between karst and non-karst nature reserves—with a special reference to Guizhou province, China. *Sustainability* 13:2442. doi: 10.3390/su13052442

Chen, Y., Xiong, K., Ren, X., and Cheng, C. (2022). An overview of ecological vulnerability: a bibliometric analysis based on the web of science database. *Environ. Sci. Pollut. Res.* 29, 12984–12996. doi: 10.1007/s11356-021-17995-1

Chen, J., Yang, X., Yin, S., Wu, K., Deng, M., and Wen, X. (2018). The vulnerability evolution and simulation of social-ecological systems in a semi-arid area: a case study of Yulin City, China. *J. Geogr. Sci.* 28, 152–174. doi: 10.1007/s11442-018-1465-1

Cheng, F., Lu, H., Ren, H., Zhou, L., Zhang, L., Li, J., et al. (2017). Integrated emergy and economic evaluation of three typical rocky desertification control modes in karst areas of Guizhou Province, China. *J. Clean. Prod.* 161, 1104–1128. doi: 10.1016/j.jclepro.2017.05.065

Colburn, L. L., Jepson, M., Weng, C., Seara, T., Weiss, J., and Hare, J. A. (2016). Indicators of climate change and social vulnerability in fishing dependent communities along the eastern and gulf coasts of the United States. *Mar. Policy* 74, 323–333. doi: 10.1016/j.marpol.2016.04.030

Dasgupta, S., and Badola, R. (2020). Indicator-based assessment of resilience and vulnerability in the Indian Himalayan region: a case study on socio-economy under different scenarios. *Sustainability.* 12:6938. doi: 10.3390/su12176938

Easterling, D. R., Meehl, G. A., Parmesan, C., Changnon, S. A., Karl, T. R., and Mearns, L. O. (2000). Climate extremes: observations, modeling, and impacts. *Science* 289, 2068–2074. doi: 10.1126/science.289.5487.2068

Foley, J. A., DeFries, R., Asner, G. P., Barford, C., Bonan, G., Carpenter, S. R., et al. (2005). Global consequences of land use. *Science* 309, 570–574. doi: 10.1126/science.1111772

Ford, D., and Williams, P. D. (2013). *Karst hydrogeology and geomorphology*. New Jersey, USA: John Wiley & Sons.

Gallopín, G. C. (2006). Linkages between vulnerability, resilience, and adaptive capacity. *Global. Environ. Chang.* 16, 293–303. doi: 10.1016/j.gloenvcha.2006.02.004

Ghosh, M., and Ghosal, S. (2021). Climate change vulnerability of rural households in flood-prone areas of Himalayan foothills, West Bengal, India. *Enviro. Dev. Sustain.* 23, 2570–2595. doi: 10.1007/s10668-020-00687-0

Guo, J., and Huang, Y. (2016). Assesment of ecosystem vulnerability in pingtan county based on AHP and fuzzy comprehensive evaluation. *Prot. Forest Sci. Technol.* 9, 18–21. doi: 10.13601/j.issn.1005-5215.2016.09.006

Guo, B., Jiang, L., Luo, W., Yang, G., and Ge, D. (2017). Study of an evaluation method of ecosystem vulnerability based on remote sensing in a southwestern karst mountain area under extreme climatic conditions. *Acta Ecol. Sin.* 37, 7219–7231. doi: 10.5846/stxb201608111651

Guo, B., Zang, W., and Luo, W. (2020). Spatial-temporal shifts of ecological vulnerability of Karst Mountain ecosystem-impacts of global change and anthropogenic interference. *Sci. Total Environ.* 741:140256. doi: 10.1016/j.scitotenv.2020.140256

Guo, B., Zhou, Z., Su, W., Chen, Q., and Wei, X. (2014). Evaluation of ecological vulnerability of karst grassland based on grid GIS. *Bull. Soil Water Conserv.* 34, 204–207. doi: 10.13961/j.cnki.stbctb.2014.02.043

Hagenlocher, M., Renaud, F. G., Haas, S., and Sebesvari, Z. (2018). Vulnerability and risk of deltaic social-ecological systems exposed to multiple hazards. *Sci. Total Environ.* 631-632, 71–80. doi: 10.1016/j.scitotenv.2018.03.013

Han, H., Liu, Y., Gao, H., Zhang, Y. J., Wang, Z., and Chen, X. Q. (2020). Tradeoffs and synergies between ecosystem services: a comparison of the karst and non-karst area. *J. Mt. Sci.* 17, 1221–1234. doi: 10.1007/s11629-019-5667-5

Hong, W., Jiang, R., Yang, C., Zhang, F., Su, M., and Liao, Q. (2016). Establishing an ecological vulnerability assessment indicator system for spatial recognition and management of ecologically vulnerable areas in highly urbanized regions: a case study of Shenzhen, China. *Ecol. Indic.* 69, 540–547. doi: 10.1016/j.ecolind.2016.05.028

Hu, X., Ma, C., Huang, P., and Guo, X. (2021). Ecological vulnerability assessment based on AHP-PSR method and analysis of its single parameter sensitivity and spatial autocorrelation for ecological protection–a case of Weifang City, China. *Ecol. Indic.* 125:107464. doi: 10.1016/j.ecolind.2021.107464

Huang, G. (2019). Functions, problems and countermeasures of China's rural ecosystems. *Chin. J. Eco-Agric.* 27, 177–186. doi: 10.13930/j.cnki.cjea.180582

Huang, X., Huang, X., Cui, C., and Yang, X. (2014). The concept, analytical framework and assessment method of social vulnerability. *Prog. Geogr.* 33, 1512–1525. doi: 10.11820/dlkxjz.2014.10.008

Jamshed, A., Birkmann, J., Rana, I. A., and McMillan, J. M. (2020). The relevance of city size to the vulnerability of surrounding rural areas: an empirical study of flooding in Pakistan. *Int. J. Disaster Risk Reduct.* 48:101601. doi: 10.1016/j.ijdrr.2020.101601

Ji, C., Xiong, K., Yu, Y., Zhang, Y., and Yang, C. (2020). Photosynthetic characteristics and environmental response of plants in rocky desertification area of karst plateaus. *Southwest. Chin. J. Agr. Sci.* 33, 747–753. doi: 10.16213/j.cnki.scjas.2020.4.010

Jia, Y., Hu, J., Xie, S., Qiao, H., and Liu, D. (2021). Vulnerability and influence mechanisms of social-ecosystem in poor mountains tourism destinations. *Hum. Geogr.* 36, 155–164. doi: 10.13959/j.issn.1003-2398.2021.01.018

Jiang, Z., Li, X., Zeng, F., Qiu, S., Deng, Y., Luo, W., et al. (2009). Study of fragile ecosystem reconstruction technology in the karst Peak-Cluster Mountain. *Acta Geosci. Sin.* 30, 155–166. doi: 10.3321/j.issn:1006-3021.2009.02.003

Kan, A., Li, G., Yang, X., Zeng, Y. L., Tesren, L., and He, J. (2018). Ecological vulnerability analysis of Tibetan towns with tourism-based economy: a case study of the Bayi District. *J. Mt. Sci.* 15, 1101–1114. doi: 10.1007/s11629-017-4789-x

Kang, H., Tao, W., Chang, Y., Zhang, Y., Xuxiang, L., and Chen, P. (2018). A feasible method for the division of ecological vulnerability and its driving forces in southern Shaanxi. *J. Clean. Prod.* 205, 619–628. doi: 10.1016/j.jclepro.2018.09.109

Karuppusamy, B., Leo George, S., Anusuya, K., Venkatesh, R., Thilagaraj, P., Gnanappazham, L., et al. (2021). Revealing the socio-economic vulnerability and multi-hazard risks at micro-administrative units in the coastal plains of Tamil Nadu, India. *Geomat. Nat. Haz. Risk* 12, 605–630. doi: 10.1080/19475705.2021.1886183

Keshavarz, M., and Moqadas, R. S. (2021). Assessing rural households' resilience and adaptation strategies to climate variability and change. *J. Arid Environ.* 184:104323. doi: 10.1016/j.jaridenv.2020.104323

Koehn, L. E., Nelson, L. K., Samhouri, J. F., Norman, K. C., Jacox, M. G., Cullen, A. C., et al. (2022). Social-ecological vulnerability of fishing communities to climate change: a US west coast case study. *PLoS One* 17:e0272120. doi: 10.1371/journal.pone.0272120

Lee, C. K. F., Duncan, C., Owen, H. J. F., and Pettorelli, N. (2018). A new framework to assess relative ecosystem vulnerability to climate change. *Conserv. Lett.* 11:e12372. doi: 10.1111/conl.12372

Li, H. (2020). Rural settlements research from the perspective of resilience theory. *Sci. Geogr. Sin.* 40, 556–562. doi: 10.13249/j.cnki.sgs.2020.04.007

Li, Y., Fan, Q., Wang, X., Xi, J., Wang, S., and Yang, J. (2015). Spatial and temporal differentiation of ecological vulnerability under the frequency of natural hazard based on SRP model: a case study in Chaoyang county. *Sci. Geogr. Sin.* 8, 120–126. doi: 10.1007/s12182-011-0124-2

Li, Y., Hou, J., and Xie, D. (2002). The recent development of research on karst ecology in Southwest China. *Sci. Geogr. Sin.* 3, 365–370. doi: 10.3969/j.issn.1000-0690.2002.03.019

Li, H., Hui, Y., and Pan, J. (2022). Evolution and influencing factors of social-ecological system vulnerability in the wuling mountains area. *Int. J. Environ. Res. Public Health* 19:11688. doi: 10.3390/ijerph191811688

Li, Q., Shi, X., and Wu, Q. (2021). Effects of protection and restoration on reducing ecological vulnerability. *Sci. Total Environ.* 761:143180. doi: 10.1016/j.scitotenv.2020.143180

Li, H., and Song, W. (2021). Spatiotemporal distribution and influencing factors of ecosystem vulnerability on Qinghai-Tibet plateau. *Int. J. Environ. Res. Public Health* 18:6508. doi: 10.3390/ijerph18126508

Liu, S., Ge, J., Li, W., and Bai, M. (2020). Historic environmental vulnerability evaluation of traditional villages under geological hazards and influencing factors of adaptive capacity: a district-level analysis of Lishui, China. *Sustainability.* 12:2223. doi: 10.3390/su12062223

Liu, Y., and Li, Y. (2017). Revitalize the world's countryside. *Nature* 548, 275–277. doi: 10.1038/548275a

Liu, C., Lv, D., Chen, H., and Nie, Y. (2014). Causes for the eco-environment vulnerability of the karst area in Southwest China. *J. Geol. Haz. Environ. Pres.* 25, 49–53. doi: 10.3969/j.issn.1006-4362.2014.02.010

Liu, H., Wang, N., Xie, J., and Zhu, J. (2014). Assessment of ecological vulnerability based on fuzzy comprehensive evaluation in Weihe River basin. *J. Shenyang Agric. Univ* 45, 73–77. doi: 10.3969/j.issn.1000-1700.2014.01.016

Liu, H. L., Willems, P., Bao, A. M., Wang, L., and Chen, X. (2016). Effect of climate change on the vulnerability of a socio-ecological system in an arid area. *Glob. Planet. Chang.* 137, 1–9. doi: 10.1016/j.gloplacha.2015.12.014

Lu, Q., Zhao, Y., and Ge, Y. (2019). Vulnerability assessment of land system in karst mountainous area basedon grid: a case of puding county in Guizhou. *Environ. Sci. Technol.* 42, 221–229. doi: 10.19672/j.cnki.1003-6504.2019.09.032

Luo, D., and Zhang, H. (2018). Grey incidence analysis method for regional drought vulnerability. *J. North China Univ. Water Resour. Electr. Power.* 39, 61–67. doi: 10.3969/j.issn.1002-5634.2018.03.011

Malekmohammadi, B., and Jahanishakib, F. (2017). Vulnerability assessment of wetland landscape ecosystem services using driver-pressure-state-impact-response (DPSIR) model. *Ecol. Indic.* 82, 293–303. doi: 10.1016/j.ecolind.2017.06.060

Malmborg, K., Sinare, H., Enfors Kautsky, E., Ouedraogo, I., and Gordon, L. J. (2018). Mapping regional livelihood benefits from local ecosystem services assessments in rural Sahel. *PLoS One* 13:e0192019. doi: 10.1371/journal.pone.0192019

Marín, A. I., Andreo, B., and Mudarra, M. (2015). Vulnerability mapping and protection zoning of karst springs. Validation by multitracer tests. *Sci. Total Environ.* 532, 435–446. doi: 10.1016/j.scitotenv.2015.05.029

Meng, L., Huang, J., and Dong, J. (2018). Assessment of rural ecosystem health and type classification in Jiangsu province, China. *Sci. Total Environ.* 615, 1218–1228. doi: 10.1016/j.scitotenv.2017.09.312

Miller Hesed, C. D., Van Dolah, E. R., and Paolisso, M. (2020). Engaging faith-based communities for rural coastal resilience: lessons from collaborative learning on the Chesapeake Bay. *Clim. Chang.* 159, 37–57. doi: 10.1007/s10584-019-02638-9

Mu, Y., Liu, Z., Li, Y., and Zhu, D. (2021). Characteristics of soil temperature variation in karst area and its relationship with environmental factors. *Acta Ecol. Sin.* 41, 2738–2749. doi: 10.5846/stxb201911102370

Nandy, S., Singh, C., Das, K. K., Kingma, N. C., and Kushwaha, S. P. S. (2015). Environmental vulnerability assessment of eco-development zone of great Himalayan National Park, himachal Pradesh, India. *Ecol. Indic.* 57, 182–195. doi: 10.1016/j.ecolind.2015.04.024

Pandey, R., Jha, S. K., Alatalo, J. M., Archie, K. M., and Gupta, A. K. (2017). Sustainable livelihood framework-based indicators for assessing climate change vulnerability and adaptation for Himalayan communities. *Ecol. Indic.* 79, 338–346. doi: 10.1016/j.ecolind.2017.03.047

Polsky, C., Neff, R., and Yarnal, B. (2007). Building comparable global change vulnerability assessments: the vulnerability scoping diagram. *Global Environ. Chang.* 17, 472–485. doi: 10.1016/j.gloenvcha.2007.01.005

Qiu, S., Peng, J., Dong, J., Wang, X., Ding, Z., Zhang, H., et al. (2021). Understanding the relationships between ecosystem services and associated social-ecological drivers in a karst region: a case study of Guizhou Province, China. *Prog. Phys. Geogr.* 45, 98–114. doi: 10.1177/0309133320933525

Ren, W., Xiong, K., Ying, B., and Xiao, J. (2020). Assessment of the impact factors of farmers' livelihood vulnerability under different landforms in karst are- as: a case study of Huajiang and Salaxi. *J. Ecol. Rural. Environ.* 36, 442–449.

Shu, Y., Peng, W., and Zhou, P. (2020). Vulnerability assessment of agro-ecological environment in karst mountain based on set pair analysis model of grey trigonometrically whitening weight. *Chin. J. Appl. Ecol.* 31, 2680–2686. doi: 10.13287/j.1001-9332.202008.014

Silva, M., Pennino, M., and Lopes, P. (2019). Social-ecological trends: managing the vulnerability of coastal fishing communitie. *Ecol. Soc.* 24:4. doi: 10.5751/ES-11185-240404

Su, W., and Zhu, X. (2000). The ecological environment fragility in karst mountainous area of Guizhou province. *Mt. Res.* 5, 429–434. doi: 10.16089/j.cnki.1008-2786.2000.05.015

Tai, X., Xiao, W., and Tang, Y. (2020). A quantitative assessment of vulnerability using social-economic-natural compound ecosystem framework in coal mining cities. *J. Clean. Prod.* 258:120969. doi: 10.1016/j.jclepro.2020.120969

Tang, J., Xiong, K., Chen, Y., Wang, Q., Ying, B., and Zhou, J. (2022). A review of village ecosystem vulnerability and resilience: implications for the rocky desertification control. *Int. J. Environ. Res. Public Health* 19:6664. doi: 10.3390/ijerph19116664

Tessema, K. B., Haile, A. T., and Nakawuka, P. (2021). Vulnerability of community to climate stress: an indicator-based investigation of upper Gana watershed in Omo gibe basin in Ethiopia. *Int. J. Disaster Risk Reduct.* 63:102426. doi: 10.1016/j.ijdrr.2021.102426

Tian, Y., and Chang, H. (2012). Bibliometric snalysis of research progress on ecological vulnerability in China. *Acta Geograph. Sin.* 67, 1515–1525. doi: 10.11821/xb201211008

Tian, Y., Xiang, Q., and Wang, P. (2013). Regional coupled humannatural systems vulnerability and its evaluation indexes. *Geogr. Res.* 32, 55–63. doi: 10.11821/yj2013010006

Touza, J., Lacambra, C., Kiss, A., Amboage, R. M., Sierra, P., Solan, M., et al. (2021). Coping and adaptation in response to environmental and climatic stressors in Caribbean coastal communities. *Environ. Manag.* 68, 505–521. doi: 10.1007/s00267-021-01500-y

Vitousek, P. M., Mooney, H. A., Lubchenco, J., and Melillo, J. M. (1997). Human domination of Earth's ecosystems. *Science* 277, 494–499. doi: 10.1126/science.277.5325.494

Wang, Q., Xiong, K., Zhou, J., Xiao, H., and Song, S. (2023). Impact of land use and land cover change on the landscape pattern and service value of the village ecosystem in the karst desertification control. *Front. Env. Sci* 11:141. doi: 10.3389/fenvs.2023.1020331

Wang, Q., Yin, M. H., Yang, X. Z., and Yao, Z. (2019). Spatio-temporal evolution and impact mechanism of socioecological system vulnerability in poor mountainous tourist distinations: taking dabie mountain area as example. *Acta Geogr. Sinica.* 74, 1663–1679. doi: 10.11821/dlxb201908013

Wang, D., and Yu, L. (2005). The quantitative assessment of ecological frangibility in karst areas. *J. Nanjing For. Univ.* 6, 23–26. doi: 10.3969/j.issn.1000-2006.2005.06.006

Wang, L., Zhang, Y., Zhang, J., Liu, C., and Wang, G. (2022). Assessment of water resources vulnerability and identification of its contribution factors in typical dry year in Henan Province. *Hydro-Sci. Eng.*, 1–10. doi: 10.12170/20211015001

Wang, Q., Zhao, X., Pu, J., Yue, Q., Chen, X., and Shi, X. (2021). Spatial-temporal variations and influencing factors of eco-environment vulnerability in the karst region of Southeast Yunnan, China. *Chin. J. Appl. Ecol.* 32, 2180–2190. doi: 10.13287/j.1001-9332.202106.018

Wang, C., Zhou, Z., Chen, Q., Feng, Q., and Zhu, C. (2022). Study on the livelihood vulnerability of the poor relocated households in karst area: a case study of Liupanshui area. *Agriculture* 12:1577. doi: 10.3390/agriculture12101577

Xenarios, S., Nemes, A., Sarker, G. W., and Sekhar, N. U. (2016). Assessing vulnerability to climate change: are communities in flood-prone areas in Bangladesh more vulnerable than those in drought-prone areas? *Water Resour. Rural Dev.* 7, 1–19. doi: 10.1016/j.wrr.2015.11.001

Xiong, K., and Chen, Q. (2010). Discussion on karst rocky desert evolution trend based on ecologically comprehensive treatment. *Carsol. Sin.* 29, 267–273. doi: 10.3969/j.issn.1001-4810.2010.03.008

Xiong, K., and Chi, Y. (2015). The problems in southern China karst ecosystem in southern of China and its countermeasures. *Ecol. Econ.* 31, 23–30. doi: 10.3969/j.issn.1671-4407.2015.01.006

Xiong, K., Li, P., and Zhou, Z. (2002). *A typical study on remote sensing-GIS of karst desertification in Guizhou province*. Geological Publishing House: Beijing, China.

Xiong, K., Mei, Z., Peng, X., and Lan, A. (2006). Integrated management of the karst rocky desertification areas—a case study of huajiang karst gorge. *GZ. For. Sci. Technol.* 34, 5–8.

Xu, Y., Qiu, X., Yang, X., Lu, X., and Chen, G. (2020). Disaster risk management models for rural relocation communities of mountainous southwestern China under the stress of geological disasters. *Int. J. Disast. Risk. Re.* 50:101697. doi: 10.1016/j.ijdrr.2020.101697

Yang, M. (1990). On the fragility of karst environment. *Yn. Geogr. Environ. Res.* 1, 21–29.

Yang, R., and Pan, Y. (2021). Rural vulnerability in China: evaluation theory and spatial patterns. *J. Geogr. Sci.* 31, 1507–1528. doi: 10.1007/s11442-021-1909-x

Yu, H. (2022). A multi-scale approach to mapping conservation priorities for rural China based on landscape context. *Environ. Dev. Sustain.* 24, 10803–10828. doi: 10.1007/s10668-021-01884-1

Zhang, J., Li, J., Liu, S., Liu, J., and Yang, Y. (2017). The vulnerability of ecosystem and evaluation system construction of Xiangshangang Bay. *J. Mar. Sci.* 35, 74–81. doi: 10.3969/j.issn.1001-909X.2017.02.008

Zhang, K., Sun, X., Jin, Y., Liu, J., Wang, R., and Zhang, S. (2020). Development models matter to the mutual growth of ecosystem services and household incomes in developing rural neighborhoods. *Ecol. Indic.* 115:106363. doi: 10.1016/j.ecolind.2020.106363

Zhang, F., Tan, H., Zhao, P., Gao, L., Ma, D., and Xiao, Y. (2022). What was the spatiotemporal evolution characteristics of high-quality development in China? A case study of the Yangtze River economic belt based on the ICGOS-SBM model. *Ecol. Indic.* 145:109593. doi: 10.1016/j.ecolind.2022.1095930

Zhang, M., Wang, K., Liu, H., Zhang, C., Yue, Y., and Qi, X. (2018). Effect of ecological engineering projects on ecosystem services in a karst region: a case study of Northwest Guangxi, China. *J. Clean. Prod.* 183, 831–842. doi: 10.1016/j.jclepro.2018.02.102

Zhao, L., and Hou, R. (2019). Human causes of soil loss in rural karst environments: a case study of Guizhou, China. *Sci. Rep.* 9, 1–11. doi: 10.1038/s41598-018-35808-3

Zhao, J., Ji, G., Tian, Y., Chen, Y., and Wang, Z. (2018). Environmental vulnerability assessment for mainland China based on entropy method. *Ecol. Indic.* 91, 410–422. doi: 10.1016/j.ecolind.2018.04.016

Zhu, Z., Wang, J., Hu, M., and Jia, L. (2019). Geographical detection of groundwater pollution vulnerability and hazard in karst areas of Guangxi Province, China. *Environ. Pollut.* 245, 627–633. doi: 10.1016/j.envpol.2018.10.017

Zuo, T., Zhang, F., Zhang, J., Gao, L., and Yu, S. (2022). Rocky desertification poverty in Southwest China: Progress, challenges and enlightenment to rural revitalization. *J. Geogr. Sci.* 32, 1357–1382. doi: 10.1007/s11442-022-2001-x

frontiers | Frontiers in Ecology and Evolution

TYPE Original Research
PUBLISHED 12 May 2023
DOI 10.3389/fevo.2023.1178609

OPEN ACCESS

EDITED BY
Guoqi Wen,
Laval University, Canada

REVIEWED BY
Wang Huasen,
Zhejiang Agriculture and Forestry University, China
Yahui Guo,
Beijing Normal University, China

*CORRESPONDENCE
Shuyan Li
✉ lsy_126com@126.com
Wei Ma
✉ mawei02@caas.cn

RECEIVED 03 March 2023
ACCEPTED 20 April 2023
PUBLISHED 12 May 2023

CITATION
Peng J, Lu L, Noor MA, Li S, Ma W and Wang J (2023) Mid-season lodging modulates photosynthesis, evapotranspiration, and dry matter accumulation and distribution simulated by the optimized model in maize.
Front. Ecol. Evol. 11:1178609.
doi: 10.3389/fevo.2023.1178609

Mid-season lodging modulates photosynthesis, evapotranspiration, and dry matter accumulation and distribution simulated by the optimized model in maize

Jiyong Peng[1,2], Liang Lu[3], Mehmood Ali Noor[3,4], Shuyan Li[1,2]*, Wei Ma[3]* and Jing Wang[5]

[1]Henan Institute of Meteorological Science, Zhengzhou, China, [2]Key Laboratory of Agrometeorological Support and Applied Technique, China Meteorological Administration, Zhengzhou, China, [3]Chinese Academy of Agricultural Sciences Institute of Crop Sciences, Beijing, China, [4]Institute of Environmental & Agricultural Sciences, Faculty of Life Sciences, University of Okara, Renala Khurd, Punjab, Pakistan, [5]College of Resources and Environmental Sciences, China Agricultural University, Beijing, China

Introduction: Mid-season lodging in maize (*Zea mays* L.) often restricts grain yield potential and is a great hurdle in improving production efficiency. The aim of this research was to study the effects of lodging on photosynthesis, evapotranspiration, dry matter accumulation, and distribution in a maize population.

Methods: We examined the effects of lodging on photosynthesis, dry matter accumulation, and distribution of maize in Zhengzhou Agro-meteorological station in August 2016, following a strong wind lodging process. Based on observational data of crops, meteorology, and CO_2/H_2O flux from milk maturity to maturity of maize in a normal growth year (2017), a model of population photosynthesis and evapotranspiration of maize under normal growth conditions was constructed. The validated model was used to simulate the theoretical value of photosynthesis and evapotranspiration in lodging years (2016), then the measured value of population photosynthesis and evapotranspiration after lodging was calculated based on the measured data of CO_2/H_2O flux from milk maturity to maturity of maize, and the difference between the simulated value and the measured value of population photosynthesis and evapotranspiration in lodging years (2016) was compared and analyzed. The correlation between dry matter accumulation and population photosynthetic accumulation was examined in order to estimate the reduction of dry matter accumulation after lodging. The effect of lodging on dry matter accumulation, distribution, and yield was analyzed using field biomass data. The population photosynthesis model and evapotranspiration model could accurately simulate the characteristics of normal growth conditions of summer maize.

Results: The population photosynthesis model absolute error between the simulated value and the measured values in 2017 was −0.43mgm^{-2} s^{-1}, and the relative error was −3.3%; the evapotranspiration model absolute error between the simulated value and the measured values in 2017 was −0.005mm·30min^{-1}, and the relative error was −10.7%. In 2016, the measured value of photosynthesis after lodging was significantly lower than the simulated value, and the daily average population photosynthesis rate decreased by 13.99mgm^{-2} s^{-1} or 53%. Under the same condition, the daily average evapotranspiration decreased by 1.03mmd^{-1} or 28%. The lodging process altered the accumulation and distribution of dry matter in maize. The dry weight of the stem

and sheath increased by 5.5% and the ear weight decreased by 10.9% after lodging, compared to without lodging but there was no significant effect on leaf dry weight. After lodging, the proportion of stem sheath distribution increased by 3.0%, while the proportion of ear distribution decreased by 3.0%. After lodging, 100-grain weight and plant grain weight decreased by 2.8 and 10.8%, respectively. According to the lodging rate and density theory of computation yield, the yield of the entire field was reduced by 5.0%.

KEYWORDS

maize lodging, CO_2 flux, evapotranspiration, population photosynthesis, dry matter partition

1. Introduction

Maize is the most widely cultivated food crop in the Huanghuai area, and its perennial sown area and yield account for more than 20% of maize in China (National Bureau Of Statistics Of China, 2018). In the growing season of maize, strong convective weather is frequent which makes lodging possible. Lodging is a critical meteorological disaster that affects the yield and quality of maize. Lodging alters the population structure and spatial distribution of leaves in maize, resulting in a mutual shielding of plants and leaves, thereby reducing the ventilation and light transmission between plants and the photosynthetic rate of the population (Alam et al., 2018; Wang et al., 2022). Furthermore, lodging destroys the grooming tissues of the stem and negatively affects the transportation of water and nutrients from roots to leaves; at the same time, the transportation of photosynthetic products to underground organs and ear filling are hindered (Elmore and Ferguson, 1999; Yoon-Sup et al., 2013; Jun et al., 2016), all of which directly affect yield and components of yield (Minami and Ujihara, 1991; Jun et al., 2017; Xue et al., 2021). Various studies have shown that lodging reduces the yield of maize by 5–25% every year, and the yield decreases by 90–120 kg hm^{-2} for every 1% increase in lodging rate (Elmore and Ferguson, 1999; Kang et al., 1999).

Lodging during grain filling can reduce the content of crude fat and crude protein in maize grains, thus affecting the quality of maize (Cao, 2016). Previous studies have made in-depth analyses of the effects of lodging on dry matter accumulation, distribution, yield, and quality of maize, as well as causes of lodging, remedial measures, and the evaluation of lodging resistance on varieties of maize (Zhang et al., 2009; Wang et al., 2011; Chen et al., 2012). However, few studies have been conducted on the various characteristics of maize photosynthetic rates and evapotranspiration after lodging; observation methods have been identified as one of the main reasons for limited research in this field. The plants become mutually shaded after lodging, so it is necessary to measure the population photosynthesis and evapotranspiration to reflect the real disaster situation on the field. At present, the recognized photosynthetic measurement systems such as LI-6800 are limited to the measurement of the photosynthetic capacity of a single leaf. Since summer maize is a high-stem crop, it is difficult to measure community photosynthesis directly. However, considerable numbers of research have been carried out on the photosynthesis of maize leaves, the characteristics of the population photosynthesis, and the establishment of photosynthesis and evapotranspiration models by numerical analysis (Yu et al., 1998; Zhang et al., 2004; Wang, 2006). The findings of this research provide new ideas for analyzing the characteristics of summer maize population photosynthesis and evapotranspiration changes after lodging.

In this study, we examined the effects of a maize lodging catastrophe at the Zhengzhou Agricultural Meteorological Experimental Station on photosynthesis, evapotranspiration, dry matter accumulation, and distribution of the maize population in August 2016. Based on the flux observation system and crop observation data of summer maize from the milk stage to the maturation stage without lodging in 2017, photosynthesis and evapotranspiration simulation models were constructed and verified under normal growth conditions. In 2016, the verified models were used to simulate the theoretical value without lodging. In addition, after lodging, according to the observed data of CO_2 flux, the actual photosynthetic rate and evapotranspiration were determined by using the carbon and water cycles theory of farmland ecosystem as the measured value, and the decrease in population photosynthesis and evapotranspiration after lodging was compared and analyzed. The Richards dry matter accumulation model was used to simulate and analyze the relationship between daily photosynthesis and daily dry matter accumulation after lodging. The dry matter accumulation after lodging was calculated by the decrease in group photosynthesis. At last, we analyzed the effects of lodging on dry matter distribution and yield formation by using field biomass data.

2. Materials and methods

2.1. Experimental site

The experimental site was located at the Zhengzhou Agro-meteorological Station, Henan Province, China (34 ° 43 ′ N, 113 ° 39 ′ E, altitude 110.4 m). The annual average temperature and precipitation at the station were 14.9°C and 670 mm, respectively. The mid-mature hybrid variety "Xundan 20" was sown in 2016 and 2017. There were no meteorological disasters during the 2017 growing season, and there were no major meteorological disasters except for a strong wind on August 25, 2016. The station experienced a strong wind at a maximum wind speed of 18.1 m s^{-1} and an hourly average wind speed of 3.8 m s^{-1} at 12:20 on August 25, 2016 (the third day after milk maturity). This time, the wind was accompanied by precipitation, with daily precipitation of 23.8 mm. Approximately half of the entire field was lodged, with broken stems mainly occurring between the third and fourth nodes, and the broken parts were approximately 20 to 30 cm away from the ground.

2.2. CO_2 flux data observation and data quality control

The CO_2 flux observation system is based on the eddy covariance system (Campbell Scientific Company of America), which also incorporates a gradient observation system and a vorticity observation system. The gradient observation system consisted of a set of PAR LITE photosynthetically active radiation sensors, five layers of air temperature and humidity probes, and four layers of wind direction anemometers. The eddy covariance system was composed of an LI-7500 CO_2/H_2O analyzer (with a height of 3 m), a CSAT3 3D ultrasonic anemometer, a CNR2 net radiation sensor, and the HFP01 soil heat flux plate. The daily maintenance and flux data download of instruments were carried out in accordance with the data format by the standers of the China Meteorological Administration. The half-hour flux data was processed in accordance with the general flux data processing method through outlier elimination, coordinate axis rotation, and WPL transformation (Vickers and Mahrt, 1997; Li et al., 2008; Xu et al., 2008). The average day and night method and nonlinear regression method were used to interpolate for the data missing due to precipitation, power failure, and other factors. As a result, the continuity of the data was ensured (Falge et al., 2001; Guo et al., 2007).

The CO_2 data was analyzed from August 22 to September 12 before and after lodging in 2016, and the data on the day of lodging (August 25) was excluded due to rainfall. In 2017, the corresponding data from milk maturity to maturity (August 28 to September 22) was selected for analysis, and the data from August 29 to 30 were excluded because of rainfall.

2.3. Investigation on lodging disaster of maize

On the second day after maize lodging (August 26, 2016), the lodging type and lodging rate were investigated. This lodging was caused by stem breakage, and 100 plants were continuously examined to record the lodging number. Based on statistical analysis and image recognition (Figure 1), it was determined that the lodging number divided by the total number of investigated plants resulted in a lodging rate of 46.0% recognition (Jia et al., 2015).

2.4. Crop observation

The data of maize growth was observed by manual methods from planting to harvest, and the agricultural meteorological observation data was completed in 2016 and 2017 (National Meteorological Administration, 1993). After lodging, lodging data was collected according to the disaster situation in 2016.

2.4.1. Observation of growth stage

This mainly included the observation of the three-leaf stage, seven-leaf stage, jointing stage, tasseling stage, milk-ripe stage, and mature stage.

2.4.2. Determination of dry matter

The samples were taken before lodging at the three-leaf stage, seven-leaf stage, jointing stage, tasseling stage, and milk ripe stage. After lodging occurred, samples were taken and determined according to "lodging" and "not lodging" in the mature period. Four measuring points were fixed in the field, 10 plants were selected continuously from each measuring point, and the height of 40 plants at each measuring point was measured, which was divided into five groups with the same date range according to the dispersion degree of data regarding plant height. Each measuring point was sampled according to the average plant height of each group as the reference height, and one plant was taken from each reference height; five plants were taken from each measuring point, which was cut off on the ground and brought back into the room. The leaves, stem sheaths, ears, and other organs were separated and dried before weighing.

Taking lodging into account, the average dry matter accumulation at the field level was calculated as follows:

$$D_{LE} = D_L \times L_r + D_{NL} \times (1 - L_r) \tag{1}$$

where D_{LE} is the average dry matter accumulation at the field level, L_r is the lodging rate (46.0%), D_L is the dry matter accumulation of lodging plants, and D_{NL} is the dry matter accumulation of non-lodging plants.

2.4.3. Determination of leaf area index

We collected leaves for leaf area measurement in the same manner for dry matter sampling as mentioned above using the length-width coefficient method:

$$LS_i = \sum_{i=1}^{n} L_i \times D_i \times k \tag{2}$$

where LS_i is the leaf area per plant (cm^2), L_i is leaf length (cm), D_i is leaf width (cm), and k is the leaf area correction coefficient, which is 0.70. The leaf area index LAI was obtained by multiplying the leaf area per plant by the number of plants per square meter.

2.4.4. Yield investigation and theoretical yield calculation

At the mature period of maize, four measuring points were randomly selected, and 10 plants were taken from each measuring point based on lodging and non-lodging. Plants were cut off evenly and dried in the sun and the yield component, ear length, ear diameter, total grain weight, 100-grain weight, and grain-to-stalk ratio were analyzed. The theoretical yield was calculated as:

$$Y_R = Y_{NL} + Y_L \tag{3}$$

$$Y_{NL} = SW_{NL} \times (1 - L_r) \times ED \tag{4}$$

$$Y_L = SW_L \times L_r \times ED \tag{5}$$

where Y_R is the theoretical yield ($kg{\cdot}hm^{-2}$), Y_{NL} is the yield of the non-lodging part, and Y_L is the yield of the lodging part. SW_{NL} is the grain weight of a non-lodging plant ($kg{\cdot}plant^{-1}$). L_r is the lodging rate,

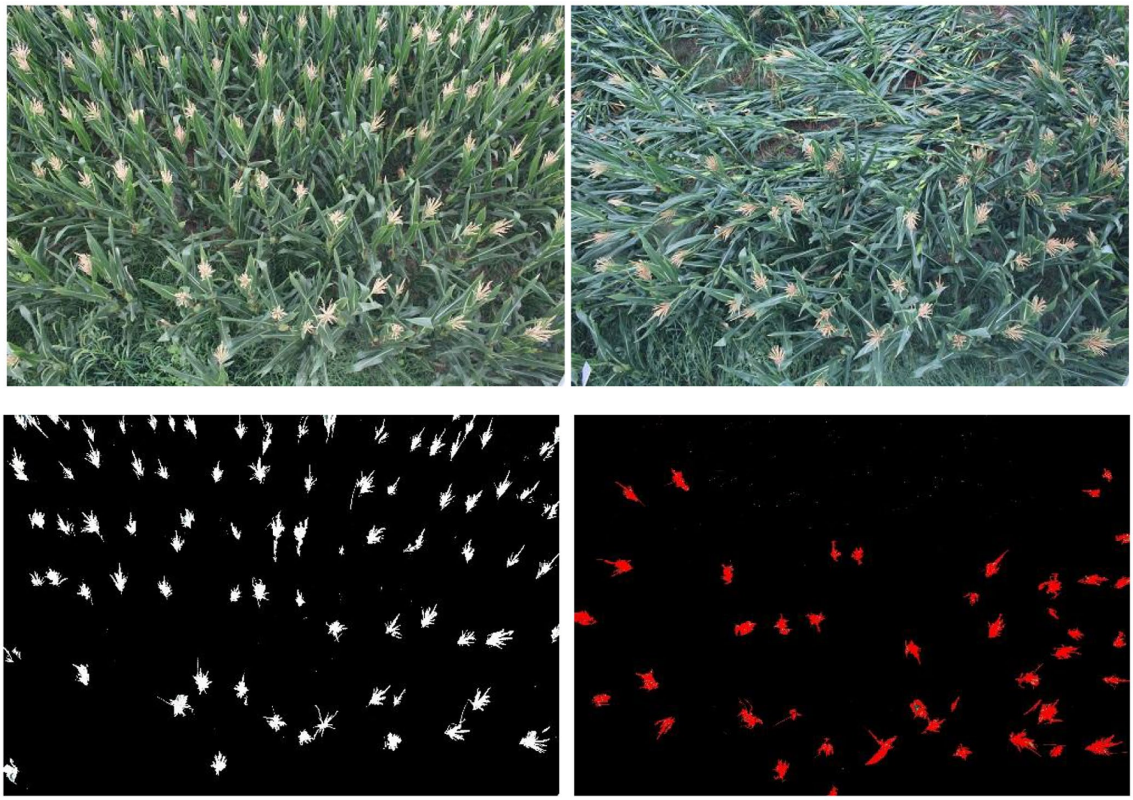

FIGURE 1
Comparison of maize before and after lodging.

which is 46.0% according to statistics. *ED* is the total planting density (plant·hm^{-2}), and S_{WL} is the grain weight of the non-lodging plant (kg·plant^{-1}).

According to the theoretical output, the yield reduction rate was calculated as follows:

$$P_r = \frac{Y_E - Y_R}{Y_E} \times 100\% \tag{6}$$

$$Y_E = SW_{NL} \times ED \tag{7}$$

P_r is the yield reduction rate (%). Y_E is the expected theoretical yield (kg·hm^{-2}).

2.5. Simulation of population photosynthesis under normal growth conditions

The crop population photosynthetic rate was equal to the difference between the total population photosynthetic rate and dark respiration rate, otherwise known as the net population photosynthetic rate, which was the simulated population photosynthetic rate under normal growth conditions:

$$A_{cm} = A - R_d \tag{8}$$

A_{cm} is the simulated value of the net photosynthetic rate of the population, A is the total photosynthetic rate of the population (mg m^{-2} s^{-1}), and R_d is the population dark breathing rate (mg m^{-2} s^{-1}), which is calculated by COLLATZ G. JAMES (Collatz et al., 1991). The total photosynthetic rate (A) of the population was simulated by the scale expansion method (Yu and Sun, 2006). Firstly, according to the modified Farquhar biochemical model of photosynthesis (Farquhar et al., 1980), the total photosynthetic rate (P) of a single leaf was calculated as:

$$P = \frac{aI + P_{\max} - \sqrt{(aI + P_{\max})^2 - 4\theta(aIP_{\max})}}{2\theta} \tag{9}$$

where α is the initial quantum efficiency (μmol μmol^{-1}), I is light intensity (μmol m^{-2} s^{-1}), P_{max} is the maximum photosynthetic rate (μmol m^{-2} s^{-1}), θ is convexity, and the value is 0.55 μmol μmol^{-1}.

Using the photosynthetic rate of a single leaf, it was then extended to the scale of crop population, and the single-leaf model was applied. The total photosynthetic rate of the population was as follows:

$$A = \int_0^L P(LAIL)\,dL \tag{10}$$

where *LAIL* is the daily leaf area index. *LAIL* is simulated by a modified Logistic equation (Peng and Yang, 2018):

$$LAIL = \frac{LAI_{\max}}{1 + e^{\left(a + b \times DS + c \times DS^2\right)}} \tag{11}$$

where LAI_{max} is the measured maximum leaf area index during the growth period, DS is the normalized accumulated temperature, and a, b, and c are the fitting parameters.

2.6. Estimation of the photosynthetic rate of measured population

Based on the carbon cycle theory of farmland ecosystems, the population photosynthetic rate can be calculated from the CO_2 flux and soil respiration as the measured value of population photosynthesis. CO_2 flux mainly includes the net photosynthesis of crops and the respiration of soil. By using the black box method, the calculation formula for the net photosynthetic rate of crop population was (Liu et al., 2015):

$$A_{cs} = F_c + R_s \tag{12}$$

where A_{cs} is the net photosynthetic rate of population (mg m^{-2} s^{-1}), and F_c is CO_2 flux (mg m^{-2} s^{-1}), which can be observed by the flux observation system. R_s is soil respiration rate (mg m^{-2} s^{-1}) which increases exponentially with the increase of soil surface temperature (T_s) (Tjkelker et al., 2001; Wang et al., 2004):

$$R_s = R_0 Q_{10}^{(Ts-25)/10} \tag{13}$$

where R_0 is the soil respiration rate (0.11 mg m^{-2} s^{-1}) when the soil temperature is 25°C, Q_{10} is a constant, the value is 2.14, and T_s is 5 cm soil temperature.

2.7. Shuttleworth–Wallace dual-source model

Shuttleworth and Wallace studied the evapotranspiration of soil surface under sparse soil cover conditions and developed a dual-source model (S-W model) consisting of vegetation and soil surface under vegetation cover with the assumption that the crop canopy was uniformly covered in vegetation.

$$\lambda ET = C_c PM_c + C_s PM_s \tag{14}$$

$$PM_s = \frac{\Delta\left(R_n - G\right) + \left[\rho C_p D - \Delta r_a^s \left(R_n - R_n^s\right)\right] / \left(r_{\mathrm{a}}^{\mathrm{a}} + r_{\mathrm{a}}^{\mathrm{s}}\right)}{\Delta + \gamma\left[1 + r_s^s / r_a^a + r_a^s\right]} \tag{15}$$

$$PM_c = \frac{\Delta\left(R_n - G\right) + \left[\rho C_p D - \Delta r_a{}^c \left(R_n - G\right)\right] / \left(r_a{}^a + r_a{}^c\right)}{\Delta + \gamma\left[1 + r_s{}^c / \left(r_a{}^a + r_a{}^c\right)\right]} \tag{16}$$

where C_cPM_c is transpiration of summer maize, C_sPM_s is the evaporation of soil， C_c is canopy coefficient, C_s is soil surface coefficient, R_n is net canopy surface radiation (W m^{-2})， G is soil heat flux, ρis is air density (kg m^{-3}), C_p is the specific heat of the air (1,012 J kg^{-1} K^{-1}), D is air saturation vapor pressure difference (hPa), γ is the dry and wet meter constant (0.67 hPa K^{-1}), $\triangle$ is the slope of saturation vapor pressure–temperature curve (hPa K^{-1}), R_n^s is the net radiation of soil surface (W m^{-2}), r_a^c is canopy resistance (s m^{-1}), r_a^c is the resistance of the canopy inner boundary (s m^{-1}), r_a^a is the height of the crop canopy, and r_a^s is aerodynamic resistance between surface and canopy height (s m^{-1}).

2.8. Model verification

The theoretical simulation value of the population photosynthetic rate calculated by Formula (8) was verified by using the measured value of the population photosynthetic rate calculated by Formula (12). The actual value of evapotranspiration is measured by the flux observation system, and the simulated value is calculated by the S-W model. The simulation result was evaluated by using Absolute Error (*AE*) and Relative Error (*RE*). The smaller the error, the higher the simulation accuracy will be.

$$AE = S_i - O_i \tag{17}$$

$$RE = \frac{\left(S_i - O_i\right)}{O_i} \times 100\% \tag{18}$$

where *AE* is the absolute relative error, *RE* is the relative error, S_i is the ith simulated value, and O_i is the ith observed value.

2.9. Estimation of dry matter accumulation

According to Richards equation, the daily growth model of maize biomass was constructed by using the measured biomass at different development stages (Zhang et al., 2018):

$$y = \frac{A}{\left[1 + \exp\left(B - Ct\right)\right]^{(1/D)}} \tag{19}$$

where y is the daily dry matter weight per unit area and the unit is g m^{-2}, A, B, C, and D are fitting parameters, and t is the normalized accumulated temperature.

As 2016 was a lodging year, according to the sampling data of lodging and non-lodging biomass, two types of daily growth biomass were simulated.

2.10. Data processing

All the data and statistical analyses were performed using SPSS Statistics package 19.0 (SPSS Inc., Chicago, IL, USA). Microsoft Excel 2016 was used for data processing and drawing.

3. Results

3.1. The effect of lodging on photosynthesis and evapotranspiration of maize population

3.1.1. Population photosynthesis simulation

Based on the observational data of maize in the normal growth year (2017) from the milk stage to the maturity stage, the simulation model of population photosynthesis was constructed, and the parameters of the model were calibrated to simulate the photosynthetic rate of the maize population under normal growth conditions (Figure 2). The simulated values of photosynthesis of normal maize farmland population were in accordance with the observed values. There was a significant positive correlation between the simulated value and the observed value, and the correlation coefficient was 0.95. The absolute error of the simulation was 0.43 mg m^{-2} s^{-1} and the relative error was −3.3%. The results showed that the model could accurately simulate the change rate in photosynthesis of the maize population from the milk stage to the mature stage under normal growth conditions.

Based on the constructed photosynthesis model of the maize population, the theoretical value of simulating the photosynthesis rate of the maize population from the milk stage to the mature stage in 2016 was taken as the control value. The differences between the measured population photosynthesis and simulated control value after lodging are shown in Figure 2. The photosynthesis of the observed population after maize lodging (August 25, 2016) was significantly lower than the simulated value, which indicated that the photosynthesis of maize farmland decreased significantly after lodging. In the period from lodging to mature harvest, the average daily photosynthesis rate decreased by 13.99 mg m^{-2} s^{-1}, with an average decrease of 53%. Among the maize population, lodging was more significant under sunny conditions (sunshine hours ≥7 h), and the rates of average daily photosynthetic activity decreased by 60 cloudy days, resulting in weak photosynthesis as a whole, and the average daily photosynthetic rate decreased by 39% after lodging.

3.1.2. Simulation of evapotranspiration by the Shuttleworth–Wallace dual-source model

The S–W dual-source model was used to calculate the evapotranspiration for summer maize from the milking to maturity stage in a normal growth year type (2017; Figure 3). The simulated and measured evapotranspiration values of summer maize in a normal year were in good agreement; the correlation coefficient was 0.88, the simulated absolute error was −0.005 mm 30 min^{-1}, and the relative error was −10.7%. The results showed that the model could accurately simulate the evapotranspiration variation from the milk stage to the maturity stage of summer maize under normal growth conditions. The S–W model was used to simulate the theoretical evapotranspiration of summer maize from the milk stage to the maturity stage in 2016 as a control, and the difference between the measured group evapotranspiration and the simulated control value after lodging was compared. After the lodging of summer maize (August 25, 2016), the measured evapotranspiration was significantly lower than the

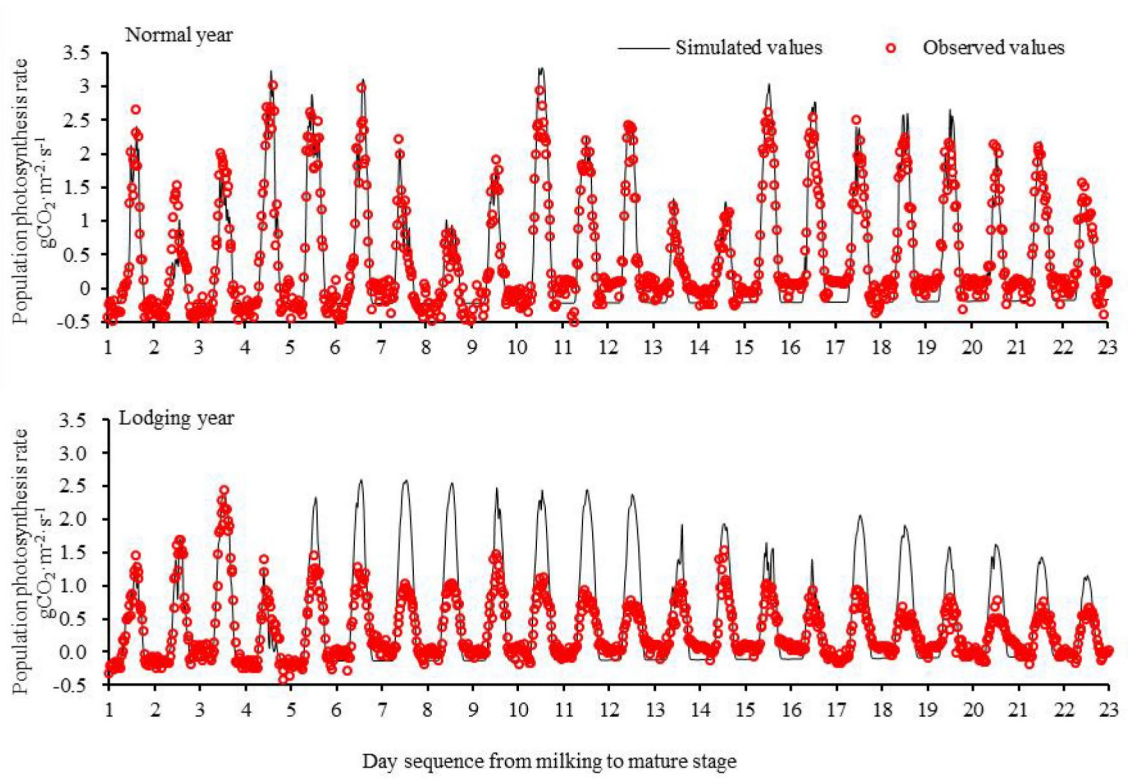

FIGURE 2
Population photosynthesis of maize from milking to mature stage in a normal year and lodging year.

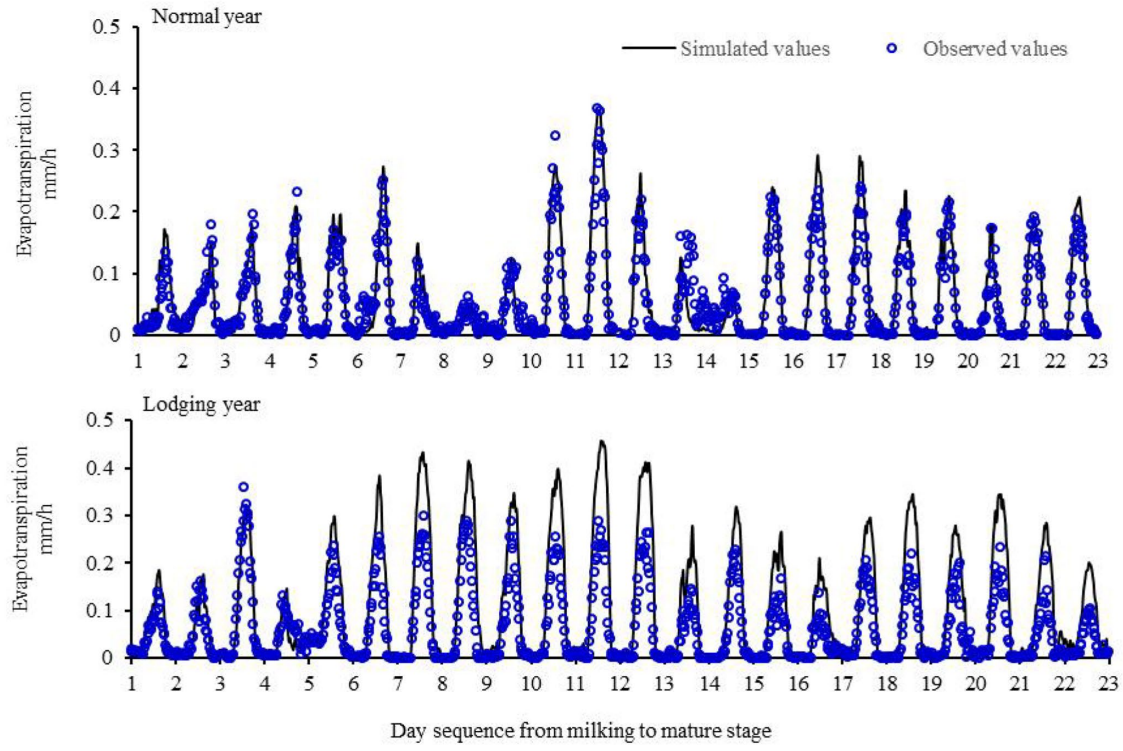

FIGURE 3
Evapotranspiration of maize from milking to mature stage in a normal year and lodging year.

simulated value, which suggested that lodging significantly reduced the evapotranspiration of summer maize. On average, the daily evapotranspiration decreased by 1.03 mm d^{-1} or 28% from lodging to harvest.

3.2. The effect of lodging on dry matter accumulation of maize

3.2.1. Estimation of dry matter accumulation of maize after lodging based on population photosynthetic model

In the study, the dry matter accumulation was simulated using the Richards model (Formula (16)) of summer corn based on dry matter sampling data in a normal year (2017) at different growth stages. As a consequence, the measured and simulated values of population photosynthesis every half hour were converted into the cumulative values of daily photosynthesis, and the daily cumulative amounts of population photosynthesis were calculated accordingly. The data in Figure 4 shows the results of correlation analysis with the accumulated amount of dry matter over the corresponding period. Under normal growth conditions, the measured and simulated values of daily population photosynthetic accumulation were significantly positively correlated with daily dry matter accumulation. The correlation coefficient between measured and simulated values of daily population photosynthetic accumulation were 0.9977 and 0.9965, respectively, which indicated that the change of daily dry matter accumulation after the milk stage of maize could be estimated by using the accumulated value of population photosynthesis.

Based on the positive correlation between photosynthesis accumulation and dry matter accumulation, the change in dry matter accumulation after lodging in 2016 was estimated. Taking the dry matter sampling data of non-lodging samples as the substitute for the Richards model of daily dry matter growth of maize, the daily dry matter growth of maize was simulated, which was taken as the "reference value of dry matter growth" under normal growth conditions. The calculated daily photosynthetic rate decreased in percentage after lodging, and multiplying the daily photosynthetic rate decreased percentage by the reference value of daily dry matter increase gave us the estimated amount of daily dry matter increase after lodging (Figure 5). After lodging, photosynthesis and daily average photosynthetic products decreased significantly, resulting in the decrease of dry matter accumulation. If lodging did not occur, the dry matter accumulation in the milk-ripe stage to the mature stage could increase by 368.2 g m^{-2}. However, lodging occurred, and it was estimated that the dry matter accumulation increased by 299.6 g m^{-2} in the milk-ripe stage, which was 68.6 g m^{-2} lower than the theoretical value. Dry matter accumulation decreased by 18.6% (Table 1).

3.2.2. Dry matter accumulation of maize after lodging based on field sampling calculation

After the disaster, samples of dry matter were taken from lodging and non-lodging plants. The changes in dry matter in maize are shown in Table 2. The total dry matter weight per unit area in the mature period increased by 181.0 g m^{-2} (lodging) and 299.8 g m^{-2} (non-lodging), and the total dry matter weight of lodging plants decreased significantly by 118.8 g·m^{-2} ($\alpha = 0.05$). According to Formula (1), the average total dry matter weight per unit area of the

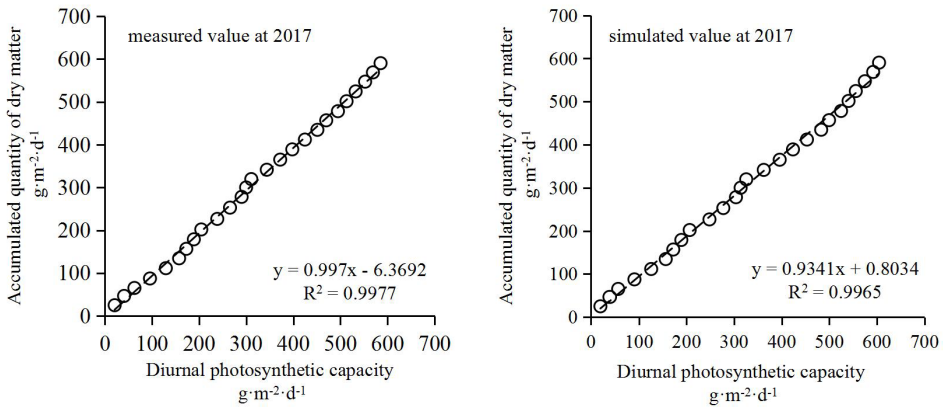

FIGURE 4
The fitting relationship between the accumulation of photosynthetic product and dry matter accumulation in normal summer maize after the milk stage.

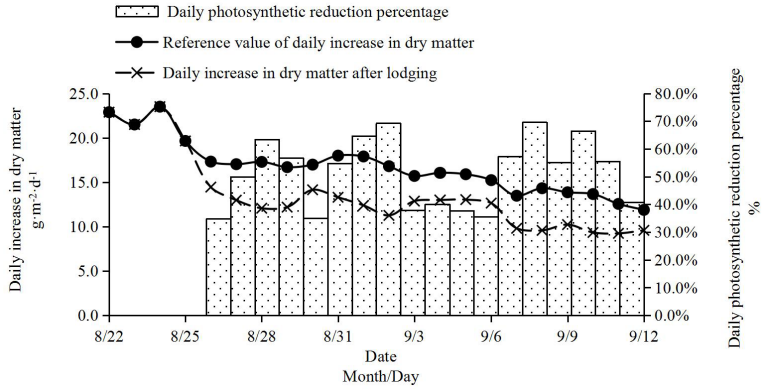

FIGURE 5
Estimation of dry matter growth after lodging.

whole field after lodging was 245.2 g·m^{-2}, which was 18.2% lower than the theoretical value without lodging. Moreover, the dry matter accumulation of field sampling results was basically consistent with the decreased range (18.6%) of dry matter accumulation estimated by population photosynthesis in 2.2.1.

3.3. The effect of lodging on dry matter distribution of maize

Compared with the milk-ripe period, the leaf dry weight at the mature stage decreased by 37.5 g m^{-2} (lodging) and 24.6 g m^{-2} (not lodging), and the stem sheath weight increased by 141.6 g m^{-2} (lodging) and 129.2 g m^{-2} (not lodging). The dry weight of ears in the mature stage increased by 77.0 g m^{-2} (lodging) and 195.2 g m^{-2} (not lodging) compared with the milk-ripe period, and the weight of ears in the lodging stage decreased significantly ($\alpha = 0.05$) by 118.2 g m^{-2}, with a decrease of 60.6%. It can be seen from the above that the decrease in the dry weight of the spike after lodging is the main reason for the decrease in total dry matter weight.

As a result of lodging, there was a significant decrease in dry matter accumulation and changes in the distribution ratio of dry matter in various organs (Table 2). After lodging, the dry matter partition ratio in stem and sheath increased significantly by 3.0%. The partition ratio of the ear significantly reduced by 3.0% after lodging than without lodging. The dry weight of aging leaves no longer increased because it was in the middle and late growth stages of maize, and the distribution ratio of lodging and non-lodging leaves had little difference. The total weight of maize plants decreased after lodging, the photosynthetic products were more distributed to the vegetative organs, and the dry matter accumulation in reproductive organs decreased, resulting in a decrease in maize yield.

3.4. The effect of lodging on maize yield

After harvest, samples were taken from lodging and non-lodging plants. The yield structure analysis of maize is shown in Table 3. As lodging occurred in the middle and late filling stages of maize, there was little difference in the ear length and ear diameter between

TABLE 1 Growth and meteorological conditions of maize in 2016 and 2017.

Year	Sowing date (month/day)	Milk date (month/day)	Maturity date (month/day)	Sunshine duration (h)	>0°C Accumulated temperature (°C·d)	Precipitation (mm)
2016	6/2	8/22	9/12	650.2	2839.0	467.6
2017	6/4	8/28	9/22	699.7	3017.4	361.0

TABLE 2 The effects of lodging on dry matter accumulation and partition ratio for organs of maize.

Dry matter weight and partition ratio	Sample type	Leaf	Stem and sheath	Ears	Total weight
Dry matter weight ($g\,m^{-2}$)	Lodging	231.6	601.8	969.6	1803
	Non-lodging	244.5	589.5	1087.8	1921.8
Dry weight partition ratio (%)	Lodging	13	33	54	-
	Non-lodging	13	30	57	-

lodging and non-lodging maize. After lodging, the weight of 100 grains of maize decreased by 0.88 g, which was significantly reduced by 2.8% ($\alpha = 0.05$), compared with without lodging. After lodging, the total grain weight of the plant decreased by 18.0 g which was significantly lower than without lodging ($\alpha = 0.05$). After lodging, the grain-to-stalk ratio of maize was significantly lower than that of non-lodging, indicating that more dry matter distribution was allocated to the stem and sheath, and the harvest index decreased. Compared with non-lodging, the theoretical yield of lodging plants decreased significantly by 1172.9 $kg\,hm^{-2}$. The yield of a whole field decreased by 539.5 $kg\,hm^{-2}$ when the lodging rate was about 46.0%, and the yield reduction rate was approximately 5.0% when the lodging rate was approximately 46.0%.

4. Discussion

The population photosynthesis model extends the physiological and ecological models at the leaf scale to the canopy scale by means of scale expansion, and the large leaf model, the two-leaf model, and the multi-layer model are widely used. In this study, the Farquhar biochemical model (1980), which is widely used, was extended to the canopy-scale photosynthesis model of large leaves. It is generally believed that the hypothesis of the big leaf model is basically valid when the leaf area index ($L \geq 3$) of the canopy is taken into account (Ren et al., 2004). At present, canopy-scale photosynthesis models mostly focus on simulating crop responses to light, temperature, water, CO_2, and other environmental factors, ignoring the simulation of the physiological and ecological processes that allow crops to adapt to the environment, and thus, the models cannot predict how crops will respond to the environment under adverse conditions. In this study, based on two aspects of crop photosynthesis and ecosystem carbon cycle combined with CO_2 flux observation data of the vorticity correlation system, the characteristic changes of group photosynthesis of maize during normal growth from milk maturity to maturity were compared and analyzed by two methods, and the model parameters were calibrated. In 2017, the simulated values of milk maturity to maturity in the normal growing season of maize were consistent with comparative values, and the change characteristics of group photosynthesis after lodging in maize in 2016 were further analyzed.

Photosynthesis is the source of dry matter accumulation and yield formation in maize, and the accumulation of photosynthetic products is generally calculated using dry matter accumulation through a model. The CO_2 assimilation module in the WOFOST model calculates the parameters of photosynthesis cumulative conversion to dry matter mass. Lizaso et al. (2005) introduced CO_2 flux observation data and used the CERES-Maize model to simulate the changes in dry matter accumulation and parameter sensitivity at the canopy scale, obtaining good simulation results. After maize lodging in 2016, the accumulation of photosynthetic products and dry matter decreased. In addition, a previous study showed that (Liu et al., 2019) parameter correction was necessary for calculating the conversion of photosynthesis accumulation of other plants into dry matter mass of plants, and the correction coefficient was not fixed, so a certain error occurred when calculating the daily dry matter accumulation through the decrease percentage of photosynthetic rate in section (2.2.1). The accumulated amount of dry matter after lodging was reduced by 18.6% calculated by daily photosynthetic rate reduction percentage, and by field sampling, the accumulated amount of dry matter after lodging was reduced by 18.2%. Although there were some errors, they were consistent.

Lodging changes the cumulative distribution of dry matter in maize. Under normal growth conditions, the vegetative organs of maize generally stop growing at the late growth stage, and the increase of dry matter in the population is mainly manifested in the accumulation of grains. Several studies have shown that the stem is the main organ for the redistribution of photosynthetic products, and the redistribution amount of stem dry matter can reach 35% of its dry weight during grain filling (Ma and Zhou, 2016). This study shows that after maize lodging, not only the photosynthesis ability of plants decreases but the accumulation of total dry matter also decreases. Moreover, the cumulative distribution law of dry matter changes, and the plant grows uprightly and in reverse, and some dry matter transfers from ear to stem (Li et al., 2015a). Several studies have shown that the earlier lodging resulted in serious yield reduction (Li et al., 2015b). On the other hand, adversity accelerates the senescence of crops, which is beneficial for their reproductive growth process, thus avoiding adversity stress and maintaining population stability (Gao et al., 2017). In this study, maize lodging occurred at the milking stage and did not have any significant effect on grain number per ear, ear length, ear diameter, and leaf dry matter distribution. There was no significant effect of lodging on yield, but it did have an effect on grain weight per ear and 100-grain weight.

TABLE 3 The effect of lodging on the yield component of maize.

Yield component	Ear length (cm)	Ear diameter (cm)	100 grain weight (g)	Total grain weight (g)	Grain-to-stalk ratio	Theoretical yield ($kghm^{-2}$)
Lodging	18.5	5.0	31.08	157.58	0.99	9706.3
Non-lodging	19.1	5.2	31.96	176.61	1.13	10879.2

The photosynthesis model of the maize population has a strong mechanism, but there are many model parameters that make it more difficult to calculate the model accurately (Zhnag et al., 2001; Zhang, 2016; An et al., 2021). Meanwhile, crop dark respiration and soil respiration are regarded as functions only depending on air temperature and soil temperature, respectively, but the model parameters are too simple, resulting in the accumulation of simulation errors (Sun et al., 2013; Chen et al., 2017; Shah et al., 2017). In addition, due to the sudden and sporadic wind lodging disaster and the poor repeatability of natural lodging, there is still a lack of observation data after large-scale lodging to verify the simulation results of population photosynthesis.

5. Conclusion

The simulation model of population photosynthesis and evapotranspiration under normal growth conditions of maize was constructed by using the Eddy-Covariance system and crop observation data during the period from milk maturity to maturity in 2017 without lodging, and the model was verified by the measured population photosynthesis calculated by CO_2/H_2O flux observation data. The results showed that the absolute error of the population photosynthesis model simulation was $-0.43\,mg\,m^{-2}\,d^{-1}$ and the relative error was −3.3% under the normal growth of maize. Under normal growth conditions, the simulated values of photosynthesis were in good agreement with the measured values. The verified model was used to simulate the theoretical population photosynthesis of maize in the lodging year (2016). Compared with the calculated measured population photosynthesis, the average daily photosynthesis decreased by $13.99\,mg\,m^{-2}\,s^{-1}$ and 53% after lodging.

Lodging reduced photosynthesis, evapotranspiration, and decreased dry matter accumulation. The dry matter accumulation of maize simulated by the Richards model was positively correlated with the population photosynthesis accumulation. The dry matter accumulation of lodging year (2016) was estimated from the population photosynthesis accumulation, and the dry matter accumulation decreased by 18.6%.

Lodging changed the distribution ratio of dry matter in maize. After lodging, the stem and sheath dry weight of maize increased by 5.5% and ear weight decreased by 10.9%, but there was no significant effect on the leaf dry weight. After lodging, the partition ratio of stem and sheath increased by 3.0% and the partition ratio of ear decreased by 3.0%. After lodging, the 100-grain weight significantly decreased by 2.8%, and the grain weight per plant decreased by 10.8%. Calculating theoretical yield according to lodging rate and density, lodging resulted in a yield reduction rate of approximately 5.0% for the whole field.

Experts have conducted extensive research on crop lodging, but the lodging process of summer maize is very complex, for example, various factors such as high or low stems. There are also meteorological factors such as strong winds or heavy precipitation and planting factors such as excessive planting density or unreasonable field management. The meteorologist, agronomists, physiologists, molecular actors, and breeders require further exploration to fix this challenging problem.

Data availability statement

The original contributions presented in the study are included in the article/supplementary materials, further inquiries can be directed to the corresponding authors.

Author contributions

JP is the first author. SL and WM are the corresponding authors. LL and MN have modified the grammar of the full text. WJ has provided technical guidance for the article. All authors contributed to the article and approved the submitted version.

Conflict of interest

The authors declare that the research was conducted in the absence of any commercial or financial relationships that could be construed as a potential conflict of interest.

Publisher's note

All claims expressed in this article are solely those of the authors and do not necessarily represent those of their affiliated organizations, or those of the publisher, the editors and the reviewers. Any product that may be evaluated in this article, or claim that may be made by its manufacturer, is not guaranteed or endorsed by the publisher.

References

Alam, S., Aaqil, K., Umair, A., Liu, H. H., and Li, J. C. (2018). Characterization of the effect of increased plant density on canopy morphology and stalk lodging risk. *Front. Plant Sci.* 9, 1–12. doi: 10.3389/fpls.2018.01047

An, S., Tanveer, M., Abbas, A., Yildirim, M., Aa, S., Mi, A., et al. (2021). Combating dual challenges in maize under high planting density: stem lodging and kernel abortion. *Front. Plant Sci.* 12:699085. doi: 10.3389/fpls.2021.699085

Cao, Q. J.. Evaluation of stalk lodging resistance of different spring maize genotypes and mechanism of its improvement by plant growth regulators (Pgrs) [D]. University Of Chinese Academy Of Sciences (Northeast Institute Of Geography And Agroecology), (2016), 23–29. (In Chinese)

Chen, S. H., Chen, H. L., Shen, X. S., Wang, C. T., Zhang, Y. L., and Liu, D. H. (2012). Effects of planting density and nitrogen application on yield and lodging of mechanized sowing maize. *Southwest China J. Agri.* 25, 805–808. doi: 10.16213/j.cnki.scjas.2012.03.031 (In Chinese)

Chen, S. T., Zou, J. W., and Hu, Z. H. (2017). Measurements and modeling of soil respiration in terrestrial ecosystems. *Ecol. Environ. Sci.* 26, 1985–1996. doi: 16258/j.cnki.1674-5906.2017.11.020 (In Chinese)

Collatz, G., James, B. J., Timothy, G. C., Berry, J. A. (1991). Physiological and environmental regulation of stomatal conductance, photosynthesis and transpiration: a model that includes a laminar boundary layer. *Agricultural & Forest Meteorology*, 54, 107–136. doi: 10.1016/0168-1923(91)90002-8

Elmore, R. W., and Ferguson, R. B. (1999). Mid-season stalk breakage in corn: hybrid and environmental factors. *J. Prod. Agric.* 12, 293–299. doi: 10.2134/jpa1999.0293

Falge, E., Baldocchi, D., Olson, R., and Anthoni, P. (2001). Gap-filling strategies for defensible annual sums of net ecosystem exchange. *Agric. For. Meteorol.* 107, 43–69. doi: 10.1016/S0168-1923(00)00225-2

Farquhar, G. D., Von Caemmere, S., and Berry, J. A. (1980). A biochemical model of photosynthetic Co_2 assimilation in leaves of C_3 species. *Planta* 149, 78–90. doi: 10.1007/BF00386231

Gao, J., Shi, J. G., Dong, S. T., Liu, P., Zhao, B., and Zhang, J. W. (2017). Effect of different light intensities on root characteristics and grain yield of maize (*Zea Mays* L.). *Sci. Agric. Sin.* 50, 2104–2113. doi: 10.3864/j.issn.0578-1752.2017.11.016 (In Chinese)

Guo, J. X., Bian, L. G., and Dai, Y. J. (2007). Measured Co_2 concentration and flux at 16m height during corn growing period on the North China plain. *Chin. J. Atmos. Sci.* 31, 695–707. doi: 10.3878/j.issn.1006-9895.2007.04.14 (In Chinese)

Jia, H. L., Wang, G., Guo, M. Z., Shah, D., Jiang, X. M., and Zhao, J. L. (2015). Methods and experiments of obtaining corn population based on machine vision. *Trans. Chin. Soc. Agri. Eng.* 31, 215–220. doi: 10.3969/j.issn.1002-6819.2015.03.028 (In Chinese)

Jun, X., Ling, G., Yingshan, Z., Hesheng, Y., Jingshan, T., and Wangfeng, Z. (2016). Effects of light intensity within the canopy on maize lodging. *Field Crop Res.* 188, 133–141. doi: 10.1016/j.fcr.2016.01.003

Jun, X., Rui-Zhi, X., Wang-Feng, Z., Ke-Ru, W., Peng, H., Bo, M., et al. (2017). Research Progress on reduced lodging of high-yield and-density maize. *J. Integr. Agric.* 16, 2717–2725. doi: 10.1016/S2095-3119(17)61785-4

Kang, M. S., Kushairi Din, A., Zhang, Y., and Magari, R. (1999). Combining ability for rind puncture resistance in maize. *Crop Sci.* 39, 368–371. doi: 10.2135/cropsci1999.0011183X0039000200011x

Li, C., He, H. L., Liu, M., Su, W., Fu, Y. L., Zhabg, L. M., et al. (2008). The design and application of Co_2 flux data processing system at China flux. *Geo-Inf. Sci.* 10, 557–565. (In Chinese)

Li, S. Y., Ma, W., Peng, J. Y., and Chen, Z. M. (2015a). Study on yield loss of maize due to lodging at the big flare stage and grain filling stage. *Sci. Agri. Sin.* 19, 3952–3964. doi: 10.3864/j.issn.0578-1752.2015.19.017 (In Chinese)

Li, S. Y., Wang, Y. X., Hu, C. D., and Yan, Y. (2015b). Effect of strong wind lodging at pre-and post-tasseling stages on growth and yield of maize. *Chin. J. Appl. Ecol.* 26, 2405–2413. doi: 10.13287/j.1001-9332.20150521.018 (In Chinese).

Liu, Y., Chen, P. M., and Chen, J. N. (2015). Progress and perspectives in studies on agro-ecosystem carbon cycle model. *Trans. Chin. Soc. Agri. Eng.* 31, 1–9. doi: 10.3969/j.issn.1002-6819.2015.03.001 (In Chinese)

Liu, Q., Xie, L. F., and Li, F. R. (2019). The spatial distribution of the needle area of planted Larix Olgensis trees. *Forests* 10, 1–17. doi: 10.3390/f10010028

Lizaso, J. I., Batchelor, W. D., Boote, K. J., and Westgate, M. E. (2005). Evaluating a leaf-level canopy assimilation model linked to Ceres-maize. *Agron. J.* 97, 734–740. doi: 10.2134/agronj2004.0172

Ma, X. Y., and Zhou, G. S. (2016). Maize biomass simulation based on dynamic Photosynthate allocation. *Chin. J. Appl. Ecol.* 27, 2292–2300. (In Chinese). doi: 10.13287/j.1001-9332.201607.026

Minami, M., and Ujihara, A. (1991). Effects of lodging on dry matter production, grain yield and nutritional composition at different growth stages in maize (*Zea Mays* L.). *Japan. J. Crop Sci.* 60, 107–115. doi: 10.1626/jcs.60.107

National Bureau Of Statistics Of China. *China Statistical Yearbook*. Beijing: China Statistics Press, (2018): 401–405. (In Chinese)

National Meteorological Administration. *Agricultural Meteorological Observation Specifications (Volume I)*. Beijing: Meteorological Press (1993): 7–30. (In Chinese)

Peng, J. Y., and Yang, G. X. (2018). Improvement of evapotranspiration models in maize field and its sensitivities analysis to the resistance parameters. *Agric. Res. Arid Areas.* 36, 55–62. doi: 10.7606/j.issn.1000-7601.2018.02.09 (In Chinese)

Ren, C. Y., Yu, G. R., Wang, Q. F., and Guan, D. X. (2004). Study on coupling model of photosynthesis and transpiration of ecosystem at canopy scale. *Sci. China Ser. D Earth Sci.* 34, 142–151. In Chinese

Shah, A. N., Tanveer, M., Rehman, A. U., Anjum, S. A., Iqbal, J., and Ahmad, R. (2017). Lodging stress in cereal—effects and management: An overview. *Environ. Sci. Pollut. Res. Vol.* 24, 5222–5237. doi: 10.1007/s11356-016-8237-1

Sun, J. W., Yuan, F. H., Guan, D. X., and Wu, J. B. (2013). Dark respiration of terrestrial vegetations: a review. *Chin. J. Appl. Ecol.* 24, 1739–1746. (In Chinese).

Tjkelker, M. G., Oleksyn, J., and Reich, P. B. (2001). Modelling respiration of vegetation: evidence for a general temperature-dependent Q10. *Glob. Chang. Biol.* 7, 223–230. doi: 10.1046/j.1365-2486.2001.00397.x

Vickers, D., and Mahrt, L. (1997). Quality control and flux sampling problems for tower and aircraft data. *J. Atmos. Ocean. Technol.* 14, 512–526. doi: 10.1175/1520-0426(1997)014<0512:QCAFSP>2.0.CO;2

Wang, J. (2006). Study on the experiment and simulation of crop growth and water heat and Co_2 transfer in agro-ecosystem. *Beijing, Chin. Acad. Sci.*, 78–90. (In Chinese)

Wang, X., Li, Y., Han, W., Song, Z., Wang, S., and Yang, J. (2022). Evaluation of root lodging resistance during whole growth stage at the plant level in maize[J]. *Sci. Rep.* 12:10375. doi: 10.1038/s41598-022-14159-0

Wang, H. L., Wu, R. H., Zhu, K., Zhang, Y. C., Zhang, Y. J., and Sun, J. W. (2011). Reviews of causes and control of maize lodging. *J. Henan Agri. Sci.* 40, 1–5. doi: 10.15933/j.cnki.1004-3268.2011.10.015 (In Chinese)

Wang, J., Yu, Q., Li, X. G., Sun, X. M., and Zhu, Z. L. (2004). Diurnal variation of winter wheat water and heat fluxes of a simulation with photosynthesis-evapotranspiration coupled model. *Chin. J. Appl. Ecol.* 11, 2077–2082. (In Chinese)

Xu, Z. W., Liu, S. M., Gong, L. J., Wang, J. M., and Li, X. W. (2008). A study on the data processing and quality assessment of the Eddy covariance system. *Adv. Earth Sci.* 23, 357–370. doi: 10.3321/j.issn:1001-8166.2008.04.005 (In Chinese)

Xue, J., Qi, B., Ma, B., Li, B., and Gou, L. (2021). Effect of altered leaf angle on maize stalk lodging resistance[J]. *Crop Sci.* 61, 689–703. doi: 10.1002/csc2.20284

Yoon-Sup, S., Adetimirin Victor, O., and Soon-Kwon, K. (2013). Observational study on the recovery from root lodging at flowering time and yield reduction in maize (*Zea Mays* L.). *Plant Breeding Biotechnol.* 1, 171–177. doi: 10.9787/PBB.2013.1.2.171

Yu, G. R., and Sun, X. M.. *Principles of Fluxes Measurement in Terrestrial Ecosystems*. Beijing: Higher Education Press, (2006): 316–324. (In Chinese)

Yu, Q., Wang, T. D., Liu, J. D., and Sun, S. F. (1998). A mathematical study on crop architecture and canopy photosynthesis I. *Model. Acta Agronomica Sinica* 24, 7–15. (In Chinese)

Zhang, Z. (2016). Simulation on Hulunbeier meadow steppe ecosystem carbon cycle dynamic and future climate scenario analysis. *Chin.Acad. Agri. Sci.*, 1–10. (In Chinese)

Zhang, J. Y., Liu, S., Song, C. Y., Gao, J. L., and Sun, L. J. (2009). Cause analysis and prevention measures of maize lodging. *Shandong Agric. Sci.* 11, 119–121. (In Chinese)

Zhang, D., Wang, J. C., Chen, H., Hunag, Z. J., and Sun, T. (2018). Effect of density on dry matter accumulation of maize and establishment of normalized simulation model. *J. Maize Sci.* 026, 58–64. doi: 10.13597/j.cnki.maize.science.20180510 (In Chinese)

Zhang, Y. Q., Yu, Q., Liu, C. M., and Wang, J. (2004). Coupled simulation of vegetation photosynthesis, canopy conductance and evapotranspiration. *Sci. China Ser. D Earth Sci.* 34, 152–160. (In Chinese)

Zhnag, Y. Q., Liu, C. M., Shen, Y. J., and Yu, H. N. (2001). Transitional calculation of carbon dioxide flux over agronomy-ecosystem. *Chin. J. Appl. Ecol.* 12, 726–730. (In Chinese)

frontiers | Frontiers in Ecology and Evolution

TYPE Original Research
PUBLISHED 12 May 2023
DOI 10.3389/fevo.2023.1179608

OPEN ACCESS

EDITED BY
Wei Zhao,
Institute of Geographic Sciences and Natural Resources Research, Chinese Academy of Sciences (CAS), China

REVIEWED BY
Yuemin Yue,
Institute of Subtropical Agriculture, Chinese Academy of Sciences (CAS), China
Chong Jiang,
Guangzhou Institute of Geography, China

*CORRESPONDENCE
Li Zhang
li.zhang@igsnrr.ac.cn

SPECIALTY SECTION
This article was submitted to Population, Community, and Ecosystem Dynamics, a section of the journal Frontiers in Ecology and Evolution

RECEIVED 04 March 2023
ACCEPTED 24 March 2023
PUBLISHED 12 May 2023

CITATION
Lv Y, Zhang L, Li P, He H, Ren X and Zhang M (2023) Ecological restoration projects enhanced terrestrial carbon sequestration in the karst region of Southwest China. *Front. Ecol. Evol.* 11:1179608. doi: 10.3389/fevo.2023.1179608

Ecological restoration projects enhanced terrestrial carbon sequestration in the karst region of Southwest China

Yan Lv[1,2,3], Li Zhang[1,2,4]*, Pan Li[5], Honglin He[1,2,4], Xiaoli Ren[1,2,4] and Mengyu Zhang[1,2,3]

[1]Key Laboratory of Ecosystem Network Observation and Modeling, Institute of Geographic Sciences and Natural Resources Research, Chinese Academy of Sciences, Beijing, China, [2]National Ecosystem Science Data Center, Institute of Geographic Sciences and Natural Resources Research, Chinese Academy of Sciences, Beijing, China, [3]University of Chinese Academy of Sciences, Beijing, China, [4]College of Resources and Environment, University of Chinese Academy of Sciences, Beijing, China, [5]School of Earth System Science, Tianjin University, Tianjin, China

The karst region of southwest China showed a significant increase in vegetation cover and vegetation carbon stocks under the implementation of a series of ecological restoration projects. However, the relative contribution of ecological restoration projects to terrestrial carbon sequestration in the context of climate change has yet to be well quantified. Here, we used the Community Land Model (CLM4.5) to investigate the trend of net ecosystem productivity (NEP) and attribution to multiple environmental factors in the karst region of southwest China during 2000–2018. The result showed that ecosystems with a significant increasing trend of NEP covered about 46% of the study region, which were mainly located in the peak forest plain region, colliculus region, peak cluster depression region, and middle-high hill region. The simulation experiments suggested that land use change associated with ecological restoration projects caused a large contribution of 53% to the increasing NEP trend, followed by CO_2 fertilization (72%), while climate factors and nitrogen deposition showed minor negative effects. Especially, the NEP trend induced by land use change in the 100 pilot counties with the implementation of rocky desertification control project was significantly higher than that in the other karst area. Moreover, moderate and high levels of restoration efforts invested into recovery led to a larger increasing trend (0.66 $gC/m^2/yr^2$ and 0.48 $gC/m^2/yr^2$) in NEP than the low efforts level (0.22 $gC/m^2/yr^2$). Our results highlight the important role of ecological restoration projects in the enhanced terrestrial carbon sequestration in the karst region of southwest China, and recommend a comprehensive assessment of ecological restoration projects for policymaking.

KEYWORDS

net ecosystem productivity, temporal variation, environmental factors, the CLM4.5 model, the ecological restoration projects

1. Introduction

The karst region of southwest China holds one of the largest continuous karsts in the world, which is highly sensitive to the increasing climate variability and extreme climate events (Kharin et al., 2013; Seddon et al., 2016). Meanwhile, the increase in population expanded the demand for natural resources and caused a severe rocky desertification (Sweeting, 2012; Delang and Yuan, 2016). Approximately 0.13 million km^2 of karst areas were transformed into rocky

landscapes from natural vegetation (Yuan, 1997; Wang et al., 2004). To combat land degradation and improve the ecological security situation, Chinese governments have invested more than 130 billion yuan in launching a series of ecological restoration projects since 1999 (Delang and Yuan, 2016). The Grain to Green Project is the most ambitious project for restoring natural vegetation and prevention of sloping farmland in human history (Ouyang et al., 2016; Xu et al., 2017). The government has also set up the rocky desertification control projects in the karst region of Southwest China since 2008, which covered from 100 pilot counties at first to all 451 rocky desertification counties in 2015. With the implementation of these ecological restoration projects, many studies have found that a recent increase in the Normalized Difference Vegetation Index (NDVI) and Leaf Area Index (LAI) (Cai et al., 2014; Xu and Zhang, 2014), aboveground biomass carbon (ABC) (Tong et al., 2020), and vegetation optical depth (VOD) (Brandt et al., 2018) in the karst region of Southwest China. This region's ecosystem quality increased simultaneously (Zhang M. et al., 2022). Estimation of the effect of ecological restoration projects on ecosystem functions (especially carbon sequestration function) in the karst region of Southwest China is crucial to the ecosystem management and performance assessment of ecological civilization construction.

Previous studies have confirmed the positive effect of ecological restoration projects on vegetation cover and vegetation carbon stocks based on different methods (Zhang et al., 2015; Zhang M. et al., 2016; Tong et al., 2017, 2018). Based on residuals between observed and predicted vegetation cover and biomass trends, Tong et al. (2017) found a direct positive effect of management in Guizhou, Yunnan, and Guangxi. Residual analysis also indicated that ecological services were improved by rocky desertification control in a typical karst region of northwest Guangxi (Zhang M. et al., 2016). The positive impacts of rocky desertification control measures on the vegetation carbon services were found in the typical karst area of northwest Guangxi through the method of canonical correspondence analysis (Zhang et al., 2015). By comparing the results of satellite products and dynamic vegetation models, Tong et al. (2018) pointed out that the areas of high ecological restoration projects have stronger positive trends in vegetation cover and vegetation carbon stocks, while the areas of little ecological restoration projects have weaker positive trends in vegetation cover and vegetation carbon stocks in Guizhou, Yunnan, and Guangxi after 2000. Besides the role of ecological restoration projects, these changes on vegetation cover and vegetation carbon stocks are also associated with other environmental drivers (Wang et al., 2014), such as changing climate, rising atmospheric CO_2 concentration, and increasing nitrogen deposition (Choi, 2004; Seabrook et al., 2011). Climatic conditions, human management, and disturbances may influence the effectiveness of ecological restoration projects. High annual rainfall and soil moisture after drought events help increase vegetation cover, especially in the areas where ecological restoration projects are implemented (Brandt et al., 2018). High investments of ecological restoration projects combined with sufficient rainfall generally increase the effectiveness of ecological restoration projects (Tong et al., 2017). However, the relative contribution of ecological restoration projects on ecosystem functions (especially carbon sequestration function) in the context of climate change and human activities in the karst region of Southwest China has not been well quantified.

The primary actions of the ecological restoration projects include expanding the natural vegetation, reducing sloping farmland, and cultivating crops on more fertile and less erodible soils (Tong et al., 2020). The implementation of ecological restoration projects directly influences the ecosystem functions (especially carbon sequestration function) through the land use change (Qin et al., 2022). The objectives of this study are to investigate the trend of NEP in the karst region of southwest China during 2000–2018, and to analyze the relative contribution from multiple environmental factors (i.e., climate change, atmospheric CO_2 concentration, nitrogen deposition, and land use change). Here, we used the Community Land Model version 4.5 (CLM4.5) to simulate the temporal variation of net ecosystem productivity (NEP) and region contribution in different karst region, and conducted a series of simulation experiments to quantify the impacts from different drivers on NEP trend.

2. Materials and methods

2.1. Study region

As one of the most typical, complex, and extensive karst landforms worldwide, the karst region of Southwest China includes Chongqing, Hubei, Hunan, Guangdong, Guangxi, Guizhou, Sichuan, and Yunnan provinces (Figure 1). With poor soil formation ability, thin soil depth, and poor surface water retention (Jiang et al., 2014), the environment in this region is vulnerable and very sensitive to climate change and anthropogenic activities (Yuan et al., 1990). Subtropical monsoon climate is the main climate types, with a mean manual temperature of 15.00°C and a mean manual precipitation of 1,100 mm. The vegetation coverage is high with a proportion of forest land and grassland equaling 82.43%. According to similarities of the karst geomorphology and its formation causes, the karst region of Southern China could be divided into eight karst regions, namely Peak forest plain region (I), Trough valley region (II), Colliculus region (III), Gorge region (IV), Peak Cluster Depression region (V), Faulted Basin region (VI), Plateau region (VII), and Middle-high Hill region (VIII) (Supplementary Table S1; Wang et al., 2015). Because of the increasing intensity of human exploitation of natural resources, about 0.13 million km^2 of karst areas were turned into rocky landscapes. A series of ecological restoration projects has been implemented to improve the environment (Tong et al., 2018). The 100 pilot counties with the implementation of rocky desertification control project since 2008 are mainly located in the regions of Colliculus (II), Gorge (IV), and Plateau (VII). According to the total area of ecological restoration projects, the 100 pilot counties are divided into three groups: (1) less than 50 km^2 (low efforts), (2) 50–100 km^2 (moderate efforts), and (3) more than 100 km^2 (high efforts) (Tong et al., 2018).

2.2. Data

The input data of CLM4.5 mainly include seven climate variables (i.e., air temperature, precipitation, relative humidity, downwelling longwave radiation, downwelling short-wave radiation, surface pressure, and wind speed), two atmospheric environment variables (i.e., atmospheric CO_2 concentration and nitrogen deposition), and other environment variables, such as plant function type, and dynamic land use and land cover change data. Climate data (1979–2018) were extracted from the high spatial and temporal resolution surface meteorological element driven dataset in China with a temporal

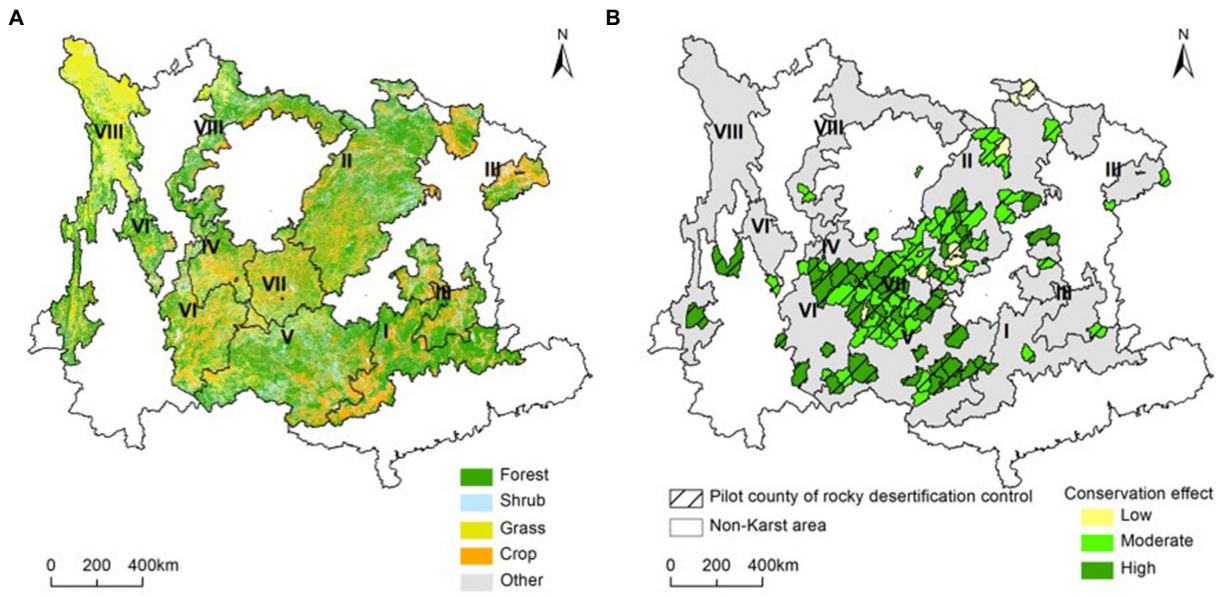

FIGURE 1
The vegetation type in karst region in Southwest China **(A)** and three groups of the 100 pilot counties of rocky desertification control since 2008 **(B)**: (1) less than 50 km^2 (low efforts), (2) 50–100 km^2 (moderate efforts), and (3) more than 100 km^2 (high efforts). I: Peak forest plain, II: Trough valley, III: Colliculus, IV: Gorge, V: Peak Cluster Depression, VI: Faulted Basin, VII: Plateau, VIII: Middle-high Hill.

resolution of 3 h and a spatial resolution of 0.1° (He et al., 2020). The atmospheric CO_2 concentration (1850–2015) with a spatial resolution of 1° comes from Mauna Loa Observatory (Lamarque et al., 2010). The atmospheric nitrogen deposition data (1980–2015) with a spatial resolution of 0.05° were calculated based on the atmospheric inorganic nitrogen wet deposition data proposed by Jia et al. (2019) and the dry and wet nitrogen deposition ratio developed by Yu et al. (2019). The plant functional type and dynamic land use and land cover changes data (1990–2015) with a spatial resolution of 0.05° were processed based on the land cover data of China (ChinaCover) produced by Wu et al. (2014) and climate variables (Wang et al., 2017) using the method reported in Bonan et al. (2018). The parameter values of ratio of leaf carbon to nitrogen for each plant functional type were revised against the inventory data (Tang Z. et al., 2018). All input data of CLM4.5 was resampled to a unified spatial resolution (0.5°). Climate data has a temporal resolution of 6 h. Other input data have a temporal resolution of 1 year. Then we could use these data to force the CLM4.5.

Modelled outputs were evaluated by estimated carbon flux production from Yao et al. (2018) and Jung et al. (2011), and field inventory data of vegetation and soil carbon density (Fang et al., 2018; Tang X. et al., 2018) in the study region. Yao et al. (2018) used a machine learning algorithm to develop a GPP dataset based on observation data from 40 stations in China and surrounding countries during 1982–2015. Jung et al. (2011) also used a machine learning algorithm to develop a terrestrial land-atmosphere energy fluxes dataset based on observation data from FLUXNET during 1982–2011. Machine learning algorithms have been applied to the upscaling of eddy covariance measurements from local to continental (Xiao et al., 2018). Therefore, these products produced by machine learning algorithms could be approximately regarded as the observed data.

We used the method in Vicente-Serrano (2006) to calculate Standardized Precipitation Index (SPI) data using monthly precipitation data (Lv et al., 2022). The SPI computed on shorter scales (e.g., 3 months) describes the short-term moisture conditions that affect the ecosystem. We used the SPI 3 to identify drought events. The drought events were extracted with SPI 3 data <−1.0, which indicates when water shortages were developing or imminent (Vicente-Serrano et al., 2014). To quantify the influence of annual water stress on the karst ecosystems, the SPI 3 products at monthly resolution were aggregated to an annual mean.

2.3. CLM4.5

2.3.1. Model description

The CLM4.5 model is a state-of-the-art land surface model for simulating bio-geophysical and bio-geochemical processes in the atmosphere-vegetation-soil continuum (Oleson et al., 2013), which has a good performance in estimating carbon and water fluxes for terrestrial ecosystems (Zhang L. et al., 2016; Li et al., 2018) and has been well applicated in China's terrestrial ecosystem (Jia et al., 2018; Lu et al., 2021; Xue et al., 2021).

2.3.2. Experiment design

We performed five simulations to assess the relative contributions of changing climate, rising atmospheric CO_2 concentration, increasing nitrogen deposition, and historical land use change on the carbon sequestration (Table 1). In simulation S1, we kept the climate driver constant for the entire period 1990–2018 and varied the other environmental factors. In simulation S2, only the atmospheric CO_2 concentration was hold constant. In simulation S3, we used the varied climatic factors, atmospheric CO_2 concentration, and land use change and held the nitrogen deposition at 1990. In simulation S4, we only kept the land use

TABLE 1 The description of simulation experiments.

Simulation experiment	Climate	Atmospheric CO_2 concentration	Nitrogen deposition	Land use change
S1	1990	1990–2018	1990–2018	1990–2018
S2	1990–2018	1990	1990–2018	1990–2018
S3	1990–2018	1990–2018	1990	1990–2018
S4	1990–2018	1990–2018	1990–2018	1990
S5	1990–2018	1990–2018	1990–2018	1990–2018

constant, while varying the other environmental factors. Finally, in simulation S5, we allowed all factors to change throughout the full simulation. The effects of each individual factor are calculated by subtracting S1, S2, S3, and S4 from simulation S5. The simulated yearly variables for gross primary productivity (GPP), ecosystem respiration (ER), and NEP from 2000 to 2018 were used for the analysis in this study.

2.3.3. Model simulation

We determined the initial conditions by first running the CLM4.5 to equilibrium using a two-stage spin-up method. Initial spin-up followed the accelerated decomposition approach for 600 simulation years with the long-term average climate and all other environmental factors. Then a normal decomposition spin-up was operated for 1,000 years using a repeating 40-year (1979–2018) cycle of climatic factors and constant other environmental factors until a dynamic equilibrium was reached. After initialization, we performed a transient run from 1901 to 2018 of the time series data of all driving factors. In this study, we choose 1990 as the base year. The annual temperature (13.64°C) and annual precipitation (1,364 mm) in 1990 are close to the multi-year average value during 1990–2018 (13.96°C and 1,370 mm). Moreover, the "base year" of emission reduction stipulated in the Kyoto Protocol is 1990. The emission reduction effect of greenhouse gases needs to be referenced and measured relative to 1990.

3. Results

3.1. Model evaluation

We evaluated modelled annual GPP by CLM4.5 with the GPP estimation extracted from the results of Yao et al. (2018) and Jung et al. (2011). Modelled annual GPP has a similar spatial pattern with the estimation based on eddy-flux observations in the karst region of Southwest China (Figures 2A–C). The Pearson correlation coefficients between GPP modelled by CLM4.5 and the estimated data of Yao et al. (2018) and Jung et al. (2011) across the eight regions were 0.94 and 0.87, respectively. For those areas with high GPP in the Peak forest plain region (I), Trough valley region (II), Colliculus region (III), Peak Cluster Depression region (V), and Plateau region (VII), the model bias for GPP varied from −8.65 to 3.35% (Figure 2D). The mean total annual GPP in the study area modelled by CLM4.5 is 1.56 Pg C/yr., which was slightly higher than that in the previous studies by 11–16%.

Figure 3 shows the comparison of observed and modelled mean vegetation carbon and soil carbon density for different forest types in the karst region of Southwest China. The CLM4.5 model could capture the variation in vegetation carbon density among different forest types but overestimate by 14.0% for ENF, 19.7% for DBF, 25.3% for MF, and 26.8% for EBF (Figure 3A). The mean values of the modelled soil carbon density were well consistent with the inventory data, with relative errors ranging from −2.6 to 3.9% for DBF, EBF, and MF, except 17.7% for ENF (Figure 3B).

3.2. Long-term trend of NEP and regional contribution

There was an increasing trend in NEP, although it was not statistically significant (0.16 Tg C/yr^2, $p = 0.87$). However, the trend of NEP showed a large spatial heterogeneity in the karst region of Southwest China. About 76% of the study region shows an increasing trend, among which 33% is significant at $p = 0.05$ level, which were mainly located in the Peak forest plain region (I), Colliculus region (III), Peak Cluster Depression region (V), and Middle-high Hill region (VIII) (Figures 4A,B). The increasing trend in NEP in these areas reached to 0.93 Tg C/yr^2 (Figure 4C), because a larger increasing rate in GPP (3.46 Tg C/yr^2) than that in ER (2.53 Tg C/yr^2). The accumulated NEP increased from 24.95 to 380.16 Tg C/yr in these areas (Figure 4C), which highlighted the important role in these areas in carbon sequestration.

The trend of NEP in different karst regions over the period 2000–2018 was shown in Figure 4D. Ecosystems in the Peak forest plain region (I), Peak Cluster Depression region (V), and Middle-high Hill region (VIII) dominated the increase in NEP, with the contribution of 28, 82, and 33%, respectively. The increasing rate of NEP in the Peak Cluster Depression region (V) was the highest (0.14 Tg C/yr^2, $p = 0.06$), followed by Peak forest plain region (I) and Middle-high Hill region (VIII) with similar trend of 0.057–0.059 Tg C/yr^2. Besides these three regions, the Plateau region (VII) also had a large contribution to the NEP trend (32%). The increases in NEP in these regions were all resulted from the higher enhancement in GPP than that in ER.

3.3. Contribution of environmental factors to the trend in NEP

Simulation experiments suggested that atmospheric CO_2 concentration (73%) and land use change (53%) dominated the increasing NEP trend, while climate change and nitrogen deposition led to the decrease in NEP (−26% and − 0.2%, respectively). CO_2 fertilization significantly stimulate NEP due to larger response of GPP than ER (3.05 vs. 2.96 Tg C/ppm), especially in the Peak forest plain region (I), Trough valley region (II), and Middle-high Hill region (VIII) (Figure 5B).

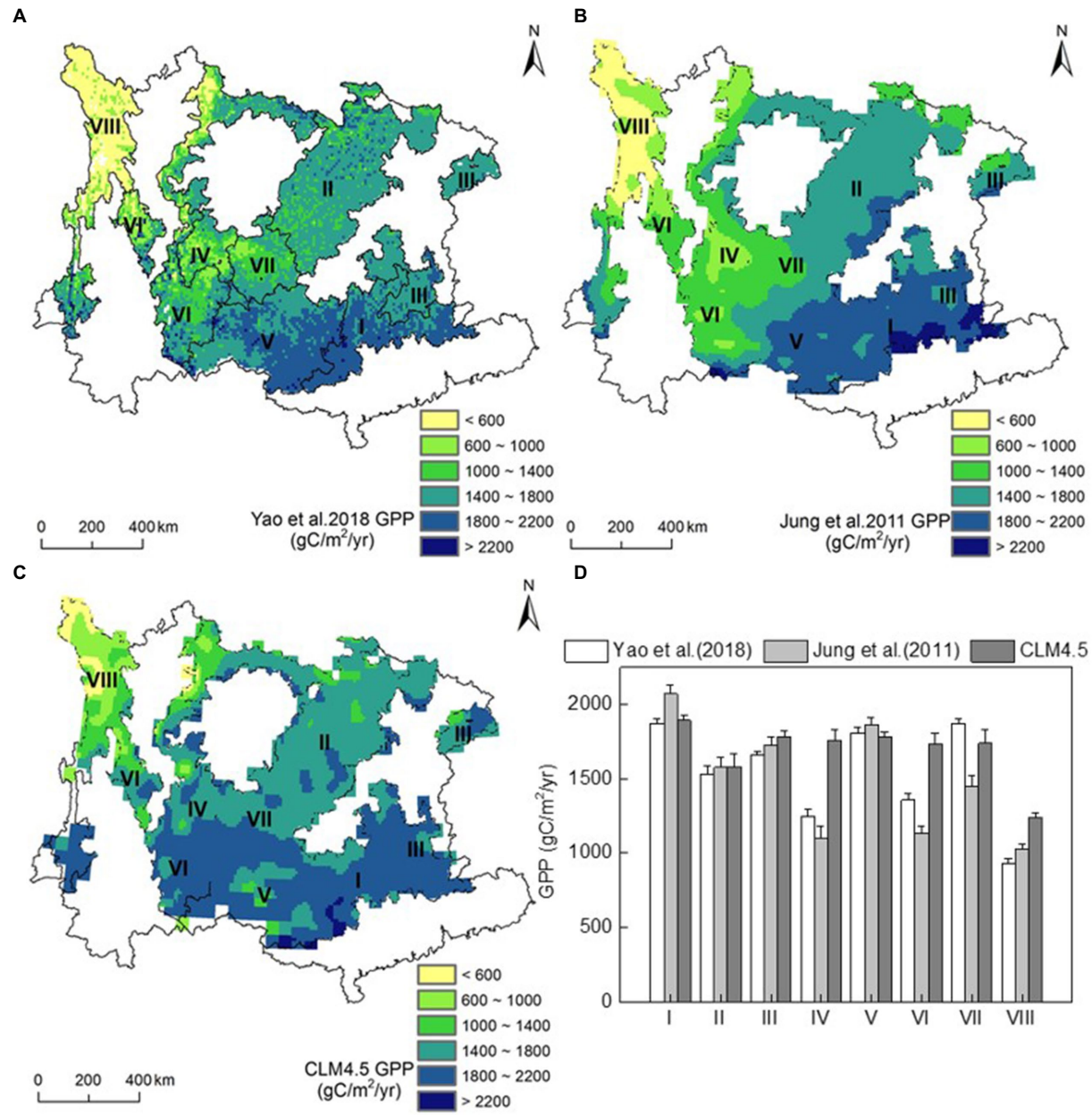

FIGURE 2
Comparison of mean gross primary productivity (GPP) between Yao et al. (2018), Jung et al. (2011), and the CLM4.5 model. The spatial pattern of mean GPP in different karst regions in Yao et al. (2018), Jung et al. (2011), and the CLM4.5 model **(A–C)**. The mean GPP in different karst regions in Yao et al. (2018), Jung et al. (2011), and the CLM4.5 model **(D)**. I: Peak forest plain, II: Trough valley, III: Colliculus, IV: Gorge, V: Peak Cluster Depression, VI: Faulted Basin, VII: Plateau, VIII: Middle-high Hill.

The increasing NEP trend induced by land use change (0.09 Tg C/yr^2, $p < 0.05$, Figure 5A) was mainly related to the large-scale afforestation (3,964 km^2), and cropland abandonment (13,517 km^2) under the implementation of a series of ecological restoration projects since 2000 (Supplementary Figure S1D). Especially in the Colliculus region (III) and Plateau region (VII), the area of afforestation is eight times that of other karst regions (Supplementary Table S3). In addition, the contribution of land use change to the NEP trend is higher than the contribution of CO_2 in the Colliculus region (III), Plateau region (VII), and Middle-high Hill region (VIII) (Figure 5B).

There was a larger increase in NEP (+0.44 gC/m^2/yr^2, $p < 0.05$, Figure 6B) induced by land use change in the 100 pilot counties of rocky desertification control than that in the other karst area due to higher trend in GPP (+0.21 gC/m^2/yr^2, $p < 0.05$) and less in ER (−0.23 gC/m^2/yr^2, $p < 0.05$). Moreover, the positive effect of land use change on NEP trend varied with ecological restoration projects efforts. The difference in impacts of land use change were analysed at the county level by dividing the 100 pilot counties of rocky desertification control into three groups according to the total ecological restoration projects areas (Figure 1B). The difference in the area of conversion of farmland into forest in the low ecological

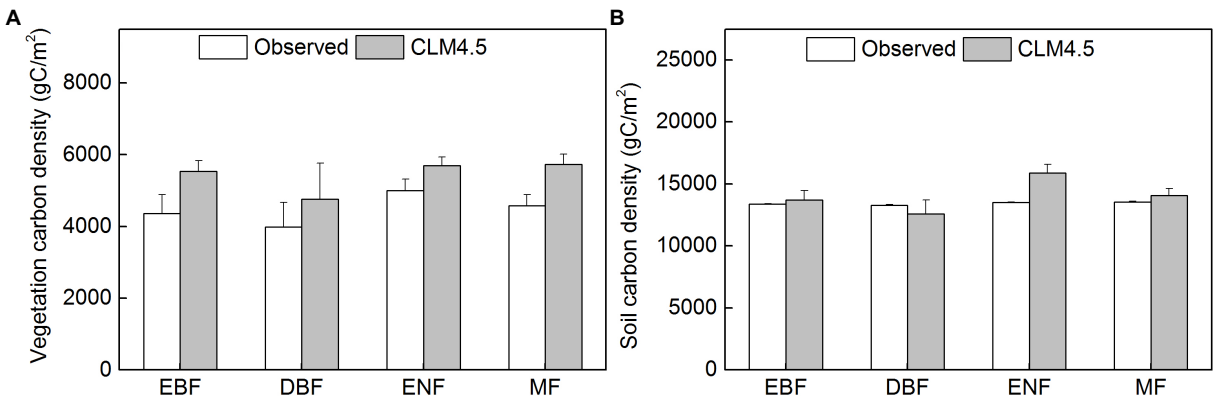

FIGURE 3
Comparison of vegetation carbon density **(A)** and soil carbon density **(B)** in different plant types in karst region of Southwest China between the observation and CLM4.5. EBF: evergreen broadleaved forest, DBF: deciduous broadleaved forest, ENF: evergreen needle leaved forest, MF: mixed forest.

restoration projects area (625 km^2) and the moderate and high ecological restoration projects areas (3,900 and 3,075 km^2, respectively) led to the difference of NEP trend driven by land use change in three groups. The NEP trend induced by land use change in the counties with moderate and high ecological restoration projects efforts (0.66 and 0.58 $gC/m^2/yr^2$, $p < 0.05$, respectively) significantly greater than those with low efforts (0.22 $gC/m^2/yr^2$, $p < 0.05$). In addition, the trend in NEP increased significantly with increasing forest coverage (Slope = 0.46, $p < 0.05$, Figure 6C) in the 100 pilot counties of rocky desertification control. These results indicated that the implementation of ecological restoration projects in the karst region of Southwest China play a remarkable role in enhancing carbon sequestration, especially in the moderate and high ecological restoration projects efforts areas. The positive NEP trend induced by land use change in counties of high ecological restoration projects efforts area was slightly lower than those with moderate efforts area, which might be associated with the drought events in 2009 and 2011. The karst region of Southwest China experience drought events in 2009 and 2011, of which 13 and 5%, respectively, in the high ecological restoration projects area (Supplementary Figure S2).

The negative effect of climate on the NEP trend in this region (−0.04 Tg C/yr^2, $p = 0.83$, Figure 5A) was mainly caused by the significant warming with the rate of 0.023°C/yr ($p < 0.05$; Supplementary Figure S1C). The increasing temperature led to a faster increase in ER (2.65 Tg C/yr^2, $p = 0.09$) than GPP (2.10 Tg C/yr^2, $p < 0.05$). This negative effect of climate was mainly in the Trough valley region (II), Colliculus region (III), and Faulted Basin region (VI) (Figure 5B). The Trough valley region (II) and Colliculus region (III) had the large increase of temperature and the high response of NEP to temperature (Supplementary Table S4). In addition, the minor contribution of nitrogen deposition to the trend in NEP was mainly due to the significant decrease of nitrogen deposition (Supplementary Table S2) and the large response of NEP to nitrogen deposition in the Trough valley region (II) (Supplementary Table S4).

4. Discussion

Southwest China has been one of the largest coherent regions with positive biomass and vegetation cover trends since 2000 (Brandt et al., 2018). Consequently, vegetation carbon sequestration has increased since 2000 as revealed by both remote sensing data (Zhang et al., 2017; Tong et al., 2020) and ecosystem process models (Zhang M. et al., 2016; Tong et al., 2018). Our study demonstrated the increase in carbon sequestration in the karst region of Southwest China during 2000–2018, especially in the Peak Forest Plain region (I), the Peak Cluster Depression region (V), and the Middle-high Hill region (VIII). This increasing trend of carbon sequestration in the karst region of Southwest China is also supported by the terrestrial land-atmosphere energy fluxes dataset from Jung et al. (2011) with a significant increasing rate of 11.74 Tg C/yr^2 ($p < 0.05$) for GPP and 5.75 Tg C/yr^2 ($p < 0.05$) for NEP in 2000–2011, and Yao et al. (2018) with the increasing rate of GPP (1.24 Tg C/yr^2, $p = 0.50$) during 2000–2015.

The increase in carbon sequestration in the karst region of southwest China has been proven to be associated with high ecological restoration projects after 2000 (Zhang M. et al., 2016; Brandt et al., 2018; Tong et al., 2018; Zhang X. et al., 2022). Our results suggested that land use change was the second large contributor to the sustained carbon sequestration besides elevated atmospheric CO_2 concentration. To alleviate ecological degradation and ameliorate regional poverty, the Chinese government has invested in a series of mitigation initiatives, which are aimed at converting farmlands and degraded lands into conservation or production forests and grasslands (Delang and Yuan, 2016). The land use change resulted in a large increase in carbon sequestration by increasing the aboveground and underground carbon density (Hong et al., 2020) and the turnover of carbon storage (Chen and Tian, 2007). With the increase of forest coverage driven by ecological restoration projects, the average ratio of the ecosystem service index increased (Zhang M. et al., 2022). With the increase of ecological restoration projects efforts, the growth rate of vegetation cover and carbon density became faster (Lv et al., 2018; Tong et al., 2018). We found the differences of increasing trend in carbon sequestration between low and other (i.e., moderate and high) ecological restoration projects efforts (Figure 6B). The positive impact of the ecological restoration projects may be influenced by climatic conditions, human management, and disturbances. The temperate climate with sufficient rainfall and high investments generally lead to the high effectiveness of ecological restoration projects in Peak Forest Plain region (I) and Peak Cluster Depression region (V) (Tong et al., 2017).

Such a positive effect of land use change on the increase of carbon sequestration in China on the national scale had been demonstrated by Tian et al. (2011) using process-based models and Houghton and

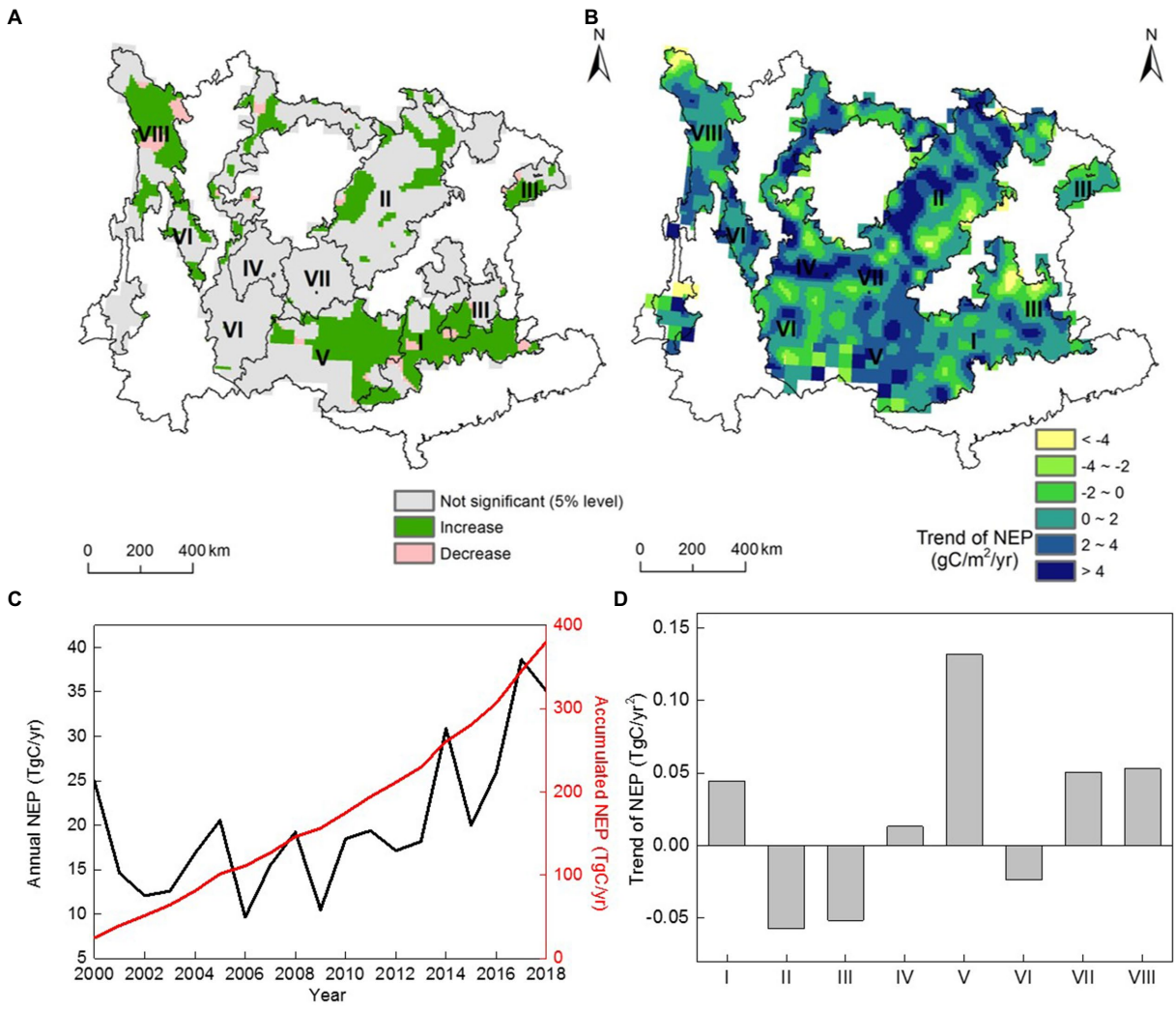

FIGURE 4
Temporal change and regional contribution of net ecosystem productivity (NEP) in karst region of Southwest China over the period 2000–2018 estimated by the CLM4.5 model. **(A)** Significance of the NEP trend in karst region of Southwest China during 2000–2018. **(B)** Temporal changes of the NEP in karst region of Southwest China during 2000–2018. **(C)** Annual NEP and accumulated NEP in the region of significant variation in NEP during 2000–2018. **(D)** Regional contribution of the NEP trend. I: Peak forest plain, II: Trough valley, III: Colliculus, IV: Gorge, V: Peak Cluster Depression, VI: Faulted Basin, VII: Plateau, VIII: Middle-high Hill.

Nassikas (2017) using the bookkeeping model but was underestimated by Jia et al. (2020) based on results of the Multi-scale Synthesis and Terrestrial Model Intercomparison Project (MsTMIP). The low contributions of land use change to GPP might be related to the underestimates of the forest area in China (33,292 km^2) in the land use change dataset produced by Hurtt et al. (2006) and Yu et al. (2022). On the other hand, the model assumptions relating to whether the productivity of secondary vegetation is smaller or larger than that of the vegetation it replaces are also important (Zhu et al., 2016). We found the land use change has a higher contribution to carbon sequestration (0.44 Tg C/yr^2) in the karst region of southwest China, compared with the effect of land use change on carbon sequestration in China (0.27 Tg C/yr^2). These results suggested that the ecological restoration projects in the karst region of southwest China play a crucial role in the increase of carbon sequestration in China. When considering the carbon emissions caused by land use change, the net biome productivity (NBP) still increased in the karst region of southwest China (1.23 Tg C/yr^2, $p = 0.28$, Supplementary Figure S3).

The effects of atmospheric CO_2 concentrations on carbon sequestration were consistent with previous studies in China (Tian et al., 2011; Jia et al., 2020) and the globe (Keenan et al., 2021) due to photosynthesis increases as CO_2 concentrations rise (Huntingford and Oliver, 2021). In contrast, climate had a negative effect on the carbon sequestration in this karst region of southwest China as shown in both this study and Tong et al. (2017), which might be due to the increase in temperature and decrease in soil water during drought events in recent years (e.g., 2009 and 2011) (Song et al., 2019). Compared to the result of Tian et al. (2011), the nitrogen deposition's contribution to carbon sequestration was lower in this study. The main reason is that the reference level of nitrogen deposition and other factors was assigned to the value in 1990 not that in 1900 as Tian et al. (2011). Right now, the nitrogen deposition level increased by 7.06 TgN/yr. than that of 1990 and 11.09 TgN/yr. than that of 1900 (data came from Tian et al., 2011) in China, but the nitrogen utilization efficiency (10.6 gC/gN) was similar to that (10.1 gC/gN) of Tian et al. (2011).

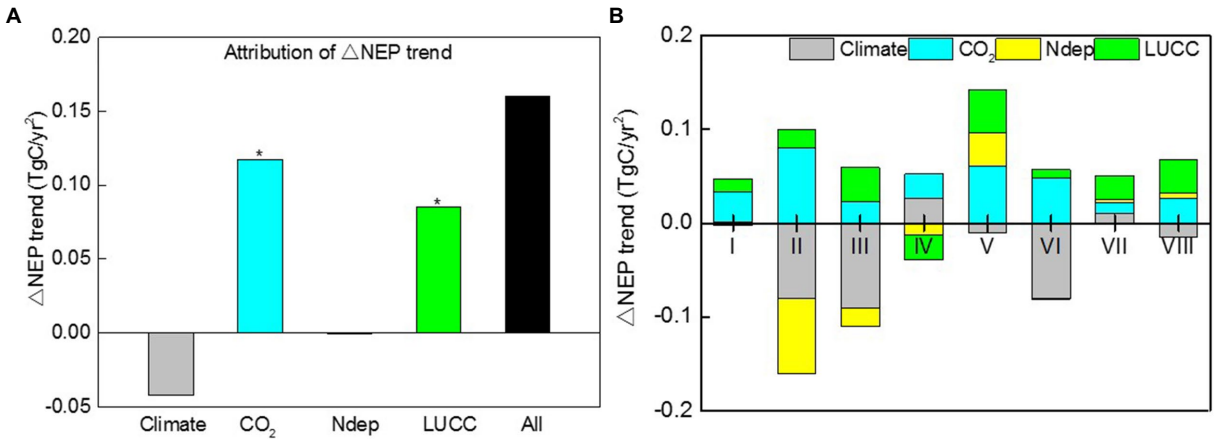

FIGURE 5
Effects of environmental factors (i.e., climatic factors (Climate), atmospheric carbon dioxide concentration (CO_2), nitrogen deposition (Ndep), land use change (LUCC), and all environmental factors (All)) on the net ecosystem productivity (NEP) trend **(A)** in karst region of Southwest China and different karst regions **(B)**. I: Peak forest plain, II: Trough valley, III: Colliculus, IV: Gorge, V: Peak Cluster Depression, VI: Faulted Basin, VII: Plateau, VIII: Middle-high Hill. * means $p<0.05$.

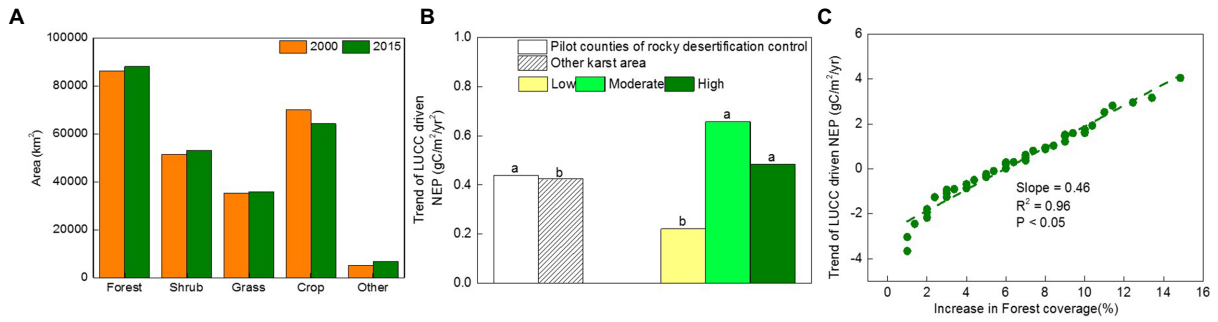

FIGURE 6
Temporal change of land use change (LUCC) in 2000 and 2015 in the 100 pilot counties of rocky desertification control **(A)**, land use change (LUCC) driven net ecosystem productivity (NEP) in the 100 pilot counties of rocky desertification control and other karst area, and in the three groups of the 100 pilot counties of rocky desertification control during 2008–2018 **(B)**, and the relationship between the increase in forest coverage and trend of LUCC driven NEP **(C)**. According to their total area of ecological restoration projects, the 100 pilot counties of rocky desertification control were divided in three groups: (1) less than 50km² (low efforts), (2) 50–100km² (moderate efforts), and (3) more than 100km² (high efforts). a and b on the bar chart mean that there is a significant difference in the trend of NEP between different groups.

Under the recommendations for formulating China's 14th five-year development plan and the long-range goals for 2035, the karst regions of southwest China will control more than 10,760 km² of rocky desertification in Hubei, Guizhou, and Yunnan provinces. In Hunan province, more than 7.50 km² of afforestation and grassland construction were carried out (Gao et al., 2021). Moreover, constructing the national rocky desert park is essential, which could realize the combination of rocky desertification control and poverty control. The implementation of these actions in 451 counties of karst desertification control will continue to increase carbon sequestration in forest and grassland, protect against soil erosion, and create a more biodiversity-rich landscape (Hogarth et al., 2013; Tong et al., 2020). Nevertheless, large-scale ecological restoration projects can have an adverse impact on the ecosystem by decreasing soil moisture and water availability (Feng et al., 2016; Jia et al., 2017; Zhao et al., 2021). Therefore, the ecological restoration projects require adjusted according to different situations. Such as, better water-conservancy areas are suitable for tropical and subtropical economic fruit species, while water-deficient areas should be planted drought tolerant savanna woody species (Zhang et al., 2012). And the benefits of ecological restoration projects should be comprehensively evaluated when considering the sustainability of ecosystems.

The impacts of multiple environmental factors on carbon sequestration have been in the spotlight of science (Qian et al., 2019; Liu et al., 2023). Based on process-based model, the simulation experiments could quantify the influence of changing climate, rising atmospheric CO_2 concentration, increasing nitrogen deposition, and historical land use change on the carbon sequestration (Tian et al., 2011; He et al., 2019). The large contribution (53%) of land use change to the increasing NEP trend in our study is similar to the result of Yu et al. (2022), who pointed out that forest expansion increased China's land carbon sink since 1980 using the simulation experiments in DLEM with a contribution of 44%. In addition, such an important role of land use change in stimulating the positive trend in carbon sequestration in China is also supported by previous studies using other approaches, such as residual analysis (Tong et al., 2017), canonical correspondence analysis (Zhang et al., 2015), comparison

of the differences between satellite products and dynamic vegetation models (Tong et al., 2018), and comparison of the differences between the baseline period and post-period (Lu et al., 2018). However, we did not include the legacy of previous land use change, which might cause uncertainty about the estimated effect of land use change. Tian et al. (2011) pointed out that the land use change could cause a change of 2.7 to 4.1% in total carbon stocks in the first half of the 20th century. These land use legacy effects in the karst regions of southwest China require further exploration in the future. Other factors, such as forest management, grazing, irrigation and disturbances, were not included in the CLM4.5 in our study. Such a comprehensive assessment of ecological restoration projects requires the strengthening of long-term observation and research, and more efforts to better simulate the effects of land cover changes and land management practices on karst ecosystems (Chen et al., 2020) in the next generation process-based models.

5. Conclusion

In this study, we investigated the trend of carbon sequestration and the impacts of environmental factors in the karst region of Southwest China during 2000–2018 using the CLM 4.5 model. Our result showed that areas with a significant trend of NEP covered about 45.6% of the study region. This increasing NEP trend was mainly contributed by the peak forest plain region, peak cluster depression region, and the middle-high hill region. We found that land use change plays an important role in stimulating the positive trend in NEP besides atmospheric CO_2 concentration in this region, while climate and nitrogen deposition had relatively small negative contributions. Moreover, with the large-scale afforestation and cropland abandonment, a notable increase in NEP was found in the 100 pilot counties of rocky desertification control project, when compared with the other karst areas. Furthermore, the areas with moderate and high ecological restoration efforts had a higher increasing rate of NEP than the low effort areas. Our study demonstrated the benefits of ecological restoration projects on carbon sequestration in the karst region of Southwest China, which could keep contributing to the achievement of China's carbon neutrality.

Data availability statement

The datasets presented in the study are shown in the article, further inquiries can be directed to the corresponding author. Climate data were extracted from the high spatial and temporal resolution surface meteorological element driven dataset in China (He et al., 2020). The atmospheric CO_2 concentration comes from Mauna Loa Observatory (Lamarque et al., 2010). The estimated carbon flux production comes from Yao et al. (2018) and Jung et al. (2011). The outputs of CLM4.5 are available upon request from Li Zhang (li.zhang@igsnrr.ac.cn).

Author contributions

YL: methodology, validation, and writing (original draft). LZ: experiment design, conceptualization, and editing. PL: investigation. HH: editing. XR: editing. MZ: editing. All authors contributed to the article and approved the submitted version.

Funding

This work was supported by the National Natural Science Foundation of China (31971512, 31988102, and 42141005).

Conflict of interest

The authors declare that the research was conducted in the absence of any commercial or financial relationships that could be construed as a potential conflict of interest.

Publisher's note

All claims expressed in this article are solely those of the authors and do not necessarily represent those of their affiliated organizations, or those of the publisher, the editors and the reviewers. Any product that may be evaluated in this article, or claim that may be made by its manufacturer, is not guaranteed or endorsed by the publisher.

Supplementary material

The Supplementary material for this article can be found online at: https://www.frontiersin.org/articles/10.3389/fevo.2023.1179608/full#supplementary-material

References

Bonan, G. B., Levis, S., Kergoat, L., and Oleson, K. W. (2018). Landscapes as patches of plant functional types: an integrating concept for climate and ecosystem models. *Global Biogeochem Cycles* 16, 5-1–5-23. doi: 10.1029/2000GB001360

Brandt, M., Yue, Y., Wigneron, J. P., Tong, X., Tian, F., Jepsen, M. R., et al. (2018). Satellite-observed major greening and biomass increase in South China karst during recent decade. *Earth's Future* 6, 1017–1028. doi: 10.1029/2018EF000890

Cai, H., Yang, X., Wang, K., and Xiao, L. (2014). Is forest restoration in the Southwest China karst promoted mainly by climate change or human-induced factors? *Remote Sens.* 6, 9895–9910. doi: 10.3390/rs6109895

Chen, A., Tang, R., Mao, J., Yue, C., Li, X., Gao, M., et al. (2020). Spatiotemporal dynamics of ecosystem fires and biomass burning-induced carbon emissions in China over the past two decades. *Geogr Sustain* 1, 47–58. https://doi:10.1016/j.geosus.2020.03.002. doi: 10.1016/j.geosus.2020.03.002

Chen, G., and Tian, H. (2007). Land use/cover change effects on carbon cycling in terrestrial ecosystems. *Chin. J. Plant Ecol.* 31, 189–204. doi: 10.17521/cjpe.2007.0024

Choi, Y. D. (2004). Theories for ecological restoration in changing environment: toward 'futuristic' restoration. *Ecol. Res.* 19, 75–81. doi: 10.1111/j.1440-1703.2003.00594_19_1.x

Delang, C. O., and Yuan, Z. (2016). *China's Grain for Green Program*. New York, United States: Springer International.

Fang, J., Yu, G., Liu, L., Hu, S., and Chapin, F. S. (2018). Climate change, human impacts, and carbon sequestration in China. *Proc. Natl. Acad. Sci. U. S. A.* 115, 4015–4020. doi: 10.1073/pnas.1700304115

Feng, X., Fu, B., Piao, S., Wang, S., Ciais, P., Zeng, Z., et al. (2016). Revegetation in China's loess plateau is approaching sustainable water resource limits. *Nat. Clim. Chang.* 6, 1019–1022. doi: 10.1038/nclimate3092

Gao, J., Li, G., Zhang, Y., and Zou, C. (2021). Analysis on Goals, Tasks and Realization Path of China's 14th Five Year Plan for Ecological and Environmental Protection. Environmental Protection. *Environmental Protection*. 49, 45–51. doi: 10.14026/j.cnki.0253-9705.2021.02.008

He, H., Wang, S., Zhang, L., Wang, J., Ren, X., Zhou, L., et al. (2019). Altered trends in carbon uptake in China's terrestrial ecosystems under the enhanced summer monsoon and warming hiatus. *Natl. Sci. Rev.* 6, 505–514. doi: 10.1093/nsr/nwz021

He, J., Yang, K., Tang, W., Lu, H., Qin, J., Chen, Y., et al. (2020). The first high-resolution meteorological forcing dataset for land process studies over China. *Sci Data*. 7:25. doi: 10.1038/s41597-020-0369-y

Hogarth, N. J., Belcher, B., Campbell, B., and Stacey, N. (2013). The role of forest-related income in household economies and rural livelihoods in the border-region of southern China. *World Dev.* 43, 111–123. doi: 10.1016/j.worlddev.2012.10.010

Hong, S., Yin, G., Piao, S., Dybzinski, R., Cong, N., Li, X., et al. (2020). Divergent responses of soil organic carbon to afforestation. *Nat. Sustain.* 3, 694–700. doi: 10.1038/s41893-020-0557-y

Houghton, R. A., and Nassikas, A. A. (2017). Global and regional fluxes of carbon from land use and land cover change 1850–2015. *Global Biogeochem. Cycles* 31, 456–472. doi: 10.1002/2016GB005546

Huntingford, C., and Oliver, R. J. (2021). Constraints on estimating the CO_2 fertilization effect emerge. *Nature* 600, 224–225. doi: 10.1038/d41586-021-03560-w

Hurtt, G. C., Frolking, S., Fearon, M. G., Moore, B., Shevliakova, E., Malyshev, S., et al. (2006). The underpinnings of land-use history: three centuries of global gridded land-use transitions, wood-harvest activity, and resulting secondary lands. *Glob. Chang. Biol.* 12, 1208–1229. doi: 10.1111/j.1365-2486.2006.01150.x

Jia, B., Luo, X., Cai, X., Jain, A., Huntzinger, D. N., Xie, Z., et al. (2020). Impacts of land use change and elevated CO_2 on the interannual variations and seasonal cycles of gross primary productivity in China. *Earth Syst. Dynam.* 11, 235–249. doi: 10.5194/esd-11-235-2020

Jia, X., Shao, M., Zhu, Y., and Luo, Y. (2017). Soil moisture decline due to afforestation across the loess plateau, China. *J. Hydrol.* 546, 113–122. doi: 10.1016/j.jhydrol.2017.01.011

Jia, B., Wang, Y., and Xie, Z. (2018). Responses of the terrestrial carbon cycle to drought over China: modeling sensitivities of the interactive nitrogen and dynamic vegetation. *Ecol. Model.* 368, 52–68. doi: 10.1016/j.ecolmodel.2017.11.009

Jia, Y., Wang, Q., Zhu, J., Chen, Z., He, N., and Yu, G. (2019). A spatial and temporal dataset of atmospheric inorganic nitrogen wet deposition in China (1996–2015). *China Sci. Data.* 4, 1–10.

Jiang, Z., Luo, W., Deng, Y., Cao, J., Qin, X., Li, Y., et al. (2014). The leakage of water and soil in the karst peak cluster depression and its prevention and treatment. *Acta Geosci. Sin.* 5, 535–542. doi: 10.3975/cagsb.2014.05.02 (In Chinese).

Jung, M., Reichstein, M., Margolis, H. A., Cescatti, A., Richardson, A. D., Arain, M. A., et al. (2011). Global patterns of land-atmosphere fluxes of carbon dioxide, latent heat, and sensible heat derived from eddy covariance, satellite, and meteorological observations. *J. Geophys. Res. Biogeosci.* 116:G3. doi: 10.1029/2010JG001566

Keenan, T. F., Luo, X., De Kauwe, M. G., Medlyn, B., Prentice, I. C., Stocker, B., et al. (2021). A constraint on historic growth in global photosynthesis due to increasing CO_2. *Nature* 600, 253–258. doi: 10.1038/s41586-021-04096-9

Kharin, V. V., Zwiers, F. W., Zhang, X., and Wehner, M. (2013). Changes in temperature and precipitation extremes in the CMIP5 ensemble. *Clim. Chang.* 119, 345–357. doi: 10.1007/s10584-013-0705-8

Lamarque, J. F., Bond, T. C., Eyring, V., Granier, C., Heil, A., Klimont, Z., et al. (2010). Historical (1850–2000) gridded anthropogenic and biomass burning emissions of reactive gases and aerosols: methodology and application. *Atmos. Chem. Phys.* 10, 7017–7039. doi: 10.5194/acp-10-7017-2010

Li, P., Zhang, L., Yu, G., Liu, C., Ren, X., He, H., et al. (2018). Interactive effects of seasonal drought and nitrogen deposition on carbon fluxes in a subtropical evergreen coniferous forest in the east Asian monsoon region. *Agric. Forest Meteorol.* 263, 90–99. doi: 10.1016/j.agrformet.2018.08.009

Liu, M., Bai, X., Tan, Q., Luo, G., Zhao, C., Wu, L., et al. (2023). Climate change enhanced the positive contribution of human activities to net ecosystem productivity from 1983 to 2018. *Front. Ecol. Evol.* 10:1101135. doi: 10.3389/fevo.2022.1101135

Lu, F., Hu, H., Sun, W., Zhu, J., Liu, G., Zhou, W., et al. (2018). Effects of national ecological restoration projects on carbon sequestration in China from 2001 to 2010. *Proc. Natl. Acad. Sci. U. S. A.* 115, 4039–4044. doi: 10.1073/pnas.1700294115

Lu, T., Zhang, J., Xue, W., Qiao, Y., Zhou, L., and Che, Y. (2021). Impacts of aerosol direct radiative forcing on terrestrial ecosystem respiration in China from 2001 to 2014. *Atmos. Res.* 260:105713. doi: 10.1016/j.atmosres.2021.105713

Lv, Y., He, H., Ren, X., Zhang, L., Qin, K., Wu, X., et al. (2022). High resistance of deciduous forests and high recovery rate of evergreen forests under moderate droughts in China. *Ecol. Indic.* 144:109469. doi: 10.1016/j.ecolind.2022.109469

Lv, Y., Zhang, L., Yan, H., Ren, X., Wang, J., Niu, Z., et al. (2018). Spatial and temporal patterns of changing vegetation and the influence of environmental factors in the karst region of Southwest China. *Acta Ecol. Sin.* 38, 8774–8786.

Oleson, K., Lawrence, D., Bonan, G., Drewniak, B., Huang, M., Koven, C. D., et al. (2013). *Technical Description of Version 4.5 of the Community Land Model (CLM), NCAR Technical Note: NCAR/TN-503+ STR*. National Center for Atmospheric Research (NCAR), Boulder, CO, USA.

Ouyang, Z., Zheng, H., Xiao, Y., Polasky, S., Liu, J., Xu, W., et al. (2016). Improvements in ecosystem services from investments in natural capital. *Science* 352, 1455–1459. doi: 10.1126/science.aaf2295

Qian, C., Shao, L., Hou, X., Zhang, B., Chen, W., and Xia, X. (2019). Detection and attribution of vegetation greening trend across distinct local landscapes under China's grain to green program: a case study in Shaanxi Province. *Catena* 183:104182. doi: 10.1016/j.catena.2019.104182

Qin, C., Li, S., Yu, G., Bass, A. M., Yue, F., and Xu, S. (2022). Vertical variations of soil carbon under different land uses in a karst critical zone observatory (CZO), SW China. *Geoderma* 412:115741. doi: 10.1016/j.geoderma.2022.115741

Seabrook, L., Mcalpine, C. A., and Bowen, M. E. (2011). Restore, repair or reinvent: options for sustainable landscapes in a changing climate. *Landscape Urban Plan.* 100, 407–410. doi: 10.1016/j.landurbplan.2011.02.015

Seddon, A. W., Macias-Fauria, M., Long, P. R., Benz, D., and Willis, K. J. (2016). Sensitivity of global terrestrial ecosystems to climate variability. *Nature* 531, 229–232. doi: 10.1038/nature16986

Song, L., Li, Y., Ren, Y., Wu, X., Guo, B., Tang, X., et al. (2019). Divergent vegetation responses to extreme spring and summer droughts in southwestern China. *Agric. Forest Meteorol.* 279:107703. doi: 10.1016/j.agrformet.2019.107703

Sweeting, M. M. (2012). *Karst in China: Its Geomorphology and Environment*, vol. *15* Springer Berlin, Heidelberg: Springer Science & Business Media.

Tang, Z., Xu, W., Zhou, G., Bai, Y., Li, J., Tang, X., et al. (2018). Patterns of plant carbon, nitrogen, and phosphorus concentration in relation to productivity in China's terrestrial ecosystems. *Proc. Natl. Acad. Sci. U. S. A.* 115, 4033–4038. doi: 10.1073/pnas.1700295114

Tang, X., Zhao, X., Bai, Y., Tang, Z., Wang, W., Zhao, Y., et al. (2018). Carbon pools in China's terrestrial ecosystems: new estimates based on an intensive field survey. *Proc. Natl. Acad. Sci. U. S. A.* 115, 4021–4026. doi: 10.1073/pnas.1700291115

Tian, H., Melillo, J., Lu, C., Kicklighter, D., Liu, M., Ren, W., et al. (2011). China's terrestrial carbon balance: contributions from multiple global change factors. *Global Biogeochem. Cycles* 25:1. doi: 10.1029/2010gb003838

Tong, X., Brandt, M., Yue, Y., Ciais, P., Rudbeck, J. M., Penuelas, J., et al. (2020). Forest management in southern China generates short term extensive carbon sequestration. *Nat. Commun.* 11:129. doi: 10.1038/s41467-019-13798-8

Tong, X., Brandt, M., Yue, Y., Horion, S., Wang, K., Keersmaecker, W. D., et al. (2018). Increased vegetation growth and carbon stock in China karst via ecological engineering. *Nat. Sustain.* 1, 44–50. doi: 10.1038/s41893-017-0004-x

Tong, X., Wang, K., Yue, Y., Brandt, M., Liu, B., Zhang, C., et al. (2017). Quantifying the effectiveness of ecological restoration projects on long-term vegetation dynamics in the karst regions of Southwest China. *Int J Appl Earth Obs.* 54, 105–113. doi: 10.1016/j.jag.2016.09.013

Vicente-Serrano, S. (2006). Differences in spatial patterns of drought on different time scales: an analysis of the Iberian Peninsula. *Water Resour. Manag.* 20, 37–60. doi: 10.1007/s11269-006-2974-8

Vicente-Serrano, S. M., Julio Camarero, J., and Azorin-Molina, C. (2014). Diverse responses of forest growth to drought time-scales in the northern hemisphere. *Glob. Ecol. Biogeogr.* 23, 1019–1030. doi: 10.1111/geb.12183

Wang, S., Liu, Q., and Zhang, D. (2004). Karst rocky desertification in southwestern China: geomorphology, landuse, impact and rehabilitation. *Land Degrad. Dev.* 15, 115–121. doi: 10.1002/ldr.592

Wang, X., Piao, S., Ciais, P., Friedlingstein, P., Myneni, R. B., Cox, P., et al. (2014). A two-fold increase of carbon cycle sensitivity to tropical temperature variations. *Nature* 506, 212–215. doi: 10.1038/nature12915

Wang, J., Wang, J., Ye, H., Liu, Y., and He, H. (2017). An interpolated temperature and precipitation dataset at 1-km grid resolution in China (2000-2012). *China Sci. Data.* 2, 73–80. doi: 10.11922/csdata.170.2016.0112

Wang, S., Zhang, X., and Bai, X. (2015). An outline of karst geomorphology zoning in the karst areas of southern China. *Mt. Res. Dev.* 33, 641–648.

Wu, B., Yuan, Q., Yan, C., Wang, Z., Yu, X., Li, A., et al. (2014). Land cover changes of China from 2000 to 2010. *Quat Sci* 34, 723–731.

Xiao, J., Zhuang, Q., Baldocchi, D. D., Law, B. E., Richardson, A. D., Chen, J., et al. (2018). Estimation of net ecosystem carbon exchange for the conterminous United States by combining MODIS and Ameri flux data. *Agric. For. Meteorol.* 148, 1827–1847. doi: 10.1016/j.agrformet.2008.06.015

Xu, W., Xiao, Y., Zhang, J., Yang, W., Zhang, L., Hull, V., et al. (2017). Strengthening protected areas for biodiversity and ecosystem services in China. *Proc. Natl. Acad. Sci. U. S. A.* 114, 1601–1606. doi: 10.1073/pnas.1620503114

Xu, E., and Zhang, H. (2014). Characterization and interaction of driving factors in karst rocky desertification: a case study from Changshun, China. *Solid Earth.* 5, 1329–1340. doi: 10.5194/se-5-1329-2014

Xue, W., Zhang, J., Ji, D., Che, Y., Lu, T., Deng, X., et al. (2021). Aerosol-induced direct radiative forcing effects on terrestrial ecosystem carbon fluxes over China. *Environ. Res.* 200:111464. doi: 10.1016/j.envres.2021.111464

Yao, Y., Wang, X., Li, Y., Wang, T., Shen, M., Du, M., et al. (2018). Spatiotemporal pattern of gross primary productivity and its covariation with climate in China over the last thirty years. *Glob. Chang. Biol.* 24, 184–196. doi: 10.1111/gcb.13830

Yu, Z., Ciais, P., Piao, S., Houghton, R. A., Lu, C., Tian, H., et al. (2022). Forest expansion dominates China's land carbon sink since 1980. *Nat. Commun.* 13:5374. doi: 10.1038/s41467-022-32961-2

Yu, G., Jia, Y., He, N., Zhu, J., Chen, Z., Wang, Q., et al. (2019). Stabilization of atmospheric nitrogen deposition in China over the past decade. *Nat. Geosci.* 12, 424–429. doi: 10.1038/s41561-019-0352-4

Yuan, D. (1997). Rock desertification in the subtropical karst of South China. *Z. Geomorphol.* 108, 81–90.

Yuan, D., Drogue, C., Dai, A., Lao, W., Cai, W., Bidaux, P., et al. (1990). Hydrology of the karst aquifer at the experimental site of Guilin in southern China. *J. Hydrol.* 115, 285–296. doi: 10.1016/0022-1694(90)90210-O

Zhang, X., Brandt, M., Yue, Y., Tong, X., Wang, K. L., and Fensholt, R. (2022). The carbon sink potential of southern China after two decades of afforestation. *Earth's Future* 10:e2022EF002674. doi: 10.1029/2022EF002674

Zhang, L., Mao, J., Shi, X., Ricciuto, D., He, H., Thornton, P., et al. (2016). Evaluation of the community land model simulated carbon and water fluxes against observations over China FLUX sites. *Agric. For. Meteorol.* 226-227, 174–185. doi: 10.1016/j.agrformet.2016.05.018

Zhang, J. L., Poorter, L., and Cao, K. F. (2012). Productive leaf functional traits of Chinese savanna species. *Plant Ecol.* 213, 1449–1460. doi: 10.1007/s11258-012-0103-8

Zhang, C., Qi, X., Wang, K., Zhang, M., and Yue, Y. (2017). The application of geospatial techniques in monitoring karst vegetation recovery in Southwest China. *Prog. Phys. Geogr.* 41, 450–477. doi: 10.1177/0309133317714246

Zhang, M., Wang, K., Liu, H., Wang, J., Zhang, C., Yue, Y., et al. (2016). Spatio-temporal variation and impact factors for vegetation carbon sequestration and oxygen production based on rocky desertification control in the karst region of Southwest China. *Remote Sens.* 8:102. doi: 10.3390/rs8020102

Zhang, M., Wang, K., Liu, H., Zhang, C., Wang, J., Yue, Y., et al. (2015). How ecological restoration alters ecosystem services: an analysis of vegetation carbon sequestration in the karst area of Northwest Guangxi, China. *Environ Earth Sci.* 74, 5307–5317. doi: 10.1007/s12665-015-4542-0

Zhang, M., Zhang, L., He, H., Ren, X., Lv, Y., and Chang, Q. (2022). Improvement of ecosystem quality in National key Ecological Function Zones in China during 2000–2015. *J. Environ. Manag.* 324:116406. doi: 10.1016/j.jenvman.2022.116406

Zhao, M., Zhang, J., Velicogna, I., Liang, C., and Li, Z. (2021). Ecological restoration impact on total terrestrial water storage. *Nat. Sustain.* 4, 56–62. doi: 10.1038/s41893-020-00600-7

Zhu, Z., Piao, S., Myneni, R. B., Huang, M., Zeng, Z., Canadell, J. G., et al. (2016). Greening of the earth and its drivers. *Nat. Clim. Chang.* 6, 791–795. doi: 10.1038/nclimate3004

frontiers | Frontiers in Ecology and Evolution

TYPE Original Research
PUBLISHED 31 May 2023
DOI 10.3389/fevo.2023.1193607

OPEN ACCESS

EDITED BY
Cuicui Jiao,
Sichuan University of Science and Engineering, China

REVIEWED BY
Min Liu,
East China Normal University, China
Wenping Yuan,
Sun Yat-sen University, China

*CORRESPONDENCE
Xiaoli Ren
✉ renxl@igsnrr.ac.cn

RECEIVED 25 March 2023
ACCEPTED 09 May 2023
PUBLISHED 31 May 2023

CITATION
Chen X, Ren X, He H, Zhang L and Lv Y (2023) Seasonal variation of ecosystem photosynthetic capacity and its environmental drivers in global grasslands.
Front. Ecol. Evol. 11:1193607.
doi: 10.3389/fevo.2023.1193607

Seasonal variation of ecosystem photosynthetic capacity and its environmental drivers in global grasslands

Xiuzhi Chen[1,2,3], Xiaoli Ren[1,2,4]*, Honglin He[1,2,4], Li Zhang[1,2,4] and Yan Lv[1,2,3]

[1]Key Laboratory of Ecosystem Network Observation and Modeling, Institute of Geographic Sciences and Natural Resources Research, Chinese Academy of Sciences, Beijing, China, [2]National Ecosystem Science Data Center, Institute of Geographic Sciences and Natural Resources Research, Chinese Academy of Sciences, Beijing, China, [3]University of Chinese Academy of Sciences, Beijing, China, [4]College of Resources and Environment, University of Chinese Academy of Sciences, Beijing, China

Ecosystem maximum photosynthetic rate (Amax) is an important ecosystem functional property, as it is critical for ecosystem productivity modeling. However, little is known about the mechanisms that regulate the seasonal variation of Amax in grasslands, one of the dominant vegetation types worldwide. In this study, we analyzed the seasonal variability of Amax of grassland sites across the globe and its environmental drivers. We found that grassland Amax had strong seasonal variations, which were influenced by the climate and agricultural management, such as grass cutting and grazing. Second, the seasonal variation of Amax at all arid grasslands [mean annual vapor pressure deficit (VPD)>10hPa] was driven more by changes in canopy physiological property (i.e., maximum photosynthetic rate per leaf area $Amax_a$) than canopy structural property (i.e., leaf area, presented by LAI), because $Amax_a$ had stronger temporal variability than LAI in these ecosystems. Third, temperature and VPD were the most influential factors for the seasonal variability of Amax and LAI, but environmental variables only explained a small proportion of the seasonal variation of $Amax_a$, which was probably because $Amax_a$ was more related to plant traits. Our findings provide new ideas for better parameterizations of Amax in terrestrial ecosystem models.

KEYWORDS

maximum photosynthetic capacity (Amax), grasslands, LAI, soil moisture, vapor pressure deficit

1. Introduction

Amax refers to ecosystem light-saturated CO_2 assimilation rates and represents the potential of an ecosystem's photosynthetic capacity. It is an important ecosystem functional property (Reichstein et al., 2014), determining ecosystem carbon assimilation. Seasonal variations in Amax are critical in determining the seasonality and magnitude of gross primary productivity (GPP) in terrestrial ecosystem modeling (Wilson et al., 2001; Medvigy et al., 2013). Therefore, understanding the seasonal variability of Amax and its drivers is vital for improving the understanding of the variability of GPP and the impact of climate change on the terrestrial ecosystem carbon cycle (Luo and Schuur, 2020).

Many studies have shown that Amax has strong seasonal variability in many ecosystem types (Hollinger et al., 1999; Zhang et al., 2006; Polley et al., 2010). Evidence suggests that environmental factors, such as light, temperature, and water, impact the seasonal variations of Amax (Zhang et al., 2006; Polley et al., 2010; Ryan et al., 2017). For example, water stress can directly affect stomatal conductance and the availability of the CO_2 substrate and thus reduce plant photosynthetic capacity (Reich et al., 2018). Leaves can adjust their photosynthetic rates to acclimate or adapt to changes in air temperature and solar radiation on intermediate to long-term timescales (Way and Yamori, 2014; Luo and Keenan, 2020). These environmental variables impact vegetation photosynthetic capacity through two different mechanisms. One is through influencing the canopy's physiological properties (i.e., the maximum photosynthesis rate per leaf area $Amax_a$) (Joswig et al., 2021), and the other is through affecting the canopy's structural properties (i.e., leaf area) (Hu et al., 2018; Li et al., 2019). Nevertheless, little literature has investigated to what extent the two mechanisms contribute to Amax.

Grasslands cover approximately 20–30% of the global land area (O'Mara, 2012), and have a great impact on the inter-annual variations in the global terrestrial carbon cycle (Poulter et al., 2014; Ahlström et al., 2015), thus it is important to understand grassland photosynthetic processes. However, knowledge of the mechanisms behind the seasonal variations in Amax of grassland ecosystems is limited. Therefore, in this study, we investigated the seasonal variations of grassland Amax. First, we derived the time series of Amax from flux measurements for 15 grassland sites in the FLUXNET 2015 dataset and analyzed its seasonal variations. Second, Amax was decomposed into leaf area index (LAI) and $Amax_a$ ($Amax = LAI \times Amax_a$), and their relative contributions to the variations of Amax were quantified. Third, we investigated the effect of environmental variables on the seasonal variations of Amax, $Amax_a$, and LAI.

2. Data and methods

2.1. Site information and meteorological data

Half-hourly eddy covariance (EC) flux data were used in this study to estimate the Amax of global grasslands. Data were retrieved from the FLUXNET 2015 Tier 1 dataset.[1] Intotal, 15 EC flux sites were analyzed in this study. These sites were selected based on the data availability (i.e., sites with more than 60% of $Amax_a$ data over the available years). Meteorological data measured alongside the flux data were also used, including soil water content (SWC), vapor pressure deficit (VPD), air temperature (Ta), and solar shortwave radiation (Rad). Detailed information for the sites used in this study is listed in Table 1.

2.2. Remote sensing data

Leaf area index data (LAI) were extracted from the moderate resolution imaging spectroradiometer (MODIS) Leaf Area Index/FPAR Products version 6.1 (MOD15A2H v061). This product was an 8-day composite dataset with a spatial resolution of 500 m. We filtered out those data points where significant clouds or snow were present, or where the data quality was poor according to the quality flags (FparLai_QC and FparExtra_QC) provided by this dataset. The average LAI of pixels within a 500 m radius around the flux tower was used to represent the LAI of the site, because Chu et al., 2021 suggested that target areas with a smaller radial distance from the flux tower tend to be less biased in representing the land surface characteristics as covered by the flux footprint climatology. Then, the LAI time series were smoothed using the Savitzky–Golay (SG) filter, which has widely been used to remove the noises in MODIS LAI data (Zhu et al., 2016; Huang et al., 2021).

Normalized difference vegetation index (NDVI) data were downloaded from the MODIS C6 (MOD13C1) which had a resolution of 16-day and 500 m. The average NDVI of pixels that are within a 500 m radius around the flux tower was used to represent the NDVI of the site. To match the temporal resolution of LAI, we interpolated the NDVI time series to the LAI dates using linear interpolation.

2.3. Estimation of ecosystem maximum photosynthetic rate

We used the daytime flux partitioning method to derive the parameters of photosynthesis and respiration. The daytime flux partitioning method uses a light response curve to fit the flux of CO_2. We followed the method proposed by Lasslop et al. (2010), with a small modification of separately estimating day-time and night-time reference respiration rates to account for light inhibition of leaf respiration (Keenan et al., 2019):

$$F_c = \frac{\alpha\beta R_g}{\alpha R_g + \beta} + F_r \tag{1}$$

where α (μmol C J^{-1}) is the canopy-scale quantum yields; β (μmol C m^{-2} s^{-1}) is canopy light-saturated CO_2 assimilation rate; R_g (W m^{-2}) is incoming shortwave radiation; and F_r (μmol C m^{-2} s^{-1}) is the ecosystem respiration term. Parameter β is estimated as an exponentially decreasing function of VPD, to account for the effect of VPD on apparent photosynthesis:

$$\beta = \begin{cases} \beta_0 \exp\left(-k\left(VPD - VPD_0\right)\right), VPD > VPD_0 \\ \beta_0, VPD < VPD_0 \end{cases} \tag{2}$$

where β_0 and k are fitted parameters and VPD_0 is set to 10 hPa, as in Lasslop et al. (2010). β_0 is the canopy light-saturated CO_2 assimilation rate after removing the influence of VPD, which is equivalent to Amax.

Ecosystem respiration F_r is described by the Lloyd and Taylor model as

$$F_r = R_{ref} \exp\left(E_0\left(\frac{1}{T_{ref} - T_0} - \frac{1}{T_{air} - T_0}\right)\right) \tag{3}$$

1 http://www.fluxnet.org/

TABLE 1 Grasslands used in this study.

Site	Latitude (°)	Longitude (°)	Elevation (m)	Mean annual Ta (°C)	Mean annual Rad (Wm^{-2})	Mean annual VPD (hPa)	Mean annual SWC (%)	Managed	References
Neustift, Austria (AT-Neu)	47.12	11.32	970	6.79	260.72	3.23	33.00	Yes	Wohlfahrt et al. (2008)
Daly River Savanna, Australia (AU-DaP)	−14.06	131.32	67	25.46	479.00	14.12	9.32	No	Beringer et al. (2011)
Emerald, Australia (AU-Emr)	−23.86	148.47	/	21.57	441.29	13.02	10.54	/	/
Riggs Creek, Australia (AU-Rig)	−36.65	145.58	162	15.57	393.46	8.95	21.61	Yes	Beringer et al. (2016)
Sturt Plains, Australia (AU-Stp)	−17.15	133.35	225	26.15	503.88	20.94	10.08	No	Beringer et al. (2011)
Ti Tree East, Australia (AU-TTE)	−22.29	133.64	553	24.31	489.92	24.69	2.61	No	Beringer et al. (2016)
Chamau, Switzerland (CH-Cha)	47.21	8.41	393	9.48	265.09	2.83	53.00	Yes	Zeeman et al. (2010)
Früebüel, Switzerland (CH-Fru)	47.12	8.54	982	7.63	266.98	2.16	45.37	Yes	Rogger et al. (2022)
Monte Bondone, Italy (IT-MBo)	46.01	11.05	1,550	5.21	310.40	2.34	48.55	Yes	Marcolla et al. (2011)
ARM USDA UNL OSU Woodward Switchgrass 1, USA (US-AR1)	36.43	−99.42	611	15.26	402.37	9.02	20.16	No	Raz-Yaseef et al. 2015
ARM Southern Great Plains control site-Lamont, USA (US-ARc)	35.55	−98.04	424	15.67	401.50	7.80	20.14	No	Raz-Yaseef et al. (2015)
Goodwin Creek, USA (US-Goo)	34.25	−89.87	87	16.15	352.87	4.78	32.66	Yes	Runkle et al. (2017)
Santa Rita Grassland, USA (US-SRG)	31.79	−110.83	1,291	18.77	462.02	16.40	7.38	No	Scott et al. (2015)
Vaira Ranch, USA (US-Var)	38.41	−120.95	129	15.83	416.44	10.44	12.23	No	Ma et al. (2007)
Walnut Gulch Kendall Grasslands, USA (US-Wkg)	31.74	−109.94	1,531	17.29	471.20	14.94	6.84	No	Scott et al. (2010)

where R_{ref} (μmol C m^{-2} s^{-1}) is the reference respiration rate at the reference temperature (T_{ref} = 15°C) and E_0 (°C) is the temperature sensitivity. T_{air} is the air temperature and the parameter T_0 (°C) is set to a constant of −46.02°C following Lloyd and Taylor (1994).

To get the seasonal variations of the parameters in the above model, we fitted the equations above to a dynamic window of 2–14 days of Fc depending on the availability of flux measurements, and assumed that every day in the same time window has the same daily parameters. We retrieved the time series of all parameters in the above model (i.e., α, β_0, k, R_{ref}, and E_0) for each site by implementing Equations (1)–(3) using the REddyProc R package.[2] The estimated Amax time series were smoothed with a nonparametric method for estimating regression surfaces (LOESS).

The light-saturated photosynthetic rate per unit leaf area ($Amax_a$) was calculated as the ratio of Amax to LAI. The unit of Amax is μmol m^{-2} ground area s^{-1} and the unit of $Amax_a$ is μmol m^{-2} leaf area s^{-1}. Then, the reason why the ratio of Amax to LAI is $Amax_a$ is demonstrated in Equation (4):

2 https://github.com/bgctw/REddyProc

$$\frac{Amax}{LAI} = \frac{\mu mol\ m^{-2}\ ground\ area\ s^{-1}}{\frac{m^2\ leaf\ area}{m^2\ ground\ area}} = \frac{\mu mol\ m^{-2}\ ground\ area\ s^{-1} \times m^2\ ground\ area}{m^2\ leaf\ area} = \frac{\mu mol\ s^{-1}}{m^2\ leaf\ area} = \mu mol\ m^{-2}\ leaf\ area\ s^{-1} = Amax_a \quad (4)$$

2.4. Statistical analyses

We used linear regression coefficients to quantify the environmental control on the seasonal variations in Amax, $Amax_a$, and LAI. Environmental variables included air temperature (Ta), solar radiation (Rad), SWC, VPD, and day length (Dlen). Day length was defined as the number of hours with Rad >4 W m^{-2} each day. The effects of other environmental factors were also analyzed, but the other environmental factors did not show significant effects on Amax, $Amax_a$, or LAI. For $Amax_a$, we also added NDVI into the independent variables, because environmental variables had little explanatory power for $Amax_a$.

Data used for the seasonal analysis were integrated for every adjacent and non-overlapped eight-day window. Because the time series were multiyear, we divided the 8-day time series each year by the annual mean of that year to remove the inter-annual variations in the variables (Baldocchi et al., 2021). To make the regression coefficients of different variables comparable, we applied z-score standardization to the normalized time series before we conducted the linear regression.

The log–log scaling slope analysis was used to quantify the relative contribution of $Amax_a$ and LAI to variations in Amax because $Amax_a$ and LAI are related to Amax in a multiplicative manner (i.e., Amax = $Amax_a$ × LAI) (Renton and Poorter, 2011). The relative contributions of $Amax_a$ and LAI can be calculated as the regression coefficient of log(Amax) in the following equations:

$$\log(Amax_a) = a_{Amax_a} + b_{Amax_a} * \log(Amax) \quad (5)$$

$$\log(LAI) = a_{LAI} + b_{LAI} * \log(Amax) \quad (6)$$

where a_{Amaxa}, a_{LAI}, b_{Amaxa}, and b_{LAI} are coefficients of the linear regression between Amax and $Amax_a$ and LAI, in which b_{Amaxa} and b_{LAI} represent the relative contribution of $Amax_a$ and LAI to the variations of Amax. $b_{Amaxa} + b_{LAI}$ will always equal 1. If b_{Amaxa} is close to 1 and b_{LAI} is close to 0, then $Amax_a$ is largely responsible for variations in Amax, whereas if b_{Amaxa} is close to 0 and b_{LAI} is close to 1, then LAI is largely responsible for variations in Amax. If b_{Amaxa} and b_{LAI} are both close to 0.5, then $Amax_a$ and LAI are similarly responsible. More information about the derivation and effectiveness of this method can be found in Renton and Poorter (2011).

3. Results

3.1. Seasonal patterns of Amax, $Amax_a$, and LAI

The seasonal dynamics of Amax, $Amax_a$, and LAI and their multiyear averages for each site are shown in Figure 1 and Table 2, respectively. Amax had strong seasonal variations, mainly showing unimodal curves over the season. Amax at North Hemisphere sites usually exhibited a cyclical character each year, but some grasslands in Australia had variable temporal patterns of Amax, which were different for each year, such as at AU-Emr, AU-Stp, and AU-TTE. The seasonal pattern of $Amax_a$ varied substantially among sites. CH-Cha and IT-MBo did not exhibit any clear seasonal trend in $Amax_a$, while $Amax_a$ at other sites had strong seasonal variations, and often had a similar trend with Amax over the growing season. LAI also varied a lot over the season.

The climate influenced the seasonal patterns of Amax, $Amax_a$, and LAI. In grasslands located in no dry season climate according to Köppen-Geiger climate classification (e.g., AT-Neu, CH-Cha, CH-Fru, IT-MBo, US-AR1, US-ARc, and US-Goo), Amax, $Amax_a$, and LAI were higher in higher temperature and radiation season. In contrast, in arid or dry summer sites, the seasonal pattern of Amax, $Amax_a$, and LAI was driven more by water availability (Figure 2). For example, at the US-SRG, US-Var, and US-Wkg sites, Amax was significantly greater during higher water availability periods, but lower in high temperature and radiation periods because of the associated low water availability.

In addition to climate, agricultural management practices also impacted the seasonal variation of Amax, $Amax_a$, and LAI. At sites under intensive management practices (i.e., AT-Neu, CH-Cha, CH-Fru, IT-MBo, US-Goo), the unimodal curve of Amax and LAI changed by grass cutting and grazing, which can reduce Amax and LAI. As shown in the seasonal patterns of Amax at these sites, Amax decreased after each cutting or grazing event and later gradually recovered, which added fluctuation into the unimodal seasonal pattern of Amax (Figure 1). For example, at the AT-Neu site, the meadow was cut three times a year, the three cuts taking place between DOY 153 ~ 167, DOY 204 ~ 224, and DOY 264 ~ 301 (Wohlfahrt et al., 2008). We can observe decreases and recovery of Amax and $Amax_a$ around the three cutting periods in our estimated Amax and $Amax_a$ time series (Figure 1). After each cutting, the grassland could not recover to the same level of Amax as before cutting. Therefore, Amax was decreasing with each of the three cuttings. A similar pattern was also observed in IT-MBo, CH-Cha, and CH-Fru.

3.2. Relative contribution of $Amax_a$ and LAI to the seasonal variation in Amax

$Amax_a$ and LAI jointly influenced the seasonal variations of Amax (b_{Amaxa} and $b_{LAI} \neq 0$) at all sites (Table 3). $b_{LAI} > 0.5$ at all managed sites, except CH-Cha, meaning that LAI contributed more to the seasonal variations in Amax than $Amax_a$ at these sites, which might be because cutting and grazing caused more changes in LAI than in $Amax_a$.

We investigated the effect of air dryness on the relative contribution of LAI to Amax, and we found that $b_{LAI} < 0.5$ and

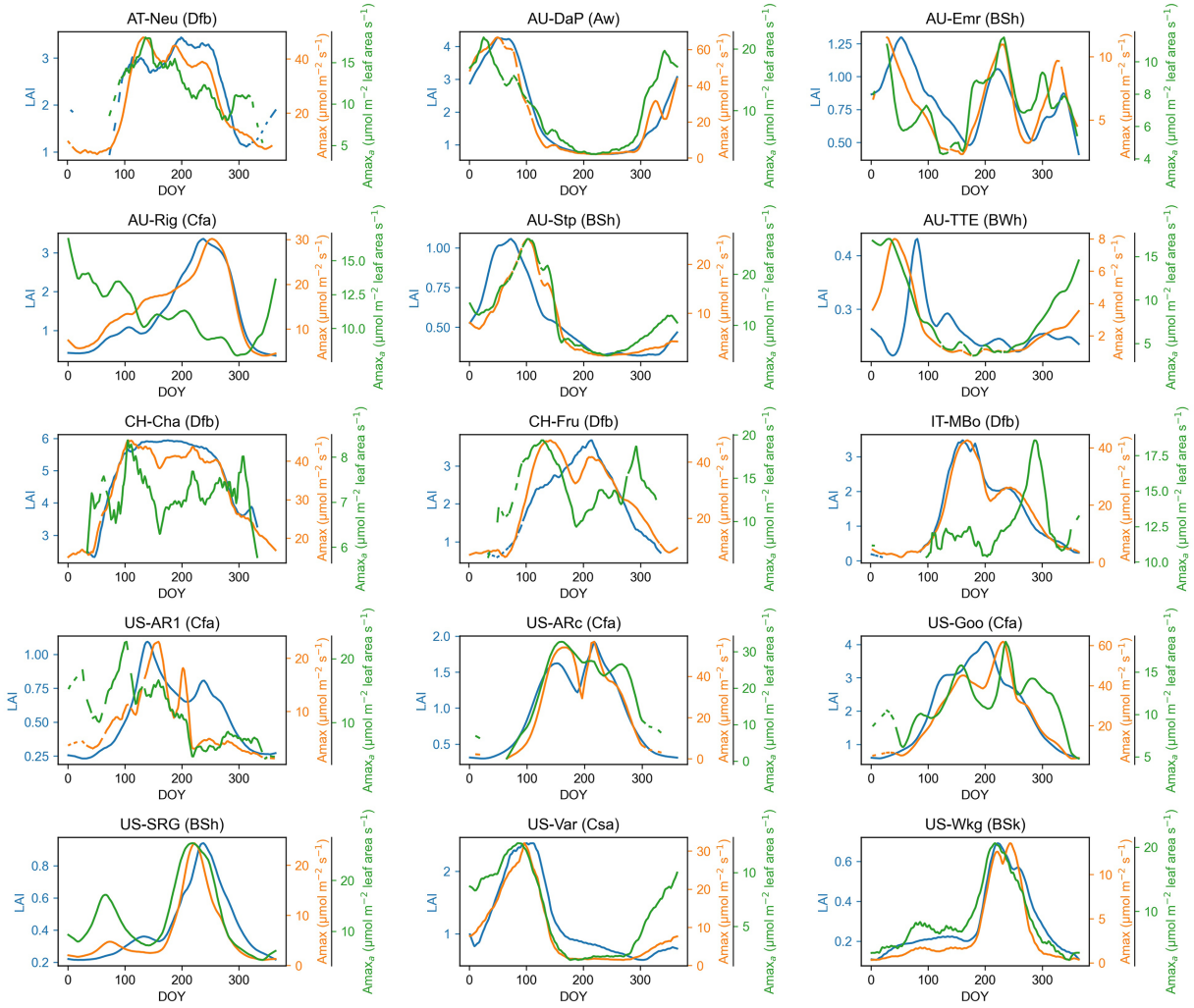

FIGURE 1
Seasonal patterns of maximum photosynthetic capacity (Amax), maximum photosynthetic capacity per leaf area (Amax$_a$), and leaf area index (LAI) for each grassland site. The time series presented in the graph are smoothed with a nonparametric method for estimating regression surfaces (LOESS). The abbreviation after each site name is the Köppen-Geiger climate classification dataset (Beck et al., 2018). Aw, Tropical, savannah; BSh, Arid, steppe, hot; BSk, Arid, steppe, cold; BWh, Arid, desert, hot; Cfa, Temperate, no dry season, hot summer; Csa, Temperate, dry summer, hot summer; Dfb, Cold, no dry season, warm summer.

TABLE 2 Ecosystem maximum photosynthetic capacity (Amax), maximum photosynthetic capacity per leaf area (Amax$_a$), and leaf area index (LAI) for each grassland.

Site	Amax	Amax$_a$	LAI
AT-Neu	46.24	17.31	3.68
AU-DaP	56.56	20.27	3.43
AU-Emr	12.7	13.27	1.29
AU-Rig	29.57	15.19	3.27
AU-Stp	16.29	19.58	0.96
AU-TTE	5.65	14.51	0.41
CH-Cha	48.45	9.2	6.05
CH-Fru	46.93	20.12	3.52
IT-MBo	39.73	16.12	3.5
US-AR1	18.95	20.75	1.04
US-ARc	56.33	32.62	1.75
US-Goo	50.77	17.62	3.63
US-SRG	19.72	23.31	0.83
US-Var	25.37	12.16	2.14
US-Wkg	10.34	18.06	0.57

Amax, Amax$_a$, and LAI were calculated as the multiyear averages of the 90th percentile of the variables each year for each site.

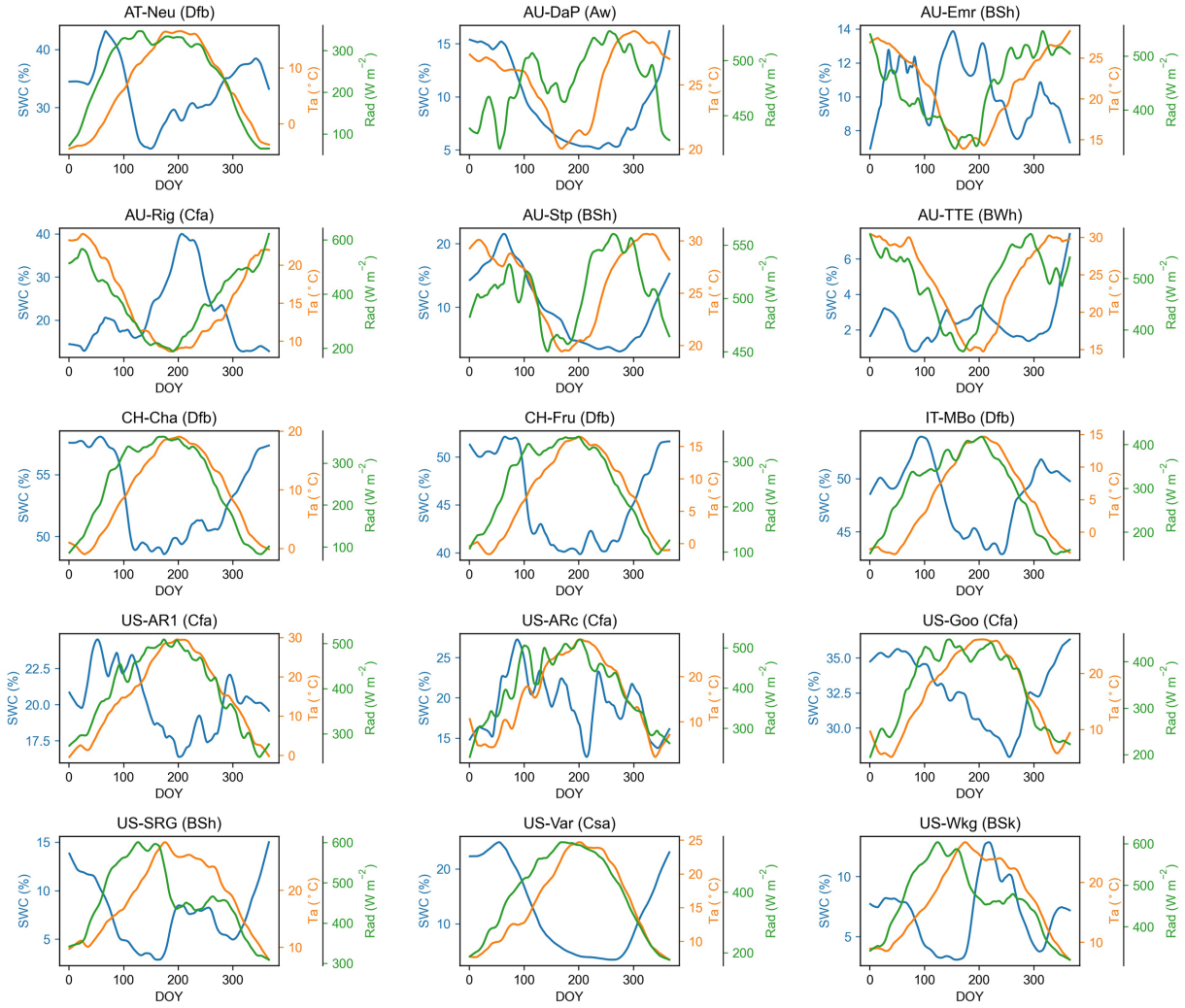

FIGURE 2
Seasonal patterns of air temperature (Ta), solar radiation (Rad), and soil water content (SWC) for each grassland site. The time series presented in the graph are smoothed with a nonparametric method for estimating regression surfaces (LOESS). The abbreviation after each site name is the Köppen-Geiger climate classification dataset (Beck et al., 2018). Aw, Tropical, savannah; BSh, Arid, steppe, hot; BSk, Arid, steppe, cold; BWh, Arid, desert, hot; Cfa, Temperate, no dry season, hot summer; Csa, Temperate, dry summer, hot summer; Dfb, Cold, no dry season, warm summer.

$b_{Amaxa} > 0.5$ in all arid grasslands (mean annual VPD > 10 hPa), which indicated that $Amax_a$ had more influence on Amax than LAI in these sites. In comparison, among moist grassland sites (mean annual VPD < 10 hPa), there were LAI-driven sites and $Amax_a$-driven sites (Figure 3).

To explain the difference between arid and moist grasslands in the relative contribution of LAI and $Amax_a$ to Amax, we further investigated the relationship of b_{Amaxa} with the relative magnitude of the seasonal variability of $Amax_a$ and LAI and the relationship of mean annual VPD and SWC with the seasonal variability of $Amax_a$ and LAI (Figure 4). We found that at sites where $CV_{Amaxa} > CV_{LAI}$, $Amax_a$ contributed more to the seasonal variations of Amax than LAI ($b_{Amaxa} > 0.5$), and $b_{Amaxa} < 0.5$ at sites where $CV_{Amaxa} < CV_{LAI}$ (Figure 4). Sites with $CV_{Amaxa} > CV_{LAI}$ tended to have higher mean annual VPD (Figure 4A). Therefore, $Amax_a$ dominated the seasonal variation of Amax at sites with higher mean annual VPD. Mean annual SWC did not show any correlation with the relative magnitude of CV_{Amaxa} and CV_{LAI}, but grasslands with higher mean annual SWC had lower absolute CV_{Amaxa} (Figure 4B).

3.3. Effects of environmental factors on the seasonal variations of Amax and its components $Amax_a$ and LAI

Among the environmental variables, air temperature (Ta) showed strong control effects for the seasonal variations of $Amax_a$, LAI, and Amax (Table 4), with Ta having the largest absolute regression coefficient with them in most sites. Air dryness (VPD) also greatly influenced the seasonal variations of $Amax_a$, LAI, and Amax, especially for grasslands with a mean annual VPD > 10 hPa. It was consistently negatively associated with them at all sites. However, SWC, representing soil water condition, had a much smaller impact on $Amax_a$, LAI, and Amax. It positively correlated with them at all arid

TABLE 3 Relative contribution of $Amax_a$ and LAI to the seasonal variation in Amax.

Site	b_{LAI}	b_{Amaxa}
AT-Neu	0.56	0.44
AU-DaP	0.43	0.57
AU-Emr	0.42	0.58
AU-Rig	0.98	0.02
AU-Stp	0.4	0.6
AU-TTE	0.28	0.72
CH-Cha	0.31	0.69
CH-Fru	0.72	0.28
IT-MBo	0.92	0.08
US-AR1	0.33	0.67
US-ARc	0.4	0.6
US-Goo	0.59	0.41
US-SRG	0.43	0.57
US-Var	0.35	0.65
US-Wkg	0.41	0.59

b_{LAI} represents the relative contribution of LAI to Amax, and b_{Amaxa} represents the relative contribution of $Amax_a$ to Amax. $b_{LAI}+b_{Amaxa}=1$. If $b_{LAI}>0.5$, LAI contributes more to Amax than $Amax_a$; otherwise, $Amax_a$ contributes more to Amax.

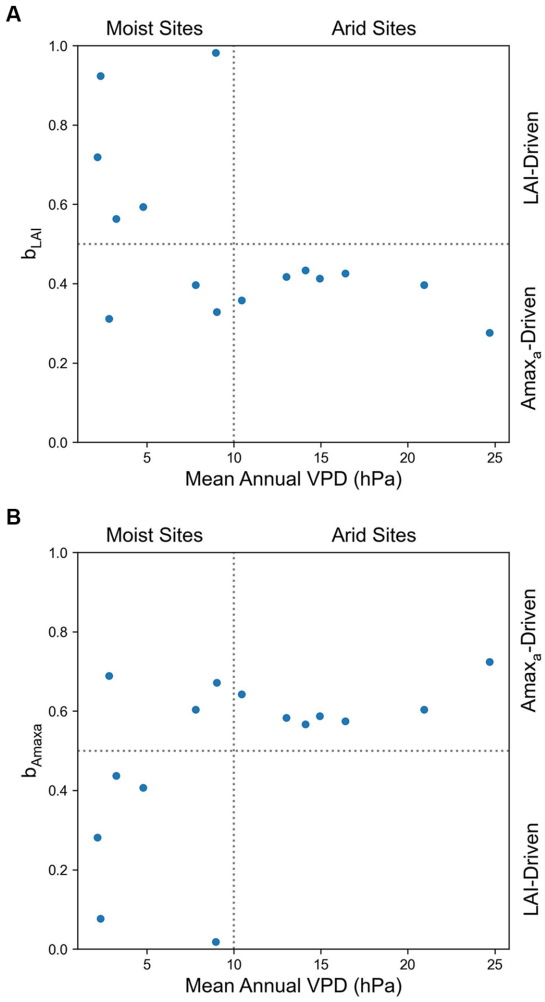

FIGURE 3
Effects of mean annual VPD on the relative contribution of **(A)** LAI (b_{LAI}) and **(B)** $Amax_a$ (b_{Amaxa}) to the seasonal variation of Amax. $b_{LAI}+b_{Amaxa}=1$.

sites, but negatively correlated with them at some moist sites. Solar radiation and photoperiod were positively correlated with $Amax_a$, LAI, and Amax at many sites.

Environmental variables explained on average 38, 70, and 62% of the seasonal variations in $Amax_a$, LAI, and Amax, respectively, which suggested environmental variables had a greater impact on LAI than on $Amax_a$. Therefore, environmental factors affected the seasonal variations of Amax mainly through its impact on LAI rather than through its impact on $Amax_a$.

Environmental variables had little explanatory power for $Amax_a$, except a few arid grasslands (i.e., AU-DaP, AU-TTE, US-Var, US-Wkg) where environmental factors can account for over 50% variance of $Amax_a$. The low average R^2 across sites suggested that environmental factors could affect $Amax_a$, but were not the main drivers for the seasonal variations of $Amax_a$. We further investigated whether vegetation greenness (represented by NDVI) was better correlated with $Amax_a$ and found that the average R^2 for $Amax_a$ with NDVI as one of the independent variables was 0.44, which was slightly greater than without NDVI. Coefficients of NDVI for $Amax_a$ were significant at 11 of the 15 sites. These results suggested that the seasonal variations of $Amax_a$ cannot be well explained by classical environmental factors, but may be more correlated with variations in plant traits such as pigment contents.

4. Discussion

4.1. Relative contribution of $Amax_a$ and LAI to the seasonal variation in Amax

Our results suggested that $Amax_a$ and LAI jointly determined the seasonal dynamics of Amax. The seasonal variation of Amax at all arid grasslands (mean annual VPD > 10 hPa) was driven more by changes in $Amax_a$ than LAI, but the drivers of Amax for the moist grasslands (mean annual VPD < 10 hPa) were bimodal in that some sites were $Amax_a$-driven and others LAI-driven. The relative contribution of $Amax_a$ and LAI to Amax was related to the relative magnitude of the temporal variability (CV) of $Amax_a$ and LAI, which in turn, was influenced by mean annual VPD.

Annual air dryness influenced the relative magnitude of CV_{Amaxa} and CV_{LAI} from two aspects. On one hand, mean annual VPD was negatively correlated with LAI (the correlation coefficient between them was-0.77, $p<0.001$), suggesting that drier grasslands tended to have lower LAI, and hence the magnitude of temporal variation in LAI would be smaller. On the other hand, VPD could affect leaf photosynthetic capacity directly by its control on leaf stomatal conductance (Fu et al., 2022), and indirectly by its impact on leaf traits. Moreover, environmental variables explained a large proportion of the variance in $Amax_a$ in arid grasslands (Table 4) compared with wetter grasslands, which also suggested $Amax_a$ in arid grasslands were more sensitive to changes in the environment. Therefore, lesser LAI and greater sensitivity of $Amax_a$ to

TABLE 4 Results (regression coefficients) of linear regression analysis with 8-day average Amax, $Amax_a$, and LAI as dependent and 8-day average Ta, Rad, SWC, VPD, and Dlen as independent variables.

Site	Coefficients	Ta	Rad	SWC	VPD	Dlen	R^2	Log
AT-Neu	Amax	0.37***	−0.19**	−0.14***	−0.03	0.77***	0.79	
	$Amax_a$	−0.57**	−0.25	−0.08	0.26*	0.97***	0.39	Yes
	LAI	0.9***	0.39***	−0.06	−0.51***	0.43***	0.57	Yes
AU-DaP	Amax	0.28***	0.27***	0.1	−0.84***	0.17**	0.84	Yes
	$Amax_a$	0.16	0.18*	0.04	−0.71***	0.24*	0.59	Yes
	LAI	0.32***	0.53***	0.1	−1.02***	0.07	0.79	Yes
AU-Emr	Amax	−0.06	0.61**	−0.07	−0.83**	0.56*	0.21	Yes
	$Amax_a$	−0.53*	0.1	−0.25	−0.03	0.42	0.12	Yes
	LAI	0.8***	0.92***	0.23*	−1.35***	0.05	0.39	Yes
AU-Rig	Amax	0.06	0.36*	0.28***	−0.99***	0.01	0.65	Yes
	$Amax_a$	1.35***	0.15	0.08	−0.62**	−0.73***	0.27	
	LAI	−0.41**	0.31*	0.26***	−0.65***	0.21	0.65	Yes
AU-Stp	Amax	0.77***	0.26***	0.22*	−0.72***	−0.26**	0.48	Yes
	$Amax_a$	0.77***	0.29***	0.06	−0.8***	−0.06	0.4	Yes
	LAI	0.53***	0.2***	0.46***	−0.45***	−0.46***	0.54	Yes
AU-TTE	Amax	1.09***	0.2	0	−0.88***	0.42**	0.63	Yes
	$Amax_a$	0.85***	0.09	0.08	−0.54**	0.44**	0.65	Yes
	LAI	1.08***	0.28**	−0.05	−0.79***	−0.32*	0.3	Yes
CH-Cha	Amax	0.61***	0.23*	0.08	−0.46***	0.4***	0.56	
	$Amax_a$	0.28	−0.02	0.19*	−0.15	0.04	0.05	
	LAI	0.5***	0.2*	−0.02	−0.37***	0.73***	0.67	
CH-Fru	Amax	0.48***	−0.22***	−0.17***	−0.17***	0.67***	0.72	
	$Amax_a$	−0.94***	0.28	0.1	0.15	0.05	0.21	Yes
	LAI	0.66***	−0.12	−0.15***	−0.2***	0.71***	0.73	
IT-MBo	Amax	0.52***	−0.18*	−0.08*	−0.12*	0.65***	0.66	
	$Amax_a$	0.24	0.3*	0.07	−0.26**	−0.64***	0.19	Yes
	LAI	0	−0.11	0.01	−0.04	1.01***	0.73	
US-AR1	Amax	0.22	0.14	0.03	−0.49***	0.62**	0.4	Yes
	$Amax_a$	−0.47	0.05	−0.03	−0.42*	0.86***	0.23	
	LAI	0.76***	0.08	0.03	−0.42***	0.43***	0.84	Yes
US-ARc	Amax	0.96***	−0.22	−0.08	−0.22	0.58***	0.65	
	$Amax_a$	1.34***	−0.05	−0.14	−0.66**	0.25	0.58	
	LAI	0.85***	−0.05	−0.08*	−0.42***	0.54***	0.91	Yes
US-Goo	Amax	0.84***	0.6***	0.04	−0.54***	−0.06	0.66	
	$Amax_a$	0.66***	0.69***	−0.11	−0.76***	−0.36	0.21	
	LAI	0.63***	0.26***	−0.02	−0.27***	0.35***	0.91	Yes
US-SRG	Amax	1.53***	0.39***	0.28***	−1.12***	−0.05	0.7	Yes
	$Amax_a$	0.93***	0.41***	0.41***	−0.86***	0.23*	0.5	Yes
	LAI	1.8***	0.25***	0.06	−1.09***	−0.33***	0.76	Yes
US-Var	Amax	−0.18	0.33***	0.61***	−0.54***	0.36***	0.67	Yes
	$Amax_a$	−0.26**	0.15*	0.52***	−0.34***	0.11	0.7	Yes
	LAI	−0.09	0.48***	0.58***	−0.54***	0.65***	0.62	Yes
US-Wkg	Amax	1.63***	0.48***	0.03	−1.14***	−0.21**	0.69	Yes
	$Amax_a$	1.25***	0.4***	0.07	−0.86***	−0.04	0.56	Yes
	LAI	1.75***	0.43***	0.04	−1.25***	−0.37***	0.71	Yes

Ta, air temperature; Rad, solar radiation; SWC, soil water content; VPD, vapor pressure deficit; Dlen, day length. For some regression, dependent variables are $\log_e$-transformed according to the normality of regression residuals. *$p < 0.05$, **$p < 0.01$, ***$p < 0.001$.

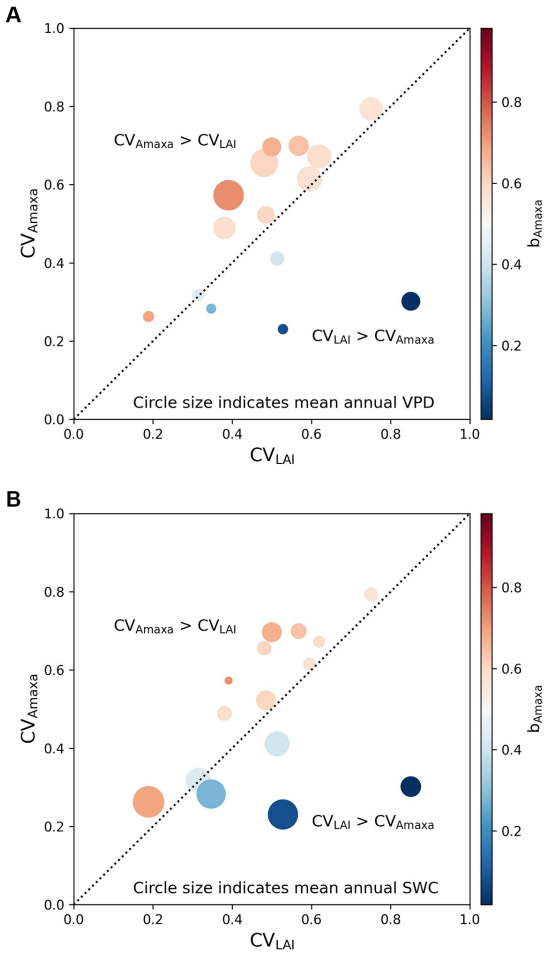

FIGURE 4
Effects of the relative magnitude of the temporal variability of $Amax_a$ (CV_{Amaxa}) and LAI (CV_{LAI}) on the contribution of $Amax_a$ to Amax (b_{Amaxa}) with circle size indicates **(A)** mean annual VPD and **(B)** mean annual SWC. The color indicates the contribution of $Amax_a$ to Amax (b_{Amaxa}). b_{Amaxa}>0.5 represents the seasonal variation of Amax is driven more by $Amax_a$, while b_{Amaxa}<0.5 represents the seasonal variation of Amax is driven more by LAI. The black dotted line is a 1:1 line.

environmental variables in arid grasslands resulted in a greater contribution of $Amax_a$ to Amax.

4.2. Effects of environmental factors on the seasonal variations of Amax, $Amax_a$, and LAI

At the seasonal scale, air temperature and air dryness were the driving factors for the variation in Amax. Other studies also identified the two factors as the most important factors to regulate grassland C fluxes (Polley et al., 2010; Scott et al., 2015; Wang et al., 2019). We also found that VPD was more correlated with Amax than SWC at the seasonal scale, which was also observed in previous studies (Ryan et al., 2017; Fu et al., 2022). The possible reason for this higher correlation of VPD and Amax at the seasonal scale could be related to the non-linear relationship between SWC and Amax, as suggested by previous studies (Xu and Zhou, 2011; Fu et al., 2022). Xu and Zhou (2011) found that the Amax of two grass species was enhanced under moderate soil moisture with reductions under both severe water deficit and excessive water conditions. Fu et al. (2022) suggested that Amax was also non-linearly correlated with soil moisture at the ecosystem scale, while VPD was consistently negatively related to Amax.

The environmental factors used in our study can explain the variances in LAI better than Amax and $Amax_a$. The explanatory power (R^2) of linear regression can be impacted by intensive management practices or other irregular natural events, such as fire and extreme temperatures (Moore et al., 2016). For some sites, such as AT-Neu, IT-MBo, CH-Cha, and CH-Fru, previous studies at these sites have demonstrated that management practices, like cutting, grazing, and fertilization, can obscure the response of photosynthesis to environmental variables (Wohlfahrt et al., 2008; Zeeman et al., 2010; Marcolla et al., 2011; Rogger et al., 2022).

In our study, environmental variables only explained a small proportion of variance in $Amax_a$ on the 8-day scale, much less than that of Amax and LAI, which is probably because canopy photosynthetic capacity per leaf area ($Amax_a$) was controlled more by leaf traits, such as nitrogen (N) and chlorophyll (Chl) content, than by environmental factors, compared with Amax and LAI. According to its definition in our study, $Amax_a$ is the average of the maximum photosynthetic rate per leaf area of individual plants in the ecosystem, or more precisely, all plants within the footprint of the flux tower, a variable independent of the ecosystem structure embedded in LAI and intrinsically related to individual plants. Reichstein et al. (2014) have summarized that environmental variables can account for only a fraction of the temporal and spatial variance of flux-derived ecosystem functional properties (EFP), e.g., seasonal carbon-use efficiency and light-saturated gross primary production (similar to Amax), and suggested that a substantial part of the variation in EFP would be explained by plant traits. Furthermore, Feng and Dietze (2013) examined the relationship between the seasonal variation of Amax and leaf traits on 25 grassland species. They found that leaf N and Chl content significantly correlated with leaf Amax in both mass-and area-based manner. Therefore, we thought that the large unexplained variance in $Amax_a$ was related to plant traits.

4.3. Uncertainties

There are still some uncertainties in our estimation and analysis. The LAI data and Amax estimates used in this study had some uncertainty, which could propagate into $Amax_a$. To reduce the uncertainty of LAI, we tested whether the radius we used to extract LAI from the MODIS LAI dataset could have impacted the temporal dynamics of LAI. We extracted the average LAI of pixels within a 250, 500, 1,000, and 3,000 m radius centered at the flux tower. We found that these buffer sizes did not have much impact on the temporal dynamics in LAI. Then we assessed the influence of the uncertainty of the LAI dataset on $Amax_a$. Following He et al. (2014), we calculated the relative uncertainty in $Amax_a$ induced by the uncertainty in LAI, which was expressed as the standard deviation for each LAI observation provided by the MODIS LAI dataset. The result (Table 5) showed that on average, the uncertainty in LAI could introduce 27.28% of uncertainty in $Amax_a$.

TABLE 5 The uncertainty in $Amax_a$ induced by the uncertainty in LAI.

Site	The relative uncertainty of $Amax_a$ (%)
AT-Neu	23.16
AU-DaP	24.99
AU-Emr	23.24
AU-Rig	27.62
AU-Stp	40.35
AU-TTE	49.32
CH-Cha	12.74
CH-Fru	17.69
IT-MBo	18.09
US-AR1	24.85
US-ARc	19.05
US-Goo	14.35
US-SRG	45.01
US-Var	21.73
US-Wkg	46.95
Average	27.28

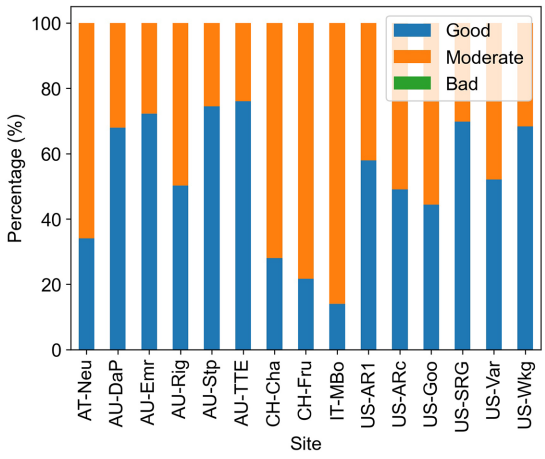

FIGURE 5
Percentage of the different qualities of the Amax estimates. High quality means all parameters in the fitted curve are within a reasonable range, moderate quality means the light response curve is fitted but some of the parameters are out of the reasonable range, and low quality means the light response curve cannot be well constrained using available data in 2weeks.

The uncertainty of Amax estimates was assessed by the fitting quality flag provided by the REddyProc package. The results were shown in Figure 5. On average, each site had 52% of the Amax estimates that were of good quality, 48% of moderate quality, and no bad quality estimates.

Data availability statement

The original contributions presented in the study are included in the article/supplementary material, further inquiries can be directed to the corresponding author.

Author contributions

XC: conceptualization, methodology, formal analysis, and writing (original draft). XR: conceptualization and editing. HH: conceptualization. LZ and YL: editing. All authors contributed to the article and approved the submitted version.

Funding

This work was supported by the National Natural Science Foundation of China (No. 42030509) and the Special Project on National Science and Technology Basic Resources Investigation of China (No. 2021FY100705).

Conflict of interest

The authors declare that the research was conducted in the absence of any commercial or financial relationships that could be construed as a potential conflict of interest.

Publisher's note

References

Ahlström, A., Raupach, M. R., Schurgers, G., Smith, B., Arneth, A., Jung, M., et al. (2015). The dominant role of semi-arid ecosystems in the trend and variability of the land CO_2 sink. *Sci.* 348, 895–899. doi: 10.1126/science.aaa1668

Baldocchi, D., Ma, S., and Verfaillie, J. (2021). On the inter-and intra-annual variability of ecosystem evapotranspiration and water use efficiency of an oak savanna and annual grassland subjected to booms and busts in rainfall. *Glob. Chang. Biol.* 27, 359–375. doi: 10.1111/gcb.15414

Beck, H. E., Zimmermann, N. E., McVicar, T. R., Vergopolan, N., Berg, A., and Wood, E. F. (2018). Present and future Koppen-Geiger climate classification maps at 1-km resolution. *Sci. Data* 5:180214. doi: 10.1038/sdata.2018.214

Beringer, J., Hutley, L. B., Hacker, J. M., Neininger, B., and Paw U, K. T. (2011). Patterns and processes of carbon, water and energy cycles across northern Australian landscapes: from point to region. *Agric. For. Meteorol.* 151, 1409–1416. doi: 10.1016/j.agrformet.2011.05.003

Beringer, J., Hutley, L. B., McHugh, I., Arndt, S. K., Campbell, D., Cleugh, H. A., et al. (2016). An introduction to the Australian and New Zealand flux tower network – OzFlux. *Biogeosciences* 13, 5895–5916. doi: 10.5194/bg-13-5895-2016

Chu, H., Luo, X., Ouyang, Z., Chan, W. S., Dengel, S., Biraud, S. C., et al. (2021). Representativeness of Eddy-Covariance flux footprints for areas surrounding AmeriFlux sites. *Agric. For. Meteorol.* 301-302:108350. doi: 10.1016/j.agrformet.2021.108350

Feng, X., and Dietze, M. (2013). Scale dependence in the effects of leaf ecophysiological traits on photosynthesis: Bayesian parameterization of photosynthesis models. *New Phytol.* 200, 1132–1144. doi: 10.1111/nph.12454

Fu, Z., Ciais, P., Prentice, I. C., Gentine, P., Makowski, D., Bastos, A., et al. (2022). Atmospheric dryness reduces photosynthesis along a large range of soil water deficits. *Nat. Commun.* 13:989. doi: 10.1038/s41467-022-28652-7

He, H., Liu, M., Xiao, X., Ren, X., Zhang, L., Sun, X., et al. (2014). Large-scale estimation and uncertainty analysis of gross primary production in Tibetan alpine grasslands. *J. Geophys. Res. Biogeo.* 119, 466–486. doi: 10.1002/2013jg002449

Hollinger, D. Y., Goltz, S. M., Davidson, E. A., Lee, J. T., Tu, K., and Valentine, H. T. (1999). Seasonal patterns and environmental control of carbon dioxide and water vapour exchange in an ecotonal boreal forest. *Glob. Chang. Biol.* 5, 891–902. doi: 10.1046/j.1365-2486.1999.00281.x

Huang, A., Shen, R., Di, W., and Han, H. (2021). A methodology to reconstruct LAI time series data based on generative adversarial network and improved Savitzky-Golay filter. *Int. J. Appl. Earth Obs. Geoinf.* 105:102633. doi: 10.1016/j.jag.2021.102633

Hu, Z., Shi, H., Cheng, K., Wang, Y. P., Piao, S., Li, Y., et al. (2018). Joint structural and physiological control on the interannual variation in productivity in a temperate grassland: A data-model comparison. *Glob. Chang. Biol.* 24, 2965–2979. doi: 10.1111/gcb.14274

Joswig, J. S., Wirth, C., Schuman, M. C., Kattge, J., Reu, B., Wright, I. J., et al. (2021). Climatic and soil factors explain the two-dimensional spectrum of global plant trait variation. *Nat. Ecol. Evol.* 6, 36–50. doi: 10.1038/s41559-021-01616-8

Keenan, T. F., Migliavacca, M., Papale, D., Baldocchi, D., Reichstein, M., Torn, M., et al. (2019). Widespread inhibition of daytime ecosystem respiration. *Nat. Ecol. Evol.* 3, 407–415. doi: 10.1038/s41559-019-0809-2

Lasslop, G., Reichstein, M., Papale, D., Richardson, A. D., Arneth, A., Barr, A., et al. (2010). Separation of net ecosystem exchange into assimilation and respiration using a light response curve approach: critical issues and global evaluation. *Glob. Chang. Biol.* 16, 187–208. doi: 10.1111/j.1365-2486.2009.02041.x

Li, F., Peng, Y., Zhang, D., Yang, G., Fang, K., Wang, G., et al. (2019). Leaf Area Rather Than Photosynthetic Rate Determines the Response of Ecosystem Productivity to Experimental Warming in an Alpine Steppe. *J. Geophys. Res. Biogeosci.* 124, 2277–2287. doi: 10.1029/2019jg005193

Lloyd, J., and Taylor, J. A. (1994). On the temperature dependence of soil respiration. *Funct. Ecol.* 8, 315–323. doi: 10.2307/2389824

Luo, X., and Keenan, T. F. (2020). Global evidence for the acclimation of ecosystem photosynthesis to light. *Nat. Ecol. Evol.* 4, 1351–1357. doi: 10.1038/s41559-020-1258-7

Luo, Y., and Schuur, E. A. G. (2020). Model parameterization to represent processes at unresolved scales and changing properties of evolving systems. *Glob. Chang. Biol.* 26, 1109–1117. doi: 10.1111/gcb.14939

Ma, S., Baldocchi, D. D., Xu, L., and Hehn, T. (2007). Inter-annual variability in carbon dioxide exchange of an oak/grass savanna and open grassland in California. *Agric. For. Meteorol.* 147, 157–171. doi: 10.1016/j.agrformet.2007.07.008

Marcolla, B., Cescatti, A., Manca, G., Zorer, R., Cavagna, M., Fiora, A., et al. (2011). Climatic controls and ecosystem responses drive the inter-annual variability of the net ecosystem exchange of an alpine meadow. *Agric. For. Meteorol.* 151, 1233–1243. doi: 10.1016/j.agrformet.2011.04.015

Medvigy, D., Jeong, S.-J., Clark, K. L., Skowronski, N. S., and Schäfer, K. V. R. (2013). Effects of seasonal variation of photosynthetic capacity on the carbon fluxes of a temperate deciduous forest. *J. Geophysical Res. Biogeosci.* 118, 1703–1714. doi: 10.1002/2013jg002421

Moore, C. E., Brown, T., Keenan, T. F., Duursma, R. A., van Dijk, A. I. J. M., Beringer, J., et al. (2016). Reviews and syntheses: Australian vegetation phenology: new insights from satellite remote sensing and digital repeat photography. *Biogeosciences* 13, 5085–5102. doi: 10.5194/bg-13-5085-2016

O'Mara, F. P. (2012). The role of grasslands in food security and climate change. *Ann. Bot.* 110, 1263–1270. doi: 10.1093/aob/mcs209

Polley, H. W., Emmerich, W., Bradford, J. A., Sims, P. L., Johnson, D. A., Saliendra, N. Z., et al. (2010). Physiological and environmental regulation of interannual variability in CO_2 exchange on rangelands in the western United States. *Glob. Chang. Biol.* 16, 990–1002. doi: 10.1111/j.1365-2486.2009.01966.x

Poulter, B., Frank, D., Ciais, P., Myneni, R. B., Andela, N., Bi, J., et al. (2014). Contribution of semi-arid ecosystems to interannual variability of the global carbon cycle. *Nat.* 509, 600–603. doi: 10.1038/nature13376

Raz-Yaseef, N., Billesbach, D. P., Fischer, M. L., Biraud, S. C., Gunter, S. A., Bradford, J. A., et al. (2015). Vulnerability of crops and native grasses to summer drying in the U.S. southern Great Plains. *Agric. Ecosyst. Environ.* 213, 209–218. doi: 10.1016/j.agee.2015.07.021

Reich, P. B., Sendall, K. M., Stefanski, A., Rich, R. L., Hobbie, S. E., and Montgomery, R. A. (2018). Effects of climate warming on photosynthesis in boreal tree species depend on soil moisture. *Nat.* 562, 263–267. doi: 10.1038/s41586-018-0582-4

Reichstein, M., Bahn, M., Mahecha, M. D., Kattge, J., and Baldocchi, D. D. (2014). Linking plant and ecosystem functional biogeography. *Proc. Natl. Acad. Sci. U. S. A.* 111, 13697–13702. doi: 10.1073/pnas.1216065111

Renton, M., and Poorter, H. (2011). Using log-log scaling slope analysis for determining the contributions to variability in biological variables such as leaf mass per area: why it works, when it works and how it can be extended. *New Phytol.* 190, 5–8. doi: 10.1111/j.1469-8137.2010.03629.x

Rogger, J., Hörtnagl, L., Buchmann, N., and Eugster, W. (2022). Carbon dioxide fluxes of a mountain grassland: drivers, anomalies and annual budgets. *Agric. For. Meteorol.* 314:108801. doi: 10.1016/j.agrformet.2021.108801

Runkle, B. R. K., Rigby, J. R., Reba, M. L., Anapalli, S. S., Bhattacharjee, J., Krauss, K. W., et al. (2017). Delta-flux: an Eddy covariance network for a climate-smart lower Mississippi Basin. *Agric. Environ. Lett.* 2:ael2017.01.0003. doi: 10.2134/ael2017.01.0003

Ryan, E. M., Ogle, K., Peltier, D., Walker, A. P., De Kauwe, M. G., Medlyn, B. E., et al. (2017). Gross primary production responses to warming, elevated $CO_{(2)}$, and irrigation: quantifying the drivers of ecosystem physiology in a semiarid grassland. *Glob. Chang. Biol.* 23, 3092–3106. doi: 10.1111/gcb.13602

Scott, R. L., Biederman, J. A., Hamerlynck, E. P., and Barron-Gafford, G. A. (2015). The carbon balance pivot point of southwestern U.S. semiarid ecosystems: insights from the 21st century drought. *J. Geophys. Res. Biogeosci.* 120, 2612–2624. doi: 10.1002/2015jg003181

Scott, R. L., Hamerlynck, E. P., Jenerette, G. D., Moran, M. S., and Barron-Gafford, G. A. (2010). Carbon dioxide exchange in a semidesert grassland through drought-induced vegetation change. *J. Geophys. Res.* 115:G03026. doi: 10.1029/2010JG001348

Wang, N., Quesada, B., Xia, L., Butterbach-Bahl, K., Goodale, C. L., and Kiese, R. (2019). Effects of climate warming on carbon fluxes in grasslands-a global meta-analysis. *Glob. Chang. Biol.* 25, 1839–1851. doi: 10.1111/gcb.14603

Way, D. A., and Yamori, W. (2014). Thermal acclimation of photosynthesis: on the importance of adjusting our definitions and accounting for thermal acclimation of respiration. *Photosynth. Res.* 119, 89–100. doi: 10.1007/s11120-013-9873-7

Wilson, K. B., Baldocchi, D. D., and Hanson, P. J. (2001). Leaf age affects the seasonal pattern of photosynthetic capacity and net ecosystem exchange of carbon in a deciduous forest. *Plant Cell Environ.* 24, 571–583. doi: 10.1046/j.0016-8025.2001.00706.x

Wohlfahrt, G., Hammerle, A., Haslwanter, A., Bahn, M., Tappeiner, U., and Cernusca, A. (2008). Seasonal and inter-annual variability of the net ecosystem $CO_{(2)}$ exchange of a temperate mountain grassland: effects of climate and management. *J. Geophys. Res. Atmos.* 113:D08110. doi: 10.1029/2007jd009286

Xu, Z., and Zhou, G. (2011). Responses of photosynthetic capacity to soil moisture gradient in perennial rhizome grass and perennial bunchgrass. *BMC Plant Biol.* 11:21. doi: 10.1186/1471-2229-11-21

Zhang, L.-M., Yu, G.-R., Sun, X.-M., Wen, X.-F., Ren, C.-Y., Fu, Y.-L., et al. (2006). Seasonal variations of ecosystem apparent quantum yield (α) and maximum photosynthesis rate (Pmax) of different forest ecosystems in China. *Agricul. Forest Meteorology* 137, 176–187. doi: 10.1016/j.agrformet.2006.02.006

Zeeman, M. J., Hiller, R., Gilgen, A. K., Michna, P., Plüss, P., Buchmann, N., et al. (2010). Management and climate impacts on net CO_2 fluxes and carbon budgets of three grasslands along an elevational gradient in Switzerland. *Agric. For. Meteorol.* 150, 519–530. doi: 10.1016/j.agrformet.2010.01.011

Zhu, Z., Piao, S., Myneni, R. B., Huang, M., Zeng, Z., Canadell, J. G., et al. (2016). Greening of the earth and its drivers. *Nat. Clim. Chang.* 6, 791–795. doi: 10.1038/nclimate3004

frontiers | Frontiers in Ecology and Evolution

TYPE Original Research
PUBLISHED 16 June 2023
DOI 10.3389/fevo.2023.1173750

OPEN ACCESS

EDITED BY
Cuicui Jiao,
Sichuan University of Science and Engineering, China

REVIEWED BY
Hang Wang,
Southwest Forestry University, China
Zhiwei Xu,
National School of Geographical Sciences, France

*CORRESPONDENCE
Xiaoming Kang
xmkang@ucas.ac.cn
Kerou Zhang
zhangkerou1991@nwafu.edu.cn

RECEIVED 25 February 2023
ACCEPTED 01 June 2023
PUBLISHED 16 June 2023

CITATION
Yan Z, Li M, Hao Y, Li Y, Zhang X, Yan L, Kang E, Wang X, Yang A, Niu Y, Yu X, Kang X and Zhang K (2023) Effects of extreme drought on soil microbial functional genes involved in carbon and nitrogen cycling in alpine peatland. *Front. Ecol. Evol.* 11:1173750. doi: 10.3389/fevo.2023.1173750

Effects of extreme drought on soil microbial functional genes involved in carbon and nitrogen cycling in alpine peatland

Zhongqing Yan[1,2,3], Meng Li[1,2,3], Yanbin Hao[4], Yong Li[1,2,3], Xiaodong Zhang[1,2,3], Liang Yan[1,2,3], Enze Kang[1,2,3], Xiaodong Wang[1,2,3], Ao Yang[1,2,3], Yuechuan Niu[4], Xiaoshun Yu[1,2,3], Xiaoming Kang[1,2,3]* and Kerou Zhang[1,2,3]*

[1]Wetland Research Center, Institute of Ecological Conservation and Restoration, Chinese Academy of Forestry, Beijing, China, [2]Sichuan Zoige Wetland Ecosystem Research Station, Chinese Academy of Forestry, Tibetan Autonomous Prefecture of Aba, China, [3]Beijing Key Laboratory of Wetland Services and Restoration, Chinese Academy of Forestry, Beijing, China, [4]College of Life Sciences, University of Chinese Academy of Sciences, Beijing, China

Diverse microorganisms drive biogeochemical cycles and consequently influence ecosystem-level processes in alpine peatlands, which are vulnerable to extreme drought induced by climate change. However, there are few reports about the effects of extreme drought on microbial function. Here we identify microbial functional genes associated with carbon and nitrogen metabolisms of extreme drought experiments that occurred at different periods of plant growth, the results show that early extreme drought reduces the abundance of functional genes involved in the decomposition of starch and cellulose; midterm extreme drought increases the abundance of lignin decomposition functional genes; late extreme drought reduces the hemicellulose but increases cellulose decomposition functional genes. In the carbon fixation pathway, extreme drought mainly changes the abundance of functional genes involved in the reductive citrate cycle process, the 3-hydroxy propionate bi-cycle, the dicarboxylate-hydroxybutyrate cycle and the incomplete reductive citrate cycle. Among the nitrogen cycling functional genes, *amo*A involved in oxidizing ammonia to hydroxylamine significantly increases under early extreme drought; midterm extreme drought reduces *nrt*C and *nif*D genes, which participate in nitrate assimilation and nitrogen fixation, respectively; late extreme drought significantly increases *hcp* genes involved in ammonification. pH and TN had the largest effects on the carbon degradation, fixation and nitrogen cycling functional genes. The composition of microbial community structures involved in carbon fixation differed between treatments in early extreme drought. There is a good linear fit between the diversity of gene abundance and corresponding microbial communities in the reductive citrate cycle, hydroxy propionate-hydroxybutyrate cycle, dicarboxylate-hydroxybutyrate cycle and nitrogen cycling, which suggests that the functional genes and community composition

of microorganisms involved in these processes are consistent in response to extreme drought. This study provides new insights into the adaptability and response characteristics of microbial communities and functional genes in plateau peatland ecosystems to extreme drought events.

KEYWORDS

alpine peatland, extreme drought, carbon cycling, nitrogen cycling, functional genes

1 Introduction

Peatland is a carbon-rich ecosystem covering 185-423 million hectares of the earth's surface (Ribeiro et al., 2021). It is an important organic carbon (C) and nitrogen (N) pool and its C and N reserves account for 30% (ca. 644 Gt C) and 10% (8 – 15 Gt N) of the total reserves of the whole terrestrial ecosystem, respectively (Limpens et al., 2006; Wang et al., 2014). A large amount of greenhouse gases is produced and discharged due to C and N migration and transformation in peatlands (Chen et al., 2014; Yao et al., 2022). Global warming is affecting precipitation patterns in a complex way, as heating promotes evaporation, leading to soil surface drying, thus increasing the duration and intensity of drought events (Pokhrel et al., 2021). The global climate model predicts that the frequency and intensity of extreme drought events will increase in the future (Hoover and Rogers, 2016). Extreme drought has seriously affected soil biogeochemical C and N cycling and related greenhouse gas fluxes (Deng et al., 2021), leading to the loss of ecosystem functions (Du et al., 2018; Kang et al., 2018). Therefore, the fate of the large amount of C and N stored in peatland and the response of peatland to extreme drought is very important for the future climate. It is becoming increasingly apparent that in addition to drought intensity, the timing of drought has important effects on the ecosystem C and N cycling (Dietrich and Smith, 2016). Some studies have shown that drought events, occurring at different plant growth stages (i.e., rapid growth, full bloom, and decline stages), have differently influenced ecosystem production and functioning (Knapp et al., 2008; Dietrich and Smith, 2016). However, the ecological implications of greater intra-season variability of rainfall extremes have received minimal notice, especially concerning variable timing of extreme drought at different plant growth stages, which might have the largest ecological consequences.

Extreme drought events mainly lead to water stress in plants, which can alter the distribution pattern of plant biomass (Jentsch et al., 2011), cause a decrease in photosynthetic, transpiration rates (Lefi et al., 2004) and water use efficiency, then decrease in plant suitability (Loik, 2007). Extreme drought events not only directly affect plant growth, but also indirectly affect the supply of soil nutrients through changes in soil moisture content. Studies have shown that extreme drought in summer significantly reduces soil C and N mineralization, leading to a decrease in soil nutrient supply (Borken & Matzner, 2009). Soil microorganisms play an intermediary role in the key steps of all biogeochemical cycles and maintain ecosystem functions (Bell et al., 2005; Zhang et al., 2012; Bastida et al., 2021). Therefore, the effect of extreme drought events on soil water and nutrients regime is highly likely to cause changes in soil microbial activity. As the soil dries, water membranes form on soil particles, concentrating water-containing pore water components (e.g., dissolved nutrients, solutes, toxins), limiting the diffusion of stroma and extracellular enzymes and increasing interactions between microbial populations (Malik and Bouskill, 2022). There is overwhelming evidence that microorganisms will respond to drought in terms of microbial community composition and diversity (Zhou et al., 2012; Guo et al., 2020; Yuan et al., 2021). In addition, changes in microbial communities can in turn regulate soil nutrient regimes through metabolism and decomposition. Under drought conditions, microorganisms can mediate soil C sequestration and alleviate the impact of reduced soil water availability caused by climate change by increasing soil carbon sequestration (Canarini et al., 2016). Drought can reduce the decomposition of soil organic matter by reducing the characteristics of microorganisms (e.g., enzyme activity and functional gene abundance) (Alster et al., 2013; Vogel et al., 2013). Therefore, the understanding of soil microbial ecology is crucial to our ability to evaluate terrestrial C and N cycling, but the complexity of soil microbial communities and the multiple ways that they may be affected by extreme drought hinder our ability to draw clear conclusions on this topic and the metabolic kinetics and phenotypic characteristics of microbial communities are still unclear (Bardgett et al., 2008; de Vries et al., 2018), though microbial communities drive biogeochemical cycles through their specific metabolic activities.

Litter decomposition is a key link between carbon budget and nutrient cycling. In general, drought can cause a decrease in the rate constant of litter decomposition, and the decomposition of C and N in various plant litter leaves has decreased (Sardans and Penuelas, 2010). Sudden drought may have a greater effect on litter decomposition than long-term drought (García-Palacios et al., 2016). In addition, the decomposition rate of different carbon components is also inhibited to varying degrees by drought. For example, the proportion of cellulose in litter under drought treatment in the Mediterranean region increased by 10.9% compared to the ambient conditions, while the lignin content increased by 17.5% (Tu et al, 2017). Some studies suggest that drying conditions have a negative effect on soil microorganisms. Drought can lead to a decrease in soil microbial biomass, diversity

and relative abundance, thereby affecting the litter decomposition rates (Zhou et al., 2018). Therefore, understanding the decomposition, transformation, and sequestration of organic matter in soil requires a further understanding of how microbial physiology regulates the processes that control biogeochemical cycling, climate change, and ecosystem sustainability (Bardgett et al., 2008; Roth et al., 2019). Liang et al. (2017) defined two pathways (i.e., ex vivo modification and *in vivo* turnover) to jointly explain the dynamics of soil C driven by microbial catabolism and/or anabolism. However, it has been difficult to link specific taxa to these ecosystem processes and consequently predict the functional responses of soil microorganisms (Fierer, 2017). Thus, a better understanding of the diversity and abundance of microbial functional genes that predict the functional potential of soil microorganisms can link the knowledge of microbial communities to their key ecosystem functions. Soil microbial genes coding for specific enzymes related to particular ecosystem processes can help us to establish links between genetic diversity, community structure and further to ecosystem functions, such as carbon cycling through studying carbohydrate-active enzymes (CAZy) (Yang et al., 2014; Manoharan et al., 2017).

N cycling is a collection of important biogeochemical pathways mediated by microbial communities. In most northern peatlands, the slow decomposition of dead plant material returns organic N to the soil and causes peat accumulation (Moore, 2002). Microbial conversion of N is usually described as a cycling consisting of denitrification, nitrification, nitrogen fixation and dissimilatory nitrate reduction to ammonium (DNRA) (Glaze et al., 2022). Drought stresses directly or indirectly affect the ecosystem N cycling (Deng et al., 2021). The effect of drought on net N mineralization and flux in soils of different climates, soil, and ecosystem types varies (Hartmann et al., 2013). The increase in duration and intensity of drought is usually related to N mineralization, mobility, and a decrease in the plant uptake rate of inorganic nutrients (Deng et al., 2021). Recent efforts have focused on characterizing functional genes involved in multiple N cycling processes using genetic approaches and relating genetic information to ecosystem functioning. It has been made clear that *amo*A genes regulate the availability of inorganic N and the production of N_2O through nitrification, while *nir*K and *nir*S genes are involved in NO_3^- consumption and N_2O production, *nos*Z genes mediate the conversion of N_2O to N_2 during denitrification (Dai et al., 2020). Tu et al. (2017) have also correlated soil N cycling with microbial genetic data, which were mainly concentrated in a few gene families by PCR. Petersen et al. (2012) analyzed nitrification and denitrification processes across a vegetation gradient in Alaska by qPCR amplification of gene families including *amo*A, *nir*K/S, and *nos*Z, and suggested that the abundance of these functional genes can be used as good predictors for biogeochemical process rates. Drought was reported to affect the diversity and composition of microbial communities, and therefore the abundance of functional genes related to N cycling in arable land (Banerjee et al., 2016) and pasture soils (Radl et al., 2015). However, comprehensive surveys of genes involved in all N cycling processes in peatland ecosystems under extreme drought events have rarely been carried out.

The Qinghai-Tibet Plateau has large soil C and N stocks that turn over at low rates (Chen et al., 2013; Fu et al., 2021). In alpine peatland soils, microbial metabolism is limited by harsh environments, such as low temperatures or oxygen levels, and microorganisms are less able to decompose and recover soil organic material. The purpose of this study is to conduct a prospective study on whether the functional genes involved in the process of C and N cycling changed significantly after extreme drought events using metagenomics methods and to explore which specific processes and microbial groups are most affected. To address these objectives, an *in-situ* field extreme drought simulation experiment was conducted for five years in an alpine peatland ecosystem was performed and the functional genes of soil C and N cycling were screened in detail. Finally, we explore the role of drought-affected microbial communities in the C and N cycling at the genetic level.

2 Materials and methods

2.1 Study area experimental design and soil sampling

The location of the peatland investigated in this research is at an altitude of 3430 m above sea level, located in the Zoige plateau (33° 47′56.61″ N, 102°57′28.43″ E) on the northeast edge of the Qinghai-Tibet Plateau. The largest alpine peatland in the world is found in this area due to the region's unique climatic and hydrological regimes and its geomorphologic and soil conditions (Ma et al., 2016). The mean annual temperature and mean annual precipitation are -1.7°C to 3.3°C and 650 mm to 750 mm, respectively and 90% of the annual precipitation occurs from April to September. The soil is highland peat soil. For this study, the vertical depth of peat at the study site was approximately 1.2 m. The SOC content was between 179 $g{\cdot}kg^{-1}$ to 276 $g{\cdot}kg^{-1}$ and the soil pH was between 6.8 to 7.2. The vegetation was primarily composed of *Carex meyeriana*, *Koeleria tibetica*, *Carex muliensis*, *Eriophorum gracile*, *Blysmus sinocompressus*, and *Carex secbrirostris*.

The extreme drought events were designed by statistical extremity concerning a historical reference period (extreme value theory) independent of biological effects. We focused on one extreme drought event, not a long-term drought, so local rainfall statistics at the study site have been collected over the past 50 years (China Meteorological Data Network). Daily rainfall of ≤ 3 mm is defined as non-effective rainfall and the minimum duration of non-effective rainfall during the study period was set to 32 days (where the days without effective rainfall are the duration of the drought) (Jentsch et al., 2011), which has the same design idea with the previous research(Zhou et al., 2019). Different periods of extreme drought events were applied during the growing season. The experiment consisted of a control (CK) with ambient precipitation and then different periods of extreme drought. The names and dates of three drought periods were: early drought (ED) from June 18 to July 20, 2019; midterm drought (MD) from July 20 to August 23, 2019; and late drought (LD) from August 23 to September 25, 2019, following 5 years of continuous extreme drought events from 2014 to 2018.

Precipitation was excluded from the study site using a transparent awning (length × width × height: 2.5 m × 2.5 m × 1.8 m). The light transmittance of the shelter material was more than 90%. Each drought treatment consisted of three replicate plots of 2 m × 2 m each, and these were selected randomly in the study field. The iron plates around each experimental community are smashed into the ground for 1m to prevent the lateral flow of water. During rain, roof water was collected with gutters along the shelter awning and transported 50 m downhill of the experimental site, and after each extreme drought event, we removed the shelters and then allow the extreme drought plots to receive natural precipitation. Three soil cores of 0–20 cm in depth were collected and mixed from each plot at the end of each simulated extreme drought period (i.e., ED, MD and LD). One part of the soil samples was transported to the laboratory in coolers with dry ice and then were stored at −80°C for later DNA extraction, the other part was passed through a 2–mm sieve to remove the plant roots and determine soil biochemical properties.

2.2 Measurements of soil properties

The soil pH was determined in a 1:2.5 soil/water solution using a pH meter. soil water content (SWC) was determined using the oven-drying method. Soil ammonium (NH_4^+) and nitrate (NO_3^-) concentrations were determined by the colorimetric method. Soil organic carbon (SOC) was determined by the rapid dichromate oxidation-titration method. Dissolved organic carbon (DOC) was measured using a continuous-flow analyzer. Soil total nitrogen (TN) was determined by the Kjeldahl procedure. These have already been demonstrated in our previous research (Kang et al., 2022; Yan et al., 2022).

2.3 DNA extraction, library construction, and metagenomic sequencing

Total genomic DNA was extracted from the soil samples using the E.Z.N.A.® Soil DNA Kit (Omega Bio-tek, Norcross, GA, U.S.) according to the manufacturer's instructions. The concentration and purity of extracted DNA were determined using TBS-380 and NanoDrop2000, respectively. DNA extract quality was checked using 1% agarose gel.

DNA extract was fragmented to an average size of about 400 bp using Covaris M220 (Gene Company Limited, China) for paired-end library construction. A paired-end library was constructed using NEXTFLEX Rapid DNA-Seq (Bioo Scientific, Austin, TX, USA). Adapters containing the full complement of sequencing primer hybridization sites were ligated to the blunt-end of fragments. Paired-end sequencing was performed on an Illumina NovaSeq (Illumina Inc., San Diego, CA, USA) at Majorbio Bio-Pharm Technology Co., Ltd. (Shanghai, China) using NovaSeq Reagent Kits according to the manufacturer's instructions (www.illumina.com). Sequence data associated with this project have been deposited in the NCBI Short Read Archive database (Accession Number: SRP368675).

2.4 Sequence quality control and genome assembly

The data were analyzed on the free online platform, Majorbio Cloud Platform (www.majorbio.com). The paired-end Illumina reads were trimmed of adaptors, and low-quality reads (length<50 bp or with a quality value <20 or having N bases) were removed by fastp (Chen et al., 2018) (https://github.com/OpenGene/fastp, version 0.20.0). Metagenomics data were assembled using MEGAHIT (Li et al., 2015) (https://github.com/voutcn/megahit, version 1.1.2), which makes use of succinct de Bruijn graphs. Contigs with a length being or over 300 bp were selected as the final assembling result, and then the contigs were used for further gene prediction and annotation.

2.5 Gene prediction, taxonomy, and functional annotation

Open reading frames (ORFs) from each assembled contig were predicted using MetaGene (Noguchi et al., 2006) (http://metagene.cb.k.u-tokyo.ac.jp/). The predicted ORFs with length being or over 100 bp were retrieved and translated into amino acid sequences using the NCBI translation table (http://www.ncbi.nlm.nih.gov/Taxonomy/taxonomyhome.html/index.cgi?chapter=tgencodes#SG1. A non-redundant gene catalog was constructed using CD-HIT (Fu et al., 2012) (http://www.bioinformatics.org/cd-hit/,version4.6.1) with 90% sequence identity and 90% coverage. Reads after quality control were mapped to the non-redundant gene catalog with 95% identity using SOAPaligner (Li et al., 2008) (http://soap.genomics.org.cn/, version 2.21), and gene abundance in each sample was evaluated.

Representative sequences of non-redundant gene catalog were aligned to the NCBI and NR databases with an e-value cutoff of $1e^{-5}$ using Diamond (Buchfink et al., 2015) (http://www.diamondsearch.org/index.php, version 0.8.35) for taxonomic annotations. The KEGG annotation was conducted using Diamond (Buchfink et al., 2015) (http://www.diamondsearch.org/index.php, version 0.8.35) against the Kyoto Encyclopedia of Genes and Genomes database (http://www.genome.jp/keeg/) with an e-value cutoff of $1e^{-5}$.

2.6 Statistical analyses

Independent sample t-tests were used to analyze the functional genes related to C and N affected by extreme drought in different periods. Linear discriminant analysis (LDA) effect size analysis (LEfSe) was conducted using the Galaxy server (http://huttenhower.sph.harvard.edu/galaxy) to analyze the microbial communities at genus level affected by extreme drought in different periods, and the linear fitting variance was used to test the consistency of microbial community and functional gene diversity. Constrained ordination (redundancy analysis, RDA) was used to investigate the relationships between soil factors and the functional genes involved in C degradation, C fixation and N cycling. The differences of microbial

community structure between the control and extreme drought treatments were determined using non-metric multidimensional scaling analysis (NMDS) in the "vegan" package of R software. Analysis of variance was performed by SPSS 26.0, and the figures were drawn with OriginPro.

3 Results

3.1 The effects of extreme drought on C cycling functional genes

In this study, a total of 65 functional genes (Table S1) responsible for the process of soil C decomposition were selected and 116 functional genes involved in the soil C sequestration pathway were detected (Table S2).

Extreme drought significantly affected many important microbial functional genes involved in C decomposition (Figure 1). Specifically, the functional genes involved in Chitin, Pectin and Aromatics decomposition were not significantly affected by ED. *npl*T significantly decreased ($P < 0.05$) by 23.73% in the ED, and the abundance of the PGM3 gene changed from 0.38% to 0, which participated in the decomposition of starch, and the abundance of *bgl*B gene involved in cellulose decomposition was significantly reduced ($P < 0.05$) by 6.16%; In the MD, *pmm-pgm* and *xyn*B were significantly reduced ($P < 0.05$) by 5.08% and 7.52%, while *tre*S and *gmu*G were significantly increased ($P < 0.05$) by 4.58% and 42.28%, they participated in the decomposition of starch and hemicellulose, and the *glx* gene involved in the decomposition of Lignin was changed from 0 to 4.55%. The *abf*1 gene significantly decreased ($P < 0.05$) by 56.89%, but the glucan 1, 3-beta-glucosidase (EC: 32.1.58) significantly increased ($P < 0.05$) by 84.94%. These are involved in the decomposition of hemicellulose and cellulose, respectively. In general, the ED reduced the abundance of functional genes involved in the decomposition of starch and cellulose, and the MD increased the abundance of genes involved in the decomposition of Lignin, but had different effects on the functional genes involved in the different processes of the decomposition of starch and cellulose. The LD reduced the functional genes involved in the decomposition of hemicellulose, but increased the functional genes involved in the decomposition of cellulose.

Extreme drought also significantly affected many important functional genes involved in different C fixation pathways (Figure 2), including the reductive citrate cycle, the 3-hydroxypropionate bi-cycle, the dicarboxylate-hydroxybutyrate cycle and the incomplete reductive citrate cycle, while the hydroxy propionate-hydroxybutyrate cycle, the reductive acetyl-CoA pathway, and the phosphate acetyltransferase-acetate kinase pathway were almost unchanged. In the ED, *kor*C decreased by 30.78% and 28.39% ($P < 0.05$) in the Reductive citrate cycle and in the Incomplete reductive citrate cycle, respectively. The abundance of E4.2.1.2B, participating in the 3-Hydroxypropionate bi-cycle process, increased significantly by 3.18%. In the MD, *sdh*C in the reductive citrate cycle, the 3-hydroxy propionate bi-cycle and the dicarboxylate-hydroxybutyrate cycle significantly increased ($P < 0.05$) by 7.63%, 9.42%, and 6.57%, respectively. *mch* and *smt*A1 decreased significantly ($P < 0.05$) by 18.58% and 19.78%, respectively, while K15052 increased significantly ($P < 0.05$) by 38.46% in the 3-Hydroxypropionate bi-cycle. In the LD, *suc*C significantly decreased ($P < 0.05$) by 4.61% in the Dicarboxylate-hydroxybutyrate cycle.

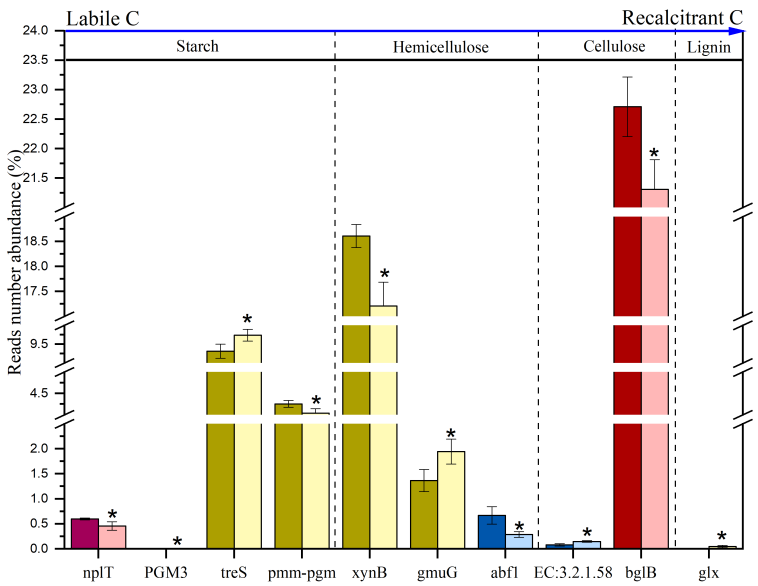

FIGURE 1
Significantly changed C degradation functional genes are compared between extreme drought and control sites. CK: light color; Extreme drought: dark color; Red: ED; Yellow: MD; Blue: LD. Error bars represent standard error (n = 3). The differences between extreme drought and control sites were analyzed by two-tailed paired t-tests. *$P < 0.05$.

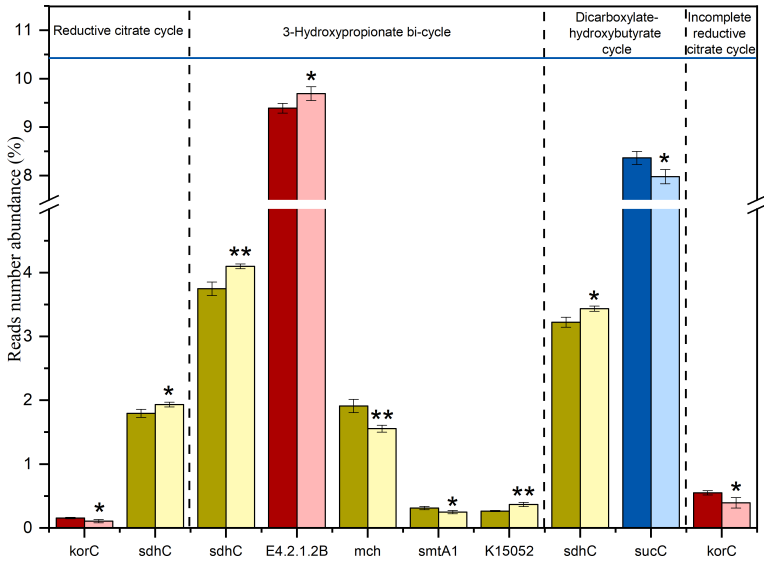

FIGURE 2
Significantly changed C degradation functional genes compared between extreme drought test plots and control test plots. CK: light color; Extreme drought: dark color Red: ED; Yellow: MD; Blue: LD. Error bars represent standard error (n = 3). The differences between extreme drought and control sites were analyzed using two-tailed paired t-tests. $^{**}P < 0.01$, $^{*}P < 0.05$.

Results of the RDA indicated that microbial functional genes involved in C degradation and fixation across the different treatments could be distinguished by soil factors (Figure 3). pH and TN had the largest effects on the C degradation and fixation functional genes. The first axis described 52.38% of the variation in microbial C degradation functional genes, and the second axis explained 4.26% of the variation. The first axis described 37.21% of the variation in microbial C fixation functional genes, and the second axis explained 4.58% of the variation.

3.2 The effects of extreme drought on N cycling functional genes

In this study, a total of 50 genes (Table S3) related to the N cycling were detected, including those associated with ammonification, nitrate assimilation, assimilatory N reduction, dissimilatory N reduction, nitrification, denitrification and N fixation. In different periods of extreme drought, the affected functional genes and their response processes were different (Figure 4). When the ED event occurred, the abundance of the ammonia oxidation key gene of nitrification (*amo*A) in the extreme drought soil increased significantly by 55.32% compared with the control ($P < 0.05$). This gene is responsible for oxidizing ammonia to hydroxylamine. The abundance of *nrt*C and *nif*D genes of soil microorganisms significantly decreased by 13.51% and 25.21%, respectively, compared with the control under the MD ($P < 0.05$), they participate in the process of nitrate assimilation and N fixation respectively. In the LD, the abundance of *hcp* genes involved in the soil amelioration process was significantly reduced by 57.78% compared with the control ($P < 0.05$). Results of the RDA indicated that pH, TN and NO_3^- had the largest effects on the N

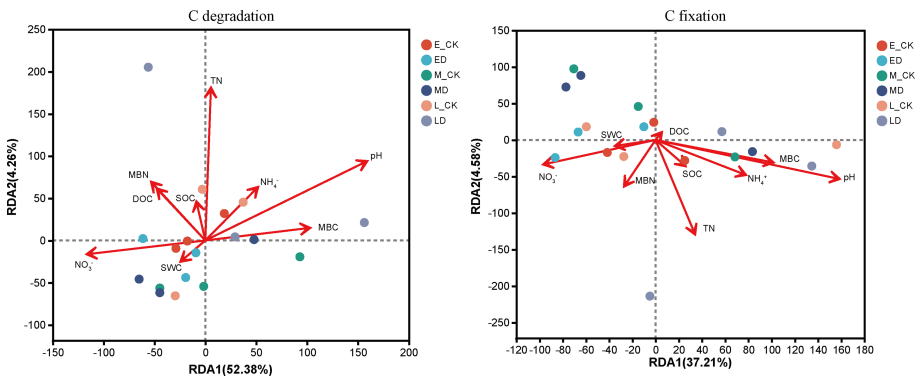

FIGURE 3
Ordination biplots of redundancy analysis (RDA) showing the relationship of C degradation and fixation functional genes to soil characteristics at 0–20 cm soil layers.

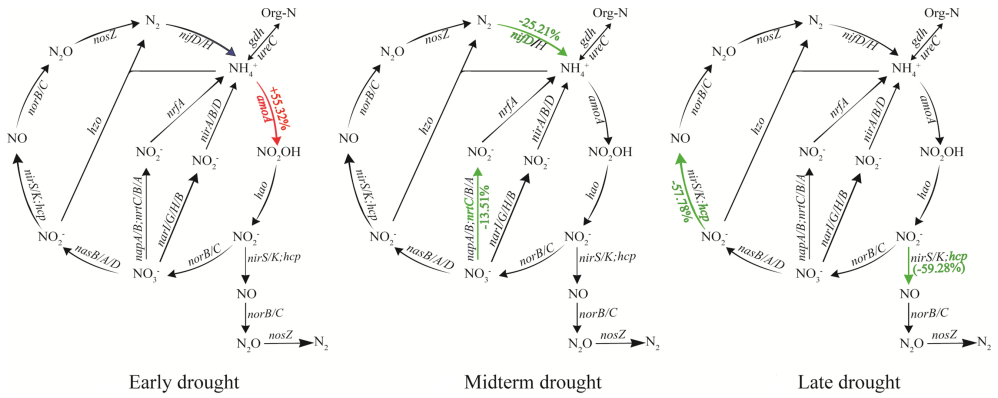

FIGURE 4
The extreme drought effect on N cycling genes. The percentages in brackets indicate changes in average abundances of functional genes between extreme drought and control sites. Red and green represent the increase and decrease in the average abundance by extreme drought, respectively.

cycling functional genes. The first axis described 20.62% of the variation in microbial C degradation functional genes, and the second axis explained 12.59% of the variation (Figure 5).

3.3 The effects of extreme drought on soil microbial communities

In all the samples in this study, the detection numbers at different community classification levels were that Domain: 4; Kingdom: 7; Phylum: 87; Class: 161; Order: 293; Family: 501; Genus: 1631; Species: 6269. The co-occurrence relationship between the sample and the microbial community (Phylum and Genus level) is shown in Figure 6. At the Phylum level, the dominant communities were mainly Proteobacteria, Actinobacteria, Acidobacteria and Chroroflexi. They accounted for about 40%, 20%, 9% and 3% of all communities in the different drought treatments.

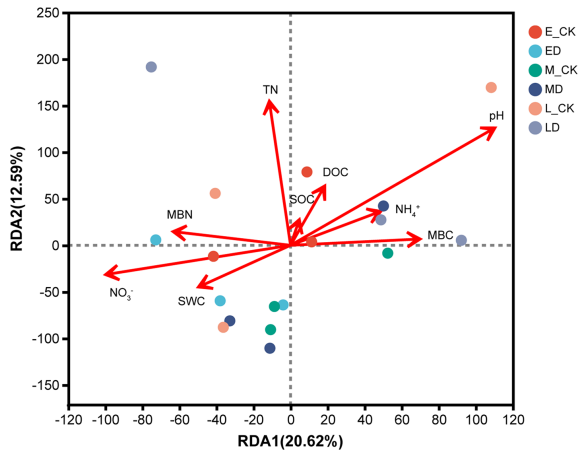

FIGURE 5
Ordination biplots of redundancy analysis (RDA) showing the relationship of N cycling functional genes to soil characteristics at 0–20 cm soil layers.

Extreme drought also significantly affected many microbial groups at the genus level (Figure 7). In the ED, MD and LD, there were 32, 41 and 2 microbial communities at the genus level that changed significantly, indicating that the impact of ED and MD on microbial community structure was stronger than that of LD. Among microbial communities that have undergone significant changes, extreme drought during different periods leads to different directions of change in microbial communities. ED reduced the abundance of 90.63% of microbial communities, while MD increased the abundance of 95.12% of microbial communities. LD significantly reduced the community abundance of *Thermobacterium* and *Gallionella*. In addition, only ED significantly reduced the composition of the *Mycobacteriaceae*, which belongs to Archaea. In other treatments, there were no significant changes in the Archaea or Fungal categories, indicating that extreme drought mainly changed the composition of bacterial groups.

Based on the abundance information of species and function, α diversity of species and function were calculated, respectively, and linear regression analysis was performed to evaluate the consistency of species and function. In this study, the microbial communities of some C sequestration processes exhibited good consistency with the corresponding functional genes, including the reductive citrate cycle, the hydroxypropionate-hydroxybutylate cycle and the dicarboxylate-hydroxybutyrate cycle (Table 1), The associated linear fits were $y=1.643X+0.8031$ ($R^2 = 0.37$, $P < 0.01$), $y=0.7463X+4.9030$ ($R^2 = 0.28$, $P < 0.05$) and $y=0.6539X+4.2184$ ($R^2 = 0.24$, $P < 0.05$), respectively. The species and functional gene α diversity of the N cycling also showed good consistency, and the linear fit was $y=0.3084X+4.8109$ ($R^2 = 0.28$, $P < 0.05$). NMDS analyses showed that the composition of microbial community structures involved in C fixation differed between treatments in early extreme drought (Figure 8), while the microbial community structure involved in C degradation and N cycling has little change under extreme drought treatment in different periods. Furtherly, the relative contributions of the top ten functional genes to microbial communities involved in C degradation, C fixation and N cycling processes (Figure 9) showed that as the abundance of microbial communities decreased, although the composition of related functional genes changed, the functional

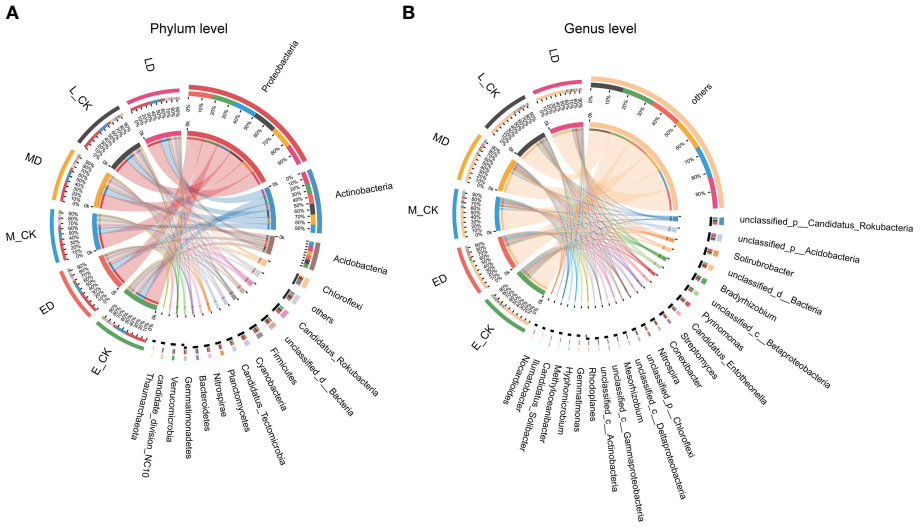

FIGURE 6
Co-occurrence relationship between samples and species. **(A)** Microbial community at phylum level; **(B)** Microbial community at genus level.

categories did not show significant changes, indicating a complex relationship between microbial community composition and functional gene abundance. The changes in population abundance were not consistent with the changes in function.

4 Discussion

4.1 Extreme drought changed C cycling functional genes

Microorganisms have two distinct and critical roles in controlling terrestrial C fluxes i.e., facilitating the release of C into the atmosphere through their catabolic activities, but also blocking it by stabilizing it into a form that is not easily decomposed (Liang and Balser, 2011; Liang et al., 2017). Microbial necromass rather than standing biomass may be a better indicator of microbial contributions to soil C pools, and research increasingly shows a substantial microbial role in the sequestration of C into stable soil C pools (Ludwig et al., 2015).

Our research showed that different periods of extreme drought events have different effects on the functional genes involved in organic C decomposition. After five years of extreme drought, only 15.38% of the selected key functional genes show significant changes. The impact of extreme drought on the different organic matter has certain complexities, and the time of occurrence of

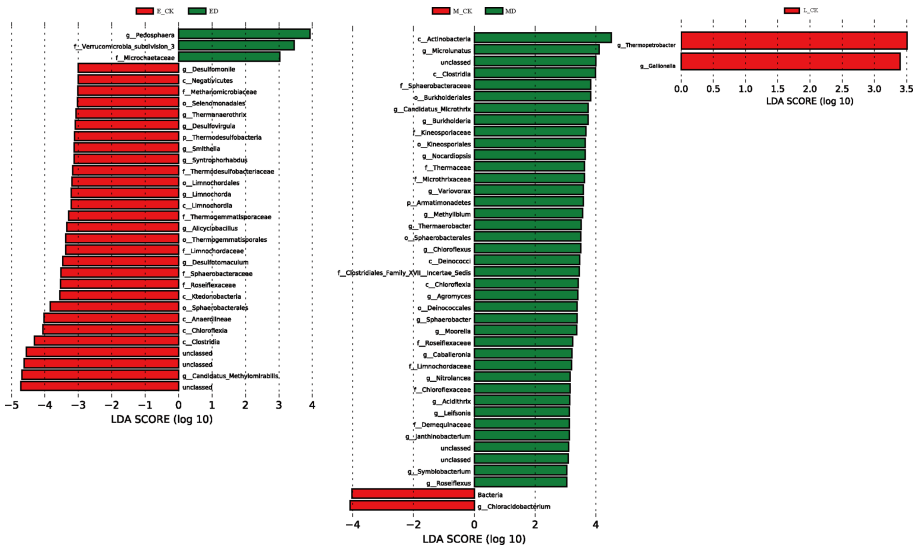

FIGURE 7
A linear discriminant analysis effect size (LEfSe) method identifies the responses of soil microbial abundant taxa under extreme drought treatment. The threshold on the logarithmic LDA score was 3.0. Red indicates a significant increase in abundance in CK plots, and green indicates a significant increase in abundance in extreme drought plots. The replicate (n = 3).

TABLE 1 Regression relationship of α diversity (Shannon index) for species at the genus level and their corresponding functions in different processes.

Categary	Subcategary	P value	R^2	Formula
C degradation	Starch	0.7094	0.0089	
	Hemicellulose	0.2977	0.0675	
	Cellulose	0.8325	0.0028	
	Chitin	0.0854	0.1735	
	Pectin	0.4307	0.0392	
	Aromatics	0.7814	0.0049	
	Lignin	0.4307	0.0392	
C fixation	Reductive citrate cycle	0.0077	0.3664	y=1.643X+0.8031
	3-Hydroxypropionate bi-cycle	0.3362	0.0578	
	Hydroxypropionate-hydroxybutylate cycle	0.0235	0.2811	y=0.7463X+4.9030
	Dicarboxylate-hydroxybutyrate cycle	0.0389	0.2402	y=0.6539X+4.2184
	Reductive acetyl-CoA pathway	0.4449	0.0369	
	Phosphate acetyltransferase-acetate kinase pathway	0.102	0.1582	
	Incomplete reductive citrate cycle	0.1383	0.132	
N cycling	N cycling	0.0239	0.2801	y=0.3084X+4.8109

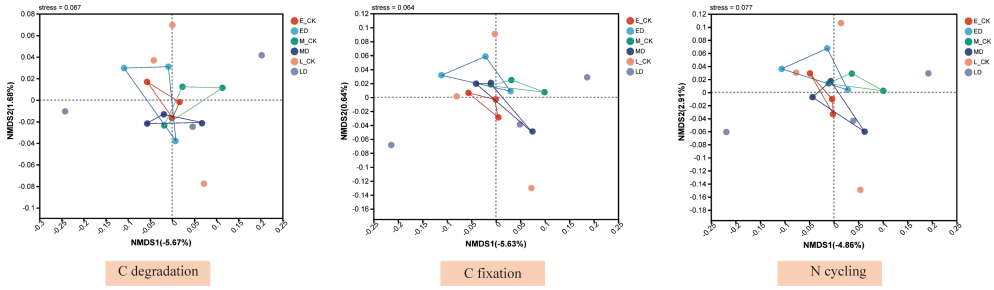

FIGURE 8
Non−metric multidimensional scaling (NMDS) ordination of the microbial community involved in C degradation, C fixation and N cycling at different treatments. The Bray−Curtis distance matrix based on the abundance of microbial community at genus level was used to determine the compositional variation.

extreme drought events within the seasonal cycle plays an important role. In addition, although the changing trend of functional genes is also not consistent, our research showed that the change of functional genes for the decomposition of labile C is relatively complex, and the functional genes for the decomposition of lignin are significantly increased. The production of extracellular degrading enzymes may be reduced under drought conditions because of the lower rate of return of decomposition products due to diffusion limitations (Sardans and Penuelas, 2010). The microbial community is very sensitive to changes in precipitation conditions and even a slight precipitation event can cause rapid microbial response (Nielsen and Ball, 2015). Yue et al. (Yue et al., 2015) used gene chips to study soil microorganisms in alpine meadows and noted that the relative abundance of catabolic genes related to C and N cycling decreased with the increase of temperature, with the most obvious change being in genes related to stable C. Our study also suggests that drought significantly increases the catabolic genes related to lignin and has complex effects on labile C such as cellulose and hemicellulose. This is consistent with research that has indicated that extreme drought promotes more gene expression in microorganisms degrading stable C, and reduces the long-term stability of soil C. Due to the huge diversity of microorganisms and the unclear ecological functions of most species, detection methods for specific

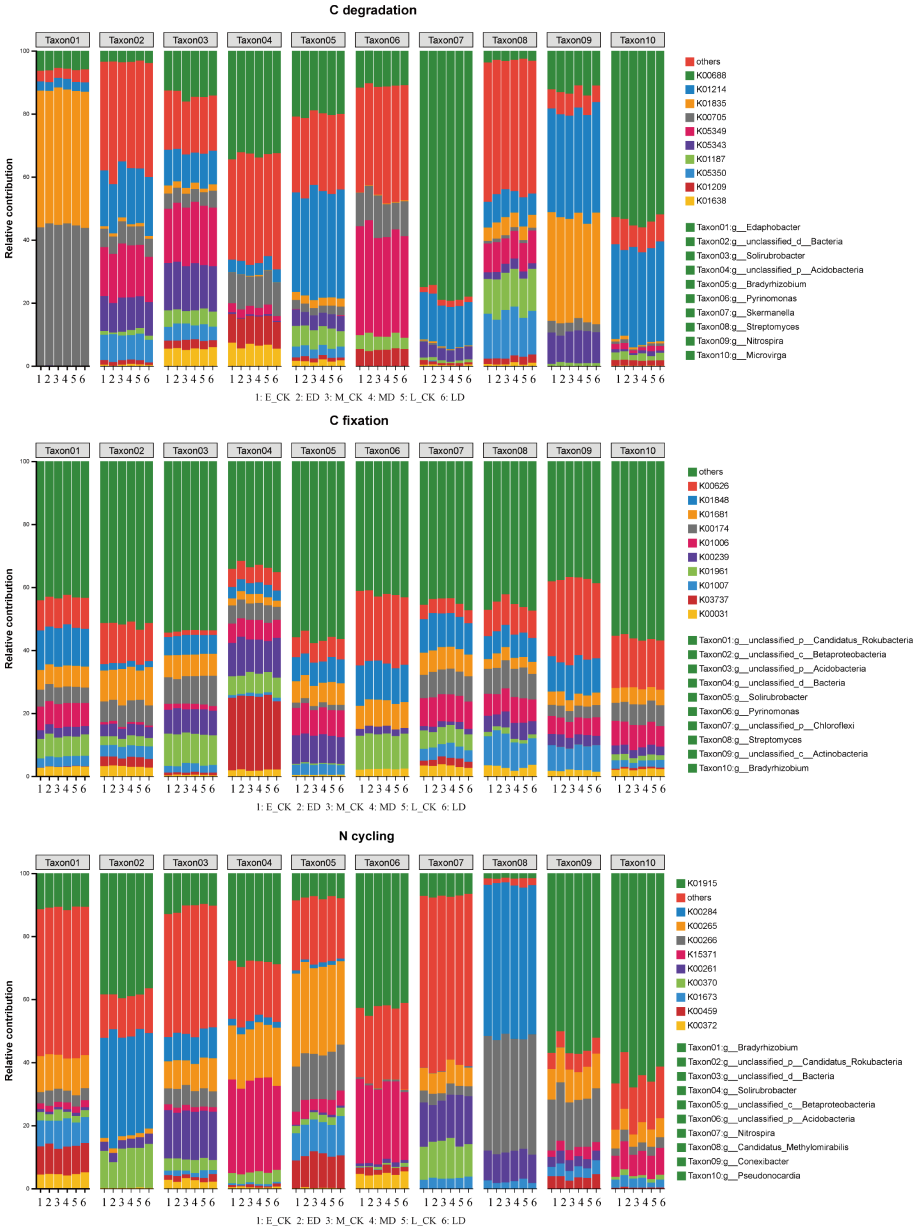

FIGURE 9
The relative contributions of the top ten functional genes to microbial communities involved in C degradation, C fixation and N cycling processes. The taxonomy of the bacterial communities is shown at the genus level, and the relative contributions are represented by different colors.

functional microbial groups need to be greatly improved (Rinke et al., 2013).

Similar to the decomposition process of soil organic matter, the genes involved in the C fixation process exhibited different changes for different extreme drought periods, although the response trend of related processes was not consistent, indicating that the response of microorganisms to extreme drought is very complex. However, it is difficult to deduce the change direction of the final C fixation capacity from the change of a certain function. Assimilation of CO_2 by soil autotrophic microorganisms is an important process of the soil C cycling, particularly in vegetation-constrained ecosystems with environmental stresses such as on the Tibetan Plateau which is characterized by low temperature and high UV radiation levels. Lynn et al. (2017) showed that the C sequestration rate of autotrophic microorganisms in wetland soil was 85.1 mg C m^{-2} d^{-1}, and that of autotrophic microorganisms in grassland and woodland soil was 21.9 mg C m^{-2} d^{-1} and 32.9 mg C m^{-2} d^{-1}, respectively. Precipitation and latitude together accounted for 76.00% difference in soil C sequestration microbial metabolic pathways in differently vegetated areas. In addition, oxygen sensitivity can also one of the reasons for differences in CO_2 sequestration pathways (Liu et al., 2016).

4.2 Extreme drought changed N-related functional genes involved in ammonia oxidation, N fixation, nitrate assimilation and denitrification processes

In our study, *nir*K and *nir*S genes in denitrifying microbial communities for reducing nitrite (NO_2^-) to nitric oxide (NO), and *nos*Z genes in denitrifying bacterial communities for reducing N_2O to N_2 (Jetten, 2008; Levy-Booth et al., 2014) were not affected by extreme drought. This may greatly influence the nitrification and denitrification rates and associated N_2O emissions. Keil et al. (Keil et al., 2015) used qPCR to study microbial communities. Their results showed that the abundance of *nir*K, *nir*S and *nos*Z all changed, while the abundance of the *nos*Z denitrifying gene decreased by 3.1%, which was greatly affected by drought. Hartmann et al. (Hartmann et al., 2013) studied the response of soil N cycling microorganisms to simulated drought through qPCR. Drought increased the N mineralization rate by 14%, and reduced the relative abundance of denitrification gene *nir*S by 7%. In an incubation experiment, it was found that under both flooded and non-flooded conditions, warming increased the N mineralization rate, which was reflected in the increase of denitrification rate and the abundance of copper reductase (*nir*K) (Gao et al., 2009; Fang et al., 2021).

Snider et al. (2015) documented significant changes in denitrification gene abundance (*nir*S, *nos*Z), which increased after heavy rainfall events increased WFPS from < 40% to > 70%, consistent with large fluxes of N_2O. A meta-analysis found that the effect sizes of *nir*K and *nos*Z showed a U-shaped relationship with the effect sizes of soil moisture (Li et al., 2020), contrary to the belief that lower soil moisture and correspondingly higher soil oxygen concentration may inhibit *nir*K and *nos*Z genes under drought conditions (Delgado-Baquerizo et al., 2014; Homyak et al., 2017). Although our experiment was carried out continuously for 5 years, rewetting during the period of non-shielding may play a great role in the recovery of microorganisms. Some studies have pointed out that the significant resistance and/or resilience of the functional microbial community participating in the N cycling to extreme weather events may indicate that the microorganisms in silt are better adapted to the expected pressure conditions (Hammerl et al., 2019).

Ammonia oxidation is the first step of nitrification, which is the key process in the global N cycling and forms nitrate through microbial activities (Leininger et al., 2006). We observed an increase in abundance of *amo*A genes from the ED plots. This suggests that the ammonia oxidation process increases after extreme drought events. Che et al. (2017) used N cycling gene abundance (*amo*A) to find that a major shift in the N cycling led to a five-fold increase in nitrobacteria during grassland degradation in Tibet. Nitrification produces easily leached nitrates, which are the limiting substrate for denitrification in alpine meadows (Xie et al., 2014). Therefore, nitrates increase during periods of high soil moisture or in moist soil microhabitats. However, it has also been reported that both ammoxidation archaea (AOA) abundance and community composition are unaffected by drought, supporting earlier observations of AOA resistance to drought stress (Gleeson et al., 2010) and AOA's good adaptation to a wide range of growing conditions and substrate concentrations (Schleper, 2010). Our study did not distinguish between AOA and AOB, but the increase of overall gene abundance indicates that extreme drought events in peatland may enhance the ammonia oxidation process. Previous studies have reported that although total N concentration sharply decreases under drought, the availability of soluble organic N and mineral N significantly increases, thereby promoting plant N absorption in the short term (Rennenberg et al., 2009). The opposite research results suggest that drought does not affect the inorganic N content in the soil, even under long-term drought treatment. Part of the reason for these two results is the difference in drought intensity and timing (Hartmann et al., 2013). We demonstrated that the soil pH, TN and NO_3^- had the largest effects on the N cycling functional genes (Figure 5).

4.3 Relationship between microbial community composition and functional potential

Most biogeochemical transformations appear to be mediated by a limited set of metabolic pathways in multiple taxa (Louca et al., 2018). We still do not know the appropriate solutions to establish links between microbial diversity and ecosystem processes in order to be able to capture the taxonomic distribution, metabolic capacity and response to environmental perturbations of microorganisms, although the diversity of microbes is incredible (Gans et al., 2005). The relationship between microbial biodiversity and ecosystem function is mainly inferred by measuring the change of species diversity and community composition derived using the marker gene method, but this inference does not explain the causal relationship between microbial diversity and ecosystem function (Krause et al., 2014). Research on the relationship between microbial biodiversity and ecosystem function needs to further characterize the functional performance and role of microorganisms in the ecosystem (Wang et al., 2019).

Our results showed that the composition of microbial community structures involved in C fixation function differed between treatments in early extreme drought (Figure 8). In addition to the derailed ecosystem function and microbial community function mentioned above, microbial taxonomic composition and functional potential may not always be linearly correlated. In our study, microbial community diversity involved in the N cycling process exhibited a good linear relationship with functional gene diversity, and only 3 out of 7 microbial C fixation processes had a good linear relationship. However, the diversity of genes involved in soil C degradation screened by us showed no linear relationship with the corresponding microbial communities, indicating that the decomposition of organic matter was involved in the decoupling between microbial groups and genes. This may be caused by different microbial groups having the same functional genes. This separation of microbial functional and taxonomic composition raises key questions about the relative spatial and temporal value of information on microbial phylogenetic diversity versus metabolic diversity of functional microorganisms for understanding biogeochemical reactions (Wertz et al., 2007).

For microorganisms performing relatively "extensive" functions, such as the decomposition and turnover of organic matter, the recombination of functional gene diversity (i.e. the functional potential of the community) does not necessarily lead to changes in ecosystem functions, such as decomposition rate (Allison and Martiny, 2008; Miki et al., 2014). A recent meta-analysis based on a metagenomic dataset of 365 samples worldwide revealed a consistent pattern in the relative frequencies of eight metabolic pathways associated with N transformation, hinting at the ability of metagenomic approaches to make potential inferences about the role of microorganisms in mediating biogeochemical cycles (Nelson et al., 2016). Studies have shown strong evidence to support the hypothesis of functional redundancy in soil microorganisms, as the degree of variation in microbial taxonomic composition is greater than the functional potential based on metagenomic gene abundance in global terrestrial ecosystems (Chen et al., 2022). In the future, we need to further integrate macro genomics, experimental culture and field measurement technology to link the information on microbial classification, phylogeny and functional genes with the measured phenotypic traits and environmental preferences (Barberan et al., 2017).

5 Conclusion

In this study, it was shown that under extreme drought conditions, microbial communities with low abundance underwent more significant changes than those with high abundance, and the abundance of functional genes involved in related processes showed a similar pattern, pH and TN had the largest effects on microbial functional genes. Changes in α diversity of microbial communities and functional genes were consistent in some C fixation processes and N cycling. In summary, progress has been made in understanding the potential negative impacts and positive contributions of soil microorganisms to extreme drought by considering the direct and indirect impacts of climate change on microorganisms and the ability of such impacts to amplify or inhibit key processes in the C and N cycling, despite uncertainties in predicting ecosystem function. We believe that in the future it will be necessary to link microbial ecology with whole-ecosystem scale flux measurements and C cycling feedback models. It is possible for ecosystem models to make better predictions of the ecosystem effects of future extreme drought by better evaluating microorganisms' functional capacity and response.

Data availability statement

The datasets presented in this study can be found in online repositories. The names of the repository/repositories and accession number(s) can be found in the article/Supplementary Material.

Author contributions

ZY, XK, YL, KZ and YH contributed to the conception and design of the study. EK, XZ and XY organized the database. ZY, ML and YL performed the statistical analysis. ZY and LY wrote the first draft of the manuscript. AY, XW, and YN wrote sections of the manuscript. All authors contributed to manuscript revision, read, and approved the submitted version.

Funding

This work was supported by the National Natural Science Foundation of China (No. 32201410, 32171597, 42041005), the Fundamental Research Funds of the Chinese Academy of Forestry (No. CAFYBB2022SY041) and the Department of Science and Technology of Sichuan Province (2020YFH0131).

Acknowledgments

We would also like to acknowledge Dr. Willaim R.T. (University of North Wales) for providing language editing in the preparation of the manuscript.

Conflict of interest

The authors declare that the research was conducted in the absence of any commercial or financial relationships that could be construed as a potential conflict of interest.

Publisher's note

Supplementary material

The Supplementary Material for this article can be found online at: https://www.frontiersin.org/articles/10.3389/fevo.2023.1173750/full#supplementary-material

References

Allison, S. D., and Martiny, J. B. H. (2008). Resistance, resilience, and redundancy in microbial communities. *Proc. Natl. Acad. Sci. U.S.A.* 105, 11512–11519. doi: 10.1073/pnas.0801925105

Alster, C. J., German, D. P., Lu, Y., and Allison, S. D. (2013). Microbial enzymatic responses to drought and to nitrogen addition in a southern California grassland. *Soil Biol. Biochem.* 64, 68–79. doi: 10.1016/j.soilbio.2013.03.034

Banerjee, S., Helgason, B., Wang, L., Winsley, T., Ferrari, B. C., and Siciliano, S. D. (2016). Legacy effects of soil moisture on microbial community structure and N_2O emissions. *Soil Biol. Biochem.* 95, 40–50. doi: 10.1016/j.soilbio.2015.12.004

Barberan, A., Caceres Velazquez, H., Jones, S., and Fierer, N. (2017). Hiding in plain sight: mining bacterial species records for phenotypic trait information. *mSphere* 2 (4), e00237–17. doi: 10.1128/mSphere.00237-17

Bardgett, R. D., Freeman, C., and Ostle, N. J. (2008). Microbial contributions to climate change through carbon cycle feedbacks. *ISME J.* 2 (8), 805–814. doi: 10.1038/ismej.2008.58

Bastida, F., Eldridge, D. J., García, C., Kenny Png, G., Bardgett, R. D., and Delgado-Baquerizo, M. (2021). Soil microbial diversity–biomass relationships are driven by soil carbon content across global biomes. *ISME J.* 15 (7), 2081–2091. doi: 10.1038/s41396-021-00906-0

Bell, T., Newman, J. A., Silverman, B. W., Turner, S. L., and Lilley, A. K. (2005). The contribution of species richness and composition to bacterial services. *Nature* 436 (7054), 1157–1160. doi: 10.1038/nature03891

Borken, W., and Matzner, E. (2009). Reappraisal of drying and wetting effects on c and n mineralization and fluxes in soils. *Glob. Change Biol.* 15, 808–824. doi: 10.1111/j.1365-2486.2008.01681.x

Buchfink, B., Xie, C., and Huson, D. H. (2015). Fast and sensitive protein alignment using DIAMOND. *Nat. Methods* 12 (1), 59–60. doi: 10.1038/nmeth.3176

Canarini, A., Carrillo, Y., Mariotte, P., Ingram, L., and Dijkstra, F. A. (2016). Soil microbial community resistance to drought and links to c stabilization in an Australian grassland. *Soil Biol. Biochem.* 103, 171–180. doi: 10.1016/j.soilbio.2016.08.024

Che, R., Wang, F., Wang, W., Zhang, J., Zhao, X., Rui, Y., et al. (2017). Increase in ammonia-oxidizing microbe abundance during degradation of alpine meadows may lead to greater soil nitrogen loss. *Biogeochemistry* 136 (3), 341–352. doi: 10.1007/s10533-017-0399-5

Chen, H. H., Ma, K. Y., Lu, C. Y., Fu, Q., Qiu, Y. B., Zhao, J. Y., et al. (2022). Functional redundancy in soil microbial community based on metagenomics across the globe. *Front. Microbiol.* 13, 878978. doi: 10.3389/fmicb.2022.878978

Chen, H., Yang, G., Peng, C., Zhang, Y., Zhu, D., Zhu, Q., et al. (2014). The carbon stock of alpine peatlands on the qinghai-Tibetan plateau during the Holocene and their future fate. *Quaternary Sci. Rev.* 95, 151–158. doi: 10.1016/j.quascirev.2014.05.003

Chen, S. F., Zhou, Y. Q., Chen, Y. R., and Gu, J. (2018). Fastp: an ultra-fast all-in-one FASTQ preprocessor. *Bioinformatics* 34 (17), 884–890. doi: 10.1093/bioinformatics/bty560

Chen, H., Zhu, Q., Peng, C., Wu, N., Wang, Y., Fang, X., et al. (2013). The impacts of climate change and human activities on biogeochemical cycles on the qinghai-Tibetan plateau. *Glob. Change Biol.* 19 (10), 2940–2955. doi: 10.1111/gcb.12277

Dai, Z., Yu, M., Chen, H., Zhao, H., Huang, Y., Su, W., et al. (2020). Elevated temperature shifts soil n cycling from microbial immobilization to enhanced mineralization, nitrification and denitrification across global terrestrial ecosystems. *Glob. Change Biol.* 26 (9), 5267–5276. doi: 10.1111/gcb.15211

Delgado-Baquerizo, M., Maestre, F. T., Escolar, C., Gallardo, A., Ochoa, V., Gozalo, B., et al. (2014). Direct and indirect impacts of climate change on microbial and biocrust communities alter the resistance of the n cycle in a semiarid grassland. *J. Ecol.* 102 (6), 1592–1605. doi: 10.1111/1365-2745.12303

Deng, L., Peng, C., Kim, D.-G., Li, J., Liu, Y., Hai, X., et al. (2021). Drought effects on soil carbon and nitrogen dynamics in global natural ecosystems. *Earth Sci. Rev.* 214, 103501. doi: 10.1016/j.earscirev.2020.103501

de Vries, F. T., Griffiths, R. I., Bailey, M., Craig, H., Girlanda, M., Gweon, H. S., et al. (2018). Soil bacterial networks are less stable under drought than fungal networks. *Nat. Commun.* 9 (1), 3033. doi: 10.1038/s41467-018-05516-7

Dietrich, J. D., and Smith, M. D. (2016). The effect of timing of growing season drought on flowering of a dominant C4 grass. *Oecologia* 181, 391–399. doi: 10.1007/s00442-016-3579-4

Du, L., Mikle, N., Zou, Z., Huang, Y., Shi, Z., Jiang, L., et al. (2018). Global patterns of extreme drought-induced loss in land primary production: identifying ecological extremes from rain-use efficiency. *Sci. Total Environ.* 628, 611–620. doi: 10.1016/j.scitotenv.2018.02.114

Fang, X., Zheng, R., Guo, X., Fu, Q., Fan, F., and Liu, S. (2021). Yak excreta-induced changes in soil microbial communities increased the denitrification rate of marsh soil under warming conditions. *Appl. Soil Ecol.* 165, 103935. doi: 10.1016/j.apsoil.2021.103935

Fierer, N. (2017). Embracing the unknown: disentangling the complexities of the soil microbiome. *Nat. Rev. Microbiol.* 15, 579–590. doi: 10.1038/nrmicro.2017.87

Fu, L. M., Niu, B. F., Zhu, Z. W., Wu, S. T., and Li, W. Z. (2012). CD-HIT: accelerated for clustering the next-generation sequencing data. *Bioinformatics* 28 (23), 3150–3152. doi: 10.1093/bioinformatics/bts565

Fu, B., Ouyang, Z., Shi, P., Fan, J., Wang, X., Zheng, H., et al. (2021). Current condition and protection strategies of qinghai-Tibet plateau ecological security barrier. *Bull. Chin. Acad. Sci.* 36 (11), 1298–1306.

Gans, J., Wolinsky, M., and Dunbar, J. (2005). Computational improvements reveal great bacterial diversity and high metal toxicity in soil. *Science* 309 (5739), 1387–1390. doi: 10.1126/science.1112665

Gao, J. Q., Ouyang, H., Xu, X. L., Zhou, C. P., and Zhang, F. (2009). Effects of temperature and water saturation on CO_2 production and nitrogen mineralization in alpine wetland soils. *Pedosphere* 19 (1), 71–77. doi: 10.1016/S1002-0160(08)60085-5

García-Palacios, P., Prieto, I., Ourcival, J. M., and Hattenschwiler, S. (2016). Disentangling the litter quality and soil microbial contribution to leaf and fine root litter decomposition responses to reduced rainfall. *Ecosystems* 19 (3), 490–503. doi: 10.1007/s10021-015-9946-x

Glaze, T. D., Erler, D. V., and Siljanen, H. M. P. (2022). Microbially facilitated nitrogen cycling in tropical corals. *ISME J.* 16 (1), 68–77. doi: 10.1038/s41396-021-01038-1

Gleeson, D. B., Mueller, C., Banerjee, S., Ma, W., Siciliano, S. D., and Murphy, D. V. (2010). Response of ammonia oxidizing archaea and bacteria to changing water filled pore space. *Soil Biol. Biochem.* 42 (10), 1888–1891. doi: 10.1016/j.soilbio.2010.06.020

Guo, X., Gao, Q., Yuan, M., Wang, G., Zhou, X., Feng, J., et al. (2020). Gene-informed decomposition model predicts lower soil carbon loss due to persistent microbial adaptation to warming. *Nat. Commun.* 11 (1), 4897. doi: 10.1038/s41467-020-18706-z

Hammerl, V., Kastl, E. M., Schloter, M., Kublik, S., Schmidt, H., Welzl, G., et al. (2019). Influence of rewetting on microbial communities involved in nitrification and denitrification in a grassland soil after a prolonged drought period. *Sci. Rep.* 9, 2280. doi: 10.1038/s41598-018-38147-5

Hartmann, A. A., Barnard, R. L., Marhan, S., and Niklaus, P. A. (2013). Effects of drought and n-fertilization on n cycling in two grassland soils. *Oecologia* 171 (3), 705–717. doi: 10.1007/s00442-012-2578-3

Homyak, P. M., Allison, S. D., Huxman, T. E., Goulden, M. L., and Treseder, K. K. (2017). Effects of drought manipulation on soil nitrogen cycling: a meta-analysis. *J. Geophys. Res. Biogeosci.* 122 (12), 3260–3272. doi: 10.1002/2017JG004146

Hoover, D. L., and Rogers, B. M. (2016). Not all droughts are created equal: the impacts of interannual drought pattern and magnitude on grassland carbon cycling. *Glob. Change Biol.* 22 (5), 1809–1820. doi: 10.1111/gcb.13161

Jentsch, A., Kreyling, J., Elmer, M., Gellesch, E., Glaser, B., Grant, K., et al. (2011). Climate extremes initiate ecosystem-regulating functions while maintaining productivity. *J. Ecol.* 99 (3), 689–702. doi: 10.1111/j.1365-2745.2011.01817.x

Jetten, M. S. M. (2008). The microbial nitrogen cycle. *Environ. Microbiol.* 10 (11), 2903–2909. doi: 10.1111/j.1462-2920.2008.01786.x

Kang, E., Li, Y., Zhang, X., Yan, Z., Zhang, W., Zhang, K., et al. (2022). Extreme drought decreases soil heterotrophic respiration but not methane flux by modifying the abundance of soil microbial functional groups in alpine peatland. *Catena.* 212, 106043. doi: 10.1016/j.catena.2022.106043

Kang, X., Yan, L., Cui, L., Zhang, X., Hao, Y., Wu, H., et al. (2018). Reduced carbon dioxide sink and methane source under extreme drought condition in an alpine peatland. *Sustainability* 10), 4285. doi: 10.3390/su10114285

Keil, D., Niklaus, P. A., von Riedmatten, L. R., Boeddinghaus, R. S., Dormann, C. F., Scherer-Lorenzen, M., et al. (2015). Effects of warming and drought on potential N_2O emissions and denitrifying bacteria abundance in grasslands with different land-use. *FEMS Microbiol. Ecol.* 91 (7), fiv066. doi: 10.1093/femsec/fiv066

Knapp, A. K., Beier, C., Briske, D. D., Classen, A. T., Luo, Y., and Reichstein, M. (2008). Consequences of more extreme precipitation regimes for terrestrial ecosystems. *BioScience* 58, 811–821. doi: 10.1641/B580908

Krause, S., Le Roux, X., Niklaus, P. A., Van Bodegom, P. M., Lennon, J. T., Bertilsson, S., et al. (2014). Trait-based approaches for understanding microbial biodiversity and ecosystem functioning. *Front. Microbiol.* 5, 251. doi: 10.3389/fmicb.2014.00251

Lefi, E., Medrano, H., and Cifre, J. (2004). Water uptake dynamics, photosynthesis and water use efficiency in field-grown medicago arborea and medicago citrina under prolonged Mediterranean drought conditions. *Ann. Appl. Biol.* 144, 299–307. doi: 10.1111/j.1744-7348.2004.tb00345.x

Leininger, S., Urich, T., Schloter, M., Schwark, L., Qi, J., Nicol, G. W., et al. (2006). Archaea predominate among ammonia-oxidizing prokaryotes in soils. *Nature* 442 (7104), 806–809. doi: 10.1038/nature04983

Levy-Booth, D. J., Prescott, C. E., and Grayston, S. J. (2014). Microbial functional genes involved in nitrogen fixation, nitrification and denitrification in forest ecosystems. *Soil Biol. Biochem.* 75, 11–25. doi: 10.1016/j.soilbio.2014.03.021

Li, R. Q., Li, Y. R., Kristiansen, K., and Wang, J. (2008). SOAP: short oligonucleotide alignment program. *Bioinformatics* 24 (5), 713–714. doi: 10.1093/bioinformatics/btn025

Li, D. H., Liu, C. M., Luo, R. B., Sadakane, K., and Lam, T. W. (2015). MEGAHIT: an ultra-fast single-node solution for large and complex metagenomics assembly *via* succinct de bruijn graph. *Bioinformatics* 31 (10), 1674–1676. doi: 10.1093/bioinformatics/btv033

Li, L. F., Zheng, Z. Z., Wang, W. J., Biederman, J. A., Xu, X. L., Ran, Q. W., et al. (2020). Terrestrial N_2O emissions and related functional genes under climate change: a global meta-analysis. *Glob. Change Biol.* 26 (2), 931–943. doi: 10.1111/gcb.14847

Liang, C., and Balser, T. C. (2011). Microbial production of recalcitrant organic matter in global soils: implications for productivity and climate policy. *Nat. Rev. Microbiol.* 9 (1), 75. doi: 10.1038/nrmicro2386-c1

Liang, C., Schimel, J. P., and Jastrow, J. D. (2017). The importance of anabolism in microbial control over soil carbon storage. *Nat. Microbiol.* 2 (8), 17105. doi: 10.1038/nmicrobiol.2017.105

Limpens, J., Heijmans, M. M. P. D., and Berendse, F. (2006). *Boreal Peatland ecosystems*. Eds. R. K. Wieder and D. H. Vitt. (Berlin, Heidelberg: Springer Berlin Heidelberg), 195–230.

Liu, J. F., Mbadinga, S. M., Sun, X. B., Yang, G. C., Yang, S. Z., Gu, J. D., et al. (2016). Microbial communities responsible for fixation of CO_2 revealed by using mcrA, cbbM, cbbL, fthfs, fefe-hydrogenase genes as molecular biomarkers in petroleum reservoirs of different temperatures. *Int. Biodeter. Biodegr.* 114, 164–175. doi: 10.1016/j.ibiod.2016.06.019

Loik, M. E. (2007). Sensitivity of water relations and photosynthesis to summer precipitation pulses for artemisia tridentata and purshia tridentata. *Plant Ecol.* 191, 95–108. doi: 10.1007/s11258-006-9217-1

Louca, S., Polz, M. F., Mazel, F., Albright, M. B. N., Huber, J. A., O'Connor, M. I., et al. (2018). Function and functional redundancy in microbial systems. *Nat. Ecol. Evol.* 2 (6), 936–943. doi: 10.1038/s41559-018-0519-1

Ludwig, M., Achtenhagen, J., Miltner, A., Eckhardt, K. U., Leinweber, P., Emmerling, C., et al. (2015). Microbial contribution to SOM quantity and quality in density fractions of temperate arable soils. *Soil Biol. Biochem.* 81, 311–322. doi: 10.1016/j.soilbio.2014.12.002

Lynn, T. M., Ge, T., Yuan, H., Wei, X., Wu, X., Xiao, K., et al. (2017). Soil carbon-fixation rates and associated bacterial diversity and abundance in three natural ecosystems. *Microb. Ecol.* 73 (3), 645–657. doi: 10.1007/s00248-016-0890-x

Ma, K., Liu, J. G., Balkovic, J., Skalsky, R., Azevedo, L. B., and Kraxner, F. (2016). Changes in soil organic carbon stocks of wetlands on china's zoige plateau from 1980 to 2010. *Ecol. Model.* 327, 18–28. doi: 10.1016/j.ecolmodel.2016.01.009

Malik, A. A., and Bouskill, N. J. (2022). Drought impacts on microbial trait distribution and feedback to soil carbon cycling. *Funct. Ecol.* 36 (6), 1442–1456. doi: 10.1111/1365-2435.14010

Manoharan, L., Kushwaha, S. K., Ahrén, D., and Hedlund, K. (2017). Agricultural land use determines functional genetic diversity of soil microbial communities. *Soil Biol. Biochem.* 115, 423–432. doi: 10.1016/j.soilbio.2017.09.011

Miki, T., Yokokawa, T., and Matsui, K. (2014). Biodiversity and multifunctionality in a microbial community: a novel theoretical approach to quantify functional redundancy. *Proc. R Soc. Lond B Biol. Sci.* 281 (1776), 20132498. doi: 10.1098/rspb.2013.2498

Moore, P. D. (2002). The future of cool temperate bogs. *Environ. Conserv.* 29 (1), 3–20. doi: 10.1017/S0376892902000024

Nelson, M. B., Martiny, A. C., and Martiny, J. B. H. (2016). Global biogeography of microbial nitrogen-cycling traits in soil. *Proc. Natl. Acad. Sci. U.S.A.* 113 (29), 8033–8040. doi: 10.1073/pnas.1601070113

Nielsen, U. N., and Ball, B. A. (2015). Impacts of altered precipitation regimes on soil communities and biogeochemistry in arid and semi-arid ecosystems. *Glob. Change Biol.* 21 (4), 1407–1421. doi: 10.1111/gcb.12789

Noguchi, H., Park, J., and Takagi, T. (2006). MetaGene: prokaryotic gene finding from environmental genome shotgun sequences. *Nucleic Acids Res.* 34 (19), 5623–5630. doi: 10.1093/nar/gkl723

Pokhrel, Y., Felfelani, F., Satoh, Y., Boulange, J., Burek, P., Gädeke, A., et al. (2021). Global terrestrial water storage and drought severity under climate change. *Nat. Clim. Change* 11 (3), 226–233. doi: 10.1038/s41558-020-00972-w

Radl, V., Kindler, R., Welzl, G., Albert, A., Wilke, B.-M., Amelung, W., et al. (2015). Drying and rewetting events change the response pattern of nitrifiers but not of denitrifiers to the application of manure containing antibiotic in soil. *Appl. Soil Ecol.* 95, 99–106. doi: 10.1016/j.apsoil.2015.06.016

Ribeiro, K., Pacheco, F. S., Ferreira, J. W., de Sousa-Neto, E. R., Hastie, A., Krieger Filho, G. C., et al. (2021). Tropical peatlands and their contribution to the global carbon cycle and climate change. *Glob. Change Biol.* 27 (3), 489–505. doi: 10.1111/gcb.15408

Rinke, C., Schwientek, P., Sczyrba, A., Ivanova, N. N., Anderson, I. J., Cheng, J. F., et al. (2013). Insights into the phylogeny and coding potential of microbial dark matter. *Nature* 499 (7459), 431–437. doi: 10.1038/nature12352

Roth, V. N., Lange, M., Simon, C., Hertkorn, N., Bucher, S., Goodall, T., et al. (2019). Persistence of dissolved organic matter explained by molecular changes during its passage through soil. *Nat. Geosci.* 12 (9), 755. doi: 10.1038/s41561-019-0417-4

Sardans, J., and Penuelas, J. (2010). Soil enzyme activity in a Mediterranean forest after six years of drought. *Soil Sci. Soc Am. J.* 74 (3), 838–851. doi: 10.2136/sssaj2009.0225

Schleper, C. (2010). Ammonia oxidation: different niches for bacteria and archaea? *ISME J.* 4 (9), 1092–1094. doi: 10.1038/ismej.2010.111

Snider, D., Thompson, K., Wagner-Riddle, C., Spoelstra, J., and Dunfield, K. (2015). Molecular techniques and stable isotope ratios at natural abundance give complementary inferences about N_2O production pathways in an agricultural soil following a rainfall event. *Soil Biol. Biochem.* 88, 197–213. doi: 10.1016/j.soilbio.2015.05.021

Tu, Q. C., He, Z. L., Wu, L. Y., Xue, K., Xie, G., Chain, P., et al. (2017). Metagenomic reconstruction of nitrogen cycling pathways in a CO_2- enriched grassland ecosystem. *Soil Biol. Biochem.* 106, 99–108. doi: 10.1016/j.soilbio.2016.12.017

Vogel, A., Eisenhauer, N., Weigelt, A., and Scherer-Lorenzen, M.. (2013). Plant diversity does not buffer drought effects on early-stage litter mass loss rates and microbial properties. *Glob. Change Biol.* 19 (9), 2795–2803. doi: 10.1111/gcb.12225

Wang, M., Chen, H., Wu, N., Peng, C., Zhu, Q., Zhu, D., et al. (2014). Carbon dynamics of peatlands in China during the Holocene. *Quaternary Sci. Rev.* 99, 34–41. doi: 10.1016/j.quascirev.2014.06.004

Wang, J.-T., Egidi, E., Li, J., and Singh, B. K. (2019). Linking microbial diversity with ecosystem functioning through a trait framework. *J. Biosci.* 44 (5), 109. doi: 10.1007/s12038-019-9928-9

Wertz, S., Degrange, V., Prosser, J. I., Poly, F., Commeaux, C., Guillaumaud, N., et al. (2007). Decline of soil microbial diversity does not influence the resistance and resilience of key soil microbial functional groups following a model disturbance. *Environ. Microbiol.* 9 (9), 2211–2219. doi: 10.1111/j.1462-2920.2007.01335.x

Xie, Z., Le Roux, X., Wang, C., Gu, Z., An, M., Nan, H., et al. (2014). Identifying response groups of soil nitrifiers and denitrifiers to grazing and associated soil environmental drivers in Tibetan alpine meadows. *Soil Biol. Biochem.* 77, 89–99. doi: 10.1016/j.soilbio.2014.06.024

Yan, Z., Kang, E., Zhang, K., Hao, Y., Wang, X., Li, Y., et al. (2022). Asynchronous responses of microbial CAZymes genes and the net CO2 exchange in alpine peatland following 5 years of continuous extreme drought events. *ISME Commun.* 2, 115. doi: 10.1038/s43705-022-00200-w

Yang, Y., Gao, Y., Wang, S., Xu, D., Yu, H., Wu, L., et al. (2014). The microbial gene diversity along an elevation gradient of the Tibetan grassland. *ISME J.* 8, 430–440. doi: 10.1038/ismej.2013.146

Yao, Z., Yan, G., Ma, L., Wang, Y., Zhang, H., Zheng, X., et al. (2022). Soil C/N ratio is the dominant control of annual N_2O fluxes from organic soils of natural and semi-natural ecosystems. *Agric. For. Meteorol.* 327, 109198. doi: 10.1016/j.agrformet.2022.109198

Yuan, M. M., Guo, X., Wu, L., Zhang, Y., Xiao, N., Ning, D., et al. (2021). Climate warming enhances microbial network complexity and stability. *Nat. Clim. Change* 11 (4), 343–U100. doi: 10.1038/s41558-021-00989-9

Yue, H., Wang, M., Wang, S., Gilbert, J. A., Sun, X., Wu, L., et al. (2015). The microbe-mediated mechanisms affecting topsoil carbon stock in Tibetan grasslands. *ISME J.* 9 (9), 2012–2020. doi: 10.1038/ismej.2015.19

Zhang, X., Zhao, X., and Zhang, M. (2012). Functional diversity changes of microbial communities along a soil aquifer for reclaimed water recharge. *FEMS Microbiol. Ecol.* 80 (1), 9–18. doi: 10.1111/j.1574-6941.2011.01263.x

Zhou, C., Biederman, J. A., Zhang, H., Li, L., Cui, X., Kuzyakov, Y., et al. (2019). Extreme-duration drought impacts on soil CO_2 efflux are regulated by plant species composition. *Plant Soil* 439 (1-2), 357–372. doi: 10.1007/s11104-019-04025-w

Zhou, S., Huang, C., Xiang, Y., Tie, L., Han, B., and Scheu, S. (2018). Effects of reduced precipitation on litter decomposition in an evergreen broad-leaved forest in Western China. *For. Ecol. Manage.* 430, 219–227. doi: 10.1016/j.foreco.2018.08.022

Zhou, J., Xue, K., Xie, J., Deng, Y., Wu, L., Cheng, X., et al. (2012). Microbial mediation of carbon-cycle feedbacks to climate warming. *Nat. Clim. Change* 2 (2), 106–110. doi: 10.1038/nclimate1331

frontiers | Frontiers in Ecology and Evolution

TYPE Review
PUBLISHED 13 July 2023
DOI 10.3389/fevo.2023.1189059

OPEN ACCESS

EDITED BY
Huakun Zhou,
Chinese Academy of Sciences (CAS), China

REVIEWED BY
Jia Lu,
China Institute of Water Resources and Hydropower Research, China
Zi-jian Xie,
Chinese Research Academy of Environmental Sciences, China

*CORRESPONDENCE
Guirui Yu
yugr@igsnrr.ac.cn

RECEIVED 18 March 2023
ACCEPTED 26 June 2023
PUBLISHED 13 July 2023

CITATION
Zhang T, Chen Z, Jiao C, Zhang W, Han L, Fu Z, Sun Z, Liu Z, Wen Z and Yu G (2023) Using the dynamics of productivity and precipitation-use efficiency to detect state transitions in Eurasian grasslands. *Front. Ecol. Evol.* 11:1189059. doi: 10.3389/fevo.2023.1189059

Using the dynamics of productivity and precipitation-use efficiency to detect state transitions in Eurasian grasslands

Tianyou Zhang[1], Zhi Chen[2,3,4], Cuicui Jiao[5], Weikang Zhang[2], Lang Han[6], Zheng Fu[7], Zhongyi Sun[8], Zhaogang Liu[2,3], Zhongming Wen[1] and Guirui Yu[2,3,4]*

[1]College of Grassland Agriculture, Northwest A&F University, Xianyang, Shaanxi, China, [2]Key Laboratory of Ecosystem Network Observation and Modeling, Institute of Geographic Sciences and Natural Resources Research, Chinese Academy of Sciences, Beijing, China, [3]College of Resources and Environment, University of Chinese Academy of Sciences, Beijing, China, [4]Yanshan Earth Critical Zone and Surface Fluxes Research Station, University of Chinese Academy of Sciences, Beijing, China, [5]College of Economics, Sichuan University of Science and Engineering, Yibin, China, [6]Institute of Surface-Earth System Science, School of Earth System Science, Tianjin University, Tianjin, China, [7]Laboratoire des Sciences du Climat et de l'Environnement, LSCE/IPSL, CEA-CNRS-UVSQ, Université Paris-Saclay, Gif-sur-Yvette, France, [8]College of Ecology and Environment, Hainan University, Haikou, China

In the face of accelerated global dryland expansion and grassland degradation, signaling grassland ecosystem state transitions is an ongoing challenge in ecology. However, there is still a lack of effective indicators and understanding of the mechanisms of grassland ecosystem state transitions at the continental scale. Here, we propose a framework that links ecosystem function-based indicators and critical slowing down (CSD) theory to reveal grassland state transitions. Across precipitation gradients, we quantified the statistical characteristics and spatial patterns in ANPP and PUE dynamics (variability, asymmetry, and sensitivity to precipitation and temperature) in Eurasian grasslands. We show that the CV_{ANPP}, CV_{PUE}, A_{ANPP}, A_{PUE}, $S_{PUE\text{-}P}$, and $S_{ANPP\text{-}P}$ of temperate steppes were significantly higher than those of alpine steppes, while the $S_{PUE\text{-}T}$ and $S_{ANPP\text{-}T}$ were the inverse. In temperate grasslands, A_{ANPP}, A_{PUE}, and $S_{ANPP\text{-}P}$ indicated the transition of typical steppes, and CV_{ANPP}, A_{PUE}, and $S_{PUE\text{-}T}$ indicated the transition from meadow to typical steppes. In alpine grasslands, A_{PUE} indicated the transition between alpine deserts and alpine steppes, and A_{ANPP} and $S_{ANPP\text{-}P}$ indicated the transition between alpine steppes and meadow steppes. The interannual variability of precipitation strongly affected xerophyte proportion and demographic processes, which control state transitions in low-resilience grasslands. Community structures and limiting factors (nutrient, light, and/or temperature) regulate state transitions in high-resilience grasslands. Our results demonstrate that function-based indicators are predictive of impending state transitions of temperate and alpine grasslands, highlighting the complementation of ANPP and PUE dynamics that have the potential for predicting grassland ecosystem regime shifts and their underlying mechanisms.

KEYWORDS

Eurasian grasslands, precipitation-use efficiency, productivity, regime shift, state transitions

1 Introduction

With the impacts of global warming and human activities, planetary boundaries have already been overstepped (Lenton et al., 2019; Lade et al., 2020). Climate factors are undergoing abrupt change at different spatiotemporal scales (Wang et al., 2020; Duffy et al., 2021). With global warming-accelerated drying, dryland ecosystems risk regime shifts without warning in structural and functional states and recovery from perturbations requires more time (Arani et al., 2021; Rietkerk et al., 2021). As one of the main types of terrestrial ecosystem, grassland ecosystems maintain the habitat for various wildlife and contribute to human well-being (Berdugo et al., 2020; Bardgett et al., 2021). However, grassland ecosystems are sensitive to climate change and face increasing risk of state transitions, which could have catastrophic impacts on ecosystem services (Berdugo et al., 2020; Maurer et al., 2020; Dietz et al., 2021). Therefore, indicators to predict state transitions and explore the underlying ecological mechanisms are necessary to cope with the regime shifts of grassland ecosystems caused by global climate change.

State transitions occur in a system when it is forced outside the basin of attraction of the original state, allowing a perturbation to trigger self-propelled change toward a contrasting state (Liu et al., 2019; Rietkerk et al., 2021). This phenomenon has been extensively applicated in ecological research, such as the sudden collapse of coral ecosystems (Hughes et al., 2018), the rapid degradation of arid ecosystems (Berdugo et al., 2020), and lake eutrophication (Liu et al., 2017; Su et al., 2021). The critical slowing down (CSD) theory of dynamical systems has provided a theoretical foundation for understanding ecosystem state transitions (Scheffer et al., 2009). The theory suggests that ecosystems subject to low resilience, with high variability, asymmetry, and sensitivity to external environment perturbations, and those systems in a state near the critical threshold (tipping point) are most likely to undergo a state transition (Scheffer et al., 2009; Clements and Ozgul, 2018). Experimental perturbations and natural time series have demonstrated that CSD-based indicators (e.g., variability, asymmetry, and temporal autocorrelation) are useful metrics to serve as potential metrics of systems undergoing a state transition (Carpenter and Brock, 2006; Dakos et al., 2012; Hu et al., 2018). Consistent with the theory, eigenvalue, skewness, variability, sensitivity, and autocorrelation estimated from a state variable increase abruptly before a regime shift occurs (Ratajczak et al., 2018; Cheng et al., 2021; Liang et al., 2021). However, these metrics are directly derived from general theoretical expectations and, as such, lack a link to specific ecological mechanisms (Dakos et al., 2015; Hu et al., 2022). Exploring useful indicators and ecological mechanisms in practice remains a big challenge for those concerned about implementing effective coping measures.

Aboveground net primary productivity (ANPP), as a principal ecosystem function, determines energy flow and facilitates carbon-water cycles within ecosystems (Haberl et al., 2014). ANPP dynamics (e.g., inter-annual variability and asymmetric and climatic sensitivity) have been used as indicators, identifying state transitions caused by demographic and limiting factors at the regional scale (Scheffer et al., 2009; Hu et al., 2018). Recent research has provided empirical support for the usefulness of ANPP dynamics as metrics of state transitions in grassland and forest ecosystems (Hu et al., 2018; Liu et al., 2019). Precipitation-use efficiency (PUE), as an aspect of ecosystem function–environment (Hu et al., 2022), represents the adaptive strategies of xerophyte proportion changes to cope with precipitation resource changes, especially in grassland ecosystems (Hu et al., 2010; Gherardi and Sala, 2019; Zhang et al., 2021). Therefore, PUE may be useful for identifying grassland state transitions. We suppose that the complementation of ANPP and PUE dynamics probably has more potential to detect state transitions and understand the underlying ecological mechanisms of grassland ecosystems. However, we still lack the combination of ANPP and PUE dynamics to detect grassland state transitions and reveal the underlying ecological mechanisms at the continental scale.

Eurasian grasslands have a large and continuous spatial distribution, a wide range of environment gradients, and various types of grassland, which will serve as an indispensable and ideal natural laboratory for understanding the indicators of state transitions and shifting ecological mechanisms at the continental scale. Here, we present a framework connecting ANPP and PUE dynamics to detect the state transitions of grassland ecosystems (Figure 1). Our framework focuses on the spatial variation in ANPP and PUE dynamics for variability, asymmetry, and climatic sensitivity along with precipitation. In our study, we hypothesize that intensified precipitation restrictions will lead to ecosystem states approaching the critical threshold (i.e., tipping point) and trending toward the alternative state. If there is a peak point in the spatial pattern of the ANPP and PUE dynamics along the mean annual precipitation (MAP) and corresponding to the shift of grassland type, the dynamic indicators can serve as metrics for state transitions.

We integrated field surveys of ANPP, the long-term Normalized Difference Vegetation Index (NDVI), and annual precipitation to produce long-term ANPP and PUE datasets from 1982 to 2021, then calculated the ANPP and PUE dynamics (variability, asymmetry, and sensitivity to precipitation and temperature) at each pixel in Eurasian grasslands. The main objectives of this study were to identify: (1) the spatial pattern and statistical characteristics of ANPP and PUE dynamics for variability, asymmetry, and climatic sensitivity in Eurasian grasslands; (2) the spatial pattern of ANPP and PUE dynamics along the MAP in temperate and alpine grasslands; and (3) effective indicators of ANPP and PUE dynamics to detect state transitions of grassland ecosystems in Eurasia. Moreover, we aimed to understand the shifting ecological mechanisms underlying ANPP and PUE dynamics related to abiotic and biotic factors that could help optimize regional grassland management strategies for achieving sustainable development.

2 Materials and methods

2.1 Study area

The Eurasian grasslands are located in the middle latitude region of the Northern Hemisphere (30°N ~ 55°N, 30°E ~ 125°E)

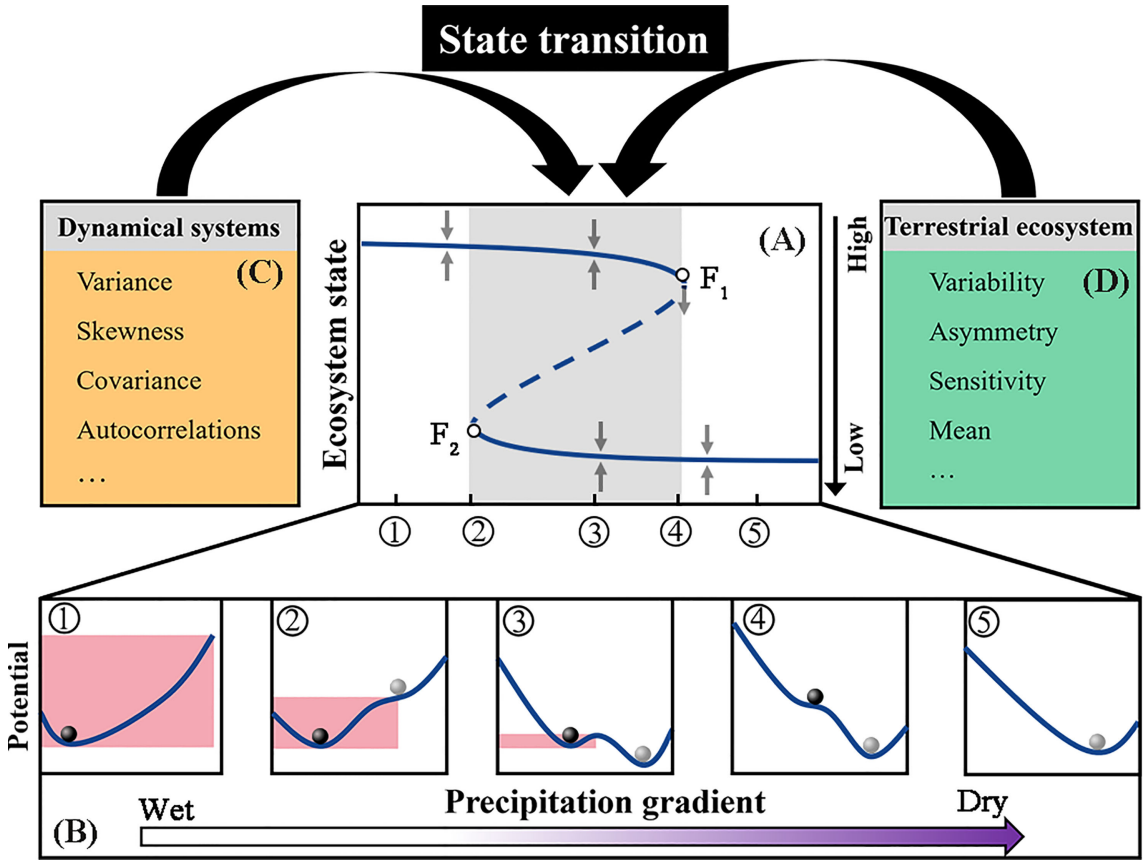

FIGURE 1
Schematic illustration of alternative stable states by means of ball-and-cup diagrams representing the stability properties at different external conditions. In **(A)**, the upper branch represents one stable ecosystem state, and the lower branch represents another stable state. Ecosystems are in one state of the upper branch under external disturbances (φ). Ecosystems are in two transitional states under external disturbances (κ-μ), where, in ecosystem states near the tipping point (for example point F_1 or point F_2), minor disturbances may cause a significant shift. Ecosystems are in one state of a lower branch under external disturbances (⑤). **(B)** shows the corresponding ball-and-cup explanations of alternative stable states at the different external conditions from ① to ⑤. In **(C)**, the temporal variance, skewness, covariance, and autocorrelation in state and functional variables serve as CSD state-based indicators of dynamical systems. In **(D)**, we assume that these CSD function-based indicators (variability, asymmetry, and climatic sensitivity) can also potentially serve as metrics of state transitions in terrestrial ecosystems.

(Figure 2A). The precipitation and temperature gradients are from 70 mm to 1030 mm and −9 to 15°C, respectively (Zhang et al., 2020). We used the International Geosphere-Biosphere Program (IGBP) terrestrial ecoregions map (Olson et al., 2001), Moderate Resolution Imaging Spectroradiometer (MODIS) production (https://lpdaac.usgs.gov/), and vegetation classification map of China (http://www.geodata.cn/) to obtain the geographical extent and grassland types. Previous research showed that the response of ANPP and PUE to precipitation is distinct in water-limited temperate steppes and temperature-limited alpine grasslands (Guo et al., 2015; Zhang et al., 2020). We hypothesize that ANPP and PUE dynamics have contrasting spatial patterns with MAP in temperate and alpine grasslands, respectively. According to the geographical environment and plant compositions of Eurasian grasslands, they could be divided into two categories: temperate grasslands (i.e., temperate desert steppes (TDS), typical steppes (TTS), and meadow steppes (TMS)) and alpine grasslands (i.e., alpine desert steppes (ADS), alpine steppes (AS), and alpine meadow steppes (AMS)) (Figure 2A). Desert steppes are characterized by short shrubs, semi-shrubs, and low diversity (Zhang et al., 2016). Typical steppes are dominated by relatively meso-xerophytic species. Meadows are located in the sub-humid district and have the highest coverage and biodiversity, which is dominated by mesophyte species (*Artemisia frigida, Agropyron cristatum* and *Stipa baicalensis*, etc.) (Hu et al., 2018). Alpine desert steppes are characterized by xerophyte species (*Ceratoides compacta* and *Stipa purpurea* etc.) with low productivity. Alpine steppes and meadows are mainly composed of drought-resistant and hardy species (*Alpine forbs*, *Carex moorcroftii*, *Stipa purpurea*, etc.) (Yang et al., 2010). The grassland types have clear divides and represent different ecosystem states along the MAP (Figures 2B, C), allowing us to diagnose if there are signals in the ANPP and PUE dynamics that correspond to state transitions.

2.2 *In situ* measured ANPP data

In this study, we collected three datasets of ANPP observations. This field sampling data approximates the ANPP of grassland ecosystems. The first ANPP dataset was extracted from published

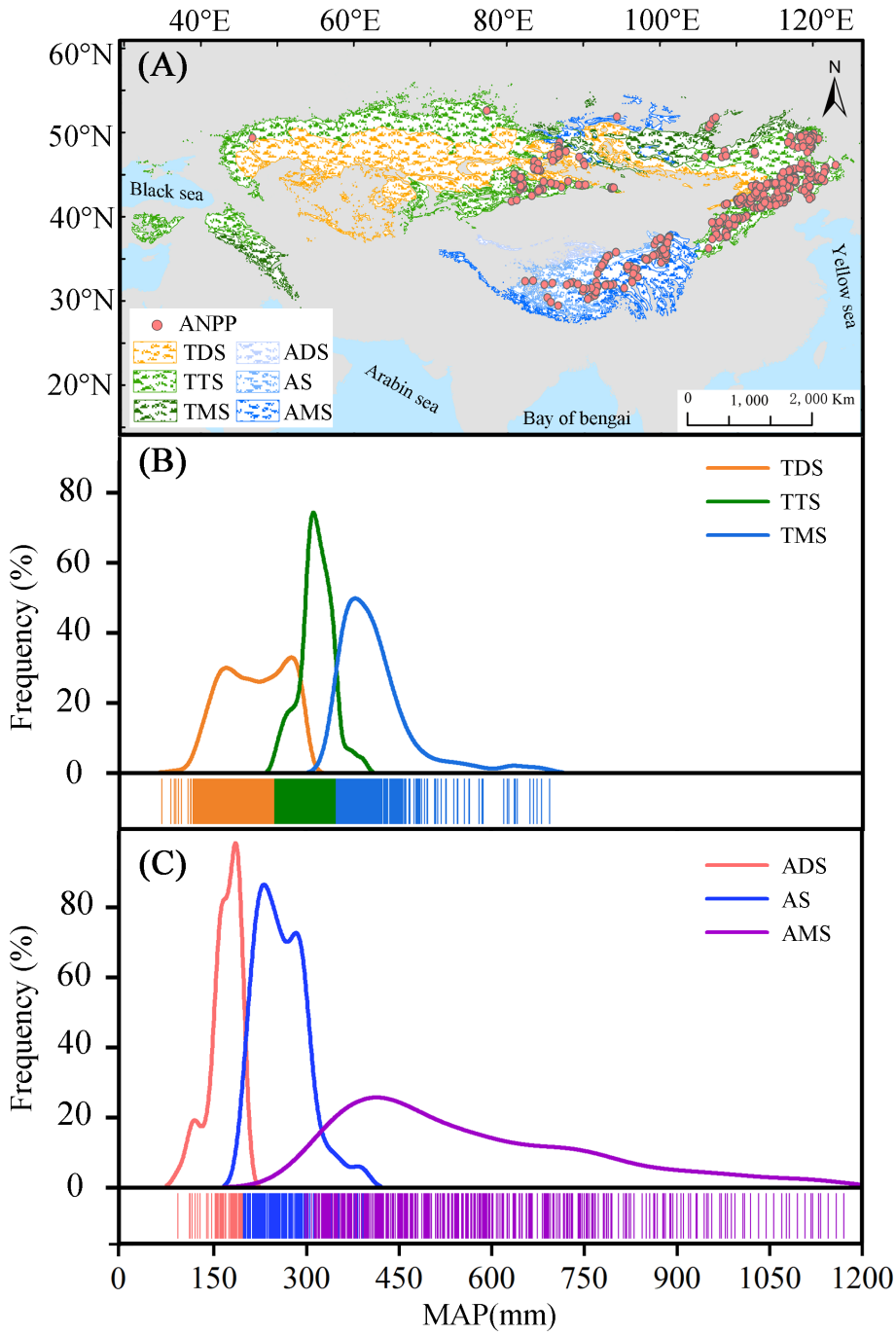

FIGURE 2
Spatial distributions of grassland types and measured aboveground net primary productivity (ANPP) **(A)**; the frequency distributions of mean annual precipitation (MAP) in temperate grasslands **(B)** and alpine grasslands **(C)**. TDS, TTS, TMS, ADS, AS, and AMS represent the six grassland types, i.e., temperate desert steppes, temperate typical steppes, temperate meadow steppes, alpine desert steppes, alpine steppes, and alpine meadow steppes, respectively.

literature, in which the AGB was measured at 267 sites on the Eurasian grasslands during July and August of 2002–2004 (Yang et al., 2010). The second ANPP dataset was supported by the Ministry of Agriculture of China (Hu et al., 2010). A background survey was organized in the peak growing seasons of 1983–1995 to study the forage yield of the region, in which the ANPP was measured at 503 sites on the Eurasian grasslands. The third dataset was extracted from the Oak Ridge National Laboratory (ORNL) (seven sites) and obtained directly from field surveys (81 sites) (Jiao et al., 2017). A total of 858 sites were selected from three sources (Figure 2A), which were used to estimate the long-term ANPP remote sensing products in Eurasian grasslands.

2.3 ANPP and PUE estimations from remote sensing products

The Global Inventory Modeling and Mapping Studies Normalized Difference Vegetation Index (GIMMS NDVI) and Moderate Resolution Imaging Spectroradiometer NDVI (MODIS13A2) data were used to construct the empirical mode between ANPP measurements and their corresponding NDVI at the sites. Specifically, we used the biweekly NDVI with a spatial resolution of 8 km from the GIMMS group as derived from the Advanced Very High Resolution Radiometer (AVHRR) from 1982 to 2015 (http://ecocast.arc.nasa.gov/data/pub/gimms/3g.v1/). The preprocessing of GIMMS NDVI remote sensing images consisted of 15-day maximum-value compositions (MVC), corrected to reduce the effects of residual clouds, the solar zenith angle, viewing geometry, and atmospheric perturbations (Jiao et al., 2017; Chen et al., 2019).

The MODIS NDVI product (MOD13A2) comes from the National Aeronautics and Space Administration (NASA, https://lpdaacsvc.cr.usgs.gov), with a temporal resolution of 16 days and a spatial resolution of 1 km. The MODIS NDVI data were corrected for cloud cover, atmosphere, and solar elevation angle (Liu et al., 2022). The bilinear interpolation method was used to resample the data to the spatial resolution of the GIMMS NDVI (Parker et al., 1983). Previous studies showed that seasonally integrated NDVI are more direct measures of vegetation activity, and therefore, frequently estimate ANPP (Verma et al., 2014; Maurer et al., 2020). We compared and found that the GIMMS and MODIS $NDVI_{int}$ had some linearity errors in the years between 2004 and 2013 (Figure 3A). We established an empirical relationship between the GIMMS and MODIS $NDVI_{int}$ ($R^2 = 0.93$) (Figure 3B). Then, we recalibrated the MODIS $NDVI_{int}$ and obtained the long-term $NDVI_{int}$ from 1982 to 2021 in the study area.

The NDVI is highly correlated to biomass across spatial scales and commonly used to estimate the quantities of vegetation ANPP in grasslands (Hu et al., 2018; Maurer et al., 2020). For these reasons, we established the relationship between ground-based measurements of ANPP and integrated NDVI during the growing season. A significant exponential relationship between measured ANPP and the corresponding integrated NDVI for the growing season was derived as (Figure 4):

$$ANPP = 24.20e^{0.47NDVI_{int}} \left(R^2 = 0.61, n = 858, P < 0.01\right)$$

With this relationship, ANPP was estimated for the entire study region based on long-term NDVI data from 1982 to 2021. The PUE was produced by the ratio of ANPP to the corresponding annual precipitation at each pixel during 1982 to 2021 in Eurasian grasslands (Zhang et al., 2021).

2.4 Precipitation and temperature data

The monthly precipitation and temperature data (0.5° × 0.5°) from 1982 to 2021 were obtained from the Climate Research Unit 4.06 dataset (CRU) (https://crudata.uea.ac.uk/cru/data/hrg/cru_ts_4.06/) (Harris et al., 2020). We calculated the annual precipitation and temperature from the monthly datasets. MAP was calculated as a multi-year averaged value from 1982 to 2021. The nearest neighbor interpolation method was used to resample the data to the spatial resolution of ANPP (8 km at the equator) for subsequent analysis (Parker et al., 1983).

2.5 ANPP and PUE dynamics for variability, asymmetry, and sensitivity

The ANPP and PUE dynamics for variability, asymmetry, and precipitation and temperature sensitivity were calculated based on the inter-annual ANPP and PUE data of the remote sensing products. The interannual variability in ANPP and PUE was calculated as the coefficient of variation in ANPP (CV_{ANPP}) and PUE (CV_{PUE}), namely, the ratio of standard deviation of the mean with long-term ANPP and PUE at each pixel from 1982 to 2021 (Knapp and Smith, 2001; Hu et al., 2018), according to

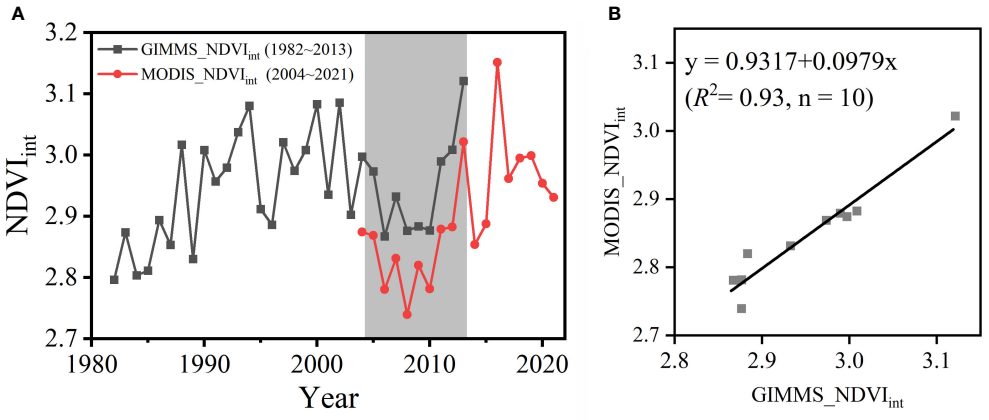

FIGURE 3
Comparisons NDVI between the $GIMMS\_NDVI_{int}$ and $MODIS\_NDVI_{int}$ from 1982 to 2021 in the entire Eurasian grasslands. **(A)** The time series of ANPP of the $GIMMS\_NDVI_{int}$ and $MODIS\_NDVI_{int}$. **(B)** The linear relationships between ANPP of the $GIMMS\_NDVI_{int}$ and $MODIS\_NDVI_{int}$ from 2003 to 2013.

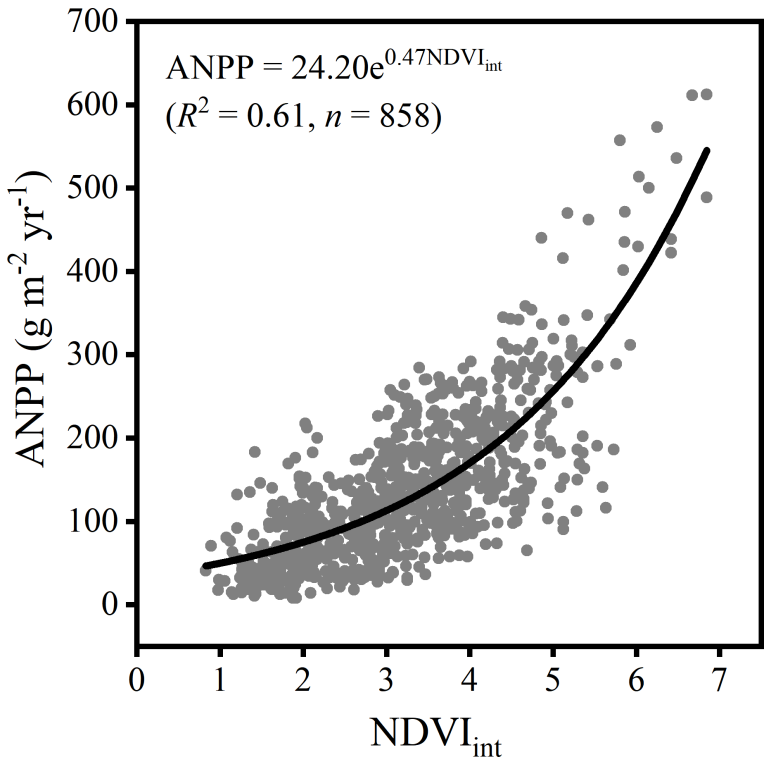

FIGURE 4
Regression function between the $NDVI_{int}$ and measured ANPP.

$$CV_{X(1982-2021)} = \frac{\sqrt{\frac{\sum_t (X_t - \bar{X})}{\bar{X}}}}{t-1}, X = ANPP, PUE \quad (1)$$

where CV is the coefficient of variation, X is ANPP, PUE, t is the year from 1982 to 2021, and $\bar{X}$ is mean value of variables.

Asymmetry (A) as an indicator is broadly analogous with skewness in system dynamics. With the disturbance of environmental factors, resilience decreases with increasing A (Wu et al., 2018; Al-Yaari et al., 2020). We estimated A as

$$A_X = \frac{X_{max} - \bar{X}}{\bar{X} - X_{min}}, X = ANPP, PUE \quad (2)$$

where A_X is the asymmetry of ANPP (A_{ANPP}) and PUE (A_{PUE}), X_{max} is the maximum and X_{min} is the minimum of ANPP and PUE during 1982–2021. An A value > 1 implies that ANPP gains in wet/warm years are larger than reduced in dry/cold years, and vice versa. The A value equal to 1 means the ecosystem is in a stable equilibrium state. The greater the degree of the ecosystem state deviating from the equilibrium is characterized by the deviation degree of A to 1, which indicates the ecosystem state is closer to the tipping point.

An ecosystem state closer to the tipping point responds more sensitively (S) to external perturbations (Hu et al., 2022; Zeng et al., 2022). To evaluate the sensitivity of ecosystems to climate variability, we estimated the response of ANPP and PUE to precipitation (S_{ANPP-P}, S_{PUE-P}) and temperature (S_{ANPP-T}, S_{PUE-T}) for each pixel during 1982–2021 using a multiple regression method (He et al., 2019):

$$y' = \delta^{int} \tilde{n} AP' + \gamma^{int} \tilde{n} AT' + \epsilon \quad (3)$$

where y' is the detrended anomaly of the ensemble mean of ANPP and PUE. AP' and AT' are the detrended anomalies of annual precipitation and temperature, respectively. δ^{int} and γ^{int} represent the sensitivity of ANPP and PUE to climate factors, respectively, and ε is the residual error.

In addition to the variability and asymmetry of ANPP and PUE, we also calculated the annual precipitation variability (CV_P) and asymmetry (A_P) to evaluate the effect that precipitation dynamics plays in determining the ecosystem state.

The spatial pattern of ANPP and PUE dynamics were mapped using ArcGIS 10.7 software. The multiple regression analysis was achieved using Sigmaplot 14.0 software.

2.6 Data processing and methodology

We calculated the arithmetic average and standard error value of ANPP and PUE dynamics (CV_{ANPP}, CV_{PUE}, A_{ANPP}, A_{PUE}, S_{ANPP-P}, S_{ANPP-T}, S_{PUE-P}, S_{PUE-T}) at 20 mm intervals in the MAP. The simple line regression analysis was applied to explore the spatial pattern of ANPP and PUE dynamics with MAP, according

10.3389/fevo.2023.1189059

to Equation (4):

$$y = \alpha + \beta MAP + \xi \quad (4)$$

where y is ANPP or PUE dynamics, MAP is mean annual precipitation, α is the constant term, β is the regression coefficient for MAP, and ξ is the residual error.

We also used a piecewise linear regression model to diagnosis the critical threshold of ANPP and PUE dynamics (CV_{ANPP}, CV_{PUE}, A_{ANPP}, A_{PUE}, S_{ANPP-P}, S_{ANPP-T}, S_{PUE-P}, S_{PUE-T}) in response to MAP (Hu et al., 2018), determined by the least square error. According to Equation (5):

$$y = \begin{cases} \beta_0 + \beta_1 MAP + \epsilon, t \le \alpha \\ \beta_0 + \beta_1 t + \beta_2 (MAP) - \alpha + \epsilon, t \ge \alpha \end{cases} \quad (5)$$

where y is the ANPP and PUE dynamics, and MAP is the mean annual precipitation. α is the value of the turning point. β_0 is the constant term. β_1 and β_2 are the regression coefficients for MAP. A t-test was applied to test the null hypothesis "β_2 is not different from zero".

3 Results

3.1 Spatial pattern and statistical characteristics of ANPP and PUE dynamics in Eurasian grasslands

Our results showed that the range of CV_{ANPP}, A_{ANPP}, S_{ANPP-P}, and S_{ANPP-T} in Eurasian grasslands were 0.02–0.56, 0.3–3.1, −0.05–0.32, and −12–21, respectively (Figures 5A–D). A high CV_{ANPP} and S_{ANPP-P} were found in the northern typical and meadow steppes. In contrast, a low CV_{ANPP} and S_{ANPP-P} were found in the southern desert grasslands and alpine grasslands (Figures 5A, C). The CV_{PUE}, A_{PUE}, S_{PUE-P}, and S_{PUE-T} varied from 0.02 to 0.45, 0.4 to 3.2, −0.006 to 0, and −0.05 to 0.28, respectively (Figures 5E–H). A high S_{PUE-P} and S_{PUE-T} occurred in the eastern temperate grasslands. A low S_{PUE-P} and S_{PUE-T} appeared in the desert steppes and southwestern alpine steppes (Figures 5G, H). However, the spatial distribution of A_{ANPP}, S_{ANPP-T}, CV_{PUE}, and A_{PUE} showed no clear rule of territorial differentiation.

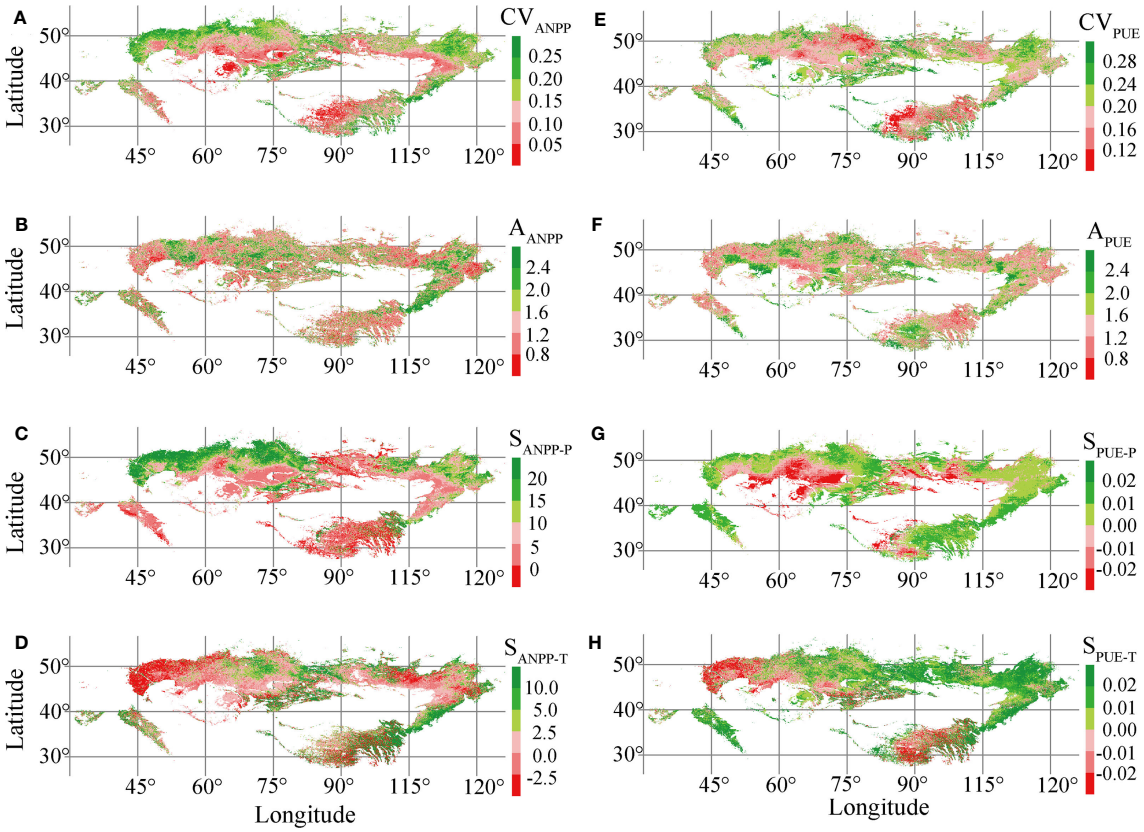

FIGURE 5
Spatial distribution of interannual variability of aboveground net primary production (CV_{ANPP}) **(A)** and precipitation use efficiency (CV_{PUE}) **(E)**, ANPP asymmetry (A_{ANPP}) **(B)** and PUE asymmetry (A_{PUE}) **(F)**, ANPP precipitation sensitivity (S_{ANPP-P}) **(C)** and PUE precipitation sensitivity (S_{PUE-P}) **(G)**, and ANPP temperature sensitivity (S_{ANPP-T}) **(D)** and PUE temperature sensitivity (S_{PUE-T}) **(H)** in Eurasian grasslands.

The magnitude of ANPP and PUE dynamics of temperate grasslands were generally larger than those of alpine grasslands (Supplementary Figure S1). In temperate grasslands, the magnitude of CV_{ANPP}, $S_{ANPP\text{-}T}$, CV_{PUE}, $S_{PUE\text{-}P}$, and $S_{PUE\text{-}T}$ in desert steppes were generally lower than in meadow steppes, while the magnitude of A_{ANPP} and A_{PUE} was the converse (Figure 6). We also found that the magnitude of $S_{ANPP\text{-}P}$ in typical steppes was larger than in desert and meadow steppes (Figure 6C). In alpine grasslands, the magnitude of CV_{ANPP}, $S_{ANPP\text{-}T}$, CV_{PUE}, and $S_{PUE\text{-}P}$ in alpine desert steppes were significantly lower than alpine meadows (Figures 6A, D, E, G), while the magnitude of A_{ANPP} was the converse (Figure 6B). It is worth noting that the $S_{ANPP\text{-}P}$ and $S_{PUE\text{-}T}$ in alpine steppes were lower than in alpine desert and meadow steppes (Figures 6C, H). We also found that the ANPP and PUE sensitivity to precipitation were positive and negative values, respectively. In addition, the ANPP and PUE sensitivities to temperature had positive and negative values, respectively. These results indicated that ANPP and PUE dynamics have different meanings in grassland state transitions.

3.2 Spatial patterns of ANPP and PUE dynamics with MAP in temperate and alpine grasslands

In temperate grasslands, the spatial patterns of CV_{ANPP}, A_{ANPP}, $S_{ANPP\text{-}P}$, A_{PUE}, and $S_{PUE\text{-}T}$ appeared as peaks along the MAP, which were consistent with the transition of grassland types (Figures 7A–C, F, H). A_{ANPP}, $S_{ANPP\text{-}P}$, and A_{PUE} peaked at the regime shift of typical steppes (Figures 7B, C, F), indicating it was an available CSD-based indicator for state transitions between the desert and typical steppes. In addition, the spatial patterns of CV_{ANPP}, A_{ANPP}, and $S_{PUE\text{-}T}$ appeared as peaks at the transition zone between the typical and meadow steppes (Figures 7A, B, H). On the contrary, $S_{ANPP\text{-}T}$, CV_{PUE}, and $S_{PUE\text{-}P}$ showed no peaks corresponding to regime shifts between grassland types along the MAP (Figures 7D, E, G), indicating it failed to capture state transitions in temperate grasslands. These results showed that CV_{ANPP}, A_{ANPP}, $S_{ANPP\text{-}P}$, A_{PUE}, and $S_{PUE\text{-}T}$ were effective indicators for state transitions of temperate grasslands.

We found that the spatial pattern of ANPP and PUE dynamics with the MAP differed in alpine and temperate grasslands (Figures 7, 8). In alpine grasslands, A_{PUE} peaked at the dry edge of alpine steppes (Figure 8F), indicating A_{PUE} was an available CSD-based indicator for the state transition between alpine desert and alpine steppes. In addition, A_{ANPP} and $S_{ANPP\text{-}P}$ peaked at the wet edge of alpine steppes and near the critical zone between alpine steppes and alpine meadows (Figures 8B, C). The CV_{ANPP}, CV_{PUE}, and $S_{PUE\text{-}P}$ showed an increasing trend with MAP and did not peak corresponding to the transition interval of grassland types (Figures 8A, E, G). Although the spatial pattern of $S_{ANPP\text{-}T}$ and $S_{PUE\text{-}T}$ appeared as peaks along the MAP (Figures 8D, H), it was inconsistent with ecotone, and thus also could not indicate state transitions in temperate grasslands. These results showed that $S_{ANPP\text{-}P}$, A_{PUE}, and A_{ANPP} were available indicators for state transitions of alpine grasslands.

4 Discussion

4.1 Ecological significance of variability, asymmetry, and sensitivity of ANPP and PUE

Overall, we found that the ANPP and PUE dynamics (e.g., CV_{ANPP}, $S_{ANPP\text{-}T}$, CV_{PUE}, $S_{PUE\text{-}P}$, and $S_{PUE\text{-}T}$) in desert steppes were

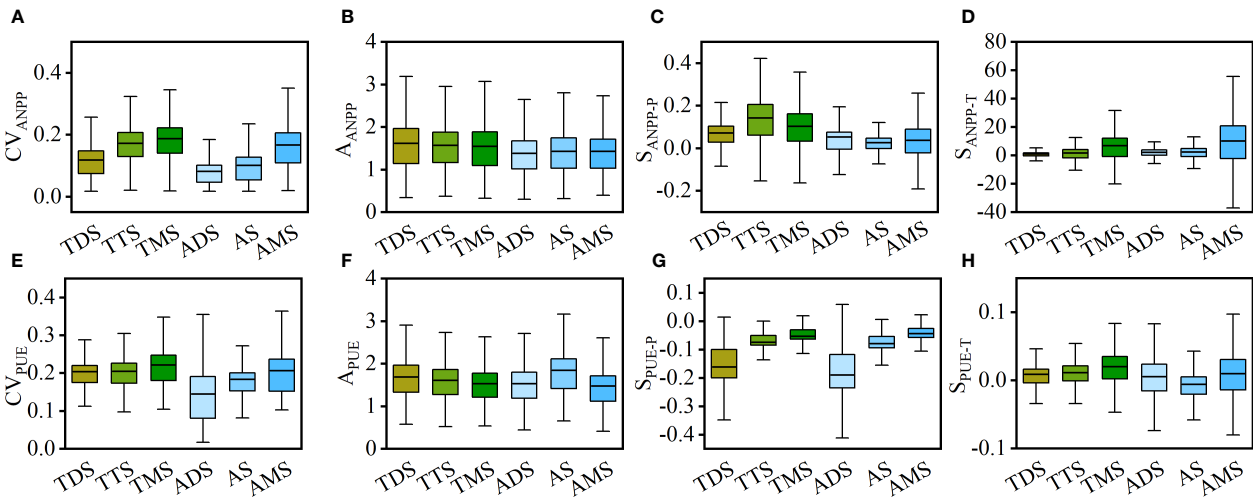

FIGURE 6
Statistical characteristics of interannual variability of aboveground net primary production (CV_{ANPP}) **(A)** and precipitation use efficiency (CV_{PUE}) **(E)**, ANPP asymmetry (A_{ANPP}) **(B)** and PUE asymmetry (A_{PUE}) **(F)**, ANPP precipitation sensitivity ($S_{ANPP\text{-}P}$) **(C)** and PUE precipitation sensitivity ($S_{PUE\text{-}P}$) **(G)**, and ANPP temperature sensitivity ($S_{ANPP\text{-}T}$) **(D)** and PUE temperature sensitivity ($S_{PUE\text{-}T}$) **(H)** in temperate and alpine grasslands. TDS, TTS, TMS, ADS, AS, and AMS represent the six grassland types, i.e., temperate desert steppes, temperate typical steppes, temperate meadow steppes, alpine desert steppes, alpine steppes, and alpine meadow steppes, respectively.

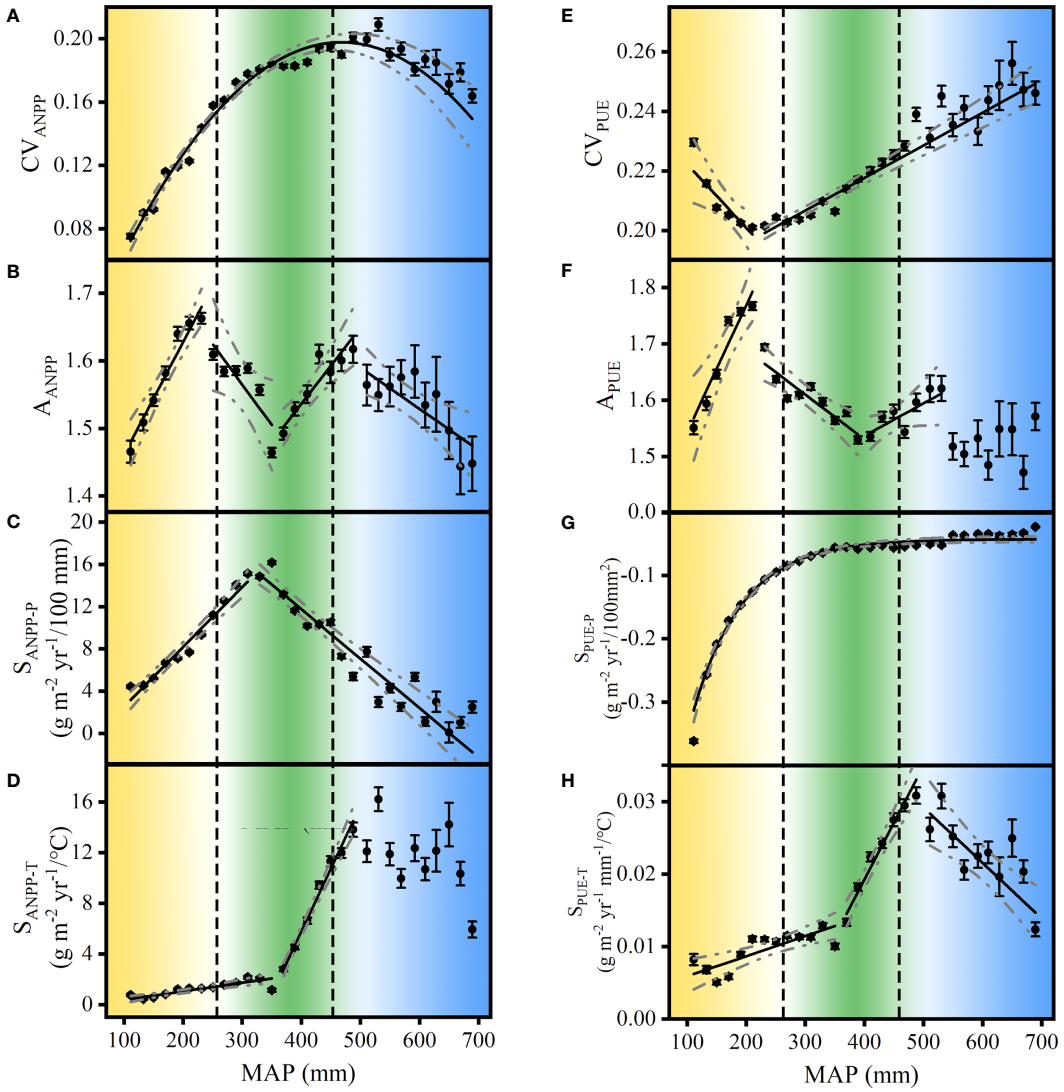

FIGURE 7
Spatial pattern of interannual variability of aboveground net primary production (CV_{ANPP}) **(A)** and precipitation use efficiency (CV_{PUE}) **(E)**, ANPP asymmetry (A_{ANPP}) **(B)** and PUE asymmetry (A_{PUE}) **(F)**, ANPP precipitation sensitivity (S_{ANPP-P}) **(C)** and PUE precipitation sensitivity (S_{PUE-P}) **(G)**, and ANPP temperature sensitivity (S_{ANPP-T}) **(D)** and PUE temperature sensitivity (S_{PUE-T}) **(H)** along the mean annual precipitation (MAP) in Eurasian temperate grasslands. The broken lines with ANPP and PUE dynamics denote 95% confidence intervals for the regressions. The vertical dashed lines denote the edge of the desert and typical steppes at 280 mm and 450 mm, respectively (based on Figure 2B). The data exemplified were bin-average at 20 mm MAP intervals. Yellow, green, and blue represent the three grassland types, i.e., temperate desert steppes, typical steppes, and meadow steppes, respectively.

generally lower than in meadow steppes in temperate and alpine grasslands, respectively (Figure 6). It is likely because the short xerophytic species and low diversity in deserts are adapted the low precipitation and poor nutrient availability, causing low ANPP and PUE dynamics (Davidowitz, 2002; Huang et al., 2015; Hu et al., 2022). On the contrary, meadow steppes are characterized by the highest coverage and abundant biodiversity, likely causing the high variability and sensitivity of ANPP and PUE to climate change (Bai et al., 2004; Wang et al., 2005; Guo et al., 2015). These results were consistent with previous analyses based on long-term observations of ANPP dynamics in temperate grasslands (Zhou et al., 2006).

We have also found that the magnitude of A_{ANPP} and A_{PUE} in desert steppes were larger than typical and meadow steppes in temperate grasslands (Figure 6). The A_{ANPP} and A_{PUE} were positive values, which suggested a more significant decrease of ANPP and PUE in dry years than increases in wet years (Knapp and Smith, 2001; Zhou et al., 2006; Wu et al., 2018). Previous research showed that the hysteresis effects of soil moisture of earlier years alleviate the substantial declines of ANPP and PUE, meaning that A_{ANPP} and A_{PUE} in the dry region were larger than in the wet region (Sala et al., 2012; Petrie et al., 2018). In dry regions, the hysteresis effects of soil moisture from previous years was limited. In contrast, in a wet region, other resources such as soil nutrient availability, light, or temperature limitations associated with wet periods countervailed the effect of increased precipitation on ANPP and PUE (Wu et al., 2018).

In addition, we found that CV_P in desert steppes was generally larger than in meadow steppes (Supplementary Figure S2). Collectively, we demonstrated that ANPP and PUE dynamics

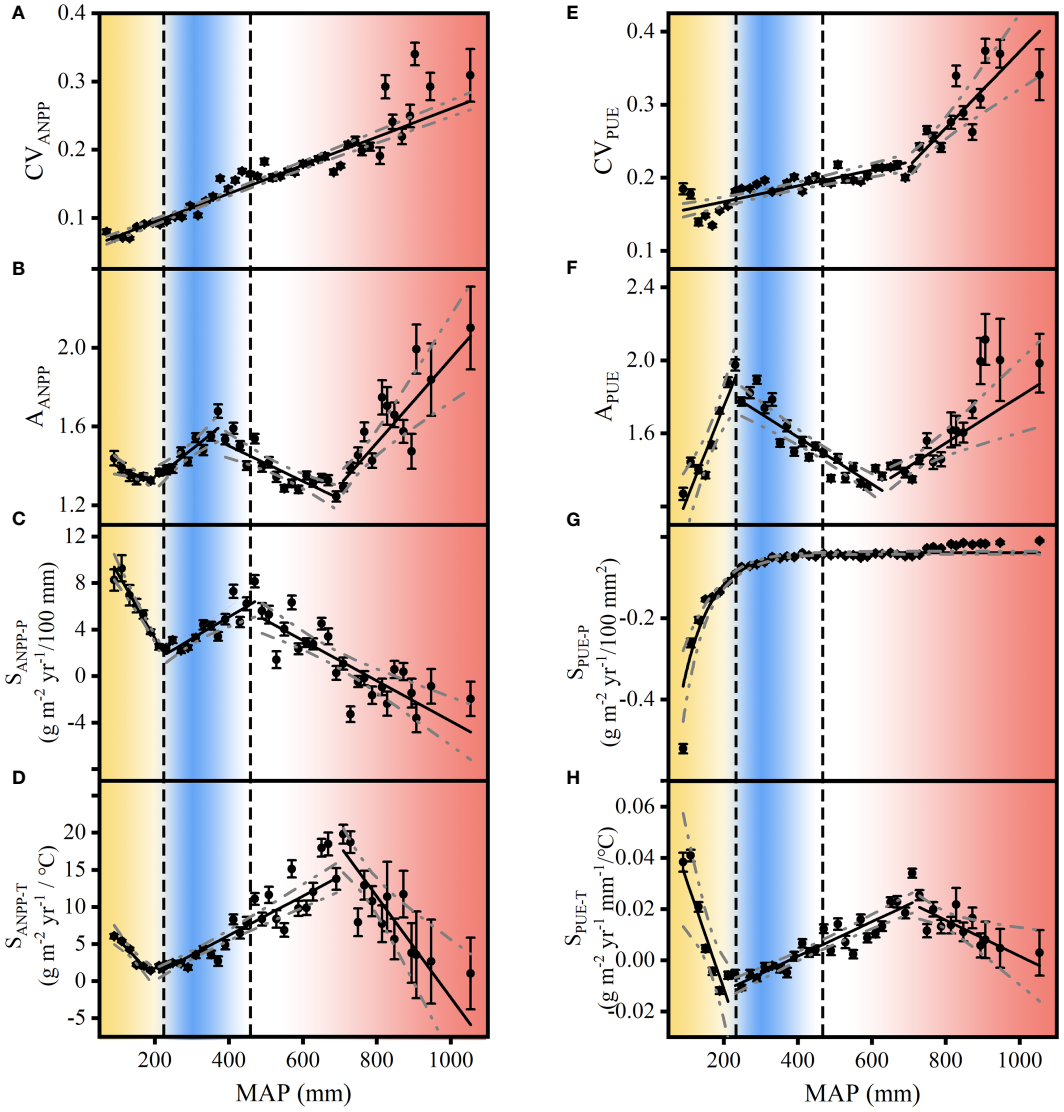

FIGURE 8
Spatial pattern of interannual variability of aboveground net primary production (CV_{ANPP}) **(A)** and precipitation use efficiency (CV_{PUE}) **(E)**, ANPP asymmetry (A_{ANPP}) **(B)** and PUE asymmetry (A_{PUE}) **(F)**, ANPP precipitation sensitivity (S_{ANPP-P}) **(C)** and PUE precipitation sensitivity (S_{PUE-P}) **(G)**, and ANPP temperature sensitivity (S_{ANPP-T}) **(D)** and PUE temperature sensitivity (S_{PUE-T}) **(H)** along the mean annual precipitation (MAP) in Eurasian alpine grasslands. The broken lines with ANPP and PUE dynamics denote 95% confidence intervals for the regressions. The vertical dashed lines indicate the edge of alpine desert steppes and alpine steppes at 200 mm and 400 mm, respectively (based on Figure 2C). The data illustrated were bin-average at 20 mm MAP intervals. Yellow, blue, and red represent the three grassland types, i.e., alpine desert steppes, alpine steppes, and alpine meadow steppes, respectively.

were available to indicate the stability and resilience of grassland ecosystems. Abiotic and biotic factors are essential factors influencing the variability, asymmetry, and climatic sensitivity of ANPP and PUE in grassland ecosystems (Hector et al., 2010; Willis et al., 2018).

4.2 Underlying ecological mechanisms shape the spatial patterns of ANPP and PUE dynamics

We found that the CV_{ANPP} exhibited an initial ascending and then declining spatial pattern with MAP in temperate grasslands (Figure 7A), while it increased with MAP in alpine grasslands (Figure 8A). These results were consistent with previous analyses based on long-term observations of ANPP dynamics in temperate grasslands (Knapp and Smith, 2001; Hu et al., 2018). In our study, we once again illustrated the relationship between CV_{ANPP} and precipitation and enhanced robustness by using long-term remote sensing products and climate data sets of grassland ecosystems on a large spatial scale. In addition, CV_{PUE} and CV_{ANPP} had reverse spatial patterns along the MAP in temperate grasslands, and were consistent in alpine grasslands (Figures 8A, E). It is worth noting that the CV_{ANPP}, CV_{PUE}, and CV_{AP} were inconsistent with MAP in temperate and alpine grasslands (Supplementary Figure S3). This result showed that CV_{ANPP} was not completely controlled by spatial patterns in CV_P.

The A_{ANPP} exhibited a piecewise mode with MAP and peaked at the wet edge of temperate desert, typical, and alpine steppes in Eurasian grasslands. In this region, precipitation strongly shaped xerophyte proportion and demographic processes, which could cause the transition between shrub and steppe (Huxman et al., 2004; Liu et al., 2012; Zhang et al., 2020). These results were consistent with the spatial pattern of A_{ANPP} in desert and typical steppes of temperate grasslands (Hu et al., 2018). In addition, the A_{PUE} showed a similar piecewise pattern with MAP in temperate and alpine grasslands and peaked at the moist edge of temperate and alpine desert steppes. We suggested that the ANPP gains in rainy years were larger than reduced in lower rainfall years and intensified with the MAP in desert steppes. Conversely, ANPP gains in wet years and reductions in dry years could be offset, causing A_{ANPP} to decrease with the MAP in meadow steppes (Wilcox et al., 2017; Wu et al., 2018). In addition, the spatial pattern of A_{ANPP} and A_{PUE} was inconsistent with A_P in temperate and alpine grasslands, respectively (Figure S3). Consequently, we inferred that the proportion of opportunistic species, demographic, and ecosystem traits regulated the asymmetry of ANPP and PUE in temporal (Huxman et al., 2004; Luo et al., 2017).

The $S_{ANPP\text{-}P}$ peaked at the moist edge of temperate desert and alpine steppes (Figures 7C; 8C), where the importance of ecosystem traits and xerophyte proportion on ecosystem temporal dynamics of ANPP and PUE were higher. We also found that $S_{PUE\text{-}T}$ peaked at the wet edge of alpine steppes (Figure 8H), where light, temperature, ecosystem traits, and soil nutrient limitations on ANPP and PUE dynamics were higher (Guo et al., 2015; Ganjurjav et al., 2016). In addition, low temperature and soil nutrients limited the ability of plants to use soil moisture and caused the decline of $S_{ANPP\text{-}P}$ and $S_{ANPP\text{-}T}$ in temperate and alpine meadow steppes (Kou et al., 2020).

4.3 Indicators of grasslands ecosystem state transitions at the continental scale

Our study confirmed that ANPP and PUE dynamics are useful indicators in detecting state transitions at the continental scale. ANPP as a principal ecosystem function has been demonstrated, but PUE is rarely mentioned (Hu et al., 2018; Berdugo et al., 2020). The adaptive strategies of communities to precipitation are important for understanding state transitions, especially in grassland ecosystems (Knapp et al., 2017; Wu et al., 2018; Wang et al., 2022). We based our study on the magnitude of ANPP and PUE dynamics magnitude and divided temperate and alpine grasslands into low and high resilience states, respectively (Figure 9). Spatial patterns of ANPP and PUE dynamics with MAP were used to analyze state transitions of low and high resilience in Eurasian grasslands. Notably, we found that the complementation of ANPP and PUE dynamics was helpful in identifying state transitions and understanding its underlying ecological mechanisms in Eurasian grasslands.

In our study, A_{ANPP}, A_{PUE}, and $S_{ANPP\text{-}P}$ peaked at the wet edge of desert steppes (Figure 7C), and CV_{ANPP}, A_{ANPP}, and $S_{PUE\text{-}T}$ peaked at the moist edge of typical steppes (Figures 7B, E, H). Thus, these grassland types lie functionally approach a state transition in temperate grasslands. A_{PUE} peaked at the edge of alpine desert steppes (Figures 8C, G), and A_{ANPP} and $S_{ANPP\text{-}P}$ peaked at the wet edge of alpine steppes (Figure 8D), all of which peaked at the transition region in alpine grasslands. A previous study showed that CV_{ANPP} and A_{ANPP} could indicate state transitions between desert and typical steppes, and $S_{ANPP\text{-}P}$ was available to detect typical and meadow steppe regime shifts in temperate grasslands (Hu et al., 2018). We suggest that CV_P and xerophyte proportion explained the relative state transitions in low resilience grassland ecosystems (Gherardi and Sala, 2019; Deng et al., 2021; Hu et al., 2022). Community (species traits, composition, and competition) and limiting factors (light, temperature, and nutrients) regulate the relative abrupt transition of high resilience grassland ecosystems (Kou et al., 2020; Sun et al., 2021) (Figure 9). Note that, although MAP itself has a clear threshold between grassland types (Figures 2B, C), ecosystems may be undergoing a state transition without detectable signals in precipitation changes (Scheffer et al., 2009; Lenton, 2011; Hou et al., 2021). In addition, we also found that the ANPP and PUE dynamics closely linked to precipitation are a promising complementary method for understanding the underlying mechanisms.

Overall, ANPP and PUE dynamics were predictive of critical state transitions of grassland ecosystems, and this was our motivation for connecting function-based indicators and CSD to identify state transitions. However, not all indicators could serve as metrics of state transition. For instance, CV_{PUE}, $S_{PUE\text{-}P}$, and $S_{ANPP\text{-}T}$ did not peak corresponding to the transitions between grassland types. Note that the theory predicts positive feedback for the cascading effects of multiple elements (species, soil water, plant biomass, root system, and water uptake, etc.) as a critical fundamental mechanism for state transition (Grace et al., 2007; Estiarte et al., 2016; De Boeck et al., 2018). Unfortunately, we lacked the data to assess the connection between the dynamics and feedback. Furthermore, the quality and quantity of data, as well as the temporal and spatial scales, all affected the robustness of the indicators (Dakos et al., 2015; Rietkerk et al., 2021). In future research, we would further consider the feedback processes of ecosystems, and use long-term *in situ* observation data to explore the indicators for state changes in terrestrial ecosystems at the continental scale.

5 Conclusion

With long-term ANPP and PUE remote sensing products, our study proposed a theoretical basis for ecosystem function-based indicators to detect state transitions in Eurasian grasslands. We greatly extended the analysis of ANPP and PUE dynamics across the conterminous Eurasia grasslands, thereby firmly establishing functional ecosystem indicators to signal state transitions at the continental scale. Of greater significance, we have comprehensively confirmed valuable indicators for state transitions, and revealed its underlying ecological mechanisms in low and high resilience in Eurasian grasslands. CV_{ANPP}, A_{ANPP}, A_{PUE}, $S_{ANPP\text{-}P}$, and $S_{PUE\text{-}T}$ displayed distinct spatial patterns, with peaks signaling state transitions of grassland ecosystems. We highlight the essential roles of hydrothermal conditions, community

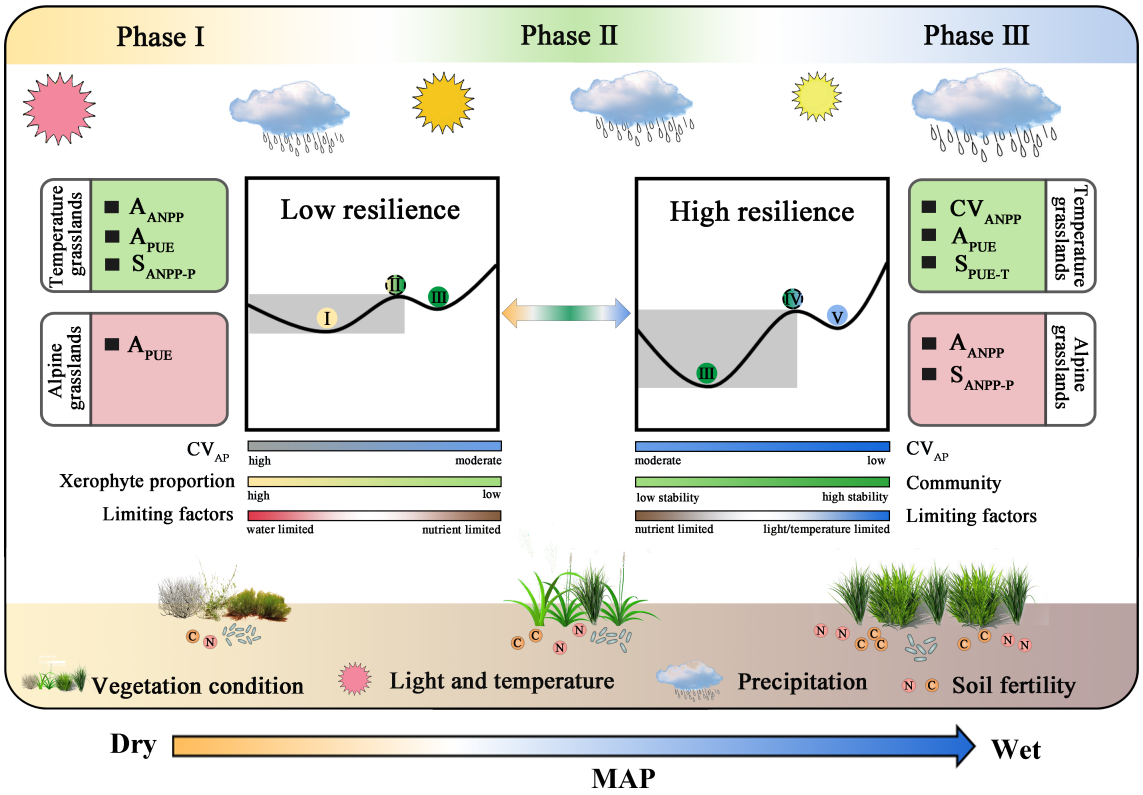

FIGURE 9
Schematic illustration of early warning signals and ecological mechanisms of state transitions in the processes underlying their distribution along MAP. Precipitation, light/temperature, and species composition regulated high and low resilience state transitions in Eurasian grasslands. In the inner rectangular list, peak ANPP asymmetry (A_{ANPP}), PUE asymmetry (A_{PUE}), and ANPP precipitation sensitivity (S_{ANPP-P}) signal transitions at the edge of desert steppes of low resilience temperate grasslands. Interannual variability of ANPP (CV_{ANPP}), A_{PUE}, and PUE temperature sensitivity (S_{PUE-T}) peak at the transition of high resilience temperate grasslands. A_{PUE} signals transitions of the low resilience alpine grasslands. A_{ANPP} and S_{ANPP-P} signal transitions of the high resilience alpine grasslands. Precipitation and xerophyte proportion controlled state transitions in low resilience grasslands. Community structure and limiting factors (nutrient, light, and/or temperature) regulated state transitions in high resilience grasslands. Low and high resilience represent the desert and meadow steppes in temperate and alpine grasslands, respectively. Phase I, II, and III correspond to desert steppes, typical steppes, and meadow steppes in temperate grasslands, respectively, or alpine desert steppes, alpine steppes, and alpine meadow steppes in alpine grasslands, respectively.

structures, and limiting factors in regulating ecosystem state transitions. We suggest that grassland management strategies and climate change research focus on areas that are highly vulnerable to climate variability and are changing rapidly due to multiple factors in the grassland transition zone.

Author contributions

TZ and GY conceived the article. TZ, WZ, CJ, LH, and ZL performed the statistical analyses. ZF, ZS, ZW, ZC, and GY drafted the manuscript. All authors contributed to the article and approved the submitted version.

Funding

This study was supported by the National Natural Science Foundation of China (32201344, 41991234, 42141005, 31988102), National Key Research and Development Program of China (2017YFA0604803), Young Talents Project of Institute of Geographic Sciences and Natural Resources Research (2021RC004), Science and Technology Basic Investigation Program of China (2019FY101302), and Startup Research Program of Northwest A&F University (2452021105).

Conflict of interest

The authors declare that the research was conducted in the absence of any commercial or financial relationships that could be construed as a potential conflict of interest.

Publisher's note

Supplementary material

The Supplementary Material for this article can be found online at: https://www.frontiersin.org/articles/10.3389/fevo.2023.1189059/full#supplementary-material

References

Al-Yaari, A., Wigneron, J.-P., Ciais, P., Reichstein, M., Ballantyne, A., Ogee, J., et al. (2020). Asymmetric responses of ecosystem productivity to rainfall anomalies vary inversely with mean annual rainfall over the conterminous united states. *Global Change Biol.* 26 (12), 6959–6973. doi: 10.1111/gcb.15345

Arani, B. M. S., Carpenter, S. R., Lahti, L., van Nes, E. H., and Scheffer, M. (2021). Exit time as a measure of ecological resilience. *Science* 372 (6547), 1168–116+. doi: 10.1126/science.aay4895

Bai, Y. F., Han, X. G., Wu, J. G., Chen, Z. Z., and Li, L. H. (2004). Ecosystem stability and compensatory effects in the inner Mongolia grassland. *Nature* 431 (7005), 181–184. doi: 10.1038/nature02850

Bardgett, R. D., Bullock, J. M., Lavorel, S., Manning, P., Schaffner, U., Ostle, N., et al. (2021). Combatting global grassland degradation. *Nat. Rev. Earth Environ.* 2 (10), 720–735. doi: 10.1038/s43017-021-00207-2

Berdugo, M., Delgado-Baquerizo, M., Soliveres, S., Hernandez-Clemente, R., Zhao, Y., Gaitan, J. J., et al. (2020). Global ecosystem thresholds driven by aridity. *Science* 367 (6479), 787–78+. doi: 10.1126/science.aay5958

Carpenter, S. R., and Brock, W. A. (2006). Rising variance: a leading indicator of ecological transition. *Ecol. Lett.* 9 (3), 308–315. doi: 10.1111/j.1461-0248.2005.00877.x

Chen, J. M., Ju, W., Ciais, P., Viovy, N., Liu, R., Liu, Y., et al. (2019). Vegetation structural change since 1981 significantly enhanced the terrestrial carbon sink. *Nat. Commun.* 10. doi: 10.1038/s41467-019-12257-8

Cheng, L., Lu, N., Wang, M., Fu, B., and Xu, Z. (2021). Alternative biome states of African terrestrial vegetation and the potential drivers: a continental-scale study. *Sci. Tot. Environ.* 800. doi: 10.1016/j.scitotenv.2021.149489

Clements, C. F., and Ozgul, A. (2018). Indicators of transitions in biological systems. *Ecol. Lett.* 21 (6), 905–919. doi: 10.1111/ele.12948

Dakos, V., Carpenter, S. R., Brock, W. A., Ellison, A. M., Guttal, V., Ives, A. R., et al. (2012). Methods for detecting early warnings of critical transitions in time series illustrated using simulated ecological data. *PloS One* 7 (7), e41010. doi: 10.1371/journal.pone.0041010

Dakos, V., Carpenter, S. R., van Nes, E. H., and Scheffer, M. (2015). Resilience indicators: prospects and limitations for early warnings of regime shifts. *Philos. Trans. R. Soc. B-Biol. Sci.* 370 (1659), 20130263. doi: 10.1098/rstb.2013.0263

Davidowitz, G. (2002). Does precipitation variability increase from mesic to xeric biomes? *Global Ecol. Biogeog.* 11 (2), 143–154. doi: 10.1046/j.1466-822X.2002.00271.x

De Boeck, H. J., Bloor, J. M. G., Kreyling, J., Ransijn, J. C. G., Nijs, I., Jentsch, A., et al. (2018). Patterns and drivers of biodiversity-stability relationships under climate extremes. *J. Ecol.* 106 (3), 890–902. doi: 10.1111/1365-2745.12897

Deng, Y., Li, X., Shi, F., and Hu, X. (2021). Woody plant encroachment enhanced global vegetation greening and ecosystem water-use efficiency. *Global Ecol. Biogeog.* 30 (12), 2337–2353. doi: 10.1111/geb.13386

Dietz, S., Rising, J., Stoerk, T., and Wagner, G. (2021). Economic impacts of tipping points in the climate system. *Proc. Natl. Acad. Sci. United States America* 118 (34), e2103081118. doi: 10.1073/pnas.2103081118

Duffy, K. A., Schwalm, C. R., Arcus, V. L., Koch, G. W., Liang, L. L., and Schipper, L. A. (2021). How close are we to the temperature tipping point of the terrestrial biosphere? *Sci. Adv.* 7 (3), eaay1052. doi: 10.1126/sciadv.aay1052

Estiarte, M., Vicca, S., Penuelas, J., Bahn, M., Beier, C., Emmett, B. A., et al. (2016). Few multiyear precipitation-reduction experiments find ashift in the productivity-precipitation relationship. *Global Change Biol.* 22 (7), 2570–2581. doi: 10.1111/gcb.13269

Ganjurjav, H., Gao, Q., Gornish, E. S., Schwartz, M. W., Liang, Y., Cao, X., et al. (2016). Differential response of alpine steppe and alpine meadow to climate warming in the central qinghai-Tibetan plateau. *Agric. For. Meteorol.* 223, 233–240. doi: 10.1016/j.agrformet.2016.03.017

Gherardi, L. A., and Sala, O. E. (2019). Effect of interannual precipitation variability on dryland productivity: a global synthesis. *Global Change Biol.* 25 (1), 269–276. doi: 10.1111/gcb.14480

Grace, J. B., Anderson, T. M., Smith, M. D., Seabloom, E., Andelman, S. J., Meche, G., et al. (2007). Does species diversity limit productivity in natural grassland communities? *Ecol. Lett.* 10 (8), 680–689. doi: 10.1111/j.1461-0248.2007.01058.x

Guo, Q., Hu, Z., Li, S., Yu, G., Sun, X., Zhang, L., et al. (2015). Contrasting responses of gross primary productivity to precipitation events in a water-limited and a temperature-limited grassland ecosystem. *Agric. For. Meteorol.* 214, 169–177. doi: 10.1016/j.agrformet.2015.08.251

Haberl, H., Erb, K.-H., and Krausmann, F. (2014). Human appropriation of net primary production: patterns, trends, and planetary boundaries. *Annu. Rev. Environ. Resour.* 39, 363–391.

Harris, I., Osborn, T. J., Jones, P., and Lister, D. (2020). Version 4 of the CRU TS monthly high-resolution gridded multivariate climate dataset. *Sci. Data* 7 (1), 1-18. doi: 10.1038/s41597-020-0453-3

He, H., Wang, S., Zhang, L., Wang, J., Ren, X., Zhou, L., et al. (2019). Altered trends in carbon uptake in china's terrestrial ecosystems under the enhanced summer monsoon and warming hiatus. *Natl. Sci. Rev.* 6 (3), 505–514. doi: 10.1093/nsr/nwz021

Hector, A., Hautier, Y., Saner, P., Wacker, L., Bagchi, R., Joshi, J., et al. (2010). General stabilizing effects of plant diversity on grassland productivity through population asynchrony and overyielding. *Ecology* 91 (8), 2213–2220. doi: 10.1890/09-1162.1

Hou, E., Litvak, M. E., Rudgers, J. A., Jiang, L., Collins, S. L., Pockman, W. T., et al. (2021). Divergent responses of primary production to increasing precipitation variability in global drylands. *Global Change Biol.* 27 (20), 5225–5237. doi: 10.1111/gcb.15801

Hu, Z., Dakos, V., and Rietkerk, M. (2022). Using functional indicators to detect state changes in terrestrial ecosystems. *Trends Ecol. Evol.* 37(12), 1036–1045 doi: 10.1016/j.tree.2022.07.011

Hu, Z., Guo, Q., Li, S., Piao, S., Knapp, A. K., Ciais, P., et al. (2018). Shifts in the dynamics of productivity signal ecosystem state transitions at the biome-scale. *Ecol. Lett.* 21 (10), 1457–1466. doi: 10.1111/ele.13126

Hu, Z., Yu, G., Fan, J., Zhong, H., Wang, S., and Li, S. (2010). Precipitation-use efficiency along a 4500-km grassland transect. *Global Ecol. Biogeog.* 19 (6), 842–851. doi: 10.1111/j.1466-8238.2010.00564.x

Huang, G., Li, Y., and Padilla, F. M. (2015). Ephemeral plants mediate responses of ecosystem carbon exchange to increased precipitation in a temperate desert. *Agric. For. Meteorol.* 201, 141–152. doi: 10.1016/j.agrformet.2014.11.011

Hughes, T. P., Anderson, K. D., Connolly, S. R., Heron, S. F., Kerry, J. T., Lough, J. M., et al. (2018). Spatial and temporal patterns of mass bleaching of corals in the anthropocene. *Science* 359 (6371), 80–8+. doi: 10.1126/science.aan8048

Huxman, T. E., Smith, M. D., Fay, P. A., Knapp, A. K., Shaw, M. R., Loik, M. E., et al. (2004). Convergence across biomes to a common rain-use efficiency. *Nature* 429 (6992), 651–654. doi: 10.1038/nature02561

Jiao, C., Yu, G., Ge, J., Chen, X., Zhang, C., He, N., et al. (2017). Analysis of spatial and temporal patterns of aboveground net primary productivity in the Eurasian steppe region from 1982 to 2013. *Ecol. Evol.* 7 (14), 5149–5162. doi: 10.1002/ece3.3027

Knapp, A. K., Ciais, P., and Smith, M. D. (2017). Reconciling inconsistencies in precipitation-productivity relationships: implications for climate change. *New Phytol.* 214 (1), 41–47. doi: 10.1111/nph.14381

Knapp, A. K., and Smith, M. D. (2001). Variation among biomes in temporal dynamics of aboveground primary production. *Science* 291 (5503), 481–484. doi: 10.1126/science.291.5503.481

Kou, D., Yang, G., Li, F., Feng, X., Zhang, D., Mao, C., et al. (2020). Progressive nitrogen limitation across the Tibetan alpine permafrost region. *Nat. Commun.* 11 (1), 3331. doi: 10.1038/s41467-020-17169-6

Lade, S. J., Steffen, W., De Vries, W., Carpenter, S. R., Donges, J. F., Gerten, D., et al. (2020). Human impacts on planetary boundaries amplified by earth system interactions. *Nat. Sustain.* 3 (2), 119–128. doi: 10.1038/s41893-019-0454-4

Lenton, T. M. (2011). Early warning of climate tipping points. *Nat. Climate Change* 1 (4), 201–209. doi: 10.1038/nclimate1143

Lenton, T. M., Rockstroem, J., Gaffney, O., Rahmstorf, S., Richardson, K., Steffen, W., et al. (2019). Climate tipping points - too risky to bet against. *Nature* 575 (7784), 592–595. doi: 10.1038/d41586-019-03595-0

Liang, M., Cao, R., Di, K., Han, D., and Hu, Z. (2021). Vegetation resistance and resilience to a decade-long dry period in the temperate grasslands in China. *Ecol. Evol.* 11 (15), 10582–10589. doi: 10.1002/ece3.7866

Liu, Y., Kumar, M., Katul, G. G., and Porporato, A. (2019). Reduced resilience as an early warning signal of forest mortality. *Nat. Climate Change* 9 (11), 880–88+. doi: 10.1038/s41558-019-0583-9

Liu, Y., Li, Z., Chen, Y., Li, Y., Li, H., Xia, Q., et al. (2022). Evaluation of consistency among three NDVI products applied to high mountain Asia in 2000–2015. *Remote Sens. Environ.* 269, 112821. doi: 10.1016/j.rse.2021.112821

Liu, R., Pan, L.-P., Jenerette, G. D., Wang, Q.-X., Cieraad, E., and Li, Y. (2012). High efficiency in water use and carbon gain in a wet year for a desert halophyte community. *Agric. For. Meteorol.* 162, 127–135. doi: 10.1016/j.agrformet.2012.04.015

Liu, J., Rhland, K. M., Chen, J., Xu, Y., Chen, S., Chen, Q., et al. (2017). Aerosol-weakened summer monsoons decrease lake fertilization on the Chinese loess plateau. *Nat. Climate Change* 7 (3), 190–19+. doi: 10.1038/nclimate3220

Luo, Y., Jiang, L., Niu, S., and Zhou, X. (2017). Nonlinear responses of land ecosystems to variation in precipitation. *New Phytol.* 214 (1), 5–7. doi: 10.1111/nph.14476

Maurer, G. E., Hallmark, A. J., Brown, R. F., Sala, O. E., and Collins, S. L. (2020). Sensitivity of primary production to precipitation across the united states. *Ecol. Lett.* 23 (3), 527–536. doi: 10.1111/ele.13455

Olson, D. M., Dinerstein, E., Wikramanayake, E. D., Burgess, N. D., Powell, G. V. N., Underwood, E. C., et al. (2001). Terrestrial ecoregions of the worlds: a new map of life on earth. *Bioscience* 51 (11), 933–938. doi: 10.1641/0006-3568(2001)051[0933:Teotwa]2.0.Co;2

Parker, J., Kenyon, R. V., and Troxel, D. E. (1983). Comparison of interpolating methods for image resampling. *IEEE Trans. Med. Imaging* 2 (1), 31–39. doi: 10.1109/tmi.1983.4307610

Petrie, M. D., Peters, D. P. C., Yao, J., Blair, J. M., Burruss, N. D., Collins, S. L., et al. (2018). Regional grassland productivity responses to precipitation during multiyear above- and below-average rainfall periods. *Global Change Biol.* 24 (5), 1935–1951. doi: 10.1111/gcb.14024

Ratajczak, Z., Carpenter, S. R., Ives, A. R., Kucharik, C. J., Ramiadantsoa, T., Stegner, M. A., et al. (2018). Abrupt change in ecological systems: inference and diagnosis. *Trends Ecol. Evol.* 33 (7), 513–526. doi: 10.1016/j.tree.2018.04.013

Rietkerk, M., Bastiaansen, R., Banerjee, S., van de Koppel, J., Baudena, M., and Doelman, A. (2021). Evasion of tipping in complex systems through spatial pattern formation. *Science* 374 (6564), 169–16+. doi: 10.1126/science.abj0359

Sala, O. E., Gherardi, L. A., Reichmann, L., Jobbagy, E., and Peters, D. (2012). Legacies of precipitation fluctuations on primary production: theory and data synthesis. *Philos. Trans. R. Soc. B-Biol. Sci.* 367 (1606), 3135–3144. doi: 10.1098/rstb.2011.0347

Scheffer, M., Bascompte, J., Brock, W. A., Brovkin, V., Carpenter, S. R., Dakos, V., et al. (2009). Early-warning signals for critical transitions. *Nature* 461 (7260), 53–59. doi: 10.1038/nature08227

Su, H., Wang, R., Feng, Y., Li, Y., Li, Y., Chen, J., et al. (2021). Long-term empirical evidence, early warning signals and multiple drivers of regime shifts in a lake ecosystem. *J. Ecol.* 109 (9), 3182–3194. doi: 10.1111/1365-2745.13544

Sun, Y., Yang, Y., Zhao, X., Tang, Z., Wang, S., and Fang, J. (2021). Global patterns and climatic drivers of above- and belowground net primary productivity in grasslands. *Sci. China-Life Sci.* 64 (5), 739–751. doi: 10.1007/s11427-020-1837-9

Verma, M., Friedl, M. A., Richardson, A. D., Kiely, G., Cescatti, A., Law, B. E., et al. (2014). Remote sensing of annual terrestrial gross primary productivity from MODIS: an assessment using the FLUXNET la thuile data set. *Biogeosciences* 11 (8), 2185–2200. doi: 10.5194/bg-11-2185-2014

Wang, S. P., Niu, H. S., Cui, X. Y., Jiang, S., Li, Y. H., Xiao, X. M., et al. (2005). Plant communities - ecosystem stability in inner Mongolia. *Nature* 435 (7045), E5–E6. doi: 10.1038/nature03862

Wang, C., Wang, Z.-H., and Sun, L. (2020). Early-warning signals for critical temperature transitions. *Geophys. Res. Lett.* 47 (14), e2020GL088503. doi: 10.1029/2020gl088503

Wang, Y., Xiao, J., Li, X., and Niu, S. (2022). Global evidence on the asymmetric response of gross primary productivity to interannual precipitation changes. *Sci. Tot. Environ.* 814, 152786. doi: 10.1016/j.scitotenv.2021.152786

Wilcox, K. R., Shi, Z., Gherardi, L. A., Lemoine, N. P., Koerner, S. E., Hoover, D. L., et al. (2017). Asymmetric responses of primary productivity to precipitation extremes: a synthesis of grassland precipitation manipulation experiments. *Global Change Biol.* 23 (10), 4376–4385. doi: 10.1111/gcb.13706

Willis, K. J., Jeffers, E. S., and Tovar, C. (2018). What makes a terrestrial ecosystem resilient? a complex set of biotic and abiotic factors determines the resilience of an ecosystem. *Science* 359 (6379), 988–989. doi: 10.1126/science.aar5439

Wu, D., Ciais, P., Viovy, N., Knapp, A. K., Wilcox, K., Bahn, M., et al. (2018). Asymmetric responses of primary productivity to altered precipitation simulated by ecosystem models across three long-term grassland sites. *Biogeosciences* 15 (11), 3421–3437. doi: 10.5194/bg-15-3421-2018

Yang, Y., Fang, J., Fay, P. A., Bell, J. E., and Ji, C. (2010). Rain use efficiency across a precipitation gradient on the Tibetan plateau. *Geophys. Res. Lett.* 37, 1-5. doi: 10.1029/2010gl043920

Zeng, X., Hu, Z., Chen, A., Yuan, W., Hou, G., Han, D., et al. (2022). The global decline in the sensitivity of vegetation productivity to precipitation from 2001 to 2018. *Glob Chang Biol.* 28 (22), 6823–6833. doi: 10.1111/gcb.16403

Zhang, T., Chen, Z., Zhang, W., Jiao, C., Yang, M., Wang, Q., et al. (2021). Long-term trend and interannual variability of precipitation-use efficiency in Eurasian grasslands. *Ecol. Indic.* 130, 108091. doi: 10.1016/j.ecolind.2021.108091

Zhang, C., Lu, D., Chen, X., Zhang, Y., Maisupova, B., and Tao, Y. (2016). The spatiotemporal patterns of vegetation coverage and biomass of the temperate deserts in central Asia and their relationships with climate controls. *Remote Sens. Environ.* 175, 271–281. doi: 10.1016/j.rse.2016.01.002

Zhang, T., Yu, G., Chen, Z., Hu, Z., Jiao, C., Yang, M., et al. (2020). Patterns and controls of vegetation productivity and precipitation-use efficiency across Eurasian grasslands. *Sci. Tot. Environ.* 741, 140204. doi: 10.1016/j.scitotenv.2020.140204

Zhou, H. K., Zhou, L., Zhao, X. Q., Liu, W., Li, Y. N., Gu, S., et al. (2006). Stability of alpine meadow ecosystem on the qinghai-Tibetan plateau. *Chin. Sci. Bull.* 51 (3), 320–327. doi: 10.1007/s11434-006-0320-4

frontiers | Frontiers in Ecology and Evolution

TYPE Original Research
PUBLISHED 17 August 2023
DOI 10.3389/fevo.2023.1148910

OPEN ACCESS

EDITED BY
Cuicui Jiao,
Sichuan University of Science and Engineering, China

REVIEWED BY
Nicolas Diaz-Kloch,
Trent University, Canada
Juan-Jose Jiménez-Osornio,
Universidad Autónoma de Yucatán, Mexico

*CORRESPONDENCE
Hu Du
hudu@isa.ac.cn
Wanxia Peng
wxpeng@isa.ac.cn

RECEIVED 20 January 2023
ACCEPTED 27 July 2023
PUBLISHED 17 August 2023

CITATION
Su L, Du H, Zeng F, Wang H, Lu M, Luo L, Peng W and Song T (2023) Habitat associations of woody plant species in evergreen–deciduous broadleaf karst forests in southwest China.
Front. Ecol. Evol. 11:1148910.
doi: 10.3389/fevo.2023.1148910

Habitat associations of woody plant species in evergreen–deciduous broadleaf karst forests in southwest China

Liang Su[1,2,3], Hu Du[1,2]*, Fuping Zeng[1,2], Hua Wang[4], Menzhen Lu[1,2], Liujuan Luo[5], Wanxia Peng[1,2]* and Tongqing Song[1,2]

[1]Key Laboratory of Agro-ecological Processes in Subtropical Region, Institute of Subtropical Agriculture, Chinese Academic of Sciences, Changsha, China, [2]Guangxi Key Laboratory of Karst Ecological Processes and Services, Huanjiang Observation and Research Station of Karst Ecosystem, Chinese Academic of Sciences, Huanjiang, China, [3]Hunan Research Academy of Environmental Sciences, Institute of Water Ecology and Environment, Changsha, China, [4]College of Resources & Environment, Hunan Agricultural University, Changsha, China, [5]Management Center for Guangxi Mulun National Nature Reserve, Huanjiang, China

The effects of habitat filtering on community assembly have been extensively researched, and topography has been identified as a critical factor influencing the spatial distribution of trees. In this study, a 25-ha plot was established in karst evergreen–deciduous broadleaf forests in southwestern China. Eight topographical factors were used to divide plots into four habitat types, i.e., hilltop, steep slope, gentle slope, and depression, using a multivariate regression tree. A total of 85 evergreen and deciduous tree species were recorded in these four habitats and classified into three life stages, the differentiation of which was assessed using torus-translation tests. A total of 65 species significantly positively associated with at least one habitat and 79 species significantly negatively associated with at least one habitat were identified. Most species, whether evergreen or deciduous, exhibited a positive correlation with steep slopes, whereas relatively few species were adapted to depressions. Moreover, the percentage of evergreen species positively associated with hilltops and steep slopes was higher than that of deciduous species. Both evergreen and deciduous species showed an increasing percentage of positive correlation with hilltops from the sapling stage to the mature stage. However, more evergreen species grew on steep slopes in the sapling stage, whereas deciduous species grew in the mature stage. Canonical correspondence was used to analyze the relationship between species and the eight topographical factors. Regardless of life form or life stage, results showed that species distribution was significantly affected by topography. Furthermore, the distribution of evergreen species on sapling-stage trees was found to be more influenced by topography, whereas deciduous species were more influenced by topography in the mature stage. Finally, elevation was identified as the most crucial topographical factor affecting species distribution.

KEYWORDS

environmental heterogeneity, habitat filtering, life form, species distribution, topography, karst forests

1 Introduction

The coexistence of species has long been a central focus of community ecology research (Nakashizuka, 2001; Wright, 2002; Silvertown, 2004), with niche differentiation and species diffusion limitation theories being among the most important in this regard (Whitfield, 2002; Lai et al., 2009). According to the niche theory, community structure is affected by environmental heterogeneity and the interactions between species, with each species carving out unique niches to avoid competitive exclusion (Chesson, 2000; Potts et al., 2002). Therefore, environmental factors, such as topography and soil, can shape the distribution of species through their species-level associations with habitats (Whittaker, 1956). Thus, it is important to investigate species–habitat associations at the community scale.

Previous research has demonstrated that niche differentiation plays a critical role in community maintenance and species coexistence at various scales (Clark et al., 1999; Tuomisto et al., 2003; Potts et al., 2004). However, the association between a single species and its habitat is often not determined during the early stages of seed germination or seedling growth but rather undergoes developmental changes at different life stages (Webb & Peart, 2000; Yamada et al., 2006; Comita et al., 2007; Lai et al., 2009). Moreover, the adaptability of specific species to particular habitats may not be constant, as their response to extreme weather events and global changes can vary (Condit et al., 1995). In addition, topography has been identified as a crucial driver of habitat diversity and variations in soil moisture and nutrient levels (Harms et al., 2001; Daws et al., 2002; Sorensen et al., 2006; John et al., 2007), which are essential for plant growth and development. In this respect, karst areas, which are characterized by a complex topography consisting of cliffs, caves, and sinkholes, as well as variable climate conditions (Clements et al., 2006), offer a diverse range of ecological niches that promote high species diversity. As a result, the uniqueness of the karst ecosystem makes it an especially valuable reservoir of biodiversity (Schilthuizen et al., 2004).

The phenology of leaves is of great importance in community appearance, understory environment, litter decomposition, and ecosystem productivity, as leaves are the main site of plant photosynthesis (Quigley & Platt, 2003). Deciduous tree species can avoid damage and the effects of adverse environmental conditions, such as low temperatures and drought, on growth by shedding leaves (Reich et al., 2004; Poorter & Markesteijn, 2008). Previous studies have shown that plants with different life forms have differences in leaf nutrient uptake efficiencies (Liu et al., 2006). Typically, deciduous species have a higher rate of nitrogen mineralization than evergreen species (Malhi et al., 2010), which are often found in barren habitats and, thus, considered to have higher nutrient re-uptake efficiencies (Chapin & Kedrowski, 1983; Chapin & Moilanen, 1991).

Southwest China is one of the three largest karst regions in the world (Jiang et al., 2014). The area features a distinctive evergreen–deciduous broadleaf forest, which boasts a complex community structure, high species diversity, and unique habitat heterogeneity (Du et al., 2017). However, the mechanisms underlying the species' coexistence in local-scale plots were unclear, and consequently, based on studies conducted on Barro Colorado Island, Panama, we surveyed a 25-ha forest plot in Mulun National Natural Reserve in 2014. Our hypotheses are that there are significant species–habitat associations in the karst evergreen–deciduous broadleaf forest and that topographical factors significantly affect species distribution. Furthermore, we assume that the percentage of species–habitat association ratio for evergreen species in slope habitats is lower than that of deciduous species. We anticipate that this result will be evident even in the mature stage. The results of this study will serve as a foundation for future research on the structure of tree communities in the highly heterogeneous, species-rich karst evergreen–deciduous broadleaf forest. This study will also aid in preserving the vulnerable ecosystem in the area.

2 Material and methods

2.1 Study area

The study was conducted in the Mulun National Natural Reserve (MNNR) (25°07′01″–25°12′22″N, 107°54′01″–108°05′51″E), located in the northwest of Huanjiang County, Guangxi Province, Southwest China. The study area's maximum elevation is 1,028.0 m. The region has an annual average temperature of 15.7°C, January has an average temperature of 10.1°C, July has an average temperature of 28°C, the minimum temperature is 5.2°C, the frost-free period is 290 days, the average annual sunshine is 1,451 h, the average relative humidity is 70%, the average evaporation is 1,571.1 mm, the and average annual rainfall is 1,389.1 mm, with precipitation from April to September accounting for 70% of the annual total (Du et al., 2017). The geomorphological type comprises depressions between the karst hills. The soil is mainly dark or brown calcareous soil developed over carbonate rocks, which is a non-zonal shallow soil with high rock exposure, and the pH ranges from 7.06 to 7.68 (Du et al., 2019).

In 2014, we established a 25-ha (500 m × 500 m) forest plot within the MNNR. We subdivided the plot into a grid of 625 cells, each of which was 20 m × 20 m in size. Within these grids, we measured plant characteristics and topographical factors, i.e., elevation, slope, and slope aspect, as previously described by Condit (1998). This plot belongs to the Chinese Forest Biodiversity Monitoring Network (CForBio) and is currently the largest forest plot in the karst region, with elevations ranging from 442.6 m to 651.4 m and slopes ranging from 0.12° to 66.97° (Du et al., 2017) (Figure 1).

2.2 Data collection

In the year of plot establishment, we mapped the individuals of all tree species with a diameter at breast height (DBH) ≥ 1 cm and tagged them following standard field procedures of the Center for Tropical Forest Science (CTFS). The first census documented 144,552 free-standing individual trees. The region is characterized by a subtropical mixed evergreen deciduous broadleaf forest, dominated by *Cryptocarya microcarpa* F. N. Wei and *Lindera communis* Hemsl. Other important species include *Itoa orientalis* Hemsl, *Platycarya*

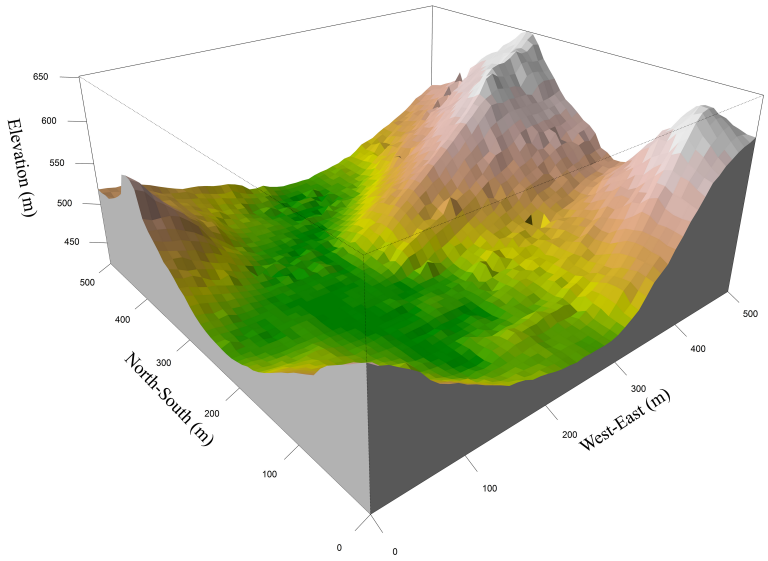

FIGURE 1
Topographic map of the 25-ha forest dynamics plot in Mulun, south of China.

longipes Wu, *Decaspermum gracilentum* (Hance) Merr. et Perry, *Brassaiopsis glomerulata* (Bl.) Regel, *Diospyros dumetorum* W. W. Smith, and *Clausena dunniana* Levl. (Lu et al., 2021).

Trees were divided into the sapling, juvenile, and mature stages based on DBH (Bagchi et al., 2011). Within each species, trees were ranked by DBH, and the 99th percentile (DBH99) was determined. All trees with a DBH > $DBH99^{2/3}$ were classified as the mature stage, trees with a DBH < $DBH99^{1/2}$ were classified as saplings, and those with a $DBH99^{1/2}$ ≤DBH < $DBH99^{2/3}$ were classified as juveniles (Guo et al., 2017). The species–habitat associations were examined for those species with individual stems greater than 25 in the sapling, juvenile, and mature stages. In total, 85 species including 52 evergreen species and 33 deciduous species were included (Supplementary Table S1).

In terms of topographical factors, average elevation (ELE), slope (SLO), aspect (ASP), convexity (CON), soil thickness (STK), rock outcrop ratio (ROC), topographic wetness index (TWI), and altitude above channel (ACH) were used as eight major topographical factors. The first four factors were computed following the methods described by Du et al. (2017), and the remaining factors were assessed following Liu et al. (2020). TWI and ACH were used to quantify topographical control on hydrological processes, where the TWI was calculated as the ratio of the area upslope from any given point on the landscape to the local slope at that point, and the ACH was calculated as the vertical distance from the channel network (Punchi-Manage et al., 2013); these two indicators make up the lack of hydrology.

2.3 Statistical analysis

2.3.1 Multivariate regression tree analysis

For species–habitat association analysis, we used a multivariate regression tree (MRT) to classify habitats into four categories, i.e., hilltop, steep slope, gentle slope, and depression (Supplementary Figures S1, S2). We computed the MRT procedure using the "mvpart" package. The data are presented in Table 1.

2.3.2 Species–habitat association analysis

To determine the association between a species and a particular type of habitat, we used the torus-transformation test, which is the most commonly used method in this regard (Harms et al., 2001), with a slight modification as described by Comita et al. (2007). This test entails calculating the probability of the true distribution of a species in each habitat under the condition of random distribution and determining whether a species is significantly correlated with a certain type of habitat based on probability. Detailed descriptions of the test can be found in a paper published by Harms et al. (2001). Our field survey obtained a species abundance data matrix for 625 samples in three size classes. We computed the torus-transformation test using the *tt_test* function of the "fgeo" package. Using canonical correspondence analysis (CCA) in the "vegan" package (Oksanen et al., 2020), we assessed the influence of topographical factors, and we used the Monte Carlo permutation test to evaluate their significance. We used the hierarchical partitioning method to distinguish a single topographical factor's contribution via the "rdacca.hp" package in R (Lai et al., 2022). We performed all the above analyses in R4.0.2 (Team, 2020).

3 Results

3.1 Topographical habitat types and their characteristics

The forest plot covers a topographically heterogeneous area that contains two small peaks and a complete depression. The cross-

TABLE 1 The characteristic parameters of habitat categories in the 25-ha Mulun permanent plot.

Habitat category	A: Hilltop	B: Steep slope	C: Gentle slope	D: Depression
Total area (ha)	4.56	8.08	6.32	6.04
Average elevation (m)	576.02 ± 28.87	501.35 ± 18.67	459.90 ± 6.81	448.64 ± 1.53
Slope (°)	50.77 ± 6.39	41.41 ± 9.32	25.78 ± 10.25	9.02 ± 6.21
Aspect	−0.23 ± 0.58	−0.24 ± 0.74	0.08 ± 0.77	0.01 ± 0.72
Convexity (m)	2.09 ± 3.77	−0.67 ± 1.94	−0.86 ± 1.31	−0.73 ± 0.86
Rock outcrop (%)	63.65 ± 23.96	60.82 ± 24.67	57.98 ± 26.57	22.05 ± 23.40
Soil thickness (cm)	16.97 ± 8.24	14.91 ± 7.54	17.13 ± 9.59	34.92 ± 14.06
TWI	2.67	2.16	2.85	3.52
ACH (m)	5.94	10.48	3.46	0.97
Individual	159.33 ± 74.91	198.37 ± 86.28	172.32 ± 74.23	129.53 ± 64.21
Shannon index	1.64 ± 0.81	1.68 ± 0.57	1.38 ± 0.41	1.03 ± 0.32
Patrick index	32.72 ± 13.70	35.06 ± 13.14	26.34 ± 14.89	20.82 ± 13.42

TWI, topographic wetness index; ACH, altitude above channel.

validation relative error (CVRE) value of the MRT analysis was approximately 0.716 (Supplementary Figure S1). Hilltop was exposed to limestones characterized by high rock exposure, received direct sunlight, and was dry. The steep slope was the largest of the assessed Mulun habitats, whereas the gentle slope was located at the foot of the hill and contained large amounts of rubble and a number of caves, and the depression was low-lying and moist. With respect to tree density, steep slopes and the depression were found to have the highest and lowest densities, respectively (Supplementary Figure S2). The Shannon–Wiener index values (species diversity per quadrat) ranged from 1.03 (depression habitats) to 1.68 (steep slope habitats), whereas the values of the Patrick index (species richness per quadrat) ranged from 20.82 to 35.06. Steep-slope habitats had both the highest species richness and diversity (Table 1).

3.2 Associations of species with the four habitat types

Based on the torus-translation test analysis, only *Pistacia weinmannifolia* J. Poisson ex Franch among the total 85 species was neither positively nor negatively associated with any of the four habitat types, whereas 65 (75.6%) species were positively associated with at least one habitat, and 79 (91.9%) species were negatively associated with at least one habitat. Furthermore, 44 species showed a positive association with steep slopes, whereas only *C. microcarpa* F. N was positively associated with depression. However, most species were negatively associated with depression habitats.

We conducted separate analyses for evergreen and deciduous species and found that 73.1% of evergreen species and 79.4% of deciduous species were positively associated with at least one habitat. Species in two life forms showed similar habitat association distributions, with a higher percentage found on slopes or hilltops and a lower percentage in depressions. However, evergreen species were found to have a higher percentage of growth on hilltops and steep slopes than deciduous species, whereas the percentage of evergreen species growing on gentle slopes was lower than that of deciduous species. There was little difference between the evergreen and deciduous species in terms of their habitat association with depressions.

The percentage of evergreen and deciduous species growing on hilltops increased from the sapling stage to the mature stage. Among all species and evergreen species in particular, the highest percentage of sapling stage trees was found on steep slopes, whereas deciduous species had the highest percentage on mature stage trees. Additionally, both evergreen and deciduous species had the highest number of mature-stage trees on gentle slopes and in depressions (Figure 2).

3.3 The relationship between species distribution and topographical factors

Species distribution patterns as explained by CCA for all, evergreen, and deciduous species were similar. Regardless of life form or life stage, the permutation test showed that species distribution was significantly affected by topographic factors. When all, evergreen, and deciduous species were taken into consideration, topographical factors explained approximately 20.4%, 21.0%, and 18.2% of the variation, respectively (Table 2). The first axis explains most of the explainable parts across different stages (Figure 3) (Supplementary Figure S2). Among the eight topographic factors, ELE was the most important factor affecting species distribution in different life forms and stages, followed by SLO, CON, and ROC. Topographic factors explained the most variation in evergreen species at the sapling stage and deciduous species at the mature stage while explaining the least variation in evergreen and deciduous species at the juvenile stage (Table 2).

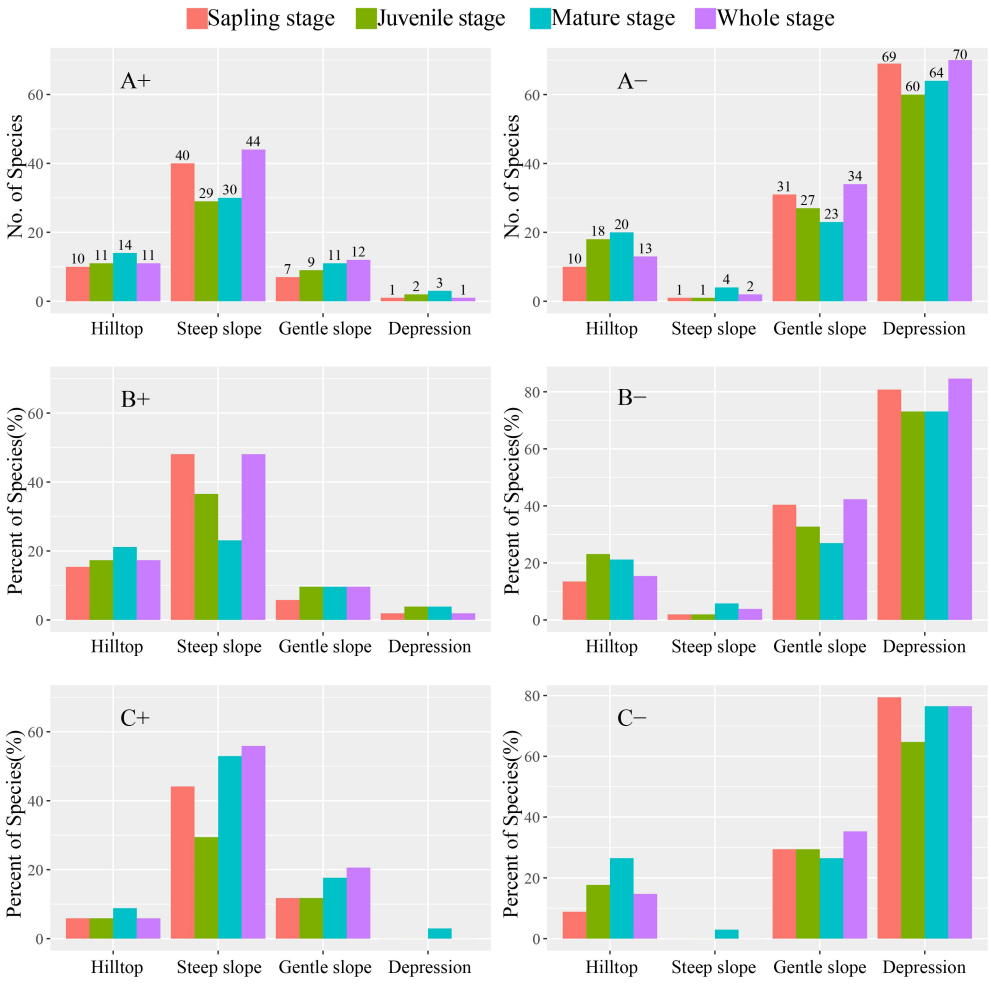

FIGURE 2
Number and percent of species in different stages positively and negatively associated with the four habitat types. **(A)** Whole, **(B)** evergreen, and **(C)** deciduous species. "+" and "−" indicate positive and negative, respectively.

4 Discussion

4.1 Topographic habitat types and their characteristics

Karst, in southwest China, is characterized by large slopes and high rock exposure, which contribute to high habitat heterogeneity (Su et al., 2019). Although the habitat tends to be more homogeneous at the 20-m scale, a diverse range of niche types are widely distributed throughout the entire experiment plot because of the strong fragmentation of karst (Harms et al., 2001; Punchi-Manage et al., 2013; Guo et al., 2017). Along a hilltop-depression gradient within the MNNR, different habitat types occur. Our MRT analysis resulted in a CVRE value of 0.716, which is similar to values reported in previous studies (Kanagaraj et al., 2011; Punchi-Manage et al., 2013). Our study found that four habitat classifications covered most of the observed topographical variation. Given the spatial distribution of ecological factors (e.g., light, temperature, soil moisture, and soil nutrients), the differentiation of topography creates diverse habitats that contribute to distinct patterns of plant diversity and spatial distribution (Sorensen et al., 2006; John et al., 2007; Kanagaraj et al., 2011). On steep slopes, sunlight is more likely to penetrate the forest floor, thereby facilitating the regeneration and survival of a larger number and more diverse species. As a result, we found that steep slopes had the highest diversity index among the four habitat types assessed, whereas depressions tended to be more suitable for a small number of shade-tolerant plants (Table 1).

4.2 Habitat associations of species and the importance of topographical factors

We conducted torus-translation tests to examine the association between species with a DBH ≥ 1 cm and a density higher than 25 individuals in the 25-ha MNNR plot. The result showed that 84 (98.8%) species were significantly associated with at least one habitat type, with 65 (75.6%) and 79 (91.9%) species showing positive and negative associations, respectively. Values of 98.8% were compared with significant species–habitat association in the

TABLE 2 Canonical correspondence analysis (CCA).

	Total inertia	Variation explained	CCA1 (%)	CCA2 (%)	R^2	Permutation test p-value	Individual % of total explained variation							
							ELE	SLO	ASP	CON	ROC	STK	TWI	ACH
All species														
Sapling stage	6.019	17.9%	0.700 (12.53)	0.226 (4.05)	0.800	0.001	28.83%	24.58%	4.69%	15.25%	8.49%	8.83%	4.58%	4.58%
Juvenile stage	9.311	11.7%	0.672 (7.86)	0.250 (2.93)	0.721	0.001	28.72%	28.72%	4.36%	16.07%	9.66%	8.46%	5.56%	4.27%
Mature stage	7.590	14.3%	0.671 (9.60)	0.250 (3.58)	0.719	0.001	29.58%	21.53%	5.28%	12.57%	10.69%	9.58%	6.18%	4.24%
Whole stage	5.228	20.4%	0.683 (13.93)	0.230 (4.69)	0.810	0.001	29.17%	23.43%	4.80%	14.80%	9.31%	8.82%	5.15%	4.61%
Evergreen species														
Sapling stage	5.738	19.7%	0.726 (14.30)	0.246 (4.85)	0.730	0.001	31.01%	22.63%	3.79%	16.16%	9.19%	7.68%	4.04%	5.25%
Juvenile stage	9.986	11.7%	0.704 (8.24)	0.288 (3.37)	0.569	0.001	31.37%	20.51%	4.02%	15.90%	10.94%	8.29%	4.96%	4.19%
Mature stage	13.933	8.6%	0.696 (5.99)	0.304 (2.61)	0.466	0.001	31.28%	19.30%	4.07%	10.12%	13.37%	9.53%	6.86%	5.70%
Whole stage	5.416	21.0%	0.715 (15.02)	0.254 (5.33)	0.754	0.001	31.00%	21.95%	3.90%	15.57%	10.10%	8.00%	4.57%	5.00%
Deciduous species														
Sapling stage	5.783	10.1%	0.378 (3.82)	0.114 (1.15)	0.500	0.001	27.30%	26.80%	5.20%	18.30%	4.50%	8.50%	6.10%	3.00%
Juvenile stage	8.634	8.4%	0.487 (4.09)	0.163 (1.37)	0.445	0.001	29.64%	25.42%	6.51%	16.99%	5.42%	9.64%	5.30%	1.57%
Mature stage	6.105	14.3%	0.602 (8.61)	0.194 (2.77)	0.616	0.001	31.33%	22.66%	6.78%	13.43%	8.25%	10.70%	4.20%	2.38%
Whole stage	4.140	18.2%	0.513 (9.34)	0.157 (2.86)	0.711	0.001	28.45%	26.96%	6.52%	15.25%	5.75%	9.50%	5.47%	2.21%

ELE, average elevation; SLO, slope; ASP, aspect; CON, convexity; STK, soil thick; ROC, rock outcrop ratio; TWI, topographic wetness index; ACH, altitude above channel.

10.3389/fevo.2023.1148910

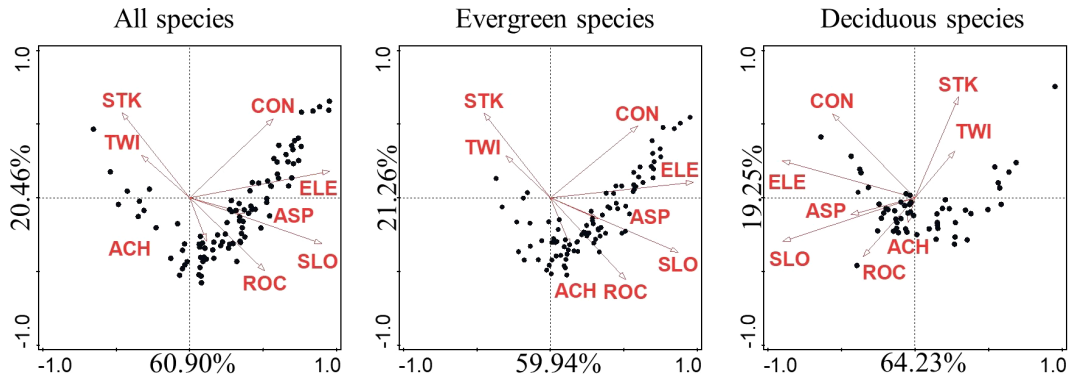

FIGURE 3
CCA diagram showing the relationship of species with the eight topographic factors. The black dots represent species. The percentage on the CCA axis represents the fraction of total explained variation. ELE, average elevation; SLO, slope; ASP, aspect; CON, convexity; STK, soil thick; ROC, rock outcrop ratio; TWI, topographic wetness index; ACH, altitude above channel; CCA, canonical correspondence analysis.

BCI, Sinharaja in the tropics, and Gutianshan in the subtropics at 33%, 79%, and 86%, respectively (Harms et al., 2001; Gunatilleke et al., 2006; Lai et al., 2009). However, our study found a lower percentage of positive associations (75.6%) when compared to Nonggang (85.1%), a tropical karst area in the same region (Guo et al., 2017). Only *P. weinmannifolia* J. Poisson ex Franch showed no clear habitat associations, likely due to its rapid growth and adaptability. Furthermore, we found that the distribution of 24 dominant species with importance > 1 was significantly correlated with habitat type (Du et al., 2017). These results suggest that species distribution in karst forests is strongly influenced by their responses to the environment, promoting strong habitat filtering. However, Baldeck et al. (2013) suggested that habitat filtering is stronger during the early stages of growth (DBH < 1 cm), leading to an underestimation of the percentages of species–habitat associations.

In this study, we found that most of the assessed species demonstrated a stronger species–habitat association on steep slopes, gentle slopes, and hilltops, whereas species growing in depressions were less common (Figure 2). Although the extent of the depression in the study plot was greater than that of hilltops (Table 1), the lack of sunlight in depressions limits plant survival, resulting in only a large number of shade-tolerant plants such as *C. microcarpa* F. N. Guo et al. (2017) suggested that the greater dependence of karst species on sunlight and their higher adaptability for higher elevations contribute to the higher abundance and diversity of species on slopes and hilltops. Consistent with this premise, we observed a greater number of species–habitat associations on steep slopes, which are characterized by greater sunlight exposure and a larger number of niches.

The number of species positively associated with hilltops increased from the sapling stage to the mature stage (Figure 2), indicating that while hilltops in karst areas are suitable for the growth and survival of trees, the greater abundance of pioneer species will be gradually replaced by other species during succession. Webb et al. (2002) and Wu et al. (2017) found that seed dispersal and seedling establishment are more likely to occur in moist habitats in a Bornean rainforest. In contrast, we recorded the highest number of species positively associated with steep slopes in the sapling stage, suggesting that species–habitat associations vary significantly according to different life stages (Battaglia et al., 2000; Dovciak et al., 2003). Negative density dependence in survival is incompatible with genetic shifts in resource requirements (Lusk, 2004; Comita et al., 2007). Our results show that the percentage of deciduous species at the mature stage was higher than that of evergreen species on steep slopes. This is because deciduous tree species have a greater requirement for sunlight, leading to higher tree height (Brando, 2018). Additionally, the crown coverage of dense species assemblages in depressions tends to create unfavorable conditions for deciduous tree growth (Malhi et al., 2010). Contrastingly, we found that both evergreen and deciduous species had the highest number in the mature stage on gentle slopes and depression, consistent with the result of the hilltops, which further shows that the germination of species was under strong environmental stress. These findings are generally consistent with those of previous studies (Comita et al., 2007; Bagchi et al., 2011; Hu et al., 2012), suggesting that species–habitat associations are largely influenced by the size class in a heterogeneous environment.

Based on our observations, there is little difference in the species–habitat associations of deciduous and evergreen species, except for a higher percentage of deciduous species growing on steep slopes at the mature stage (Figure 2). However, those observed differences may be attributed to the uniqueness of the karst study plot and strong niche differentiation (Guo et al., 2017). Furthermore, the results of CCA (Table 2) indicated that while topographical factors can explain the lower variation at juvenile trees, the distributions of the sapling, juvenile, and mature stages were relatively similar, further confirming the strong habitat filtering association with the karst ecosystem. Similar studies have suggested that seed dispersal may be the main driver of habitat change among different species (Comita et al., 2007; Kanagaraj et al., 2011). Therefore, in further studies, it is necessary to pay more attention to seed dispersal and seedling distribution. Furthermore, given the ecological fragility of karst areas and the fact that plants are primarily adapted to porous limestone bedrock and are highly sensitive to human activities, it is imperative to develop sound land-use regulations to protect biodiversity and prevent the further degradation of karst habitats.

5 Conclusion

Our study reveals that habitat heterogeneity plays an important role in maintaining diversity in the evergreen–deciduous broadleaf karst forests. The association between species and their habitats was found to be the strongest on slopes and hilltops and the weakest in depressions. Hilltops were suitable for tree growth and survival to maturity. Our results show that the proportion of evergreen species at the sapling stage was the highest on steep slopes, while deciduous species were dominant at the mature stage. Moreover, ELE emerged as the most important topographical factor affecting species distribution in the MNNR plot.

Data availability statement

The datasets generated during and/or analyzed during the current study are available from the corresponding author on reasonable request. Requests to access the datasets should be directed to hudu@isa.ac.cn.

Author contributions

HD, FZ, WP, and TS conceived and designed the experiments. HD, LS, LL, and ML conducted the experiments. LS, HD, and HW discussed the results. LS wrote the manuscript. The authors read and approved the final manuscript.

Funding

National Key Research and Development Program of China (2022YFF1300703), National Natural Science Foundation of China (42071073, 31971487), Youth Innovation Promotion Association of the Chinese Academy of Sciences (2021366), Guangxi Key Research and Development Program (AB17129009), and Hechi Distinguished Expert Program to FZ.

Acknowledgments

The authors thank two reviewers for helpful remarks on an earlier version of the paper.

Conflict of interest

The authors declare that the research was conducted in the absence of any commercial or financial relationships that could be construed as a potential conflict of interest.

Publisher's note

Supplementary material

The Supplementary Material for this article can be found online at: https://www.frontiersin.org/articles/10.3389/fevo.2023.1148910/full#supplementary-material

References

Bagchi, R., Henrys, P. A., Brown, P. E., Burslem, D. F. R. P., Diggle, P. J., Gunatilleke, C. V. S., et al. (2011). Spatial patterns reveal negative density dependence and habitat associations in tropical trees. *Ecology* 92, 1723–1729. doi: 10.1890/11-0335.1

Baldeck, C. A., Harms, K. E., Yavitt, J. B., John, R., Turner, B. L., Valencia, R., et al. (2013). Habitat filtering across tree life stages in tropical forest communities. *Proc. R. Soc B* 280, 20130548. doi: 10.1098/rspb.2013.0548

Battaglia, L. L., Fore, S. A., and Sharitz, R. R. (2000). Seedling emergence, survival and size in relation to light and water availability in two bottomland hardwood species. *J. Ecol.* 88, 1041–1050. doi: 10.1046/j.1365-2745.2000.00518.x

Brando, P. (2018). Tree height matters. *Nat. Geosci.* 11, 390–391. doi: 10.1038/s41561-018-0147-z

Chapin, F. S., and Kedrowski, R. A. (1983). Seasonal changes in nitrogen and phosphorus fractions and autumn retranslocation in evergreen and deciduous Taiga trees. *Ecology* 64, 376–391. doi: 10.2307/1937083

Chapin, F. S., and Moilanen, L. (1991). Nutritional controls over nitrogen and phosphorus resorption from Alaskan birch leaves. *Ecology* 72, 709–715. doi: 10.2307/2937210

Chesson, P. (2000). Mechanisms of maintenance of species diversity. *Annu. Rev. Ecol. Syst.* 31, 343–366. doi: 10.1146/annurev.ecolsys.31.1.343

Clark, D. B., Palmer, M. W., and Clark, D. A. (1999). Edaphic factors and the landscape-scale distributions of tropical rain forest trees. *Ecology* 80, 2662–2675. doi: 10.1890/0012-9658(1999)080[2662:efatls]2.0.co;2

Clements, R., Sodhi, N. S., Schilthuizen, M., and Ng, P. K. L. (2006). Limestone karsts of southeast Asia: Imperiled arks of biodiversity. *Bioscience* 56, 733–742. doi: 10.1641/0006-3568(2006)56[733:lkosai]2.0.co;2

Comita, L. S., Condit, R., and Hubbell, S. P. (2007). Developmental changes in habitat associations of tropical trees. *J. Ecol.* 95, 482–492. doi: 10.1111/j.1365-2745.2007.01229.x

Condit, R. (1998). *Tropical forest census plots: methods and results from Barro Colorado Island, Panama and a comparison with other plots* (Berlin: Springer).

Condit, R., Hubbell, S. P., and Foster, R. B. (1995). Mortality-rates of 205 neotropical tree and shrub species and the impact of a severe drought. *Ecol. Monogr.* 65, 419–439. doi: 10.2307/2963497

Daws, M. I., Mullins, C. E., Burslem, D., Paton, S. R., and Dalling, J. W. (2002). Topographic position affects the water regime in a semideciduous tropical forest in Panama. *Plant Soil* 238, 79–90. doi: 10.1023/a:1014289930621

Dovciak, M., Reich, P. B., and Frelich, L. E. (2003). Seed rain, safe sites, competing vegetation, and soil resources spatially structure white pine regeneration and recruitment. *Can. J. For. Res.-Rev. Can. Rech. For.* 33, 1892–1904. doi: 10.1139/x03-115

Du, H., Hu, F., Zeng, F., Wang, K., Peng, W., Zhang, H., et al. (2017). Spatial distribution of tree species in evergreen-deciduous broadleaf karst forests in southwest China. *Sci. Rep.* 7, 15664. doi: 10.1038/s41598-017-15789-5

Du, H., Liu, L., Su, L., Zeng, F., Wang, K., Peng, W., et al. (2019). Seasonal changes and vertical distribution of fine root biomass during vegetation restoration in a karst area, Southwest China. *Front. Plant Sci.* 9. doi: 10.3389/fpls.2018.02001

Gunatilleke, C. V. S., Gunatilleke, I. A. U. N., Esufali, S., Harms, K. E., Ashton, P. M. S., Burslem, D. F. R. P., et al. (2006). Species-habitat associations in a Sri Lankan dipterocarp forest. *J. Trop. Ecol.* 22, 371–384. doi: 10.1017/s0266467406003282

Guo, Y., Wang, B., Mallik, A. U., Huang, F., Xiang, W., Tao, D., et al. (2017). Topographic species-habitat associations of tree species in a heterogeneous tropical karst seasonal rain forest, China. *J. Plant Ecol.* 10, 450–460. doi: 10.1093/jpe/rtw057

Harms, K. E., Condit, R., Hubbell, S. P., and Foster, R. B. (2001). Habitat associations of trees and shrubs in a 50-ha neotropical forest plot. *J. Ecol.* 89, 947–959. doi: 10.1046/j.0022-0477.2001.00615.x

Hu, Y. H., Lan, G. Y., Sha, L. Q., Cao, M., Tang, Y., Li, Y. D., et al. (2012). Strong Neutral Spatial Effects Shape Tree Species Distributions across Life Stages at Multiple Scales. *PloS One* 7, e38247. doi: 10.1371/journal.pone.0038247

Jiang, Z., Lian, Y., and Qin, X. (2014). Rocky desertification in Southwest China: Impacts, causes, and restoration. *Earth-Sci. Rev.* 132, 1–12. doi: 10.1016/j.earscirev.2014.01.005

John, R., Dalling, J. W., Harms, K. E., Yavitt, J. B., Stallard, R. F., Mirabello, M., et al. (2007). Soil nutrients influence spatial distributions of tropical tree species. *Proc. Natl. Acad. Sci. United States America* 104, 864–869. doi: 10.1073/pnas.0604666104

Kanagaraj, R., Wiegand, T., Comita, L. S., and Huth, A. (2011). Tropical tree species assemblages in topographical habitats change in time and with life stage. *J. Ecol.* 99, 1441–1452. doi: 10.1111/j.1365-2745.2011.01878.x

Lai, J. S., Mi, X. C., Ren, H. B., and Ma, K. P. (2009). Species-habitat associations change in a subtropical forest of China. *J. Veg. Sci.* 20, 415–423. doi: 10.1111/j.1654-1103.2009.01065.x

Lai, J. S., Zou, Y., Zhang, J. L., and Peres-Neto, P. R. (2022). Generalizing hierarchical and variation partitioning in multiple regression and canonical analyses using the rdacca.hp R package. *Methods Ecol. Evol.* 13, 782–788. doi: 10.1111/2041-210X.13800

Liu, C., Berg, B., Kutsch, W., Westman, C. J., Ilvesniemi, H., Shen, X., et al. (2006). Leaf litter nitrogen concentration as related to climatic factors in Eurasian forests. *Glob. Ecol. Biogeogr.* 15, 438–444. doi: 10.1111/j.1466-822x.2006.00251.x

Liu, L., Zeng, F. P., Song, T. Q., Wang, K. L., and Du, H. (2020). Stand structure and abiotic factors modulate karst forest biomass in Southwest China. *Forests* 11. doi: 10.3390/f11040443

Lu, M. Z., Du, H., Song, T. Q., Peng, W. X., Su, L., Zhang, H., et al. (2021). Drivers of tree survival in an evergreen-deciduous broadleaf karst forest in southwest China. *For. Ecol. Manage.* 499, 119598. doi: 10.1016/j.foreco.2021.119598

Lusk, C. H. (2004). Leaf area and growth of juvenile temperate evergreens in low light: species of contrasting shade tolerance change rank during ontogeny. *Funct. Ecol.* 18, 820–828. doi: 10.1111/j.0269-8463.2004.00897.x

Malhi, Y., Silman, M., Salinas, N., Bush, M., Meir, P., and Saatchi, S. (2010). Introduction: Elevation gradients in the tropics: laboratories for ecosystem ecology and global change research. *Glob. Change Biol.* 16, 3171–3175. doi: 10.1111/j.1365-2486.2010.02323.x

Nakashizuka, T. (2001). Species coexistence in temperate, mixed deciduous forests. *Trends Ecol. Evol.* 16, 205–210. doi: 10.1016/s0169-5347(01)02117-6

Oksanen, J., Blanchet, F. G., Kindt, R., Legendre, P., Minchin, P., O'hara, R., et al. (2020). *Community ecology package* (R package version 2.5-7 2).

Poorter, L., and Markesteijn, L. (2008). Seedling traits determine drought tolerance of tropical tree species. *Biotropica* 40, 321–331. doi: 10.1111/j.1744-7429.2007.00380.x

Potts, M. D., Ashton, P. S., Kaufman, L. S., and Plotkin, J. B. (2002). Habitat patterns in tropical rain forests: A comparison of 105 plots in Northwest Borneo. *Ecology* 83, 2782–2797. doi: 10.2307/3072015

Potts, M. D., Davies, S. J., Bossert, W. H., Tan, S., and Nur Supardi, M. N. (2004). Habitat heterogeneity and niche structure of trees in two tropical rain forests. *Oecologia* 139, 446–453. doi: 10.1007/s00442-004-1525-3

Punchi-Manage, R., Getzin, S., Wiegand, T., Kanagaraj, R., Gunatilleke, C. V. S., Gunatilleke, I. A. U. N., et al. (2013). Effects of topography on structuring local species assemblages in a Sri Lankan mixed dipterocarp forest. *J. Ecol.* 101, 149–160. doi: 10.1111/1365-2745.12017

Quigley, M. F., and Platt, W. J. (2003). Composition and structure of seasonally deciduous forests in the Americas. *Ecol. Monogr.* 73, 87–106. doi: 10.1890/0012-9615(2003)073[0087:casosd]2.0.co;2

Reich, P. B., Uhl, C., Walters, M. B., Prugh, L., and Ellsworth, D. S. (2004). Leaf demography and phenology in Amazonian rain forest: A census of 40000 leaves of 23 tree species. *Ecol. Monogr.* 74, 3–23. doi: 10.1890/02-4047

Schilthuizen, M., Hoekstra, R. F., and Gittenberger, E. (2004). Hybridization, rare alleles and adaptive radiation. *Trends Ecol. Evol.* 19, 404–405. doi: 10.1016/j.tree.2004.06.005

Silvertown, J. (2004). Plant coexistence and the niche. *Trends Ecol. Evol.* 19, 605–611. doi: 10.1016/j.tree.2004.09.003

Sorensen, R., Zinko, U., and Seibert, J. (2006). On the calculation of the topographic wetness index: evaluation of different methods based on field observations. *Hydrol. Earth Syst. Sci.* 10, 101–112. doi: 10.5194/hess-10-101-2006

Su, L., Du, H., Zeng, F., Peng, W., Rizwan, M., Nunez-Delgado, A., et al. (2019). Soil and fine roots ecological stoichiometry in different vegetation restoration stages in a karst area, southwest China. *J. Environ. Manage.* 252, 109694. doi: 10.1016/j.jenvman.2019.109694

Team, R.C (2020). *R: A Language and Environment for Statistical Computing*.

Tuomisto, H., Ruokolainen, K., and Yli-Halla, M. (2003). Dispersal, environment, and floristic variation of western Amazonian forests. *Science* 299, 241–244. doi: 10.1126/science.1078037

Webb, C. O., Ackerly, D. D., McPeek, M. A., and Donoghue, M. J. (2002). Phylogenies and community ecology. *Annu. Rev. Ecol. Syst.* 33, 475–505. doi: 10.1146/annurev.ecolsys.33.010802.150448

Webb, C. O., and Peart, D. R. (2000). Habitat associations of trees and seedlings in a Bornean rain forest. *J. Ecol.* 88, 464–478. doi: 10.1046/j.1365-2745.2000.00462.x

Whitfield, J. (2002). Neutrality versus the niche. *Nature* 417, 480–481. doi: 10.1038/417480a

Whittaker, R. H. (1956). Vegetation of the great smoky mountains. *Ecol. Monogr.* 26, 1–69. doi: 10.2307/1943577

Wright, J. S. (2002). Plant diversity in tropical forests: a review of mechanisms of species coexistence. *Oecologia* 130, 1–14. doi: 10.1007/s004420100809

Wu, H., Franklin, S. B., Liu, J. M., and Lu, Z. J. (2017). Relative importance of density dependence and topography on tree mortality in a subtropical mountain forest. *For. Ecol. Manage.* 384, 169–179. doi: 10.1016/j.foreco.2016.10.049

Yamada, T., Tomita, A., Itoh, A., Yamakura, T., Ohkubo, T., Kanzaki, M., et al. (2006). Habitat associations of Sterculiaceae trees in a Bornean rain forest plot. *J. Veg. Sci.* 17, 559–566. doi: 10.1111/j.1654-1103.2006.tb02479.x

Frontiers in
Ecology and Evolution

Ecological and evolutionary research into our natural and anthropogenic world

This multidisciplinary journal covers the spectrum of ecological and evolutionary inquiry. It provides insights into our natural and anthropogenic world, and how it can best be managed.

Discover the latest Research Topics

See more →

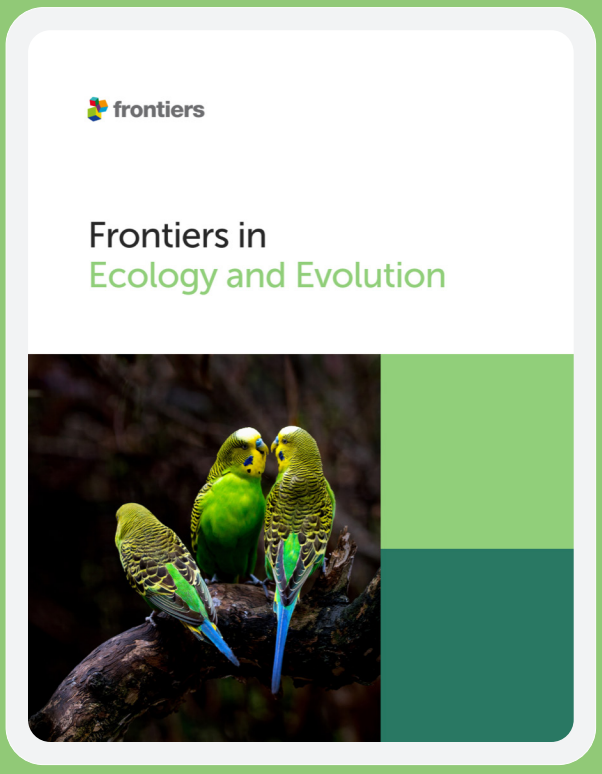

Frontiers

Avenue du Tribunal-Fédéral 34
1005 Lausanne, Switzerland
frontiersin.org

Contact us

+41 (0)21 510 17 00
frontiersin.org/about/contact